



**MAG**

MATHEMATICAL  
APPROACHES TO  
GEOPHYSICS

# Theoretical Glaciology

Kolumban Hutter

D. Reidel Publishing Company  
Dordrecht / Boston / Lancaster

Terra Scientific Publishing Company  
Tokyo, Japan

## **THEORETICAL GLACIOLOGY**

# **MATHEMATICAL APPROACHES TO GEOPHYSICS**

**Editor:**

**T. RIKITAKI** (*Nihon University*)

**Co-Editor:**

**M. HAZEWINKEL** (*Mathematics Centre, Amsterdam*)

**KOLUMBAN HUTTER**

*Federal Institute of Technology, Zurich*

# Theoretical Glaciology

**Material Science of Ice and the  
Mechanics of Glaciers and Ice Sheets**

**D. Reidel Publishing Company**



A MEMBER OF THE  
KLUWER ACADEMIC PUBLISHERS GROUP

**Dordrecht / Boston / Lancaster**



**Terra Scientific Publishing Company**  
Tokyo, Japan

**Library of Congress Cataloging in Publication Data**

Hutter, Kolumban.  
Theoretical glaciology.



(Mathematical approaches to geophysics)

Includes bibliographies and index.

1. Glaciology. I. Title. II. Series.

**GB2403.2.H88 1983 551.3'1 83-4479**

ISBN 978-94-015-1169-8 ISBN 978-94-015-1167-4 (eBook)

DOI 10.1007/978-94-015-1167-4

---

Published by D. Reidel Publishing Company,  
P.O. Box 17, 3300 AA Dordrecht, Holland,  
in co-publication with Terra Scientific Publishing Company, Tokyo, Japan

Sold and distributed in the U.S.A. and Canada  
by Kluwer Academic Publishers,  
190 Old Derby Street, Hingham, MA 02043, U.S.A.,  
in Japan by Terra Scientific Publishing Company,  
307 Shibuyadai-haim, 4-17 Sakuragaoka-cho, Shibuya-ku, Tokyo 150, Japan

In all other countries, sold and distributed  
by Kluwer Academic Publishers Group,  
P.O. Box 322, 3300 AH Dordrecht, Holland

All Rights Reserved

Copyright © 1983 by D. Reidel Publishing Company, Dordrecht, Holland

Softcover reprint of the hardcover 1st edition 1983

No part of the material protected by this copyright notice may be reproduced or utilized  
in any form or by any means, electronic or mechanical, including photocopying,  
recording or by any information storage and retrieval system,  
without written permission from the copyright owner

*to  
Barbara  
Bettina + Katja*

## TABLE OF CONTENTS

ACKNOWLEDGEMENTS	xiii
PREFACE	xv
INTRODUCTION	xix
SYMBOLS AND NOTATION	xxvii
PART I. FUNDAMENTAL PHYSICS AND MATERIALS TECHNOLOGY OF ICE	
<b>Chapter 1. General Concepts</b>	3
1. Introduction	3
2. Equations of Balance	4
3. Material Response	18
(a) General constitutive relations, simple materials	18
(b) The rule of material objectivity	20
(c) Material symmetry	22
(d) Constitutive response for isotropic bodies	25
(e) Materials with bounded memory – some constitutive representations	27
(f) Incompressibility	30
(g) Some representations of isotropic functions	30
4. The Entropy Principle	33
(a) The viscous heat-conducting compressible fluid	34
(b) The viscous heat-conducting incompressible fluid	37
(c) Pressure and extra stress as independent variables	38
(d) Thermoelastic solid	39
(e) Final remarks	40
5. Phase Changes	41
(a) Phase changes for a viscous compressible heat-conducting fluid	42

(b) Phase changes for a viscous incompressible heat-conducting fluid	46
References	46
<b>Chapter 2. A Brief Summary of Constitutive Relations for Ice</b>	<b>48</b>
1. Preliminary Remarks	48
2. The Mechanical Properties of Hexagonal Ice	49
(a) The crystal structure of ordinary ice	49
(b) The elastic behavior of hexagonal ice	52
(c) The inelastic behavior of single-crystal ice	56
3. The Mechanical Properties of Polycrystalline Ice	60
(a) The elastic behavior of polycrystalline ice	60
(b) Linear viscoelastic properties of polycrystalline ice	63
(α) General theory	63
(β) Experimental results	77
(c) Non-linear viscous deformation and creep	81
(α) Results of creep tests	81
(β) Generalization to a three-dimensional flow law	85
(γ) Other flow laws	91
4. The Mechanical Properties of Sea Ice	99
(a) The phase diagram of standard sea ice and its brine content	100
(b) Elastic properties	103
(c) Other material properties	105
References	110

**PART II. THE DEFORMATION OF AN ICE MASS UNDER ITS OWN WEIGHT**

<b>Chapter 3. A Mathematical Ice-flow Model and its Application to Parallel-sided Ice Slabs</b>	<b>119</b>
1. Motivation and Physical Description	119
2. The Basic Model – Its Field Equations and Boundary Conditions	122
(a) The field equations	124
(α) Cold ice region	124
(β) Temperate ice region	126
(b) Boundary conditions	131
(α) At the free surface	132
(β) Along the ice-water interface	136
(γ) Along the bedrock surface	138
(δ) Along the melting surface	143
3. The Response of a Parallel-sided Ice Slab to Steady Conditions	145
(a) Dimensionless forms of the field equations	148
(b) Parallel-sided ice slab, a first approximation to glacier and ice-shelf flow dynamics	154
(α) Velocity and temperature fields $\bar{x}$ -independent	155

## TABLE OF CONTENTS

ix

( $\beta$ ) Extending and compressing flow	166
( $\gamma$ ) Floating ice shelves	179
<b>4. Concluding Remarks</b>	<b>183</b>
<b>References</b>	<b>184</b>
<b>Chapter 4. Thermo-mechanical Response of Nearly Parallel-sided Ice Slabs Sliding over their Bed</b>	<b>188</b>
1. Motivation	188
2. The Basic Boundary-value Problem and its Reduction to Linear Form	190
3. The Solution of the Boundary-value Problems	199
(a) Zeroth-order problem	199
(b) First-order problem	200
( $\alpha$ ) Harmonic perturbation from uniform flow for a zero accumulation rate	202
( $\beta$ ) Analytic solution for a Newtonian fluid	204
( $\gamma$ ) Numerical solution for non-linear rheology	208
( $\delta$ ) Effect of a steady accumulation rate	212
( $\varepsilon$ ) A historical note on a previous approach	214
( $\eta$ ) The first-order temperature problem	215
(c) Numerical results for steady state	218
( $\alpha$ ) Transfer of bottom protuberances to the surface	220
( $\beta$ ) Basal stresses	230
( $\gamma$ ) Surface velocities	236
( $\delta$ ) Effect of a steady accumulation rate	240
4. Remarks on Response to a Time-dependent Accumulation Rate	242
5. Surface-wave Stability Analysis	243
(a) The eigenvalue problem	244
(b) Discussion of results	249
6. Final Remarks	252
<b>References</b>	<b>253</b>
<b>Chapter 5. The Application of the Shallow-ice Approximation</b>	<b>256</b>
1. Background and Previous Work	256
2. Derivation of the Basal Shear-stress Formula by Integrating the Momentum Equations over Ice Thickness	260
(a) Derivation	260
(b) The use of the basal shear-stress formula in applied glaciology	264
3. Solution of the Ice-flow Problem using the Shallow-ice Approximation	268
(a) Governing equations	268
(b) Shallow-ice approximation	270
(c) Construction of the perturbation solution	274

## TABLE OF CONTENTS

(d) Results	282
(e) Temperature field	289
4. Theoretical Steady-state Profiles	292
(a) Earlier theories and their limitations	292
(b) Surface profiles determined by using the shallow-ice approximation	298
5. An Alternative Scaling – a Proper Analysis of Dynamics of Ice Sheets with Ice Divides	309
(a) Finite-bed inclination	314
(b) Small-bed inclination	316
(c) Illustrations	321
References	330

**Chapter 6. The Response of a Glacier or an Ice Sheet to Seasonal and Climatic Changes**

	<b>333</b>
1. Statement of the Problem	333
2. Development of the Kinematic Wave Theory	336
(a) Full non-linear theory	336
(b) Perturbation expansion – linear theory	341
(c) An estimate for the coefficients $C$ and $D$	342
(d) Boundary and initial conditions	346
3. Theoretical Solutions for a Model Glacier	346
(a) Solutions neglecting diffusion	347
(b) Theoretical solutions for a diffusive model	353
( $\alpha$ ) Coefficient functions for the special model	353
( $\beta$ ) Solution for a step function	355
( $\gamma$ ) General solution for uniform accumulation rate	363
( $\delta$ ) The inverse problem – calculation of climate from variations of the snout	367
4. General Treatment for an Arbitrary Valley Glacier	369
(a) Fourier analysis in time	370
( $\alpha$ ) Low-frequency response	371
( $\beta$ ) High-frequency response	373
( $\gamma$ ) Use of the results	374
(b) Direct integration methods	375
5. Derivation of the Surface-wave Equation from First Principles – Non-linear Theory	377
(a) Surface waves in the shallow-ice approximation	379
( $\alpha$ ) Integration by the methods of characteristics	382
( $\beta$ ) An illustrative example	392
( $\gamma$ ) A remark on linearization	398
( $\delta$ ) Effects of diffusion	400
(b) Remarks regarding time-dependent surface profiles in ice sheets	403

## TABLE OF CONTENTS

xi

(c) Long waves in an infinite ice slab – Is accounting for diffusion enough?	404
(α) Basic equations	405
(β) Construction of perturbation solutions	407
(γ) Numerical results	416
6. Concluding Remarks	420
References	421
<b>Chapter 7. Three-dimensional and Local Flow Effects in Glaciers and Ice Sheets</b>	<b>424</b>
1. Introduction	424
2. Effect of Valley Sides on the Motion of a Glacier	425
(a) Solutions in special cases	428
(α) Exact solutions for the limiting cases	428
(β) Solution for a slightly off-circular channel	431
(γ) A note on very deep and wide channels	434
(b) A useful result for symmetrical channels with no boundary slip	438
(c) Numerical solution – discussion of results	441
3. Three-dimensional Flow Effects in Ice Sheets	450
(a) Basic equations	451
(b) Decoupling of the stress-velocity problem from the problem of surface profile	455
(c) The equation describing the surface geometry	460
(d) The margin conditions	461
4. Variational Principles	462
(a) Fundamental variational theorem	463
(b) Variational principle for velocities	467
(c) Reciprocal variational theorem	468
(d) Maximum and minimum principles	471
(e) Adoption of the variational principles to ice problems	474
5. Discussion of Some Finite-element Solutions	476
References	482
<b>Appendix. Detailed Calculations Pertaining to Higher-order Stresses in the Shallow-ice Approximation</b>	<b>484</b>
AUTHOR INDEX	490
SUBJECT INDEX	494

## **ACKNOWLEDGEMENTS**

Most graphs contained in this book and taken from other works are redrawn. Nevertheless, thanks are due to the following for permission to reproduce diagrams and photographs indicated in the text: Dr W. F. Budd (5.4); Dr G. C. K. Clarke (3.8, 3.17, 3.18, 3.20, 3.21, 3.22, 3.23, 3.24, 3.25); Dr J. W. Glen (2.2, 2.4, 2.5, 2.14, 2.15, 2.20); Dr A. Higashi (2.6); Dr A. Iken (7.17, 7.18, 7.19); Dr M. Mellor (2.13); Dr L. W. Morland (5.17, 5.19, 5.20, 5.21, 5.22, 5.23); Dr J. W. Nye (6.4, 6.8, 6.10, 7.5, 7.6, 7.9, 7.10, 7.11, 7.12, 7.14, 7.15); Dr W. S. B. Paterson (5.15); Dr C. Richardson (2.25); Dr S. Steinemann (2.16, 2.17, 2.18); Dr D. E. Thompson (4.22, 4.23, 4.24); Dr W. Weeks (2.26, 2.27, 2.29, 2.30, 2.31, 2.32); Dr J. Weertman (3.18); Dr D. A. Yuen (3.15, 3.16).

Academic Press, Inc. (5.15); American Geophysical Union (3.8, 3.17, 3.18, 3.20, 3.21, 3.22, 3.23, 3.24, 3.25); Dover Publications, Inc. (2.1); International Association of Hydrological Sciences (2.20, 5.4); International Glaciological Society (7.17, 7.18, 7.19); Japan Institute of Metals (2.6); Naval Civil Engineering Laboratories (2.26); The Royal Society (2.21, 6.4); Schweizerische Naturforschende Gesellschaft (2.16, 2.17, 2.18); U.S. Army Cold Region Science and Engineering Laboratory (2.2, 2.14, 2.15).

## PREFACE

The purpose and scope of this book on *theoretical glaciology* is outlined in the Introduction. Its aim is to study the theoretical aspects of 'ice mechanics' and the 'dynamics of ice masses in a geophysical environment'. For the mature reader, the book can serve as an introduction to glaciology. However, this is not what I would regard as advisable. Glaciology is an interdisciplinary science in which many special scientific disciplines play their part, from descriptive geography to fairly abstract mathematics. Advancement will evolve from a merger of two or more branches of scientific specialization.

In the last 20 years, several researchers in different fields of glaciology have written books emphasizing the aspects of their specialities and I have listed some which are known to me at the end of the Introduction. When glancing through these books, one recognizes that the mathematical aspects of glaciology are generally glossed over and, to date, there seems to be nothing available which concentrates on these. Therefore, I have written this book in an effort to close the gap and no apologies are offered for the mathematical emphasis. Rather, I believe that this neglect has, to a certain extent, aggravated progress in the modelling of glaciology problems. The mechanics of ice, the fluid dynamics of glaciers and ice masses in particular, and of ice in its geophysical environment in general, are so complex that a presentation of the most important aspects of the 'theoretical' literature from a unified concept might enhance and simplify our understanding. In doing so, I found that the mathematics of ice creep and the fluid dynamics of glaciers and large ice masses indeed allows the deduction of known results from a common basis, but the study also indicates that many problems – for which the more applied glaciologists would like to have answers – have not been touched mathematically so far. It is possible therefore that this book raises more queries than it gives answers to the questions posed by glaciologists. If it really does, I would interpret this as a tacit compliment.

I seriously started writing this book in 1979 when I had the occasion to spend a leave of absence at the University of Arizona, Tucson, as a teacher of mechanics. I am grateful to Dean R. H. Gallagher for the appointment

making the plan possible. Although precursors to Chapters 1, 2 and parts of Chapter 7 were available as notes from lectures held at Memorial University, St Johns, Newfoundland, and the Technical University, Vienna, Chapters 1 to 6 were drafted in 1979/1980 in Tucson. I am grateful to Professors R. A. Seebass and S. Yakowitz for their enthusiasm in my work and for the discussions we had in seminars and during many lunch breaks. I am particularly thankful to Prof. Yakowitz for his friendship and encouragement that kept me going while spending endless hours in writing and erasing. Chapter 7 was wholly written in Zurich, and so were the amendments and extensions of Chapter 3, 5 and 6. I thank Prof. Vischer of the Laboratory of Hydraulics, Hydrology and Glaciology for permitting me to use part of my working time for this project and, in particular, for his permission to allow me to use the secretarial and drawing staff of the laboratory for typing and drawing purposes.

The contents have been tested in lectures, and certainly profited from this involvement. Two such experiences have already been mentioned. Influential were the applied mathematics seminars on fluid dynamics of glaciers at the University of Arizona, Tucson, which Prof. R. A. Seebass kindly organized for me. I am grateful to the audience of these seminars for the discussions that influenced my early writings. The book has further profited from an invitation by the authorities of the Stephan Banach International Mathematical Center in Warsaw to teach a course on 'Mathematical Models and Methods in Contemporary Mechanics' in the spring of 1981. I am grateful to their organizing committee and in particular, to Prof. K. Wilmanski for the invitation and to the participants of the lectures, for it gave me the occasion to go through the entire manuscript once more and to make further amendments and eliminate further misprints. Several scientists have, either directly or indirectly, helped to improve the manuscript. Dr Morland of the University of East Anglia has criticized in detail Chapters 1 and 2 and suggested many improvements and he and Dr Fowler of the University of Dublin have kindly let me see unpublished work done by them and their co-authors. These have found their way into the writing. Prof. G. C. K. Clarke of the University of British Columbia, Vancouver, has discussed with me the problem of thermal instability and sent me amended graphs of his work on such instabilities. Dr A. Iken from the Laboratory of Hydraulics, Hydrology and Glaciology has helped me in tracing the finite element literature on glacier flow problems. I would also like to thank my former students Drs Hofer, Spring, and Raggio from whom I have learned more than many supervisors generally admit can be learned from students.

It is not particularly easy to write in English which is not my native language, but I have tried very hard. Parts of the manuscript were screened by Drs T. Davies, G. Smart, and B. Straughan, but unfortunately I failed

to find somebody to look through the entire manuscript. The publishers, D. Reidel Publishing Company, have taken on this responsibility. I am deeply thankful to them and, in particular, to Prof G. Csanady of Woods Hole Oceanographic Institution, for giving me the chance to publish this work, and to make it the way it looks now.

I wish to thank all those who helped me through the task. Mesdame, S. Thomas, B. Stier, M. Coray, M. Gassler and Mr F. Langenegger took the burden in Tucson and Zurich, respectively, to disentangle my 'interplanetary' handwriting (as Langenegger says) and Mrs J. Wiederkehr, Mr C. Bucher and Mr W. Nobs produced the final drawings. I am particularly grateful to Mr Langenegger for not hesitating to make every effort to minimize my involvement with the editing, to Messrs Wiederkehr and Bucher for their good and efficient work, and to the latter for the proof that 'doing it' aside of all the other work is simply a matter of organization. Finally, Mr Th. Scheiwiller assisted me in reading through the proofs, and I gratefully acknowledge his help.

My wife Barbara and my daughters have spent endless hours from early morning to late night, weekdays and weekends, on their own. They deserve my gratitude; it is therefore a pleasure for me to dedicate this book to these three women in my life.

K. Hutter  
Zurich,  
*February 1983*

## INTRODUCTION

This book is designed as a comprehensive ‘mathematical’ introduction to the science of the behavior of glaciers and ice sheets in their geophysical environment. As the last two or three decades have witnessed, a large impetus in fundamental understanding of the field of glaciology in its broadest meaning, various specialized branches of glaciology have developed and moved ahead in their own directions. Geography, geomorphology, geophysics, material science, continuum mechanics, meteorology, physics, oceanography, and applied mathematics, to name a few, are sciences distinct in their basic training and aims, in which glaciology may legitimately be treated as a field of specialization. Because of such interdisciplinary character, progress in the subject often seems to be aggravated by barriers that exist among various scientific disciplines if simply because of the differences in vocabulary. I do not believe that this book will be able to lift *all* these walls, but the intention is to stand up for clear unification of the mathematical description of problems that may be collectively summarized under the term ‘*ice mechanics*’. Even within this limited understanding, the field of glaciology is so diverse that it is, in general, very difficult for the non-specialist to be able to grasp arguments or theories let alone be able to solidly judge the appropriateness of these arguments or theories. For instance, the material scientist’s concern has, during the last two decades, been concentrated on testing basically one-dimensional specimens of ice grown under various conditions. These specimens are subjected to ideal stress states such as uniaxial compression or simple shear under constant stress or constant strain rate. Creep curves are then published characterizing the material but attempts to use these creep curves to derive a constitutive relationship relating stress with the deformation that is typified by the creep curves are unsatisfactory. It is, however, clear that creep curves performed under a constant stress and strain rate should be reproducible from a mathematical model describing both experimental outcomes as the response of one and only one material. Further, ice flow in its geophysical environment is three- or, at least, two-dimensional and a constitutive relationship for this bi- or tri-axial situation must be found. Uniaxial and shear stress tests do not suffice to deduce a three-dimensional stress relation.

It is at this point that modern methods of continuum mechanics can help constructively. These methods were and still are being developed in the context of rheology and it is well known that (experimental) viscometry has profited tremendously from the fundamental studies of general constitutive theories. In this regard the present status of the material science of ice is unsatisfactory and is in the process of just leaving its virginity. One goal of this book is to make the reader aware of the usefulness of merging modern constitutive theory with material science.

It would appear strange that as an appropriate constitutive relationship for the two- and three-dimensional response of ice under creeping motion is not available, this book goes on, in its third chapter and beyond, to study the flow and deformation of glacier and ice-sheet models in which firm knowledge of a three-dimensional constitutive relationship is vital. The reason is that ice flow processes in the geophysical environment take place under typical time scales for which the detailed behavior of the creep curves discussed above are irrelevant! On the basis of this cognition, glaciers and ice sheets are postulated or assumed to behave as a very viscous fluid much like honey. Such fluids, known as non-Newtonian liquids, have been clearly understood for nearly 30 years and during this time glaciology literature has been enriched by articles in which mechanical aspects of glacier and ice sheet flows were presented. The first analyses aimed at a description of ice flow by studying simple geometries, such as the plane motion of a strictly parallel-sided ice slab, using purely mechanical models. Thermal effects were either set aside or, when temperature was allowed to vary within the ice region, simplifications were introduced which allowed uncoupling of the mechanical from the thermal fields. Furthermore, although it was recognized that glaciers and ice sheets occur in essentially two different forms, *temperate* and *cold*, the theoretical formulations of these two thermodynamic states were not clearly differentiated. The terms ‘temperate’ and ‘cold’ hereby mean ice that is everywhere at the melting temperature and ice that is colder, respectively. Accordingly, glacier or ice sheets are called temperate or cold depending on whether the ice is at or below the melting temperature. Glaciers can, however, also be *polythermal* which means that they constitute two thermodynamically different zones, one temperate the other cold, separated by a transition surface. A satisfactory mathematical formulation of the thermomechanical response of polythermal glaciers does not yet exist but consistent descriptions of the response of wholly cold or wholly temperate ice regions are available.

Scrutiny of available literature dealing with the thermomechanical aspects of glaciers and ice sheets reveals that problems of flow and temperature distribution are mostly treated in an uncoupled fashion and are often loaded with (hidden) *ad-hoc* assumptions. When stress and velocity distributions are of interest, the temperature distribution is assumed to be known. On the

other hand, for questions of temperature distributions the velocity and stress fields are regarded as known, thereby achieving a separation of the energy equation from the mechanical equations. In reality, ice flow and temperature distribution problems are interrelated and uncoupling, while not direct, can often be justified by the application of an iterative solution procedure for the full thermomechanical problem. Many *ad-hoc* theories can be explained this way and indeed, by deriving these formulations from first principles, they become physically more transparent and easier to understand, notwithstanding that assumptions can clearly be stated and delimited.

A typical example belonging to this class is the formula known to (almost) every glaciologist, for shear stress at the base of an ice sheet or glacier. This formula says that basal shear stress is proportional to local depth and to the slope angle of the top surface relative to the horizontal, directly above the point under consideration. This relationship between stress, depth and surface angle arises in almost every piece of work on glacier and ice sheet flow. It is as highly respected as if it were one of the Ten Commandments set before us on a stone slab by some glaciological Moses. The formula has been subject to heresy and extensions to it have been presented by the most prominent scientists in the field. Yet these studies, right or wrong, mostly fail to derive the formula for basal shear stress from first principles by either not stating clearly its range of validity, or else by not deriving it as a first approximation from an approximation scheme. Such rational derivations are possible and have been presented, indeed, they clearly state the fundamental assumptions that the formula is based upon and have paved the route for improvements. These derivations show that stress is not at all as an important quantity as has been emphasized. What is of relevance are physically-measurable quantities such as velocity components and strain-rates and temperature, from which stress is obtained as a derived quantity. In my opinion, this should be emphasized much more than is currently the practice in glaciology.

Whereas questions of stress, velocity and temperature distribution are relatively clearly understood so that their presentation in this book merely necessitates a collection of the available literature in a form that is easily accessible from one single set of basic equations, this is not the case for problems dealing with the derivation of the *geometry* of glaciers and ice sheets. The mathematical problem of determining the surface geometry, either steady-state or time-dependent, is still not clearly understood. Usual attempts to prove a satisfactory understanding of the steady-state ice sheet geometry by comparing existing profiles with theoretically-determined surface profiles are misleading, if not wrong. However, a sound theoretical treatment of determination of the surface profile from a combination of the kinematic surface condition with the kinematic boundary condition at the base and the balance laws of mass and momentum is possible. What emerges is

the *kinematic wave equation* in which the mass flux is related to a force balance statement. In the general case, the emerging equation is a nonlinear evolution equation for the surface geometry, of which the form depends on the order of approximation to which stress and velocity components are determined. For the lowest order, the simple forward wave equation emerges and for first order, the convection-diffusion equation results but further analysis of the problem indicates that dispersion or even higher-order effects should be accounted for. However, whereas derivation of the differential equation for the surface profile seems to be straightforward, it is very difficult to derive appropriate boundary conditions at the head and the snout of a glacier and indeed present knowledge is not satisfactory in this regard for the motion of surface bulges travelling down-glacier still cannot be analysed with the simultaneous inclusion of temporary advances and retreats of glacier snouts.

Whereas the mathematical subtleties encountered in the analysis of glacier-flow problems can be explained by looking at plane deformation, three-dimensional analyses are necessary as soon as quantitative information is sought. Such three-dimensional problems often defy an analytic, or semi-analytic procedure; numerical techniques are needed at a more or less early stage of the study. Nonetheless, it is not necessary to hastily dig into computer applications. A good example of this is the three-dimensional study of ice-sheet flow. By invoking the assumption of slowly varying geometry, the full three dimensional equations can be considerably simplified and may in this reduced form, be more accessible to numerical exploration than the full equations.

The content of the book is as follows: Chapter 1 presents the general background of continuum mechanics. The balance laws of mass, momenta and energy are presented along with the constitutive theory. It is shown how constitutive relationships are postulated and how the postulated material relations are reduced to be independent of the observer, to reflect certain symmetries and to conform with the second law of thermodynamics. In view of the importance of processes at melting, phase changes are given more attention than is usually the case in books dealing with continuum mechanics.

Chapter 2 then presents a review of mechanical properties of ice. No claim is made that the review is complete but an attempt is made to link the material scientist's view as much as possible with the methods of continuum mechanics. Chapters 1 and 2 together give a fair appraisal of the techniques and knowledge available to the material scientist of ice. It is also believed that these two chapters are most likely to be of interest to every glaciologist.

Chapter 3 presents a continuum model for a polythermal glacier or ice sheet. The field equations and boundary conditions at the free surface, base, ice-water interface, and transition surface between cold and temperate ice, are derived. Equations are then put into non-dimensional form and the

first simple applications, dealing with the motion and temperature distribution in a strictly parallel-sided slab resting on a horizontal or inclined flat bed are presented. This very simple geometry already allows analysis of the flow and temperature distribution in ice slopes and ice shelves and gives the possibility of discussing the very difficult problem of thermal instability.

Chapters 4 to 6 continue the analysis of glacier and ice-sheet models by allowing the surface and bottom geometry to vary with position and time. First, in Chapter 4, steady-state, nearly parallel sided ice slabs are analysed and it is shown how small bottom protuberances are transferred to the top and how the stress and velocity distribution is affected by the bed and surface undulations. A similar study is made of the temperature distribution and finally a stability analysis of small amplitude surface waves is made. Common to all these studies is the assumption that bottom and top surfaces are such that the geometry of the ice slope deviates only slightly from a strictly parallel-sided ice slab. Such analyses give useful information on processes with length scales which are small with respect to the overall length of the sheet.

This restriction is relaxed in Chapter 5 which presents an analysis of ice flow (and temperature distribution) for length scales comparable to the entire length or dominant horizontal extent of the glacier or ice sheet. Simplifications must, however, be introduced in order to be able to extract explicit information from the complicated non-linear thermomechanical problem. The essential idea is to ignore local effects such as sudden changes in topography and to assume that both the top and bottom surfaces *slowly vary* with position. This assumption allows a drastic reduction in the complexity of the equations resulting in approximate analyses of steep glaciers flowing only in one direction and ice sheets which possess ice divides.

It is in Chapter 5 that the shear stress formula mentioned earlier is closely investigated. It is also in this chapter that the problem of steady-state glacier and ice-sheet geometry is formulated. Both questions have kept mathematical modellers in glaciology busy for a long time. By invoking the assumption of slowly varying geometry, the effects of the longitudinal strain rate gradient on the distribution of the stresses, find their natural explanation; similarly a natural and rational procedure can be found to derive the equations governing steady-state surface profiles. There are, however, many unanswered questions relating to the determination of the profile of a glacier or an ice sheet which indicates that much research is still left until a full mathematical description of glacier geometry is possible.

Whereas Chapter 5 deals with steady-state geometry, Chapter 6 concentrates upon time-dependent processes. At first an appraisal of the linear theory of kinematic waves is given as it was developed by Nye. This study is then complemented by a non-linear treatment of surface waves on glaciers and ice sheets. This non-linear formulation will prove to be useful in future.

more complete studies of waves on glaciers and, by exploring its first consequences, we hope to generate the interest of the more mathematically-inclined reader. There is still a wealth of many unanswered basic questions whose solution must be awaited before successful treatment of waves on glaciers is possible.

Whereas ice flow and temperature distributions are assumed to be plane in Chapters 4 to 6, we conclude in Chapter 7 with a brief study of three-dimensional effects. Three basic problems are treated, namely rectilinear flow in channels, two-dimensional horizontal spreading of ice sheets, and the variational principles that apply to the non-linear laws used in the preceding chapters. The first problem serves to demonstrate that valley sides have a non-negligible effect on the flow and reduce the stresses by a considerable amount. In the second problem it is demonstrated as to how difficult it is to formulate (and explore) a theory of multi-dimensional ice sheet flow. The variational principles, finally, pave the route to numerical finite element techniques of which the most relevant problems are briefly stated. However, the variational principles are also helpful from another point of view, as they permit the construction of upper and lower bounds for many other problems.

Whereas many important topics are not touched upon, some new and I hope enlightening results are presented for the first time in this book. Among these, I mention the developments in some aspects of steady- and unsteady-surface geometry in Chapters 5, 6 and 7. That which is new can after all be checked by the reader himself, however, I should offer apologies for the many omissions that have obviously been made. Firstly, a word on literature citations. The cited references are highly selective. Naturally, 'theoretical' work receives more consideration than 'applied' work. This is not a valuation but rather an emphasis. I have mentioned only those references which I felt at the time of writing were either relevant to the particular questions at hand or else would give the reader additional background information. Less weight was assigned to older literature than to the more recent works, simply to facilitate the reader in his own literature search. To all authors of important papers that have been omitted, I would like to offer my apologies. Secondly, some important topics were either entirely deleted or hardly touched upon. The most serious omission is that little is said about the role of water in temperate glaciers. This omission includes the detailed presentation of a sliding law. However, since the mathematics of sliding and a general (and correct!) analysis of water in temperate ice are extremely difficult, I have decided to leave further sophisticated treatment of this topic to another study. For the time being, the reader is advised to peruse the basic literature and to accept my *ad-hoc* formulation of sliding as a possibility subject to revision.

It is hoped that glaciologists who model ice flow problems will find this

book useful. The mathematically-weak student or scientist should be warned that reading will most probably not be easy and progress therefore slow but if he succeeds in reading through several chapters, I hope he will experience the same enlightenment that I did when studying and disentangling the scattered literature; namely that there is a rational, unified approach making the dynamics of ice masses a challenging field in non-Newtonian fluid mechanics. The applied mathematician interested in glaciology on the other hand, may miss mathematical rigor and find large parts of the book wordy, however, despite these disadvantages I trust he will find a wealth of unsolved problems and unanswered questions which hopefully will challenge him in his own studies.

The reader, scientist or student, is expected to know basic 'engineering mathematics', including Cartesian tensors, differential equations, elements of asymptotic theories and continuum mechanics. While a systematic training in these topics is not necessary because the mathematical background is developed along with the particular problem at hand, a first year graduate level engineering mathematics training (or equivalent) should suffice for this book to serve as a basis for graduate courses in geophysics, engineering, or applied mathematics. To the engineer, the first two chapters can form the basis for training in continuum mechanics and some aspects of material science; on the other hand, Chapters 3 to 7 (with a brief introductory glance over the important parts of the first two chapters) can serve as a basis for a semester course in theoretical glaciology to students of mathematics, geophysics, meteorology, environmental fluid mechanics, and so on. The investment of endless hours of writing this book will have been well worthwhile if it proves not only useful as a basis for graduate classes, but also as a reference for the scientist.

## REFERENCES

- Colbeck, S. C. (ed.), *Dynamics of Snow and Ice Masses*, Academic Press, 1980.  
Hobbs, P. V., *Ice Physics*, Clarendon Press, Oxford, 1974.  
Lliboutry, L. A., *Traité de Glaciologie*, Tome 1, Masson, Paris, 1964.  
Lliboutry, L. A., *Traité de Glaciologie*, Tome 2, Masson, Paris, 1965.  
Michel, B., *Ice Mechanics*, Les presses de l'Université Laval, Quebec, 1978.  
Paterson, W. S. B., *The Physics of Glaciers*, Pergamon Press, Oxford, 2nd Edn. 1981.  
Shumskiy, P. A., *Dynamic Glaciology*. Transl. from the Russian, Amerind Publishers, 1978.  
Sugden, D. E. and John, B. S., *Glaciers and Landscapes*, Edward Arnold, London, 1976.

## SYMBOLS AND NOTATION

$A, \mathcal{A}$	rate factors in stress-stretching relation
$\mathbf{A}, \mathcal{A}$	matrices arising in vector two-point boundary-value problems (Chapter 4)
$\mathbf{A}_{(n)}$	$n$ th Rivlin–Ericksen tensor
$\mathbb{A}$	Arrhenius number (Chapter 3)
$\mathfrak{U}$	dimensionless accumulation rate in stretched variables
$\mathfrak{a}, \mathfrak{a}_\perp, \mathfrak{a}$	accumulation rate functions
$\mathfrak{a}_M^\perp$	melting rate function
$da, dA$	surface elements in the present and reference configuration, respectively
$B$	glacier width
$B, \mathcal{B}$	power law constants in the stress-stretching relationship
$\mathcal{B}, \mathcal{B}_t, \mathcal{B}_R$	body, in its present and reference configurations
$\partial \mathcal{B}, \partial \mathcal{B}_t, \partial \mathcal{B}_R$	corresponding body surfaces
$\mathbf{b}$	time-dependent vector
$\mathbf{C}$	right Cauchy–Green deformation tensor
$\mathcal{C}$	basal sliding coefficient
$\mathfrak{C}$	fourth-rank tensor of elastic constants
$\mathfrak{C}$	(kinematic) wave velocity
$\mathbf{C}$	$6 \times 6$ matrix of elasticity coefficients
$\mathbb{C}$	dimensionless basal friction number
$\mathbb{C}_M$	dimensionless coefficient in basal sliding law close to margin
$C, c$	phase speeds
$c_p$	specific heat
$c_w$	drag coefficient
$c_t = -dT_M/dp$	pressure-melting constant
$c_x$	mass fraction of constituent $x$
$D, d$	ice sheet thickness
$\mathbf{D} = D_{ij}$	stretching tensor = tensor of strain rates
$D_{(I)}, D_{(II)}, D_{(III)}$	invariants of stretching tensor
$D, \mathfrak{D}$	diffusivities

$\mathbb{D}, \mathbb{D}_w$	dimensionless diffusion numbers
$E$	Young's modulus
$E_z$	elastic constants
$\mathbf{E}$	Lagrangian strain tensor
$\mathcal{E}$	exponential integral
$\mathfrak{E}$	coefficient arising in the surface-wave equation
$\mathbb{E}, \mathbb{E}_w$	energy dissipation number
$e_{ijk}$	permutation symbol
$F$	depth averaged longitudinal force
$\mathbf{F} = F_{iA}$	tensor of deformation gradient
$\mathcal{F}$	transfer or filter function
$\mathfrak{F}$	dimensionless creep response function, coefficient arising in the surface-wave equation
$\mathbb{F}$	Froude number, creep response function in stretched coordinates
$\mathbf{f} = f_i$	external body force
$\mathbf{f}, \mathbf{f}'$	vectors in general two-point boundary-value problems (Chapter 4)
$G_\alpha$	coefficient of relaxation functions
$\mathcal{G}, \mathcal{G}, \mathcal{G}_\alpha$	relaxation functions
$\mathfrak{G}$	coefficient arising in the surface-wave equation
$\mathbb{G}$	'Glen' number
$g$	gravity constant
$g = 1/T$	coldness
$\mathbf{g}$	vector of gravity acceleration, or temperature gradient
$\mathbf{g}'$	vector arising in general two-point boundary-value problem
$H$	Heaviside function
$H_n$	functions arising in the determination of steady-state perturbed ice thickness (Chapter 6)
$\mathcal{H}$	Fourier-transformed perturbed ice thickness function
$\mathfrak{H}$	coefficient arising in the surface-wave equation, functional arising in variational principle for stresses enthalpy, Planck's constant
$h$	Perturbed ice depths
$h_1, h_1^\infty$	time averages of the function
$\langle h \rangle_i$	symbol for a general integral
$I$	counting index
$i$	Jacobian of the tensor of deformation gradient
$J$	creep functions of linear viscoelasticity
$\mathcal{J}, \mathcal{J}, \mathcal{J}_z$	functional, arising in variational principle for velocities
$\mathfrak{J}$	diffusive flux
$\mathcal{K}$	fourth-rank tensor of linear viscosities
$k$	bulk modulus, Boltzmann's constant

$\mathbb{K}$	dimensionless constant arising in a particular creep response function
$L$	latent heat of fusion
$L, L^*$	characteristic lengths
$\mathbb{L}$	'fusion number'
$m$	exponent arising in the power law sliding law
$M$	'Clausius–Clapeyron number'
$n$	brine content
$\mathbf{n}$	unit normal vector
$N, Nu$	Nusselt numbers
$\mathbf{O}$	orthogonal transformation
$\mathcal{O}$	order symbol
$\mathbf{P} = P_{AB}$	deformation gradient from one reference configuration to another
$\mathcal{P}, \mathcal{P}_t, \mathcal{P}_R$	parts of a body
$\mathbb{P}, \mathbb{P}r$	Prandtl number
$p$	pressure
$Q$	activation energy, volume flux
$\mathbf{Q} = Q_A$	heat flux vector (reference configuration)
$Q_i$	coefficients arising in accumulation rate function
$\mathcal{Q}$	Fourier transform of the function $q$
$\mathfrak{Q}$	functional for heat flux
$\mathbb{Q}$	dimensionless heat flux
$q$	flux (general)
$\mathbf{q} = \mathbf{q}_i$	heat flux vector (present configuration)
$R$	radius
$\mathbf{R}$	rotation tensor
$\text{Re}$	Reynolds number
$r$	radial coordinate
$r_o$	longitudinal stretching
$S$	depth-averaged longitudinal force, cross-sectional area
$S_k$	parameter arising in the determination of surface variations (Chapter 6)
$\mathcal{S}$	singular surface
$\mathcal{S}, \mathcal{S}_s, \mathcal{S}_w$	bounding surface (free surface, ice-water interface etc.)
$\mathbf{S}$	$6 \times 6$ -matrix of elastic compliances
$s$	variable characterizing the past history, Laplace-transform variable, flux function of the accumulation rate function (Chapters 5, 6)
$T$	(abs) temperature
$T_M$	melting temperature
$T_i$	coefficients arising in the perturbation shear-stress formula of the shallow-ice approximation
$T_x, T_y$	dimensionless shear stress

$\mathbf{T} = T_{iA}$	first Piola–Kirchhoff stress tensor
$\mathbf{T}^P = T_{AB}^P$	second Piola–Kirchhoff stress tensor
$\mathfrak{T}$	characteristic time
$\mathfrak{T}$	function(al) for Piola–Kirchhoff stress tensor
$t$	time variable
$\mathbf{t} = t_{ij}$	Cauchy stress tensor
$\mathbf{t}^E = t_{ij}^E$	extra stress tensor
$\mathbf{t}' = t'_{ij}$	Cauchy stress deviator
$t_{(I)}, t_{(II)}, t_{(III)}$	stress tensor invariants
$\tau'$	dimensionless time (arising in the shallow-ice approximation)
$U$	characteristic velocity (Chapter 3); stretched velocity (Chapters 5–7; velocity potential for external body force (Chapter 7))
$U_w$	ocean current speed
$\mathbb{U}$	dimensionless ocean current speed
$\mathbf{u} = u_i$	velocity vector
$u_g$	gliding velocity
$u_s$	sliding velocity
$V$	stretched velocity component
$\gamma$	volume
$\partial\mathcal{V}$	boundary of $\gamma$
$d\gamma, dV$	volume increments
$v, \mathbf{V}$	velocity component, velocity vector
$W$	stretched velocity component
$\mathbf{W}$	skewsymmetric part of velocity gradient
$w$	mass fraction of water in temperate ice (= moisture content) (Chapter 3); velocity component (Chapter 7); width-to-depth ratio in symmetrical cross-sections (Chapter 7)
$X_A$	Cartesian coordinates (reference configuration)
$\mathcal{X}$	coefficient arising in two-point boundary-value problems, characterizing sliding (Chapter 4)
$x, \mathbf{x} = x_i$	Cartesian coordinates (present configuration)
$\dot{x}_i$	velocity vector
$y$	transverse coordinate
$y_M$	transverse coordinate describing the melting surface
$y_B$	transverse coordinate describing the base
$y_S$	transverse coordinate describing the free surface
$y_W$	transverse coordinate describing the ice-water interface
$z$	transverse horizontal coordinate
$Z$	temperature ratio
$\alpha$	wave number
$\alpha, \alpha_S$	inclination angles of free surface

$\beta, \beta', \beta''$	coefficients arising in constitutive relations for stress deviators (Chapter 2)
$\beta$	inclination angle of basal surface
$\Gamma, \hat{\Gamma}$	potentials for viscous stress
$\gamma$	mean inclination angle, shear rate, specific entropy production
$\Delta$	finite difference increment
$\delta$	small parameter
$\delta_{ij}$	Kronecker delta
$\varepsilon$	specific internal energy, longitudinal strain, small parameter
$\boldsymbol{\varepsilon}$	6-vector of strains
$\zeta$	auxiliary variable, dimensionless horizontal coordinate
$\eta$	specific entropy, viscosity, dimensionless transverse variable
$\eta_s$	surface deflection
$\Theta$	stress perturbation amplitude (Chapter 4)
$\Theta_{(1)}, \Theta_{(2)}$	temperature variables
$\theta$	dimensionless coldness
$\vartheta$	dimensionless temperature
$\kappa, \hat{\kappa}$	symbol characterizing configuration
$\boldsymbol{\kappa}$	tensor of heat conductivity
$\Lambda$	function describing basal sliding
$\lambda$	Lame's first constant, wavelength expansion coefficient (Chapter 6)
$\mu$	viscosity, chemical potential, Lamé's second constant (shear modulus), shallow-ice perturbation parameter
$\mu_k$	expansion parameter in frequency space
$\nu$	Poisson's ratio, frequency of occurrence
$\nu_k$	expansion parameter in frequency space
$\xi$	dimensionless longitudinal variable, integration variable
$\Pi^\Psi, \pi^\psi$	productions of $\Psi(\psi)$ in the reference (present) configuration
$\bar{\omega}^\psi$	surface production of $\psi$
$\rho, \rho_R$	mass density
$\sum,$	summation sign, stress perturbation amplitude (Chapter 4)
$\Sigma^\Psi, \sigma^\psi$	supply of $\Psi(\psi)$ in the reference (present) configuration
$\sigma$	normal stress, characteristic time
$\sigma_f$	failure strength
$\sigma$	6-vector of stresses
$\tau$	dimensionless time, dimensionless shear-stress retardation (relaxation) time
$\tau'_{(II)}$	dimensionless second-stress deviator invariant
$\Phi$	stress function
$\phi_i$	coefficients arising in the constitutive relations for stress deviator

$\Phi^\Psi, \phi^\psi$	flux of $\Psi(\psi)$ through body surface in the reference (present) configuration
$\varphi, \varphi_{\bar{x}}, \varphi_\Theta, \left. \varphi \right. \atop \varphi_{U_0}, \varphi_{V_0}$	phase shift functions
$\varphi$	angle
$\chi = \chi_i$	deformation function (motion)
$\Psi, \psi$	general physical quantity refering to the reference and present configurations, respectively, stream functions
$\psi_h$	free enthalpy
$\psi_n, \psi_\sigma$	functions describing boundary conditions (Chapter 7)
$\Omega$	dimensionless frequency
$\Omega_i$	functions arising in a Newtonian flow problem (Chapter 4)
$\omega$	frequency
$\frac{d}{dt}$	material (total) time derivative
$\frac{D}{Dt}$	time derivative following a moving singular surface
$\frac{\partial}{\partial x}$	partial derivative
$\llbracket a \rrbracket = a^+ - a^-$	jump of the quantity $a$ across a singular surface
$\nabla$	nabla operator
$\nabla T$	material gradient of $T$
$\nabla^2$	Laplacian (operator)
*	convolution operator $(f * g)(t) = \int_0^t f(\xi)g(t - \xi)d\xi$
$\circ$	convolution operator $(f \circ g)(t) = \int_0^t f(t - \xi) \frac{dg(\xi)}{d\xi} d\xi$

**PART I**

**FUNDAMENTAL PHYSICS AND MATERIALS  
TECHNOLOGY OF ICE**

## **Chapter 1**

### **GENERAL CONCEPTS**

#### *1. Introduction*

Basic to ice mechanics – be it the theory of glacier flow, the response of floating ice plates to external loading, ice drifting and ice ridging, or the very practical questions of ice forces on structures – are the fundamental laws of continuum physics. These consist of the *balance laws* of mass, momentum, angular momentum, and energy, and indeed, there is no essential problem in glaciology in which use of one or more of these laws is not made. Not all of them would necessarily be used for answering the questions in mind. For instance, in the so-called ‘mass balance’ of a glacier, one only makes use of the law of conservation of mass. A similar situation prevails when one is investigating the response of a glacier to changes in climate. Of course, in such situations the true picture is oversimplified, and the neglect of certain physical laws might have to be bought at the expense of accuracy, or must be compensated by introducing phenomenological statements which replace the neglected balance laws. However, the simplifications in the physical picture and the replacement of certain basic balance laws by phenomenological statements often leads to drastic mathematical reductions yielding detailed physical insight that could not otherwise be obtained. As an example we mention that the distribution of stress and velocity in an ice sheet is often determinable without simultaneously searching for the temperature distribution. Alternatively, the temperature distribution may be determined independently from that of velocity. In either case, some assumptions about the neglected fields must be made, assumptions motivated by experimental observations or by some sort of plausibility arguments.

This brings us naturally to the second set of fundamental laws which, apart from the balance laws, must be formulated.

What we have in mind are the *phenomenological relations*. They occur in all theories in which equations resulting from physical principles do not suffice to integrate the system of equations at hand. When all physical principles are exploited, additional equations, which close the system, can only come from experimental observations. They are usually given as

material response relations, but this is, as we have just seen, not necessarily the case. For instance, to say that ice is a non-linear viscous fluid is a statement about the material behavior of ice; but to relate the mass flux of a valley glacier through a valley cross-section to its depth is a statement characterizing the glacier as a whole. In this chapter, we shall discuss the material response only.

With regard to the constitutive response, ice can be regarded as a viscous fluid, an elastic, viscoelastic or ideally plastic solid, and so on. In other words, there is not just a single material response for ice. *The response also depends on the physical process one is dealing with.* In glaciers, ice is almost always treated as a heat-conducting non-linear viscous fluid. In problems of bearing capacity of floating ice sheets, we may regard it as an elastic, viscoelastic, or plastic solid. Here we shall not discuss all the possibilities, because this would fill an entire volume on its own. Rather, we are interested in the general form of the constitutive response that is possible when one particular material response is postulated, and in bringing to the reader's attention the very useful tools of modern rational continuum mechanics, at least as far as ice mechanics is concerned. In this respect no completeness is intended, and interested readers are referred to the pertinent literature; e.g., Müller [5], Truesdell and Toupin [9], Truesdell and Noll [10], Chadwick [1], Truesdell [8]. Moreover, particular applications will be reserved until Chapter 2.

In what follows we shall use the classical methods of continuum physics. Cartesian tensor notation is used with the usual notation. Subscripts indicate, if not otherwise stated, vector and tensor components in a Cartesian frame of reference. The summation convention is used according to which summation is understood over doubly-repeated indices. Super-imposed dots denote time derivatives at a fixed material particle, and an index following a comma denotes partial differentiation with respect to that coordinate.

## 2. Equations of Balance

All dynamical statements of classical continuum physics can be presented in the form of a general balance law. To derive this, let  $\mathcal{B}$  be a body with boundary  $\partial\mathcal{B}$ , see Figure 1.1. Usually, the particles  $X$  of the body are visualized by referring them to a Cartesian coordinate system of a Euclidean three space. Each particle may then be represented by its place  $X_A$  ( $A = 1, 2, 3$ ). The union of all places  $X_A$  is the picture of  $\mathcal{B}$  in the Euclidean space. It is called  $\mathcal{B}_R$ , the *reference configuration* of  $\mathcal{B}$ . To describe the motion of a body it suffices to describe the position of all of its particles. At time  $t$ , the mapping of  $\mathcal{B}$  in the Euclidean space is given by  $\mathcal{B}_t$ . It is not necessary that  $\mathcal{B}_t$  is referred to the same frame of Cartesian coordinates. The coordinates of a particle  $X$  in  $\mathcal{B}_t$ , which is called the *present configuration*, will be denoted by

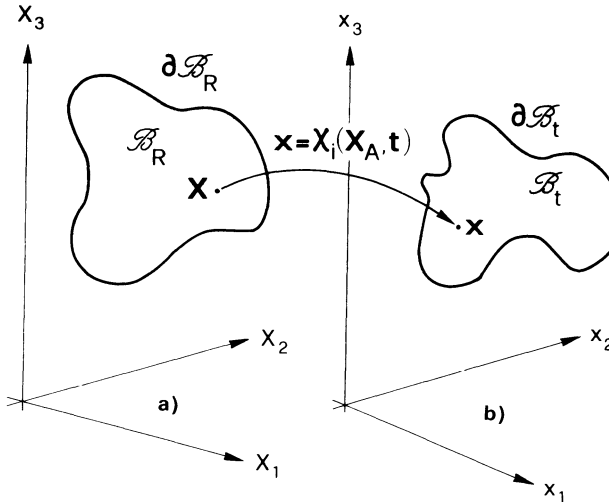


FIG. 1.1. Explaining the body configurations and the motion. (a) is the reference configuration and (b) is the present configuration.

$x_i$  ( $i = 1, 2, 3$ ). The motion of a body is defined as the mapping  $X_A \rightarrow x_i$ . It is obvious that this is also a function of time, viz.,

$$x_i = \chi_i(X_A, t). \quad (1.1)$$

We assume the function  $\chi_i$  to be differentiable and invertible.

A reader not familiar with these concepts may regard the reference configuration as the initial position of the body and the present configuration as a snap-shot of it at time  $t$ . It is then clear that the present configuration is, in general, different for different times and that the coordinates  $x_i$  of a particle are different from  $X_A$ , even when the coordinate triad in the reference and present configuration are chosen to be the same. It should be stressed, however, that although the above interpretations are helpful for the new reader, they are by no means general; in particular, the reference configuration need not be the initial configuration and the two triads need not coalesce. If, for instance, a cube of snow is, by some mechanism, deformed into a sphere, it is appropriate to describe it in its reference state by a set of Cartesian coordinates and in its deformed (present) state by spherical coordinates. In practice, such general cases will hardly occur.

Any physical quantity,  $\Psi$  say, can be regarded as a function of place  $X_A$  and time  $t$  or else as a function of position  $x_i$  and time  $t$ . Mathematically,

$$\Psi = \hat{\Psi}(X_A, t) = \tilde{\Psi}(x_i, t). \quad (1.2)$$

Of course, it does not matter which point of view one takes, because either one of (1.2) can be transformed to the other by using (1.1) or the inverse

relation, which we assumed to exist. Usually one does not differentiate between a function and its value. Then (1.2) would read

$$\Psi = \Psi(X_A, t) = \Psi(x_i, t). \quad (1.3)$$

When arguments are written, (1.3) does not provide any confusion. On the other hand, when the arguments are left out, there is no way of differentiating between a function and its value and so one must be very careful. For instance, the *material time derivative* of a quantity  $\Psi$  is defined as its time rate of change *at a fixed particle*:

$$\dot{\Psi} := \frac{d\Psi}{dt} := \frac{\partial \hat{\Psi}}{\partial t} = \frac{\partial \tilde{\Psi}}{\partial t} + \tilde{\Psi}_{,i} v_i, \quad (1.4)$$

where

$$v_i := \dot{x}_i = \frac{dx_i}{dt} = \frac{\partial \chi_i}{\partial t}. \quad (1.5)$$

In the notation of (1.3), (1.4) would read

$$\frac{\partial \Psi}{\partial t} = \frac{\partial \Psi}{\partial t} + \Psi_{,i} v_i.$$

This is not only confusing, but pure nonsense.

To avoid such complications and still be able to maintain the sloppy notation of not making a function different from its value, it is usually stated once and for all what functions one is looking at. If  $X_A$  and  $t$  are regarded as the independent variables, then one works with the *material* or *Lagrangian description*. When  $x_i$  and  $t$  are the independent variables, this is the *spatial* or *Eulerian formulation*.

In subsequent developments, in line with this notation functions of the Lagrangian variables will frequently be written in capital letters and functions of the Eulerian variables in small letters.

With these preliminary remarks we are now able to derive the general balance law for a physical quantity  $\Psi$ . In the spatial description, it has the following form:

$$\frac{d}{dt} \int_{\mathcal{B}_t} \psi \, dv = \oint_{\partial \mathcal{B}_t} \varphi_i^\psi \, da_i + \int_{\mathcal{B}_t} \pi^\psi \, dv + \int_{\mathcal{B}_t} \sigma^\psi \, dv. \quad (1.6)$$

In the above,  $dv$  and  $da_i$  are the volume and vectorial surface elements, respectively. The quantities  $\psi$ ,  $\pi^\psi$  and  $\sigma^\psi$  may be tensor-valued quantities of any (but equal) order.  $\varphi_i^\psi$  is then a tensor of one order higher than  $\psi$ , a fact which must be taken for granted here. It can be shown to be a necessity if a local equation is to follow from (1.6), see Wang and Truesdell, [13]. More precisely, the integrand in the first term of the right-hand side may be

written as  $\varphi_{(\mathbf{n})}^\psi da$ , where  $da$  is the scalar surface element and the index  $\mathbf{n}$  indicates that the surface term  $\varphi_{(\mathbf{n})}^\psi$  depends only on the unit normal vector of the surface at that point. It is the content of *Cauchy's lemma* that  $\varphi_{(\mathbf{n})}^\psi = \varphi_i^\psi n_i$ , where  $\varphi_i^\psi$  is a tensor of one order higher than  $\varphi_{(\mathbf{n})}^\psi$ . Consequently,  $\varphi_{(\mathbf{n})}^\psi da = \varphi_i^\psi n_i da = \varphi_i^\psi da_i$ , as stated in (1.6). As an example, consider the boundary tractions  $\mathbf{t}_{(\mathbf{n})}$  and the (Cauchy) stress  $t_{ij}$ . Then, according to the above rule,  $t_i^{(\mathbf{n})} = t_{ij}n_j$ . On the other hand, if  $\varphi_{(\mathbf{n})}^\psi$  is the heat flow  $q_{(\mathbf{n})}$  through the boundary then  $q_{(\mathbf{n})} = q_i n_i$ , where  $q_i$  must be interpreted as the heat flux vector.

On the left-hand side of (1.6) stands the time rate of change of  $\psi$  when integrated over the entire body. This time rate of change must be balanced by the three terms on the right. The first is a surface term and is called the (total) *flux*  $\varphi_i^\psi$  of the quantity  $\psi$  through the surface  $\partial\mathcal{B}_t$  of the body  $\mathcal{B}$  in its present configuration  $\mathcal{B}_t$ . The remaining two terms are volume integrals of two quantities.  $\pi^\psi$  is called the *production of  $\psi$  in  $\mathcal{B}_t$* , and  $\sigma^\psi$  is the *supply of  $\psi$  to  $\mathcal{B}_t$* . Hence, the time rate of change of  $\psi$  in  $\mathcal{B}_t$  is balanced by its flux, its production and its supply. The balance equation (1.6) may appear to be a rather difficult physical statement, but it is not. In the general form stated above, it is rather quite trivial, for a quantity in a body can, clearly, increase only by its flux through the boundary, its production within the body and its supply by outside agents. To give an example, let  $\psi$  be the mass density of water in an ice-water mixture. In this case  $\varphi_i^\psi$  denotes the flux of water mass through the body surface,  $\pi^\psi$  is the production of water within the body which is produced by melting. Finally  $\sigma^\psi$  would be the water supplied by external sources. This term obviously vanishes.

Equation (1.6) is stated in the Eulerian description. Of course, there is a material counterpart to it, which reads

$$\frac{d}{dt} \int_{\mathcal{B}_R} \Psi dV = \oint_{\partial\mathcal{B}_R} \Phi_B^\Psi dA_B + \int_{\mathcal{B}_R} \Pi^\Psi dV + \int_{\mathcal{B}_R} \Sigma^\Psi dV. \quad (1.7)$$

Here  $dV$  and  $dA_B$  are the volume and surface increments of the Lagrangian formulation, and in line with the notation introduced earlier to differentiate between the Eulerian and Lagrangian formulations, we have used capital letters to designate quantities in the material description.

It is easy, in principle, to relate (1.6) and (1.7), but before this correspondence is made explicit, the introduced concepts will now be applied to the specific balance laws of classical physics. These are the balance laws of mass, momentum, angular momentum, energy, and entropy. Perhaps the best way of writing them down is by listing the individual quantities in a table. Table 1.1 contains them. The physical significance of the quantities occurring in this table is as follows:  $\rho_R$  and  $\rho$  are the *mass densities* in the reference and present configurations, respectively.  $\dot{x}_i$  or  $v_i$  is the *velocity vector*,  $t_{ij}$  the *Cauchy stress tensor* and  $T_{iA}$  the *first Piola-Kirchhoff stress*

TABLE 1.1. Physical interpretation of the various quantities in the balance laws

Balance law	$\Psi$	$\psi$	$\phi_A^\psi$	$\varphi_i^\psi$	$\sum^\psi$	$\sigma^\psi$	$\Pi^\psi$	$\pi^\psi$
Balance of mass	$\rho_R$	$\rho$	0	0	0	0	0	0
Balance of momentum	$\rho_R \dot{x}_j$	$\rho v_i$	$T_{jA}$	$t_{ji}$	$\rho_R f_j$	$\rho f_j$	0	0
Balance of angular momentum*	$x_{[k} \rho_R \dot{x}_{j]}$	$x_{[k} \rho v_{j]}$	$x_{[k} T_{j]A}$	$x_{[k} t_{j]i}$	$x_{[k} \rho_R f_{j]}$	$x_{[k} \rho f_{j]}$	0	0
Balance of energy	$\rho_R \left( \frac{\dot{x}_k \dot{x}_k}{2} + \varepsilon \right)$	$\rho \left( \frac{v_i v_i}{2} + \varepsilon \right)$	$-Q_A + T_{iA} \dot{x}_i$	$-q_i + t_{ij} v_j$	$\rho_R (f_j \dot{x}_j + r)$	$\rho (f_j v_j + r)$	0	0
Balance of entropy	$\rho_R \eta$	$\rho \eta$	$-\frac{Q_A}{T}$	$-\frac{q_i}{T}$	$\frac{\rho_R r}{T}$	$\frac{\rho r}{T}$	$\rho_R \gamma$	$\rho \gamma$

\*Bracketed indices denote the antisymmetric part of a tensor, e.g.  $t_{[ij]} = \frac{1}{2}(t_{ij} - t_{ji})$ .

*tensor.*  $f_i$  denotes the *external body force* per unit mass,  $\varepsilon$  the *specific internal energy*;  $q_i$  and  $Q_A$  are the *heat flux vectors* in the spatial and material descriptions, respectively, and  $r$  is the *heat supplied* by external sources.  $\eta$  is the *specific entropy*,  $T$  the *absolute temperature* and  $\gamma$  the *entropy production*. In all balance laws except the balance of entropy, the production term is assumed to vanish. It is with respect to this property that mass, momentum, angular momentum, and energy are said to be *conserved*. On the other hand, there are situations in which mass, momentum, angular momentum, and energy are not necessarily conserved. For instance, in a mixture of ice-water in which phase changes may occur, the mass of the water and that of ice is not conserved, although the sum of both, the total mass, must be. We shall encounter such a situation in a later chapter.

For clarity, we shall now further explain the contents of Table 1.1. For instance, in the *mass balance equation* the physical quantity is the density  $\rho$  (or  $\rho_R$ ). Its flux through the boundary of the body must vanish, because there is no flux of matter through a material surface. Mass cannot be supplied to a body from the outside either and neither is there any mass production in a one-component body. This explains the first row in Table 1.1.

Next, let the physical quantity under consideration be *momentum*. One then has  $\psi = \rho v_i$  or  $\Psi = \rho_0 \dot{x}_i$ . According to Newton's second law, the time rate of change of momentum of the entire body is balanced by the forces acting within the body and on its surface. The body forces can be expressed as the volume integral of the specific forces  $\rho f_j$  (or  $\rho_0 f_j$ ) and are usually of external origin (electromagnetic and gravity forces). Thus, these forces can be interpreted as a momentum supply. In a one-component material there are no internal body forces, but in a mixture such internal forces do exist and can influence the physical processes. To see this, consider a powder snow avalanche. It consists of snow particles and air; these two components may be regarded as the constituents of a binary mixture. For each of the constituents a balance law of momentum may be written down, and it seems clear that the air exerts an aerodynamic viscous drag which influences the motion of the snow particles. Alternatively, an equal but opposite force is exerted by the snow particles on the air influencing its motion within the avalanche. These equilibrating forces are internal and must for each constituent thus be regarded as momentum production. Finally, surface tractions are acting on every body boundary, and their vectorial sum is the total surface force exerted on the body. As seen in connection with Cauchy's lemma, these tractions can be related to the stress tensor. It is this tensor which, in the balance law of momentum plays the role of momentum flux. Since  $t_j^{(n)} = t_{jk} n_k = T_{jA} N_A$ , it is seen that the stress tensors in the material and spatial descriptions are not the same, even though the traction  $t_j^{(n)}$  is the same. The stress tensor  $t_{ij}$  in the Eulerian formulation is called the *Cauchy stress tensor* and that in the material description the *first Piola-*

*Kirchhoff stress tensor.* This completes the identification of Newton's second law with the general balance law (1.6) and (1.7).

The various terms for the balance law of angular momentum are easily obtained from those of linear momentum if it is observed that in a non-polar theory angular momentum is simply the moment of momentum. With this interpretation in mind all terms in the third row of Table 1.1 are easily identifiable.

To proceed, let the physical quantity  $\psi$  now be the *total specific energy*, that is the sum of kinetic and internal energy. The flux of energy through the boundary of the body must then also consist of two parts; the heat flux and the mechanical work of the surface forces. Here the second term is usually called the power of working of the surface forces. The negative sign in the heat-flux term stems from the fact that heat flux is positive as an outflux. Finally, the supply of energy is the sum of the power of working of the volume forces and of the heat supply by outside agents. A possible candidate for the latter is radiation.

This brings us now to the *entropy balance*. In accord with common practice we have chosen

$$\begin{aligned} \text{entropy flux} &= \frac{\text{heat flux}}{\text{absolute temperature}}, \\ \text{entropy supply} &= \frac{\text{heat supply}}{\text{absolute temperature}}, \end{aligned}$$

but have left entropy production  $\gamma$  unspecified. Readers not familiar with irreversible thermodynamics may regard the above choices as postulates occurring in a balance law for a quantity called entropy. As long as no specification is introduced for this quantity, it cannot represent any physical notion. It is, however, the expression of the *second law of thermodynamics* that entropy production cannot be negative, i.e.,  $\gamma \geq 0$ , for any single process a body might undergo. We shall return to this postulate later in this chapter.

Although the Lagrangian and Eulerian descriptions are not used simultaneously, it is nevertheless advantageous to relate the variables in the two descriptions. This amounts to a transformation of Equation (1.6) into (1.7), or vice versa.

To this end we must simply transform the volume and surface elements in (1.6) to their corresponding Lagrangian counterparts. To demonstrate the procedure for the volume increments  $dv$  and  $dV$ , recall the following formula for the determinant of a  $3 \times 3$ -matrix  $F_{iA}$ :

$$e_{ABC}(\det \mathbf{F}) = e_{ijk} F_{iA} F_{jB} F_{kC}, \quad (1.8)$$

which we list without proof.  $e_{ABC}$  and  $e_{ijk}$  are the permutation symbols,

defined by

$$e_{ABC} = \begin{cases} 1, & \text{if } ABC \text{ are an even permutation of } 1, 2, 3, \\ -1, & \text{if } ABC \text{ are an odd permutation of } 1, 2, 3, \\ 0, & \text{otherwise.} \end{cases}$$

A similar definition holds also for  $e_{ijk}$ .

Consider now the increment  $dx_i$ . It can be related to  $dX_A$  by

$$dx_i = \chi_{i,A} dX_A = F_{iA} dX_A. \quad (1.9)$$

Here  $F_{iA}$ , defined by

$$F_{iA} = \chi_{i,A} = \frac{\partial \chi_i}{\partial X_A} \quad (1.10)$$

is the *deformation tensor*, to which formula (1.8) may be applied. Consider now the volume increment  $dv$  spanned by the three vector increments  $dx_i^{(\alpha)}$  ( $\alpha = 1, 2, 3$ ), see Figure 1.2.

Remembering the formula for a volume of three vectors

$$dv = |e_{ijk} dx_i^{(1)} dx_j^{(2)} dx_k^{(3)}|$$

we may use (1.9) to write this as

$$\begin{aligned} dv &= |e_{ijk} F_{iA} F_{jB} F_{kC} dX_A^{(1)} dX_B^{(2)} dX_C^{(3)}| \\ &= |\det \mathbf{F}| |e_{ABC} dX_A^{(1)} dX_B^{(2)} dX_C^{(3)}| \end{aligned}$$

Hence

$$dv = |\det \mathbf{F}| dV. \quad (1.11)$$

Henceforth, we shall frequently denote  $\det \mathbf{F}$  by  $J$ :

$$J = \det \mathbf{F}. \quad (1.12)$$

In much the same way, using only two vector increments  $dx^{(1)}$  and  $dx^{(2)}$ , the vectorial surface element  $da = dx^{(1)} \times dx^{(2)}$ , where the operator  $\times$  denotes the cross-product, can be formed and related to a corresponding formula

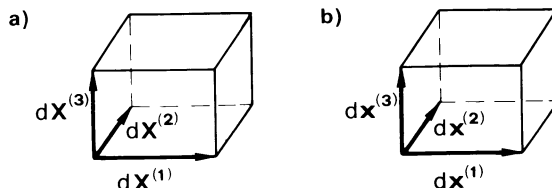


FIG. 1.2. Volume element formed by three linearly independent vector increments, explaining the derivation of formula (1.11). (a) is the reference configuration and (b) is the present configuration.

in the reference configuration. Indeed, starting from the formulas

$$da_i = e_{ijk} dx_j^{(1)} dx_k^{(2)}, \quad dA_B = e_{BCD} dX_C^{(1)} dX_D^{(2)}$$

we may show that

$$da_k = J F_{Bk}^{-1} dA_B. \quad (1.13)$$

In the above,  $F_{Bj}^{-1}$  is the inverse of  $F_{iB}$  which must exist according to our assumption that the motion  $\chi_i(\cdot)$  is invertible.

Formula (1.13) is not yet in a form suitable to be used in Equation (1.6); for the surface in (1.6) is closed. It is tacitly understood in this surface integral that the increment  $da_i$  is oriented such that it is an outward normal. It is left to the reader as an exercise to demonstrate that under the transformation (1.9) outward normals go over into outward normals only if  $\operatorname{sgn} J > 0$ . For  $\operatorname{sgn} J < 0$  outward normals are transformed into inward normals. Hence, to transform outward normals into outward normals, we must replace (1.13) by

$$da_k = |J| F_{Bk}^{-1} dA_B \quad (1.14)$$

whenever the surface under consideration is closed. Equation (1.11) allows us to write

$$\begin{aligned} \frac{d}{dt} \int_{\mathcal{B}_t} \psi dv &= \frac{d}{dt} \int_{\mathcal{B}_R} \psi |J| dV = \frac{d}{dt} \int_{\mathcal{B}_R} \Psi dV, \\ \int_{\mathcal{B}_t} (\sigma^\psi + \pi^\psi) dv &= \int_{\mathcal{B}_R} (\sigma^\psi + \pi^\psi) |J| dV = \int_{\mathcal{B}_R} (\Sigma^\psi + \Pi^\psi) dV \end{aligned} \quad (1.15)$$

so that the following relations hold

$$\Psi = |J|\psi, \quad \Sigma = |J|\sigma, \quad \Pi = |J|\pi \quad (1.16)$$

with the obvious inversions

$$\psi = |J^{-1}|\Psi, \quad \sigma = |J^{-1}|\Sigma, \quad \pi = |J^{-1}|\Pi. \quad (1.17)$$

Analogously and in view of (1.14)

$$\oint_{\partial\mathcal{B}_t} \varphi_i^\psi da_i = \oint_{\partial\mathcal{B}_R} \varphi_i^\psi |J| F_{Bi}^{-1} dA_B = \oint_{\partial\mathcal{B}_R} \Phi_B^\psi dA_B, \quad (1.18)$$

whence follows

$$\Phi_B^\psi = |J| F_{Bi}^{-1} \varphi_i^\psi \quad \text{or} \quad \varphi_i^\psi = |J^{-1}| F_{iA} \Phi_A^\psi. \quad (1.19)$$

The Equations (1.15) through (1.19) establish the connection of physical quantities in the material and spatial description.

We now turn back to the balance laws (1.6) and (1.7) respectively. They are written down above for the entire body, but generally *one postulates that*

they apply to any part  $\mathcal{P}$  of it. Hence (1.6) may be replaced by

$$\frac{d}{dt} \int_{\mathcal{P}_t} \psi \, dv = \oint_{\partial \mathcal{P}_t} \varphi_i^\psi \, da_i + \int_{\mathcal{P}_t} (\sigma^\psi + \pi^\psi) \, dv. \quad (1.20)$$

This is still a *global* statement, but because it applies for all  $\mathcal{P} \subset \mathcal{B}$  it can be transformed into *local* form. To this end, the various integrand fields are assumed to be differentiable. For such a case we may, in the first term on the right, use the divergence theorem:

$$\oint_{\partial \mathcal{P}_t} \varphi_i^\psi \, da_i = \int_{\mathcal{P}_t} \varphi_{i,i}^\psi \, dv. \quad (1.21)$$

The term on the left-hand side, on the other hand, may be written as

$$\frac{d}{dt} \int_{\mathcal{P}_t} \psi \, dv = \int_{\mathcal{P}_t} \dot{\psi} \, dv + \int_{\mathcal{P}_t} \psi (dv)^\cdot. \quad (1.22)$$

Using (1.8) and (1.11) it is straightforward to show that

$$(dv)^\cdot = |J|^\cdot \, dV = (\operatorname{sgn} J) \dot{J} \, dV = v_{i,i} \, dv, \quad (1.23)$$

where

$$v_i = \dot{x}_i \quad \text{and} \quad v_{i,i} = \dot{x}_{i,i} \quad (1.24)$$

Using (1.23), relation (1.22) becomes

$$\frac{d}{dt} \int_{\mathcal{P}_t} \psi \, dv = \int_{\mathcal{P}_t} (\dot{\psi} + v_{i,i} \psi) \, dv = \int_{\mathcal{P}_t} \left( \frac{\partial \psi}{\partial t} + (\psi v_i)_i \right) \, dv. \quad (1.25)$$

This result is known as the *transport theorem*. Substituting (1.21) and (1.25) into (1.20), one obtains

$$\int_{\mathcal{P}_t} \left\{ \frac{\partial \psi}{\partial t} + (\psi v_i)_i - \varphi_{i,i}^\psi - \sigma^\psi - \pi^\psi \right\} \, dv = 0$$

which must hold for all  $\mathcal{P}_t$ . Hence

$$\dot{\psi} := \frac{\partial \psi}{\partial t} + (\psi v_i)_i = \varphi_{i,i} + \sigma^\psi + \pi^\psi. \quad (1.26)$$

This is the local form of the balance law (1.20). Note that all fields are variables of  $x_i$  and  $t$ . Apparently, the differentiability of the fields involved and the postulate that the global balance law is valid for any part of the body, are sufficiently stringent to derive it. Of course, differentiability is not always satisfied; the inferences that can be drawn from such weaker postulates are also physically important and will be treated below.

As is the case for the Eulerian description, there is also a local balance

law in the Lagrangian formulation. We leave it as an exercise for the reader to show that the local form of the balance law in the material description assumes the form

$$\dot{\Psi} := \frac{\partial \Psi}{\partial t} = \Phi_{A,A}^\Psi + \Sigma^\Psi + \Pi^\Psi. \quad (1.27)$$

As opposed to (1.26), here all field variables are functions of  $X_A$  and  $t$ . This is formally the reason that the material time derivative is simpler in (1.27) than in (1.26).

In what follows we shall make use primarily of the *local forms* of the balance laws. It is thus helpful to state them explicitly, and substitution of the quantities in Table 1.1 into the local balance laws (1.26) or (1.27) reveals the following expressions for the conservation laws of mass, momentum, angular momentum, energy, and for entropy balance.

*(a) In the spatial description*

Balance of mass,

$$\frac{\partial \rho}{\partial t} + (\rho v_i)_{,i} = \frac{d\rho}{dt} + \rho v_{i,i} = 0.$$

Balance of momentum,

$$\rho \frac{dv_i}{dt} = t_{ij,j} + \rho f_i.$$

Balance of angular momentum:

$$t_{ij} = t_{ji} \quad \text{or} \quad t_{[ij]} = 0. \quad (1.28)$$

Balance of energy,

$$\rho \frac{d\epsilon}{dt} = t_{ij} D_{ij} - q_{i,i} + \rho r.$$

Balance of entropy,

$$\rho \frac{d\eta}{dt} + \left( \frac{q_i}{T} \right)_{,i} - \frac{\rho r}{T} = \rho \gamma.$$

*(b) In the material description*

Balance of mass

$$\rho_R = \rho_R(\mathbf{X}).$$

Balance of momentum

$$\rho_R \frac{d\dot{x}_i}{dt} = T_{iA,A} + \rho_R f_i. \quad (1.29)$$

Balance of angular momentum

$$F_{[iA} T_{j]A} = 0.$$

Balance of energy

$$\rho_R \frac{d\epsilon}{dt} = T_{iA} \dot{F}_{iA} - Q_{A,A} + \rho_R r.$$

Balance of entropy

$$\rho_R \frac{d\eta}{dt} + \left( \frac{Q_A}{T} \right)_{,A} = \frac{\rho_R r}{T} = \rho_R \gamma.$$

In these equations it is tacitly understood that all quantities in (1.28) are functions of  $x_i$  and  $t$  while those in (1.29) are functions of  $X_A$  and  $t$ . Furthermore,

$$D_{ij} = v_{(i,j)} = \frac{1}{2}(v_{i,j} + v_{j,i}) \quad (1.30)$$

is called the *stretching tensor* or the *tensor of strain rate*, and it is obvious that the balance law of mass in the material description (1.29), does not constitute an essential equation, because  $\rho_R$  is a given function of place. Nevertheless, the actual density  $\rho$  may in this case be obtained from (1.28)<sub>1</sub> by integration. One obtains

$$\rho = \rho_R J. \quad (1.31)$$

Since  $J$  is known, once the motion  $\chi_i(\cdot)$  is determined (1.31) is an equation for  $\rho$ .

In the above derivation of the physical laws, an approach of ‘reduction’ was used to deduce local, point forms from the global, integral forms of the balance laws. This ‘reduction’ involved only mathematical assumptions so that the integral forms of the balance laws should be regarded as the essential physical statements. Early derivations of the conservation laws of mass, momentum, etc., were generally directly stated in their local forms. Newton’s second law for a continuum was first used by Euler in such a local form and was derived from some rudimentary atomic models by Cauchy. The local balance law of momentum is therefore often called the *Euler–Cauchy equation*.

The advantage of introducing the balance laws in integral form is that they can also be applied to situations when the field variables are not differentiable. Physically, such situations are important, and we shall see that the relations, which can be deduced from such weaker statements will, for instance, describe shocks, boundary conditions, and phase-change relations. Such phase-change relations are repeatedly met in the glaciological literature. To give but one example, consider the freezing of a lake or the ocean. Depending on the thermal state at the ice-water interface, water will either

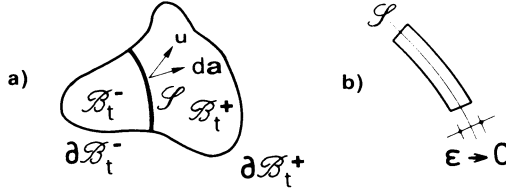


FIG. 1.3. (a) Singular surface  $\mathcal{S}$  separating the body in two parts and moving with velocity  $u_i$ ; (b) ‘pillbox’ volume surrounding the singular surface  $\mathcal{S}$ .

freeze and the plate thickness will grow, or else melting of the ice will occur and give rise to an ablation.

We thus assume now that there exists a smooth surface  $\mathcal{S}$  in the body at which the fields involved may suffer a *finite* jump. Except for its smoothness, the surface  $\mathcal{S}$  is arbitrary. In particular, it need not be material and therefore possesses its own velocity  $u_i$  (in the Eulerian description), see Figure 1.3. Further, let  $da_i$  be the vectorial surface element of  $\mathcal{S}$  defined in such a way that it points into  $\mathcal{B}_t^+$ . It is obvious that non-differentiability of the fields at  $\mathcal{S}$  prevents us from applying the divergence and transport theorems (1.21) and (1.25). However, we may write

$$\begin{aligned} \frac{d}{dt} \int_{\mathcal{B}_t} \psi dv &= \frac{d}{dt} \int_{\mathcal{B}_t^+} \psi^+ dv + \frac{d}{dt} \int_{\mathcal{B}_t^-} \psi^- dv \\ &= \int_{\mathcal{B}_t^+} \frac{\partial \psi^+}{\partial t} dv + \int_{\mathcal{B}_t^+} \psi^+ v_i da_i - \int_{\mathcal{S}} \psi^+ u_i da_i + \\ &\quad + \int_{\mathcal{B}_t^-} \frac{\partial \psi^-}{\partial t} dv + \int_{\mathcal{B}_t^-} \psi^- v_i da_i + \int_{\mathcal{S}} \psi^- u_i da_i. \end{aligned} \quad (1.32)$$

Hence

$$\frac{d}{dt} \int_{\mathcal{B}_t} \psi dv = \int_{\mathcal{B}_t} \frac{\partial \psi}{\partial t} dv + \int_{\mathcal{B}_t} \psi v_i da_i - \int_{\mathcal{S}} [\psi u_i] da_i \quad (1.33)$$

This is the form of the transport theorem which holds when  $\psi$  suffers a finite jump on a smooth singular surface. It is seen that the bracketed term has been defined as

$$[\psi] = \psi^+ - \psi^-. \quad (1.34)$$

Substituting (1.33) into (1.20) yields

$$\begin{aligned} &\int_{\mathcal{B}_t} \frac{\partial \psi}{\partial t} dv + \int_{\mathcal{B}_t} \psi v_i da_i - \int_{\mathcal{S}} [\psi u_i] da_i \\ &= \oint_{\partial\mathcal{B}_t} \varphi_i^\psi da_i + \int_{\mathcal{B}_t} (\sigma^\psi + \pi^\psi) dv. \end{aligned} \quad (1.35)$$

The jump conditions follow from (1.35) by selecting as the integration region a suitable region  $\mathcal{P}$ . We choose that indicated in Figure 1.3b; this is a ‘pillbox’-shaped volume surrounding the singular surface. The mantle of the pillbox is assumed to be small and its height is reduced to zero in such a way that the lower and upper faces will in the limit coincide with the singular surface. Because it is assumed that *all fields remain bounded from above*, all volume integrals in (1.35) will vanish as the volume  $\mathcal{P}$  is reduced to zero. On the other hand, the surface integrals become

$$\oint_{\partial\mathcal{B}_t} \psi v_i \, da_i = \int_{\mathcal{S}} [\psi v_i] \, da_i, \quad \int_{\partial\mathcal{B}_t} \phi_i^\psi \, da_i = \int_{\mathcal{S}} [\phi_i^\psi] \, da_i,$$

whence follows

$$[\phi_i^\psi] n_i - [\psi(v_i - u_i)n_i] = 0. \quad (1.36)$$

Here,  $n_i$  denotes the unit vector normal to  $\mathcal{S}$  and pointing into the positive part of the body. When applied to the quantities in Table 1.1 the jump conditions (1.36) imply

$$\begin{aligned} & [\rho(v_i - u_i)n_i] = 0, \quad [[t_{ij}n_j]] - [[\rho v_i(v_j - u_j)n_j]] = 0, \\ & [[t_{ij}v_i n_j - q_i n_i]] - \left[ \rho \left( \varepsilon + \frac{v^2}{2} \right) (v_i - u_i)n_i \right] = 0, \\ & \left[ \frac{q_i n_i}{T} \right] + [[\rho \eta(v_j - u_j)n_j]] \geq 0. \end{aligned} \quad (1.37)$$

When the singular surface is material, then  $u_i = v_i$  and Equations (1.37) reduce to the usual Neumann-type boundary conditions.

The reader should very well be aware that Equations (1.36) and (1.37) are based on the hypothesis that volume integrals of field quantities vanish as the volume is shrunk to zero. More generally, one could, for instance, assume that in the above pillbox argument the production term would not remain bounded on the singularity surface. Allowing singularities such that  $\int_{\mathcal{P}_t} \pi^\psi \, dv \rightarrow \tilde{\omega}^\psi < \infty$  as the pillbox volume is shrunk to zero, would result in Equation (1.36) in which the right-hand side is replaced by  $\tilde{\omega}^\psi$ . This quantity plays the role of a *surface production* of  $\psi$  on  $\mathcal{S}$ . While it is common practice to ignore this term in the balance laws of mass, momenta, and energy, one often assumes a non-vanishing surface entropy production which, according to the second law of thermodynamics is non-negative. This is the reason why the fourth of Equations (1.37) has the strong inequality sign.

The balance laws (1.28) or (1.29) do not suffice, in general, to determine the field quantities involved, even when complemented by initial and boundary conditions. To arrive at field equations they must be complemented by additional equations, so-called phenomenological relations. Generally, these describe the material response. In what follows, we shall discuss the way

in which constitutive relations are postulated. Only afterwards shall we specialize them to the material ‘ice’.

Before we pass on to the postulation of constitutive relations, the most important results so far will be summarized. These results are comprised in Equations (1.28), (1.29) and (1.37). The former two sets of equations are the local balance laws of mass, momentum, moment of momentum, energy, and entropy in the spatial and material description, respectively. Apart from the entropy balance law, these laws will be used when temperature, velocity, and stress fields are analyzed. In many situations the temperature field and the stress and velocity fields may decouple, so that one of these can be determined on the basis that the other is prescribed. For many ice-flow problems in glaciers and ice sheets, for instance, the temperature field may be regarded as known so that stresses and velocities can be determined independently. On the other hand, a reasonable postulation or approximate determination of the velocity field might make an independent integration of the energy equation possible. Only rarely will a simultaneous determination of the stress, velocity, and temperature fields be necessary.

The local balance laws have been listed in both the spatial and material description because, depending upon the physical problem at hand, ice is regarded as a fluid or a solid, respectively. Mathematically, fluids are best described in the Eulerian description; solids, on the other hand, are preferably handled in the Lagrangian description. In glacier and ice-sheet flow problems ice is regarded as a viscous fluid, whereas in floating ice plates problems, a solid model is more appropriate.

To the new reader, the presentation of the jump conditions of mass, momentum, energy, and entropy listed in Equations (1.37), might not seem necessary. Yet we shall see that a reasonably sound derivation of phase-change relations for ice-water is only possible, if proper jump conditions are introduced. Incidentally, Equations (1.37) are given in the Eulerian description. Analogous relations could also be derived in the Lagrangian formulation. They are not used in the sequel, however, and so will not be presented.

### 3. Material Response

#### (a) General constitutive relations, simple materials

As stated above, the balance laws will now be complemented by constitutive relations. Experience teaches us that stress, heat flux, and internal energy in a body depend on the present and past values of the motion  $\chi_i$ , temperature  $T$  and density  $\rho$ . This dependence is different for different materials. In the spatial description, to which we shall restrict ourselves in this section, this means generally that stress, heat flux, and internal energy at the position  $x_i$  and time  $t$  must depend on the histories of  $\chi_i$ ,  $T$  and  $\rho$  in the

entire body. Hence, we may write

$$\psi = \hat{\psi}^{\infty}_{s=0} (\chi_i(Y_A, t-s), T(Y_A, t-s), \rho(Y_A, t-s)), \quad (1.38)$$

where  $\psi$  stands for stress  $t_{ij}$ , heat flux  $q_i$  and internal energy  $\varepsilon$  and  $\hat{\psi}(\cdot)$  denotes a functional over the entire body  $\mathcal{B}_t$  and the entire past history  $0 \leq s < \infty$ . When  $\hat{\psi}(\cdot)$  is the material functional for stress,  $\hat{\psi}(\cdot) = \hat{t}_{ij}(\cdot)$ , it is tacitly assumed that the symmetry relation (1.28)<sub>3</sub> is obeyed in the functional relation, which is tantamount to the statement that angular momentum is satisfied identically. In the functional relation (1.38) the history dependence is symbolically indicated by writing  $s = 0$  below and  $\infty$  above the letter denoting the functional, and it is understood that  $s$  varies from zero to infinity.

Analogously, the symbol  $Y_A \in \mathcal{B}_t$  indicates that the independent variable  $Y_A$  in the variable set of the respective functional may be any point within the body  $\mathcal{B}_R$ . Of course, each material is characterized by its own set of functionals  $\hat{t}_{ij}, \hat{q}_i$  and  $\hat{\varepsilon}$ , yet it is impossible in general to determine these functionals for a particular material, say ice. A given set of relations (1.38) rather *defines* a material.

In the form in which the relations (1.38) appear, the material equations describe nonlocal and hereditary effects in the most general sense possible. They appear as very complex and difficult in this generality and will virtually be intractable to explicit calculations even in the most simple initial boundary value problem, but in general it is clear how one has to proceed: The relations (1.38) are postulated for the stress tensor, the heat flux vector and the internal energy and then substituted in the balance laws (1.28). What results is a set of five functional differential equations for the fields  $\chi_i, T$  and  $\rho$ . These equations are called the *field equations*. For prescribed initial and boundary conditions and for a given external body force  $f_i$  and heat source term  $r$  one might be able to find solutions. *Every such solution to the field equations is called a thermodynamic process.*

Their construction will concern us in most of the subsequent chapters. *In this section, however, we are concerned with the methods of postulating constitutive relations and reducing them to their thermodynamically-admissible form.*

The theory of reducing postulated constitutive relations to their thermodynamically-admissible minimal form is known as ‘material theory’ or thermodynamics. There exist definite rules as to how such reductions are performed, of which the most important are:

- (i) constitutive relations describing the material response must be independent of the observer,
- (ii) in case a body possesses certain symmetries, these properties should be exploited in the material equations,

- (iii) the constitutive relations should obey the *second law of thermodynamics*, which is generally stated as an entropy principle.

In the following, we shall briefly indicate what restrictions emerge from the above invariance and symmetry requirements for the material functionals of stress, heat flux, and energy. In so doing, we shall restrict ourselves to *simple materials*. In such a material the functional response of a particle  $X_A$  does not depend on the histories of the motion  $\chi_i$ , temperature  $T$ , and density  $\rho$  in the entire body, but only on those of the motion, temperature, and density of the particle and the particles in the immediate neighborhood of it. Since a function in the neighborhood of  $X_A$  is determined by its value and the value of its gradient at  $X_A$ , the material response functional (1.38) may be written as

$$\psi(\mathbf{X}) = \hat{\psi}_{s=0}^{\infty} (\chi_{\kappa}(\mathbf{X}, t-s), F_{kB}(\mathbf{X}, t-s), T(\mathbf{X}, t-s), T_{,B}(\mathbf{X}, t-s), \rho(\mathbf{X}, t-s), \rho_{,B}(\mathbf{X}, t-s)) \quad (1.39)$$

where

$$\rho_{,B} = \frac{\partial \rho}{\partial X_B}, \quad T_{,B} = \frac{\partial T}{\partial X_B}. \quad (1.40)$$

The representation (1.39) is still too general to describe a simple material. It is characterized by the condition that *density gradients do not occur in the set of independent constitutive variables*. In view of (1.31), which reads  $\rho = \rho_R J$ , the density is known once the motion is determined, which simply means that  $\rho$  may also be deleted as an independent variable, so that a simple material is given by the constitutive relations

$$\psi = \hat{\psi}_{s=0}^{\infty} (\chi_{\kappa}(\mathbf{X}, t-s), F_{kB}(\mathbf{X}, t-s), T(\mathbf{X}, t-s), T_{,B}(\mathbf{X}, t-s)), \quad (1.41)$$

### (b) *The rule of material objectivity*

We have stated above that material equations should be independent of the observer. To understand what is meant by this, let  $x_i$  be the coordinates of a point referring to a given Cartesian basis. Further, let  $x_i^*$  be the coordinates with respect to another basis moving relative to the first one, according to

$$x_i^* = O_{ij}(t)x_j + b_i(t). \quad (1.42)$$

Here,  $O_{ij}(t)$  is a time-dependent orthogonal matrix, and  $b_i(t)$  is a time-dependent vector. A transformation (1.42) is called a *Euclidean transformation*. It is shown in texts of continuum mechanics that the balance laws (1.8) are invariant under such transformations, provided that  $\rho, \epsilon, T$  transform as

scalars,  $q_i$  transforms as a vector, and  $t_{ij}$  transforms as a tensor; such transformation properties will be assumed to hold. It means that the following relations must be fulfilled:

$$\begin{aligned}\varepsilon^* &= \varepsilon, & \rho^* &= \rho, & T^* &= T, \\ q_i^* &= O_{ij}q_j, & t_{ij}^* &= O_{ik}O_{jl}t_{kl}.\end{aligned}\quad (1.43)$$

However, the balance laws are *not* frame indifferent, because when transforming them from an inertial to a non-inertial frame, frame-dependent terms occur as, e.g., in the acceleration (Coriolis acceleration).

This result implies that constitutive functionals for stress, heat flux, and internal energy, need not be frame indifferent, in general. Indeed, they could depend on the frame dependent terms  $\mathbf{O}$  and  $\mathbf{b}$  in such a way that this dependence vanishes whenever the frame of reference is inertial. However, *it is the conjecture of the rule of material frame indifference that all material functionals be frame indifferent.* (This rule is motivated by experience since it has never been found to be violated.\*). Explicitly, it states that the functional form of the material response functional does not depend on the observer frame. In other words, whether written in the starred or unstarred quantities, the response functionals must formally be the same. Mathematically this can be expressed as follows. In the two systems one has

$$\psi = \hat{\psi}_{s=0}^{\infty} (\chi_{\kappa}(t-s), F_{kB}(t-s), T(t-s), T_{,B}(t-s)), \quad (1.44)$$

$$\psi^* = \hat{\psi}_{s=0}^{\infty} (\chi_{\kappa}^*(t-s), F_{kB}(t-s), T^*(t-s), T_{,B}^*(t-s)). \quad (1.45)$$

In general, the starred and unstarred functionals may differ, but material frame indifference requires that

$$\hat{\psi}^*(\cdot) = \hat{\psi}(\cdot),$$

where the arguments are those of (1.44) and (1.45), respectively.

Using the above relations and the transformations (1.43) it is shown in texts on continuum mechanics, see, e.g., Müller [5], Truesdell and Noll [10], Wang and Truesdell [14], that the constitutive functionals do not depend on the motion  $\chi$  and can depend on the deformation gradient  $\mathbf{F}$  only in a certain specific way. An important role is thereby played by the *right Cauchy–Green deformation tensor*

$$C_{AB} = F_{iA}F_{iB} \quad (1.46)$$

\*Modern investigations in statistical mechanics seem to indicate that this might not be so. Müller in [6] presents calculations which indicate that the principle of material frame indifference is not satisfied in the expressions for stress and heat flux when derived from statistical mechanics; yet Truesdell [11] rejects that these relations be constitutive relations at all, thereby maintaining the principle.

and the *second Piola–Kirchhoff stress tensor*  $T_{AB}^P$  and the *material heat flux*  $Q_A$ , which are defined by

$$T_{AB}^P = |J| F_{Ai}^{-1} F_{Bj}^{-1} t_{ij}, \quad Q_A = |J| F_{Ai}^{-1} q_i \quad (1.47)$$

or inversely by

$$t_{ij} = \frac{1}{|J|} F_{iA} F_{jB} T_{AB}^P, \quad q_i = \frac{1}{|J|} F_{iA} Q_A. \quad (1.48)$$

In terms of these variables functional relations for stress, heat flux, and internal energy, which obey the rules of material frame indifference, can have either one of the following forms:

For the material variables,

$$\begin{aligned} T_{AB}^P &= \underset{s=0}{\overset{\infty}{\mathfrak{T}_{AB}^P}}(C_{DE}(t-s), T(t-s), T_D(t-s)), \\ Q_A &= \underset{s=0}{\overset{\infty}{\mathfrak{Q}_A^P}}(\text{---}), \\ \varepsilon &= \underset{s=0}{\overset{\infty}{\hat{\varepsilon}}}(\text{---}). \end{aligned} \quad (1.49)$$

and those in the Eulerian description

$$\begin{aligned} t_{ij} &= F_{iA} F_{jB} \underset{s=0}{\overset{\infty}{\mathfrak{T}_{AB}^P}}(C_{DE}(t-s), T(t-s), T_D(t-s)), \\ q_i &= F_{iA} \underset{s=0}{\overset{\infty}{\mathfrak{Q}_A^P}}(\text{---}), \\ \varepsilon &= \underset{s=0}{\overset{\infty}{\hat{\varepsilon}}}(\text{---}). \end{aligned} \quad (1.50)$$

The functionals  $\mathfrak{T}_{AB}^P$ ,  $\mathfrak{T}_{AB}$  and  $\mathfrak{Q}_A^P$ ,  $\mathfrak{Q}_A$  could be related to each other by use of Equations (1.47) or (1.48). We leave the proof of this as an exercise to the reader. As far as objectivity is concerned, no further reduction of Equations (1.49) and (1.50) is possible. But this is not to say that these are the only objective form of constitutive relations. In fact, there are others, and we may frequently use them without proof.

### (c) Material symmetry

Natural ice is a hexagonal crystal. It is therefore obvious that material properties must reflect this symmetry. Polycrystalline ice, on the other hand, may be regarded as a conglomerate of randomly-oriented crystals and may, on length scales which are large as compared to the grain size, be assumed isotropic. In such a material the response is said to be independent of the direction. To make these statements more precise and to exploit their

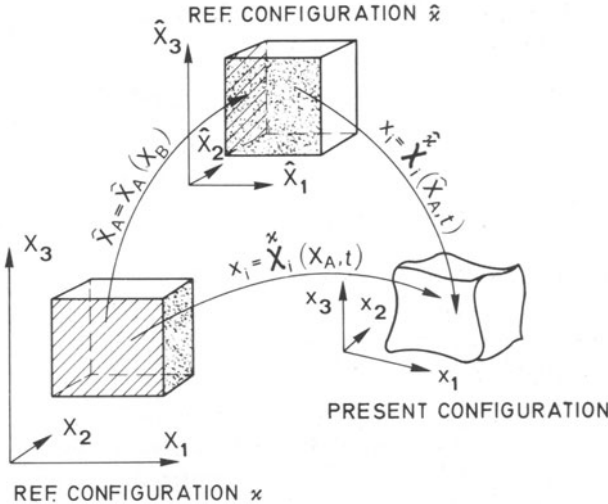


FIG. 1.4. Explaining the motion from two different configurations.

consequences, denote by  $\kappa$  and  $\hat{\kappa}$  two different reference configurations, with respect to which a particle  $X$  has the coordinates  $X_A$  and  $\hat{X}_A$ , respectively, see Figure 1.4. The transformation from one reference configuration to the other may be a rotation, translation or even more general transformation. In any case, it is assumed to be known and invertible. Thus the relations

$$\hat{X}_A = \hat{X}_A(X_B), \quad P_{AB} := \frac{\partial \hat{X}_A}{\partial X_B} \quad (1.51)$$

are known and non-singular so that  $P_{AB}^{-1}$  exists. Depending on which material representation one is looking at, one may write

$$x_i = \chi_i(\mathbf{X}, t) = \hat{\chi}_i(\hat{\mathbf{X}}, t), \quad T = \hat{T}(\mathbf{X}, t) = \hat{T}(\hat{\mathbf{X}}, t), \quad (1.52)$$

where the superscript designates the reference configuration. The deformation and temperature gradients of the two representations may be related to each other. Indeed (1.51) and (1.52) reveal that

$$\begin{aligned} \hat{F}_{iA} &= \frac{\partial \hat{\chi}_i}{\partial \hat{X}_A} = \frac{\partial \chi_i^\kappa}{\partial X_B} \frac{\partial X_B}{\partial \hat{X}_A} = F_{iB} P_{BA}^{-1}, \\ \hat{T}_{,A} &= \frac{\partial \hat{T}}{\partial \hat{X}_A} = \frac{\partial T^\kappa}{\partial X_B} \frac{\partial X_B}{\partial \hat{X}_A} = T_{,B} P_{BA}^{-1}. \end{aligned} \quad (1.53)$$

Deformation and temperature gradients, therefore, depend on the configuration. It follows that this must also be the case for the constitutive functionals.

For instance,

$$\begin{aligned}\psi &= \hat{\psi}^{\kappa} \left( \underset{s=0}{\overset{\infty}{F}}_{kA}(\mathbf{X}, t-s), T(\mathbf{X}, t-s), \underset{,B}{T}(\mathbf{X}, t-s) \right) \\ &= \hat{\psi}^{\hat{\kappa}} \left( \underset{s=0}{\overset{\infty}{F}}_{kA}(\hat{\mathbf{X}}, t-s), \hat{T}(\hat{\mathbf{X}}, t-s), \underset{,B}{T}(\hat{\mathbf{X}}, t-s) \right).\end{aligned}\quad (1.54)$$

Using (1.52) and (1.53), we may also write

$$\begin{aligned}\psi &= \hat{\psi}^{\kappa} \left( \underset{s=0}{\overset{\infty}{F}}_{kA}(\mathbf{X}, t-s), T(\mathbf{X}, t-s), \underset{,B}{T}(\mathbf{X}, t-s) \right) \\ &= \hat{\psi}^{\hat{\kappa}} \left( \underset{s=0}{\overset{\infty}{F}}_{kB}(\mathbf{X}, t-s) P_{BA}^{-1}, T(\mathbf{X}, t-s), \underset{,B}{T}(\mathbf{X}, t-s) P_{BA}^{-1} \right).\end{aligned}\quad (1.55)$$

To introduce the concept of material symmetry, consider a particle which at time  $t = -\infty$  was in configuration  $\kappa$  and subsequently suffered certain histories of the deformation gradient  $F_{iA}$ , temperature  $T$  and temperature gradient  $T_{,B}$ . At time  $t$  the material response functional for stress, heat flux, or internal energy is then given by

$$\psi = \hat{\psi}^{\kappa} \left( \underset{s=0}{\overset{\infty}{F}}_{kA}(\mathbf{X}, t-s), T(\mathbf{X}, t-s), \underset{,B}{T}(\mathbf{X}, t-s) \right). \quad (1.56)$$

Next, consider the same particle but now in configuration  $\hat{\kappa}$  at  $t = -\infty$ . Assume that it experiences the same histories of the deformation gradient, temperature, and temperature gradient as before, but now from configuration  $\hat{\kappa}$ . Because  $\hat{\psi}^{\kappa}(\cdot)$  and  $\hat{\psi}^{\hat{\kappa}}(\cdot)$  are not the same functionals in general, it follows that the value of the variable  $\psi$  under this situation will not be the same as before. Should coincidence occur, however, it is said that *the particle is isotropic with respect to transformations  $\kappa \rightarrow \hat{\kappa}$* . The condition for this to be the case is

$$\begin{aligned}\hat{\psi}^{\kappa} \left( \underset{s=0}{\overset{\infty}{F}}_{kA}(\mathbf{X}, t-s), T(\mathbf{X}, t-s), \underset{,A}{T}(\mathbf{X}, t-s) \right) \\ = \hat{\psi}^{\hat{\kappa}} \left( \underset{s=0}{\overset{\infty}{F}}_{kA}(\mathbf{X}, t-s), T(\mathbf{X}, t-s), \underset{,A}{T}(\mathbf{X}, t-s) \right).\end{aligned}\quad (1.57)$$

Notice that the arguments in both functionals are the same and therefore may be identified with either one of the configurations  $\kappa, \hat{\kappa}$ . If we choose  $\hat{\kappa}$ , use (1.53) in (1.55) and apply the emerging result in (1.57), we obtain

$$\begin{aligned}\hat{\psi}^{\kappa} \left( \underset{s=0}{\overset{\infty}{F}}_{kA}(\mathbf{X}, t-s), T(\mathbf{X}, t-s), \underset{,A}{T}(\mathbf{X}, t-s) \right) \\ = \hat{\psi}^{\kappa} \left( \underset{s=0}{\overset{\infty}{F}}_{kB}(\mathbf{X}, t-s) P_{BA}, T(\mathbf{X}, t-s), \underset{,B}{T}(\mathbf{X}, t-s) P_{BA} \right).\end{aligned}\quad (1.58)$$

The matrices  $\mathbf{P}$ , for which (1.58) applies, are called symmetry (or isotropy) transformations. Candidates for such transformations are rotations (orthogo-

nal transformations). Often the constitutive functionals remain invariant even under the so called *unimodular* transformations. These are all those transformations, for which  $\det \mathbf{P} = \pm 1$ . But we know of no case where (1.58) would be satisfied for more general transformations than the latter ones.

(d) *Constitutive response for isotropic bodies*

We are now in a position to define the conditions of isotropy. If a body possesses a configuration  $\kappa$ , in which the isotropy condition (1.58) applies for all *orthogonal transformations*, we say that the body is *isotropic with respect to  $\kappa$* . Of course, the configuration to which this property applies is a special one, which is why it is called the *natural* or unperturbed configuration. We shall henceforth always assume that the body under consideration possesses a natural configuration.\* The constitutive functionals of an isotropic body necessarily satisfy the condition

$$\begin{aligned} & \hat{\tilde{t}}_{ij}^{\infty}(F_{kA}(\mathbf{X}, t-s), T(\mathbf{X}, t-s), T_{,A}(\mathbf{X}, t-s)) \\ &= \hat{\tilde{t}}_{ij}^{\infty}(F_{kA}(\mathbf{X}, t-s)Q_{AB}, T(\mathbf{X}, t-s), T_{,B}(\mathbf{X}, t-s)Q_{BA}) \end{aligned} \quad (1.59)$$

etc., where  $Q_{AB}$  is an orthogonal matrix and where the superscript  $\kappa$  has been omitted. We may combine the isotropy condition (1.59) with the requirements following from the rule of material frame indifference, Equation (1.43)<sub>5</sub>,  $\mathbf{t} = \mathbf{O}\mathbf{t}^*\mathbf{O}^T$ . In this equation  $\mathbf{t}$  and  $\mathbf{t}^*$  may be replaced by their respective constitutive functionals; moreover,  $\mathbf{O}$  is an arbitrary orthogonal matrix, and one may, in particular, choose  $\mathbf{O} = \mathbf{Q}$ , where  $\mathbf{Q}$  is time-independent. Combining the resulting relation with Equation (1.59) gives

$$\begin{aligned} & \hat{\tilde{t}}_{ij}^{\infty}(F_{kB}(\mathbf{X}, t-s)Q_{BA}, T(\mathbf{X}, t-s), T_{,B}(\mathbf{X}, t-s)Q_{BA}) \\ &= Q_{kl}Q_{lj} \hat{\tilde{t}}_{kl}^{\infty}(Q_{pq}F_{qA}(\mathbf{X}, t-s), T(\mathbf{X}, t-s), T_{,B}(\mathbf{X}, t-s)). \end{aligned} \quad (1.60)$$

\*The concept of symmetry or isotropy is a complex one, and the literature in applied engineering science is full of confusion. Often statements are made that a body becomes anisotropic under applied loads. Such statements are meaningless for a simple body, because the symmetry properties of a material body are always referred to a certain reference configuration. What authors tacitly imply by the above ill-posed statements is a change of configuration. For instance, wave propagation in an otherwise unconstrained body might be described by a linear isotropic elastic constitutive response. If, on the other hand, small perturbation wave propagation of the same body, now subjected to a given large prestress, is analyzed, a proper description of the motion around this new prestressed configuration might very well be described by an anisotropic response model. It is clear from this that, once the reference configuration is chosen, the symmetry properties of the body do not change.

As a last step we make the following substitution:

$$\begin{aligned} F_{kB} Q_{BA} &\rightarrow F_{kA} \Rightarrow F_{kA} \rightarrow F_{kB} Q_{AB}, \\ T_{,B} Q_{BA} &\rightarrow T_{,A} \Rightarrow T_{,B} \rightarrow T_{,A} Q_{BA} = Q_{BA} T_{,A}, \end{aligned}$$

This is permissible, because (1.60) must hold for all fields of the deformation and temperature gradients. Thus (1.60) becomes

$$\begin{aligned} Q_{ik} Q_{jl} \hat{\int}_{s=0}^{\infty} (F_{pq}(\mathbf{X}, t-s), T(\mathbf{X}, t-s), T_{,B}(\mathbf{X}, t-s)) \\ = \hat{\int}_{s=0}^{\infty} (Q_{pq} F_{qB}(\mathbf{X}, t-s) Q_{BA}, T(\mathbf{X}, t-s), Q_{BA} T_{,A}(\mathbf{X}, t-s)). \end{aligned} \quad (1.61)$$

Similar relations can also be derived for the constitutive functionals of heat flux and internal energy. When written in symbolic notation these, together with (1.61), read

$$\begin{aligned} \hat{\mathbf{t}} \int_{s=0}^{\infty} (\mathbf{Q}\mathbf{F}(\mathbf{X}, t-s)\mathbf{Q}^T, T(\mathbf{X}, t-s), \mathbf{Q}\nabla T(\mathbf{X}, t-s)) \\ = \mathbf{Q} \hat{\mathbf{t}} \int_{s=0}^{\infty} (\mathbf{F}(\mathbf{X}, t-s), \mathbf{T}(\mathbf{X}, t-s), \nabla T(\mathbf{X}, t-s))\mathbf{Q}^T, \\ \hat{\mathbf{q}} \int_{s=0}^{\infty} (\mathbf{Q}\mathbf{F}(\mathbf{X}, t-s)\mathbf{Q}^T, T(\mathbf{X}, t-s), \mathbf{Q}\nabla T(\mathbf{X}, t-s)) \\ = \mathbf{Q} \hat{\mathbf{q}} \int_{s=0}^{\infty} (\mathbf{F}(\mathbf{X}, t-s), \mathbf{T}(X, t-s), \nabla T(\mathbf{X}, t-s))\mathbf{Q}^T, \\ \hat{\mathbf{e}} \int_{s=0}^{\infty} (\mathbf{Q}\mathbf{F}(\mathbf{X}, t-s)\mathbf{Q}^T, T(\mathbf{X}, t-s), \mathbf{Q}\nabla T(\mathbf{X}, t-s)) \\ = \hat{\mathbf{e}} \int_{s=0}^{\infty} (\mathbf{F}(\mathbf{X}, t-s), \mathbf{T}(X, t-s), \nabla T(\mathbf{X}, t-s))\mathbf{Q}^T, \end{aligned} \quad (1.62)$$

where  $\nabla$  designates the Nabla operator with respect to the reference coordinates,  $\nabla T = \partial T / \partial \mathbf{X}$ .

Functionals which satisfy the conditions (1.62) are called *tensorial, vectorial, and scalar isotropic functionals* with respect to orthogonal transformations. All functionals satisfying these relations represent constitutive relations of isotropic bodies. It is obvious that the identities (1.62) will yield drastic restrictions on the constitutive functionals. In the following section we shall list them for the special case that the material response does not depend on the entire histories of the deformation gradient, temperature, and temperature gradient, but only on their values in the neighborhood of the present time.

Before we turn to that, we would like to draw the reader's attention to the fact that conditions (1.62) must hold for any isotropic body be it a solid

or a fluid. Yet, we expect that there must be additional conditions which allow us to characterize a body as a solid and a fluid, respectively.

Indeed, according to Noll [10], a fluid is characterized by the condition that the matrix  $\mathbf{P}$  of the symmetry condition (1.58) be *unimodular*, while for a solid, this matrix must be orthogonal (a special unimodular transformation). This difference may then be used to show that *the response functionals of fluids can depend on the present value of the deformation gradient only through its determinant*. Since the determinant of  $\mathbf{F}$  is proportional to the density  $\rho$ , see (1.31), it follows that constitutive relations of fluids must be functions of the present value of  $\rho$  and functionals of the past history of the deformation gradient:  $\mathbf{F}(t-s)$ ,  $0 < s < \infty$  (note this is an open interval).

(e) *Materials with bounded memory – some constitutive representations*

In the preceding calculations we were exclusively dealing with *simple* materials in their broadest sense of the definition. Most descriptions of the material response are not that complex. Indeed, in most situations one is dealing with less complexity. The key idea for a further reduction of the constitutive functionals is the concept of *fading memory*. A material may not remember all of its past history it has undergone. In fact, it is conceivable that there are materials whose memory is bounded.

To express the boundedness of a memory let  $h(t-s)$  be an analytic function of its argument, and let  $0 \leq s < \infty$ . For small  $s$ ,  $h$  may then be represented by a truncated Taylor series :

$$h(t-s) \simeq \sum_{n=0}^N \frac{(-1)^n}{n!} \left. \frac{\partial^n h(t-s)}{\partial s^n} \right|_{s=0} s^n. \quad (1.63)$$

For small  $s$  (well within the radius of convergence of the above Taylor series) the truncated series (1.63) approximates the true function  $h$  quite accurately. Generally, the larger the  $N$ , the better is the approximation. If the memory of the material does not go beyond  $s = T_s$  and  $T_s$  lies inside the radius of convergence, the history of  $h$  in a response functional beyond  $s = T_s$  does not influence the response functional. Thus, the history of  $h$  may then be replaced by the  $N + 1$  variables:

$$\overset{(n)}{h}(t) = (-1)^n \left. \frac{\partial^n h(t-s)}{\partial s^n} \right|_{s=0}, \quad (n = 0, 1, \dots, N). \quad (1.64)$$

If the memory of the material is such that  $N$  derivatives of the form (1.64) are needed, one says that the material is of the *rate type of degree  $N$  with respect to the variable  $h$* . If the material is of the rate type in all its variables, the constitutive functionals become constitutive functions. For instance

$$\psi(t) = \hat{\psi}(\mathbf{F}(\mathbf{X}, t), \dot{\mathbf{F}}(\mathbf{X}, t), T(\mathbf{X}, t), \nabla T(\mathbf{X}, t)) \quad (1.65)$$

is a constitutive equation of the rate type of degree 1 with respect to the

deformation gradient and of degree 0 with respect to the remaining variables. It is easy to see how (1.65) may be generalized. For instance, a material characterized by constitutive relations of the form

$$\psi = \hat{\psi}(\mathbf{F}, \dot{\mathbf{F}}, \dots, {}^{(N_F)}\mathbf{F}, T, \dot{T}, \dots, {}^{(N_T)}T, \nabla T, (\nabla T), \dots, {}^{(N_{\nabla T})}(\nabla T)), \quad (1.66)$$

is of the rate type in all its variables. The degrees  $N_F$ ,  $N_T$  and  $N_{\nabla T}$  need not be the same. Special cases are as follows:

(α) If we set  $N_R = N_T = N_{\nabla T} = 0$ , we obtain

$$\begin{aligned} \mathbf{t} &= \hat{\mathbf{t}}(\mathbf{F}, T, \nabla T), & \mathbf{T}^P &= \mathfrak{T}^P(\mathbf{C}, T, \nabla T), \\ \mathbf{q} &= \hat{\mathbf{q}}(\text{---}), \quad \text{or} \quad \mathbf{Q} = \mathfrak{Q}^P(\text{---}), \\ \boldsymbol{\varepsilon} &= \hat{\boldsymbol{\varepsilon}}(\text{---}), & \boldsymbol{\varepsilon} &= \hat{\boldsymbol{\varepsilon}}(\text{---}), \end{aligned} \quad (1.67)$$

the constitutive relations of a *thermoelastic* body, where the expressions on the left are the general, non-objective relations and those on the right are the objective counter-parts listed in (1.49). Deleting the temperature gradient in (1.67) would correspond to an *elastic* material with a temperature dependence. Omitting both, the temperature and its gradient as a constitutive variable results in the classical constitutive relations of a *purely elastic body*.

(β) A *viscous thermoelastic* body is defined by  $N_F = 1$ ,  $N_T = 0$ ,  $N_{\nabla T} = 0$ ; hence

$$\begin{aligned} \mathbf{t} &= \hat{\mathbf{t}}(\mathbf{F}, \dot{\mathbf{F}}, T, \nabla T), & \mathbf{T}^P &= \mathfrak{T}(\mathbf{C}, \dot{\mathbf{C}}, T, \nabla T), \\ \mathbf{q} &= \hat{\mathbf{q}}(\text{---}), \quad \text{or} \quad \mathbf{Q} = \mathfrak{Q}(\text{---}), \\ \boldsymbol{\varepsilon} &= \hat{\boldsymbol{\varepsilon}}(\text{---}), & \boldsymbol{\varepsilon} &= \hat{\boldsymbol{\varepsilon}}(\text{---}). \end{aligned} \quad (1.68)$$

(γ) In the representations (1.67) and (1.68), no distinction is made as to whether the body under consideration is a solid or a fluid although the relations on the right of (1.67) and (1.68) pertain to solids. In view of the comments at the end of the last subsection, the constitutive relation of a fluid can depend on the present value of the deformation gradient only through its determinant (which is proportional to the density). A *thermoelastic fluid* is therefore characterized by the constitutive functions

$$\mathbf{t} = \hat{\mathbf{t}}(\rho, T, \text{grad } T), \quad \mathbf{q} = \hat{\mathbf{q}}(\text{---}), \quad \boldsymbol{\varepsilon} = \hat{\boldsymbol{\varepsilon}}(\text{---}). \quad (1.69)$$

As is customary in symbolic notation, we have written here *grad* for the spatial gradient,  $(\text{grad } T)_i = T_{,i}$ . Alternatively, we have used above  $\nabla$  for the material gradient,  $(\nabla T)_A = T_{,A}$ .

(δ) To obtain the constitutive relations appropriate for a *viscous heat*

conducting fluid, we start from Equation (1.38). Noticing that

$$F_{iA} = (x_{i,A}) = \dot{x}_{i,A} = v_{i,A} = v_{i,j} F_{jA}, \quad T_{,A} = T_{,i} F_{iA}$$

it is seen that the constitutive equations for a viscous fluid may be written as  $\psi = \hat{\psi}(\rho, v_{i,j}, T, T_{,i})$ . Moreover, using the rule of material frame indifference, it may be shown that the constitutive function cannot depend on the spatial velocity gradient  $L_{ij} \equiv v_{i,j}$  but only on its symmetric part (1.30).  $L_{(ij)} = D_{ij}$ . Hence

$$\psi = \hat{\psi}(\rho, D_{ij}, T, T_{,i}) \quad (1.70)$$

The constitutive relations (1.70) are not yet in the simplest form possible. For that purpose one must exploit the conditions which follow from isotropy. We shall do this below. Here it may suffice to mention that they embrace nonlinear viscous behavior. Fluids characterized by this nonlinearity are called *Maxwellian* or *non-Newtonian fluids*. On the other hand, linear behavior is generally referred to as *Newtonian* behavior. If, moreover, constitutive relations are also linear with respect to the temperature gradient, the emerging field equations are called the *Navier–Stokes equations*.

In certain problems of transient creep, another model of viscous heat conducting fluids is appropriate, namely a material which with respect to  $\mathbf{D}$  is of the rate type of degree  $N$ . Such a material possesses constitutive relations of the form

$$\psi = \hat{\psi}(\rho, \mathbf{D}, \dot{\mathbf{D}}, \ddot{\mathbf{D}}, \dots, \overset{(N)}{\mathbf{D}}, T, \nabla T). \quad (1.71)$$

It can be shown that  $\mathbf{D}^{(m)}$ ,  $m = 1, \dots, N$ , are not frame indifferent measures. These are given by the symmetric *Rivlin–Ericksen tensors*  $\mathbf{A}_{(n)}$  which are defined by the recurrence relations (see Truesdell and Noll [10])

$$\begin{aligned} \mathbf{A}_{(1)} &= 2\mathbf{D}, \\ \mathbf{A}_{(n+1)} &= \dot{\mathbf{A}}_{(n)} + \mathbf{L}^T \mathbf{A}_{(n)} + \mathbf{A}_{(n)} \mathbf{L}, \quad (\text{where } L_{ij} \equiv v_{i,j}). \end{aligned} \quad (1.72)$$

A Rivlin–Ericksen fluid of degree  $N$  is then characterized by the constitutive relations

$$\psi = \hat{\psi}(\rho, \mathbf{A}_{(1)}, \dots, \mathbf{A}_{(n)}, T, \text{grad } T).$$

Clearly, for  $N = 1$ , this fluid agrees with the heat conducting fluid listed in (1.70).

Still further generalizations are possible (and needed to interpret creep data). Such generalizations would be functional relationships among stress, stretching, and objective measures for the time derivatives of both. The reader may easily show that

$$\mathbf{t}_{(1)} = \dot{\mathbf{t}} + \mathbf{t}(\mathbf{W} + \mathbf{D}) + (\mathbf{D} - \mathbf{W})\mathbf{t} \quad (1.73)$$

in which  $\mathbf{W}$  is the skewsymmetric part of the velocity gradient, is an objective

stress rate. A constitutive relation for stress could also involve this stress rate. In modern creep test interpretations, this is indeed so, as a relation between  $\mathbf{t}$ ,  $\mathbf{t}_{(1)}$ ,  $\mathbf{A}_{(1)}$ ,  $\mathbf{A}_{(2)}$ , and  $T$  is established.

(f) *Incompressibility*

All foregoing calculations have been performed on the tacit assumption that the material under consideration be compressible. For an incompressible material the density is constant for all time, which may be interpreted as a constraint condition. The constitutive relations (1.70) and similar previous ones are then inappropriate. In an incompressible body, constitutive relations cannot depend on density. Similarly, density disappears as an unknown in the balance laws. Hence, when using the above constitutive approach we have lost one field variable. This is serious because there would now be one field equation more than there are field variables. The system of field equations would no longer be integrable. To obtain field equations from the balance laws and appropriate constitutive relations, a different approach to the postulation of phenomenological laws must therefore be taken. The procedure is to introduce the variable lost by the constraint condition in the constitutive relation of stress by writing  $t_{ij} = t_{ij}^0 + t_{ij}^E$ , and to postulate a constitutive relation for the stress  $t_{ij}^E$  only.  $t_{ij}^0$  is then a basic field variable introduced to compensate for the 'lost' field  $\rho$ , yet,  $t_{ij}^0$  are six fields. Hence, a criterion is needed, by which  $t_{ij}^0$  can be reduced to one variable. Truesdell [10] has formulated such a postulate. It reads: *The constraint stress  $t_{ij}^0$  performs no work in any motion satisfying the constraint equation*, which is simply the incompressibility condition  $v_{i,i} = 0$ . It is shown in texts on continuum mechanics that this 'workless constraint postulate' requires that  $t_{ij}^0 = -p \delta_{ij}$ . Consequently

$$t_{ij} = -p \delta_{ij} + t_{ij}^E. \quad (1.74)$$

As expected,  $p$  is called the pressure and  $t_{ij}^E$  is given by a constitutive functional to which the constitutive theory presented above may be applied. The field equations in an incompressible material are now the balance laws of mass, momentum, and energy in which the constitutive relationships for stress, heat flux, and internal energy have been substituted. The emerging equations contain as unknowns the motion, pressure, and temperature. The number of these unknowns is the same as was encountered in the theory of compressible bodies. Hence, the difficulty of having too many equations and not enough unknowns is resolved.

(g) *Some representations of isotropic functions*

In subsection d the restrictions of isotropy imposed on the constitutive relations were discussed, but no attempt was made to exploit these. Generally, such an exploitation is very difficult, and we have no intention of demon-

ing this reduction in this book and shall limit our attention to the presentation of the results for the simple case that constitutive relations are isotropic *functions* of a symmetric tensor, vector, and scalar. More complicated cases can be taken from the pertinent literature, see Smith [7] and Wang [13]. Constitutive relations of this complexity have the form  $\psi = \hat{\psi}(\mathbf{D}, T, \mathbf{g} \equiv \nabla T)$  and are in this form appropriate for an *incompressible viscous heat-conducting fluid*. In the following,  $\mathbf{D}$ ,  $\nabla T$  and  $T$  will be assumed to be a symmetric tensor, vector, and scalar, which may not necessarily have the physical meaning suggested by this fluid.

Tensorial, vectorial and scalar functions must satisfy the identities (1.62) for all orthogonal matrices  $\mathbf{Q}$ . Exploiting these relations for constitutive relations of the form  $\psi = \hat{\psi}(\mathbf{D}, T, \mathbf{g})$  shows that the heat flux vector  $q_i$  and the Cauchy stress tensor  $t_{ij}$  are expressible as \*

$$\begin{aligned} q_i &= \alpha g_i + \beta D_{ij} g_j + \gamma (\mathbf{D}^2)_{ij} g_j, \\ t_{ij} &= a \delta_{ij} + b D_{ij} + c (\mathbf{D}^2)_{ij} + d g_i g_j + \\ &\quad + e g_k D_{k(i} g_{j)} + f g_k (\mathbf{D}^2)_{k(i} g_{j)}, \end{aligned} \quad (1.75)$$

where the coefficients  $\alpha, \beta, \gamma$  and  $a, b, d, e, f$  and the free energy  $\varepsilon$  are functions of the following scalar valued variables:

$$T, D_I, D_{II}, D_{III}, \mathbf{g} \cdot \mathbf{g}, \mathbf{g} \cdot \mathbf{Dg}, \mathbf{g} \cdot \mathbf{D}^2 \mathbf{g}. \quad (1.76)$$

Here,  $D_I$ ,  $D_{II}$  and  $D_{III}$  are the three invariants of the symmetric tensor  $\mathbf{D}$  expressible as

$$\begin{aligned} D_{(I)} &= \text{tr } \mathbf{D} = D_{ii}, \\ D_{(II)} &= D_{11} D_{22} + D_{22} D_{33} + D_{33} D_{11} - D_{12}^2 - D_{23}^2 - D_{31}^2, \\ D_{(III)} &= \det \mathbf{D}. \end{aligned} \quad (1.77)$$

The meaning of the remaining variables is evident from (1.76). It can be seen that the heat flux vector depends *linearly* on the temperature gradient  $\mathbf{g}$  but contains two non-linear terms as the stretching tensor  $\mathbf{D}$  arises together with  $\mathbf{g}$ . The coefficient  $\alpha = -\kappa$  is the heat conductivity, and a constitutive relation of the form  $q_i = -\kappa g_i$  is called the isotropic Fourier's law of heat conduction. In the constitutive relation of stress, the coefficient  $a = -p$  is the pressure and  $b = \mu$  the viscosity, whereas the remaining coefficients do not have separate names. In a constitutive theory, where stress does not depend on temperature gradient, only the first three terms on the right-hand side of (1.75)<sub>2</sub> survive with coefficients which are only functions of

\*An easy derivation of these formulas is given by Müller. The method is to look at the scalars  $q_i \phi_i, t_{ij} \phi_{ij}$ , where  $\phi_i$  and  $\phi_{ij}$  are arbitrary and to require that these scalars have the same values for all orthogonal matrices  $\mathbf{Q}$ . The procedure uses theorems of matrix algebra, such as the Cayley–Hamilton theorem, see Greub [2], van der Waerden [12].

the first four variables of the list (1.76). This is an important special case known as Reiner–Rivlin fluid and it embraces most of the constitutive relationships encountered in glaciology.

The set (1.76) of scalar variables formed with  $\mathbf{D}$ ,  $\mathbf{g}$  and  $T$  is complete in the sense that there are no fewer and no more, but it is not the only possible set of independent scalar combinations. For instance, the invariants  $D_1$ ,  $D_{\text{II}}$  and  $D_{\text{III}}$  can be combined to form other invariants. Another such possible set is, for instance,

$$D_1 = \text{tr } \mathbf{D}, \quad D_2 = \frac{1}{2} \text{tr} (\mathbf{D}^2), \quad D_3 = \frac{1}{6} \text{tr} (\mathbf{D}^3). \quad (1.78)$$

This alternative set is frequently used in the literature. For an incompressible body  $\mathbf{t}$  in (1.75) must be replaced by  $\mathbf{t}^E$ . The coefficient  $a$  should in this case, not be confused with the pressure. In fact, since pressure is arbitrary, any isotropic part of  $t_{ij}$  may be absorbed into it without loss of generality. That is, the constitutive relation determines only the deviatoric stress  $t_{ij}^E$ , and the condition  $t_{ii}^E = 0$  relates the coefficients arising in (1.75). For a *Reiner–Rivlin fluid* the condition is  $3a + 2cD_2 = 0$ , in which  $D_1 = 0$  has been used. Thus (1.75) becomes

$$t_{ij}^E = bD_{ij} + c[(\mathbf{D}^2)_{ij} - \frac{2}{3}D_2\delta_{ij}] \quad (1.79)$$

where  $b$  and  $c$  are functions of  $D_2$  and  $D_3$  and the temperature  $T$ .

Isotropic constitutive functions of the form (1.75) are not sufficient to interpret creep-curve data accurately, and so it seems appropriate to mention what complexity would be needed in isotropic constitutive relationships to approximate such data mathematically by materially-objective constitutive relations. To this end we restrict our attention to the constitutive relation for the stress tensor of an incompressible body. Our aim is to generalize the Reiner–Rivlin fluid by including, in a constitutive relationship for  $\mathbf{t}^E$ , objective measures for strain rates and stress rates. In view of (1.72) one has  $\mathbf{A}_{(2)} = 2\mathbf{D} + 4\mathbf{D}^2 + 2(\mathbf{DW} - \mathbf{WD})$  as expression for the second Rivlin–Ericksen tensor but since  $\mathbf{D}^2$  is objective by itself, an alternative objective measure for the strain rate is also

$$\mathbf{M} = 2\dot{\mathbf{D}} + 2(\mathbf{DW} - \mathbf{WD}). \quad (1.80)$$

Thus, one has the general constitutive postulate  $\mathbf{t}^E = \hat{\mathbf{t}}^E(t_{(1)}^E, \mathbf{D}, \mathbf{M}, T)$ , in which  $\hat{\mathbf{t}}^E(\cdot)$  is an objective isotropic function of the three symmetric tensors  $t_{(1)}^E$ ,  $\mathbf{D}$  and  $\mathbf{M}$ . Its complete explicit form could be written down by consulting the literature, see, e.g., Smith [7], but the formula would be very lengthy and nothing could be learned from it. We thus restrict ourselves to an isotropic function, which is *linear* in  $t_{(1)}^E$  and  $\mathbf{M}$ . This can be shown to yield the relation

$$a\mathbf{t}^E + dt_{(1)}^E = b\mathbf{D} + c[\mathbf{D}^2 - \frac{2}{3}D_2\mathbf{1}] + e\mathbf{M} \quad (1.81)$$

in which  $a, b, c, d, e$  are functions of all the scalar invariants that can be formed with the four symmetric tensors. The constitutive relation (1.81) must still satisfy the traceless condition. Since in view of (1.73)  $\text{tr}(\mathbf{t}_{(1)}^E) = 2 \text{tr}(\mathbf{t}^E \mathbf{D})$  and because all remaining terms in (1.81) are traceless, an alternative relation is

$$\begin{aligned} a\mathbf{t}^E + d[\mathbf{t}_{(1)}^E - \frac{2}{3}\text{tr}(\mathbf{t}^E \mathbf{D})\mathbf{1}] \\ = b\mathbf{D} + c[\mathbf{D}^2 - \frac{2}{3}D_2\mathbf{1}] + e\mathbf{M} \end{aligned} \quad (1.82)$$

with a different coefficient  $d$ . There are too many scalar invariants of the four tensors that practical considerations would allow to consider all of them as possible variables in the coefficients  $a$  through  $d$ . The most obvious ones are  $D_2, D_3, \dot{D}_2, \dot{D}_3$  (see (1.78)) and the corresponding invariants of the stress deviator  $S_2 \equiv \frac{1}{2}\text{tr}\mathbf{t}_E^2, S_3 = \frac{1}{6}\text{tr}\mathbf{t}_E^3$  and  $\dot{S}_2$  and  $\dot{S}_3$ . In a paper by Morland and Spring\* these dependencies were included in an attempt to mathematically describe creep data obtained from tests of constant strain rate and constant stress, but these tests were not sufficient to evaluate all dependencies in the coefficient functions (1.82). For this purpose, multiaxial tests are necessary.

#### 4. The Entropy Principle

The foregoing analysis makes no use of thermodynamic considerations, and indeed of the three statements on pages 19, 20 we have so far only dealt with the first two. The exploitation of the second law of thermodynamics is also part of the material theory and it would strictly belong in Section 3. Thermodynamic requirements are so important, however, that we prefer to present them in a separate section.

Basic to the second law of thermodynamics is the balance law of entropy which, in the Eulerian description, reads as follows

$$\rho \frac{d\eta}{dt} + \left( \frac{q_i}{T} \right)_{,i} - \frac{\rho r}{T} = \rho\gamma \quad (1.83)$$

$\eta$  is the entropy,  $q_i/T$  the entropy flux,  $r/T$  the entropy supply and  $\gamma$  the entropy production. Statistical mechanics suggests that the entropy production cannot be negative,  $\gamma \geq 0$ . This inequality is the expression of the *second law of thermodynamics*. In a body it must be satisfied whatever process the body is subjected to.  $\gamma \geq 0$  implies

$$\rho \frac{d\eta}{dt} + \left( \frac{q_i}{T} \right)_{,i} - \frac{\rho r}{T} \geq 0, \quad (1.84)$$

which, in modern continuum thermodynamics, is called the *Clausius–Duhem inequality*.

\*Viscoelastic fluid relation for the deformation of ice', *Cold Regions Sci. Tech.*, 4 (1981), 225–268.

The Clausius–Duhem inequality is not the only dissipation postulate that is used in modern continuum thermodynamics. There are many others, some of which do not even involve entropy as a field variable. We shall restrict our considerations to the above form, but refer the interested reader to an article by Hutter [3], in which the various forms of the second law of thermodynamics are critically reviewed.

The entropy principle is a statement concerning the exploitation of the Clausius–Duhem inequality. We shall follow here the approach of modern rational thermodynamics, according to which the entropy inequality (1.84) must be satisfied for every thermodynamic process. A thermodynamic process is thereby a solution of the field equations which have been defined in Section 3.

The fact that the specific body force  $\rho f_i$  and the energy supply  $\rho r$  are external source terms, which can be chosen at will, implies that corresponding to the given acceleration, stress, internal energy and its rate of change, stretching tensor and heat flux, there is always a body force  $\rho f_i$  and heat supply  $\rho r$ , which guarantee that the momentum equation

$$\rho \dot{v}_i = t_{ij,j} + \rho f_i \quad (1.85)$$

and the energy equation

$$\rho \dot{\epsilon} = t_{ij} D_{ij} - q_{i,i} + \rho r \quad (1.86)$$

are identically satisfied. Hence, one can choose in a body arbitrary histories of the motion (and of the deformation gradient), of the temperature and its gradient and still can find the appropriate body force and heat supply terms such that (1.85) and (1.86) are satisfied identically. Consequently, when satisfying the entropy inequality (1.84) identically for all thermodynamic processes, the momentum and energy equations do not form restrictions. However the continuity equation may have to be considered as a side condition. We shall demonstrate the procedure using the viscous, heat-conducting compressible fluid as an example, but shall only list the results for other simple materials that are of some importance in ice mechanics.

#### (a) *The viscous heat-conducting compressible fluid*

Fluids are treated in the Eulerian description, so that the field equations are

$$\begin{aligned} \dot{\rho} + \rho v_{i,i} &= 0, & t_{ij} &= \hat{t}_{ij}(\rho, D_{kl}, T, T_{,k}), \\ \rho \dot{v}_i &= t_{ij,j} + \rho f_i, & q_i &= \hat{q}_i(\text{---}), \\ \rho \dot{\epsilon} &= t_{ij} D_{ij} - q_{i,i} + \rho r, & \epsilon &= \hat{\epsilon}(\text{---}). \end{aligned} \quad (1.87)$$

The Clausius–Duhem inequality contains a new variable, the entropy  $\eta$ . Since it is not determined by the field equations, a constitutive relation must

be established for it. It is reasonable to choose the same set of independent variables (rule of *equipresence*), so that

$$\eta = \hat{\eta}(\rho, D_{kl}, T, T_{,i}). \quad (1.88)$$

A direct exploitation of the Clausius–Duhem inequality (1.84) is not appropriate because it contains the term  $\rho r$ , which may be assigned arbitrarily. We eliminate it using the energy Equation (1.87)<sub>3</sub> and then obtain

$$\rho(T\dot{\eta} - \dot{\varepsilon}) + t_{ij} \cdot D_{ij} - \frac{q_i T_{,i}}{T} \geq 0. \quad (1.89)$$

Using (1.88) and applying the chain rule it follows from (1.89) that

$$\begin{aligned} \rho \left[ \dot{\rho} \left( T \frac{\partial \hat{\eta}}{\partial \rho} - \frac{\partial \hat{\varepsilon}}{\partial \rho} \right) \dot{\rho} + \left( T \frac{\partial \hat{\eta}}{\partial T} - \frac{\partial \hat{\varepsilon}}{\partial T} \right) \dot{T} + \left( T \frac{\partial \hat{\eta}}{\partial D_{ij}} - \frac{\partial \hat{\varepsilon}}{\partial D_{ij}} \right) \dot{D}_{ij} + \right. \\ \left. + \left( T \frac{\partial \hat{\eta}}{\partial T_{,i}} - \frac{\partial \hat{\varepsilon}}{\partial T_{,i}} \right) (T_{,i})' \right] + D_{ij} t_{ij} - \frac{q_i T_{,i}}{T} \geq 0. \end{aligned} \quad (1.90)$$

This inequality must be satisfied identically for all thermodynamic processes, that is for all solutions of the field Equations (1.87). As was explained before, since  $\rho f_i$  and  $\rho r$  may be assigned arbitrary values, any values may be chosen for  $\rho, D_{ij}, T, T_{,i}$  and their space and time derivatives; we may thereby still be able to satisfy (1.87)<sub>2,3</sub> identically. However,  $\dot{\rho}$  cannot be chosen arbitrarily as the balance equation of mass, (1.87)<sub>1</sub> must be fulfilled, implying that  $\dot{\rho} = -\rho D_{ij} \delta_{ij}$ . Substituting this value for  $\dot{\rho}$  into inequality (1.90), a new inequality emerges, which is explicitly linear in  $\dot{T}, (T_{,i})', D_{ij}$ . Since these may have any arbitrary values, the inequality would be violated unless the coefficients of these quantities vanish.\* This argument yields the following conditions:

$$\frac{\partial \hat{\eta}}{\partial T} = \frac{1}{T} \frac{\partial \hat{\varepsilon}}{\partial T}, \quad \frac{\partial \hat{\eta}}{\partial T_{,i}} = \frac{1}{T} \frac{\partial \hat{\varepsilon}}{\partial T_{,i}}, \quad \frac{\partial \hat{\eta}}{\partial D_{ij}} = \frac{1}{T} \frac{\partial \hat{\varepsilon}}{\partial D_{ij}}. \quad (1.91)$$

There remains the residual inequality

$$\Gamma \equiv \left[ t_{ij} - \rho^2 \left( T \frac{\partial \hat{\eta}}{\partial \rho} - \frac{\partial \hat{\varepsilon}}{\partial \rho} \right) \delta_{ij} \right] D_{ij} - \frac{q_i T_{,i}}{T} \geq 0. \quad (1.92)$$

By cross-differentiation of the relations (1.91) it can be shown that

$$\frac{\partial \hat{\eta}}{\partial T_{,i}} = \frac{\partial \hat{\eta}}{\partial D_{ij}} = \frac{\partial \hat{\varepsilon}}{\partial T_{,i}} = \frac{\partial \hat{\varepsilon}}{\partial D_{ij}} = 0.$$

\*The general form of the inequality is  $A\alpha + \beta \geq 0$ , where  $A$  and  $\beta$  are independent of  $\alpha$ , and  $\alpha$  may have any arbitrarily-assigned value. It is seen by inspection that the choice  $\alpha = -(1/A)(\beta + \varepsilon)$ ,  $\varepsilon > 0$  will violate the inequality.

Hence,  $\hat{\varepsilon}$  and  $\hat{\eta}$  cannot be functions of  $T_{,i}$  and  $D_{ij}$ :

$$\varepsilon = \hat{\varepsilon}(\rho, T), \quad \eta = \hat{\eta}(\rho, T). \quad (1.93)$$

Next we define *thermostatic equilibrium*. This is defined as a time-independent thermodynamic process with uniform temperature and velocity distribution. Hence, in thermostatic equilibrium, which will be characterized by the index  $|E$ ,  $D_{ij} = T_{,i} = 0$ . It follows from (1.92) that  $\Gamma|_E = \Gamma_{\min} = 0$ . Hence  $\Gamma$  assumes its minimum in thermostatic equilibrium. From the theory of extrema of functions of several variables we then conclude that

$$\left. \frac{\partial \Gamma}{\partial D_{ij}} \right|_E = 0, \quad \left. \frac{\partial \Gamma}{\partial T_{,i}} \right|_E = 0 \quad (1.94)$$

and that the matrix  $\mathbf{A}$

$$\mathbf{A} = \left[ \begin{array}{cc} \frac{\partial^2 \Gamma}{\partial D_{ij} \partial D_{kl}} & \frac{\partial^2 \Gamma}{\partial D_{ij} \partial T_{,k}} \\ \frac{\partial^2 \Gamma}{\partial D_{ij} \partial T_{,k}} & \frac{\partial^2 \Gamma}{\partial T_{,i} \partial T_{,j}} \end{array} \right]_E \quad (1.95)$$

is positive-semi definite. The relations (1.94) imply that

$$q_{i|E} = 0, \quad t_{ij|E} = -p\delta_{ij}, \quad \text{with} \quad p = \rho^2 \left( \frac{\partial \hat{\varepsilon}}{\partial \rho} - T \frac{\partial \hat{\eta}}{\partial \rho} \right). \quad (1.96)$$

The equilibrium heat flux vanishes and the equilibrium stress is isotropic,  $p$  is the pressure, and it is seen from (1.93) that it is a function of density and temperature. The result (1.96) may also be taken as motivation for the decomposition  $t_{ij} = -p\delta_{ij} + t_{ij}^E$ , where  $t_{ij}^E$  is the *extra stress*. Its constitutive equation has the form (1.87)<sub>4</sub> and in terms of it, the second of Equations (1.96) reads  $t_{ij|E}^E = 0$ . Thus, in thermodynamic equilibrium, both heat flux and extra stress vanish. Moreover, (1.91) and Equation (1.96)<sub>3</sub> for the pressure may be used to derive the total differential of  $\eta$  as follows:

$$d\eta = \frac{1}{T} \left\{ \frac{\partial \hat{\varepsilon}}{\partial T} dT + \left( \frac{\partial \hat{\varepsilon}}{\partial \rho} - \frac{p}{\rho^2} \right) d\rho \right\}. \quad (1.97)$$

This is the Gibbs relation for a compressible heat-conducting viscous fluid.

To draw conclusions from (1.95), it is advantageous to write down extra stress and heat flux in their most general form appropriate for an isotropic fluid. With a notation, which differs slightly from that of (1.75), we may write

$$\begin{aligned} q_i &= -\kappa\delta_{ij} + q_1 D_{ij} T_{,j} + q_2 D_{ij} D_{jk} T_{,k}, \\ t_{ij}^E &= \alpha\delta_{ij} + 2\mu D_{ij} + t_2 D_{ik} D_{kj} + \tau T_{,i} T_{,j} + \\ &\quad + t_4 T_{,k} D_{k(i} T_{,j)} + t_5 T_{,k} D_{kl} D_{l(i} T_{,j)} \end{aligned} \quad (1.98)$$

with  $\alpha|_E = 0$ .

The coefficients  $\kappa, q_1, q_2, \alpha, \mu, t_2, \tau, t_4$  and  $t_5$  are functions of the variables (1.76)  $T$  and  $\rho$ . Substituting (1.98) into (1.95) and performing the differentiations required for the evaluation of (1.95) gives

$$\mathbf{A} = \begin{bmatrix} \frac{\partial \alpha}{\partial D_{kl}} \Big|_E \delta_{ij} + 2\mu \Big|_E \delta_{ik} \delta_{jl} & \frac{\partial \alpha}{\partial T_{,k}} \Big|_E \delta_{ij} \\ \frac{\partial \alpha}{\partial T_{,k}} \Big|_E \delta_{ij} & \frac{\kappa}{T} \Big|_E \end{bmatrix} \quad (1.99)$$

A necessary (but not sufficient) condition for this to be positive-semidefinite is  $\kappa \geq 0$ ; but, in general, it cannot be concluded that  $\mu \geq 0$ . This would only be possible when  $(\partial \alpha / \partial D_{kl})|_E = 0$  or  $(\partial \alpha / \partial T_{,k})|_E = 0$ . In spite of this, it is generally assumed that  $\kappa > 0$  and  $\mu > 0$ .

*(b) The viscous heat conducting incompressible fluid*

Glacier ice is almost always considered to be a viscous heat-conducting incompressible fluid. The field equations of such a fluid are

$$\begin{aligned} v_{i,i} &= 0, & t_{ij}^E &= \hat{t}_{ij}^E(T, T_{,k}, D_{kl}), \\ \rho \dot{v}_i &= -p_{,i} + t_{ij,j}^E + \rho f_i, & q_i &= \hat{q}_i(T, T_{,k}, D_{kl}), \\ \rho \dot{e} &= t_{ij}^E D_{ij} - q_{i,i} + \rho r, & \varepsilon &= \hat{\varepsilon}(T, T_{,k}, D_{kl}), \end{aligned} \quad (1.100)$$

and the entropy inequality reads

$$\rho \dot{\eta} + \left( \frac{q_i}{T} \right)_{,i} \geq \frac{\rho r}{T} \quad \text{with} \quad \eta = \hat{\eta}(T, T_{,k}, D_{kl}). \quad (1.101)$$

Notice that a constitutive relation has been postulated here for the extra stress tensor  $t_{ij}^E$ . Since any isotropic stress may be absorbed in the pressure, this extra stress may, without loss of generality, be assumed as a stress deviator, satisfying  $t_{ii}^E \equiv 0$ . Notice that (1.101) must hold for all thermodynamic processes, and this implies that (1.100)<sub>1</sub> must be used as a side condition to (1.101). Thus we add  $\bar{p}v_{i,i} = \bar{p}D_{ij}\delta_{ij}$  to the left-hand side of (1.101), where  $\bar{p}$  is a Lagrangian parameter identical to the pressure. The calculations parallel now the procedure outlined in the last section. In a first step,  $r$  is eliminated between the energy equation and the extended Clausius–Duhem inequality, and the constitutive functions (1.100)<sub>4,5,6</sub> are substituted in the emerging inequality. This inequality is linear in the variables  $\dot{T}, (T_{,k})'; D_{kl}^*$ , which may have arbitrarily assigned values. Thus, the coefficients of these variables must vanish, and this requires that

$$\varepsilon = \hat{\varepsilon}(T), \quad \eta = \hat{\eta}(T), \quad d\eta = \frac{1}{T} d\varepsilon. \quad (1.102)$$

Internal energy and entropy are only functions of the temperature. The

residual inequality is

$$t_{ij}^E D_{ij} - \frac{q_i T_{,i}}{T} \geq 0 \quad (1.103)$$

and implies that in thermostatic equilibrium, where  $D_{ij} \equiv T_{,i} \equiv 0$ ,  $t_{ij|E}^E = q_{i|E} = 0$ . The general form of the constitutive relations for heat flux and stress is again as shown in (1.98), but with  $\alpha \equiv 0$  and satisfying the condition  $t_{ij}^E \equiv 0$ , or

$$t_2 D_{ik} D_{ik} + \tau T_{,i} T_{,i} + t_4 T_{,k} D_{ik} T_{,i} + t_5 T_{,k} D_{kl} E_{li} T_{,i} \equiv 0. \quad (1.104)$$

It thus follows from (1.99) that in thermostatic equilibrium  $\kappa|_E \geq 0$  and  $\mu|_E \geq 0$ .

(c) *Pressure and extra stress as independent variables*

In the constitutive postulates of the preceding sections, motion, temperature (and density) were regarded as the independent constitutive variables, whereas stress, heat flux, internal energy, and entropy were regarded as the dependent constitutive variables. This need not necessarily be so, and another equally-popular formulation regards pressure, temperature, temperature gradient, and extra stress as independent variables, and stretching heat flux, internal energy, and entropy, as the dependent ones,

$$\psi = \hat{\psi}(p, T, T_{,k}, t_{kl}^E), \quad (1.105)$$

where  $\psi$  stands for  $D_{ij}$ ,  $q_i$ ,  $\varepsilon$  and  $\eta$ . When comparing (1.105) with the constitutive relations (1.87) of a compressible viscous fluid, it is seen that in (1.105) the pressure plays the role of the density and the extra stress  $t_{ij}^E$  plays that of the stretching tensor. It follows that in the constitutive relations for an incompressible fluid of the form (1.105), the pressure would be absent from the set of independent variables. The key to the exploitation of the entropy inequality is to write  $t_{ij} = -p \delta_{ij} + t_{ij}^E$ , to introduce *enthalpy*  $h$  and *free enthalpy*  $\psi_h$ , defined by

$$h := \varepsilon + \frac{p}{\rho}, \quad \psi_h := \varepsilon + \frac{p}{\rho} - T\eta = h - T\eta \quad (1.106)$$

and to postulate constitutive relations of the form (1.105) for  $D_{ij}$ ,  $q_i$ ,  $\varepsilon$ ,  $\eta$ ,  $h$  and  $\psi_h$ . The Clausius–Duhem inequality then leads to the results that  $\varepsilon$ ,  $\eta$ ,  $h$  and  $\psi_h$  are functions of the pressure and temperature only,  $\psi_h = \hat{\psi}_h(p, T)$ , etc. with

$$\eta = -\frac{\partial \hat{\psi}_h}{\partial T}, \quad \frac{1}{\rho} = \frac{\partial \hat{\psi}_h}{\partial p}, \quad d\eta = \frac{1}{T} \left\{ dh - \frac{dp}{\rho} \right\}. \quad (1.107)$$

We see that the enthalpy function plays the same role here as does the internal energy when  $T$  and  $\rho$  are the independent variables.

The above applies to a compressible fluid. For an *incompressible fluid*, the pressure would not occur as an independent variable in the variable

set (1.105). Using an approach akin to the one above, it can then be shown that  $t_{kl}^E$  may be identified with the deviator and

$$\varepsilon = \hat{\varepsilon}(T), \quad \eta = \hat{\eta}(T), \\ D_{ij} = \hat{D}_{ij}(T, T_{,k}, t_{kl}^E), \quad q_i = \hat{q}_i(\text{---}), \quad (1.108)$$

where in thermostatic equilibrium, defined by the conditions  $t_{ij}^E = 0$  and  $T_{,k} = 0$ , both  $q_i$  and  $D_{ij}$  must vanish.

The constitutive relations (1.108) embrace those used to date in theoretical glacier studies as a special case. Special among these is that the function  $\hat{D}_{ij}(\cdot)$  is assumed to be independent of the temperature gradient and, furthermore, that  $\hat{q}_i(\cdot)$  does not depend on  $t_{kl}^E$ , and  $T$  and is linear in the temperature gradient. Generally, one also assumes that  $\hat{\varepsilon}(T)$  is a linear function of  $T$ . Under these restrictive assumptions one obtains

$$\varepsilon = c(T - T_0), \quad D_{ij} = \hat{D}_{ij}(t_{kr}^E T), \quad q_i = -\kappa T_{,i}. \quad (1.109)$$

$c$  is called *specific heat* and  $\kappa$  the *heat conductivity*, and Equation (1.109)<sub>3</sub> is Fourier's law of heat conduction. Clearly, in a viscous fluid, the function  $\hat{D}_{ij}(\cdot)$  must also satisfy the conditions for an isotropic tensor-valued function, as treated in Section 3g. With temperature gradients not being present as independent variables in (1.109), it follows from the second of the relations (1.75), where the  $t_{kl}^E$  and  $D_{ij}$  above are denoted in Equations (1.75) as  $D_{kl}$  and  $t_{ij}$ , respectively, that

$$D_{ij} = h(\cdot)\delta_{ij} + f(\cdot)t_{ij}^E + g(\cdot)t_{ik}^Et_{kj}^E, \quad (1.110)$$

in which  $f(\cdot)$ ,  $g(\cdot)$  and  $h(\cdot)$  are functions of the second and third stress invariants of the deviator  $t_{ij}^E$  and of the temperature. There is still a further restriction that Equation (1.110) must fulfil. Since for an incompressible body trace  $\mathbf{D} = 0$ , the right-hand side of (1.110) must vanish when the trace is formed. This gives  $3h(\cdot) + g(\cdot)\text{tr}(\mathbf{t}^E)^2$ , where  $\text{tr}(\mathbf{t}^E) = 0$ . Hence,

$$D_{ij} = -\frac{1}{3}\text{tr}(\mathbf{t}^E)^2g(\cdot)\delta_{ij} + f(\cdot)t_{ij}^E + g(\cdot)t_{ik}^Et_{kj}^E$$

which is the most general form of constitutive relationship for stress of the class listed in (1.108). We shall return to this law in Chapter 2.

#### (d) Thermoelastic solid

In bearing capacity problems of floating ice plates, ice is often regarded as a thermoelastic solid. The field equations of such a body are

$$\begin{aligned} T_{AB}^P &= \mathfrak{T}_{AB}^P(C_{CD}, T, T_{,C}), \\ \rho_R \ddot{x}_i &= T_{iA,A} + \rho_R f_i, & Q_A &= \mathfrak{Q}_A(C_{CD}, T, T_{,C}), \\ \rho_R \dot{\varepsilon} &= T_{iA} \dot{F}_{iA} - Q_{A,A} + \rho_R r, & \varepsilon &= \hat{\varepsilon}(C_{CD}, T, T_{,C}). \end{aligned} \quad (1.111)$$

Notice that the continuity equation plays no role here, since the balance of mass results in the statement  $\rho_R = \rho_R(\mathbf{X})$ . Furthermore,  $T_{iA}$  and  $T_{AB}^P$  are

the first and second Piola–Kirchhoff stress tensors, related by

$$T_{iA} = F_{iB} T_{AB}^P, \quad (1.112)$$

and  $C_{AB} = F_{iA} F_{iB}$  is the right Cauchy–Green deformation tensor. With the aid of the Lagrangian form of the Clausius–Duhem inequality,

$$\rho_R \dot{\eta} + \left( \frac{Q_A}{T} \right)_{,A} \geq \frac{\rho_R r}{T}, \quad \eta = \hat{\eta}(C_{AB}, T, T_{,A}) \quad (1.113)$$

it may be shown by a procedure analogous to the previous ones, that  $\varepsilon, \eta$  and  $T^P$  are functions of  $\mathbf{C}$  and  $T$  only,  $\varepsilon = \hat{\varepsilon}(\mathbf{C}, T)$ , etc., and that  $1/T$  is the integrating factor of the Pfaffian form

$$d\eta = \frac{1}{T} \left\{ \frac{\partial \hat{\varepsilon}}{\partial T} dT + \left( \frac{\partial \hat{\varepsilon}}{\partial C_{AB}} - \frac{1}{\rho_R} \mathfrak{T}_{AB}^P \right) dC_{AB} \right\}. \quad (1.114)$$

This is the *Gibbs relation* of a thermoelastic body. If the constitutive relations for  $\varepsilon$  and  $T^P$  are known, it allows the determination of the entropy. Alternatively, by introducing the *Helmholtz free energy*

$$\psi = \varepsilon - T\eta = \hat{\psi}(C_{AB}, T), \quad (1.115)$$

one may deduce the relations

$$\eta = - \frac{\partial \hat{\psi}}{\partial T}, \quad T_{AB}^P = \frac{\partial \hat{\psi}}{\partial C_{AB}}, \quad (1.116)$$

demonstrating that  $\psi$  serves as a thermodynamic potential for entropy and the second Piola–Kirchhoff stress tensor. Moreover, the residual inequality is  $Q_A T_{,A} \geq 0$ ; in thermodynamic equilibrium, which is defined as a process with  $T_{,B} \equiv 0$ , it implies  $Q_{A|E} \equiv 0$ . This condition is satisfied, provided that

$$Q_A = -\kappa_{AB} T_{,B}, \quad (1.117)$$

where  $\kappa_{AB}$  is, in general, a function of  $\mathbf{C}, T$  and  $\nabla T$  and is called the *tensor of heat conductivity*. The residual inequality, thus, reduces to

$$\kappa_{(AB)} T_{,A} T_{,B} \geq 0,$$

where parentheses indicate symmetrization. This inequality states that  $\kappa_{(AB)}$  must be positive-semidefinite. Nothing can be concluded from the above about the skew-symmetric part of  $\kappa_{AB}$ . It is the expression of the so-called *Onsager reciprocity relations* that  $\kappa_{[AB]} \equiv 0$ . Henceforth, this assumption will tacitly be made.

#### (e) Final remarks

In the above treatment of the entropy principle, we only considered constitutive relations with bounded memory. We saw that its exploitation

was relatively straightforward; no extreme mathematical complexities arose. The situation is different for materials which have hereditary effects. There, a rigorous treatment of the second law of thermodynamics requires the knowledge of functional analysis. We do not assume that the reader is familiar with the latter and, therefore, refrain from presenting the theory. When dealing with viscoelasticity and other material behavior with hereditary effects, however, the constitutive relations will be presented in a thermodynamically-admissible form.

The reader might ask himself what he has learned from the above derivations. Our purpose was to demonstrate that general continuum physics can offer substantial insight into the possible forms constitutive relations might assume. Material scientists dealing with ice often restrict themselves to uniaxial compression/tension or simple shear tests of a specimen and rarely give much thought as to whether these tests suffice for the determination of constitutive relationships governing arbitrary stress states. The above treatment should have taught us that establishing a constitutive relation for a material might proceed along the following lines: Preliminary experiments in simple shear or compression will indicate which class of constitutive relations should best be postulated from a continuum physics point of view. Using the above demonstrated principles, these postulated relations can be reduced to their thermodynamically-admissible form. In the last step it is left to the material scientist to determine by experiment the unspecified coefficient functions occurring in the reduced constitutive relationships. This step might be extremely difficult, and it will often require further simplifications. But, in most cases, it will be seen that simple compression or shear tests are not sufficient to determine the unspecified coefficient functions at hand.

Unfortunately, material science in ice physics has largely neglected such considerations. Multiaxial stress tests are hardly ever performed, leaving virtually no possibility of checking whether the very restricted constitutive relations do indeed rightly model multidimensional stress states. These are important, however; in Chapter 2 we shall have the occasion to see this.

### 5. Phase Changes

In certain aspects of ice mechanics, phase changes play a decisive role. As an example we mention water flow through a glacier. If its temperature is close to or at melting point, the heat available in the water might be used to melt some ice. It is important, therefore, that the mechanism of phase change is thoroughly understood. Of course the form of phase-change relations will depend on the material behavior of the two phases. Ice may be regarded as a solid or a fluid (in the mathematical sense defined above)

and, whereas water certainly is a fluid, its material response is not defined by this statement. The most important case in glaciology is when both phases are regarded as *viscous compressible heat-conducting fluids*. We shall now treat this case.

Basic to the derivation of the phase-change relations will be the jump conditions derived in Section 2 and listed in Equations (1.37).

(a) *Phase changes for a viscous compressible heat-conducting fluid*

Consider a body consisting of two phases which are separated at a surface. We regard this surface to be singular. By this we mean that any field quantity defined in the body may suffer a finite jump when the surface is crossed. The limit values of a quantity may not, therefore, be the same when the surface is approached from either the left or the right. Furthermore, we do not assume the surface to be material and this implies that the surface points move with their own velocity, which we call  $u_i$ . The jump conditions which must be satisfied at such surfaces are listed in (1.37). We define a *surface of phase change* as a special singular surface at which the temperature and tangential velocity are continuous. Thus

$$[T] = 0 \quad \text{and} \quad [v_{\parallel} t_i] = 0, \quad (1.118)$$

where  $v_{\parallel}$  is the speed tangential to  $\mathcal{S}$  and  $t_i$  denotes a unit vector in the direction of  $v_{\parallel}$  and tangential to the singular surface. With (1.118)<sub>1</sub> and the use of (1.37)<sub>1,2</sub> in (1.37)<sub>3</sub> the jump conditions (1.37) assume the form\*

$$\begin{aligned} [\rho(v_i - u_i)n_i] &= 0, & [t_{ij}n_j] + [\rho v_i(v_j - u_j)n_j] &= 0, \\ [q_i n_i] &= \left[ \frac{1}{\rho} t_{ij} n_i n_j - \varepsilon - \frac{1}{2}(v_k - u_k)(v_k - u_k) \right] \rho(v_p - u_p)n_p, \\ \frac{1}{T} [q_i n_i] + [\rho \eta(v_j - u_j)n_j] &= 0. \end{aligned} \quad (1.119)$$

To prove (1.119)<sub>3</sub>, notice that (1.37)<sub>3</sub> may also be written as

$$\begin{aligned} [q_i n_i] &= [t_{ij} v_i n_j] - [\varepsilon + \frac{1}{2}(v_k - u_k)(v_k - u_k)] \rho(v_i - u_i)n_i - \\ &\quad - [v_k u_k] \rho(v_i - u_i)n_i - \frac{3}{2}[u_k u_k] \rho(v_i - u_i)n_i. \end{aligned} \quad (1.120)$$

Since  $[u_k] = 0$ , the last term in this equation vanishes and the second but last term may be written as

$$\begin{aligned} [v_k u_k] \rho(v_i - u_i)n_i &= [v_k] u_k \rho(v_i - u_i)n_i = -[t_{ki} n_i u_k], \\ [t_{ij} v_i n_j] + [v_k u_k] \rho(v_i - u_i)n_i &= [t_{ij} (v_i - u_i)n_j]. \end{aligned} \quad (1.121)$$

Since we assume the tangential velocity to be continuous, we may set

$$v_i = v_k n_k n_i + v_{\parallel} t_i, \quad u_i = u_k n_k n_i + u_{\parallel} g_i.$$

\*We assume vanishing surface entropy production.

Here  $u_{\parallel}$  is the component of the velocity  $u_i$  in the surface  $\mathcal{S}$  and  $g_i$  a unit vector parallel to it. Hence

$$\begin{aligned} \llbracket t_{ij}(v_i - u_i)n_j \rrbracket &= \llbracket t_{ij}n_i n_j(v_k - u_k)n_k \rrbracket + v_{\parallel} \llbracket t_{ij}n_i t_i \rrbracket - u_{\parallel} \llbracket t_{ij}g_i n_j \rrbracket \\ &= \left[ \frac{1}{\rho} t_{ij}n_i n_j \right] \rho(v_k - u_k)n_k + v_{\parallel} \llbracket v_i t_i \rrbracket \rho(v_j - u_j)n_j + \\ &\quad + u_{\parallel} \llbracket v_i g_i \rrbracket \rho(v_j - u_j)n_j \end{aligned} \quad (1.122)$$

In this formula,  $v_i t_i$  is the tangential velocity which is continuous and  $v_i g_i$  is the projection of  $v_i$  onto the direction of  $g_i$ , which lies in  $\mathcal{S}$  as well. This projection is also continuous so that the last two terms on the right of (1.122) vanish. Substitution of this result into (1.121) and the latter into (1.120) yields (1.119)<sub>3</sub>.

In thermostatic equilibrium  $q_{i|E} = 0$ . This then implies that the right-hand side of (1.119)<sub>3</sub> must vanish in this case. This can be achieved by setting to zero either one of the factors on the right-hand side. We require that in thermostatic equilibrium  $v_i = u_i$ , because the other alternative would lead to unreasonable results. Consequently, *the surface of phase change in thermostatic equilibrium is material*.

Next we evaluate the jump in entropy. This is now easy. Indeed from a combination of (1.119)<sub>1,3,4</sub> we obtain

$$\llbracket \eta \rrbracket + \frac{1}{T} \left[ \frac{t_{ij}n_i n_j}{\rho} - \varepsilon - \frac{1}{2}(v_k - u_k)(v_k - u_k) \right] = 0. \quad (1.123)$$

When both phases are in thermostatic equilibrium (1.119)<sub>2</sub> and (1.123) imply

$$\begin{aligned} \llbracket t_{ij}|_E n_j \rrbracket &= \llbracket -p|_E n_i \rrbracket = 0 \rightarrow \llbracket p|_E \rrbracket = 0, \\ \llbracket \eta|_E \rrbracket &= \frac{1}{T} \left[ \frac{p|_E}{\rho} + \varepsilon \right] = \frac{1}{T} \left\{ p|_E \left[ \frac{1}{\rho} \right] + \llbracket \varepsilon \rrbracket |_E \right\}. \end{aligned} \quad (1.124)$$

These are important relations. (1.124)<sub>2</sub> is usually written as

$$\llbracket \mu|_E \rrbracket := \left[ \varepsilon|_E - T\eta|_E + \frac{p|_E}{\rho} \right] = 0, \quad (1.125)$$

where  $\mu_E$  is called the *equilibrium chemical potential*. If the two phases are in equilibrium, their chemical potentials are equal.

Another somewhat more familiar form of (1.125) is

$$T \llbracket \eta|_E \rrbracket = \llbracket \varepsilon|_E \rrbracket + p|_E \left[ \frac{1}{\rho} \right]. \quad (1.126)$$

The left-hand side of (1.126) is called the *latent heat of fusion* and is generally

denoted by  $L$ . Thus,

$$L|_E = [\varepsilon|_E] + p|_E \left[ \frac{1}{\rho} \right]. \quad (1.127)$$

It consists of two terms, firstly the energy jump and, secondly, the power of working of the stresses due to the volume change. Notice further the similarity of (1.124)<sub>2</sub> with the Gibbs relation (1.97) which at a constant temperature reads

$$d\eta_{T=\text{const}} = \frac{1}{T} \left\{ \frac{\partial \varepsilon}{\partial (1/\rho)} + p \right\} d\left(\frac{1}{\rho}\right). \quad (1.128)$$

Here, we have regarded  $\varepsilon$  as a function of  $1/\rho$  rather than  $\rho$ . Another formula that follows from (1.124)<sub>2</sub> is the *melting pressure formula*. If we solve (1.124)<sub>2</sub> for  $p|_E$ , what obtains reads as follows

$$p|_E = \frac{T[\eta|_E] - [\varepsilon|_E]}{[1/\rho]} = \frac{L|_E - [\varepsilon|_E]}{[1/\rho]}. \quad (1.129)$$

The interpretation of this equation is simplified if we look at the two relations

$$[p|_E] = 0 \quad \text{and} \quad [\mu|_E] = 0 \quad (1.130)$$

more closely.  $p|_E$  and  $\mu|_E$  are functions of  $\rho_I$ ,  $\rho_{II}$  and  $T(\rho_I, \rho_{II})$  denote the densities of the two phases. Hence, at a given temperature the relations (1.130) may be used to determine  $\rho_I$  and  $\rho_{II}$  as functions of  $T$ . Once these densities are known, (1.129) may be used to calculate  $p|_E$  as a function of temperature alone. Hence the right-hand side of (1.129) is a function of temperature only:

$$p|_E = \hat{p}|_E(T) = \frac{L|_E - [\varepsilon|_E]}{[1/\rho]}. \quad (1.131)$$

This equation may now be used to calculate  $dp|_E/dT$ . What results after some calculations is the *Clausius–Clapeyron equation*.

$$\frac{d\hat{p}|_E}{dT} = \frac{[\eta|_E]}{[1/\rho]} = \frac{[\varepsilon|_E] + p|_E [1/\rho]}{T [1/\rho]}. \quad (1.132)$$

Of particular interest in ice mechanics is a different version of the Clausius–Clapeyron equation, namely

$$\frac{dT}{d\hat{p}_E} = -c = \frac{T [1/\rho]}{[\varepsilon|_E] + p|_E [1/\rho]}. \quad (1.133)$$

Since the temperature variations in problems involving phase changes are usually small,  $c$  in (1.133) is regarded as a constant.

Most of the above calculations have been performed for two fluids

which are in thermostatic equilibrium. In non-equilibrium, the chemical potential must be defined by

$$\mu := T\eta + \frac{t_{ij}n_i n_j}{\rho} - \varepsilon - \frac{1}{2}(v_k - u_k)(v_k - u_k) \quad (1.134)$$

and the relations (1.124) must now be replaced by

$$\begin{aligned} \llbracket \rho(v_i - u_i)n_i \rrbracket &= 0, \\ \llbracket t_{ij}n_j \rrbracket + \llbracket \rho v_i(v_j - u_j)n_j \rrbracket 0, \quad \llbracket \mu \rrbracket &= 0. \end{aligned} \quad (1.135)$$

The exploitation of these equations has never been achieved. This is the reason why one usually assumes near equilibrium behavior and sets  $u_i - v_i \simeq 0$ . In this approximation, all results are similar to the previous ones. In particular, we may write the approximate relations

$$\llbracket t_{ij}n_j \rrbracket \simeq 0, \quad \llbracket \eta \rrbracket + \frac{1}{T} \left[ \frac{t_{ij}n_i n_j}{\rho} - \varepsilon \right] \simeq 0. \quad (1.136)$$

Hence

$$L = T\llbracket \eta \rrbracket \simeq \llbracket \varepsilon \rrbracket - t_{ij}n_i n_j \left[ \frac{1}{\rho} \right]. \quad (1.137)$$

Since  $t_{ij}n_i n_j$  is the stress normal to the surface of phase change, we may write

$$P_N = -t_{ij}n_i n_j \quad (1.138)$$

and now obtain a pressure-melting formula

$$P_N \simeq \frac{L - \llbracket \varepsilon \rrbracket}{\llbracket 1/\rho \rrbracket}. \quad (1.139)$$

Hence, we see that in contrast to the Clausius–Clapeyron equation in thermostatic equilibrium, it is not the pressure entering this formula, but the normal force exerted on the surface of phase change  $P_N$  (it is positive as a pressure and negative as a tension). This result has already been derived by Kamb [4] by methods of classical reversible thermodynamics.

Consider, finally a body consisting of a *mixture* of two compressible viscous heat-conducting fluids. We think of the two fluids as being ice and water and assume that on one side of the surface of the phase change, the ice (at the melting temperature) and water will coexist while on the other side, only the component ice, say, will be present. For the mixture as a whole, the jump conditions (1.119) are still valid in this case, so that in particular  $\llbracket \mathbf{q} \cdot \mathbf{n} \rrbracket = -T\llbracket \eta \rrbracket \rho(\mathbf{v} - \mathbf{u}) \cdot \mathbf{n}$ , where  $\eta = \eta_{\text{water}} + \eta_{\text{ice}}$ . Only  $\eta_{\text{water}}$  will suffer a jump. Denoting the mass fraction of water in the ice-water

mixture by  $w$  we have

$$\eta_{\text{ice}} = (1 - w)\eta, \quad \eta_{\text{water}} = w\eta \quad (1.140)$$

and consequently, since  $L = T[\eta]$ ,

$$[\mathbf{q} \cdot \mathbf{n}] = -Lw(\rho(\mathbf{v} - \mathbf{u}) \cdot \mathbf{n}), \quad \text{ice on both sides.} \quad (1.141)$$

On the other hand, if water is separated from an ice-water mixture

$$[\mathbf{q} \cdot \mathbf{n}] = -L(1 - w)(\rho(\mathbf{v} - \mathbf{u}) \cdot \mathbf{n}), \quad \text{water on both sides.} \quad (1.142)$$

Both formulas can be combined as

$$[\mathbf{q} \cdot \mathbf{n}] = -L[w](\rho(\mathbf{v} - \mathbf{u}) \cdot \mathbf{n}), \quad (1.143)$$

where  $w$  is the mass fraction of water on either side of the surface of singularity. This important formula will be used in Chapter 3.

(b) *Phase changes for a viscous incompressible heat-conducting fluid*

The jump conditions (1.119) are independent of the material, and it is readily seen that the same also holds true for all remaining results up to and including (1.124). Equation (1.124)<sub>2</sub>,

$$[\eta|_E] = \frac{1}{T} \left\{ p|_E \left[ \frac{1}{\rho} \right] + [\varepsilon|_E] \right\},$$

however, leads to an inconsistency unless  $[1/\rho] = 0$ . The inconsistency follows from the fact that  $\varepsilon$  and  $\eta$  are functions of  $T$  only while  $p|_E$  may have any value. Hence, an incompressible material cannot, in a phase change, suffer a jump in density. Hence,

$$[\eta|_E] = \frac{1}{T} [\varepsilon|_E].$$

Of course, there cannot be a pressure-melting formula and a Clausius–Clapeyron formula in an incompressible material.

It is now also clear how the phase change relations should read, when the two phases are, say, a viscous fluid and a thermoelastic solid. We leave their derivation to the reader. Often in ice mechanics, ice is treated as an incompressible material but phase-change relations are those of a compressible one. As the above derivations show, this is strictly incorrect and must be regarded as a simplification which can only be justified by the fact that the errors induced thereby are negligibly small.

## REFERENCES

1. Chadwick, P., *Continuum Mechanics, Concise Theory and Problems*, George Allen and Unwin, London, 1976.

2. Greub, W., *Linear Algebra*, Springer Verlag, Berlin, Heidelberg, New York, 1960.
3. Hutter, K., The foundations of thermodynamics, its basic postulates and implications. A review of modern thermodynamics, *Acta Mechanica*, **27**, 1–54, 1977.
4. Kamb, B., The thermodynamic theory of non-hydrostatically stressed solids. *J. Geophys. Res.* **66**, 259–271, 1961.
5. Müller, I., *Thermodynamik, Die Grundlagen der Materialtheorie*, Bertelsmann Universitätsverlag, 1973.
6. Müller, I., On the frame dependence of stress and heat flux. *Arch. Ration. Mech. Anal.*, **45**, 241–250, 1972.
7. Smith, G. E., On isotropic integrity bases. *Arch. Ration. Mech. Anal.*, **18**, 282–292, 1965.
8. Truesdell, C., *Rational Continuum Mechanics*. Vols. I and II. Academic Press, New York, San Francisco, London, 1977, 1978.
9. Truesdell, C. and R. A. Toupin, The classical field theories. in *Handbuch der Physik*, Vol. III/1, edited by S. Flügge, Springer-Verlag, Berlin, 1960.
10. Truesdell, C. and W. Noll, The nonlinear field theories of mechanics. in *Handbuch der Physik*, Vol. III/3, edited by S. Flügge, Springer-Verlag, Berlin, 1965.
11. Truesdell, C. and R. G. Muncaster, *Fundamentals of Maxwell's Kinetic Theory of a Simple Monatomic Gas. Treated as a Branch of Rational Mechanics*, Academic Press, New York, 1980.
12. Van der Waerden, *Algebra I und II*, Heidelberger Taschenbuch, Springer-Verlag, Berlin, Heidelberg, New York, 1971.
13. Wang, C. C., A new representation theorem for isotropic functions: An answer to Professor G. F. Smith's criticism of my papers on representations for isotropic functions. *Arch. Ration. Mech. Anal.*, **36**, 166–223, 1970.
14. Wang, C. C. and C. A. Truesdell, *Introduction to Rational Elasticity*. Noordhoff International Publishing, Leyden, 1973.

## **Chapter 2**

### **A BRIEF SUMMARY OF CONSTITUTIVE RELATIONS FOR ICE**

#### *1. Preliminary Remarks*

In Chapter 1 the constitutive theory was treated from a rather general point of view and no specific details were given about ice as a material. Here, we give a brief summary of its constitutive response from a view-point of material science. No claim of completeness will be made, however.

As already stipulated in Chapter 1, ice cannot be regarded as a material with a single unique constitutive response. When ice is subjected to external forces its response depends on the physical nature of the applied forces as well. Depending on the characteristic times of the physical processes, ice may behave as an elastic or viscoelastic solid or as a viscous fluid etc. Its material properties may further depend on the orientation so that in these instances its anisotropy should be taken into account. Impurities such as bubbly air and water inclusions or dislocations and internal cracks may also have an effect on its response.

On a microscale, ice is a hexagonal crystal to which the theories of physical crystallography may be applied. The properties on this scale are of primary importance in engineering applications, although one rarely encounters pure crystal behavior *in situ*. In glaciers, the individual crystals are clustered into grains and are randomly oriented with no apparent preference on any direction. The grain size is usually smaller than the characteristic differential lengths which are relevant in the description of its deformation. Hence, to describe the flow mechanism of glaciers, ice may be regarded as an isotropic body. We shall see that for most purposes, a viscous fluid model is accurate enough. On the other hand, wave propagation problems, especially the seismic response of a glacier to artificially-induced waves, can be treated by assuming that ice is an elastic solid. In this regard, the progress of the transformations of snow to ice at a given place may be relevant, because primary and secondary wave speeds depend on density. In the upper layers of a glacier, there is a more or less smooth transition from snow to firn to ice. The density of the latter is highest ( $0.85 \text{ gr cm}^{-3}$  or larger) and may increase slightly with depth.

At greater depths in the Antarctic or Greenland ice caps, glacier ice is

subjected to extreme stresses consisting of a combination of pressure and shear, giving rise to stress-induced recrystallizations. Because of non-isotropy in the stress distribution, a stress-dependent anisotropy is introduced. Strictly, therefore, the material response in ice sheets should account for these. So far this has not been done, although experimental investigations describing the phenomenon do exist, see Lile [66]\*.

In lake ice, the response largely depends on crystal growth. Generally, there are two preferred directions of crystal growth, manifested by the fact that the *c*-axis (see later) of the ice crystals is oriented either vertically or horizontally. The two orientations lead to two different mechanical behaviors but, generally, length scales of changes in orientation are not large enough to clearly identify the two different mechanical behaviors. With regard to dynamics such as the dynamic response of floating ice plates to moving vehicles, an elastic model is accurate enough, but quasistatic processes should be treated with a viscoelastic model. For questions of bearing capacity, a non-linear viscous or plastic model might be more appropriate. If floating sea ice is considered instead, nothing essential changes, compared to lake ice, except that now salinity plays a major role. As a consequence, material properties of sea ice plates vary substantially with depth, effectively resulting in an orthotropic structure of the plates. Depending on temperature, sea ice contains a larger or smaller fraction by volume of sphere- or cylinder-like inclusions of brine, which must influence the overall response of the ice. Consequently, we cannot strictly speak of a material behavior of sea ice, because the response of the brine also depends on the thermodynamic state of the environment.

These examples should suffice to illustrate that one can look at the response of ice from different points of view. No one mathematical representation is likely to be applicable to every situation. The problem under consideration rather prescribes the type of material response that should be applied.

In what follows, we shall describe the most important mechanical models that are used in glaciology, thereby restricting ourselves to the mechanical properties of ice. We shall not mention all pertinent literature. The reader is chiefly referred to two monographs on the physics and mechanics of ice by J. W. Glen [32] and to the treatises *Ice Physics* by Hobbs, [45], and *Ice Mechanics* by Michel [75].

## 2. *The Mechanical Properties of Hexagonal Ice*

### (a) *The crystal structure of ordinary ice*

The phase of ice stable at ordinary low pressures is known as ice *I*. There are two variants of its structure which are closely related to each

\*A first attempt at stress induced anisotropy has been given only recently by Spring and Morland [104a].

other. One is *hexagonal* in its symmetry and is known as ice *Ih*, the other is *cubic* and is known as ice *Ic*. The hexagonal phase is obtained by freezing water at a given temperature. It is the form which is familiar to most people and is for this reason known as ‘ordinary’ ice, which we shall only be concerned with here. Its crystallographic structure can be seen in the hexagonal symmetry of many snow crystals (see Figure 2.1 with photographs of snow-flakes).

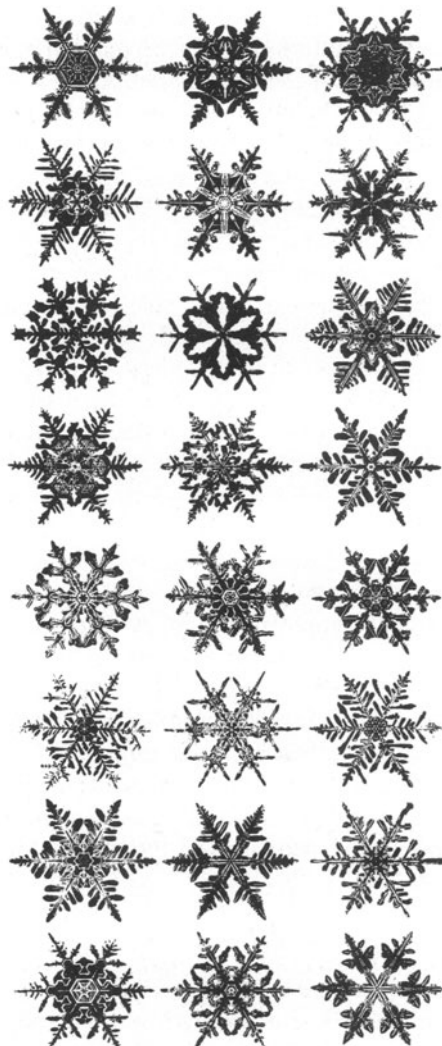


FIG. 2.1. Photographs of snowflakes reproduced from the Bentley and Humphreys-Atlas. See also *Symmetry in Science and Arts* [101].

In its crystal structure, the water molecules of ice  $Ih$  are arranged such that each water molecule has four nearest neighbors positioned very close to the vertices of a regular tetrahedron centered on the water molecule considered, see Figure 2.2a. If we consider two particular water molecules joined by a line parallel to the hexad axis, I and II say, then the three neighbors of II are vertically above the corresponding neighbors of I. If we draw the projection of the whole structure to a plane perpendicular to the hexad axis (see Figures 2.2b, c), the stacking sequence is  $ABBAABBA\dots$ .

For many purposes, such as ultrasonic wave propagations, the ice crystal can be considered as an elastic body with temperature-dependent constants of elasticity. In other instances when larger quasistatic loadings are applied, the crystal behaves as a viscous or plastic body. It is the second behavior that is of importance in glaciological applications. Below we shall discuss both behaviors.

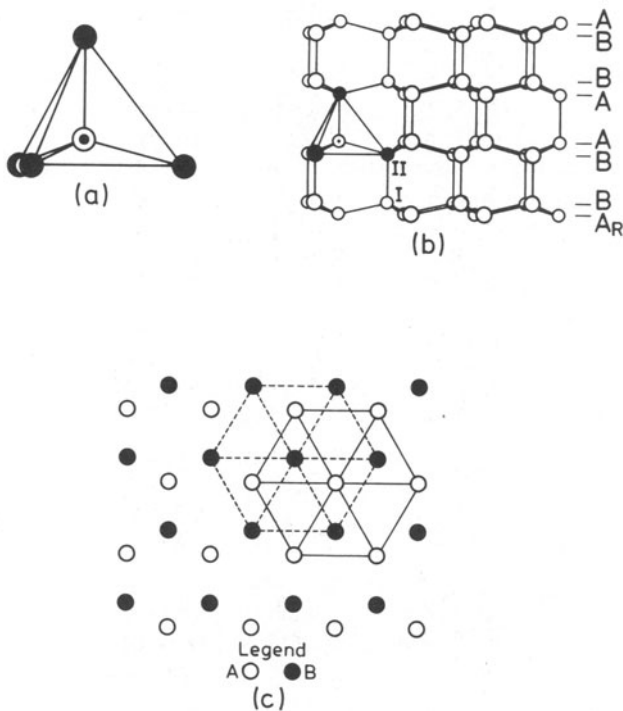


FIG. 2.2. The arrangement of water molecules in ordinary ice, from Glen [32] (with changes). (a) Each water molecule has four nearest neighbors arranged very closely to the positions of the vertices of a regular tetrahedron. (b) The molecules in the planes  $A$  are all vertically above the molecules in  $A_R$ . Conversely, the molecules in the planes  $B$  are all above those in  $B_R$ . The vertical is called the *hexad* or *c-axis*. (c) Projection of the structure of ice  $Ih$  on the basal plane.

(b) *The elastic behavior of hexagonal ice*

A body is called elastic if the constitutive response of the Cauchy stress depends on the deformation gradient only. In the notation of Chapter 1.

$$\mathbf{t} = \hat{\mathbf{t}}(\mathbf{F}). \quad (2.1)$$

In material science one usually includes temperature as a variable, implying that the emerging theory includes some effects of thermoelasticity. However, this temperature dependency is less general than in a thermoelastic body and does not even include thermal stresses. In the following, we shall regard temperature simply as a parameter and we shall not express it explicitly, thereby considering the constitutive response as being elastic whose response function may parametrically depend on temperature.

Constitutive relations are subject to the rule of material frame indifference, and when this is used in (2.1) it is found that the second Piola–Kirchhoff stress tensor  $\mathbf{T}^P$  (see (1.67)) may be written as

$$\mathbf{T}^P = \hat{\mathbf{T}}^P(\mathbf{E}), \quad (2.2)$$

where

$$\mathbf{E} = \frac{1}{2}(\mathbf{C} - \mathbf{I}) \quad \text{and} \quad \mathbf{C} = \mathbf{F}^T \mathbf{F}.$$

$\mathbf{C}$  is the right Cauchy–Green deformation tensor and  $\mathbf{E}$  the *Lagrangian strain tensor*. Another objective form of (2.1) would be

$$\mathbf{t} = \mathbf{R} \hat{\mathbf{t}}(\mathbf{E}) \mathbf{R}^T, \quad (2.3)$$

where  $\mathbf{R}$  is the rotation tensor defined implicitly by

$$\mathbf{F} = \mathbf{R} \mathbf{U}, \quad \mathbf{C} = \mathbf{U}^2.$$

Thermodynamic arguments further show that stress is derivable from a free energy  $\psi$ . This free energy serves as a thermodynamic potential to the stresses in the sense that (see (1.116))

$$T_{AB}^P = \frac{\partial \hat{\psi}}{\partial E_{AB}} \quad (2.4)$$

It thus suffices to postulate a constitutive relation for the scalar function  $\hat{\psi}(\mathbf{E})$ .

In (2.2) and (2.3) we regard  $\hat{\mathbf{T}}^P(\cdot)$  and  $\hat{\mathbf{t}}(\cdot)$  as functions of  $\mathbf{E}$  rather than  $\mathbf{C}$ , because in a rigid body motion  $\mathbf{C} = \mathbf{I}$  and hence  $\mathbf{E} = \mathbf{0}$ . Under all these rigid motions,  $\mathbf{T}^P = \hat{\mathbf{T}}^P(\mathbf{0})$ , so that the stress cannot be distinguished from the stress tensor for a body at rest. Clearly, since the constitutive functions generally depend on the reference configuration, the value of the stress tensor at rest  $\hat{\mathbf{T}}^P(\mathbf{0})$ , also depends on this configuration. For each particle, there is a configuration in which  $\hat{\mathbf{T}}^P(\mathbf{0}) = \mathbf{0}$ , and when these configurations coincide for all the particles of the body, the body is said to be *homogeneous*. We assume this to be the case and are therefore free to choose as a reference configuration

that configuration for which  $\hat{T}^P(\mathbf{0}) = 0$ . The body is then said to be in its *natural state*. In most applications, such a natural state is assumed to exist from the outset.

The above applies to all elastic materials, linear or non-linear. In material science, one usually assumes small deformations from the reference state and then may linearize (2.2) or (2.3). We prefer here to look at the more general non-linear theory of an elastic solid, whose constitutive relation for stress is linear in the Lagrangian strain tensor. Thus, the free energy function is quadratic and may be written as

$$\psi = \hat{\psi}(\mathbf{E}) = \frac{1}{2} \mathcal{C}_{ABCD} E_{AB} E_{CD}, \quad (2.5)$$

in which  $\mathcal{C}$  is a fourth-rank tensor which, in view of the symmetry relations of  $E_{AB}$  and the differentiability of  $\hat{\psi}[\partial^2 \hat{\psi} / \partial E_{AB} \partial E_{CD} = \partial^2 \hat{\psi} / \partial E_{CD} \partial E_{AB}]$ , must satisfy the symmetry relations

$$\mathcal{C}_{ABCD} = \mathcal{C}_{BACD} = \mathcal{C}_{ABDC} = \mathcal{C}_{CDAB}. \quad (2.6)$$

This reduces the number of independent coefficients to 21. The stress tensor corresponding to (2.5) can be obtained by differentiation, according to (2.4); this gives

$$T_{AB}^P = \mathcal{C}_{ABCD} E_{CD}. \quad (2.7)$$

So far, no symmetry properties of the body have been invoked. However, ice *Ih* is hexagonal enjoying this symmetry. Figure 2.3 shows such a crystal in its natural state in two indistinguishable reference configurations. One is obtained from the other by a rotation of  $60^\circ$  about the *c*-axis. It is apparent that all indistinguishable configurations are obtained by first rotating the coordinate system by the angles  $n\pi/6$ ,  $n = 1, 2, \dots, 6$  and, second, by a change

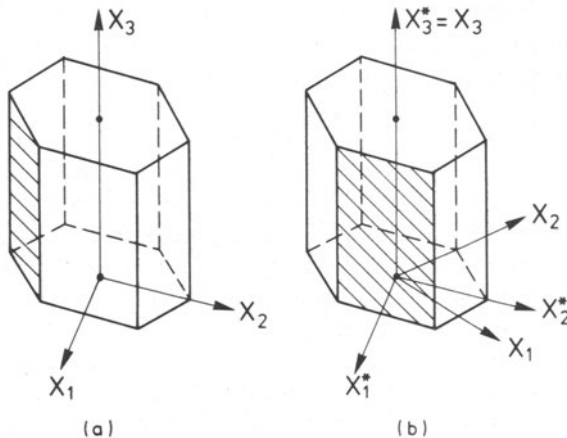


FIG. 2.3. Two indistinguishable reference configurations. The crystal in Figure 2.3b is rotated relative to the crystal in Figure 2.3a by an angle  $\pi/3$ .

of orientation of the coordinate system in the planes perpendicular to the  $c$ -axis. Since the free energy is a scalar, its value must be the same for all deformations starting from indistinguishable reference configurations,  $\psi = \hat{\psi}(\mathbf{E}) = \hat{\psi}(\mathbf{E}^*)$ . The exploitation of this condition is routine and will therefore not be given here, but it is clear that restrictions on the coefficients  $\mathcal{C}$  will emerge. These conditions are usually formulated in matrix notation using the following definitions:

$$\begin{aligned}\boldsymbol{\sigma} &= (T_{11}^P, T_{22}^P, T_{33}^P, T_{23}^P, T_{31}^P, T_{12}^P), \\ \boldsymbol{\varepsilon} &= (E_{11}, E_{22}, E_{33}, E_{23}, E_{31}, E_{12}).\end{aligned}\quad (2.8)$$

Relations (2.5) and (2.7) then become

$$\boldsymbol{\sigma} = \mathbf{C}\boldsymbol{\varepsilon}, \quad \Psi = \frac{1}{2}\boldsymbol{\varepsilon}^T \mathbf{C} \boldsymbol{\varepsilon}. \quad (2.9)$$

$\mathbf{C}$  is a symmetric  $6 \times 6$  matrix having, at most, 21 independent coefficients. Ice  $Ih$  is characterized by five independent elastic constants, and in a coordinate system where the  $X_3$  axis is parallel to the  $c$  axis and the  $X_1$  and  $X_2$  axes are symmetry axes of the crystal in its basal plane, the matrix  $\mathbf{C}$  is given by

$$\mathbf{C} = \begin{bmatrix} C_{11} & C_{12} & C_{13} & 0 & 0 & 0 \\ C_{12} & C_{11} & C_{13} & 0 & 0 & 0 \\ C_{13} & C_{13} & C_{33} & 0 & 0 & 0 \\ 0 & 0 & 0 & C_{44} & 0 & 0 \\ 0 & 0 & 0 & 0 & C_{44} & 0 \\ 0 & 0 & 0 & 0 & 0 & \frac{1}{2}(C_{11} - C_{12}) \end{bmatrix}. \quad (2.10)$$

Equations (2.9) together with elastic constants (2.10) characterize *Hooke's law* for a hexagonal crystal.

The pure elastic behavior of single crystals is due to (i) changes in intermolecular distances under an applied force and (ii) to dislocation and disinclination movements, the latter being more likely under permanent loading conditions than under dynamically-applied forces. For this reason, the elastic constants of ice deduced from high-frequency measurements (which will be referred to as *dynamic* values) are more reliable than the static values, since fewer imperfections move and, therefore, fewer inelastic deformations occur. Moreover, and as follows from the fading memory property (see viscoelastic behavior, below), the dynamic values should be larger than their corresponding static ones.

Measurements have been made on both the static and dynamic elastic constants. They are reviewed by Hobbs [45], although here we confine ourselves to mentioning articles, by Dorsey [21], Mantis [70], Gold [35, 36] and Voytkovskiy [111], which all give results on static moduli. The dynamic elastic constants have been determined at various temperatures  $T$  from

measurements of the sound velocities in specific directions of the crystals using an ultrasonic pulse method. Such measurements were performed by Jona and Scherrer [55], Schaefer and Bergmann [99], Green and McKinnon [38], Bass *et al.* [6] and others. There have, however, also been theoretical predictions (see Penny [84]) using the theory of lattice dynamics of Born and Begbie [11]. Penny's values of the dynamical constants agree remarkably with those determined by others.

The dynamic constants listed below are valid in the temperature range  $0 \geq T \geq -140^\circ\text{C}$  and are those of Dantl [19]. They are listed as reliable by both Glen [32] and Hobbs [45]:

$$\begin{aligned} C_{11} &= 1.2904(1 - 1.489 \times 10^{-3}T - 1.85 \times 10^{-6}T^2) \times 10^{10} \text{ N m}^{-2} \pm 0.3\% \\ C_{12} &= 0.5622(1 - 1.874 \times 10^{-3}T) \times 10^{10} \text{ N m}^{-2} \pm 7\% \\ C_{13} &= 0.6487(1 - 2.072 \times 10^{-3}T - 3.62 \times 10^{-6}T^2) \times 10^{10} \text{ N m}^{-2} \pm 2\% \\ C_{33} &= 1.4075(1 - 1.629 \times 10^{-3}T - 2.93 \times 10^{-6}T^2) \times 10^{10} \text{ N m}^{-2} \pm 0.4\% \\ C_{44} &= 0.2819(1 - 1.601 \times 10^{-3}T - 3.62 \times 10^{-6}T^2) \times 10^{10} \text{ N m}^{-2} \pm 0.7\%. \end{aligned} \quad (2.11)$$

Frequently, it is more convenient to work with compliances rather than with elasticities. These are defined by  $\mathbf{S} := \mathbf{C}^{-1}$

It follows from (2.10) that the matrix  $\mathbf{S}$  is given by

$$\mathbf{S} = \begin{bmatrix} S_{11} & S_{12} & S_{13} & 0 & 0 & 0 \\ S_{12} & S_{22} & S_{13} & 0 & 0 & 0 \\ S_{13} & S_{13} & S_{33} & 0 & 0 & 0 \\ 0 & 0 & 0 & S_{44} & 0 & 0 \\ 0 & 0 & 0 & 0 & S_{44} & 0 \\ 0 & 0 & 0 & 0 & 0 & 2(S_{11} - S_{12}) \end{bmatrix} \quad (2.12a)$$

and it is not hard to show that

$$\begin{aligned} S_{11} + S_{12} &= \frac{C_{33}}{C}, & S_{11} - S_{12} &= \frac{1}{C_{11} - C_{12}}, \\ S_{13} &= \frac{C_{13}}{C}, & S_{33} &= \frac{C_{11} + C_{12}}{C}, & S_{44} &= \frac{1}{C_{44}} \end{aligned} \quad (2.12b)$$

where

$$C := C_{33}(C_{11} + C_{12}) - 2C_{13}^2.$$

With these formulas, the elements of  $\mathbf{S}$  are readily deduced from the elasticities. If the emerging formulas are approximated by quadratic polynomials, the following relations are obtained, Dantl (19).

$$\begin{aligned}
 S_{11} &= 1.040(1 + 1.070 \times 10^{-3}T + 1.87 \times 10^{-6}T^2) \times 10^{-10} \text{ m}^2 \text{ N}^{-1} \pm 1\% \\
 S_{12} &= -0.442(1 + 0.463 \times 10^{-3}T - 2.06 \times 10^{-6}T^2) \times 10^{-10} \text{ m}^2 \text{ N}^{-1} \pm 6\% \\
 S_{13} &= -0.189(1 + 1.209 \times 10^{-3}T + 6.15 \times 10^{-6}T^2) \times 10^{-10} \text{ m}^2 \text{ N}^{-1} \pm 20\% \\
 S_{33} &= 0.848(1 + 1.405 \times 10^{-3}T + 4.66 \times 10^{-6}T^2) \times 10^{-10} \text{ m}^2 \text{ N}^{-1} \pm 1\% \\
 S_{44} &= 3.342(1 + 1.505 \times 10^{-3}T + 4.04 \times 10^{-6}T^2) \times 10^{-10} \text{ m}^2 \text{ N}^{-1} \pm 1\%.
 \end{aligned} \tag{2.13}$$

Notice that the value of  $C_{13}$  is less accurate than the other  $C_{AB}$  and that, consequently, those  $S_{AB}$  which involve  $C_{13}$  are also less accurate. All elasticities are of the order of  $10^{10} \text{ N m}^{-2}$  which confirms the earlier measurements of other authors.

Clearly, the above values are those appropriate for ice in single-crystal form. Polycrystalline ice will have elastic properties which are close to some average of these, depending on the relative amounts of different crystal orientations in the polycrystalline aggregate.

### (c) The inelastic behavior of single-crystal ice

In general, the response of ice to an applied stress is not completely elastic. There are always effects of dissipation present, as can be seen, for instance, from the attenuation of mechanical vibrations. To account for such damping effects, the elastic model is replaced by a viscoelastic model. In these, the stress at a given place and time does not only depend on the corresponding strain and time, but on its entire history. Material scientists, however, restrict themselves, generally, to a material behavior with a bounded memory by postulating, for the stress tensor, a *linear* constitutive relation of the rate type of degree 1 (see Chapter 1, Section 3e). The second Piola–Kirchhoff stress tensor may then be written as

$$T_{AB}^P = \mathcal{C}_{ABCD} E_{CD} + \mathcal{K}_{ABCD} \dot{E}_{CD} \tag{2.14}$$

with coefficients  $\mathcal{C}_{ABCD}$  and  $\mathcal{K}_{ABCD}$  possibly depending on temperature. The tensor  $\mathcal{C}$  has been determined in (2.11).  $\mathcal{K}$  is not fully known, although some inferences about its form could be drawn from the logarithmic decrement measurements of the mechanical vibrations of ice samples, which are known. Of course,  $\mathcal{K}$  must show the symmetry of hexagonal crystals, and thus only five components of  $\mathcal{K}$  are linearly independent. On the basis of the postulation that viscoelastic behavior is isotropic, although the elastic part may not be, these can be reduced to two independent components, so that two experiments suffice for its determination. This is still too general and has not been done to our knowledge. Hence, further reduction is necessary. Besides *isotropy*, one may also postulate that there is *no bulk viscosity* reducing

the tensor  $\mathcal{K}$  finally to the form

$$\mathcal{K}_{ABCD} = \mu\{\delta_{AC}\delta_{BD} + \delta_{AD}\delta_{BC} - \frac{2}{3}\delta_{AB}\delta_{CD}\}, \quad (2.15)$$

where  $\delta_{AB}$  is the second-order unit tensor, and where  $\mu$  is called *viscosity*.

The reduction of  $\mathcal{K}$  for an isotropic body proceeds along the same lines, as was demonstrated for the hexagonal crystal. Here, it must be inquired whether any configuration that is obtained from the unstrained state by an arbitrary rotation about any axis, is a possible reference-configuration. If this is done

$$\mathcal{K}_{ABCD} = \lambda\delta_{AB}\delta_{CD} + \mu(\delta_{AC}\delta_{BD} + \delta_{AD}\delta_{BC}) \quad (2.16)$$

is obtained. The postulation of no bulk viscosity then requires  $\mathcal{K}_{ABCD}\dot{E}_{KK}\delta_{CD} = 0$  implying  $(3\lambda + 2\mu) = 0$ , or  $\lambda = -\frac{2}{3}\mu$ . A single experiment suffices for the determination of the viscosity constant  $\mu$ . Measurements are usually confined to the harmonic excitation of crystal bars under uniaxial strain or stress. If the excitation is in the direction of the *c* axis, (2.14) and (2.15) imply  $\sigma = C_{33}\varepsilon + \frac{4}{3}\mu\dot{\varepsilon}$ . This differential equation is equivalent to the 'Volterra-type' integral relation

$$\varepsilon = \frac{1}{C_{33}} \int_0^t \left[ 1 - \exp\left(-\frac{(t-t')}{\tau}\right) \right] \frac{d\sigma(t')}{dt'} dt' \text{ with } \tau = \frac{4\mu}{3C_{33}}. \quad (2.18)$$

The integral function in brackets is called the *creep function* and  $\tau$  is the *relaxation* or *retardation time*. It is this quantity which is usually determined by experiments. The following formula, good for H<sub>2</sub>O-ice, is quoted by Hobbs [43]:\*  $\tau = 6.9 \times 10^{-16} \exp(0.57 \text{ eV}/kT)$  (in [s]). Here,  $k$  is the Boltzmann constant and  $T$  the absolute temperature. It allows determination of  $\mu$ .

More important than anelastic effects in applied glaciology, is the behavior of ice crystals under large quasistatic loads. The deformation under such conditions is usually referred to as being *plastic*, a term that is inappropriate, at least if the notion of plasticity is associated with the existence of a yield surface. *It is experimentally proven that ice does not have a yield surface.* The behavior may be more accurately called viscous. Such deformations are referred to as *creep* if they occur under constant stress. Numerous creep tests have been performed under a number of different stressing conditions, including tension, compression, bending, shear, and combined stress states. Deformations may most easily be envisaged by modeling the ice crystal as a deck of cards (see Hobbs [45]), in which the contact surfaces are identified with the basal planes. There are numerous

\*1 eV = 23.06 kcal mol<sup>-1</sup> = 96.2 kJ mol<sup>-1</sup> = 1.6 × 10<sup>-19</sup> J,  
 $k = 1.381 \times 10^{-16}$  erg K<sup>-1</sup> = 1.381 × 10<sup>-23</sup> J K<sup>-1</sup>

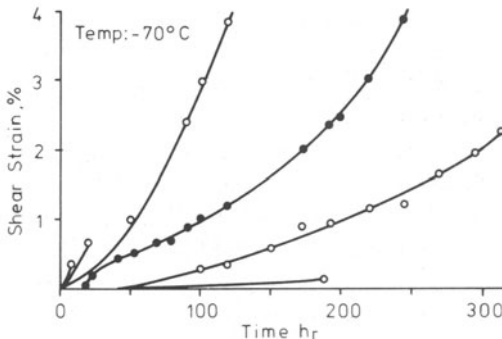


FIG. 2.4. Creep curves of ice single crystals deformed under various stresses at  $-70^{\circ}\text{C}$ . (From Jones and Glen [56].)

configurations of applied forces where the cards slide easily one over the other, and only a few where this is impossible.

Many detailed investigations have been undertaken, but we can only mention the most important ones. They are Glen and Perutz [33], Steinemann [105], Griggs and Coles [40], Jellinek and Brill [54], Rigsby [96], Glen and Jones [34], [56]. The general result of the tests performed by these authors is that the specimen deforms by sliding along the basal planes, unless the shear stress is very low; the rate at which such a slip occurs increases with time. Typical creep curves for basal sliding are shown in Figure 2.4. They clearly indicate the above-mentioned increase of creep rate with time.

If, instead of applying a constant stress or loading, creep tests are performed with a crystal whose strain is kept constant and the stresses (or better still, the total forces) are then measured to ensure the constant rate of deformation, then conventional stress-strain curves can be obtained. Stress-strain curves of single ice crystals obtained at a constant strain rate

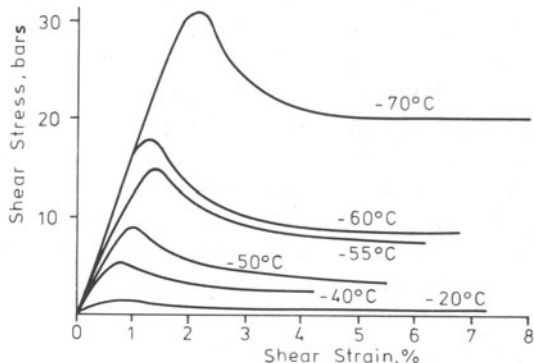


FIG. 2.5. Stress strain curves of single ice crystals obtained at a strain rate of  $2.7 \times 10^{-7} \text{ s}^{-1}$  and various temperatures. (From Jones and Glen [56].)

are shown in Figure 2.5. With a growing strain rate, stress increases, first monotonically, then reaches a certain maximum, and finally drops, reaching an asymptotic value. This behavior is in agreement with what one expects from creep tests of constant stress. Since, in these experiments, the strain rate increases with time, one would expect that the stress needed to keep it constant would decrease. But this behavior is different from conventional stress-strain curves of many materials, for these generally possess a rather distinct transition from the linear elastic behavior at low strains to a more or less pronounced flow level. For large strains, stress-strain curves increase further, thus giving rise to *strain hardening*. Ice crystals are characterized by *strain weakening* or *strain softening* effects.

Mathematically, the strain rate in a creep test can be related to stress. The most familiar law is a power law, where the strain rate *at a given strain* is proportional to the stress raised to the power  $n$ . If stress is called  $\sigma$  and strain rate  $\dot{\varepsilon}$ , this relation has the form

$$\dot{\varepsilon} = \tilde{A} \operatorname{sgn}(\sigma) |\sigma|^n \quad (2.19)$$

where  $\tilde{A}$  and  $n$  are constants, the first of which may depend on temperature. To account for this, one usually postulates an *Arrhenius-type* of relationship

$$\dot{\varepsilon} = \operatorname{sgn}(\sigma) A \exp\left(-\frac{Q}{kT}\right) |\sigma|^n, \quad (2.20)$$

where  $Q$  is the so-called *activation energy*,  $k$  the *Boltzmann constant* and  $T$  the absolute temperature. For temperatures between  $-50$  and  $-10^\circ\text{C}$ , the activation energy is  $0.68 \text{ eV}^*$  and  $n \gtrsim 3$ .

If creep tests are performed under conditions of very low shear stress at the basal plane, sliding occurs at other planes. Figure 2.6 shows the stress-

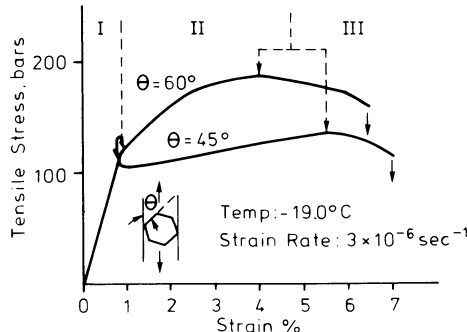


FIG. 2.6. Stress-strain curves for non-basal glide of ice single crystals with various orientations. The tensile axis lies in the basal plane. (From Higashi *et al.* [44].)

\*See the footnote on p. 57.

strain curves for a tension test under a constant strain rate, when the specimen was under tension. The stress-strain curves are quite different from the previous ones which apply when slip occurs in the basal planes, and they look much like the stress-strain curves of usual metals. The angle  $\theta$  in Figure 2.6 is that between the  $a$ -axis<sup>†</sup> and the applied tensile stress and is depicted in the insert. Three different stages of curves are indicated. Stage I is nearly linear and reversible with a relatively steep slope which ends in slight yielding. In stage II the stress required to maintain a constant strain rate increases with increasing strain and strain hardening occurs. In stage III, the stress slowly decreases until fracture occurs. This stage is characterized by *strain softening*. The power law (2.20) remains valid but now  $n \geq 2.7$ .

There are many more features that have been studied in single ice crystals, see Hobbs [45], but none of these applies to arbitrary strain and under combined stresses. The above power laws are therefore, at most, a hint as to the class of constitutive relations that might be postulated to describe the deformation of single ice crystals under combined loadings. We shall refrain from any speculations in this regard and directly pass on to the description of polycrystalline ice.

### 3. The Mechanical Properties of Polycrystalline Ice

Polycrystalline ice is an aggregate of randomly-oriented grains of single ice crystals. It is thus clear that polycrystalline ice deforms much more slowly under otherwise similar conditions than do single crystals. The reason is that deformations along the basal planes of polycrystalline ice are blocked by neighboring ice crystals. As was the case for  $Ih$  ice crystals, polycrystalline ice may be considered to be an elastic, viscoelastic or viscoplastic body, dependent on the physical processes under consideration. Since the orientation of the crystals is random, polycrystalline ice can, for many purposes, be regarded as an isotropic material. Anisotropy effects are introduced, only when recrystallizations occur under high stresses.

#### (a) The elastic behavior of polycrystalline ice

We consider a body of polycrystalline ice. Characteristic lengths and the processes involved are assumed to be of the order of several grain diameters so that the mechanical behavior of a single grain is only important insofar as it interacts with neighboring grains and contributes on a scale of several grain diameters to an isotropic state of stress. On this intermediate scale, the *linear* stress-strain relationship reduces to the classical isotropic *Hooke's law*

$$T_{AB}^P = \mathcal{C}_{ABCD} E_{CD}, \quad \mathcal{C}_{ABCD} = \lambda \delta_{AB} \delta_{CD} + \mu (\delta_{AC} \delta_{BD} + \delta_{AD} \delta_{BC}), \quad (2.21)$$

<sup>†</sup> The  $a$ -axis is an axis within the basal plane. Its direction is tangential to a side of the hexagonal crystal.

TABLE 2.1. Equivalence of elastic constants

Constants	$\lambda$	$\mu$	$E$	$v$	$k$
$\lambda, \mu$			$\frac{\mu(3\lambda + 2\mu)}{\lambda + \mu}$	$\frac{\lambda}{2(\lambda + \mu)}$	$\lambda + \frac{2}{3}\mu$
$\lambda, v$		$\frac{\lambda(1 - 2v)}{2v}$	$\frac{\lambda(1 + v)(1 - 2v)}{v}$		$\frac{\lambda(1 + v)}{3v}$
$\lambda, k$		$\frac{3}{2}(k - \lambda)$	$\frac{9k(k - \lambda)}{3k - \lambda}$	$\frac{\lambda}{3k - \lambda}$	
$\mu, E$		$\frac{\mu(E - 2\mu)}{3\mu - E}$		$\frac{E}{2\mu} - 1$	$\frac{\mu E}{3(3\mu - E)}$
$\mu, v$		$\frac{2\mu v}{1 - 2v}$	$2\mu(1 + v)$		$\frac{2\mu(1 + v)}{3(1 - 2v)}$
$\mu, k$	$k - \frac{2}{3}\mu$		$\frac{9k\mu}{3k + \mu}$		$\frac{3k - 2\mu}{2(3k + \mu)}$
$E, v$		$\frac{Ev}{(1 + v)(1 - 2v)}$	$\frac{E}{2(1 + v)}$		$\frac{E}{3(1 - 2v)}$
$E, k$		$\frac{3k(3k - E)}{9k - E}$	$\frac{3kE}{9k - E}$		$\frac{3k - E}{6k}$
$v, k$		$\frac{3kv}{1 + v}$	$\frac{3k(1 - 2v)}{2(1 + v)}$	$3k(1 - 2v)$	

$\lambda, \mu$  are the Lamé constants,  $E$  and  $v$  Young's modulus and Poisson's ratio and  $k$  the compression or bulk modulus.  $\mu$  agrees with the common shear modulus.

where  $\lambda$  and  $\mu$  are the Lamé constants, which may depend parameterically on temperature. Equation (2.21) tacitly assumes that the body possesses a natural state; in other words the stress is zero at vanishing strain. Of course, a nonlinear elastic response could also be considered, but this has never been done and it is not clear whether it would be realistic.

The tensor of elastic constants listed in (2.21) is formally identical with the tensor  $\mathcal{K}$  listed in (2.16), but with different meanings of the constants  $\lambda$  and  $\mu$ . Incidentally, these constants are one possible pair to choose out of many. Young's modulus  $E$  and Poisson's ratio  $v$  would be another. Table 2.1 lists the most important pairs of elasticity constants and the relations which allow the transformation from one pair to another.

The determination of the elasticity constants of linear elastic polycrystalline ice can be achieved by averaging the elasticity constants of single-crystal ice over all directions in space. This has been done, and Röthlisberger [97] summarizes the work of several authors.\* Figure 2.7 is a direct inter-

\*The averaging process is essentially a mixture theory of randomly oriented small single crystals developed by Voigt [109] in 1910. It determines the Lamé constants as functions of the elastic moduli of the hexagonal crystal. It is worth noting that this theory was also adopted by Penny

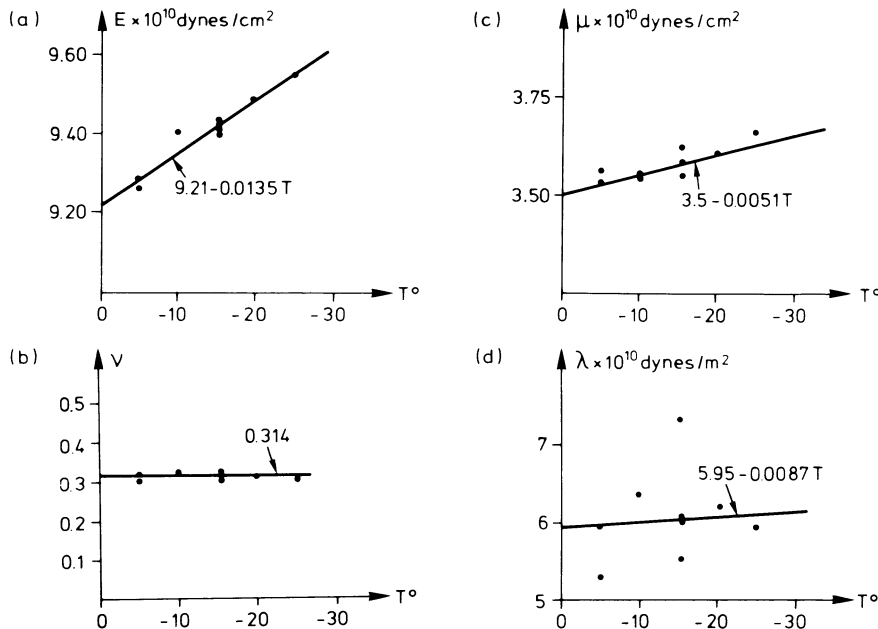


FIG. 2.7. Young's modulus (a), Poisson's ratio (b), and the Lamé constants (c), (d) of polycrystalline ice according to the data collected by Roethlisberger [97] and the linear temperature fit by Hutter [46].

pretation of the data collected by Röthlisberger. It is seen that to a good order of approximation, the Poisson ratio may be assumed independent of temperature. Furthermore, whereas  $E$ ,  $\mu$  and  $v$  do not show considerable scatter,  $\lambda$ , the first Lamé constant, does. Clearly, this is an indication that the temperature-dependency of polycrystalline ice may safely be neglected. Nevertheless, in an attempt to obtain this dependency, Hutter [46] constructed a least square fit of the data collected by Röthlisberger and obtained the following relations :

$$\begin{aligned} E(T) &= 9.2 \times (1 - 0.00146T) \times 10^9 \text{ N cm}^{-2} \\ v(T) &= 0.314 \\ \mu(T) &= 3.5 \times (1 - 0.00146T) \times 10^9 \text{ N cm}^{-2} \\ \lambda(T) &= 5.95 \times (1 - 0.00146T) \times 10^9 \text{ N cm}^{-2} \end{aligned} \quad (2.22)$$

[84] to evaluate two atomic constants of a lattice dynamic theory from measurements of Young's modulus and Poisson's ratio of polycrystalline ice, which then were used to predict theoretically the elastic moduli of a single ice crystal with good agreement with experiments! Kröner gives another approach, see *Zeitschrift für Physik*, E. Kröner: Berechnung der elastischen Konstanten des Vielkristalles aus den Konstanten des Einkristalles; Vol. 151 (1958), 504–511. See also [58].

$T$  must be given in centigrade degrees and the range of validity of (2.22) is  $0 \geq T \geq -20^\circ\text{C}$ . The order of magnitude agrees well with the more recent data (2.11) for hexagonal single ice crystals.

Clearly, the above values as averages over all directions of single-crystal elasticities must be considered as upper bounds to the real values of the elastic constants of polycrystalline ice. Impurities, such as defects along grain boundaries and entrained air bubbles, cause the above values to be somewhat lower in certain cases. However, since these are not controllable effects which are small, in general the relations (2.22) may be considered to yield reliable values. In the higher regions of glacier ice, however, density effects come into play which are significant in the interpretation of seismograms. This is the reason why in these instances glacier ice cannot simply be considered as ordinary polycrystalline ice. Here, an explicit dependency of ice on density is essential. Röthlisberger [97] gives more details.

(b) *Linear viscoelastic properties of polycrystalline ice\**

(x) *General theory.* At moderately low stresses below 1 bar =  $10^5 \text{ N m}^{-2}$  and slowly applied forces, polycrystalline ice may be considered to be a linear viscoelastic body. Provided that applied loads are not too high, the usual tests can be made using creep or vibration on specimens in pure bending or tension. The first systematic treatment of viscoelastic behavior of ice goes back to Jellinek and Brill [54]. Other experimental investigations, not on laboratory polycrystalline ice but on glacier ice from the Greenland ice cap, are reported by Nakaya [77]. These investigations used mechanical models such as springs and dashpots arranged in parallel fashion and in series. We believe that such a method is outdated and that a more mathematical approach to determine relaxation and creep functions is appropriate. Below, we give a brief account of this more recent approach; yet we shall not be able to report data on many of the phenomenological constants which appear, mainly because of a lack of available experimental results. Nevertheless, viscoelastic response is important, because it is a reasonable description of floating lake and sea ice when quasistatic loads are applied. In many engineering applications, such as the installation of parking places, transportation of goods and recreation on floating ice, one may have to make use of viscoelasticity theory. It is therefore important that the viscoelastic behavior of ice is further studied experimentally. I hope that the

\*There are many books and expository articles on viscoelasticity. Of the older ones, Bland [10], Gross [41] and Zener [121] must be mentioned. More modern treatments are those of Findley, Lai and Oranen [25], Pipkin [86], Christensen [18], Gurtin and Sternberg [42] and, in the nonlinear viscoelastic case, Lockett [67]. Historically visco-elasticity goes back to Volterra [110], who appears to have been the first in establishing a constitutive relation of the hereditary type (2.23). A thorough thermodynamic foundation of the theory of viscoelasticity can be found in Coleman [16] and Day [20].

following theoretical investigation may serve as a stimulus to the experimentalist.

To derive the stress-strain relationship of linear visco-elasticity, let  $dT_{AB}^P(t)$  be the stress increment which is induced at a particle by a strain increment  $dE_{CD}(t')$  which lies at a time interval  $t - t' = s$  in the past. In a linear theory, this stress increment must be linearly related to the strain increment, so that a relation of the form

$$dT_{AB}^P(t) = \mathcal{G}_{ABCD}(t, s) dE_{CD}(t - s). \quad (2.23)$$

applies.  $\mathcal{G}_{ABCD}$  is the elastic tensor which, in general, is a function of both  $s$  and  $t$ . It is called *relaxation function* and in usual viscoelasticity formulations is independent of  $t$ , which excludes the possibility of *aging*. Henceforth, we shall restrict our attention to this special case.

Summation over the entire past history prior to time  $\tau = t$ , i.e., from  $s = \infty$  to  $s = 0$ , gives

$$\begin{aligned} T_{AB}^P(t) &= - \int_0^\infty \mathcal{G}_{ABCD}(s) \frac{dE_{CD}(t-s)}{ds} ds = \mathcal{G}_{ABCD}(0) E_{CD}(t) + \\ &\quad + \int_0^\infty \frac{d\mathcal{G}_{ABCD}(s)}{ds} E_{CD}(t-s) ds. \end{aligned} \quad (2.24)$$

Here, the minus sign in front of the first integral stems from an interchange of the upper and lower integration limits. Moreover, the second expression has been obtained from the first by an integration by parts, which can only be performed provided that the integrand functions  $\mathcal{G}_{ABCD}$  and  $E_{CD}$  are differentiable. In this integration by parts, it was assumed that  $\mathcal{G}_{ABCD}(\infty) E_{CD}(-\infty) \equiv 0$  requiring that for finite and bounded strain  $\mathcal{G}_{ABCD}(s)$  must approach the zero value or else  $E_{CD}(-\infty)$  must vanish as  $s$  tends to infinity. There are representations which are different from those listed in (2.24). For instance, by a change of variables one may easily show that an equivalent representation for the stress tensor is

$$T_{AB}^P(t) = \int_0^\infty \mathcal{G}_{ABCD}(t-s) \frac{dE_{CD}(s)}{ds} ds. \quad (2.25)$$

Often a material particle suffers zero strain history for all times  $t < 0$ . The upper limit in the integral at the far right in Equations (2.24) and (2.25) can then be replaced by  $t$ . Because of the importance of this special case a special operator notation is used, namely

$$T_{AB}^P(t) = \mathcal{G}_{ABCD}(t) \circ E_{CD}(t), \quad (2.26)$$

where  $\circ$  is called the *Stieltjes convolution operator* defined by

$$\mathcal{G}(t) \circ E(t) \equiv \int_0^t \mathcal{G}(t-s) \frac{dE(s)}{ds} ds \equiv \mathcal{G}(0) E(t) + \int_0^t \frac{d\mathcal{G}(s)}{ds} E(t-s) ds. \quad (2.27)$$

In polycrystalline *isotropic* ice, symmetry conditions require that

$$\mathcal{G}_{ABCD}(s) = \lambda(s)\delta_{AB}\delta_{CD} + \mu(s)(\delta_{AC}\delta_{BD} + \delta_{AD}\delta_{BC}), \quad (2.28)$$

where  $\lambda(s)$  and  $\mu(s)$  are relaxation functions which play the same role in linear viscoelasticity as do the Lamé constants in the theory of linear elasticity. Once these functions are known, the viscoelastic response of polycrystalline ice is determined.

There is a formulation of stress-strain relationship which is dual to (2.25). It is the inverse relation of the form

$$E_{AB}(t) = \int_{-\infty}^t \mathcal{J}_{ABCD}(t-s) \frac{dT_{CD}^P(s)}{ds} ds = \mathcal{J}_{ABCD}(t) \circ T_{CD}^P(t). \quad (2.29)$$

$\mathcal{J}_{ABCD}$  are again response functions; they are called *creep functions*. It can be shown by thermodynamic arguments that the representation using relaxation functions is derivable from a free energy, called the Helmholtz energy. Alternatively, (2.29) is derivable from a different thermodynamic potential, the *enthalpy*, which can be obtained from the free energy by a Legendre transformation.

Both relaxation and creep functions have easy physical interpretations. To find these, let us look at simple shear or simple tension for which (2.25) and (2.29) assume the form

$$\sigma(t) = \mathcal{G}(t) \circ \varepsilon(t), \quad \varepsilon(t) = \mathcal{J}(t) \circ \sigma(t). \quad (2.30)$$

$\sigma$  and  $\varepsilon$  represent stress and strain. For each of these cases, a Gedanken experiment will be performed. In the first, we apply a constant stress from  $t = 0$  onward, so that

$$\sigma(t) = \begin{cases} 0, & t < 0, \\ 1, & t \geq 0. \end{cases} \quad (2.31)$$

This is a Heaviside function whose derivative is given by the  $\delta$ -function. Equation (2.30)<sub>2</sub> thus becomes, in this case,

$$\varepsilon(t) = \int_0^t \mathcal{J}(t-s) \delta(s) ds = \mathcal{J}(t).$$

If, therefore, strain is plotted as a function of time, the creep function is obtained. Consider instead an experiment in which strain is kept constant so that

$$\varepsilon(t) = \begin{cases} 0, & t < 0, \\ 1, & t \geq 0. \end{cases} \quad (2.32)$$

Here (2.30)<sub>1</sub> immediately implies

$$\sigma(t) = \mathcal{G}(t).$$

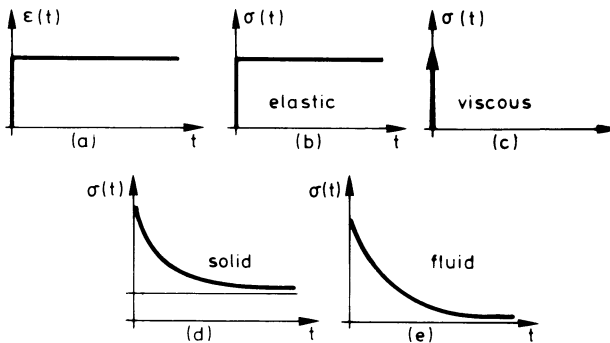


FIG. 2.8. Results of creep tests at constant strain. The graphs of  $\sigma$  as a function of time directly yield the relaxation function. (a) strain history, (b)–(e) various corresponding stress histories = relaxation functions.

In such experiments, plotting the applied force as a function of time, gives directly the relaxation function. Typical relaxation and creep functions are shown in Figures 2.8 and 2.9. In Figure 2.8a the strain history is plotted which leads directly to the relaxation function. If the body were elastic, the corresponding stress history would be as shown in Figure 2.8b. If it were an ideal viscous fluid, the stress corresponding to the strain history (2.32) would be instantly infinite. Real materials are neither ideally elastic nor ideally viscous. Their relaxation functions show a behavior, as in Figures 2.8d and 2.8e. In the situation of Figure 2.8d, the final stress after an infinitely long time is bounded away from zero. Such a body is called a *solid*. If at infinitely long times the stress has relaxed to zero, it is a *fluid*.

Figure 2.9 shows the results obtained for creep tests at constant stress. Figures 2.9b and 2.9c show what could be obtained as creep functions for an ideally elastic and linear viscous body. In these instances the creep function

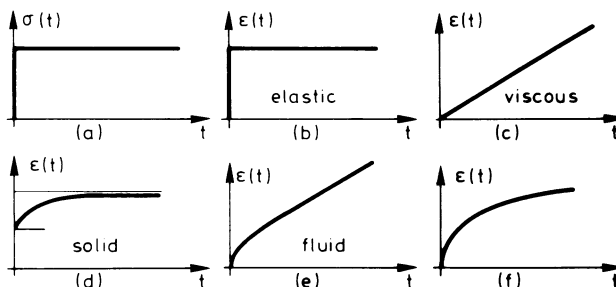


FIG. 2.9. Results of creep tests at constant stress. The graphs of  $\epsilon$  as a function of time directly yield the creep functions. (a) stress-history, (b) creep function for an elastic body, (c) for a viscous fluid, (d) for a solid, (e) for a fluid and (f) for a material which cannot be characterized as solid or as fluid.

would have to be a step function and a linear function, respectively. The rate of increase of  $\mathcal{J}(t)$  in the viscous case could easily be related to the viscosity  $\eta$ :  $\dot{\varepsilon}(t) = \sigma t / \eta$ . Real materials behave rather as shown in Figures 2.9d–f.

The creep function of a solid starts at a finite value and reaches a finite level asymptotically as  $t \rightarrow \infty$ . The initial jump in strain can be interpreted as an instantaneous elastic response. In very fast processes, this is recognizable almost to the exclusion of other responses. For infinitely slow processes, on the other hand, the actual creep curve can be replaced by its asymptote, so that such processes may again be treated elastically, but with elasticities which are different from those of very fast processes. If as  $t \rightarrow \infty$ , the strain rate is constant, one calls the material a fluid. If, on the other hand, the behavior of the creep function is as in Figure 2.9f the material is neither a linear solid nor a linear fluid. It may be called fluid-like.

The above description explains why material scientists concentrate so intensely on the performing of creep tests. Creep curves directly yield the creep functions of a linear viscoelastic model. Moreover, they give relatively easy access to the decision as to whether a body under certain processes behaves more like a solid than a fluid and *vice versa*. For a solid they also give indications as to whether the elastic behaviors for very fast and very slow processes differ considerably. This latter point needs clarification. To this end, consider the strain histories  $\varepsilon(t)$  and  $\varepsilon_\alpha = \varepsilon(\alpha t)$ .  $\varepsilon_\alpha$  represents the same process as  $\varepsilon(t)$ , but for  $0 < \alpha < 1$  it is *retarded* and for  $1 < \alpha < \infty$  it is *accelerated*. The stress due to such a process is

$$\sigma_\alpha = \int_{-\infty}^t \mathcal{G}(t-s) \frac{d\varepsilon(\alpha s)}{d\alpha s} ds = \int_{-\infty}^{\alpha t} \mathcal{G}\left(\frac{\alpha t - s'}{\alpha}\right) \frac{d\varepsilon(s')}{ds'} ds'.$$

Consider a very slow process,  $\alpha \rightarrow 0$ . For fixed  $t$ , then the argument of the relaxation function is very large (and positive). Hence, for most arguments the value of  $\mathcal{G}(\cdot)$  does not differ much from  $\mathcal{G}(\infty)$ , which is the constant  $\mathcal{G}_\infty$ , thus to 0th order in  $\alpha$

$$\sigma_{\alpha \rightarrow 0} \sim \mathcal{G}_\infty \cdot \varepsilon(\alpha t).$$

This is Hooke's law with Young's modulus  $\mathcal{G}_\infty$ . If, on the other hand, very fast processes are looked at, one obtains

$$\sigma_{\alpha \rightarrow \infty} \sim \mathcal{G}(t)\varepsilon(\alpha t) = \mathcal{G}\left(\frac{\tau}{\alpha}\right)\varepsilon(\tau) \sim \mathcal{G}(0)\varepsilon(\alpha t).$$

This is again an elastic response, but with a different Young's modulus. In Figure 2.8d,  $\mathcal{G}(0)$  is given by the interception of the creep curve with the ordinate;  $\mathcal{G}_\infty$  is represented by the horizontal asymptote.

In order to determine the linear viscoelastic response functions of

an *isotropic* body, one must perform two experiments, say a creep test under tension and another one under shear. These two tests then give either the relaxation functions  $\lambda(s)$  and  $\mu(s)$  or the corresponding creep functions. For practical reasons, it is interesting to know how the relaxation functions can be determined from the creep functions and *vice versa*. Such transformation rules will absolve us from performing creep tests at both constant stress and strain, or they give us a means of checking whether functional representations of one particular data-fit will also sufficiently match the other. To find these relations, notice that for a material which has been in a natural state for  $t < 0$  and has suffered a deformation only for  $t \geq 0$ , Equations (2.26) and (2.29) may be interpreted in terms of a Laplace convolution integral\*

$$F(t) = \int_0^t g(t-s)h(s) ds = g(t)*h(t). \quad (2.33)$$

It is known from the theory of Laplace transforms that in the transformed plane the convolution operation  $*$  goes over into a simple product. Denoting Laplace transforms by overbars, using formulas (2.35) of the footnote and considering the fact that the material is assumed to be in a natural state for  $t < 0$ , the reader may deduce the relations

$$\begin{aligned} \overline{T_{AB}^P}(s) &= \overline{\mathcal{G}_{ABCD}(t) \cdot E_{CD}(t)} = s \overline{\mathcal{G}_{ABCD}(s)} \overline{E_{CD}(s)}, \\ \overline{E_{AB}}(s) &= \overline{\mathcal{J}_{ABCD}(t) \cdot T_{CD}^P(t)} = s \overline{\mathcal{J}_{ABCD}(s)} \overline{T_{CD}^P(s)}. \end{aligned} \quad (2.36)$$

The Laplace transform of the Stieltjes convolution  $\circ$  of two functions is the product of the Laplace transforms of the functions multiplied with  $s$ . The relations (2.36) are very important ones, because they essentially establish a one-to-one relationship between the constitutive relations of linear elasticity (see (2.21)) and the Laplace transform of the corresponding relationships of linear viscoelasticity. The correspondence is

$$\mathcal{C}_{ABCD} \rightarrow s \overline{\mathcal{G}_{ABCD}}, \quad \mathcal{S}_{ABCD} \rightarrow s \overline{\mathcal{J}_{ABCD}}.$$

\*The reader is assumed to be familiar with the basic theory of Fourier and Laplace transforms. Elementary treatment of these transforms are given in any book on mathematical methods in engineering and physics, such as Greenberg [39], Kaplan [57], Sokolnikov and Redheffer [104] and others. As examples we mention: If  $f(t)$ ,  $t > 0$ , does not grow faster than exponentially as  $t \rightarrow \infty$  the Laplace transform and its inverse are given by

$$\bar{f}(s) := \int_0^\infty f(t) e^{-st} dt, \quad f(t) = \frac{1}{2\pi i} \int_{\gamma-i\infty}^{\gamma+i\infty} \bar{f}(s) e^{st} ds, \quad (2.34)$$

where integration in the inversion integral is along a vertical line in the complex  $s$ -plane. Using (2.34), it may be shown that

$$\overline{\frac{df}{dt}} = sf(s) - f(0), \quad \overline{g * h} = \overline{g(s)} \cdot \overline{h(s)}. \quad (2.35)$$

It gives rise to the *elastic-viscoelastic correspondence principle*. According to this, *quasistatic* solutions of linear viscoelastic problems can be constructed by replacing, in the static solution of a linear elasticity problem, the elastic moduli by the corresponding above-indicated products. The viscoelastic solution is thereafter obtained by an inverse Laplace transform. Because many boundary-value problems of linear elasticity have already been solved, the corresponding viscoelasticity problems are then ‘merely’ a problem of inverse Laplace transforms. A proof of the correspondence principle, which was first given by Read [94], can be found, e.g., in Christensen’s book [18].

Combining the two relations (2.36) yields relations between the Laplace transforms of the relaxation and creep functions, namely

$$s^2 \overline{\mathcal{G}_{ABCD}(s)} \overline{\mathcal{J}_{CDEF}(s)} = \delta_{AE} \delta_{BF}. \quad (2.37)$$

By knowing the Laplace transforms of the relaxation functions, those of the creep functions can then be calculated from (2.37), and the determination of the creep functions then remains a matter of Laplace inversion, for which general programs are available. Conversely, having determined the creep functions, their Laplace transforms then allow us to calculate those of the relaxation functions. For isotropic materials, one may substitute relation (2.28) and a similar one for the creep functions. Equation (2.37) then reduces to a set of two equations relating the two relaxation functions with the two creep functions. However, it turns out to be simpler if one works with the *deviatoric* stresses and strains

$$T'_{AB} := T_{AB}^P - \frac{1}{3} T_{CC}^P \delta_{AB}, \quad E'_{AB} := E_{AB} - \frac{1}{3} E_{CC} \delta_{AB}, \quad (2.38)$$

and the traces  $T_{AA}^P$  and  $E_{AA}$  as basic variables. Equations (2.36) and (2.37) may then be shown to be equivalent to

$$T'_{AB} = \mathcal{G}_1 \circ E'_{AB}, \quad T_{AA}^P = \mathcal{G}_2 \circ E_{AA} \quad (2.39)$$

with

$$\mathcal{G}_1 = \frac{\mu}{2}, \quad \mathcal{G}_2 = (3\lambda + 2\mu). \quad (2.40)$$

The inverse relations of (2.39) are simply

$$E'_{AB} = \mathcal{J}_1 \circ T'_{AB}, \quad E_{AA} = \mathcal{J}_2 \circ T_{AA}^P \quad (2.41)$$

and the creep functions  $\mathcal{J}_\alpha$  are related to the relaxation functions  $\mathcal{G}_\alpha$  by

$$\overline{\mathcal{J}_\alpha} = \frac{1}{s^2 \overline{\mathcal{G}_\alpha}}, \quad (2.42)$$

equivalent to (2.37).

Equation (2.42) is one of the forms of relationship between the relaxation and creep functions we were looking for. The disadvantage of the formula is

that Laplace transforms must be performed to obtain a simple relationship. In analytic calculations, the use of Laplace inversions may be appropriate, but when calculations have to be performed numerically, Laplace transforms are not necessarily the most convenient method to evaluate creep from relaxation functions and *vice versa*. In this case, a direct use of (2.26) and (2.29) is more convenient. One basic relationship between the  $\mathcal{J}_x$ 's and  $\mathcal{G}_x$ 's is found by noticing that if the strain history is  $\mathcal{J}_x(t)$ , then the corresponding stress history must be  $H(t)$ , where  $H(t)$  is the unit step function. (Compare the discussions of Figures 2.8 and 2.9.) Thus, from (2.39) and the definition of the Stieltjes convolution (2.27),

$$H(t) = \mathcal{G}_x(t)\mathcal{J}_x(0) + \int_{0^+}^t \mathcal{G}_x(t-\tau) \frac{d\mathcal{J}_x(\tau)}{d\tau} d\tau.$$

If  $\mathcal{J}_x(0) \neq 0$  we may alternatively write

$$\mathcal{G}_x(t) = \frac{H(t)}{\mathcal{J}_x(0)} + \frac{1}{\mathcal{J}_x(0)} \int_{0^+}^t \mathcal{G}_x(t-\tau) \frac{d\mathcal{J}_x(\tau)}{d\tau} d\tau. \quad (2.43)$$

This is a *Volterra integral equation of the second kind* for  $\mathcal{G}_x$  when  $\mathcal{J}_x$  is known. The dual equation is obtained from (2.41) by applying a unit-step-strain history  $H(t)$  for which the stress history is  $\mathcal{G}_x(t)$ . This yields

$$\mathcal{J}_x(t) = \frac{H(t)}{\mathcal{G}_x(0)} + \frac{1}{\mathcal{G}_x(0)} \int_{0^+}^t \mathcal{J}_x(t-\tau) \frac{d\mathcal{G}_x(\tau)}{d\tau} d\tau, \quad (2.44)$$

which is again a Volterra integral equation of the second kind for  $\mathcal{J}_x(t)$ , if  $\mathcal{G}_x(t)$  is known.

There are standard solution techniques by which the Volterra integral Equations (2.43) and (2.44) can be solved. Such techniques are discussed, for instance, by Lovitt [68] and Tricomi [108]. In this connection, it might be worth noting that in solving these equations, approximate solution techniques suffice, since creep or relaxation functions are determined by experiments which always give rise to a certain error.

The reader may regard the above analysis as somewhat mathematical and perhaps superfluous, since for actual calculations of stress and strain, one only needs the creep or relaxation function but not both. However, the serious material scientist, attempting to find a linear viscoelastic constitutive relation for ice, will perform creep tests for both and thus has to find mutually-consistent mathematical expressions for the creep and relaxation functions. In this process he may well find that a satisfactory dual fit is not possible, which would force him to abandon the postulate of *linear* viscoelastic behavior. Undoubtedly such information is very useful.

On time scales in the order of minutes and less, creep tests may be inappropriate, since the viscous effects cannot be well detected by them.

Nevertheless, they are still of significance, as can be inferred from load tests on floating lake ice. To cover this short-time response, experimentalists often consider the steady-state response of a specimen when the latter is driven by harmonic excitation. If  $E$  is strain and  $T$  is stress in any one of the relations (2.39) or (2.41) one may write  $E = E^0 \exp(i\omega t)$ ,  $T = T^0 \exp(i\omega t)$ , in which  $\omega$  is the driven frequency and indexed quantities are complex amplitudes. Substituting these relations into the constitutive relationship,  $T = \mathcal{G} \circ E$  will yield a linear relation between the amplitudes  $T^0$  and  $E^0$ , and the reader may easily show that

$$\begin{aligned} T^0 &= \mathcal{G}^*(i\omega)E^0, \\ \mathcal{G}^*(i\omega) &= \mathcal{G}^\infty + i\omega \int_0^\infty \tilde{\mathcal{G}}(y) \exp(-i\omega y) dy \end{aligned} \quad (2.45)$$

in which  $\mathcal{G}^\infty = \mathcal{G}(\infty)$  and  $\tilde{\mathcal{G}} = \mathcal{G} - \mathcal{G}^\infty$ . The function  $\mathcal{G}^*(i\omega)$  is called the *complex modulus* and has real and imaginary parts which are given by

$$\begin{aligned} \mathcal{G}_{\text{Re}}^* &= \mathcal{G}^\infty + \omega \int_0^\infty \tilde{\mathcal{G}}(y) \sin \omega y dy, \\ \mathcal{G}_{\text{Im}}^* &= \omega \int_0^\infty \tilde{\mathcal{G}}(y) \cos \omega y dy. \end{aligned} \quad (2.46)$$

The integrals in these expressions are Fourier-sine and Fourier-cosine transforms, and the inversions can be shown to be (see, e.g., [18])

$$\begin{aligned} \mathcal{G}(t) &= \frac{2}{\pi} \int_0^\infty \frac{\mathcal{G}_{\text{Re}}^*(\omega) \sin \omega t}{\omega} d\omega, \\ \tilde{\mathcal{G}}(t) &= \frac{2}{\pi} \int_0^\infty \frac{\mathcal{G}_{\text{Im}}^*(\omega) \cos \omega t}{\omega} d\omega. \end{aligned} \quad (2.47)$$

The usefulness of these formulas is as follows: In an experiment one can, for instance, prescribe  $E^\circ$  (as a real quantity) and  $\omega$  and will then measure the modulus of  $T^\circ$  and the phase angle by which  $T^\circ$  lags behind  $E^\circ$ ,

$$\begin{aligned} \text{mod } T^0 &= |\mathcal{G}^*(i\omega)| = (\mathcal{G}_{\text{Re}}^{*2} + \mathcal{G}_{\text{Im}}^{*2})^{1/2}, \\ \tan(\varphi(T^0)) &= \mathcal{G}_{\text{Im}}^*/\mathcal{G}_{\text{Re}}^*, \end{aligned} \quad (2.48)$$

and from these and (2.47) by numerically inverting the Fourier-sine and Fourier-cosine integrals, the relaxation function can be determined. A comparison of the two functions obtained with (2.47) may again serve as a test of the accuracy of the data or the appropriateness of the model. In a rudimentary form, this method was essentially used by Nakaya [77].

Classical methods of viscoelasticity do not use the integral relationships (2.26) and (2.29) as constitutive equations relating stress and strain. In that ap-

proach, one starts from rheological models consisting of springs and dashpots arranged in parallel and in series, and from these one establishes differential relationships for stress and strain and their time derivatives. This approach may have served its purpose, but we believe that it is outdated and bears, despite its advantage, several shortcomings. One of these is that rheological models are much less general than is the integral approach. The relaxation functions which emerge from this treatment are, indeed, very special.

Simple rheological models are shown in Figure 2.10. Clearly, these models are one-dimensional and cannot be applied to a continuum, but if the relaxation and creep functions of a body have the same structure as those of the models, one says that the continuum behaves as a Maxwell or Kelvin body, etc. The rheological model in Figure 2.10a is a composition of the two separated models shown in Figure 2.10b. The model at the top of Figure 2.10b is called a Maxwell body. It consists of a spring and a dashpot arranged in series. In the other rheological model of Figure 2.10b, the spring and dashpot are parallelly arranged; this model is a Kelvin or Voigt body. In the terminology introduced in connection with Figures 2.8 and 2.9, the Maxwell body is a fluid and the Kelvin body a solid. Of course, there are many more possible combinations – arranging Maxwell units parallelly results in the generalized Maxwell fluid and arranging Kelvin units in series yields the generalized Kelvin body – each of them characterizing a certain material behavior. But unfortunately, while to every model there corresponds a certain material behavior, there may be several models to a certain typical material,

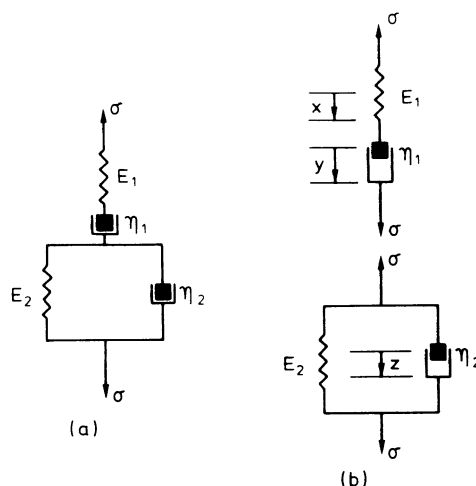


FIG. 2.10. Ice model of Jellinek and Brill, the so called Burgers model. (a) in its natural state, and (b) deformed and separated into the two units.

the models being different in the combination of springs and dashpots, see [25]. In ice mechanics, only the most simple combinations have been considered. Some authors use the Maxwell model, Nakaya [77], Nevel [78]. In the context of ice research, one of the most complex models has been introduced by Jellinek and Brill [54]. It consists of a Maxwell and a Kelvin body arranged in series (Figure 2.10a) and is known as *Burgers model*. What results, as we shall see, is a fluid. It is noteworthy that the Burgers model was proposed by De Quervain [92] as early as 1946, as a reliable model for snow. Recently, Nevel [79] introduced a rheological model consisting of a Maxwell unit and two Kelvin units, all arranged in series. The special feature is that one of the Kelvin units has a negative value of its spring constants. We shall discuss this case below.

Stress-strain relationships emerging from rheological models are usually expressed in terms of differential equations. To see how these are obtained, let us consider the ice model suggested by Jellinek and Brill and shown in Figure 2.10a, where the model is in its natural state. The separations are displayed in Figure 2.10b in the deformed state, and the elongations of springs and dashpots are denoted by  $x$ ,  $y$  and  $z$ , respectively. The entire elongation,  $\varepsilon$ , is  $\varepsilon = x + y + z$  and the force-deformation relations for the separated units are  $\sigma = E_1 x$ ,  $\sigma = \eta_1 \dot{y}$  and  $\sigma = E_2 z + \eta_2 \dot{z}$ . Eliminating  $x$ ,  $y$ ,  $z$  between these four equations yields the differential equation

$$\frac{\eta_2}{E_1} \ddot{\sigma} + \left( 1 + \frac{E_2}{E_1} + \frac{\eta_2}{\eta_1} \right) \dot{\sigma} + \frac{E_2}{\eta_1} \sigma = E_2 \dot{\varepsilon} + \eta_2 \ddot{\varepsilon} \quad (2.49)$$

between stress  $\sigma$  and strain  $\varepsilon$ .

More generally, all rheological models with a finite number of spring-dashpot combinations are representable in the form

$$P_{(n)}(\sigma) = P_{(m)}(\varepsilon), \quad \text{where} \quad P_{(n)}(\cdot) = \sum_{j=1}^n a_j \frac{d^j(\cdot)}{dt^j}, \quad a_n \neq 0 \quad (2.50)$$

in which  $m$  and  $n$  are integers, which need not necessarily be the same, and  $P_{(n)}(\cdot)$  is a polynomial differential operator. It should be observed that the differential relationship (2.50) is not sufficient to characterize the model at hand. Since higher time derivatives of stress and strain occur, initial conditions for  $(n - 1)$  stress and  $(m - 1)$  strain derivatives must be prescribed along with (2.50). These conditions require that at  $t = 0$ , all derivatives of  $\sigma$  and  $\varepsilon$  equal to and higher than 2 vanish.

To construct the relaxation function associated with (2.50) we note that the Laplace transformed stress-strain relation reads  $\bar{\sigma} = s \mathcal{G}(s) \bar{\varepsilon}$ . Hence, performing a Laplace transform with (2.50) reveals  $P_{(n)}(s) \bar{\sigma} = P_{(m)}(s) \bar{\varepsilon}$ . [In the Laplace-transformed domain, the polynomials are functions of the transform variable  $s$ , because in view of the initial conditions  $\partial^P \sigma(t)/\partial t^P = s^P \bar{\sigma}(s)$ .]

Hence,

$$\bar{\mathcal{G}}(s) = \frac{P_{(m)}(s)}{sP_{(n)}(s)} \quad \text{or} \quad \mathcal{G} = \frac{1}{2\pi i} \int_{\gamma-i\infty}^{\gamma+i\infty} e^{st} \frac{P_{(m)}(s)}{sP_{(n)}(s)} ds. \quad (2.51)$$

The integrand function is algebraic; its singularities are poles. It then follows from the residue theorem of complex variable theory that (see, e.g., [104])

$$\mathcal{G}(t) = \sum_{\text{Residues}} \left( \frac{P_{(m)}(s)}{sP_{(n)}(s)} e^{st} \right). \quad (2.52)$$

It is physically obvious that poles cannot lie in the positive half plane, because  $\mathcal{G}$  would then grow exponentially with increasing time. This would mean that strain of the distant past would affect present stress more than does strain in the recent past. This is in conflict with our common experience that the memory of the material fades in time. It can further be shown that the poles must lie on the negative real  $s$  axis, see Figure 2.11, with the possibility of one pole at the origin  $s = 0$ . The corresponding contribution to the relaxation function is constant in time. A solid is therefore characterized by a pole at the origin. Denoting these poles with  $s_i$  and their negative inverse as relaxation or retardation times  $t_i = -1/s_i$ , it immediately follows that

$$\mathcal{G}(t) = \sum_{\text{Residues}} \mathcal{G}_i \exp(-t/t_i) \quad (2.53)$$

as a relaxation function of the general polynomial constitutive relation (2.50).

As an example, consider the Burgers model with its differential relationship (2.49); the polynomials have the degrees  $m = n = 2$  and it is readily shown that

$$\bar{\mathcal{G}} = \frac{E_2 + s\eta_2}{(s - s_1)(s - s_1)} \frac{E_1}{\eta_2}, \quad (2.54)$$

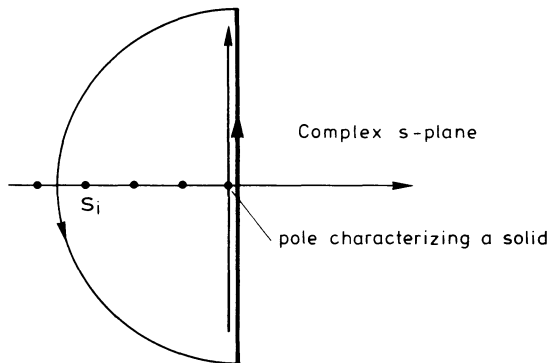


FIG. 2.11. Bromwich contour and positions of residues for the evaluation of  $G(t)$ .

where

$$s_{1,2} = \frac{E_1}{2\eta_2} \left\{ - \left( 1 + \frac{E_2}{E_1} + \frac{\eta_2}{\eta_1} \right) \pm \sqrt{\left( 1 + \frac{E_2}{E_1} + \frac{\eta_2}{\eta_1} \right)^2 - 4 \frac{E_2 \eta_2}{E_1 \eta_1}} \right\}$$

Thus,  $\mathcal{G}$  has two simple poles on the negative real axis and, consequently,  $\mathcal{G}$  must be the sum of two exponentials. Indeed, by collecting residues, the reader may show by himself that

$$\begin{aligned} \mathcal{G} &= G_1 e^{-t/t_1} + G_2 e^{-t/t_2}, \\ G_1 &= \frac{1}{R} (E_2 + s_1 \eta_2), \quad t_1 = -s_1^{-1}, \\ G_2 &= \frac{1}{R} (E_2 + s_2 \eta_2), \quad t_2 = -s_2^{-1}, \\ R &= \sqrt{\left( 1 + \frac{E_2}{E_1} + \frac{\eta_2}{\eta_1} \right)^2 - 4 \frac{E_2 \eta_2}{E_1 \eta_1}}. \end{aligned} \tag{2.55}$$

The relaxation functions to most rheological models can be constructed in this way. There are exceptions, notably the Kelvin solid. On the other hand, the result (2.53) suggests a method of constructing relaxation functions from creep tests at a constant stress. The idea is to fit the test data by a sum of exponentials  $\mathcal{G} = \sum_{n=0}^N \mathcal{G}_n \exp(-t/t_n)$ . The determination of the amplitudes  $\mathcal{G}_n$  and the relaxation times  $t_n$  is referred to as the problem of *separation of exponentials*, and it is known to be notoriously difficult. Accurate data must be known if one tries to fit these with more than two or three exponential functions, see Lanczos [60]. Since most rheological models happen to give relaxation functions which are a sum of exponentials, this indicates that creep tests will hardly improve the ice model of Jellinek and Brill.

The separation of exponentials being difficult, one may just attempt the opposite and try to ‘smear’ over a certain range of relaxation times. In other words, one assumes a continuous distribution of Maxwell units arranged in parallel fashion so that, instead of (2.53), one obtains

$$\mathcal{G}(t) = \int_{\tau_1}^{\tau_2} F(\tau) \exp\left(-\frac{t}{\tau}\right) d\tau, \tag{2.56}$$

where  $F$  is a continuous amplitude function of the relaxation function. Now, it is no longer the separation of exponentials one has to determine, but rather the function  $F(\tau)$  and the relaxation times  $\tau_1$  and  $\tau_2$ . This choice was also considered by Jellinek and Brill and they choose  $F(\tau) = c/\tau$ ; this yields

$$\mathcal{G}(t) = c [\mathcal{E}_1(t/\tau_1) - \mathcal{E}_1(t/\tau_2)],$$

where

$$\mathcal{E}_1(t) = \int_t^\infty \frac{1}{x} \exp(-x) dx \tag{2.57}$$

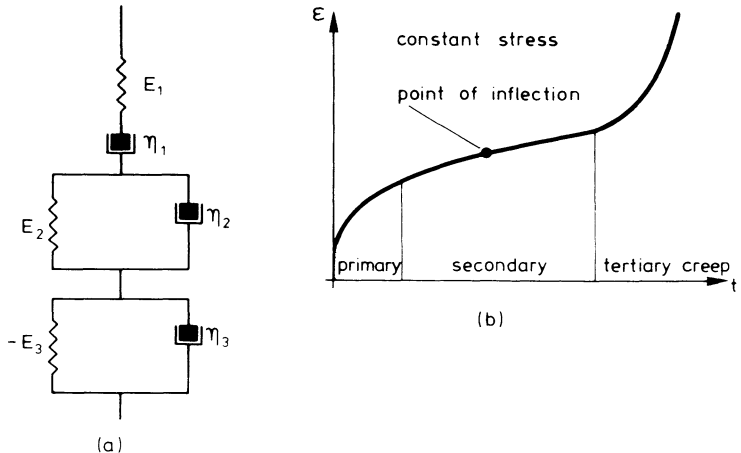


FIG. 2.12. (a) Nevel's ice model [79], (b) typical creep curve of ice under compression (schematic).

is the exponential integral. The problem of separating many exponentials in the interval  $(\tau_0, \tau_2)$  has been reduced here to finding three unknown parameters. Numerical values will be given in the next section.

Finally, we present the viscoelastic body proposed by Nevel [79]. His model, shown in Figure 2.12a, represents a series-arrangement of a Burgers model with a Kelvin unit. Nevel's conjecture is that within the realm of a linear constitutive relationship, this model describes all features of the creep curve sketched in Figure 2.12b. The creep curve of this figure contains all the characteristic properties of material ice. Accordingly, for a very small time, the strain rate is large and decelerates with increasing time. This stage is called *primary creep*. There is an intermediate domain for which the strain rate is approximately constant. Clearly, a minimum strain rate is obtained at the inflection point. The domain where the actual creep curve can be replaced by a straight line through the point of inflection is known as *secondary creep*. At large times, the strain rate accelerates and it is reasonable to assume that another steady-state strain rate will be approached. This domain is called *tertiary creep*.<sup>\*</sup> The location of the point of inflection depends on stress, in general, implying that a proper description of the constitutive response of ice is non-linear. For low stresses, however, the creep curve may be assumed to be stress-independent.

To derive the relaxation and creep functions of Nevel's rheological model, one proceeds as demonstrated with the Burgers model, derives the differential relationship between  $\sigma$  and  $\epsilon$  and then uses (2.52). This will result in a sum of three exponentials, as given in (2.53). For the relaxation functions to have the fading memory property, the relaxation times must necessarily be positive,

<sup>\*</sup>A negative spring constant  $-E_3$  is needed to obtain this accelerating tertiary creep.

which can be shown to be the case only if

$$E_3 < \frac{E_1 E_2}{E_1 + E_2}. \quad (2.58)$$

Since Nevel provides no numerical values for his phenomenological coefficients, it cannot be judged whether (2.58) would be fulfilled. This is a disadvantage, while another is that three exponentials are very difficult to separate. To model secondary and tertiary creep, Nevel deletes the Maxwell unit. However, such a model requires both spring constants to be positive, if the relaxation function should have the fading memory property and not grow exponentially. Nevel's [79] creep model, therefore, is not appropriate for ice. Furthermore, experimental evidence, to be discussed in detail below, indicates that tertiary creep is only attained at large stresses for which a non-linear constitutive relationship must be postulated. Attempts to this effect have been undertaken by Morland and Spring [76a, 104a].

(β) *Experimental results.* The best early creep tests of polycrystalline ice are due to Jellinek and Brill [54] who made constant stress-creep tests with circular cylinders under tension.

The polycrystalline ice, so-called *snow ice*, was prepared by filling troughs with tap water to a certain height. Snow of a narrow particle size range was then sieved into the water until the surface was dry. This mixture was frozen at  $-5^{\circ}\text{C}$ . The outer layers were subsequently cut away from the specimen and rectangular blocks were cut from the remainder. The grains of the ice were distributed irregularly and their effective diameter was 1–2 mm. Experiments were also performed on Alaskan glacier ice and on single-crystal ice. This is particularly interesting because it demonstrates that there is no difference between the artificial snow ice and glacier ice.

Tension test experiments were performed at  $-5$ ,  $-10$  and  $-15^{\circ}\text{C}$  and various strain- versus time-curves at constant stress were determined. A close fit of the data was obtained with the model of Figure 2.10, with values of  $E_1$ ,  $E_2$  and  $\eta_1$ ,  $\eta_2$  as listed in Table 2.2. Relaxation functions are as shown in (2.55); the amplitudes  $G_1$  and  $G_2$  and the relaxation times  $t_1$  and  $t_2$  have been calculated and are also shown in Table 2.2. Actually, Jellinek and Brill did not determine the relaxation, but rather the creep function of their rheological model. It is easily shown that the latter is given by

$$\mathcal{J} = \left( \frac{1}{E_1} + \frac{t}{\eta_1} \right) + \frac{1}{E_2} (1 - e^{-t/\tau}). \quad (2.59)$$

It is composed of a constant term, a term linear in time, and an exponential term. The first two members on the right-hand side of (2.59) are the contribution of the Maxwell unit, the others are due to the Kelvin unit. The relaxation time is given by  $\tau = 2\eta_2(1 + v)/E_2$ , where  $v$  is Poisson's ratio.

TABLE 2.2. Viscoelastic constants according to Jellinek and Brill

Jellinek and Brill generalized their approach to include a continuous distribution of relaxation times between  $\tau_1$  and  $\tau_2$  and thus wrote

$$\mathcal{J}(t) = \frac{1}{E_1} + \frac{t}{\eta_1} + \int_{\tau_1}^{\tau_2} F(\tau)(1 - e^{-t/\tau}) d\tau. \quad (2.60)$$

This representation corresponds to a Maxwell unit in series with an infinitely long generalized Kelvin body, whose relaxation times vary between  $\tau_1$  and  $\tau_2$  and whose spring constants are given by the reciprocal of  $F(\tau)$ . They chose  $F(\tau) = c/\tau$  and then deduced that

$$\mathcal{J}(t) = \frac{1}{E_1} + \frac{t}{\eta_1} + c \left\{ \ln \left( \frac{\tau_2}{\tau_1} \right) + \mathcal{E}_1 \left( \frac{t}{\tau_1} \right) - \mathcal{E}_1 \left( \frac{t}{\tau_2} \right) \right\}, \quad (2.61)$$

where  $\mathcal{E}_1$  is the exponential integral defined in (2.57).

An optimal fit to the data was also obtained for this function and the results are listed in Table 2.3. The representation (2.61) bears the disadvantage that the relaxation function is difficult to determine and may be mathematically so intractable so as to become virtually useless for mathematical analysis. As can be seen from Table 2.3, the experimental variations in the  $\tau_1$  and  $\tau_2$  values are too large to permit recognition of their proper temperature relationship. The  $t_1$  values are fairly constant, but the other constants vary appreciably.

TABLE 2.3. Viscoelastic constants of the creep function (2.59) according to Jellinek and Brill [54].

$T$ (°C)	$E_1$ (dyn cm <sup>-2</sup> ) $\times 10^6$	$\eta_1$ (poise) $\times 10^{14}$	$\tau_1$ (s)	$\tau_2$ (s) $\times 10^2$	$c$ (cm <sup>2</sup> dyn <sup>-1</sup> ) $\times 10^{-8}$
-5°	6.1	6.4	0.18	1.6	3.6
	7.7	6.1	2.8	1.0	3.8
	7.0	5.5	...	...	...
	5.9	2.1	4.6	2.1	3.9
	2.7	2.1	1.8	1.4	7.7
	2.0	1.8	0.4	...	8.0
	6.1	1.8	0.2	...	4.6
	3.4	2.4	1.0	...	3.8
-10°	4.5	4.3	0.2	3.5	3.6
	3.7	4.0	1.0	2.4	3.0
	3.8	3.1	2.6	1.1	2.6
-15°	5.6	5.4	1.6		1.8
	5.6	7.0	2.8		2.0
	4.2	5.1	0.9	ca. 1	...
	6.2	7.2	2.6		2.3
	6.1	6.6	1.1		6.0
	4.3	9.3	2.8		3.2

The relaxation functions of the form (2.59) and (2.61), as determined by Jellinek and Brill, correspond to Young's modulus in elasticity. In isotropic viscoelasticity, a second constant is needed. Such a second constant could be provided by a further experiment, say under simple shear. Yet such complementary experiments were not performed by Jellinek and Brill. Consequently, to obtain a full set of viscoelastic response functions, a further assumption must be made. The usual procedure is to make a postulate regarding the Poisson ratio, and it is common to assume it to be time-independent, namely

$$\nu = 0.314 \quad \text{or approximately} \quad \nu = 0.3.$$

In summary, we may thus use the following relaxation functions:

Young's Modulus:

$$E(t) = G_1 e^{-t/t_1} + G_2 e^{-t/t_2}, \quad (2.62)$$

of which the constants are listed in Table 2.2.

Poisson's ratio:

$$\nu = 0.314.$$

That the Poisson ratio should be constant is a special condition which must imply constraints on the other relaxation functions. We leave it as an exercise to the reader, using the elastic-viscoelastic correspondence principle, to show that

$$\mathcal{G}_1(t) = \frac{1}{1+\nu} E(t), \quad \mathcal{G}_2(t) = \frac{1}{1-2\nu} E(t) \quad (2.63)$$

are relaxation functions appropriate for the deviatoric stress and the trace, given in (2.39).

It is unfortunate that experiments frequently give only a partial indication of the material properties, so that in the end the experimentally determined phenomenological quantities do not suffice to describe the stress completely.\* In a way the relations (2.63) corroborate this as they are based on the (albeit reasonable) assumption that Poisson's ratio is a constant. A similar assumption was also used by Nevel [78] in an attempt to interpret load-test data of floating lake ice. Nevel's assumption is  $\nu = \frac{1}{2}$ , which is tantamount to saying that ice is incompressible.

Finally, it must be emphasized here that linear elastic and viscoelastic behavior can only be appropriate for stresses below a certain level. Jellinek

\*In fact, most of the information about the constitutive equations for ice under creeping motion stems from uniaxial tension and compression tests. A literature survey of these and other results can be found in Kuo [59] and Shumskiy [102]. Screening these surveys and the respective literature has not given any further information for the case of linear viscoelasticity as to the completion of creep tests under uniaxial compression and simple shear by multiaxial stress tests.

and Brill [54] set this limit at  $10^5 \text{ Pa} (\text{N m}^{-2}) = 1 \text{ bar}$ . This is very limited, and according to modern literature (see Mellor [74]), nearly all practically significant loads are in the non-linear stress-strain range.

(c) *Non-linear viscous deformation and creep*

( $\alpha$ ) *Results of creep tests.* At large stresses and for very slow processes, as for instance quasistatic load histories and deformations of glaciers under their own weight, polycrystalline ice must be treated as an isotropic plastic body. Creep tests on polycrystalline ice have been made by many workers, notably Glen [29–34], Steinemann [105], Gold [35–37], Jellinek [54], Mellor, Smith and Testa [72], [73a, b] and others. The state of the art is also reviewed by Kuo [59], Shumskiy [102] and Mellor [74]. The commonly used stress systems are tension, compression, and pure shear, although combined states of stress have also been looked at. Creep curves of polycrystalline ice are quite different from the corresponding curves of single ice crystals. Unlike the latter, creep curves of polycrystalline ice initially decelerate. Typical curves for different specimens under the same conditions are shown in Figure 2.13, in which a constant stress is applied during a time of the order of 100 to 150 h. Qualitatively, most results seem to be in agreement with the findings of Figure 2.13, but it seems likely that at all stresses, if the tests were continued long enough, a steady-state rate would be reached. In Figure 2.13, the onset of this steady state can clearly be seen. More evidence for it is provided by Figures 2.14 and 2.15 in which creep curves for randomly-oriented polycrystalline ice are shown in Figure 2.14 at various stresses but at constant temperature, and in Figure 2.15 at various

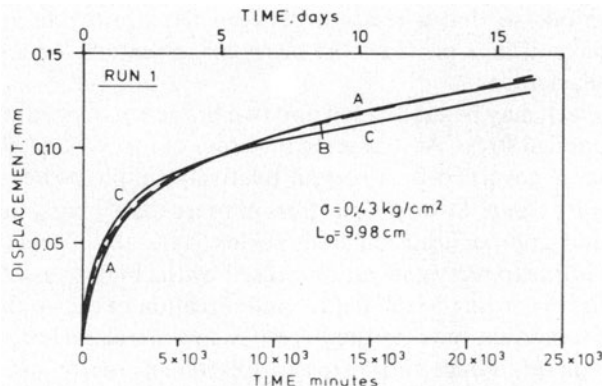


FIG. 2.13. Low-stress creep curves for fine-grained ice whose crystal orientation was initially random. Constant axial compressive test. (From Mellor and Testa [73a].)

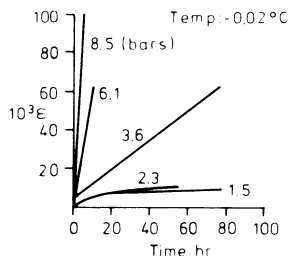


FIG. 2.14. Creep curves of randomly-oriented polycrystalline ice under various stresses. (From Glen [32].)

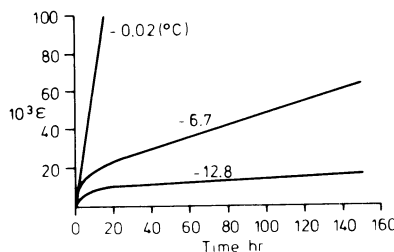


FIG. 2.15. Creep curves of randomly-oriented polycrystalline ice at various temperatures under a stress of 6 bar. (From Glen [32].)

temperatures but at constant stress. The initial decelerated creep in the left-hand corner of these figures is called *transient creep* and the other domain, after the specimen has been subjected to external loadings for a longer time, is called *steady creep*. It is this part that has mostly been studied, because it is of practical significance. Glacier ice is under a certain state of stress for very long periods so that a relation between the strain rate and stress at steady-creep conditions provides the necessary essentials for a constitutive response of glacier ice.

Steady creep may be subdivided into two branches, depending on the domain of the applied stress. At stresses in the order of 1 to 10 bars ( $10^5$  –  $10^6$  Pa), the creep rate is governed by a certain relatively simple power law. This is called *secondary creep*. At very high stress of more than 7 bars, the creep rate accelerates and approaches a different steady state, the *tertiary creep*. The acceleration is due to recrystallization caused by the high stresses. Recrystallization occurs according to the nature and direction of the applied stress so that polycrystalline ice under tertiary creep is, in general, no longer isotropic. Experiments on this induced anisotropy are extremely scarce and attempts to determine flow laws are virtually nonexistent, see Lile [66], Morland and Spring [76a, 104a].

The flow laws of Figures 2.14 and 2.15 only indicate transient and

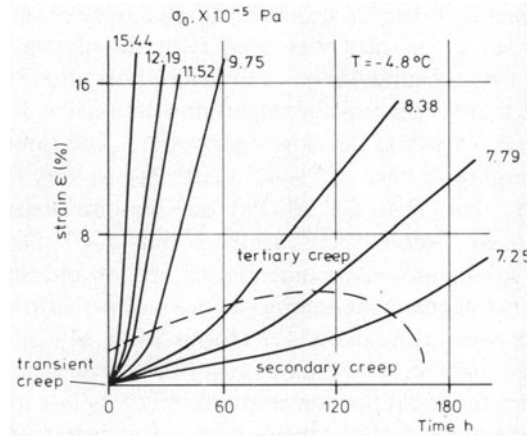


FIG. 2.16. Creep curves for polycrystalline ice at  $-4.8^{\circ}\text{C}$  under various stresses.  
(From Steinemann [105].)

secondary creep. If a different scale is chosen and creep curves under high stresses are drawn, tertiary creep becomes visible, see Figure 2.16.

Prompted by the above observations, there are three possible ways of identifying a flow law:

- (i) In the first law, one tries to relate stress, strain, and its rates for the entire-creep domain of accelerated and steady-state creep. Such a law would amount to mathematically representing creep curves at a constant stress and strain rate.
- (ii) In the second law, one tries to relate the stress and strain rate for the entire *steady*-creep domain and must therefore assume that the specimen has been under the considered state of stress for a very long time. At high stress, the actual creep rate may be larger than the minimum creep rate because of the recrystallization that commences in tertiary creep. In this state, ice ceases to remain isotropic.
- (iii) In the third flow law, one is restricting attention to secondary creep before any recrystallization has occurred. This law relates to the deformation of similar ice at all stresses.

Creep in glaciers takes place under conditions where steady tertiary or secondary creep apply. Analytically, the laws for cases (ii) and (iii) are usually represented by a power law of the form (2.19) or (2.20) but with different coefficients and exponents than hexagonal ice. The power law

$$\dot{\epsilon} = \tilde{A} \operatorname{sgn}(\sigma) |\sigma|^n \quad (2.64)$$

was suggested by Glen and, for this reason, is called *Glen's flow law* in glaciology. In metallurgy, it was introduced in 1929 by Norton [80]. The

value of  $n$  obtained by Glen for steady-state secondary creep was 4.2; if the minimum observed creep rate was used with no allowance for further deceleration, the value obtained was 3.2. Other authors also obtain values of  $n$  between 2 and 4, there is general agreement now to use  $n = 3$ , although Glen concludes that  $n \approx 3.5$  would be more appropriate. The range of validity is from 1 bar to roughly 15 bars ( $10^5 - 1.5 \times 10^6$  Pa). At very low stresses not higher than 1 to 2 bars ( $1$  to  $2 \times 10^5$  Pa), one may approximate the creep behavior by a linear viscous relationship so that  $n = 1$ . Newtonian creep behavior at low strain rates is documented by Mellor and Smith [103] and others, but there is disagreement among various authors as to whether experiments at low stresses are reliable, see Hobbs [45]. My opinion is that a dependence other than the power law must hold at very small strain rates simply because no real material can respond infinitely fast to applied strain rates. Such an argument would favour Newtonian behavior. At very high stresses where recrystallization occurs, the power law may be applied again but  $n$  may assume values here as high as 10.

The temperature-dependency of the strain rate is postulated to follow an Arrhenius type of relationship so that

$$\dot{\epsilon} = \text{sgn}(\sigma) A \exp\left(-\frac{Q}{kT}\right) |\sigma|^n \quad (2.65)$$

with activation energies in the order of 0.52–0.72 eV. At high temperatures, some authors have reported activation energies that are somewhat higher.

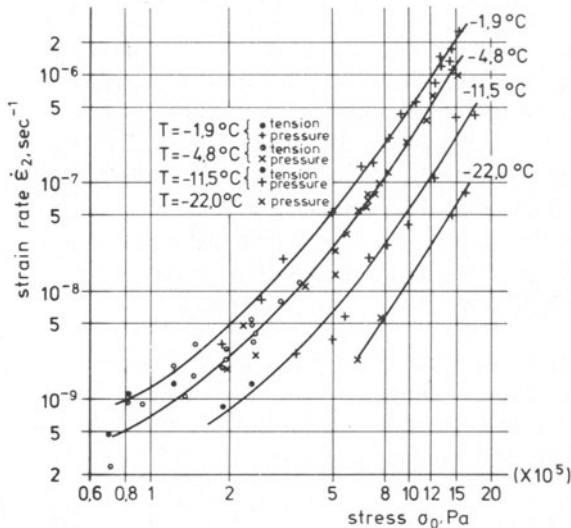


FIG. 2.17. Steady strain rate during secondary creep for polycrystalline ice as a function of stress. (From Steinemann [105].)

On a log-log plot, the power law (2.65) should be representable as a straight line. Experimentally, this is only nearly corroborated, as can clearly be seen from Figures 2.17 and 2.18, which show stress-strain-rate plots at various temperatures and for secondary and tertiary creep, respectively. It is for this reason that Steinemann proposed a flow law other than the power law, namely

$$\dot{\epsilon} = \text{sgn}(\sigma) A \exp\left(-\frac{Q}{kT}\right) f(|\sigma|) = \text{sgn}(\sigma) A \exp\left(-\frac{Q}{kT}\right) |\sigma|^{n(\sigma,n)},$$

where  $n$  varies from about 1.9 to 4.8 in secondary creep and reaches values as high as 10 in tertiary creep. Other authors, see, e.g., [32] [72] [76], have also concluded that the theoretically-based Arrhenius function is not appropriate to temperatures above 263 K. Smith and Morland [102a] summarize this research and propose an alternative temperature-dependence which is also thought to be appropriate in the practically-important temperature range, see Section  $(\beta)$  below.

$(\beta)$  *Generalization to a three-dimensional flow law.* The experimental information provided by the creep tests at steady-state creep and the power law by which stress and strain rates in these actual tests are matched, do not make a constitutive relation that could be used in the analysis of three-dimensional deformation states. On the basis of rather mild assumptions, Glen's flow law may, however, be generalized to a three-dimensional law. There were essentially two attempts to achieve this. One generalization is due to Nye [82] and is simple and the other one is due to Glen [31].

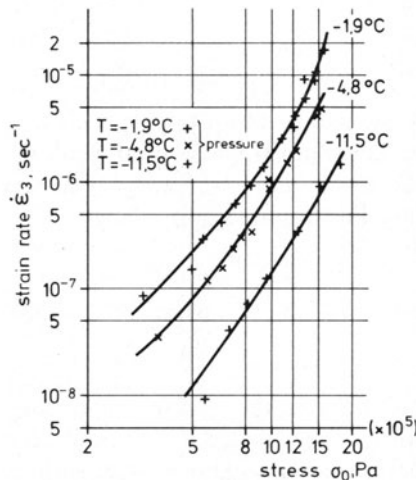


FIG. 2.18. Steady strain rate for tertiary creep of polycrystalline ice as a function of stress. (From Steinemann [105].)

The basic postulate is that polycrystalline ice is an incompressible non-linear viscous fluid. Experiments by Rigsby [96] demonstrated that hydrostatic pressure does not affect the flow law, which is justification for treating ice as incompressible. The general constitutive relation for such a fluid was obtained in Chapter 1. If it is heat-conducting, the constitutive relation of the deviatoric stress is given by

$$t'_{ij} = \hat{t}'_{ij}(\mathbf{D}, T, \nabla T), \quad (2.66)$$

where  $\mathbf{D}$  is the stretching tensor and  $T$  the temperature. The dependency on the temperature gradient is thought to be irrelevant in the constitutive relation of the stress tensor. It is common usage in glaciology to write stretching as a function of the stress. If we invert (2.66) as a function of  $\mathbf{D}$ , and also omit a dependency on temperature gradient, then

$$D_{ij} = \hat{D}_{ij}(\mathbf{t}', T) \quad (2.67)$$

is obtained, which is a form of the constitutive relation used by Nye and Glen. Ice being a fluid, the constitutive function  $\hat{D}_{ij}(\cdot)$  must be an isotropic tensor-valued function of its arguments. The methods by which such functions can be reduced to their appropriate form were given in Chapter 1. As can easily be deduced from (1.75), one necessarily has

$$D_{ij} = A\delta_{ij} + Bt'_{ij} + C t'_{ik} t'_{kj}, \quad (2.68)$$

where  $A$ ,  $B$  and  $C$  are scalar-valued functions of the temperature and the two invariants of the stress deviator  $t'_{ij}$ :

$$A = \hat{A}(t'_{(III)}, t'_{(III)}, t), \text{ etc.} \quad (2.69)$$

where

$$t'_{(II)} = \frac{1}{2} t'_{ij} t'_{ij}, \quad t'_{(III)} = \frac{1}{6} t'_{ik} t'_{kj} t'_{ji}.$$

Equation (2.68) is not yet in a form appropriate for ice, because the latter was postulated to be an incompressible material. Since the change in volume is proportional to  $\text{tr } \mathbf{D}$ , the latter must vanish if the constitutive relation (2.68) is to correctly model incompressibility. Thus

$$3A + 2Ct'_{(II)} = 0.$$

This relation can be used to eliminate  $A$  from (2.68), which yields

$$D_{ij} = -\frac{2}{3}t'_{(II)}C\delta_{ij} + Bt'_{ij} + C t'_{ik} t'_{kj}. \quad (2.70)$$

This is the most general form that the relation connecting the stress deviator and stretching can have under the stated assumptions. It contains two arbitrary functions of two stress measures and the temperature, and *these cannot be determined from any series of tests using only one kind of loading conditions, for example, compression tests*. In order to perform calculations, in

three dimensions, Nye added the further assumptions that (i) the third invariant of the stress tensor had no effect on the material response and (ii) that under a state of stress, the components of stress deviator and stretching tensor are proportional. This requires that  $C = 0$  and, furthermore, that  $B$  is only a function of the second invariant of the stress deviator  $t'_{(II)}$  and the temperature so that

$$D_{ij} = \hat{B}(t'_{(II)}, T)t'_{ij}. \quad (2.71)$$

Nye in his derivation, did not include the dependency on temperature.

So far, no use has been made of the results obtained with creep tests and, in order to invoke the conditions implied by these, we consider several simple experimental situations: (i) simple shear, (ii) simple tension or compression, and (iii) a state of stress of simultaneous shear and compression (see Figure 2.19a). We shall look at the third case only because the other two stress states can be derived from the latter by merely imposing special conditions. Denoting the shear stress by  $\tau$  and the uniaxial compression by  $P$ , the stress tensor and its deviator as indicated in the coordinate system of Figure 2.19a, can be written as

$$(t_{ij}) = \begin{pmatrix} 0 & \tau & 0 \\ \tau & -P & 0 \\ 0 & 0 & 0 \end{pmatrix}, \quad (t'_{ij}) = \begin{pmatrix} P/3 & \tau & 0 \\ \tau & -\frac{2}{3}P & 0 \\ 0 & 0 & P/3 \end{pmatrix}. \quad (2.72)$$

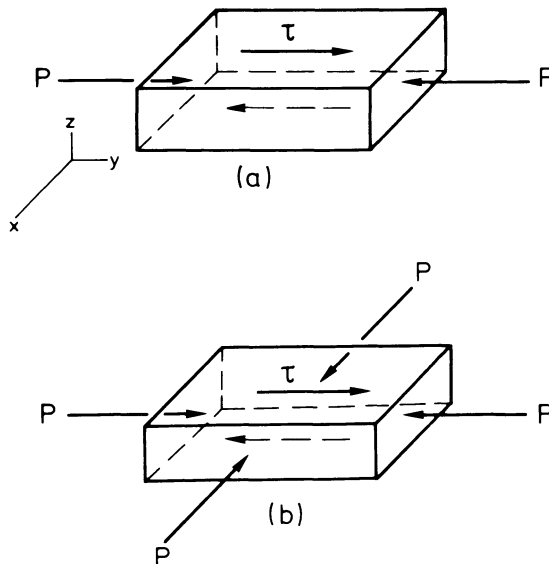


FIG. 2.19. Combined states of stresses for creep tests. (a) shear plus unilateral compression, (b) shear plus equilateral compression.

The second and third invariant of the stress deviator are

$$t'_{(II)} = \frac{1}{3}P^2 + \tau^2, \quad t'_{(III)} = -\frac{P}{2}\left(\frac{2}{g}P^2 + \tau^2\right). \quad (2.73)$$

Denoting the stretching under shear by  $\dot{\gamma}$ , ( $D_{12} = 2\dot{\gamma}$ ) and the uniaxial compression stretching  $D_{11}$  by  $-\dot{\varepsilon}$ , it is easily seen that the stretching tensor  $D_{ij}$  must be given by

$$D_{ij} = \begin{pmatrix} \dot{\varepsilon}/2 & \dot{\gamma}/2 & 0 \\ \dot{\gamma}/2 & -\dot{\varepsilon} & 0 \\ 0 & 0 & \dot{\varepsilon}/2 \end{pmatrix} \quad (2.74)$$

in the evaluation of which use has been made of the fact that the material is incompressible, so that the trace of  $\mathbf{D}$  vanishes. The second and third invariants of  $\mathbf{D}$  are

$$D_{(II)} = \frac{3}{4}\dot{\varepsilon}^2 + \frac{\dot{\gamma}^2}{4}, \quad D_{(III)} = -\frac{\dot{\varepsilon}}{4}(\dot{\varepsilon}^2 + \frac{1}{2}\dot{\gamma}^2). \quad (2.75)$$

Alternatively, these invariants can also be expressed in terms of the stress-deviator invariants. To this end, one merely uses Equation (2.70). The calculations are somewhat tedious even though they are straightforward, and what obtains reads as follows:

$$\begin{aligned} D_{(II)} &= B^2 t'_{(II)} + 2BC t'_{(III)} + \frac{1}{3}C^2 t'_{(III)}, \\ D_{(III)} &= B^3 t'_{(III)} - CB^2 t'_{(II)}^2 + \frac{4}{3}BC^2 t'_{(II)} t'_{(III)} + C^3(-\frac{1}{9}t'_{(II)}^3 + t'_{(III)}). \end{aligned} \quad (2.76)$$

If  $\dot{\gamma}$  and  $\dot{\varepsilon}$  are measured as functions of  $P$  and  $\tau$ , Equations (2.73) and (2.75) yield the second and third invariants of the stress deviator and the stretching tensor, and once these are determined, relations (2.76) allow, at least in principle, the determination of the functions  $B$  and  $C$ . Hence, a combined creep test under shear and uniaxial compression should allow us to determine the three-dimensional constitutive response (2.70).

Of course, this experimental procedure does not yet prove that the constitutive relation (2.70) is, in fact, correct for ice. If  $B$  and  $C$  are determined with the approach explained above, such a test can be performed by applying an equilateral compression, see Figure 2.19b, so that the stress tensor becomes

$$t'_{ij} = \begin{pmatrix} -P & \tau & 0 \\ \tau & -P & 0 \\ 0 & 0 & 0 \end{pmatrix}. \quad (2.77)$$

By determining the second and third invariants of the stress deviator and

the stretching tensor for this state of stress and then measuring the strain rates, agreement should be obtained with Equation (2.76) within the tolerance of experimental errors, otherwise (2.70) is inappropriate. To our knowledge, nobody has gone so far in the experimental determination of the constitutive relations for polycrystalline ice.

Steinemann did perform creep tests under shear and uniaxial compression. He measured  $\dot{\gamma}$  but not  $\dot{\varepsilon}$  so that his experiments cannot be used to determine  $B$  and  $C$ . However, we can test whether Nye's simplified version (2.71) of the flow law is a reasonable one. He assumes that the components of the stress deviator and strain are proportional. In view of relations (2.72) and (2.74) this yields

$$\frac{2\tau}{\dot{\gamma}} = \frac{\frac{2}{3}P}{\dot{\varepsilon}}. \quad (2.78)$$

This equation may serve to eliminate  $\dot{\varepsilon}$  from (2.75)<sub>1</sub> (the quantity not measured by Steinemann). Thus we obtain,

$$D_{(II)} = \frac{\dot{\gamma}^2}{4} \left( 1 + \frac{P^2}{3\tau^2} \right). \quad (2.79)$$

On the other hand, (2.76)<sub>1</sub> becomes in Nye's case

$$D_{(II)} = B^2(t'_{(II)})t'_{(II)} = f\left(\frac{1}{3}P^2 + \tau^2\right) = f(t'_{(II)}). \quad (2.80)$$

If we thus plot  $\frac{1}{4}\dot{\gamma}^2 (1 + P^2/(3\tau^2))$  against  $(\frac{1}{3}P^2 + \tau^2)$  we should obtain one single curve whether or not compression is acting. Glen performed this comparison and Figure 2.20 is a copy of his results. It shows  $\log(D_{(II)})$  as a function of  $\log(t'_{(II)})$  using the data of Steinemann's tests under combined shear and compression.

It can be seen from Figure 2.20 that test data in pure shear and those under a combined state of stress do not form a single curve in this plot. Nye's postulate of the three-dimensional flow law (2.71) thus seems to be violated. Unfortunately, the matter has not been investigated any further, but Morland [76] suggests that multiaxial creep tests be performed by which the functions  $B$  and  $C$  are determined. His approach to steady creep is a modification of the above, as he uses a different set of invariants. Morland further suggests measuring directional strain rates in all three space directions, which will give a means of checking incompressibility.

A conclusion that Equation (2.71) would be inappropriate for secondary creep seems to be premature, since insufficient information is available regarding its disproof. This is one reason (the other being the easy applicability of (2.71)) why Nye's extension of Glen's flow law is still predominantly used in glaciology. Newer developments, however, point at a replacement of it. Such a replacement will be briefly discussed below. It remains here to

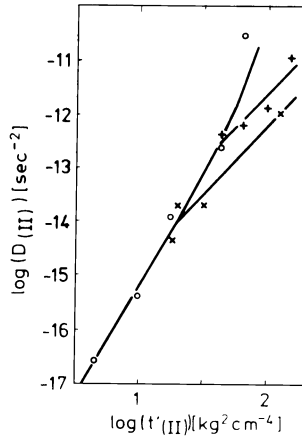


FIG. 2.20. A graph of  $\log(D_{(II)})$  against  $\log(t'_{(II)})$  using the data from Steinemann's tests under combined shear and compression. If the assumption suggested by Nye were true, all the points should lie on one curve. The symbols used for points have the following meaning: ○ points derived from tests in simple shear, × points derived from tests under a shear stress of  $4.20 \text{ kg cm}^{-2}$ , with superimposed compressive stresses from 0 to  $18 \text{ kg cm}^{-2}$ , + points derived from tests under a shear stress of  $6.59 \text{ kg cm}^{-2}$  with superimposed compressive stresses from 0 to  $18 \text{ kg cm}^{-2}$  ( $1 \text{ kg cm}^{-2} = 9.81 \text{ Pa}$ ). (From Glen [31].)

fit the coefficient function to the experimentally determined function (2.65). Since in pure shear  $P \equiv 0$ , (2.80) may be written as  $\dot{\epsilon}_{12}^2 = B^2 \tau^2$  and so a comparison with (2.65) yields

$$B = A t'^{(n-1)/2} \exp\left(-\frac{Q}{K T}\right) \quad (2.81)$$

or more generally

$$B = \tilde{A}(T) t'^{(n-1)/2}, \quad (2.81b)$$

where  $\tau^2$  has been identified with the second stress deviator invariant. Smith and Morland [102a], fitting data of Mellor and Testa [73], propose the relations

$$\tilde{A}(T) = 1 + \alpha(e^{\beta \bar{T}} - 1) \quad \text{or} \quad \tilde{A}(T) = \alpha_1 e^{\beta_1 \bar{T}} + \alpha_2 e^{\beta_2 \bar{T}}, \quad (2.82)$$

where  $T = T_0 + 20\bar{T}$  is the Kelvin temperature and  $T_0 = 273.15 \text{ K}$  and the coefficients  $\alpha$  and  $\beta$  are the constants listed in Table 2.4. They find two different 'best' fits for the second of (2.82).

Hence, we were able to determine Nye's extension of Glen's flow law of ice on the basis of simple shear tests only. The same results would also have been obtained from unilateral compression tests.

Before we go on to the discussion of how (2.71) is used to solve ice-flow

TABLE 2.4. Values for the constants  $\alpha$  and  $\beta$  arising in (2.82) according to Smith and Morland [102a].

$\alpha = 0.986$	$\beta = 6.4426$
$\alpha_1 = 0.9316$	$\beta_1 = 6.5538$
$\alpha_2 = 0.7242$	$\beta_2 = 11.9567$
$\alpha_3 = 0.0686$	$\beta_3 = 1.4410$
$\alpha_4 = 0.3438$	$\beta_4 = 2.9494$

problems, we would like briefly to touch upon certain constitutive equations which have been or could be used as material response under steady-state secondary creep.

(γ) *Other flow laws.* Glen's power law for secondary creep suggests various alternatives as possible constitutive relations for ice. In uniaxial compression, if the normal stress  $\sigma$  is plotted as a function of strain rate  $\dot{\epsilon}_{11} (= \dot{\epsilon})$ , then

$$\dot{\epsilon} = \text{sgn}(\sigma)A|\sigma|^n, \quad \sigma = \text{sgn}(\dot{\epsilon})\left[\frac{|\dot{\epsilon}|}{A}\right]^{1/n} \quad (2.83)$$

is obtained, which is a parabola of order  $n$ . For  $n = 1$ , Equation (2.83) is a *linear viscous fluid*, see Figure 2.21a. Because of the mathematical difficulties that emerge when non-linear constitutive relationships are used, certain problems in glacier flow are still solved using such a linear viscous model. As  $n$  approaches infinity, the stress-strain-rate relationship approaches the

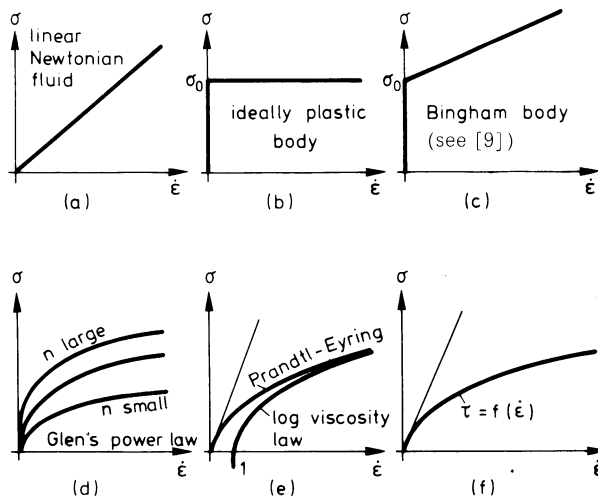


FIG. 2.21. Different types of relations between stress and stretching.

step function (Figure 2.21b). This behavior is that of an *ideally plastic body*, see Nye [82], in which, to a given stress, there is either no flow,  $\tau < \tau_0$ , or if  $\tau = \tau_0$  there is no unique stretching. When treating ice as a plastic material, the yield stress should be taken as 1 bar ( $= 10^5$  Pa). Except for certain bearing-capacity problems of floating ice plates, the plastic law has now been abandoned. Whereas the response curves of Figures 2.21a, b are far from matching experiments, more accuracy would result from the so-called *Bingham body* [9], for which there is a definite yield stress, but which shows linear behavior between stress and stretching beyond this stress, Figure 2.21c. To our knowledge, the Bingham body has never been suggested in glaciology. For finite  $n$  in the range  $1 < n < \infty$ , Equation (2.83) corresponds to one of the curves in Figure 2.21d. Initially, that is for small  $\dot{\varepsilon}$ , stress changes infinitely fast in this case, because  $d\sigma/d\dot{\varepsilon} \rightarrow \infty$  as  $\dot{\varepsilon} \rightarrow 0$ . This is a disadvantage of the power law which, apart from the observations of Steinemann that were recalled in Figures 2.17 and 2.18, calls for generalizations of Glen's flow law.

The most simple extension of Equation (2.83), since  $n$  may have integer values, is the *polynomial expansion*

$$\dot{\varepsilon} = \sum_{j=1}^N A_j(\sigma) \sigma^j, \quad (2.84)$$

a formula which, for  $N = 3$ , was proposed by Lliboutry [65]. Lliboutry showed that a better fit of Glen's 1955 data could be obtained with (2.84) than was possible with the power law. With  $A_1 \neq 0$ ,  $d\sigma/d\dot{\varepsilon}$  no longer becomes infinitely large as  $\dot{\varepsilon} \rightarrow 0$ . In fact, for small strain rates (or stresses), Equation (2.84) represents a Newtonian behavior.

Similar extensions of Glen's flow law were also independently proposed by Colbeck and Evans [15], Hutter *et al.* [50, 51, 52], Smith and Morland [102a], Thompson [107], and Williams [119]. The simplest extension is

$$\dot{\varepsilon} = A(T) f(\sigma^2) \sigma \quad (2.85a)$$

with

$$f(\sigma^2) = (\sigma^2)^{(n-1)/2} + k. \quad (2.85b)$$

It eliminates the above-mentioned singularity, but was introduced by Hutter, Thompson, and Williams for purely mathematical reasons. Yet another possibility is the so-called Prandtl–Eyring flow model, [28, 29] for which

$$\dot{\varepsilon} = \tilde{A}(T) \sinh(\beta' \sigma). \quad (2.86)$$

The function  $f$  can easily be identified and  $\tilde{A}$  is usually given as  $\tilde{A} = A' \exp(-Q/KT)$ . For small stresses, Newtonian behavior is obtained, but as stresses become large one has  $\dot{\varepsilon} \rightarrow \frac{1}{2} \tilde{A} \exp(P' \sigma)$  or, alternatively

$$\sigma = \frac{1}{\beta'} \left[ \ln \frac{\dot{\varepsilon}}{\tilde{A}(T)} \right]. \quad (2.87)$$

which was called the *logarithmic viscosity law* by Prandtl [91], see Figure 2.21e. Clearly, whereas the Prandtl–Eyring model shows the correct behavior at small stresses, this is not so for (2.87).

An alternative expression to Equation (2.85) suggested by Garofalo [27] and used by Ramseier and Dickins [93] is

$$f(\sigma^2) = \frac{[\sinh(\beta''\sqrt{\sigma^2})]^n}{\sqrt{\sigma^2}} \quad (2.88)$$

with an Arrhenius type rate factor  $\tilde{A}(T) = A'' \exp(-Q/KT)$ . For  $\beta''|\sigma| \ll 1$  the flow law (2.88) in this case becomes

$$\dot{\varepsilon} \simeq \tilde{A}(T)\beta'' \operatorname{sgn}(\sigma)|\sigma|^n$$

and thus agrees with Glen's flow law. For large values of  $\beta''|\sigma|$ , on the other hand,

$$\dot{\varepsilon} \simeq \frac{\tilde{A}(T)}{2^n} \operatorname{sgn}(\sigma) \exp(n\beta''|\sigma|)$$

is obtained, and this corresponds to the logarithmic viscosity law of Prandtl.

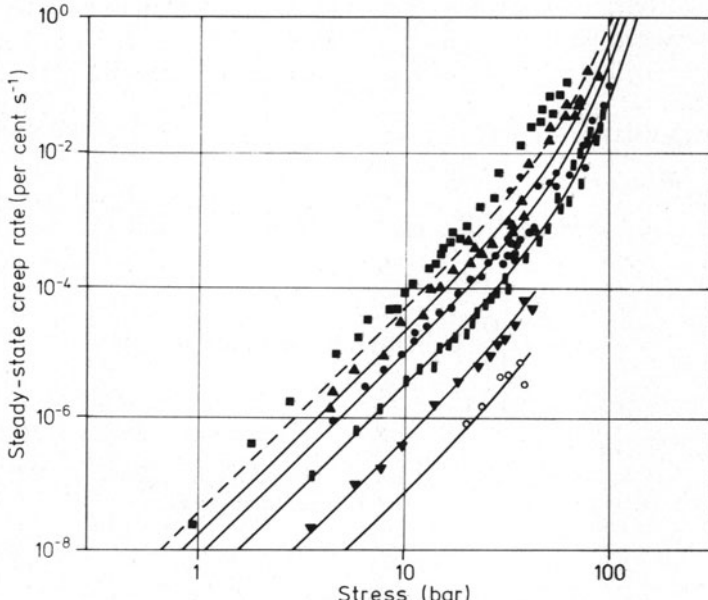


FIG. 2.22. Steady-state creep for the secondary flow of polycrystalline ice in uniaxial compression against applied stress. ■—2°C, ▲—8°C, ●—14°C, ■—22°C, ▼—34°C, ○—45°C. The curves are calculated sinh functions based on all the experimental points between –2 and –48°C. (From Barnes *et al.* [5] with changes.)

Clearly, Garofalo's formula does not remove the singularity at small stresses; thus the Prandtl–Eyring law (2.86) should probably be preferred, this in spite of the good fit of (2.88) with experimental data, see Barnes *et al.* [5]. Yet when trying to find values for the free constants  $A'$  and  $\beta'$  of (2.86) it was found that reasonable agreement between (2.86) and (2.88) could be found only for stresses below 50 bars ( $5 \times 10^6$  Pa) and that large deviations occurred between the two curves at stresses in the range from 50 to 100 bars ( $5 \times 10^6$  to  $10^7$  Pa). The steady-state creep data of Barnes *et al.* [5] are shown in Figure 2.22 together with the curve fit as obtained with formula (2.88) and the values of the parameters as shown in Table 2.5.

If a linear term is added, the behavior of the stress-strain relation at large stresses will not be affected, because the contribution from the  $\sinh^n$  term will override it. On the other hand, at low stresses, the linear term will dominate. Hence

$$\dot{\varepsilon} = A'' \exp\left(-\frac{Q}{kT}\right) \left\{ \frac{\sigma}{\mu} + \operatorname{sgn} \sigma \sinh^n(\beta'' |\sigma|) \right\} \quad (2.89)$$

incorporates both, the approximate low stress behavior as well as a good fit at high stresses.

Alternatively, the law (2.88) can be put in a form akin to the Prandtl–Eyring law by setting

$$\sinh^n(\beta'' |\sigma|) = \sinh^n(F(|\sigma|))$$

from which we easily deduce

$$\begin{aligned} F(|\sigma|) &= \sinh^{-1} \{ \sinh^n(\beta'' |\sigma|) \} \\ &= \ln \{ \sinh^n(\beta'' |\sigma|) + [1 + \sinh^{2n}(\beta'' |\sigma|)]^{1/2} \} \end{aligned} \quad (2.90)$$

so that

$$\begin{aligned} \dot{\varepsilon} &= A'' \exp\left(-\frac{Q}{kT}\right) \operatorname{sgn}(\sigma) \sinh \{ \ln [\sinh^n(\beta'' |\sigma|) + \right. \\ &\quad \left. + [1 + \sinh^{2n}(\beta'' |\sigma|)]^{1/2}] \}. \end{aligned} \quad (2.91)$$

TABLE 2.5. Values of the parameters in Equation (2.89) derived by Barnes *et al.* [1971] from their measurements on polycrystalline ice over the range 1 to 100 bar.

$A''$ (percent s <sup>-1</sup> )	$\beta''$ (bar)	$n$	$Q$ (eV)	Temperature range (°C)
$4.60 \times 10^{20}$	$2.79 \times 10^{-2}$	1.3	1.3	-2 to -8
$3.14 \times 10^{12}$	$2.54 \times 10^{-2}$	3.08	0.8	-8 to -14
$1.88 \times 10^{12}$	$2.82 \times 10^{-2}$	2.92	0.8	-14 to -22
$2.70 \times 10^{12}$	$2.62 \times 10^{-2}$	3.15	0.8	-8 to -45

Adding a quasilinear term, yields

$$\dot{\epsilon} = A'' \exp\left(-\frac{Q}{kT}\right) \operatorname{sgn}(\sigma) \sinh \left\{ \frac{|\sigma|}{\mu} + \ln [\sinh^n(\beta''|\sigma|) + [1 + \sinh^{2n}(\beta''|\sigma|)]^{1/2}] \right\}, \quad (2.92)$$

which, firstly, is now in a form resembling the Prandtl–Eyring structure, secondly agrees with the curve fitting of Barnes *et al.* and thirdly avoids the singular behavior of the Garofalo formula (2.88).

Further, polynomial fits to data from Mellor and Testa, Glen, Steinemann and others by Smith and Morland [102a] indicate that there is, in general, no common fit to data obtained by different authors on different ice specimens. Authors generally agree that above 263 K an Arrhenius-type rate factor is inappropriate but that experimental evidence is not sufficient.

On the other hand, it is worth noting that the Prandtl–Eyring law has a theoretical foundation in the so-called *rate process theory*, originally founded by Prandtl [91] and subsequently further developed, see Glasstone *et al.* [28]. The structure of the theory is different from that of Weertman [118] and makes no use of dislocation mechanisms, but it provides support for the Prandtl–Eyring law rather than Glen's flow law, as does Weertman's theory.

The Prandtl–Eyring law is sufficiently important to present its derivation. Such a derivation may, perhaps, give a clue as to the theoretical foundation of (2.92). The basis of the law is statistical mechanics. Accordingly, the body is thought to be composed of individual particles which, due to their thermal state, oscillate about an equilibrium position. Both the thermal energy and the strains (or stresses) applied to the body contribute to this motion. If sufficient energy is available, the bonds between individual particles become loose. The particles move relative to each other and form new bonds with neighboring particles. According to statistical mechanics, the thermal energy and the stresses are sources of the activation energy  $Q$ . The average thermal energy per particle is  $kT$ , where  $k$  is Boltzmann's constant and  $T$  is the absolute temperature; hence  $Q/kT$  is a measure of the activation of an individual particle. The distribution among them is described by the Boltzmann equation. Accordingly, the probability that a particle is in an energy state greater or equal to  $Q$  is

$$p(Q) = \text{constant} \cdot \exp\left(-\frac{Q}{kT}\right).$$

It may also be shown, see [28], that the mean frequency of thermal oscillations is  $kT/h$ , where  $h$  is Planck's constant. The number of times (per second),  $v$ , that any bond acquires sufficient thermal-free energy to surmount the energy

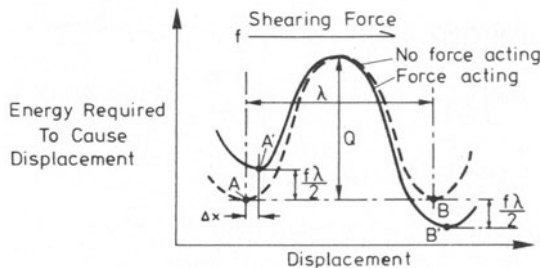


FIG. 2.23. Influence of a shearing force on energy barriers opposing particle movement.

barrier of height  $Q$  is, therefore,

$$v = \frac{kT}{h} \exp\left(-\frac{Q}{kT}\right).$$

In the absence of a directional potential such as a shearing stress, bonds are activated in all directions with equal frequency and there is no tendency for particle movement in any one direction. If, however, a shearing force  $f$  as shown in Figure 2.23, is acting, a distortion of energy barriers results. The small horizontal displacement of energy minima from  $A$  to  $A'$  and  $B$  to  $B'$ , denoted by  $\Delta x$  is instantaneous and represents an elastic deformation. As a particle oscillates through its energy minimum, and up and down the slopes of the energy barrier, the force  $f$  does work with the particle as it moves to the right, and against the particle as it moves to the left (Figure 2.23). In the case of a vibration that carries a particle to the top of an energy barrier to the right, the force contributes an energy  $f\lambda/2$ , if the barrier is symmetrical and  $\lambda$  represents the distance between successive equilibrium positions.\* The effect of force  $f$  therefore is to lower the potential barrier  $f\lambda/2$  in the direction of the force and to raise it  $f\lambda/2$  in a direction opposite to the force.

Thus, the frequency of activation for movement to the right becomes

$$\rightarrow v = \frac{kT}{h} \exp\left\{-\frac{(Q - (f\lambda/2))}{kT}\right\}$$

and to the left

$$\leftarrow v = \frac{kT}{h} \exp\left\{-\frac{(Q + (f\lambda/2))}{kT}\right\}.$$

The net frequency of displacements to the right is therefore

\*Note that in writing down this relation it was assumed that  $f$  remains constant as the particle moves to reach the top of the potential barrier.

$$\overrightarrow{v} - \overleftarrow{v} = \frac{kT}{h} \left\{ \exp \left[ \frac{-(Q - (f\lambda/2))}{kT} \right] - \exp \left[ \frac{-(Q + (f\lambda/2))}{kT} \right] \right\},$$

which yields

$$\overrightarrow{v} - \overleftarrow{v} = 2 \frac{kT}{h} \exp \left( \frac{-Q}{kT} \right) \sinh \left( \frac{f\lambda}{2kT} \right).$$

This represents the frequency of motion of a single bond. There are  $s$  number of bonds per unit length, and assuming, on the average, a displacement  $\lambda'$  occurs in the direction of  $f$  each time a bond ruptures, the total displacement per unit length must be

$$\begin{aligned} \dot{\epsilon} &= s\lambda' (\overrightarrow{v} - \overleftarrow{v}) \\ &= 2s\lambda' \frac{kT}{h} \exp \left( -\frac{Q}{kT} \right) \sinh \left( \frac{f\lambda'}{2kT} \right). \end{aligned}$$

Since  $f$  is proportional to the shear stress  $\tau$  and because the constants of the model have a phenomenological meaning, this may equally be written as

$$\dot{\epsilon} = A' \exp \left( -\frac{Q}{kT} \right) \sinh (\beta' \tau),$$

which is exactly (2.86).

From this derivation it is not difficult to see at which point the above model must be generalized to obtain the more general creep law (2.85). One must assume path-dependent restoring forces  $f = \mathfrak{F}(\lambda)$  for which case  $f\lambda/2$  in the above formulae must be replaced by  $\int_0^\lambda \mathfrak{F}(\lambda') d\lambda'$  which alternatively may be regarded as a function of  $f$ . So for such path-dependent restoring forces, one finds

$$\dot{\epsilon} = A'' \exp \left( -\frac{Q}{kT} \right) \sinh (F(\tau)),$$

where  $F$  is left undetermined. Consequently, all creep models presented above can be based on a statistical formulation – though a very weak one, see Assur [3], Hutter [48].

The flow laws of this section can be generalized to three dimensions, if Nye's postulates are invoked. In fact, Equation (2.81) may then be written as

$$D_{ij} = \tilde{A}(T) f(t'_{II}) t'_{ij} \quad (2.93)$$

with a rate factor  $\tilde{A}(T)$  usually given by the Arrhenius law and

$$\begin{aligned}
 & (t'_{(II)})^{(n-1)/2} + k, \quad \text{for (2.85)} \\
 & \frac{[\sinh(\beta''\sqrt{t'_{(II)}})]^n}{\sqrt{t'_{(II)}}}, \quad \text{for (2.89)} \\
 f(t'_{(II)}) = & \frac{1/\mu + [\sinh(\beta''\sqrt{t'_{(II)}})]^n}{\sqrt{\tau'_{(II)}}}, \quad \text{for (2.89)} \tag{2.94} \\
 & \frac{\sinh\{1/\mu\sqrt{t'_{(II)}} + \ln[\sinh^n(\beta''\sqrt{t'_{(II)}}) + [1 + \sinh^{2n}(\beta''\sqrt{t'_{(II)}})]^{1/2}]\}}{\sqrt{t'_{(II)}}} \quad \text{for (2.92).}
 \end{aligned}$$

The law (2.94)<sub>1</sub> has advantages in analytical calculation and (2.94)<sub>2,3,4</sub> can be used for numerical calculations. Incidentally, in this regard it should be observed that the singular constitutive laws will, in many numerical applications (finite elements and finite difference techniques), lead to singular numerical behavior.

So far, only viscosity has been taken into account and no elastic effects have been considered. For processes of moderately short duration, elastic effects may play some role. In this case the postulations that ice is a fluid can no longer be retained, since stress would depend on strain only through density (see Chapter 1), in which case the material would be compressible. When including elasticity effects, therefore, constitutive relations should be established for the Piola–Kirchhoff stress deviator (see Chapter 1, (1.68)), as e.g.

$$T_{AB}^{P'} = \hat{T}_{AB}^{P'}(\mathbf{E}, \dot{\mathbf{E}}, T), \tag{2.95}$$

where  $\mathbf{E}$  is the Lagrangian strain tensor and  $\dot{\mathbf{E}}$  its material time derivative. The most general isotropic tensorial function has, for this case, been derived by Smith [103] and Wang [112], yet we need not write it down, because material scientists mostly start from the postulation that the material is *viscoplastic*. In other words, the elasticity effects are formally separated from the viscous effects, according to

$$T_{AB}^P = {}_1\hat{T}_{AB}^P(\mathbf{E}, T) + {}_2T_{AB}^P(\dot{\mathbf{E}}, T). \tag{2.96}$$

The response functions may then be taken as

$${}_1\hat{T}_{AB} = \mu\{2E_{AB} - \frac{2}{3}E_{CC}\delta_{AB}\}, \quad {}_2T_{AB} = B(\dot{E}_{(II)}, T)\dot{E}_{AB}. \tag{2.97}$$

$\mu$  is the shear modulus,  $\dot{E}_{(II)} = \frac{1}{2}\dot{E}_{AB}\dot{E}_{AB}$  and  $B$  an appropriately selected function to match the creep experiments. Equations (2.96) and (2.97) satisfy the incompressibility condition. In the material science literature, (2.96) is often only written down for the shear stress or the compressive stress and seldom is any attempt made to generalize the given laws to three dimensions. A law of the form (2.96), but not necessarily with the specifications (2.97), has the capability of modelling stress-induced anisotropy.

Before concluding this section, mention should be made that the above treatment of constitutive relations for ice limits the attention to secondary steady creep. Transient, non-linear creep must most likely be modeled with a constitutive relationship involving hereditary effects, see Chapter 1. One promising class is that of materials with bounded memory; in particular, a material involving the Rivlin–Ericksen tensors  $A_{(n)}$  of degree  $n$  might be suggested. Further, stress rates could be included, as was in Chapter 1, (1.82). In fact, Morland and Spring [76, 76a, 104a] postulate a fluid and solid of the type (1.82) and (2.96) and demonstrate the uniaxial creep curves at a constant strain rate and a constant stress can be reasonably matched in the ranges of primary, secondary, and tertiary creep. The solid law exhibits stress-induced anisotropy, whereas the fluid law does not, but it should be clear that investigations which limit attention to uniaxial stress states, or to simple shear, can not serve as models for the full three-dimensional stress state. Considerations of continuum mechanics are indispensable in these instances, and promising progress in multiaxial stress states seems likely only if methods of continuum mechanics are combined with those of common material science.

#### 4. *The Mechanical Properties of Sea Ice*

The physical properties of sea ice differ from those of polycrystalline freshwater ice mainly due to higher salinity. Because of the salt content, sea ice is not a one-component material but a composite consisting of clusters of pure ice crystals, liquid brine inclusions, and solid salt. Determination of the brine content is difficult to achieve, for it depends on the amount and composition of salt present. Basically, for a given amount and composition of salt, the *phase diagram* determines, at a given temperature, the thermodynamic equilibrium state of the relative amounts of ice, water, solid salts, and salts in solution. The temperature at which the phase diagram does not allow any ice to exist is called the *melting temperature*. It is a function of the composition and amount of salt present. At temperatures below the melting point, a certain volume fraction of the original solution has crystallized as ice. It is generally the largest portion of the salt-water mixture. The other part of the original solution is still liquid and contains all the salt. This brine forms liquid voids in an otherwise pure polycrystalline ice matrix. Of course, the concentration of salt in these inclusions is higher than in the original sea water and the temperature is always at the melting point of that concentration. If this were not so, ice would melt or freeze at the boundary of the void until the remaining brine would be in thermal equilibrium. If now the temperature is lowered still further, the voids become smaller by freezing and the salt concentration becomes higher and higher. There is an upper bound of this concentration at which particular salt components can stay

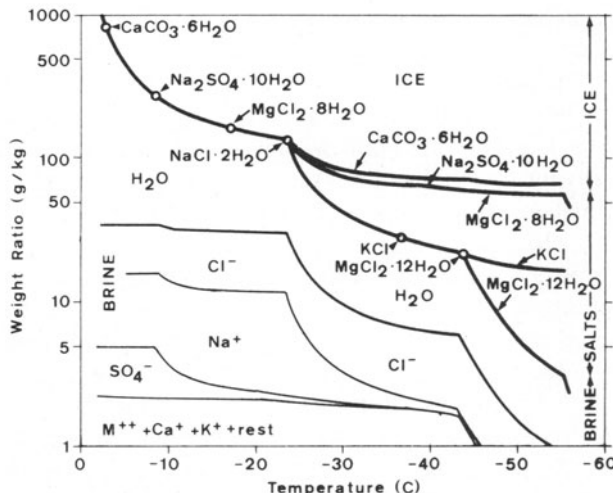


FIG. 2.24. Phase diagram for standard sea ice. (From [2].)

in solution and do not precipitate as solid salt. The temperatures at which certain components precipitate can regularly be seen as distinct discontinuities in the phase diagram (Fig. 2.24).

It is clear that the presence of brine inclusions, and at the low temperatures of the solid salts, along the grain boundaries must have an influence upon the mechanical behavior of sea ice. Of course, in order to treat sea ice as a composite, significant characteristic lengths of the physical processes must be longer than the usual mean diameters of the voids. This indicates why one usually regards ice as a mixture consisting of a fairly isotropic matrix of polycrystalline ice with randomly-oriented more or less spherical or cylindrical inclusions of brine. The resulting composite material may then be regarded as an isotropic body to which the postulates of elastic, viscoelastic, plastic, non-linear viscous behavior, may be applied. Needless to say, the phenomenological constants of such a composite must be different from those of pure polycrystalline ice. Indeed, the volume porosity of brine must play a certain role. Since in a stressed body, a cavity generates stress concentrations which generally lower the failure strength of such a specimen in comparison to a specimen without a cavity, it is to be expected, that failure strength will particularly strongly depend on brine content.

Basic relationships of the mechanical properties of sea ice have been developed, notably by Anderson [1], Assur [2, 4], Langleben [61–64], Pounder [88–90], Weeks [113–116], Savel'ev [98] and Zubov [122]. Reviews are by Assur [2] and Weeks and Assur [4, 117].

#### (a) The phase diagram of standard sea ice and its brine content

Because the actual volume fraction of brine in sea ice depends on the composition and amount of salts, and both vary within the ocean, it is impor-

tant that one agrees on a representative composition and concentration of the salts contained in sea water. Such a standardization has been introduced by Assur [2], and the ice resulting from it is called *standard sea ice*. More recent phase diagrams were introduced by Richardson [95].

As explained above, the phase diagram specifies the relative volumes of ice, brine, and solid salts that coexist in standard sea ice at thermal equilibrium at a given temperature. Figure 2.24 shows the phase diagram as presented by Assur. It gives the amount of brine, ice, and solid salt in the system and indicates the temperature of crystallization of the solid salts  $\text{CaCO}_3 \cdot 6\text{H}_2\text{O}$ ,  $\text{Na}_2\text{SO}_4 \cdot 10\text{H}_2\text{O}$ ,  $\text{NaCl} \cdot 2\text{H}_2\text{O}$ , etc. According to Weeks and Assur [117], the diagram is less reliable at temperatures below  $-35^\circ\text{C}$ . But this is no serious drawback, because sea ice is rarely colder than  $-30^\circ\text{C}$ .

The phase diagram of sea ice depends on the freezing point of brine. Since Cl is the major ion component in sea water, original determinations of the freezing point were in terms of the Cl content. The proper parameter, however, is the ratio of dissolved salts to pure water. At low concentrations, the relation is linear as can be seen from Figure 2.25. At  $-8^\circ\text{C}$ , the slope is discontinuous and the freezing point follows a different linear relationship. The discontinuity of the slope coincides with the crystallization of  $\text{NaSO}_4 \cdot 10\text{H}_2\text{O}$ . At  $-23^\circ\text{C}$ ,  $\text{NaCl} \cdot 2\text{H}_2\text{O}$  begins to precipitate. More complicated relations appear below this temperature as can be seen from Figure 2.25.

It is important to establish whether selective brine drainage causes any significant variation in the ratios of the ions in sea ice. According to Weeks and Assur [117], the current literature is inconclusive in this regard. More-

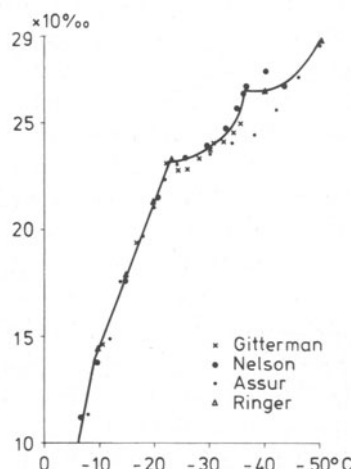


FIG. 2.25. Freezing point of brine as a function of the ratio of dissolved salts to pure water. (From Richardson [95].)

over, if brine inclusions are not isolated but connected with veins along grain boundaries, it is feasible that salt may be drained out of the composite by diffusive processes, so that the salt concentrations in the brine diminish and may ultimately cause a composition of sea water with much lower salinity than the 34‰ of standard sea ice. The literature is also inconclusive in this regard.

Assur's phase diagram can be used to derive mathematical expressions relating the volume porosity of brine, temperature, and salt content. For salt concentrations of 34‰ the following relations between volume porosity  $n$ , salt concentration  $s$ , and a temperature  $\theta$  can be derived, Hutter [49]:

$$n = \begin{cases} 0.05058(s - s_0)(-\theta)^{-0.95}, & \theta_f \geq \theta \geq -5^\circ\text{C}, \\ 0.0429(s - s_0)(-\theta)^{-0.8519}, & -5^\circ \geq \theta \geq -23^\circ\text{C}, \\ 0.00503(s - s_0)(-\theta + 21)^{-0.761}, & -23^\circ \geq \theta \geq -50^\circ\text{C}. \end{cases} \quad (2.98)$$

Here,  $s$  is the salinity (in absolute units) and  $s_0$  the amount of salt drained out. This latter parameter has a substantial influence on the material constants, as we shall see. In (2.98),  $\theta$  is not the true temperature measured in centigrades. It rather represents a temperature difference which can be written as

$$\theta = (T - T_f - T_0), \quad (2.99)$$

where  $T$  is now temperature,  $T_f$  freezing temperature at a given salinity (both in centigrade) and  $T_0$  is given by

$$T_0 = -0.04296(s - s_0)^{1.053}, \quad (\text{in centigrades}). \quad (2.100)$$

Frankenstein and Garner [26] suggest a different fit of the Assur data, namely

$$n = \begin{cases} s \frac{52.56}{T} - 2.28, & -0.5^\circ \geq T \geq -2.06^\circ, \\ s \frac{45.917}{T} + 0.930, & -2.06^\circ \geq T \geq -8.02^\circ, \\ s \frac{43.795}{T} + 1.189, & -8.2^\circ \geq T \geq -22.9^\circ, \end{cases} \quad (2.101)$$

but this bears the disadvantage that  $n(T_f) \neq 1$  in general. Calculations should therefore be based on the representations (2.98).

As a result of the presence of brine inclusions, the composite material 'pure ice + brine inclusions' gives rise to effective material constants which are functions of the material constants of pure ice at a certain temperature, the concentration of brine inclusions and their shape. In the most general situation, their mathematical determination is difficult to attempt, but certain problems have been attacked. At small concentrations, where it may be justi-

fiable to assume that interactions of brine inclusions are negligible, calculations exist for spherical and ellipsoidal holes, and rigid and fluid elastic inclusions.

Unfortunately, the mechanical properties of sea ice are not as closely known as those of freshwater ice. Detailed investigations exist for the elastic properties and for various failure strengths. Investigations regarding the relaxation functions of linear viscoelasticity and the creep behavior, as well as the dependency of these on brine content, are not available to date. These behaviors should be studied, however, if progress in the mechanical behavior of sea ice is to be made.

### (b) Elastic properties

We assume that the ice under investigation is polycrystalline with inclusions which are random in orientation and distribution. The resulting composite may then be treated as an isotropic body.

Young's modulus can either be determined by dynamic or static experiments, and generally one would expect different values for either one. Dynamic experiments either aim at determining the wave speed of propagating waves or exploring the frequency relations of bodies in different vibration modes. Weeks and Assur [117], Weeks [115], and Schwarz and Weeks [100] have reviewed the state of the art. They found that Young's modulus varies from  $1.7$  to  $5.7 \times 10^9 \text{ N m}^{-2}$  when measured by flexural waves and from  $1.7$  to  $9.1 \times 10^9 \text{ N m}^{-2}$  when determined by *in-situ* body-wave velocities. This is reasonable, for the flexural wave velocity is controlled by the overall properties of the ice sheet, while the body-wave velocity is controlled by the

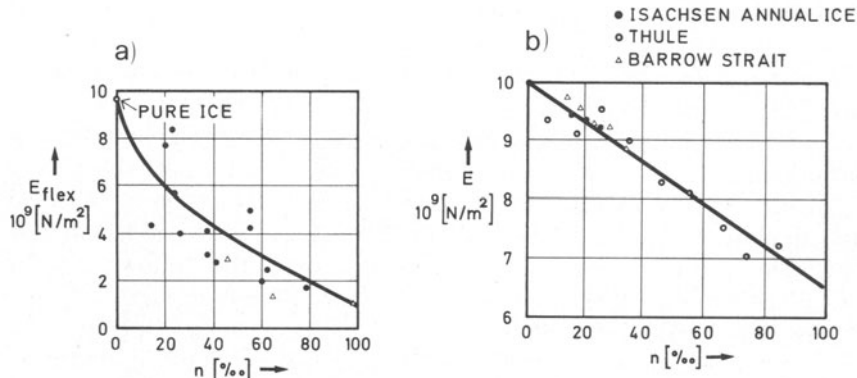


FIG. 2.26. Elastic modulus of arctic sea ice as a function of brine content (volume porosity), from [100]. (a) As determined by seismic measurements. (Anderson [1] (1958)). The three triangular points are from the static tests performed by Dykins [22]. (b) As determined by small specimen tests of Langleben and Pounder [63, 64].

the high-velocity channel in the usually colder and stronger upper portion of the ice. Figure 2.26 summarizes the experimental results of several authors. For volume porosities smaller than  $n \approx 0.15$  it seems firmly established that  $E$  varies linearly with  $n$ , as can be seen from Figure 2.26b. For higher porosities, no firm experiments are available and neither are analytical or numerical investigations. Schwarz and Weeks [100] quote recent Russian studies (Slesarenko and Frolov, 1974) which suggest that at voluminous fractions of brine content larger than 0.1, the value of  $E$  decreases more slowly, thus becoming a weak function of brine content at values in excess of 0.15. This is what one expects intuitively. Indeed, for  $n = 0$  one must necessarily have  $E = 0$ . The linear fit of Figure 2.26b may therefore be extrapolated to match these conditions. For computational purposes, such extrapolations are needed. Hutter [47, 49] uses a relationship which in the low porosity range agrees with the linear law suggested by Weeks and Assur [117]. At porosities  $n > 0.15$ , a transition to a slow decrease is used, such that  $E = 0$  for  $n = 0$ . Hutter's functional relation is

$$\frac{E}{E_0} = \begin{cases} 1 - 5n, & 0 \leq n < 0.15, \\ 47.168 \cdot (0.15 - n)^3 - 45.97 \cdot (0.15 - n)^2 + \\ + 0.5 \cdot (0.15 - n) + 0.25, & 0.15 \leq n < 0.4, \\ 0.06 \cdot (1 - n), & 0.4 \leq n \leq 1, \end{cases} \quad (2.102)$$

with

$$E_0 = 9.21 \cdot (1 - 0.00146T) \times 10^9, [\text{N m}^{-2}].$$

It would be most illuminating if this relation, especially the appropriateness of the functional relation at large porosity, could be tested by some analytical, numerical or experimental procedure.

It is perhaps noteworthy to point out that theoretical investigations regarding effective elastic moduli in a two-component mixture of elastic constituents, one of which exists as ellipsoidal inclusions, have been undertaken by various authors. The first paper dealing with the subject is probably that of Einstein [23], who evaluated the effect of a dilute suspension of spherical inclusions on the viscosity of the buck fluid, which was treated as incompressible. The incompressible fluid was subsequently further followed up for ellipsoidal rigid and liquid inclusions by Taylor [106], Batchelor [7, 8] and others. The elastic solid body with spherical holes at dilute suspension was investigated by Mackenzie [69]. The influence of an elliptical elastic inclusion on the elastic response of a solid in which it is embedded has been computed by Eshelby [24]. Wu [120] subsequently used this solution to derive a system of integral equations relating the compliances of the composite-body to those of the matrix, of the inclusions and volume concentration of these. He found that the effective elastic moduli differ for small concen-

trations from those of the matrix according to the shape of the ellipsoidal inclusions; penny-shaped inclusions have a much larger effect than elongated cylinders. Nur [81], in series of papers on the effect of cracks on the wave speeds in rocks, restricted considerations to hollow penny-shaped cracks but allowed for an arbitrary direction-distribution function of the inclusion, which may also have a nonelliptical form.

Schwarz and Weeks [100] also quote other less recent theoretical studies by Hashin, whose predictions seem not to be in conformity with the observation that deviations from the linear relation should occur at porosities as low as 0.15. It would be most illuminating if this question could be settled.

Knowledge of Young's modulus does not suffice to describe an elastic body. A second phenomenological parameter is needed. As far as the Poisson ratio is concerned, experiments seem to be inconclusive. Nevertheless, Weeks and Assur believe that

$$\nu = 0.333 + 0.06105 \cdot \exp\left(\frac{T}{5.48}\right) \quad (2.103)$$

describes the temperature-dependency appropriately. With the aid of Table 2.1, it is now relatively easy to calculate all other phenomenological constants occurring in the theory of elasticity.

Fortunately, a detailed examination of the theoretical effects of the vertical variation of the Poisson ratio through a floating ice sheet on the mechanical response of the sheet, has indicated that for most real problems it is not necessary to consider the variation of the Poisson ratio with temperature (or brine content), Hutter [47].

### (c) *Other material properties*

Unfortunately, there is very little known about the viscoelastic and plastic behavior of sea ice. In particular, no experimental investigations are available to date describing the dependence of the creep behavior on brine content. Similarly, reports are lacking in which relaxation or creep functions are presented as functions of the volume porosity of brine. Further research on these properties will fruitfully enlighten our understanding of the mechanical behavior of floating ice sheets, both qualitatively and quantitatively. On the other hand, knowledge of failure strength of sea ice is rather detailed, and tests have been performed for *compressive*, *tensile*, and *flexural strength* in general. Weeks [115] and Schwarz and Weeks [100] report results on all of these. Generally, failure strength depends on a various number of factors, such as load direction, brine content, temperature, strain rate, and specimen size.

The earliest simple laboratory compression tests on sea ice were carried

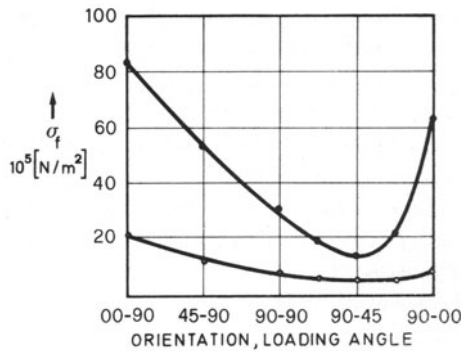


FIG. 2.27. Average failure strength in compression (solid circles) and in direct tension (open circles) versus sample orientations. On the abscissa, the first number gives the angle between the axis of the test cylinder and the vertical, the second that between the cylinder axis and the  $c$ -axis of the crystal. (From [100].)

out by Butkovich [13], who obtained strength values from vertical cores, ranging from  $7.6 \times 10^6 \text{ N m}^{-2}$  at  $-5^\circ\text{C}$  to roughly  $12 \times 10^6 \text{ N m}^{-2}$  at  $-15^\circ\text{C}$ . When horizontal cores were taken, the average values in the same temperature range were from  $2.1 \times 10^6$  to  $4.2 \times 10^6 \text{ N m}^{-2}$ . A similar orientation dependence was also observed by Peyton [85]. The ice he used had grain sizes larger than the diameter of his specimen, so that Peyton was testing single ice crystals whose strength naturally depends on the loading direction, see Figure 2.27. Schwarz and Weeks [100] report further results on compressive strength tests carried out by Schwarz, according to which higher strengths are obtained when the specimen is compressed in the horizontal rather than in the vertical direction. This points to an inconsistency and

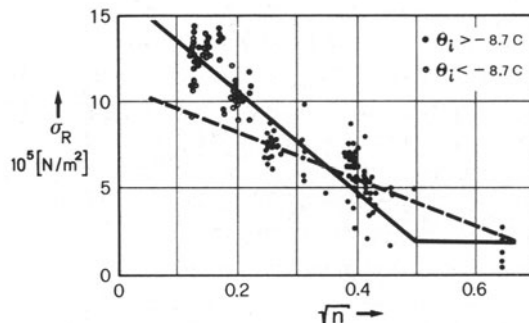


FIG. 2.28.  $\sigma_f$ , failure strength versus square root of brine ( $\sigma_f = \sigma_c / \dot{\sigma}^b$ , where  $\sigma_c$  = compressive strength,  $\dot{\sigma}$  = applied stress rate,  $b = 0.22$ ). The solid line represents Equation (2.104) for the values as listed in row 4 of Table 2.4. (From [100].)

requires a restudy of the problem. The crucial parameter that compressive strength depends upon is the volume of brine. Peyton's results [85] describing this dependency are shown in Figure 2.28.

*Tensile strength* tests on sea ice samples have been performed most comprehensively by Dykins [22] and Hawkes and Mellor [43]. The former obtained a critical dependency of the tensile strength on the loading direction relative to growth direction. In both directions, however, a distinct dependency of the failure strength on  $\sqrt{n}$  can be observed, see Figure 2.29. The functional dependence that is suggested by this figure is a linear connection of  $\sigma_f$  with  $\sqrt{n}$ .

Finally, a few words regarding flexural strength should be said. Flexural strength is not a basic material property but an index strength. It is normally obtained by either a simply-supported beam, or else a cantilever beam test. According to Schwarz and Weeks [100], these tests give nearly identical flexural strength values for sea ice (although not for fresh water ice) and may, therefore, be both regarded as reliable ones. The flexural strength is calculated from a simple elastic beam analysis. This is one of the reasons why flexural strength gives an index value.

Tests on flexural strength have been performed by many investigators, notably by Weeks and Anderson [11], Brown and Howick [12], and Butkovich [13]. The results of these authors are summarized in Figure 2.30. For low porosities, this figure suggests again a square root dependency of failure strength on brine volume. The most recent and extensive work on the flexural strength was done by Dykins [22] who tested large *in situ* beams with thicknesses of up to 2.4 m. His test results are summarized in Figure 2.31,

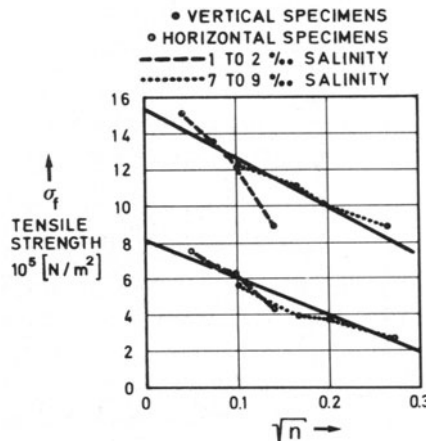


FIG. 2.29. Tensile strength of sea ice versus the square root of brine volume [22].

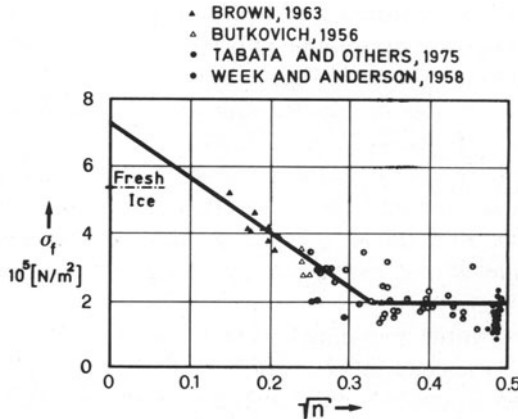


FIG. 2.30. Flexural strength measured by *in-situ* cantilever beam tests versus the square root of brine volume. (From [100].)

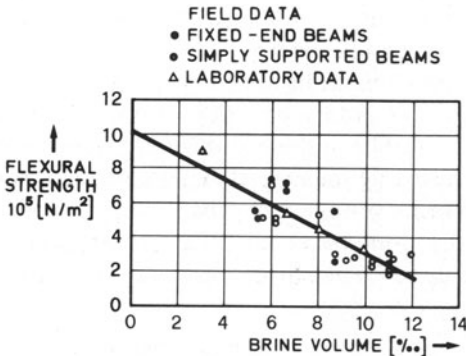


FIG. 2.31. Flexural strength as measured by fixed-end and simply-supported beams versus brine volume [22].

and conform well with Figure 2.30. The formulas of the various failure-strength mechanisms can all be put into the following form

$$\frac{\sigma_f}{\sigma_0} = 1 - \left( \frac{n}{n_0} \right)^{1/2}, \quad (2.104)$$

where  $n$  is the volume porosity of brine,  $n_0$  a pure number, and  $\sigma_0$  a stress. For the various failure modes these constants are listed in Table 2.6.

Failure strength for simple shear is also reported by Schwarz and Weeks [100], but they conclude that although a strong dependency on brine volume is observed, shear strengths must depend on load direction and strain-rate, effects that have not been quantified as yet.

Finally, it is noteworthy to mention that there exists a remarkable

TABLE 2.6. Strength data

Strength	$n_0$	$\sigma_0$ (N m <sup>-2</sup> )
Horizontal tensile strength	0.142	$8.2 \times 10^5$
Vertical tensile strength	0.311	$15.4 \times 10^5$
Flexural strength	0.209	$10.3 \times 10^5$
Compressive strength	0.275	$16.5 \times 10^5$

correlation between flexural strength and Young's modulus of elasticity. Indeed, in 1967, Weeks and Assur proposed a relationship between the elastic modulus  $E$ , the flexural strength  $\sigma_f$ , and the brine volume  $n$ , that can be obtained from the relations

$$\frac{\sigma_f}{\sigma_0} = (1 - n^{1/2})^2, \quad \frac{E}{E_0} = (1 - n^{1/2})^4$$

by eliminating  $n$ :

$$\frac{\sigma_f}{\sigma_0} = \left\{ 1 - \left[ 1 - \left( \frac{E}{E_0} \right)^{1/4} \right]^{1/2} \right\}^2. \quad (2.105)$$

This relation is remarkably well corroborated by experiments, as can be seen from Figure 2.32.

The relatively sound knowledge of the failure stress has been constructively used by Coon and Mohaghegh [17] to evaluate the axial and moment

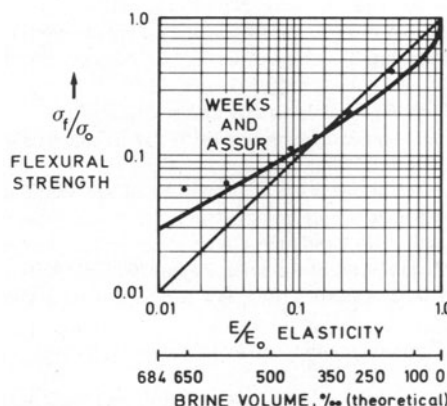


FIG. 2.32. Normalized strength versus normalized elastic modulus for saline ice [100].

capacities of floating sea ice plates as a function of the temperature distribution through the thickness of the ice sheet. This is an attempt to use limit-load analysis to evaluate the bearing capacity of sea ice plates. The lack of experiments, however, did not allow the theory to be verified.

Although a more detailed analysis of the properties of sea ice could be given, which would represent more accurately the merit of the research in this field, it is clear, that the phenomenological response of sea ice is less well known than that of freshwater ice. There is a definite need for more experimental investigations, in particular with regard to non-linear viscous behavior, and the viscoelastic response at moderate and large stresses.

#### REFERENCES

1. Anderson, D. L., A model for determining sea ice properties, in *Arctic Sea Ice*, U.S. Nat. Acad. Sci. N.R.C. Publ. 598, pp. 148–152, 1958.
2. Assur, A., Composition of sea ice and its tensile strength, in *Arctic Sea Ice*, U.S. Nat. Acad. Sci. Publ. 598, pp. 106–138, 1958.
3. Assur, A., Some promising trends in ice mechanics, *IUTAM Symposium on Physics and Mechanics of Ice*, Springer-Verlag, Berlin, pp. 1–12, 1980.
4. Assur, A. and W. F. Weeks, Growth structure and strength of sea ice, *Int. Union Geodes. and Geophys., Publ.*, **61**, 95–108, 1963.
5. Barnes, P., D. Tabor, and J. C. F. Walker, The friction and creep of polycrystalline ice, *Proc. Royal Soc. London*, **A324**, 127–156, 1971.
6. Bass, R., D. Rossberg, and G. Ziegler, Die elastischen Konstanten des Eises, *Z. Phys.*, **149**, 199–203, 1957.
7. Batchelor, G. K., The stress system in a suspension of force-free particles, *J. Fluid Mech.*, **41**, 545–570, 1970.
8. Batchelor, G. K., The stress generated in a non-dilute suspension of elongated particles by pure straining motion, *J. Fluid Mech.*, **46**, 813–829, 1971.
9. Bingham, E. C., *Fluidity and Plasticity*, New York, 1922.
10. Bland, D. R., *The Theory of Linear Viscoelasticity*, Pergamon Press, Oxford, 1960.
11. Born, M. and G. H. Begbie, Thermal scattering of X-rays by crystals: I. Dynamic foundation, *Proc. Royal Soc. London*, **A88**, 179–188, 1947.
12. Brown, J. H. and E. E. Howick, Elasticity and strength of sea ice, in *Ice and Snow-Processes, Properties and Applications*, edited by W. D. Kingery, MIT Press, Cambridge, Mass., pp. 79–106, 1963.
13. Butkowich, T. R., On the mechanical properties of sea ice, Thule, Greenland 1957, Snow Ice and Permafrost Research Establishment Research Report No. 54, 1959.
14. Butkowich, T. R. and J. K. Landauer, Creep of ice at low stresses, U.S. Army Snow, Ice and Permafrost Establishment Research Report No. 72, 1960.
15. Colbeck, S. C. and R. J. Evans, A flow law for temperate glaciers, *J. Glaciology*, **12**, 71–86, 1973.
16. Coleman, B. D., Thermodynamics of materials with memory, *Arch. Ration. Mech. Anal.*, **17**, 1–46, 1964.
17. Coon, M. and M. M. Mohaghegh, Plastic analysis of Coulomb plates and its application to the bearing capacity of sea ice, Research Report, Department of Atmospheric Sciences, University of Washington, 1974.

18. Christensen, R. M., *Theory of Viscoelasticity, An Introduction*. Academic Press, New York and London, 1971.
19. Dantl, G., Elastic moduli of ice, in *Physics of Ice*, pp. 223–230, 1969.
20. Day, W. A., The thermodynamics of simple materials with fading memory, *Springer Tract in Natural Philosophy*, **22**. Springer-Verlag, New York, Heidelberg, Berlin, 1972.
21. Dorsey, N. E., *Properties of Ordinary Water Substance*, Reinhold, New York, 1940.
22. Dykins, J. E., Ice engineering: material properties of saline ice for a limited range of Conditions. Naval Civil Engr. Lab. Tech. Rep. R.710, Port Herenence, Cal., 1971.
23. Einstein, A., Eine neue Bestimmung der Moleküldimensionen. *Ann. Phys.*, **19**, 289–301, 1906; **34**, 591–592, 1911.
24. Eshelby, J. D., The determination of the elastic field of an ellipsoidal inclusion, and related problems. *Proc. Royal Soc. London*, **A241**, 376–396, 1957.
25. Findley, W. N., J. S. Lai, and K. Onaran, *Creep and Relaxation of Nonlinear Viscoelastic Materials*, North Holland, Amsterdam, New York, Oxford, 1976.
26. Frankenstein, G. and R. Garner, Equations for determining the brine volume of sea ice from –0.5 to 22.9°C. *J. Glaciology*, **6**, 943–944, 1967.
27. Garofalo, F., An empirical relation defining the stress dependence of minimum creep rate in metals, *Trans. Metall. Soc. AIME*, **227**, 351–355, 1963.
28. Glasstone, S., K. J. Saidler, and H. Eyring, *The Theory of Rate Processes. The Kinetics of Chemical Reactions, Viscosity, Diffusion and Electrochemical Phenomena*. McGraw-Hill, New York, London, 1941.
29. Glen, J. W., Experiments on the deformation of ice. *J. Glaciology*, **2**, 111–114, 1952.
30. Glen, J. W., The creep of polycrystalline ice. *Proc. Royal Soc. London*, **A228**, 519–538, 1953.
31. Glen, J. W., The flow law of ice: A discussion of the assumptions made in glacier theory, their experimental foundations and consequences. *IASH*, **47**, 171–183, 1958.
32. Glen, J. W., Physics and mechanics of ice as a material, U.S. Army Cold Regions Research and Engineering Laboratory, Cold Regions Science and Engineering Monographs II-C 2a, b, 1974.
33. Glen, J. W. and M. F. Perutz, The growth and deformation of ice crystals. *J. Glaciology*, **2**, 397–403, 1954.
34. Glen, J. W. and S. J. Jones, The deformation of ice single crystals at low temperatures, in *Physics of Snow and Ice*, 1967, pp. 267–275.
35. Gold, L. W., Some observations on the dependence of strain on stress for ice. *Can. J. Phys.*, **36**, 1265–1276, 1958.
36. Gold, L. W. Deformation mechanisms in ice, in *Ice and Snow Processes, Properties and Applications*, edited by W. D. Kingery, MIT Press, Cambridge, Mass., pp. 8–27, 1963.
37. Gold, L. W. and A. Traetteberg, Young's modulus of ice and ice engineering problems, in *Second Symposium on Applications of Solid Mechanics*, Hamilton (Ontario), pp. 1–16, 1974.
38. Green, R. E., Jr. and L. McKinnon, Determination of the elastic constants of ice single crystals by an ultrasonic pulse method. *J. Acoust. Soc. Am.*, **28**, 1292–1293, 1956.
39. Greenberg, M. D., *Foundations of Applied Mathematics*, Prentice Hall, Englewood Cliffs, NJ, 1978.
40. Griggs, T. D. and N. E. Coles, Creep of single crystals of ice. Snow Ice and Permafrost Research Establishment Technical Report No. 11 (1954).
41. Gross, B., *Mathematical Structures of the Theories of Viscoelasticity*, Hermann, Paris, 1953.
42. Gurtin, M. E. and E. Sternberg, On the linear theory of viscoelasticity. *Arch. Ration. Mech. Anal.*, **11**, 291–356, 1962.

43. Hawkes, I. and M. Mellor, Deformation of fracture of ice under uniaxial stress. *J. Glaciology*, **11**, 103–131, 1972.
44. Higashi, A., S. Mae, and A. Fukuda, Strength of ice single crystals in relation to the dislocation structure, Proc. of Internat. Conf. on Strength of Metals and Alloys. Sept. 4–8, 1967, Tokyo (= Suppl. *Trans. Jap. Inst. Metals*, **9**, 784–789, 1968).
45. Hobbs, P. V., *Ice Physics*, Clarendon Press, Oxford, 1974.
46. Hutter, K., On the fundamental equations of floating ice. Mitteilung der Versuchsanstalt für Wasserbau, Hydrologie und Glaziologie an der ETHZ, No. 8, pp. 153, 1973.
47. Hutter, K., Floating sea ice plates and the significance of the dependence of the Poisson ratio on brine volume, *Proc. Royal Soc. London*, **A343**, 2735–2743, 1975.
48. Hutter, K., A note on rate process theory and creep response of ice. *Cold Region. Sci. Tech.*, **3**, 335–336, 1980.
49. Hutter, K., The significance of the shear rigidity and the Poisson ratio for sea ice plates. *Proc. 3rd Conf. Port and Ocean Eng. Under Arctic Conditions*, Vol. 1, pp. 247–268, 1976.
50. Hutter, K., Time-dependent surface elevation of an ice slope. *J. Glaciology*, **25**, 247–266, 1980.
51. Hutter, K., The effect of longitudinal strain on the shear stress of an ice sheet. In defence of using stretched coordinates. *J. Glaciology*, **27**, 39–56, 1981.
52. Hutter, K., Legerer, F., and Spring, U., First order stresses and deformations in glaciers and ice sheets, *J. Glaciology*, **27**, 227–270, 1981.
53. Jellinek, H. H. G., The influence of imperfections on the strength of ice. *Proc. Phys. Soc.* **71**, 797–814, 1958.
54. Jellinek, H. H. G. and R. Brill, Viscoelastic properties of ice, *J. Appl. Phys.*, **27**, 1198–1209, 1956.
55. Jona, F. and P. Scherrer, Die elastischen Konstanten von Eis-Einkristallen. *Helv. Phys. Acta*, **25**, 35–54, 1952.
56. Jones, S. J. and J. W. Glen, The mechanical properties of single crystals of pure ice. *J. Glaciology*, **8**, 463–473, 1969.
57. Kaplan, W., *Operational Methods for Linear Systems*. Addison-Wesley, Reading, Mass., Palo Alto, London, 1962.
58. Kröner, E., Statistical continuum mechanics. *International Centre for Mechanical Sciences. Courses and Lectures*, **92**, Springer-Verlag, Wien, New York, 1971.
59. Kuo, Shion-San, Stress and time effect on the creep rate of polycrystalline ice. PhD Thesis, Michigan State University, 1972.
60. Lanczos, C., *Applied Analysis*, Prentice Hall, Englewood Cliffs, 1956.
61. Langleben, M. P., Some physical properties of sea ice II, *Can. J. Phys.*, **37**, 1438–1454, 1959.
62. Langleben, M. P., Young's modulus for sea ice. *Can. J. Phys.*, **40**, 1–8, 1962.
63. Langleben, M. P. and E. R. Pounder, Elastic parameters of sea ice, in *Ice and Snow Processes, Properties and Applications*, edited by W. D. Kingery, MIT Press, Cambridge, Mass., pp. 69–78, 1963.
64. Langleben, M. P. and E. R. Pounder, Arctic sea ice of various ages. I. Ultimate strength. *J. Glaciology*, **5**, 93–98, 1964.
65. Lliboutry, L. A., The dynamics of temperate glaciers from the detailed viewpoint. *J. Glaciology*, **8**, 185–205, 1969.
66. Lile, R. C., The effect of anisotropy or the creep of polycrystalline ice. *J. Glaciology*, **21**, 475–483, 1978.
67. Lockett, F. J., *Nonlinear Viscoelastic Solids*, Academic Press, London, New York, 1972.
68. Lovitt, W. V., *Linear Integral Equations*, McGraw-Hill, New York, 1924.

69. Mackenzie, J. K., The elastic constants of a solid containing spherical holes. *Proc. Phys. Soc. London*, **B63**, 2–11, 1950.
70. Mantis, T. H. (ed.), Review of the properties of snow and ice, Snow Ice and Permafrost Research Establishment Report No. 4; 1951.
71. Mavko, G. M. and A. Nur, The effect of non-elliptical cracks on the compressibility of rocks, *J. Geophys. Res.*, **83**, 4459–4468, 1978.
72. Mellor, M. and J. H. Smith, Creep of snow and ice, in *Physics of Snow and Ice*, pp. 843–855, 1967.
- 73a. Mellor, M. and R. Testa, Creep of ice under low stress. *J. Glaciology*, **8**, 147–152, 1969.
- 73b. Mellor, M. and R. Testa, Effect of temperature on the creep of ice, *J. Glaciology*, **8**, 131–145, 1969.
74. Mellor, M., Mechanical properties of polycrystalline ice, *IUTAM Symp. on Phys. and Mech. of Ice*, edited by P. Tryde, Springer-Verlag, Berlin, pp. 217–245, 1979.
75. Michel, B., *Ice Mechanics*. Laval University Press, Québec, 1978.
76. Morland, W. L., Constitutive laws for ice. *Cold Regions Sci. Tech.*, **1**, 101–108, 1979.
- 76a. Morland, W. L. and U. Spring, Viscoelastic fluid relation for the deformation of ice. *Cold Regions Sci. Tech.*, **4**, 255–268, 1981.
77. Nakaya, U., Viscoelastic properties of snow and ice in the Greenland ice cap. Snow Ice and Permafrost Research Establishment, Research Report No. 46, 1959.
78. Nevel, D. E., Time-dependent deflection of a floating ice sheet, U.S. Army Cold Regions Research and Engineering Laboratory, Report No. 196, 1967.
79. Nevel, D. E., *Creep Theory for a Floating Ice Sheet*, U.S. Army Cold Regions Research and Engineering Laboratory Special Report No. 16–4, pp. 1–98, 1976.
80. Norton, F. H., *The Creep of Steel at High Temperature*. McGraw-Hill, New York, 1929.
81. Nur, A., Effects of stress on velocity anisotropy in rocks with cracks. *J. Geophys. Res.*, **76**, 2022–2034, 1971.
82. Nye, J. F., The flow of glaciers and ice sheets as a problem in plasticity. *Proc. Royal Soc. London*, **A213**, 546–558, 1951.
83. Nye, J. F., The flow law of ice from measurements in glacier tunnels, laboratory experiments and the Jungfraufirn experiment. *Proc. Royal Soc. London*, **A219**, 477–489, 1953.
84. Penny, A. H., A theoretical determination of the elastic constants of ice. *Proc. Cambridge Phil Soc. Math. Phys. Sci.*, **44**, 423–439, 1948.
85. Peyton, H. R., Sea ice strength, Geophysical Institute, Univ. Alaska, Report UAG-182, 1972.
86. Pipkin, A. C., *Lectures on Viscoelasticity Theory*, Applied Mathematical Sciences, Vol. 7. Springer-Verlag, New York, 1972.
87. Pounder, E. R., Mechanical strength of ice frozen from an impure melt, *Can. J. Phys.*, **36**, 363–370, 1958.
88. Pounder, E. R. and E. M. Little, Some physical properties of sea ice. I. *Can. J. Phys.*, **37**, 443–473, 1959.
89. Pounder, E. R. and P. Stalinski, Elastic properties of arctic sea ice. *Union Geodes. Geophys. Int. Publ.*, **54**, pp. 35–39, 1961.
90. Pounder, E. R. and M. P. Langleben, Arctic sea ice at various ages. II. Elastic Properties. *J. Glaciology*, **5**, 99–105, 1964.
91. Prandtl, L., Ein Gedankenmodell zur kinematischen Theorie der festen Körper. *Z. Angew. Math. Mech.*, **8**, 85–105, 1928.
92. De Quervain, M., Kristallplastische Vorgänge im Schneeaggregat. Mitt. aus dem Eidg. Inst. für Schnee und Lawinenforschung Davos-Weissfluhjoch, Teil 1/2, 1945/46.
93. Ramseier, R. O. and D. F. Dickins, A new approach to field and laboratory tests of

- tensile, compressive and flexural strength of polycrystalline fresh water ice, in *Symposium IAHR, Leningrad*, pp. 143–147, 1972.
94. Read, W. T., Stress analysis for compressible viscoelastic materials. *J. Appl. Phys.*, **21**, 671–678, 1951.
  95. Richardson, C., Phase relationship in sea ice as a function of temperature. *J. Glaciology*, **17**, 507–519, 1976.
  96. Rigsby, G. P., Effect of hydrostatic pressure on velocity of shear deformation of single crystals of ice, Snow Ice and Permafrost Research Establishment, Research Report No. 32, 1957.
  97. Roethlisberger, H., Seismic exploration in cold regions. U.S. Army Cold Region Research and Engineering Laboratory, Monograph II-A 20, 1972.
  98. Savel'ev, B. A., Properties of elasticity, viscosity and plasticity of ice, *IZd-vo Akad. Narek SSSR*, pp. 229–235, 1963.
  99. Schaefer, C. and L. Bergmann, Weitere Untersuchungen über die Beugungerscheinungen an schwingenden Kristallen: I. Experimenteller Teil, *Sber. Preuss. Akad. Wiss.*, **19**, 222–225, 1935.
  100. Schwarz, J. and W. F. Weeks, Engineering properties of sea ice. *J. Glaciology*, **19**, 499–529, 1977.
  101. Shubnikov, A. V. and V. A. Koptsik, *Symmetry in Science and Arts*. (Trans. from the Russian). Plenum Press, New York, London, 1974.
  102. Shumskiy, P. A., Ueber das Fliessgesetz in polikristallinem Eis. *Polarforschung*, **44**, 105–116, 1974.
  - 102a. Smith, G. D. and W. L. Morland, Viscous laws for the steady creep of polycrystalline ice. *Cold Regions Sci. Tech.*, **5**, 141–150, 1982.
  103. Smith, G. F., On isotropic integrity bases. *Arch. Ration. Mech. Anal.*, **17**, 281–292, 1965.
  104. Sokolnikoff, I. and R. Redheffer, *Mathematics of Physics and Modern Engineering*, 2nd eds. McGraw-Hill, New York, 1966.
  - 104a. Spring, U. and W. L. Morland, Viscoelastic solid relations for the deformation of ice. *Cold Regions Sci. Tech.*, **5**, 221–234, 1982.
  105. Steinemann, S., Experimentelle Untersuchungen zur Plastizität von Eis. *Beiträge zur Geologie der Schweiz, Hydrologie*, No. 10, 1958.
  106. Taylor, G. I., The viscosity of a fluid containing small drops of another fluid. *Proc. Royal Soc. London*, **138A**, 41–48, 1932.
  107. Thompson, D. E., Stability of glaciers and ice sheets against flow perturbations. *J. Glaciology*, **24**, 427–441, 1979.
  108. Tricomi, F. G., *Integral Equations*. Pure and Applied Mathematics. Interscience, New York, 1957.
  109. Voigt, W., *Lehrbuch der Kristallphysik*, Teubner, Leipzig, 1910.
  110. Volterra, V., Sur les équations intégralo-differentielles et leurs applications. *Acta Math.*, **35**, 295–356, 1912.
  111. Voytkovskiy, K. F., The mechanical properties of ice. *Izv. Akad. Nauk. SSSR*. (Engl. translation AMS-T-R-391, U.S. Dept. of Comm., Washington DC.) 1960.
  112. Wang, C. C., A new representation theorem for isotropic functions. An answer to Professor G. F. Smith's critique of my papers on representations for isotropic functions. *Arch. Ration. Mech. Anal.*, **36**, 166–223, 1961.
  113. Weeks, W. F., The structure of sea ice: A progress report, in *Arctic Sea Ice*, U.S. Nat. Acad. Sci. N.C.R. Publ. 598, pp. 46–98, 1958.
  114. Weeks, W. F., Tensile strength of NaCl-ice, *J. Glaciology*, **4**, 25–52, 1962.
  115. Weeks, W. F., Sea ice properties and geometry, *Arctic Ice Dynamic Joint Experiment Bulletin*, No. 34, 137–171, 1976.
  116. Weeks, W. F. and D. L. Anderson, An experimental study of strength of young sea ice, *Trans. Am. Geophys. Union*, **39**, 641–647, 1958.

117. Weeks, W. F. and A. Assur, The mechanical properties of sea ice, U.S. Cold Regions Research and Engineering Laboratory, Cold Regions Science and Engineering Report, Pt II, Sect. C3, pp. 1-67, 1967.
118. Weertman, J., The Eshelby-Shoek viscous dislocation damping mechanism applied to the steady creep of ice, in *Ice and Snow*, pp. 28-33, 1963.
119. Williams, M. F., Wave ogives as second-order effects in the creep of large ice masses. *J. Glaciology*, **24**, 509-510, 1979.
120. Wu, T. T., The effect of inclusion shape on the elastic moduli of two-phase material. *Int. J. Solids, Structures*, **2**, 9-11, 1966.
121. Zener, C., *Elasticity and Anelasticity of Metals*, University of Chicago Press, Chicago, 1948.
122. Zubov, N. N., On the problem of a floating ice layer (Trans. from the Russian), Arctic Const. Frost Effects Lab. TL-25, pp. 16-29, 1945.

**PART II**

**THE DEFORMATION OF AN ICE MASS  
UNDER ITS OWN WEIGHT**

## **Chapter 3**

# **A MATHEMATICAL ICE-FLOW MODEL AND ITS APPLICATION TO PARALLEL-SIDED ICE SLABS**

### *1. Motivation and Physical Description*

The previous chapters were devoted to the derivation of the basic principles and to the material properties of ice with no particular intention of applying the collected information to a physical problem. Here, in this chapter, attention will be focussed on a first simple application of the knowledge gained so far. In particular, an attempt is made to shed some light on the deformation mechanism and thermal conditions of glaciers and ice sheets.

Fundamental to all theoretical treatment of glacier flow is the constitutive response of ice under a slowly-varying state of stress of the order of 2 bars or more and applied over a very long period. Under such conditions, secondary and tertiary creep is the appropriate behavior. In fact, at larger depths, where the shear becomes rather high, tertiary creep must certainly be dominant and the state of stress should then influence the anisotropy of the ice. Because of the extreme difficulties one would encounter in modeling a three-dimensional version of the one-dimensional constitutive response, one usually assumes that glacier ice is an isotropic viscous fluid to which either Nye's or Glen's generalization of Glen's flow law of secondary creep may be applied.\* In the past, calculations were based on Nye's extension, because the more complex finite viscosity laws were not needed and because the additional material function that occurs in Glen's extension has never been determined.

Although valley glaciers and ice sheets are bounded objects, they may, as a first approximation, nevertheless be treated as infinitely wide, with no variations of geometry and physical properties in the direction perpendicular to the main flow. The deformation is then two-dimensional, and one may look at an ice sheet of unit thickness under plane strain, all deformations

\*What is meant here is the constitutive relationship

$$D_{ij} = -\frac{2}{3}g(\cdot)t'_{ll}\delta_{ij} + f(\cdot)t'_{ll} + g(\cdot)t'_{ik}t'_{kj}$$

between stretching tensor  $D_{ij}$  and stress deviator. In Nye's generalization of the simple power law of secondary creep  $g(\cdot) = 0$ , in Glen's extension, however,  $g(\cdot) \neq 0$ .

thereby occurring in parallel planes. Moreover, since the lengths of the sheets are generally large in comparison to their depths, the variation of the latter with a length coordinate may also be ignored. The resulting model is then an infinitely long and wide parallel-sided slab subjected to gravity forces. Such a model is geometrically simple enough so that the determination of the stress, velocity, and temperature distribution is an almost routine matter. Clearly, the finiteness of a valley glacier or an ice shelf will alter the results obtained this way. Nonetheless, the parallel-sided slab should qualitatively indicate the important physical dependencies correctly.

It was stated above that the material response will be fundamental in an appropriate description of the deformation of ice sheets and glaciers. In this regard, the state of affairs is complicated by the fact that glaciers and ice sheets are *polythermal* in general, i.e., they consist of two zones, 'cold' and 'temperate', in which the ice is respectively below and at melting point. Particular thermal limits are the so-called 'polar' or 'cold' and 'temperate' glaciers, which are defined as existing exclusively as ice in one or the other of these states. Depending upon which state exists at the base, different boundary conditions apply. Since there is no access to the base of a glacier in general and, consequently, observations at such a depth are extremely scarce, boundary conditions are essentially conjectural. There are three different types of mechanical boundary conditions which have been proposed, and each one applies under different conditions. The simplest, namely the *no-slip condition*, is believed to apply in *non-temperate cold glaciers*. In Arctic, cold glaciers, the ice at the base adheres to the basal surface. There are observations which support this point of view. On the other hand, for temperate glaciers, the heat generated by deformation causes melting of the ice. It is believed, and again there are observations which support such a conjecture (see Kamb and LaChapelle [22]), that the water at the base forms a very thin layer. The ice at the sole and at the base itself are thus not in contact with each other but are separated by a small water film of only a few microns thickness. Hence, there is virtually no friction between the base and the ice at this interface. At the true surface – the interface 'sole-bed' – *perfect slip* provides an accurate description. Thus, the ice velocity at the base is tangential to the bottom surface and there is no shear stress acting at the bed. In spite of this, a valley glacier normally does not slide catastrophically down its slope, the reason being that the undulations of the bottom surface cause pressure variations at this surface which, when resolved in the direction of the mean bed, balance the corresponding component of the gravity forces. It is intuitively clear that the exact rockbed will not govern the overall motion of the ice. This will rather follow a mean smoothed-out topography. The motion around small-scale protuberances will be confined to a relatively narrow layer, and the flow far from the sole will 'feel' the sole roughnesses as a viscous drag. This drag corresponds exactly to the component of the

pressure in the direction of the mean bed mentioned above.

There is still a third possibility for the mechanical boundary condition. To discuss it, notice that because of existing cracks, crevasses, moulinis, etc., all glaciers are essentially porous media. In temperate glaciers, many of these cavities are filled with water, and often it is appropriate to regard the glacier as a mixture of an ice matrix that is more or less continuously filled with water. Indeed, a system of internal or basal conduits often exists, as is evidenced by the main streams that ordinarily emerge at the terminus of Alpine glaciers. The water content in such glaciers is governed by the melting rate of the ice at the glacier surface and by the flow conditions encountered by the melting water as it moves through the ice. If the water table is roughly above nine-tenths of the glacier depth, then the water pressure at the base exceeds the over-burden pressure and, therefore, the glacier must become at least partially afloat. At local humps, there is still contact with the base, but there are also water pockets which separate the ice from its base. The form and extensions of these pockets is not known in advance so that the sliding mechanism must, from a mathematical point of view, be very complex. Its satisfactory treatment is still an open problem to date. We see then, that there are two possible sliding mechanisms in temperate glaciers: sliding with a thin film of water at the base is called *sliding without cavity formation*; alternatively, sliding under simultaneous formation of water pockets is called *sliding with cavity formation*. Neither will be closely investigated in this chapter.

To be complete, mention should be made of a further possibility and this is *sliding with cavitation*. In this case regelation still causes a liquid film to be built, yet no cavities are formed, but the bottom topography gives rise to contact pressures which are so low that the triple point in the phase diagram is reached; in other words, ice, water, and vapor may exist simultaneously in these points. Pressures must be extremely low for cavitation to become possible (the triple point pressure is  $\sim 0.006$  bars) and ice and base must, in particular, be sealed from the atmosphere to make it possible. Occurrence of sliding with cavitation is probably seldom but when it takes place, it is clear that the sliding velocities must be large.

The above description applies almost exclusively to *glaciers*. It is noteworthy to point out that boundary conditions of stress to be applied at the bottom ice-water interface of a floating *ice shelf*, are well defined and, unlike those in glaciers, not conjectural. In a first approximation, floating ice shelves are also parallel-sided slabs. In the direction perpendicular to the plane of deformation, in a first approximation, they may be considered as infinitely wide. If they rest on a quiescent ocean; i.e., if possible boundary-layer effects of the ocean current may be ignored, then the force exerted by the ocean on the shelf must be a normal pressure whose value is given by the hydrostatic pressure that exists at the ice-water interface.

In this discussion, any considerations regarding accumulation-ablation and thermal boundary conditions have been ignored. These are as important as the mechanical conditions. Accumulation and ablation, e.g., play an important part in the determination of the surface geometry of a glacier, and even more important, they govern the advance or retreat of a glacier at its snout. The thermal boundary conditions, on the other hand, to a large extent, determine the long-time behavior of an ice mass. As an example, consider the thermal conditions at the ice-water interface of a floating ice shelf. The ice temperature at this interface will match the water temperature in general, but the condition whether ice melts or freezes depends on the amount of heat supplied by the water to the ice and that conducted and convected upwards through the ice away from it. If the two fluxes balance, then there is neither melting nor freezing; if they do not, freezing will occur, provided that there is a heat deficiency at the interface – this corresponds to accumulation. On the other hand, melting occurs if there is a heat surplus, and this is tantamount to an ablation. It is seen that the thickness of the shelf and, therefore, its geometry is invariably tied to the thermal conditions of the environment.

The situation is slightly different at the upper free surface. Here accumulation is due solely to solid precipitation and, consequently, not directly related to a thermal condition, except that the climate must be cold enough to make solid precipitation possible. On the other hand, ablation is due to melting and evaporation, which are essential thermal conditions.

The above discussion should make it clear that the response of a glacier or ice sheet to gravity forces and external environmental conditions is a complicated thermo-mechanical problem, which needs a clear presentation of its formulation. Such formulations have been given previously; they generally represent more simple models than the one to be presented below, and have been proposed to explain certain features of the flow. Among these models, we might mention Nye's application of the kinematic wave theory to predict the advance and retreat of glaciers [39–41] (see also Chapter 6). Other models treating particular questions are by Budd [6], Grigoryan, Krass and Shumskiy [14, 57]. The theory presented below is based on a binary mixture concept and follows Hutter [14a] with results which are similar to those of Fowler and Larson [11] yet more general and more systematical.

Once the model has been presented with all its pertinent details, simplifications will be introduced whereby the reduced problems can be attacked. However, considerations will be restricted to the strictly parallel-sided slab.

## 2. *The Basic Model – Its Field Equations and Boundary Conditions*

In wide mountain glaciers and in Arctic and Antarctic floating or grounded ice sheets, the flow is often nearly two-dimensional, and so atten-

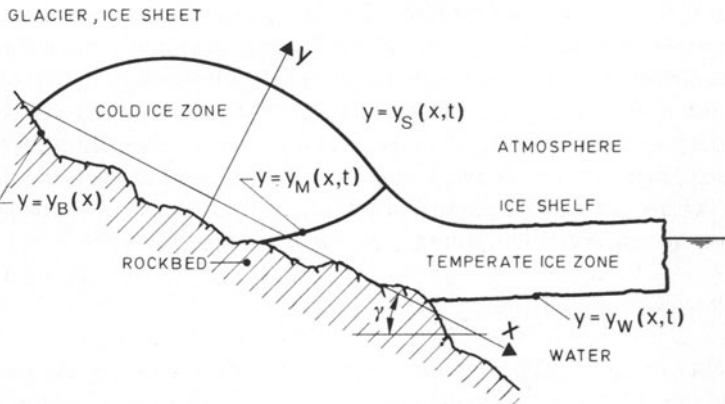


FIG. 3.1. Model glacier or ice sheet divided into a cold and a temperate ice zone, which are separated by the 'melting surface'  $y = y_M$ . The free surface, ice-bedrock interface and ice-water interface are denoted by  $y = y_S$ ,  $y = y_B$ , and  $y = y_W$ , respectively. The  $x$ -axis of the Cartesian coordinate system is parallel to the mean bedrock inclination. The figure is intended to be schematic only.

tion is mostly restricted here to ice masses whose profiles are the same for all longitudinal sections. A typical geometry of such an ice sheet is shown in Figure 3.1. Accordingly, the ice mass contains a cold ice zone, in which the temperature is below melting point, and a temperate ice zone, in which the ice is at melting point throughout. The cold and temperate zones are separated by a curve which connects two boundary points, generally at the upper and lower ice surfaces. There are three different types of boundaries that can be observed in Figure 3.1: the free surface, the ice-bedrock interface at those portions of the boundary where the ice mass is grounded, and the ice-water interface where the ice is in contact with the underlying lake or ocean water. A Cartesian coordinate system is introduced. The  $x$  axis is chosen here as parallel to the direction of the mean inclination of the grounded portion of the ice mass. The origin of the coordinate system may be chosen arbitrarily. Four different surface functions have been introduced:  $y = y_B(x)$ ,  $y = y_S(x, t)$ ,  $y = y_W(x, t)$  and  $y = y_M(x, t)$ . They denote, respectively, the surface of the ice-bedrock interface, the top surface, the surface at the ice-water interface, and the surface dividing the cold and temperate zones, henceforth to be called the melting surface. On this surface  $T = T_M$ , where  $T$  and  $T_M$  are the local ice temperature and pressure melting temperature, respectively.

Incidentally, the division of the entire ice mass into a cold zone, most of which is extended over the grounded portion of the glacier, and a temperate zone in the larger part of the floating-ice region, is intended to be schematic

in Figure 3.1 and should not indicate a common physical occurrence. Glaciers mostly have no or negligible floating portions. Often they are believed to be either cold or temperate, but not polythermal and ice shelves are hardly ever formed from temperate, but rather cold ice. Moreover, the coordinate system introduced in Figure 3.1 is naturally adjusted to the grounded portion of the ice mass with the  $x$  axis inclined to the horizontal of angle  $\gamma$ . Other choices are possible, and indeed if ice shelves are analysed, a Cartesian system with a horizontal  $x$  axis is more natural.

### (a) The field equations

( $\alpha$ ) *Cold ice region.* The common continuum mechanical model adopted for cold ice is a *non-Newtonian, viscous, heat-conducting, incompressible fluid*. The field equations are therefore

$$\begin{aligned} \operatorname{div} \dot{\mathbf{v}} &= 0, \\ \rho \dot{\mathbf{v}} &= -\operatorname{grad} p + \operatorname{div} \mathbf{t}' + \rho \mathbf{g}, \\ \rho \dot{\epsilon} &= \operatorname{tr} (\mathbf{t}' \mathbf{D}) - \operatorname{div} \mathbf{q}, \end{aligned} \quad (3.1)$$

and express the local balance of mass, momentum, and internal energy. In the above,  $\mathbf{v}$  is the velocity vector,  $\rho$  the density of ice,  $p$  pressure  $\mathbf{t}'$  symmetric Cauchy stress deviator,  $\mathbf{g}$  vector of external forces,  $\epsilon$  internal energy,  $\mathbf{q}$  heat flux vector and  $\mathbf{D} = \operatorname{sym}(\operatorname{grad} \mathbf{v})$  the stretching tensor. In the subsequent analysis, total stress will always be denoted by  $\mathbf{t}$  without an accent, thus  $\mathbf{t} = \mathbf{t}' - p\mathbf{1}$ .

The balance laws (3.1) are complemented by constitutive relations for the rate of internal energy, heat flux, and stress. Thermodynamic considerations then permit the deduction of the most general *admissible* constitutive relationships for the class of non-Newtonian fluids considered here, but for the flow of large ice masses, these are further reduced and simplified. The laws commonly adopted are

$$\begin{aligned} \rho \dot{\epsilon} &= \rho c_p \dot{T} \quad [\text{or } \rho \dot{\epsilon} = \rho \dot{\epsilon}(T_0) + \rho c_p(T - T_0)], \\ \mathbf{q} &= -\kappa \operatorname{grad} T, \\ \mathbf{D} &= \mathcal{A}(T)f(t'_{II})\mathbf{t}', \quad t'_{II} = \frac{1}{2} \operatorname{tr} \mathbf{t}'^2, \end{aligned} \quad (3.2)$$

in which  $T$  is the Kelvin temperature,  $T_0$  a reference temperature,  $c_p$  specific heat at constant pressure, and  $\kappa$  the heat conductivity of ice. Further,  $f$  is a creep response function, assumed to depend on the second stress-deviator invariant  $t'_{II}$  and  $\mathcal{A}$  is a rate factor, which depends on temperature only. In view of the small temperature range occurring in this geophysical application, a constant specific heat and a linear Fourier-type heat-conduction law are sufficiently accurate. The constitutive relationship relating stress deviator, and stretching is solved for  $\mathbf{D}$  as a function of  $\mathbf{t}'$ . It is a special case of

the more general *Reiner–Rivlin-type* constitutive law (see Chapters 1 and 2). The other important parameter in the stress-stretching law is the *rate factor*  $\mathcal{A}$ . Usual functional relationships are of the Arrhenius-type,

$$\mathcal{A} = A \exp\left(-\frac{Q}{kT}\right), \quad (3.3)$$

where  $Q$  is activation energy,  $k$  Boltzmann's constant and  $A$  a constant. It is now well established that this law is not appropriate for temperatures above 263 K. Variants of (3.3) which fit experimental data for  $263 \text{ K} < T < 273 \text{ K}$  are given by Smith and Morland (for details see Chapter 2).

In Cartesian coordinates and plane flow, denoting the ‘longitudinal’ and ‘transverse’ velocity components by  $u$  and  $v$ , respectively, Equations (3.1)–(3.3) may be written as

Balance of mass:

$$\frac{\partial u}{\partial x} + \frac{\partial v}{\partial y} = 0.$$

Balance of momentum:

$$\begin{aligned} \rho \dot{u} &= \frac{\partial t'_{xx}}{\partial x} + \frac{\partial t'_{xy}}{\partial y} - \frac{\partial p}{\partial x} + \rho g \sin \gamma = \frac{\partial t_{xx}}{\partial x} + \frac{\partial t_{xy}}{\partial y} + \rho g \sin \gamma, \\ \rho \dot{v} &= \frac{\partial t'_{xy}}{\partial x} + \frac{\partial t'_{yy}}{\partial y} - \frac{\partial p}{\partial y} - \rho g \cos \gamma = \frac{\partial t_{xy}}{\partial x} + \frac{\partial t_{yy}}{\partial y} - \rho g \cos \gamma. \end{aligned}$$

Balance of energy:

$$\rho \dot{\epsilon} = - \left( \frac{\partial q_x}{\partial x} + \frac{\partial q_y}{\partial y} \right) + t'_{ij} D_{ij}. \quad (3.4)$$

Constitutive relations:

$$\begin{aligned} D_{ij} &= A \exp\left(-\frac{Q}{kT}\right) f(t'_{II}) t'_{ij}, \\ \epsilon &= \epsilon(T_0) + c_p(T - T_0), \\ (q_x, q_y) &= -\kappa \left( \frac{\partial T}{\partial x}, \frac{\partial T}{\partial y} \right). \end{aligned}$$

Before we proceed, it should be pointed out that, strictly speaking, it is not permissible to assume ice to be incompressible and yet still presume a volume change under phase changes. Nevertheless, it is customary in these instances to maintain the basic assumption of incompressibility in the field equations, but to use the phase-change relations of a compressible heat-conducting viscous body. This is reasonable insofar as Equations (3.1)–(3.4)

can be viewed as approximations of field equations of a *compressible* viscous body in which pressure and stress deviations are the independent field variables, see Chapter 1, Section 4c. The constitutive theory then shows that of the constitutive relationships (3.2), only the expression for the internal energy changes, in that it must have the form  $\varepsilon = \hat{\varepsilon}(p, T)$ . Because in almost-incompressible bodies  $\hat{\varepsilon}(p, T)$  varies weakly with  $p$ , this latter relation may well be approximated by  $\varepsilon \approx \hat{\varepsilon}(p_{\text{mean}}, T) = \tilde{\varepsilon}(T)$ . To see which term is neglected, observe that

$$\frac{d\varepsilon}{dt} = \frac{\partial \hat{\varepsilon}}{\partial T} \frac{dT}{dt} + \frac{\partial \hat{\varepsilon}}{\partial p} \frac{dp}{dt} = c_p \frac{dT}{dt} + c_T \frac{dp}{dt}.$$

The assumption is now

$$\left| c_p \frac{dT}{dt} \right| \gg \left| c_T \frac{dp}{dt} \right|.$$

This derivation also shows that the specific heat introduced in (3.2) should be that at constant pressure and not at constant volume, as taken by Fowler and Larson [11].

When the above constitutive relations are substituted into the balance laws (3.2) the *field equations* for the unknown fields  $\mathbf{v}$  and  $T$  in the cold portion of the ice mass are obtained. For instance, the energy equation reads

$$\rho c_p \dot{T} = \kappa \nabla^2 T + 2\mathcal{A}(T)f(t'_{II})t'_{II}. \quad (3.5)$$

The second term on the right-hand side is the *dissipation*, which is often called *strain heating*. When (3.5) is viewed as a balance equation for internal energy, this term must be interpreted as the *internal energy production*.

(β) *Temperate ice region.* Temperate ice is defined to be *at melting*,  $T = T_M$ . When such ice is subject to deformation, heat generated by viscous deformation cannot simply give rise to temperature changes, because the temperature will be governed by the Clausius–Clapeyron equation, see Chapter 1, Section 5. Most frictional heat produced by ice will be used up by melting, implying that in the temperate zone there is not just temperate ice but a *binary mixture* of ice and molten water. Some of the water will be trapped by the ice, inclusions are then non-connecting. Many inclusions will, however, be connected with others, and thus water will percolate along grain boundaries, veins, cracks, and crevasses. In wholly-temperate glaciers, most water flows through moulin and the intraglacial channel system (Spring and Hutter [59, 60]). A proper mathematical description of the interaction of this discrete water flow through the continuous ice mass must be very difficult. We thus ignore this case. Controversial as this may be, hope is seen for an interaction model, which treats water and ice as separate constituents only as long as both are treated continuously. For

polythermal ice with a small water-to-ice ratio, this condition is less controversial than for wholly-temperate ice so that diffusion may be the dominant driving mechanism. A proper description of temperate ice in polythermal glaciers may thus be a mixture concept, in which the water content is treated as a *tracer*. Further, at first glance, an energy-balance statement is not important, because the melting temperature of the mixture as a whole may be related to the total pressure.

An adequate mixture concept is, therefore, one with two mass balance equations for the mixture as a whole and for the constituent water, but only one balance equation of momentum for the total mixture. If, furthermore, it is assumed that *all energy production in the mixture is instantly used up by melting*, energy production and mass production can easily be interrelated with the aid of the *latent heat of fusion*.

To make these statements better understood, the reader may recall the concept of balance laws developed in Section 2 of Chapter 1. There, the time rate of change of a physical quantity was balanced by flux, supply, and production terms; mass, momentum and energy balance of a continuous medium were deduced and it was shown that in a one-component body mass, momentum and energy are conserved in the sense that production terms must vanish. In a *binary* mixture, it is assumed that the body is made up of *two* constituents. It will also be assumed that the constituents are continuously distributed in the space filled by the body. One may then either regard each constituent as an individual body and formulate the balance laws for these, but if this is done, the production terms in the balance laws will not necessarily vanish, or else one regards the mixture as a whole and then has vanishing production terms.

Here, only mass balance will be formulated for both ice and water, while momentum is established for the mixture as a whole. The production of water then equals the annihilation (a negative production) of ice, both being governed by the melting rate. This simplistic mixture concept does not allow to differentiate between the states of stress in the ice and the water. For that, two momentum balance laws would be necessary.

To derive the balance equations of mass, let  $\rho_\alpha$  ( $\alpha = 1, 2$ ) and  $\mathbf{v}^\alpha$  be the constituent densities and velocities, respectively, and define *total mass density*  $\rho$  and *barycentric velocity*  $\mathbf{v}$  as

$$\rho = \sum_x \rho_x, \quad \rho \mathbf{v} = \sum_x \rho_x \mathbf{v}^\alpha. \quad (3.6)$$

In a mixture theory, the concept of total derivative is not unique as such derivatives can be formed with the peculiar or barycentric velocities. Of special interest here is the total derivative *with respect to the barycentric velocity*,

$$\dot{f} = \frac{\partial f}{\partial t} + \text{grad } f \cdot \mathbf{v}. \quad (3.7)$$

In terms of this, the balance laws of momentum and energy for the mixture have the form (3.1)<sub>2,3</sub>. If we denote by  $\mathfrak{C}_x$  ( $x = 1, 2$ ) the peculiar mass productions, the local balance laws of mass become

$$\frac{\partial \rho_x}{\partial t} + \operatorname{div}(\rho_x \mathbf{v}^x) = \mathfrak{C}_x, \quad \sum_x \mathfrak{C}_x = 0 \quad (x = 1, 2) \quad (3.8)$$

and may, with the aid of (3.7), be written as

$$\rho \dot{w}_x = -\operatorname{div} \mathbf{j}_x + \mathfrak{C}_x, \quad \mathbf{j}_x = \rho_x (\mathbf{v}^x - \mathbf{v}), \quad (3.9)$$

where  $w_x \equiv \rho_x / \rho$  is the *mass fraction* of constituent  $x$  and  $\mathbf{v}^x - \mathbf{v}$  is the *diffusion velocity*. More convenient than working with two equations of the type (3.9)<sub>1</sub> is to use the balance of mass for the mixture and for the constituent water. This then yields

$$\dot{\rho} + \rho \operatorname{div} \mathbf{v} = 0, \quad \rho \dot{w} = -\operatorname{div} \mathbf{j} + \mathfrak{C}, \text{ (for constituent water).} \quad (3.10)$$

Here, and henceforth, the subscript in the mass-balance equation for constituent water will be deleted as the constituent water will always be meant. The quantity  $w$  is then frequently referred to as *moisture content*.

A mixture is called incompressible when  $\dot{\rho} = 0$ . Strictly speaking, temperate ice is not incompressible because phase-change is accompanied by density changes. Density variations are therefore governed by the moisture content. It is, however, justified to ignore this variation since associated changes in bulk density are very small. The model that will be adopted for temperate ice is therefore a binary incompressible mixture obeying the equations

$$\begin{aligned} \operatorname{div} \mathbf{v} &= 0, \\ \rho \dot{\mathbf{v}} &= -\operatorname{grad} p + \operatorname{div} \mathbf{t}' + \rho \mathbf{g}, \\ \rho \dot{w} &= -\operatorname{div} \mathbf{j} + \mathfrak{C}. \end{aligned} \quad (3.11)$$

These balance laws must be complemented by constitutive relationships for the diffusive flux vector  $\mathbf{j}$ , mass production  $\mathfrak{C}$ , and stress deviator  $\mathbf{t}'$ . If all water is contained in non-connecting pockets  $\mathbf{v}^x = \mathbf{v}$  and the diffusion velocity vanishes. In this case, Equations (3.11) agree with those of Fowler and Larson [11]. Equation (3.11)<sub>3</sub> is then hyperbolic and can be shown (see later) not to permit closed melting curves. In other words, cold ice could never be enclosed by temperate ice and *vice versa*. Physically, this is somewhat unrealistic and suggests that a diffusive moisture flux having the *Fick-type* form  $\mathbf{j} = -v \operatorname{grad} w$ , with diffusivity  $v$ , or even a more general constitutive relationship, say,

$$\mathbf{j} = \hat{\mathbf{j}}(w, \operatorname{grad} w, \mathbf{D}, \mathbf{g}) \quad (3.12)$$

should be established, which changes the equation from hyperbolic to

parabolic. A dependence on  $\text{grad } w$  is likely to occur, since density jumps associated with phase changes will drive the water into the direction of smaller values of  $w$ , justifying the Fick-type constitutive relation. Even though in a first approximation the diffusivity  $v$  may be assumed to be constant, it should depend on  $w$ . The reason for this is the salt content. Because solid ice effectively rejects impurities, the (trapped) water inclusions can be rich in salts if inclusions are non-connecting. This enrichment will take place very close to the melting surface and cause the moisture content to drop quickly as that surface is approached. This suggests a boundary-layer effect and requires a moisture-dependent diffusivity, which becomes small close to the melting surface. On the length scales of glaciers and ice sheets, the thickness of the associated boundary layer is expected to be small, and thus a constant diffusivity will be assumed.

Considering the earlier assumption that all internal energy production of the mixture is used up by melting we have  $C = \text{tr}(\mathbf{t}'\mathbf{D})/L$ , where  $L$  is the *latent heat of fusion per unit volume of the mixture*. Furthermore, according to Lliboutry [28], the presence of meltwater can significantly affect the constitutive relation of stress. He concludes that the constitutive relationship (3.2)<sub>3</sub> remains formally valid, but with a rate factor which is a function of moisture content  $\mathcal{A} = \mathcal{A}(w)$ .

In summary, the constitutive relations completing the balance laws (3.11) are

$$\begin{aligned} C &= \text{tr}(\mathbf{t}'\mathbf{D})/L, \\ \mathbf{j} &= -v \text{ grad } w \quad \text{or} \quad \mathbf{j} = \mathbf{0}, \\ \mathbf{D} &= \mathcal{A}(w)f(t'_{\text{II}})\mathbf{t}'. \end{aligned} \tag{3.13}$$

Comparing Equations (3.1) and (3.2) which are valid for cold ice with (3.11) and (3.13), it is seen that, structurally, they are the same equations with the same type of couplings. The continuity equation and the momentum equations are coupled with an equation for a ‘state variable’, temperature  $T$  and moisture content  $w$ , respectively. Physically, this equation is the energy equation or the balance of mass for the water, but mathematically both equations are of a *parabolic* or *diffusion type*, provided that  $\mathbf{j} \neq \mathbf{0}$ .

Practically, there is nothing known about the numerical values of the diffusivity  $v$ , except for qualitative considerations saying that  $v$  is small. Also, only incomplete knowledge exists about the function  $\mathcal{A}(w)$  see, however, Lliboutry [28]. Most practitioners therefore assume a constant value for  $\mathcal{A}$ , thereby achieving a decoupling of the purely mechanical field equations from the diffusion equation.

As stated before, the energy equation need not be considered in the temperate ice region, since temperature  $T_M$  follows from the Clausius–Clapeyron equation. Later we shall use an expression for the heat flux vector

in the temperate region. On the basis of a Fourier-type constitutive relation one obtains

$$\mathbf{q} = -\kappa \operatorname{grad} T = -\kappa \frac{dT}{dp} \operatorname{grad} p = \kappa c_t \operatorname{grad} p, \quad (3.14)$$

$\kappa$  being the heat conductivity of the mixture. This term is so small that it can, in general, safely be ignored. Finally we mention that the theories with  $\mathbf{j} \neq \mathbf{0}$  and  $\mathbf{j} = \mathbf{0}$  are structurally very much different. In one case, the equation for the moisture content is

$$\rho \dot{w} = v \nabla^2 w + \frac{2}{L} \mathcal{A}(w) f(t_{II}) t'_{II} \quad (3.15)$$

and thus formally the same as the energy Equation (3.5). In the other case, diffusion is ignored and (3.14) is a simple evolution equation.

For future reference, it is helpful to list the special forms that the various quantities derived from stress and stretching assume under plane deformations. The stretching tensor has the form (the (+) sign indicates symmetry):

$$\begin{bmatrix} D_{xx} & D_{xy} & 0 \\ & D_{yy} & 0 \\ (+) & 0 \end{bmatrix} = \begin{bmatrix} \hat{\partial}_x u & \frac{1}{2} \left( \frac{\partial u}{\partial x} + \frac{\partial v}{\partial y} \right) & 0 \\ \frac{\partial v}{\partial y} & 0 \\ (+) & 0 \end{bmatrix}. \quad (3.16)$$

It follows from the  $D_{zz}$ -component of this relation, and from the constitutive relation of stress, that  $t'_{zz} = 0$  which implies  $t_{zz} = \frac{1}{2}(t_{xx} + t_{yy})$ . Stress tensor and deviator, therefore, have the forms

$$t_{ij} = \begin{bmatrix} t_{xx} & t_{xy} & 0 \\ t_{xy} & t_{yy} & 0 \\ 0 & 0 & \frac{1}{2}(t_{xx} - t_{yy}) \end{bmatrix}, \quad t'_{ij} = \begin{bmatrix} \frac{1}{2}(t_{xx} - t_{yy}) & t_{xy} & 0 \\ t_{xy} & \frac{1}{2}(t_{xx} - t_{yy}) & 0 \\ 0 & 0 & 0 \end{bmatrix} \quad (3.17)$$

from which the second stress-deviator invariant may be deduced as

$$t'_{II} = \frac{1}{4}(t_{xx} - t_{yy})^2 + t_{xy}^2. \quad (3.18)$$

Substituting these results in the constitutive relation for stress, (3.2)<sub>3</sub> or (3.13)<sub>3</sub>, finally, yields

$$D_{xx} = -D_{yy} = \frac{\mathcal{A}}{2} f(t'_{II})(t_{xx} - t_{yy}), \quad D_{xy} = \mathcal{A} f(t_{II}) t_{xy}. \quad (3.19)$$

Evidently,  $D_{xx} + D_{yy} = 0$ , which is the statement of incompressibility.

(b) *Boundary conditions*

The boundary surfaces (see Figure 3.1)  $y = y_S$ ,  $y = y_B$ ,  $y = y_W$  and  $y = y_M$  are not material, in general; they must therefore be regarded as *surfaces of discontinuity*. At such surfaces it is assumed that physical quantities may suffer a finite jump. In other words, whereas all quantities are assumed to be sufficiently differentiable in the regions on either side of the surface, this assumption is weakened when the surface is crossed.

A careful derivation of the jump conditions from the global-balance equations is given in Chapter 1. Jump conditions of mass, momentum, energy, and entropy are listed as Equations (1.37) and, for convenience, will be repeated below. Equation (3.11)<sub>3</sub> for the moisture content, is also a local balance equation in the sense of Chapter 1, to which a global form can be deduced, see Equations (1.33, 1.36). At a surface of discontinuity, the following jump conditions must, therefore, hold:

mass:

$$[\rho(\mathbf{v} - \mathbf{u}) \cdot \mathbf{n}] = 0,$$

momentum:

$$[\mathbf{t} \cdot \mathbf{n}] - [\rho \mathbf{v}(\mathbf{v} - \mathbf{u}) \cdot \mathbf{n}] = 0,$$

energy:

$$[(\mathbf{v} \cdot \mathbf{t} - \mathbf{q}) \cdot \mathbf{n}] - \left[ \rho \left( \varepsilon + \frac{v^2}{2} \right) (\mathbf{v} - \mathbf{u}) \cdot \mathbf{n} \right] = 0, \quad (3.20)$$

entropy:

$$\left[ \frac{\mathbf{q} \cdot \mathbf{n}}{T} \right] + [\rho \eta(\mathbf{v} - \mathbf{u}) \cdot \mathbf{n}] = 0,$$

moisture:

$$[\mathbf{j} \cdot \mathbf{n}] + [\rho w(\mathbf{v} - \mathbf{u}) \cdot \mathbf{n}] = 0.$$

With appropriate interpretations, these apply at surfaces  $\mathcal{S}$  formed by cold and temperate ice, or both. All quantities are defined except  $\mathbf{n}$  which is a unit vector perpendicular to  $\mathcal{S}$  and pointing from the negative to the positive side of  $\mathcal{S}$ ;  $\mathbf{u} \cdot \mathbf{n}$  is the speed of propagation of  $\mathcal{S}$ , and  $\mathcal{S}$  is material if  $\mathbf{u} = \mathbf{v}$ . On the other hand,  $a_{\perp} = (\mathbf{v} - \mathbf{u})^- \cdot \mathbf{n}$  is the *volume flux through  $\mathcal{S}$*  so that (3.20)<sub>1</sub> may also be written as

$$\rho^-(\mathbf{v} - \mathbf{u})^- \cdot \mathbf{n} = \rho^- a_{\perp} = \rho^+(\mathbf{v} - \mathbf{u})^+ \cdot \mathbf{n}.$$

In Section 5 of Chapter 1, a *surface of phase change* was defined as a surface of singularity for which there is no temperature jump,  $[T] = 0$ . It thus follows from Equation (3.20)<sub>4</sub> that

$$[\mathbf{q} \cdot \mathbf{n}] = -T[\eta]\rho^- a_{\perp} \quad (\text{surface of phase change}). \quad (3.21)$$

As explained in Section 5 of Chapter 1, the product  $T[\eta]$  is related to the latent heat of fusion. For the mixture concept adopted here, it was deduced that  $T[\eta] = L[w]$ , see (1.143). We shall come back to this when discussing the jump conditions at the surface  $y = y_M(x, t)$ .

The above statements are of a *dynamic nature*. However, for every moving surface there is also a *kinematic* statement. If  $S(\mathbf{x}, t) \equiv 0$  is the equation of such an orientable surface, and if this surface is *material*, it is known that  $dS/dt \equiv 0$  represents this kinematic statement and forms an evolution equation for  $S$ . For a *non-material* surface  $dS/dt$  cannot vanish, as there must be a mass flux through the surface. However, the derivative of  $S$  *following the surface* must vanish, implying that

$$\frac{\partial S}{\partial t} + \operatorname{grad} S \cdot \mathbf{u} = \frac{\partial S}{\partial t} + \operatorname{grad} S \cdot \mathbf{v}^- - \operatorname{grad} S(\mathbf{v} - \mathbf{u})^- \equiv 0$$

or

$$\left( \frac{dS}{dt} \right)^- = \operatorname{grad} S \cdot (\mathbf{v} - \mathbf{u})^- = \| \operatorname{grad} S \| ((\mathbf{v} - \mathbf{u})^- \cdot \mathbf{n}) = \| \operatorname{grad} S \| a_\perp, \quad (3.22)$$

where  $\mathbf{n} = \operatorname{grad} S / \| \operatorname{grad} S \|$  points into the positive side of  $\mathcal{S}$  (thus defining the sign of  $S(\cdot)$ ). Here the superscript  $(-)$  is important as the formula would change if it referred to quantities on the right-hand side of the surface of discontinuity.

Consider, for instance, a plane flow with  $S = y_S(x, t) - y \equiv 0$ . In this case (3.22) has the form

$$\frac{\partial y_S}{\partial t} + \frac{\partial y_S}{\partial x} u^- - v^- = \sqrt{1 + \left( \frac{\partial y_S}{\partial x} \right)^2} a_\perp = a, \quad (3.23)$$

where  $a$  is the volume flux through the surface per unit length in the  $x$ -direction and  $u^-$  and  $v^-$  are the material velocity components in the  $x$ - and  $y$ -direction, respectively. Finally, note that if  $\Sigma(\mathbf{x}, t) \equiv 0$  is an identity for a physical quantity which must hold on the singularity surface, then an equation of the form (3.22) will also hold for  $\Sigma$ . This will be used later.

With the above preliminary derivations, the presentation of boundary conditions is straightforward. Two types of conditions must be considered, the kinematic and the dynamic, and these must be established for both cold and temperate ice.

(a) *At the free surface.* Because of accumulation (nourishment due to snowing) and ablation (wastage due to surface melting) the free surface is non-material, implying that the jump conditions (3.20) and the kinematic surface equations (3.22) or (3.23) apply. The form of the thermal boundary condition varies, according to whether the ice at the surface is cold or temperate.

To formulate the boundary conditions we consider a body part consisting of ice (the negative portion), atmosphere (the positive portion) and the free surface  $S_s(\mathbf{x}, t) \equiv 0$  as the singularity surface\*. Equations (3.20) and (3.22) then yield

$$\frac{\partial S_s}{\partial t} + \operatorname{grad} S_s \cdot \mathbf{v}^- = \|\operatorname{grad} S_s\| a_\perp, \quad \text{on } S_s(\mathbf{x}, t) \equiv 0 \quad (3.24)$$

as a kinematic equation in which  $a_\perp$  is, in general, a prescribed function of position and time, and for a *cold* boundary

$$\begin{aligned} [\![\mathbf{t} \cdot \mathbf{n}]\!] &= [\![\mathbf{v}]\!] \rho^- a_\perp, \\ [\![\mathbf{q} \cdot \mathbf{n}]\!] &= - \left[ \varepsilon(T_0) + c_p(T - T_0) + \frac{v^2}{2} \right] \rho^- a_\perp + [\![\mathbf{v}]\!] \cdot \{ \mathbf{t}^+ \cdot \mathbf{n} + \mathbf{v}^- \rho^- a_\perp \}, \end{aligned} \quad (3.25)$$

as jump conditions of momentum and energy. For the derivation of these equations, no simplifying assumptions have yet been invoked. As is evident, neither traction nor normal heat flux are continuous. Both are affected by the accumulation function and the jump in velocity. The physical interpretation of (3.25)<sub>1</sub> is that the jump of traction equals the product of velocity jump and mass flux. On the other hand, (3.25)<sub>2</sub> states that heat flux normal to the boundary is balanced by atmospheric heat flux, a diffusive flux of internal and kinetic energy, and a term which can be interpreted as a power due to diffusive momentum flux. In practice, the terms on the right-hand side of (3.25) are ignored so that

$$[\![\mathbf{t} \cdot \mathbf{n}]\!] = \mathbf{0} \quad \text{and} \quad [\![\mathbf{q} \cdot \mathbf{n}]\!] = 0 \quad (3.26)$$

is obtained. With the unit exterior normal vector in plane motion given by

$$\mathbf{n} = \left( -\frac{\partial y_s}{\partial x}, 1 \right) \Big/ \sqrt{1 + \left( \frac{\partial y_s}{\partial x} \right)^2} \quad (3.27)$$

and with the atmospheric stress  $\mathbf{t}^{\text{atm}} \cdot \mathbf{n} = -p^{\text{atm}} \mathbf{n}$  the component forms of (3.26) read

$$\left. \begin{array}{l} t_{xx} \frac{\partial y_s}{\partial x} - t_{xy} = -p^{\text{atm}} \frac{\partial y_s}{\partial x}, \\ -t_{xy} \frac{\partial y_s}{\partial x} + t_{yy} = -p^{\text{atm}}, \\ \kappa \frac{\partial T}{\partial x} \frac{\partial y_s}{\partial x} - \kappa \frac{\partial T}{\partial y} = q^{\text{atm}} \sqrt{1 + \left( \frac{\partial y_s}{\partial x} \right)^2} \end{array} \right\} \text{at } y = y_s(x, t). \quad (3.28)$$

\*With this convention,  $\mathbf{n}$  is the normal vector exterior to the ice and  $a_\perp$  is positive as an ablation rate, because  $a_\perp = (\mathbf{v} - \mathbf{u})^- \cdot \mathbf{n}$  which for zero ice velocity  $\sim -\mathbf{u} \cdot \mathbf{v}$ .

For cold ice, there are two thermal quantities for which a boundary condition can be established in principle, namely surface temperature and normal heat flux. Ideally, when solving the thermal problem, the motion and temperature-distribution in the atmosphere and the glacier should be interactively determined. In such instances, a continuity of temperature and heat flux is required. However, when solving only the thermal problem in the glacier and assuming the thermal conditions in the overlying half-space to be known and prescribable, the continuity of both temperature and heat flux can no longer be fulfilled. The reason is that the energy Equation (3.5) is of a second order in the spatial variables. The procedure is then to prescribe temperature

$$T = T_s(\mathbf{x}, t) \quad \text{at} \quad S_s(\mathbf{x}, t) \equiv 0,$$

which is the boundary condition used by Fowler and Larson [11] and Grigoryan *et al.* [14], yet from a climatological point of view, it is probably rather a condition on heat flux that should be required as a boundary condition at the free surface than a prescription of the surface temperature.

A free surface at which the ice is *temperate* is a surface of phase change at which  $T = T_s = T_M$ ; thus, the temperature is a known quantity. However, Equation (3.21) must also hold. To exploit it we must distinguish the cases for which either the ice at the surface is melting, or the water is freezing. For melting, see Figure 3.2, the ice water mixture is separated from the molten water layer. In this case, Equation (1.142) applies and (3.21) reduces to  $[\mathbf{q} \cdot \mathbf{n}] = -L(1-w)\rho a_\perp$ . For freezing with  $w > 0$  (for  $w = 0$  the ice is cold) the ice water mixture is separated from a frozen ice layer and, thus, (1.141) applies. Hence  $[\mathbf{q} \cdot \mathbf{n}] = -Lw\rho^- a_\perp$ . The thermal-boundary condition is therefore

$$[\mathbf{q} \cdot \mathbf{n}] = \begin{cases} -L(1-w)\rho a_\perp, & \text{melting} \\ -Lw\rho^- a_\perp, & \text{freezing} \end{cases} \quad w > 0; \quad (3.29)$$

relating the energy jump with  $a_\perp$ ,  $L$  and  $w$ . With  $\mathbf{n}$  as shown in Figure 3.2,  $a_\perp$  is positive as an ablation [recall that  $a_\perp = (\mathbf{v} - \mathbf{u})^- \cdot \mathbf{n}$ ] which is contrary to common usage. Further,  $w$  is small and may be ignored. Equation (3.29)<sub>2</sub> agrees then with the boundary condition of cold ice  $[\mathbf{q} \cdot \mathbf{n}] = 0$ , and

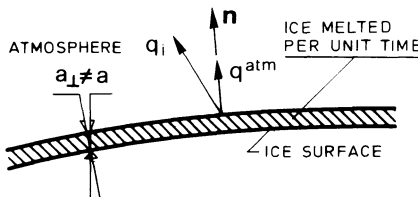


FIG. 3.2. Explaining the derivation of the surface boundary condition.

(3.29)<sub>1</sub> simply becomes  $\llbracket \mathbf{q} \cdot \mathbf{n} \rrbracket = -L\rho a_{\perp}$ . Also, for plane motion  $a_{\perp} = -a\sqrt{1 + (\partial y_s / \partial x)^2}$  (here  $a > 0$  corresponds to accumulation), (3.29)<sub>1</sub> becomes

$$apL \frac{1}{\sqrt{1 + (\partial y_s / \partial x)^2}} = q^{\text{atm}} - \frac{\kappa[(\partial T_M / \partial x)(\partial y_s / \partial x) - (\partial T_M / \partial y)]}{\sqrt{1 + (\partial y_s / \partial x)^2}}. \quad (3.29a)$$

If the ice is temperate throughout, the second term on the right can be ignored without loss of accuracy; consequently,

$$apL \approx q^{\text{atm}} \sqrt{1 + (\partial y_s / \partial x)^2}. \quad (3.29b)$$

For small inclinations, the melting rate  $a$  may directly be evaluated from  $q^{\text{atm}}$ . This explains why, at a free surface made up of temperate ice, one does not prescribe a thermal heat flux but an ablation rate in general. Equation (3.29b) relates the two.

The accumulation rate function  $a(x, t)$  depends on local weather conditions in a complicated way, and for long-term predictions of glacier and ice-sheet flows, only annual mean values, or even more extended mean values, are significant. With the coordinate system, as introduced in Figure 3.1, these mean values generally monotonically decrease with  $x$ , (see Figure 3.3). According to common procedures, the accumulation rate function  $a$  is only defined for values of  $x$  over which the ice mass extends; outside, the function is extended as the zero function. There is a point  $x_E$  which may be called the *accumulation-ablation-equilibrium point*, at which neither accumulation nor ablation occurs. It separates the mean accumulating from the mean ablating zones.

The boundary condition for the moisture content, finally, follows from (3.20)<sub>5</sub>. When  $\mathbf{j} = \mathbf{0}$  this condition is compatible with (3.20)<sub>1</sub> only provided that  $\llbracket w \rrbracket = 0$ , but when  $\mathbf{j} \neq \mathbf{0}$  one has

$$\llbracket \mathbf{j} \cdot \mathbf{n} \rrbracket = \llbracket w \rrbracket \rho^- a_{\perp} = w \rho^- a_{\perp} \quad (3.30)$$

where  $a_{\perp}$  is again positive as an ablation rate if  $\mathbf{n}$  is pointing out of the ice and where  $\mathbf{j}^+ \cdot \mathbf{n}$  is the moisture flux on the atmospheric side (usually negative).

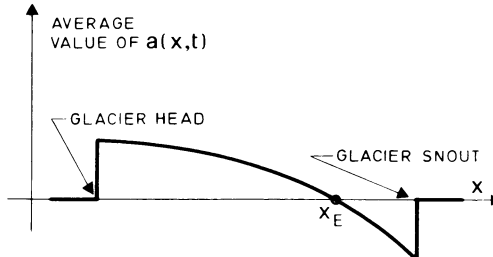


FIG. 3.3. A typical ice-accumulation function.

It must be determined from measurements of the total melting rate and estimates of the mean surface discharge; these separate identifications are difficult to determine in practice.

( $\beta$ ) *Along the ice-water interface.* Conceptually this surface is not much different from the free surface as it again separates two fluids. Since melting and freezing may occur, the ice-water interface is also non-material, but such that  $\llbracket T \rrbracket = 0$ .

Let  $S_w(x, t) \equiv 0$  be the equation of the surface; then

$$\frac{\partial S_w}{\partial t} + \text{grad } S_w \cdot \mathbf{u} = \|\text{grad } S_w\| a_w^\perp, \quad \text{on } S_w(\mathbf{x}, t) \equiv 0 \quad (3.31)$$

is the kinematic surface equation, where  $a_w^\perp$  is the melting-freezing rate which is positive for freezing. In plane flow  $S_w$  is thus defined by  $S_w = y - y_w(x, t)$  and yields

$$\frac{\partial y_w}{\partial t} + \frac{\partial y_w}{\partial x} u - v = -a_w(x, t), \quad \text{at } y = y_w(x, t), \quad (3.32)$$

With the same simplifying assumptions as in the last section, the jump conditions of momentum and energy for cold and temperate ice are

$$\llbracket \mathbf{t} \cdot \mathbf{n} \rrbracket = \mathbf{0} \quad \text{and} \quad \llbracket \mathbf{q} \cdot \mathbf{n} \rrbracket = -\rho L \llbracket w \rrbracket a_w^\perp, \quad (3.33)$$

where it is assumed that the traction and energy flux on the water side are known. Typically, on the water side  $w = 1$  and

$$\begin{aligned} (\mathbf{t} \cdot \mathbf{n})_{\text{water}} &= -p_w \mathbf{n} + \mathbf{t} \\ (\mathbf{q} \cdot \mathbf{n})_{\text{water}} &= h(T_{\text{ice}} - T_{\text{water}}), \end{aligned} \quad (3.34)$$

in which  $p_w$  is the water pressure and  $\mathbf{t}_w$  the shear traction exerted on the ice by the water. In case shear tractions are not neglected, the shear stress is set proportional to the square of the mean speed outside the boundary layer induced by the ice. Consequently  $\mathbf{t}_w = (\rho/2)c_w |\mathbf{U}_w| \mathbf{U}_w$ , where  $\mathbf{U}_w$  is the current velocity and  $c_w$  a drag coefficient whose value must be determined experimentally. On the other hand,  $h$  in Equation (3.34) is a *heat transfer coefficient* whose value depends on the flow conditions within the boundary layer beneath the ice. When  $T_{\text{ice}} = T_M$  then melting must occur,  $a_w^\perp < 0$ ; alternatively, when  $T_{\text{ice}} = T_{\text{water}} < T_M$ , one has freezing,  $a_w^\perp > 0$ . In the interval  $T_{\text{water}} < T_{\text{ice}} < T_M$  the ice adjusts its temperature to the energy budget; there is neither melting nor freezing,  $a_w^\perp = 0$ . In summary, the thermal-boundary condition at the ice-water interface has the form

$$\rho L(1-w)a_w^\perp = \begin{cases} -\mathbf{q} \cdot \mathbf{n}|_{T_{\text{ice}} = T_{\text{water}}} , & a_w^\perp > 0, w = 0, \\ 0 = h(T_{\text{ice}} - T_{\text{water}}) - \mathbf{q} \cdot \mathbf{n}|_{T_{\text{ice}}}, & a_w^\perp = 0, \\ h(T_M - T_{\text{water}}) - \mathbf{q} \cdot \mathbf{n}|_{T_{\text{ice}} = T_M}, & a_w^\perp < 0, w \neq 0, \end{cases} \quad (3.35)$$

in which  $w$  is the moisture content on the ice side. Evidently, either temperature is prescribed and then (3.35) relates the heat flux on the ice side normal to the interface to the freezing or melting rate, or else  $a_w^\perp = 0$  is known, and then the temperature on the ice side and its normal derivative are related to the (given) water temperature.

The assumption in the above was that the ice at the lower boundary is cold, or just reaches the melting point. This requires that  $T_{\text{water}} \leq T_M$ . When  $T_{\text{water}} > T_M$ , there is a layer of temperate ice close to the ice-water interface. In that case only (3.35)<sub>3</sub> applies, but  $\mathbf{q} \cdot \mathbf{n}$  is negligibly small; thus the heat transfer law determines the melting rate in this case. The jump condition for moisture (3.20)<sub>5</sub> becomes  $[\mathbf{j} \cdot \mathbf{n}] = -[w]a_w^\perp$ . Since on the water side we must have  $w \equiv 1$  throughout, and  $\mathbf{j} \equiv \mathbf{0}$ , if there is no drainage, the boundary condition of moisture at the ice water interface must be

$$\mathbf{j} \cdot \mathbf{n} - (1 - w)a_w^\perp = 0 \quad (\text{on the ice side}). \quad (3.36)$$

This completes the boundary conditions for the ice water interface.

Finally, we point out the most common functional forms of the drag coefficient  $c_w$  and the heat transfer coefficient  $h$ .

As far as drag is concerned, extensive studies have been executed to obtain precise statements when momentum transfer from the atmosphere to the free ocean or a bounded lake is considered, see Wengenfeld [70]. According to this literature, the surface shear stress not only depends on fetch but also on the surface roughness produced by the induced waves. When water flows below a floating ice plate, this motion will cause an undulating ice-water interface with wavelengths which depend on the conditions of the flow beneath the plate. It will be assumed in the following that these motion-induced waves are long, so that the ice surface acts like a smooth, flat plate, and its friction factor can be approximately represented by that of a flat plate. The momentum-integral equation for the boundary-layer flow in combination with the  $\frac{1}{7}$  power-law velocity distribution may then be used to show that

$$c_w = 0.0576 \left( \frac{U_w x}{v} \right)^{-1/5}, \quad (3.37)$$

where  $U_w$  is the ocean current speed outside the boundary layer,  $x$  is the fetch or the distance of the point under consideration measured from the leading edge of the plate and  $v$  is the kinematic viscosity of water, see Schlichting [54], Chapters 8 and 21.  $U_w x / v$  is a Reynolds number and assumes for  $U_w = 0.1 \text{ m s}^{-1}$ ,  $x = 10^4 \text{ m}$  and  $v = 2 \times 10^{-6} \text{ m}^2 \text{ s}^{-1}$  the order of magnitude  $10^9$ .

Consider next the heat transfer coefficient  $h$ . For a flat boundary, the heat transfer coefficient  $h$  can only depend on the thermal and viscous

properties of the water and its motion outside the boundary layer. For steady-state flow, simple arguments of dimensional analysis (see Bird *et al.* [2]) show that the heat transfer coefficient can be expressed as a power law relating the Nusselt, Reynolds and Prandtl numbers, provided that the flow is in the range of forced convection. An account of the analysis of the thermal boundary layer and the corresponding heat transfer problem is given by Schlichting [54] (Chapter 12). He analyses parallel flow past a flat plate at zero incident. Measuring  $x$  along the plate from the leading edge, it is demonstrated that the local Nusselt, local Reynolds and the Prandtl numbers are related by

$$\text{Nu} = a \text{Pr}^\alpha \text{Re}^\beta, \quad (3.38)$$

where

$$\text{Nu} := \frac{hx}{\kappa}, \quad \text{Pr} := \frac{\nu \rho_w c_p}{\kappa} \quad \text{Re} := \frac{U_w x}{\nu} \quad (3.39)$$

with

	$a$	$\alpha$	$\beta$	
laminar flow	0.339	$\frac{1}{3}$	$\frac{1}{2}$	
turbulent flow	0.0295	$\frac{1}{3}$	$\frac{4}{5}$	

(3.40)

For laminar flow these are restricted to Prandtl numbers larger than 10. For water at the freezing point  $\text{Pr} \approx 13.5$  so that this condition is satisfied. To obtain an order of magnitude for  $\text{Nu}$ , consider  $U_w = 10 \text{ m s}^{-1}$ ,  $x = 10^3 \text{ m}$  and  $\nu = 1.79 \times 10^{-6} \text{ m}^2 \text{ s}^{-1}$ . This yields  $\text{Re} = 5.6 \times 10^8$  and, consequently, for turbulent flow  $\text{Nu} = 7 \times 10^5$ . With  $\kappa = 7 \times 10^7 \text{ JK}^{-1} \text{ m}^{-1} \text{ a}^{-1}$  this corresponds to a heat transfer coefficient with a value  $h \approx 5 \times 10^{10} \text{ Jm}^{-2} \text{ K}^{-1} \text{ a}^{-1}$ .

(v) *Along the bedrock surface.* The development of a set of suitable boundary conditions for this surface is more involved than that for free surface or the ice-water interface. The reader may recall from the introductory remarks to this chapter that boundary conditions at the bedrock surface must not only be handled separately for cold and temperate ice, but that even for temperate ice various possibilities exist. In this regard, attention was focused on the distinction between sliding with and without cavity formation.

(i) In the *cold ice zone* and distant from the melting surface, the ice adheres to the bed. Hence the no-slip condition applies and there is no jump of momentum and heat flux,

$$[\![\mathbf{v}]\!] = \mathbf{0}, \quad [\![\mathbf{t} \cdot \mathbf{n}]\!] = \mathbf{0}, \quad [\![\mathbf{q} \cdot \mathbf{n}]\!] = 0. \quad (3.41)$$

On a *rigid bed* this implies

$$\mathbf{v} = \mathbf{0}, \quad \mathbf{q} \cdot \mathbf{n} + q^{\text{geoth}} = 0, \quad (3.42)$$

where  $q^{\text{geoth}}$  is the geothermal heat flow *into* the ice. A jump condition for  $t$  need not be written down as basal traction can be determined from (3.41)<sub>2</sub>.

(ii) In the *temperate ice zone*, the ice slides over its rockbed because of the presence of a liquid film of water that exists between the ice sole and the bed. This film acts as a lubricant and causes the ice at the boundary to slide almost 'inviscidly' over the bed. In the following, sliding with and without cavity formation need separate attention. We begin with sliding without cavity formation. On a small scale, in which the flow around the *actual* bed is looked at, sliding without cavity formation may indeed be regarded as 'inviscid'. It is, however, quite clear that the ice sufficiently distant from the rockbed will not 'feel' its small-scale undulations. These will, at most, affect the flow in the immediate neighborhood of the rockbed, see Figure 3.4. This region is called the boundary or inner flow layer. Except for regions close to the snout, this inner layer is expected to be small in comparison with the total thickness of the ice, so that attention might be restricted to the outer flow region whose flow may be determined from applying a suitable boundary condition at a smoothed boundary, see Figure 3.4. Sliding over this smoothed hypothetical rockbed is 'viscous', because the ice experience a resistive drag near the bed, due to small-scale roughness of the actual rockbed. The detailed small-scale flow of the ice over the actual rockbed profile is essentially contained in the inner layer. At its outer edge its flow should only insignificantly differ from the *outer flow* which is defined as the flow of the ice mass sliding over the smoothed-out rockbed on which a tangential stress is accordingly applied to fulfill the matching of the inner and outer flow solution.

The above ideas will not be made explicit here. It may suffice to mention that they may be made rigorous by using the methods of matched asymptotic expansions. This was first done by Fowler [9, 10a] although a consistent mathematical treatment of the problem was already presented by Kamb [21] and Nye [42, 43]. Fowler concludes that since the inner flow 'feels'

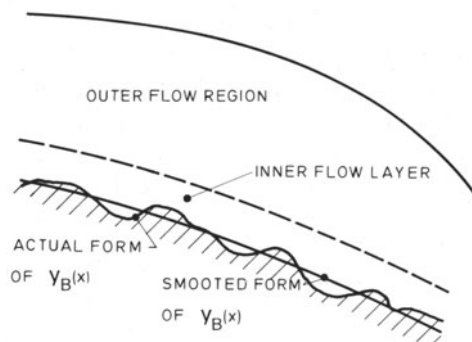


FIG. 3.4. Ice-rockbed, its actual and smoothed-out forms, explaining sliding friction.

the outer flow as a uniform shearing flow at infinity, and the outer flow ‘feels’ the inner flow as a tangential shear stress at the smoothed-out boundary, it should be possible to relate the basal shear stress at the smoothed-out boundary with the basal-sliding velocity from an examination of the inner flow problem. Hence, the following sliding law is expected to apply at the smoothed-out rockbed:<sup>\*</sup>

$$t_{sn} = f^{-1}(u_s), \quad \text{or equivalently } u_s = f(t_{sn}), \quad (3.43)$$

where  $u_s$  is the sliding velocity along the smoothed rockbed and  $t_{sn}$  is the basal shear stress, the subscripts  $s$  and  $n$  indicating the directions along and perpendicular to the smoothed rockbed surface.

Incidentally, the boundary conditions (3.42)<sub>1</sub> for cold ice and those for temperate ice (3.43), can be combined in one single formula if  $f$  is not only assumed to be a function of  $t_{sn}$ , but also of  $m = T - T_M$ . The second variable,  $m$ , allows us to interpret the relations (3.42)<sub>1</sub> and (3.43) as the generalized function shown in Figure 3.5. Accordingly,  $f$  is zero for cold ice and suddenly jumps at the melting point to a finite value.

The determination of the function  $f$  in terms of  $t_{sn}$  is one of the most challenging problems in glaciology and deserves special attention. The opinions of different authors are generally in agreement if the flow is approximated by a linear Newtonian model, but differences arise when a non-linear constitutive response is considered and when sliding with cavitation or cavity formation is analysed. Systematic ‘rational’ investigations only exist for *sliding without cavity formation*, and the following remarks pertain to these. According to the linear models (see Fowler [9, 10a], Kamb [21], Lliboutry [27], Morland [33, 34], Nye [42, 43]), the function  $f$  is linear and expressible in terms of the roughness of the bed. Hence

$$t_{sn} = Cu_s \quad (\text{linear law}) \quad (3.44)$$

with an appropriately determined constant  $C$ . Weertman [63, 66, 69] who investigated the problem for non-linear rheology first, obtains

$$t_{sn} = \frac{1}{\mathcal{C}} u_s^{1/m}, \quad \text{or} \quad u_s = \mathcal{C} t_{sn}^m, \quad (3.45)$$

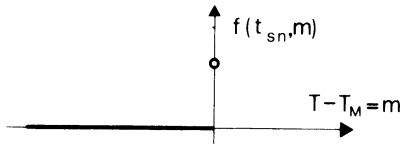


FIG. 3.5. Sliding function.

\*A full three-dimensional version of this sliding law is given in Chapter 7.

where  $m \simeq 2$  and  $\mathcal{C}$  is a function of the roughness of the bed. In fact, according to his derivation, which is based on the use of Glen's flow law, the exponent  $m$  in Equation (3.45) depends only on the exponent in Glen's flow law, whereas  $\mathcal{C}$  is merely a function of the roughness of the bed. Lliboutry [24] has challenged Weertman's approach to sliding without cavity formation, but he finds only different values for the coefficients  $\mathcal{C}$  and  $m$ . Generalizing his linear analysis, Kamb [21] on the other hand came out in support of Equation (3.45), however with slightly other interpretations of the coefficients  $\mathcal{C}$  and  $m$ . In particular, according to Kamb's results,  $m$  depends both on the material response function and on the roughness of the bed. It thus appears that for each glacier  $\mathcal{C}$  and  $m$  must be determined independently. We may leave the sliding law therefore in the undetermined form (3.45).

It appears that agreement on what form the functional relationship  $f$  should assume for temperate ice has not yet been reached. Detailed knowledge is even more lacking in cold ice close to the transition to melting, see Figure 3.5. Indeed, a relationship of the form (3.45) cannot possibly be valid in the vicinity of the bottom melting point (the intersecting point of the melting curve with the smoothed-out rockbed surface), see Figure 3.6. This holds, since  $t_{sn} \neq 0$  on the temperate side, and because any reasonable  $f$  should satisfy  $f(0) = 0$ .

A discontinuity in the boundary condition occurs at the cold temperate transition point, which will result in stress singularities. Hence the sliding law should be regularized. Hutter and Olunloyo [15, 16] propose to make

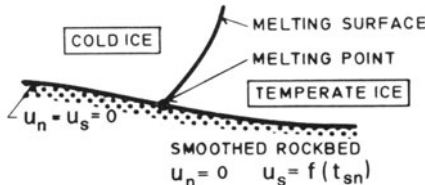


FIG. 3.6. Mechanical boundary conditions close to the melting point.

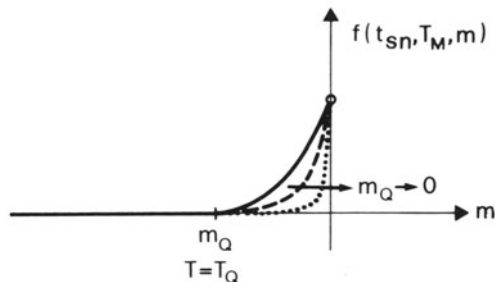


FIG. 3.7. Appropriate sliding function for polythermal glaciers near the melting point.

the  $\zeta$  position dependent with  $\zeta = 0$  at the cold-temperate transition point and prove, using a linear model, that such singularities of the stresses develop even when  $\zeta$  is continuous. Fowler and Larson [11] extend  $f$  smoothly into the cold domain by making it functionally dependent on  $T_M$  and  $m$ , see Figure 3.7, where  $f$  is continuous from the left. Fowler [9] states that in the limit as  $m_Q \rightarrow 0$  (Figure 3.7) stresses remain bounded. Thus, results depend critically on the form of the boundary conditions.

The form of  $f$  for sliding under a simultaneous formation of cavities is even more controversial. Such sliding occurs when sufficient meltwater is produced to set the water table in a glacier at roughly nine-tenths of its depth or higher. This meltwater moves through the ice in crevasses, moulin and intra- and subglacial channels (see Björnsson [3], Iken [19, 20], Matthew [31], Nye [45], Nye and Frank [46], Roethlisberger [52], Spring [58] and Spring and Hutter [59, 60]). Extensive model analyses of Lliboutry [27, 28a] indicate that  $f$  in (3.43) may cease to be the well-behaved function of Figure 3.38a (power law) and must become either multi-valued (Figure 3.8b) or grow very fast as a limit value before the shear traction is reached (Figure 3.8c). The sliding law of Figure 3.8b would give rise to a bifurcation mechanism because there are two sliding velocities to a given traction. In the model of Figure 3.8c sliding velocities could become very large. Both could explain why in certain situations glacier velocities may become 'catastrophic' (so called glacier surges). Lliboutry [27, 28a] argues that the effective pressure  $p^* = p_{\text{ice}} - p_{\text{water}}$  must enter the sliding law but no theory is presented in which  $p_{\text{ice}}$  and  $p_{\text{water}}$  would enter as independent variables.\* Weertman [66, 67, 69], on the other hand, denies such a dependence and defends his law (3.45) with an approximately adjusted constant  $\zeta$ . Because of a lack of better knowledge we may restrict our considerations to sliding without cavity formation, or postulate Equation (3.43) with a function  $f$ , as shown in Figure 3.8, as a first approximation until further investigations will prove it

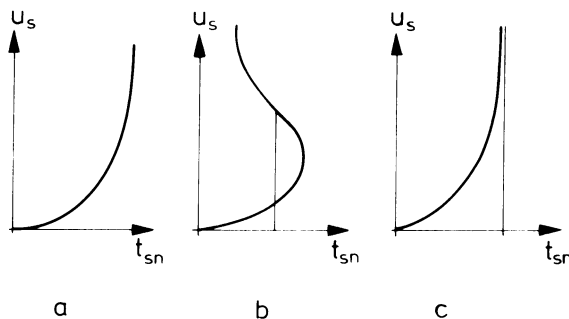


FIG. 3.8. Three possible sliding laws relating shear traction and sliding velocity.

\*Such a theory would have to start from a mixture concept in which also balance of momenta were established for ice and water separately. Such a theory must be extremely complicated.

to be insufficient as a model of sliding with a simultaneous formation of cavities.

The above considerations are only concerned with the sliding law and no other boundary conditions. The discussion also indicates that the deduction of jump conditions from (3.20) is probably controversial, since the smoothed-out surface is not a physical but a mathematical surface. Nevertheless, we now assume the mean rock bed,  $S_B \equiv 0$ , to be a rigid singular surface along which the ice slides and explore the interferences which follow from the jump conditions (3.20). Ignoring the contribution from the melting rate  $a_\perp$  the conditions are

$$\begin{aligned} \mathbf{v} \cdot \mathbf{n} &= 0, & [\![\mathbf{q} \cdot \mathbf{n}]\!] &= \mathbf{v} \cdot \mathbf{t} \cdot \mathbf{n}, \\ [\![\mathbf{t} \cdot \mathbf{n}]\!] &= \mathbf{0}, & [\![\mathbf{j} \cdot \mathbf{n}]\!] &= 0. \end{aligned} \quad (3.46)$$

The first of these is the tangency condition, the second expresses a continuity of the tractions, the third equates the jump in heat flux to the power of the frictional forces, and the fourth expresses a continuity of moisture flux. In a theory with  $\mathbf{j} \neq \mathbf{0}$ ,  $\mathbf{j} \cdot \mathbf{n}$  on the rock side is the drainage function and must be prescribed if the deformations of the ice and the rock are not interactively solved.

(d) *Along the melting surface.* A complete description of polythermal glaciers must also include transition conditions at the inner surfaces where cold ice reaches melting point. Let  $S_M(\mathbf{x}, t) \equiv 0$  be the equation of this surface. As a surface of phase change, it is not material and thus the jump conditions (3.20)<sub>1,2,5</sub> and (3.21) apply with  $T[\eta] = L[w]$ . Hence

$$\begin{aligned} [\![T]\!] &= 0, & [\![\mathbf{v} - (\mathbf{v} \cdot \mathbf{n}) \cdot \mathbf{n}]\!] &= \mathbf{0}, & [\![\mathbf{q} \cdot \mathbf{n}]\!] + L[\![w]\!] \rho^- a_M^- &= 0 \\ [\![\mathbf{t} \cdot \mathbf{n}]\!] &= [\![\mathbf{v}]\!] \rho^- a_M^\perp \simeq 0, & [\![\mathbf{j} \cdot \mathbf{n}]\!] + [\![w]\!] \rho^- a_M^\perp &= 0. \end{aligned} \quad (3.47)$$

The first two conditions express continuity of the temperature and of the tangential velocity component, the remaining three conditions are the momentum, energy and moisture jump conditions. We may also assume, with a sufficient degree of accuracy, that  $\mathbf{t} \cdot \mathbf{n}$  is continuous on  $S_M \equiv 0$ , but a similar assumption would be inappropriate for the remaining conditions. For  $\mathbf{j} \neq \mathbf{0}$  relations (3.47)<sub>3,5</sub> can be related,

$$[\![\mathbf{q} \cdot \mathbf{n}]\!] = L[\![\mathbf{j} \cdot \mathbf{n}]\!].$$

Since  $\mathbf{j}^- \equiv \mathbf{1}$  and  $(\mathbf{q} \cdot \mathbf{n})^+$  is nearly zero, because the Clausius–Clapeyron equation gives rise to very weak temperature gradients, we have

$$(\mathbf{q} \cdot \mathbf{n})^- \simeq -L(\mathbf{j} \cdot \mathbf{n})^+, \quad (\mathbf{j} \neq \mathbf{0}). \quad (3.48)$$

On the other hand, from (3.47)<sub>5</sub>, and since  $w^- = 0$

$$(\mathbf{j} \cdot \mathbf{n})^+ = -w^+ \rho^- a_M^\perp. \quad (3.49)$$

This relation implies that in a mixture theory with  $\mathbf{j} = \mathbf{0}$ , the moisture content must vanish on either side of the melting surface. In view of (3.47)<sub>4</sub>  $\mathbf{q} \cdot \mathbf{n}$  would also have to be continuous in this case. Such a theory is, however, defective, because it does not allow a solution of the following Stefan problem\*: given two ice blocks, one at a uniform temperature below melting, the other at melting. At  $t = 0$  the two blocks are brought into contact. In the ‘welded’ block the melting surface will move in time. One might wish to determine the motion of this surface. For the two blocks at rest this thermal problem can easily be established, but it has no solution when  $[w] = 0$  at the cold temperate transition surface. It follows that a theory with  $\mathbf{j} = \mathbf{0}$  is likely to be inappropriate. Nevertheless, Fowler and Larson [11] present a formulation which agrees with ours when  $\mathbf{j} = \mathbf{0}$ .

A further argument in support of having a non-trivial Fick-type moisture flux  $\mathbf{j}$  is that the field equation

$$\rho \dot{w} = \text{tr}(\mathbf{t}' \mathbf{D})/L = 2\mathcal{A}(w)f(t'_{II})t'_{II}/L \quad (3.50)$$

together with the boundary condition  $w = 0$  on  $S_M = 0$  requires that the melting surface as illustrated in Figure 3.1 is a monotonically increasing function of  $x$ , or more specifically, that the direction of the streamlines of the flow at all points along the melting surface is from the cold to the temperate ice. This assumption may be written in the form

$$\frac{\partial y_M}{\partial t} + \frac{\partial y_M}{\partial x} u - v \geq 0, \quad \text{when } y = y_M, \text{ if } T < Y_M \text{ in } y_M^\pm.$$

Here,  $y_M^\pm$  indicates ice regions just above and below  $y_M$  and the  $+(-)$  sign is associated with the  $>(<)$  inequality. The meaning of this statement becomes clear if it is recognized that for the  $>$  inequality, the material particles which are sitting immediately above  $y_M$  move though the melting surface. It follows from the theory of characteristics, see, e.g., von Mises [32] and Whitham [71], that the streamlines are the characteristics of Equation (3.50). Further, for all motions it is likely that  $\text{tr}(\mathbf{t}' \mathbf{D}) > 0$ , which we shall assume to hold. On account of the boundary condition  $w = 0$  on  $S_M = 0$ , see Figure 3.9, the moisture content can be determined in the shaded region provided  $w$  is given along the segment CD. By integration along the characteristics,  $w$  can be determined at any point on CE. Due to the stated monotonicity property,  $w_B > w_A$ ; yet the boundary condition requires  $w_B = w_A = 0$ . This is a contradiction. Hence, melting surfaces as shown in Figure 3.9 cannot exist if the moisture content is calculated from an equation of the form (3.50). Similarly, there can be no closed melting surfaces.

The above dynamic conditions must be complemented by kinematic

\*An exact solution to the Stefan problem for an ice sheet floating on water at rest is given by Carlslaw and Jeger [7a].

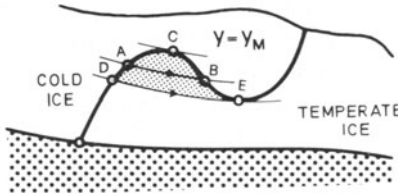


FIG. 3.9. A form of the melting surface for which no solution to Equation (3.50) can exist.

conditions. A first is

$$\left( \frac{dS_M}{dt} \right)^- = \frac{\partial S_M}{\partial t} + \text{grad } S_M \cdot \mathbf{v}^- = \| \text{grad } S_M \| a_M^\perp \quad (3.51)$$

and forms the usual kinematic surface condition. Further conditions could be deduced from any function  $f(\mathbf{x}, t)$  which is continuous and satisfies the condition  $f = \text{constant}$  on  $S_M = 0$ . Such a statement holds for temperature,  $T - T_M = 0$ , so that

$$\left( \frac{d(T - T_M)}{dt} \right)^- = \| \text{grad } (T - T_M) \| a_M^\perp \quad (3.52)$$

with  $dT_M/dp = -c_t$ , but only one of the two must be used. Which one should be adopted depends on the application. We shall use the linearized form

$$T_M = T_f - c_t(p - p_{\text{atm}}) \quad (3.53)$$

in which  $T_f$  is the freezing temperature at atmospheric pressure  $p_{\text{atm}}$ .

In conclusion, it should be said that many particulars which are important from a practical point of view have been ignored in the above description of polythermal ice. The effect of salts have not been touched upon and an equation for  $\mathbf{j}$  in which gravity enters as a parameter, has not explicitly been written down. The reason is that very little is known about these and, indeed, all authors who solve flow problems in temperate ice ignore the moisture content. This will also be the case for the remainder of this book. The reason for treating ice as a mixture model (even though a very simple one) was to demonstrate that the methods explained in Chapter 1 are the appropriate vehicle to do this. Whether the theory presented above withstands further scrutiny will have to be demonstrated by solving typical boundary-value problems. The remainder of this book will be devoted to such problems.

### 3. The Response of a Parallel-sided Ice Slab to Steady Conditions

In a first approximation, natural ice, which covers glaciers, ice sheets, and ice shelves, can be treated as infinitely long parallel-sided continua

which are subject to gravity. Clearly, the true geometries are only nearly parallel-sided; yet if the solution to the strictly parallel-sided ice slab is known, it is conceivable that some problems of the *nearly* parallel-sided slab can be treated by an appropriate perturbation scheme, taking the parallel-sided slab as a first approximation.

The restriction to such a simple geometry also implies limitations in the physical processes under consideration. In general, these have to be steady-state, although an unsteady flow configuration may be visualized in a particular case for which the thickness of the ice slab remains constant.

These are the restrictions imposed upon the flow problem under consideration: the physical processes are assumed steady in time and the ice is considered either to be temperate or else cold; polythermal ice will not be considered. Under these circumstances, the governing field equations comprise the balance of mass, momentum, energy and the constitutive relations listed in Section 2a. When referred to the coordinate system of Figure 3.10, these assume the form (see Equations (3.1) to (3.5), (3.18) and (3.19)):

$$\begin{aligned} \frac{\partial u}{\partial x} + \frac{\partial v}{\partial y} &= 0, \\ \rho \left\{ \frac{\partial u}{\partial x} u + \frac{\partial u}{\partial y} v \right\} &= \frac{\partial t_{xx}}{\partial x} + \frac{\partial t_{xy}}{\partial y} + \rho g \sin \gamma, \\ \rho \left\{ \frac{\partial v}{\partial x} u + \frac{\partial v}{\partial y} v \right\} &= \frac{\partial t_{xy}}{\partial x} + \frac{\partial t_{yy}}{\partial y} - \rho g \cos \gamma, \\ \frac{\partial u}{\partial x} &= \frac{1}{2} A \exp \left( -\frac{Q}{kT} \right) f(t'_{II})(t_{xx} - t_{yy}), \\ \frac{\partial u}{\partial y} + \frac{\partial v}{\partial x} &= 2A \exp \left( -\frac{Q}{kT} \right) f(t'_{II})t_{xy}, \\ \rho c \left\{ \frac{\partial T}{\partial x} u + \frac{\partial T}{\partial y} v \right\} &= \kappa \left( \frac{\partial^2 T}{\partial x^2} + \frac{\partial^2 T}{\partial y^2} \right) + 2A \exp \left( -\frac{Q}{kT} \right) f(t'_{II})t'_{II}, \end{aligned} \quad (3.54)$$

in which  $t'_{II} = \frac{1}{2}(t_{xx} - t_{yy})^2 + t_{xy}^2$  and where the energy Equation (3.54)<sub>6</sub> has been written for cold ice and must be replaced by Equation (3.11)<sub>3</sub> for temperate ice. In that case, the Arrhenius factor  $A \exp(-Q/kT)$  must also be replaced by  $\mathcal{A}_w$ , where  $\mathcal{A}_w$  is a function of the moisture content. Common procedure in this case is, however, to assume  $\mathcal{A}_w$  to be independent of moisture content. For such a restriction Equation (3.11)<sub>3</sub> is the only equation involving the moisture content, so that the latter can be obtained *a posteriori*. When treating temperate ice the differential equation for the moisture content may therefore in a first approximation be disregarded.

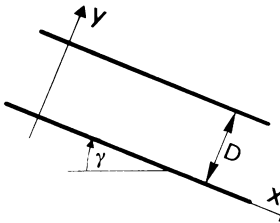


Fig. 3.10. An infinitely-long parallel-sided ice slab.

The boundary conditions to be satisfied are:

At the *ice-rock interface* [(3.45), (3.46)]:

$$\begin{aligned} u &= \mathcal{C}t_{xy}^m, & v &= 0, \\ T &= T_M, & \text{if the ice is temperate,} \\ t_{xy}u - \kappa \frac{\partial T}{\partial y} &= q^{\text{geoth}}, & \text{if the ice is cold,} \end{aligned} \quad (3.55)$$

where we have restricted considerations to Weertman-type sliding. Consequently,  $\mathcal{C} = 0$  for cold ice, which implies that the frictional heat in (3.55)<sub>4</sub> vanishes in this case:  $t_{xy}u = 0$ .

At the *free surface*, [(3.23)–(3.29)]:

$$\begin{aligned} t_{xy} &= 0, & t_{yy} &= -p^{\text{atm}}, \\ T &= T_M, & \rho La &= q^{\text{atm}}, & \left. \begin{array}{l} \text{if } q^{\text{atm}} < 0 \\ \text{if the ice is temperate,} \end{array} \right\} \\ -\kappa \frac{\partial T}{\partial y} &= q^{\text{atm}}, & T &= T_s, & \left. \begin{array}{l} \text{if the ice is cold,} \\ \text{or} \end{array} \right\} \\ v &= -a, & \text{for } a \leq 0. \end{aligned} \quad (3.56)$$

Here  $T_s$  is the prescribed surface temperature. Furthermore, of the thermal boundary conditions for cold ice, only one condition can be applied. The choice depends on the particular application in mind. Notice also that the last Equation (3.56) follows from Equation (3.23), the steady-state assumption and the requirement that the slab is parallel-sided.

At the *ice-water interface*, [(3.32)–(3.36)]:

$$\begin{aligned} t_{xy} &= \frac{\rho}{2} c_w U_w |U_w|, & t_{yy} &= -p^{\text{water}}, \\ \rho La_w + h(T_w - T_M) &= 0, & \text{if the ice is temperate,} \end{aligned}$$

$$\rho La_w = \begin{cases} -\kappa \frac{\partial T}{\partial y} \Big|_{T=T_w}, & \text{if } a_w > 0, \\ 0 = -h(T_w - T_M) - \kappa \frac{\partial T}{\partial y}, & \text{if } T_w < T < T_M, \\ -h(T_w - T_M) - \kappa \frac{\partial T}{\partial y} \Big|_{T=T_M}, & \text{if } a_w < 0, \end{cases} \quad \text{if the ice is cold}$$

$v = a_w.$  (3.57)

Reasonable boundary-value problems now consist of the field Equations (3.54) and the boundary conditions, which are either Equations (3.55) and (3.56), or (3.56) and (3.57). Before proceeding to construct solutions to these, the above set of equations will be transformed into a dimensionless form.

(a) *Dimensionless forms of the field equations*

The non-dimensionalization of the basic problem involves the finding of typical dimensional quantities to serve as scaling factors for the various dimensional variables in the problem.

An appropriate length scale is the glacier or ice sheet thickness,  $D$ , stresses may be non-dimensionalized with the overburden pressure  $\rho g D$  at zero inclination and time with a characteristic time,  $\mathfrak{T}$ . Temperatures will be scaled by introducing the dimensionless temperature according to  $T = T_f + T_0 \vartheta$ . If  $T_f$  is the freezing temperature at atmospheric pressure and  $T_0$  a temperature difference of a mean estimated ice temperature, then  $\vartheta$  assumes values between  $-1$  and  $0$ . Notation is simplified if, apart from temperature, *coldness*  $g$  is also introduced as a separate variable and defined as

$$g = \frac{1}{T}. \quad (3.58)$$

It will be made dimensionless by writing  $g = g_f - g_0 \theta$ . The choices

$$g_f = \frac{1}{T_f}, \quad g_0 = \frac{1}{T_f - T_0} - \frac{1}{T_0} \quad (3.59)$$

guarantee that the dimensionless temperature  $\vartheta$  and the coldness  $\theta$  assume the values  $(0, -1)$  simultaneously. In particular  $\vartheta$  and  $\theta$  are related by

$$\theta = \frac{1 - \mathbb{Z}}{1 + \mathbb{Z}\vartheta} \vartheta, \quad \vartheta = \frac{\theta}{1 - \mathbb{Z} - \mathbb{Z}\theta}, \quad \mathbb{Z} = \frac{T_0}{T_f}. \quad (3.60)$$

The following scalings are now introduced:

$$(x, y) = D(\bar{x}, \bar{y}), \quad t = \bar{t}/\mathfrak{T}, \quad (t_{xx}, t_{yy}, t_{xy}) = \rho g D(\sigma_x, \sigma_y, \tau),$$

$$(u, v) = U(\bar{u}, \bar{v}) = \frac{D}{\mathfrak{T}}(\bar{u}, \bar{v}), \quad T = T_f + T_0 \vartheta, \quad g = g_f - g_0 \theta. \quad (3.61)$$

The variables carrying an overhead bar and  $\sigma_x$ ,  $\sigma_y$ ,  $\tau$ ,  $\vartheta$  and  $\theta$  are dimensionless. With the exception of the energy equation the field Equations (3.54) then become

$$\begin{aligned} \frac{\partial \bar{u}}{\partial \bar{x}} + \frac{\partial \bar{v}}{\partial \bar{y}} &= 0, \\ \mathbb{F} \left\{ \frac{\partial \bar{u}}{\partial \bar{x}} \bar{u} + \frac{\partial \bar{u}}{\partial \bar{y}} \bar{v} \right\} &= \frac{\partial \sigma_x}{\partial \bar{x}} + \frac{\partial \tau}{\partial \bar{y}} + \sin \gamma, \\ \mathbb{F} \left\{ \frac{\partial \bar{v}}{\partial \bar{x}} \bar{u} + \frac{\partial \bar{v}}{\partial \bar{y}} \bar{v} \right\} &= \frac{\partial \tau}{\partial \bar{x}} + \frac{\partial \sigma_y}{\partial \bar{y}} - \cos \gamma, \\ \frac{\partial \bar{u}}{\partial \bar{x}} &= \frac{1}{2} \mathbb{G} \exp(\mathbb{A} \theta) \mathfrak{F}(\tau'_{II})(\sigma_x - \sigma_y), \\ \frac{\partial \bar{u}}{\partial \bar{y}} + \frac{\partial \bar{v}}{\partial \bar{x}} &= 2 \mathbb{G} \exp(\mathbb{A} \theta) \mathfrak{F}(\tau'_{II}) \tau, \end{aligned} \quad (3.62)$$

where

$$\mathfrak{F}(\tau'_{II}) := \frac{f(\rho^2 g^2 D^2 \tau'_{II})}{f(\rho^2 g^2 D^2)}, \quad \tau'_{II} = \frac{1}{4}(\sigma_x - \sigma_y)^2 + \tau^2 \quad (3.63)$$

are dimensionless forms of the creep response function and of the second stress deviator invariant. For Glen's flow law  $f(\tau'_{II}) = \tau'^{(k-1)/2}$ , so that  $\mathfrak{F}(\tau'_{II}) = \tau'^{(n-1)/2}$ . Moreover,

$$\begin{aligned} \mathbb{F} &:= \frac{U^2}{gD} = \frac{D}{g\mathfrak{T}^2}, \\ \mathbb{G} &:= \mathfrak{T} A \exp\left(-\frac{Q}{kT_f}\right) \rho g D f(\rho^2 g^2 D^2), \\ \mathbb{A} &:= \frac{Q}{k} g_0 = \frac{Q}{kT_f} \frac{\mathbb{Z}}{1-\mathbb{Z}}, \\ \mathbb{Z} &:= T_0/T_f \end{aligned} \quad (3.64)$$

are dimensionless characteristic numbers;  $\mathbb{F}$  can be interpreted as a *Froude number*.  $\mathbb{G}$ ,  $\mathbb{A}$  and  $\mathbb{Z}$  have no specific names; the first two could be called Glen and Arrhenius number, respectively. The latter is defined above for cold ice. For temperate ice  $A \exp(-(Q/kT)$  must be replaced by  $\mathcal{A}_w$  which in a first approximation may be assumed independent of the moisture content. Under this restrictive assumption  $\mathbb{A}$  may be set to zero and  $\mathbb{G}$  may be defined with the aid of  $\mathcal{A}_w$  rather than  $\mathcal{A}_T$ .  $\mathbb{Z}$ , finally, is a temperature ratio  $< 10^{-1}$ . To fix the dimensionless constants (3.64) no unique choice is possible.  $D \simeq 10^2$  m is a realistic mean glacier thickness but several possibilities exist

for  $U$  or  $\mathfrak{T}$ . Three different choices are directly suggested by the problem, namely

- (i) to simply assign a specific value to  $\mathbb{G} (= 1)$ ,
- (ii) to choose  $U$  according to realistic longitudinal surface velocities,
- (iii) to scale velocities with the accumulation rate ( $U = a$ ).

Case (i) is mathematically convenient, because it transforms the field equations into the most simple form; (ii) and (iii) are physically suggested. For case (ii), emphasis is laid on a proper treatment of velocity profiles and accumulation is regarded as a secondary effect. In case (iii), accumulation is regarded as important. Realistic values for surface velocities and the accumulation rate are, perhaps,  $100 \text{ m a}^{-1}$  and  $1 \text{ m a}^{-1}$ , respectively. If we choose, furthermore,  $D = 100 \text{ m}$ ,  $n = 3$  and  $\mathcal{A} = 10^{-19} \text{ dyn}^{-n} \text{ cm}^{2n} \text{ a}^{-1}$  the characteristic quantities in the three different cases assume values as listed in Table 3.1. If one scales equations with the choice (ii), one guarantees that the dimensionless velocity  $\bar{u}$  and the stresses  $\sigma_x$ ,  $\sigma_y$  are of order 1. This is numerically very convenient. For this choice,  $\mathbb{G} \simeq 0(10^2)$  which implies that an ‘undesired’ constant must be kept in Equations (3.62). It is possible to absorb this constant in a new dimensionless velocity by the transformation

$$(\bar{u}, \bar{v}) \rightarrow \frac{1}{\mathbb{G}}(\bar{u}, \bar{v}), \quad \mathbb{F} \rightarrow \frac{\mathbb{F}}{\mathbb{G}^2} \quad (3.65)$$

and it is readily seen that this simply corresponds to a non-dimensionalization of the equations according to entry (i) in Table 3.1, leading to the most simple field equations. The characteristic time in this case is  $\mathfrak{T} \simeq 10^{-2} \text{ a}$ , a few days or less, and  $U$  is much larger than typical surface velocities. Non-dimensional velocities must therefore be much smaller than unity and, indeed, they are expected to be of the order of  $10^{-2}$ . Furthermore,  $\mathbb{F}$  is very small in all the cases justifying the neglect of the local and convective acceleration terms, as compared to the stress divergence and the gravity terms in Equations (3.62)<sub>2,3</sub>. In future calculations this will always be done.

It is not clear at the moment which of the three scalings is the most appropriate one. Ideally, one would like to have *all* dimensionless fields to be of order of unity. As we have just seen, this is not possible with the scalings of the table. For case (i) the velocities are likely to be very small; in case (ii) the transverse velocity is small and in case (iii) the longitudinal velocity com-

TABLE 3.1. Orders of magnitudes for various choices of the characteristic velocity  $U$  or time  $\mathfrak{T}$

	$U$ ( $\text{m a}^{-1}$ )	$\mathfrak{T}$ (a)	$\mathbb{G}$	$\mathbb{F}$
(i)	$10^4$	$10^{-2}$	1	$10^{-10}$
(ii)	$10^2$	1	$10^2$	$10^{-14}$
(iii)	1	$10^2$	$10^4$	$10^{-18}$

ponents will be large. This suggests that one of these scalings should be combined with an appropriate stretching of coordinates. This will be done in Chapter 5. Here we simply mention that case (i) is appropriate as long as the inclination angle  $\gamma$  is not small. For  $\gamma \leq 10^{-2}$ , solutions of the boundary-value problem to be presented will react critically to the smallness of  $\gamma$ . In the remainder of this chapter we shall mostly use the scaling with  $\mathbb{G} = 1$ .

Next, the energy equation (3.54)<sub>6</sub> will be non-dimensionalized, using the scalings (3.61). This yields

$$\frac{\partial \vartheta}{\partial \bar{x}} + \frac{\partial \vartheta}{\partial \bar{x}} \bar{u} + \frac{\partial \vartheta}{\partial \bar{y}} \bar{v} = \mathbb{D} \left( \frac{\partial^2 \vartheta}{\partial \bar{x}^2} + \frac{\partial^2 \vartheta}{\partial \bar{y}^2} \right) + 2\mathbb{E}\mathbb{G} \exp(\mathbb{A}\theta) \mathfrak{F}(\tau'_{II}) \tau'_{II}, \quad (3.66)$$

where

$$\mathbb{D} = \frac{\kappa}{\rho c} \frac{\mathfrak{T}}{D^2} = \frac{1}{\frac{\rho c}{\kappa} (g\mathfrak{T})} \frac{1}{D^2} = \frac{1}{\mathbb{P}} \frac{1}{\mathbb{F}}, \quad \mathbb{E} = \frac{gD}{cT_0}. \quad (3.67)$$

$\mathbb{D}$  is a dimensionless *thermal diffusion number*,  $\mathbb{P}$  a *Prandtl number* and  $\mathbb{E}$  a dimensionless *energy dissipation number*. With the values as listed in Table 3.2, one has  $\mathbb{E} \sim 10^{-2}$ . The value of  $\mathbb{D}$ , on the other hand, depends on which

TABLE 3.2. Value for physical constants in the model

Constant	Name
$g = 9.81 \text{ m s}^{-2}$	gravity constant
$\rho = 900 \text{ kg m}^{-3}$	ice density
$\kappa = 7 \times 10^7 \text{ J K}^{-1} \text{ m}^{-1} \text{ a}^{-1}$	thermal conductivity
$Q = 1 \text{ eV} = 1.6 \times 10^{-19} \text{ J}$	activation energy
$k = 1.38 \times 10^{-23} \text{ J K}^{-1}$	Boltzmann constant
$c = 2 \times 10^3 \text{ J kg}^{-1} \text{ K}^{-1}$	specific heat at constant pressure
$c_f = 0.74 \times 10^{-2} \text{ K bar}^{-1}$	Clausius–Clapeyron constant
$L = 3.3 \times 10^{+5} \text{ J kg}^{-1}$	latent heat of fusion
$q^{\text{geoth}} = 1.6 \times 10^6 \text{ J m}^{-2} \text{ a}^{-1}$	geothermal heat
$T_f = 273.15 \text{ K}$	melting temperature at normal pressure
$T_0 = 20 \text{ K}$	mean temperature difference
$D = 100 - 500 \text{ m}$	ice thickness
$\mathfrak{T} = 10^{-2} \text{ a}$	characteristic time
$A \left( -\frac{Q}{k T_f} \right) = 0.17 \text{ bar}^{-3} \text{ a}^{-1}$	Arrhenius factor
$m = (n + 1)/2$	Exponent for basal sliding
$n = 3$	Exponent in Glen's law
$\mathcal{C} \geq 10^{-8} \text{ m}^3 \text{ N}^{-2} \text{ a}^{-1}$	frictional coefficient at rockbed
$c_w = 0.0567 \times \mathbb{R}e^{-1.5}$	hydrodynamic drag
$h \cong 5 \times 10^{10} \text{ J m}^{-2} \text{ K}^{-1} \text{ a}^{-1}$	heat transfer coefficient

of the scaling in Table 3.1 is chosen. For case (i)  $D \sim 10^{-1}$ . In all cases one can easily demonstrate that  $D \ll GE$  so that *ordinarily conduction is negligibly small as compared to dissipation*.

The omission of the conduction term should, however, be exercised with special care. It is known from the discussion of the energy equation in temperate ice that such an omission would alter the parabolic equation into a hyperbolic one. This would result in the impossibility of prescribing sufficient thermal conditions at the boundaries (since a second-order equation is replaced by a first-order equation).\*

The dimensionless forms of the boundary conditions are given by:

*At the rockbed* [see relations (3.55)]:

$$\begin{aligned}\bar{u} &= C\tau^m, \quad \bar{v} = 0, \\ \vartheta &= \vartheta_M, \quad \text{if the ice is temperate,} \\ -\frac{\partial \vartheta}{\partial \bar{y}} &= Q^{\text{geoth}}, \quad \text{if the ice is cold,}\end{aligned}\tag{3.68}$$

where

$$C = \frac{\mathcal{C}(\rho g D)^m \mathfrak{T}}{D}, \quad Q = \frac{g D}{\kappa T_0}.\tag{3.69}$$

Numerical values of  $C$  and  $Q^{\text{geoth}}$  depend on those for  $\mathcal{C}$  and  $q^{\text{geoth}}$ , but  $\kappa T_0/D \approx 1.4 \times 10^7 \text{ J m}^{-2} \text{ a}^{-1}$ .

*At the free surface* [see Equations (3.56)]:

$$\begin{aligned}\tau &= 0, \quad \sigma_y = -\bar{p}^{\text{atm}}, \\ \vartheta &= \vartheta_M, \\ \bar{a} &= \frac{1}{L} Q^{\text{atm}}, \quad \left( \text{if } Q^{\text{atm}} < 0 \right), \\ \vartheta &= \vartheta_s, \quad \text{or,} \\ \frac{\partial \vartheta}{\partial \bar{y}} &= -Q^{\text{atm}},\end{aligned}\left. \begin{array}{l} \text{if the ice is temperate,} \\ \text{if the ice is cold,} \end{array} \right\}\tag{3.70}$$

$$\bar{v} = -\frac{\mathfrak{T}}{D} a = -\bar{a},$$

where  $\bar{p}^{\text{atm}}$  is a dimensionless atmospheric pressure,  $p = \bar{p} \rho g D$ ,  $\bar{a}$  is a given dimensionless accumulation rate,  $\vartheta_M$  and  $\vartheta_s$  are dimensionless melting and surface temperatures, respectively, and where

$$L = \frac{\rho L D^2}{\mathfrak{T} \kappa T_0}\tag{3.71}$$

\*Readers familiar with the methods of matched asymptotic expansions will recognize that singular perturbation techniques are suggested.

TABLE 3.3. Dimensionless numbers introduced in the non-dimensionalization of the basic boundary value problem. Orders of magnitude follow from the assigned values of the quantities in Table 3.1 (row (i)) and from Table 3.2.

Definition	Suggested name	Order of magnitude
$\mathbb{G}$	Glen number	1 (by definition)
$\mathbb{F} = \frac{D}{g\mathfrak{T}^2}$	Froude number	$\ll 10^{-7}$
$\mathbb{A} = \frac{Q}{kT_f} \frac{T_0/T_f}{1 + T_0/T_f}$	Arrhenius number	$\sim 2$
$\mathbb{D} = \frac{\kappa\mathfrak{T}}{\rho c D^2}$	Thermal diffusion number	$\lesssim 10^{-4}$
$\mathbb{E} = \frac{gD}{cT_0}$	Energy dissipation number	$10^{-2} - 10^{-1}$
$\mathbb{C} = \frac{\mathcal{C}(\rho g D)^m \mathfrak{T}}{D}$	Basal friction number	$\sim 1 - 2$
$\mathbb{L} = \frac{\rho LD^2}{\mathfrak{T}\kappa T_0}$	Fusion number	$2 \times 10^6$
$\mathbb{N} = \frac{hD}{\kappa}$	Nusselt number	$\mathcal{O}(10^5)$
$\mathbb{U} = \frac{U_w}{\sqrt{gD}}$	Dimensionless ocean speed	$< 10^{-1}$
$\mathbb{Q} = \frac{qD}{\kappa T_0}$	Dimensionless heat flux	$\sim 1$ (for $\mathbb{Q}^{\text{geoth}}$ )
$\mathbb{M} = \frac{c_i \rho g D}{T_0}$	Clausius–Clapeyron number	$0.5 \times 10^{-2}$
$\mathbb{Z} = \frac{T_0}{T_f}$	—	$\sim 0.075$

may be called *fusion number*, which is of the order of  $10^6$ , see Table 3.3.

At the ice-water interface [see Equations (3.57)]:

$$\tau = \frac{1}{2} c_w |\mathbb{U}| \mathbb{U}, \quad \bar{\sigma}_y = -\bar{p}^{\text{water}}$$

$\mathbb{L}\bar{v} = -\mathbb{N}(\vartheta_w - \vartheta_M)$ , if the ice is temperate,

$$\mathbb{L}\bar{v} = \begin{cases} \left. \frac{\partial \vartheta}{\partial \bar{y}} \right|_{\vartheta=\vartheta_w} & \text{if } \bar{v} > 0, \\ 0 = \mathbb{N}(\vartheta_w - \vartheta) - \left. \frac{\partial \vartheta}{\partial \bar{y}} \right|_{\vartheta=\vartheta_M}, & \text{if } \vartheta_w < \vartheta < \vartheta_M, \\ \mathbb{N}(\vartheta_w - \vartheta_M) - \left. \frac{\partial \vartheta}{\partial \bar{y}} \right|_{\vartheta=\vartheta_M}, & \text{if } \bar{v} < 0, \end{cases} \quad \text{if the ice is cold. (3.72)}$$

In these formulas  $\vartheta_w$  and  $\vartheta_M$  are the dimensionless water and melting temperatures, respectively,  $p^{\text{water}}$  is a dimensionless water pressure,  $\mathbb{N} = h/\kappa$  is the Nusselt number and  $\mathbb{U} = U_w/\sqrt{gD}$ , a dimensionless ocean current speed, an order of magnitude for which is  $5 \times 10^{-2}$ . With its aid and with (3.37) an order of magnitude for the dimensionless drag  $\tau$  can be deduced. One obtains  $\tau \sim 10^{-3}x^{-1.5}$  ( $x$  in meters); where  $\tau < 10^{-3}$  for all reasonable values of fetch. Effects of ocean drag are therefore generally negligible.

The Nusselt number defined above is not the same as that defined in Equation (3.38), but it can easily be related to it:  $\mathbb{N} = \mathbb{N}_u \cdot D/x$ .

$$\mathbb{N} = \mathbb{N}_u \frac{D}{x} = \frac{D}{x} a \text{Pr}^\alpha \text{Re}^\beta, \quad (3.73)$$

where  $\text{Pr}$  and  $\text{Re}$  are the Prandtl and Reynolds numbers introduced in (3.39), and numerical values for  $a$ ,  $\alpha$  and  $\beta$  are given in (3.40). Calculations with these indicate that  $\mathbb{N}_u \gtrsim 10^6$ , so that with  $D \simeq 10^2$  m and  $x = 10^3$  m,  $\mathbb{N} \gtrsim 10^5$  is obtained. In view of the order of magnitude of the fusion number, this result is important. It implies that in the boundary conditions at the ice water interface (3.72), the conduction term is very much smaller than the contributions due to melting, freezing, and heat transfer.

Finally, a dimensionless form of the Clausius–Clapeyron equation (3.53) is

$$\vartheta_M = -\mathbb{M}\left(\frac{1}{2}(\sigma_x + \sigma_y) - \bar{p}^{\text{atm}}\right), \quad (3.74)$$

where

$$\mathbb{M} = \frac{c_t \rho g D}{T_0} \simeq 0.5 \times 10^{-2} \quad (3.75)$$

may be called Clausius–Clapeyron number.

(b) *Parallel-sided ice slab, a first approximation to glacier and ice-shelf flow dynamics*

In this section we consider a steady parallel-sided ice slab either resting on a rockbed with mean inclination angle  $\gamma$ , or floating on a quiescent ocean. The field equations describing this situation are Equations (3.62) and (3.66), yet since Froude numbers are very small, convective acceleration terms can be neglected. It follows then from the second and third equation of (3.66) that

$$\frac{\partial \sigma_x}{\partial \bar{x}} + \frac{\partial \tau}{\partial \bar{y}} + \sin \gamma = 0, \quad \frac{\partial \tau}{\partial \bar{x}} + \frac{\partial \sigma_x}{\partial \bar{y}} - \cos \gamma = 0. \quad (3.76)$$

No  $\bar{x}$ -dependency of the stress is expected in an infinite parallel-sided slab, which implies that the first members on the left-hand side of (3.76) vanish, so that on account of the boundary conditions (3.70)<sub>1,2</sub>, direct integration

reveals

$$\tau = -\sin \gamma (\bar{y} - 1), \quad \sigma_y = \cos \gamma (\bar{y} - 1) - \bar{p}^{\text{atm}}. \quad (3.77)$$

Several remarks should be made with regard to these formulas. These are so important that we list them in the form of an enumerated sequence.

(i) Notice that the only assumption made in deriving (3.77) was the  $\bar{x}$ -independency of the stresses. As a result, the shear-stress distribution and the distribution of  $\sigma_y$  – the overburden pressure – could be found without making resort to any material properties. The relations (3.77) hold irrespective of the material properties of ice.

(ii) At the rockbed,  $\bar{y} = 0$ , and for small inclinations  $\gamma$ , the basal shear stress and the overburden pressure become

$$\tau = \gamma, \quad \sigma_y = -1 - \bar{p}^{\text{atm}}, \quad (3.78)$$

or when written in dimensional coordinates

$$t_{xy} = \rho g D \gamma, \quad t_{yy} = -\rho g D - p^{\text{atm}}. \quad (3.79)$$

Consequently, the basal shear stress is proportional to the mean thickness of the ice slope,  $D$ , and to its mean surface inclination,  $\gamma^*$ . Moreover, the overburden pressure is the sum of the atmospheric pressure and the weight of the ice column above the point of consideration.

(iii) As a rule of thumb, ice may be regarded as an ideally plastic material with a yield stress of 1 bar =  $10^5$  Pa. Measuring the mean inclination of surface slopes and equating  $t_{xy}$  to the yield stress will, under such a restrictive assumption, give estimates of the thickness of the ice slope.

(iv) For  $\gamma = 0$  Equation (3.77) yields  $\tau = 0$  throughout the body. This case would correspond to a floating ice shelf. Yet in view of the boundary condition (3.72)<sub>1</sub>, such a result is in violation with the boundary condition of stress at the ice-water interface unless any friction effect due to the ocean current is neglected. Should such an omission not be permissible (as, e.g., for tabular icebergs) the above procedure is inadmissible, and stresses must become  $\bar{x}$ -dependent in order to properly account for drag.

The completion of the construction of the boundary-value problem depends on the number of further assumptions that are made. These will be discussed below in an order of increasing complexity.

(α) *Velocity and temperature fields  $\bar{x}$ -independent.* If apart from the stress fields, the velocity and temperature fields are also assumed to be  $\bar{x}$ -independent, field equations (3.62)<sub>4,5</sub> reduce to

$$\frac{\partial \bar{v}}{\partial \bar{y}} = 0, \quad \sigma_x = \sigma_y, \quad \frac{\partial \bar{u}}{\partial \bar{y}} = 2 \exp(\mathbb{A}\theta) \mathfrak{F}(\tau^2)\tau. \quad (3.80)$$

\*We shall see in a later chapter that this rule remains valid even if rock bed inclination and surface inclination angles differ from each other.

Upon substitution of (3.77), integration yields

$$\bar{u} = \mathbb{C} \sin^m \gamma + 2 \int_0^y \exp(\mathbb{A}\theta) \mathfrak{F}(\sin^2 \gamma (\xi - 1)^2) \sin \gamma (1 - \xi) d\xi, \quad \bar{v} = 0, \quad (3.81)$$

in which the boundary conditions (3.68)<sub>1,2</sub> were used and where it was assumed that the coldness  $\theta$  is known as a function of depth. It is noteworthy to point out that with the result (3.80)<sub>2</sub>, all stress components are materially independent in this case and that only the velocity field, and possibly the temperature field, depend upon the material response.\* Notice also that the second of the above results (3.81) is in violation of the last boundary condition (3.70) unless the accumulation rate is small, so that  $\bar{a} \sim 0$ . This condition is satisfied to first order, but it corresponds to the omission of a (time-independent) accumulation term. It follows that whenever accumulation is taken into account, some field variables must be  $\bar{x}$ -dependent. Moreover, Equation (3.81)<sub>1</sub> has been written to apply for cold as well as temperate ice: for the former  $\mathbb{C} = 0$ , whereas for the latter  $\mathbb{A} = 0$ .†

To determine the temperature, results (3.77) and (3.81) are substituted into the energy equation (3.66). This yields

$$\frac{d^2\vartheta}{d\bar{y}^2} + \frac{2\mathbb{E}}{\mathbb{D}} \exp(\mathbb{A}\theta) \mathfrak{F}(\sin^2 \gamma (\bar{y} - 1)^2) \sin^2 \gamma (\bar{y} - 1)^2 = 0, \quad (3.82)$$

which is a non-linear second-order differential equation for the dimensionless temperature  $\vartheta$ . Boundary conditions that must be prescribed are

$$-\frac{d\vartheta}{d\bar{y}} = \mathbb{Q}^{\text{geoth}}, \quad \text{at } \bar{y} = 0, \quad \vartheta = \vartheta_s, \quad \text{at } \bar{y} = 1, \quad (3.83)$$

provided that the basal temperature does not reach the melting temperature. When  $\vartheta = \vartheta_M$  at  $\bar{y} = 0$  a basal ice layer may become temperate. This problem is more complicated as it requires the determination of the melting surface but, so far, no one has attacked it. In Equations (3.83) we have also chosen to prescribe the surface temperature  $\vartheta_s$  at  $\bar{y} = 1$  rather than the atmospheric heat flux, because prescribing heat flux at both surfaces  $\bar{y} = 0$  and  $\bar{y} = 1$  would not make the temperature uniquely determined.

Equations (3.77), (3.81) and (3.82), (3.83) comprise the complete solution of the thermomechanical problem when temperature and velocity fields are assumed to be independent of the length coordinate. To construct the

\*It should be noticed that this statement is, strictly speaking, only partially correct, as the second of Equations (3.80) is only obtained because the constitutive relationship for stress assumes the simple form given in Equations (3.62)<sub>4,5</sub>. A more complicated nonlinear constitutive relationship, as discussed in Chapter 2, would not allow this simple conclusion.

†In a cold ice sheet which reaches the melting temperature at the base, the sliding term may also occur in Equation (3.81).

solution, the thermal problem (3.82), (3.83) is solved first, and then, in a second step, the result is used in the evaluation of the velocity field.

Solutions to the temperature boundary value problem (3.82), (3.83) must, in general, be sought numerically. To this end several procedures are possible. One possibility is to transform the second-order differential equation (3.82) into a first-order system by introducing the new variables  $\Theta_1 = d\vartheta/d\bar{y}$ ,  $\Theta_2 = \vartheta$  and using a forward integration scheme (Runge–Kutta, say), starting at  $\bar{y} = 0$  with  $\Theta_1$  satisfying the boundary condition (3.83)<sub>1</sub>, and with an estimated value  $\Theta_2$  at  $\bar{y} = 0$ . One then obtains at  $\bar{y} = 1$ , a value for  $\Theta_2$  which will generally differ from that prescribed,  $\Theta_2 = \vartheta_s$ . Calculations will have to be repeated with various values of  $\Theta_2$  at  $\bar{y} = 0$  until sufficient agreement is obtained for  $\Theta_2$  at  $\bar{y} = 1$ . A disadvantage of this shooting procedure is that the nonlinearity of the problem does not permit us to use the principle of superposition. Since numerical procedures are generally well understood for linear equations, it is advantageous to develop linear iterative schemes. Such a scheme is the method of *quasilinearization*, as described and developed by Bellman and Kalaba [1] (see also Kantorovich and Aikilov [23]).

According to the method of quasilinearization, the differential equation (3.82) is written in the form  $d^2\vartheta/d\bar{y}^2 = r(\bar{y}, \vartheta)$ , where  $r$  is the second term in (3.82). One then introduces the sequence of approximations  $\{\vartheta^{(n)}\}$  and writes the differential equation as

$$\frac{d^2\vartheta^{(n+1)}}{d\bar{y}^2} = r(\bar{y}, \vartheta^{(n+1)}) = r(\bar{y}, \vartheta^{(n)} + (\vartheta^{(n+1)} - \vartheta^{(n)})). \quad (3.84a)$$

Assuming  $|\vartheta^{(n+1)} - \vartheta^{(n)}|$  to be small, a Taylor series expansion of the function  $r$  with respect to the second variable, and truncating at the linear term, yields

$$\begin{aligned} \frac{d^2\vartheta^{(n+1)}}{d\bar{y}^2} &= r(\bar{y}, \vartheta^{(n)}) + r_{\vartheta}(\bar{y}, \vartheta^{(n)})[\vartheta^{(n+1)} - \vartheta^{(n)}], \\ \frac{d\vartheta(0)^{(n+1)}}{d\bar{y}} &= -Q^{\text{geoth}}, \quad \vartheta^{(n+1)}(1) = \vartheta_s \end{aligned} \quad (3.84b)$$

in which  $r_{\vartheta}$  is the partial derivative of  $r$  with respect to the second variable. Given the  $n$ th iterate  $\vartheta^{(n)}$ , the two-point boundary-value problem (3.84b) for  $\vartheta^{(n+1)}$  is linear and can be solved with standard techniques, see, e.g., Szidarovszki and Yakowitz [60a].

Having determined the temperature distribution, the velocity field  $\bar{u}$  is found by straightforward quadratures from Equation (3.81). For temperate ice  $A = 0$  the longitudinal velocity splits into a basal *sliding* velocity  $\bar{u}_b = C \sin \gamma^m$  and a contribution due to *gliding*  $\bar{u}_g$ ,

$$\bar{u}_g = \int_0^{\bar{y}} \mathfrak{F}(\sin^2 \gamma(\xi - 1)^2) \sin \gamma(1 - \xi) d\xi.$$

For the generalized Glen flow law (Section 3 of Chapter 2) we have

$$\delta(x) = \frac{x^{(n-1)/2} + \varepsilon}{1 + \varepsilon}, \quad \text{with } \varepsilon = \frac{k}{(\rho g D)^{n-1}}$$

and

$$\bar{u}_g(\bar{y}) = \frac{1}{1 + \varepsilon} \left\{ \frac{2 \sin^n \gamma}{n+1} [1 - (1 - \bar{y})^{n+1}] + \varepsilon \sin \gamma [1 - (1 - \bar{y})^2] \right\}, \quad (3.85)$$

a formula which for  $\varepsilon = 0$  was first derived by Nye in 1952 [36]. At the free surface  $\bar{y} = 1$ , the gliding velocity becomes

$$\bar{u}_g(1) = \frac{1}{1 + \varepsilon} \left\{ \frac{2 \sin^n \gamma}{n+1} + \varepsilon \sin \gamma \right\}.$$

In Figure 3.11, this gliding velocity is plotted against the inclination angle  $\gamma$  for the cases that  $n = 2, 3$  and, correspondingly,  $\varepsilon = 10^{-n}$ . It is seen that  $\bar{u}_g(1)$  depends strongly on  $\varepsilon$  provided that  $\gamma < 10^{-1}$  but that the curves for the two values of  $\varepsilon$  differ only marginally when  $\gamma \geq 10^{-1}$ . It can further be recognized that the curves for  $\varepsilon = 0$  and  $\varepsilon = 10^{-2}$  deviate less from each

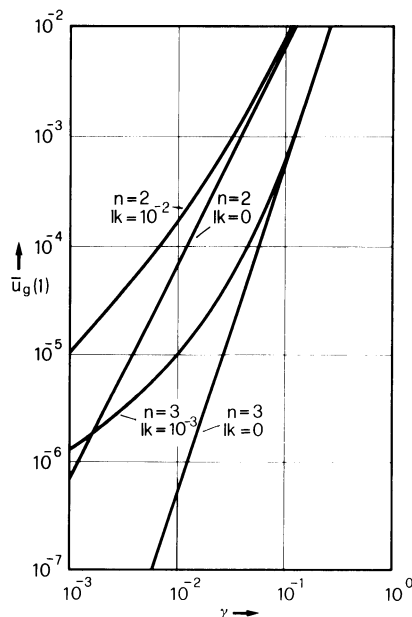


FIG. 3.11. Surface gliding speed  $\bar{u}_g(1)$  plotted as a function of  $\gamma$  for two values of the exponent  $n = (2, 3)$  and in each case for  $\varepsilon = 0$  and  $\varepsilon = 10^{-n}$ . It is seen that Newtonian behavior is important at small angles because gliding speeds for  $\varepsilon = 0$  and  $\varepsilon \neq 0$  differ considerably at these angles.

other when  $n = 2$  than when  $n = 3$ . This explains why experimentally determined exponents  $n$  of a pure power law ( $k = 0$ ) are small when determined from field data of ice sheets. Flat ice sheets must have  $1 < n < 2$  when the pure power law should adequately describe the small inclination range. On the other hand, when one is maintaining the value  $n = 3$ , the quasi-Newtonian behavior at small  $\gamma$  is important for a correct prediction of the streamwise surface velocity. The distribution of the gliding velocity across depth is shown in Figure 3.12. It is seen that the velocity distribution depends on both the exponent  $n$  and the constant  $k$ .

Classically the quasi-Newtonian behavior is neglected. At the surface

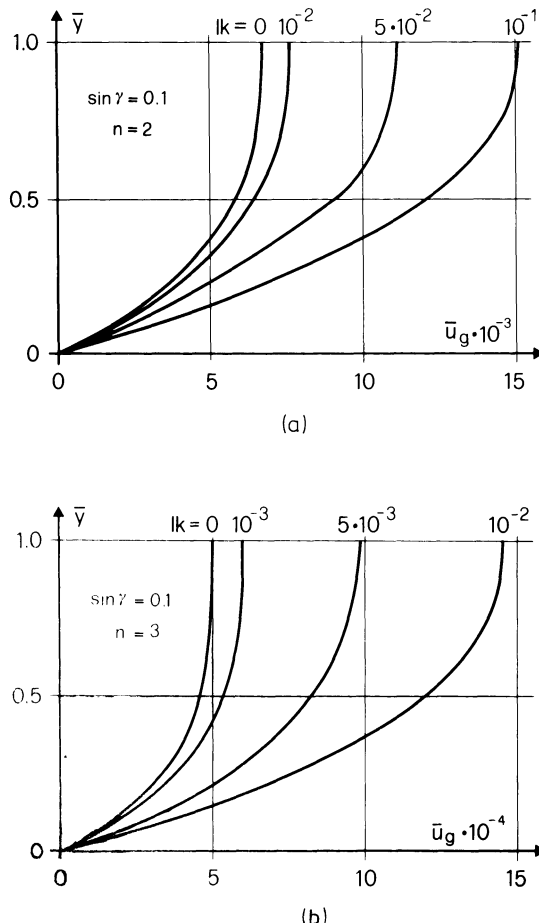


FIG. 3.12. Distribution of the gliding velocity as a function of  $\bar{y}$  and parameterized for various values of  $\bar{k}$  and two values of the power law exponent: (a)  $n = 2$  and (b)  $n = 3$ .

we may then write

$$\bar{u}_s = \mathcal{C} \sin^m \gamma + \frac{2}{n+1} \sin^n \gamma. \quad (3.86)$$

By integrating the velocity profile over the depth the *discharge* is obtained as follows :

$$\bar{q} = \mathcal{C} \sin^m \gamma + \frac{2}{n+2} \sin^n \gamma. \quad (3.87)$$

The formulas (3.86) and (3.87) were derived by Nye in 1952 [36]. Their dimensional counterparts read

$$\begin{aligned} u_s &= \mathcal{C} [\rho g D \sin \gamma]^m + \frac{2\mathcal{A}_w}{n+1} [\rho g D \sin \gamma]^n D, \\ q &= \mathcal{C} [\rho g D \sin \gamma]^m D + \frac{2\mathcal{A}_w}{n+2} [\rho g D \sin \gamma]^n D^2, \end{aligned} \quad (3.88)$$

where  $D$  is the ice sheet thickness. These equations are important in the theory of kinematic waves. Their validity is restricted to temperate ice, or ice for which the variation of the Arrhenius factor across depth is negligibly small, see Chapter 6.

The above results pertain to temperate ice for which the effects of moisture production are neglected. Consider next cold ice; here the two-point boundary value problem for temperature must be solved first and the resulting transverse temperature distribution then substituted in Equation (3.81) to obtain the velocity field. This problem was first tackled by Yuen and Schubert [72].

Results indicate that apart from surface temperature and basal heat flux, the governing parameter is the Arrhenius factor  $\mathbb{A}$ , which according to Equations (3.81) and (3.82) should affect both velocity and temperature distributions. However, transverse temperature variations are found to be nearly linear even for rather high values of the Arrhenius factor (high activation energies). This indicates that the non-linear term in the energy equation corresponding to strain heating may often be discarded. Integrating the temperature equation for  $r = 0$ , therefore, gives

$$\vartheta(\bar{y}) = \vartheta_s + \mathbb{Q}^{\text{geoth}}(1 - \bar{y}). \quad (3.89)$$

This result warrants the following remarks. Real measured temperature variations across the depth of cold, grounded ice sheets are almost never nearly linear, but rather as shown in Figure 3.13. Accordingly, the surface temperature is low and the basal temperature is high, and they are connected by a curve of just one sign in curvature. Either, temperature changes are very fast towards the bottom (which is usually the case) and moderate

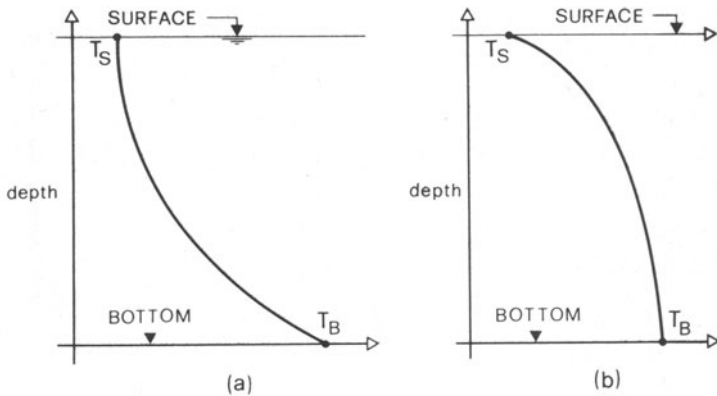


FIG. 3.13. Realistic temperature profiles in cold ice of a parallel-sided ice slab. It gives the qualitative behavior as observed in many measured temperature profiles.

close to the free surface, or vice versa. Our model of a strictly parallel-sided slab in which no fields are  $\bar{x}$ -dependent, therefore, neglects an essential parameter. It will be demonstrated in the next subsection that it is the accumulation/ablation rate that can be made responsible for an essentially non-linear distribution of temperature across depth rather than strain heating. In spite of this, the above results are useful as longitudinal velocity distributions are reasonable. A quantitative estimation of the temperature distribution on longitudinal velocities is nevertheless a worthwhile undertaking.

Since strain heating is small for most situations, the temperature distribution is governed by two input parameters, the surface temperature  $\vartheta_s$  and the geothermal heat flux  $Q^{\text{geoth}}$ , respectively. The other governing parameter, the Arrhenius factor  $\mathbb{A}$ , affects the velocity distribution. This can be demonstrated by choosing a moderate and a high value for the activation energy. Since, at a given fixed temperature, the creep response is stiffer for high activation energies than for lower ones, gliding velocities for small activation energies will be larger than for large ones. This is demonstrated in Figure 3.14. It shows a linear temperature distribution as obtained by formula (3.89) when  $\vartheta_s = -1$  and  $Q^{\text{geoth}} = 1$  (Figure 3.14a). With the aid of this temperature distribution, gliding velocities can be calculated by integrating Equation (3.81). Absolute values of dimensionless gliding velocities depend substantially on the value of the Arrhenius factor. According to Figure 3.14b, strain rates due to shear for high activation energies and close to the base are larger than for small activation energies and, correspondingly, streamwise velocity distributions are more uniform for  $\mathbb{A}$  large than for  $\mathbb{A}$  small. When velocities are normalized with the surface velocity (Figure 3.14c), the effect of large activation energies is brought about very clearly. Effects of

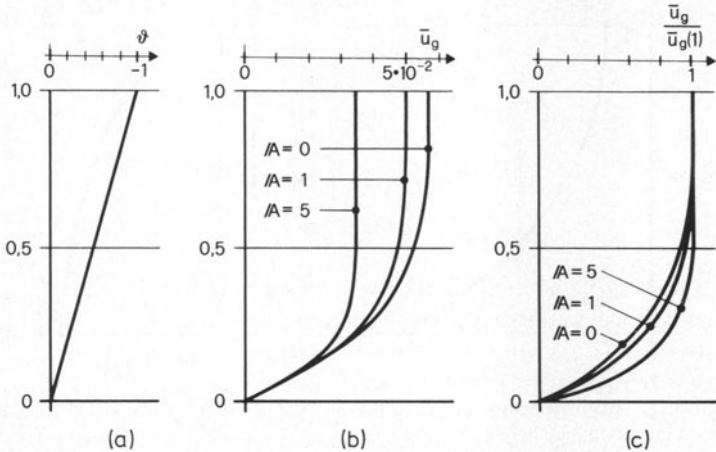


FIG. 3.14. For a linear temperature-variation (a) across the depth of the ice sheet dimensionless streamwise velocity distributions depend both in absolute value (b) and in form (c) on the value of the activation energy. The following values were chosen for the remaining physical parameters:  $Z = 0.1$ ,  $\gamma = 0.1$ ,  $n = 3$ .

temperature variations are not clearly seen in the upper half of the ice sheet, but only in the lower part close to the base. The value of the Arrhenius factor is manifested in substantial velocity differences at these lower positions.

The above findings suggest, firstly, that the effect of temperature variations on streamwise velocity is non-negligible and, secondly, that measuring transverse temperature distribution and longitudinal velocity components may allow the determination of activation energies. On the other hand, the results of Figure 3.14 indicate that an approximate velocity distribution can be obtained if measured or estimated temperature profiles are used in the integration of Equation (3.81). This was done by Hutter and Spring [17] and their results are similar to those shown in Figure 3.14.

The above results are based on a linear temperature distribution. Qualitatively, this behavior changes drastically *when strain heating is important*. Indeed, it will now be demonstrated that the boundary-value problem (3.84b) may admit multiple solutions when  $r \neq 0$ . Thus the question arises which of these steady-state solutions are physically possible or meaningful. In principle, one can solve the boundary-value problem for the temperature by prescribing for an ice sheet of a given thickness, the surface temperature and the geothermal heat flux. The output parameter is, in this case, the basal temperature. An alternative approach is to prescribe the surface and basal temperatures, and the geothermal heat flux, and to determine as the output parameter the corresponding ice sheet thickness. In this case the

temperature problem is given by

$$\begin{aligned} \frac{d^2\vartheta}{d\bar{y}^2} &= r(\bar{y}, \vartheta), \quad \vartheta \in [0, \bar{D}], \\ \vartheta(0) &= \vartheta_b, \quad \frac{d\vartheta}{d\bar{y}}(0) = -Q^{\text{geoth}}, \\ \vartheta(\bar{D}) &= \vartheta_s, \end{aligned} \quad (3.90)$$

where  $\bar{D}$  is the dimensionless, unknown thickness of the sheet (equations are now made dimensionless with an estimated thickness), and where  $r$  is given in Equation (3.82). Equations (3.90) can be treated as an initial value problem, integrating temperature from the base to the free surface. With growing  $\bar{y}$ ,  $\vartheta$  will approach  $\vartheta_s < \vartheta_b$ ;  $\bar{D}$  is determined as soon as  $\vartheta = \vartheta_s$  is obtained. Once the temperature and the depth  $\bar{D}$  are fixed, the velocity distribution follows from a modification of Equation (3.81) which now reads

$$\bar{u}(\bar{y}) = 2 \int_0^{\bar{y}} \exp(\mathbb{A}\xi) \mathfrak{F}(\sin^2 \gamma(\bar{D} - \xi)^2) \sin \gamma(\bar{D} - \xi) d\xi. \quad (3.91)$$

Yuen and Schubert [72] show that prescribing the basal temperature  $\vartheta_b$  and determining ice thickness  $\bar{D}$  rather than vice versa, is computationally advantageous, since for given surface temperature  $\vartheta_s$  and geothermal heat flux  $Q^{\text{geoth}}$ ,  $\bar{D}$  is a unique function of  $\vartheta_b$ , whereas when prescribing  $\bar{D}$  and determining  $\vartheta_b$ , the latter is double-valued. The physical constants used by Yuen and Schubert are listed in Table 3.4 and their results may be summarized as follows (we use dimensional quantities).

The overall character of the ice sheet is well described by giving its thickness  $D$ , surface velocity  $u_s$ , and basal temperature  $T_b$  for the many different environmental circumstances under which the ice sheet can exist. For these, Yuen and Schubert select, in particular,  $T_s = 218$  K,  $\gamma = 33.5^\circ$  and  $q^{\text{geoth}} = 0.0418$  W m<sup>-2</sup>. For  $u_s$ ,  $D$ , and  $T_b$  they find the relationship as

TABLE 3.4. Physical parameter values

Activation energy, $Q$	60.7, 125 kJ mol <sup>-1</sup>
Density, $\rho$	900 kg m <sup>-3</sup>
Thermal conductivity, $\kappa$	2.51 W m <sup>-1</sup> K <sup>-1</sup>
Thermal diffusivity, $\rho c/\kappa$	$1.33 \times 10^{-6}$ m <sup>2</sup> s <sup>-1</sup>
Flow-law constant (for $n = 3$ ), $A$	$3.75 \times 10^{-13}$ m <sup>6</sup> N <sup>-3</sup> s <sup>-1</sup>
Power law index, $n$	3
Surface temperature, $T_s$	218 K
Basal geothermal flux, $q^{\text{geoth}}$	41.8 mW m <sup>-2</sup>
Basal slope, $\gamma$	33.5°

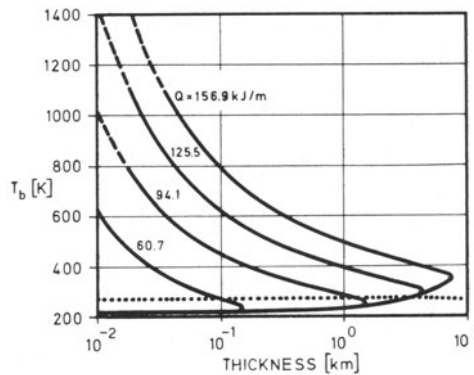


FIG. 3.15. Basal temperature  $T_b$  as a function of ice thickness  $D$ . The dotted line is the temperature at which melting occurs at the base of an ice sheet of thickness  $D$ . Parameter values are those given in Table 3.4 for indicated values of  $Q$  (From [72]).

displayed in Figures 3.15 and 3.16;  $u_s$  and  $T_b$  are seen to be double-valued functions of  $D$  in the range of  $u_s$  and  $D$  considered. Clearly, of the basal temperatures  $T_b$  in Figure 3.15, only those for which  $T_b < T_M$  are physically meaningful. But even with this limitation there is a domain for the activation energy for which the above double-valuedness of  $T_b(D)$  persists. The critical values  $u_s^*$ ,  $D^*$  and  $T_b^*$  are the points on Figures 3.15 and 3.16 which separate

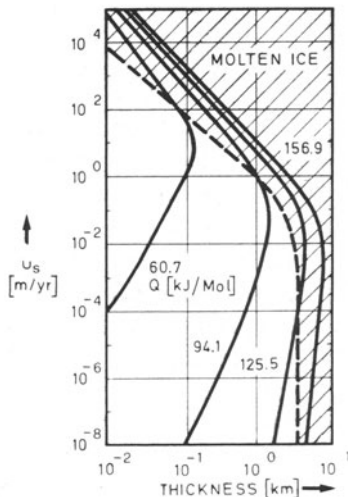


FIG. 3.16. Surface velocity  $u_s$  versus ice thickness  $D$ . The dashed line separates states at which melting occurs at the base of the ice sheet. Except for the values of  $Q$  which are indicated in the figure, all parameters have the values given in Table 3.4. (After [72].)

the curves into two branches. On the upper branch, called *supercritical* by Yuen and Schubert,  $u_s$  and  $T_b$  decrease with increasing  $D$ , while on the lower, or *subcritical* branch,  $u_s$  and  $T_b$  increase with increasing  $D$ . For a certain range of activation energies there is a maximum steady thickness, namely  $D^*$ , that can be attained by an ice sheet creeping down-slope under its own weight.

The above findings indicate that only the solutions which lie along the subcritical branch far from the critical point represent states for which there is relatively little strain heating; only for this range is the linearization of the temperature equation according to relation (3.89) permissible. For near-critical states, the full non-linear problem should be treated. Only for these states does frictional dissipation contribute substantially toward heating the ice. Figure 3.15 shows that the basal temperature of most supercritical states exceeds the melting temperature, while those of most subcritical states lie below the melting point. However, for low activation energies there are supercritical states below the melting point and for high activation energies the basal temperature may reach the melting point in the subcritical states. Moreover, only for the lowest activation energy is it possible for the subcritical states to achieve surface velocities of several meters per year.

The above results are hinged to the specific values that were assigned to the surface temperature, to the geothermal heat flux, and to the surface inclination  $\gamma$ . Yuen and Schubert [72] demonstrate that the findings do not alter qualitatively by modifying the numerical values of these physical constants. Indeed the variation of these quantities does not alter the fact that there are subcritical states at high values of activation energy which are molten while there are supercritical states at low values of the activation energy which do not involve melting. For an explicit demonstration of these results we must refer the reader to Yuen and Schubert's article.

Several remarks are in order. First, as was noted above, the temperature distribution is very nearly linear across depth even when strain heating is accounted for. This has been said to be in violation with field data. It follows that the above conclusions should be taken with some reservations. Nevertheless, for the vanishing accumulation rate they are rigorous and can, at least for this isolated case, be taken for granted. Secondly, the fact that there may exist thermal conditions and an ice sheet thickness with non-unique velocity profiles (a slow and a fast one) calls for a stability analysis of the strictly parallel-sided uniform flow considered here. An instability small perturbation analysis was performed by Yuen and Schubert [72], and they found that *neither the subcritical nor the supercritical states were instable against small perturbations*. This result does not exclude large amplitude instabilities. However, since such an analysis would again neglect the accumulation effects, results would be doubtful as a physically less-relevant problem would be solved. This was pointed out by Fowler [10]. Third, a

more realistic analysis taking accumulation into account and using accumulation as a control variable rather than depth might well render single-valued solutions. The solution of this more general problem has only recently been analysed by Fowler and Larson [12a, b], and they conclude that multiple steady states, both of which are stable, do not occur. On the contrary, in their treatment solutions are unique; one must simply regard accumulation as an input parameter.

(β) *Extending and compressing flow.* So far, no variation of velocity  $\bar{u}$  with distance  $\bar{x}$  along the glacier or ice sheet was considered. In practice, of course,  $\bar{u}$  varies along the glacier axis. It is therefore interesting to see to what extent Equations (3.62) and (3.66) admit solutions with  $\bar{x}$ -dependent longitudinal velocities. An analysis of this kind was first presented by Nye 1957 [37].

As in the previous section, it is assumed that the stresses and temperature are independent of  $\bar{x}$ ; hence, shear stress and overburden pressure are still given by Equations (3.77), yet it can no longer be concluded that  $\sigma_x = \sigma_y$ . In fact, the remaining field equations (3.62) and (3.66) become

$$\begin{aligned} \frac{\partial \bar{u}}{\partial \bar{x}} + \frac{\partial \bar{v}}{\partial \bar{y}} &= 0, \\ \frac{\partial \bar{u}}{\partial \bar{x}} &= \frac{1}{2} \exp(\mathbb{A}\theta) \mathfrak{F}(\tau'_{\text{II}})(\sigma_x - \sigma_y), \\ \frac{\partial \bar{u}}{\partial \bar{y}} + \frac{\partial \bar{v}}{\partial \bar{x}} &= 2 \exp(\mathbb{A}\theta) \mathfrak{F}(\tau'_{\text{II}})\tau, \\ \frac{\partial \vartheta}{\partial \bar{y}} \bar{v} &= \mathbb{D} \frac{\partial^2 \vartheta}{\partial \bar{y}^2} + 2\mathbb{E} \exp(\mathbb{A}\theta) \mathfrak{F}(\tau'_{\text{II}})\tau'_{\text{II}}. \end{aligned} \quad (3.92)$$

Since stresses and temperature are independent of  $\bar{x}$ , so are the right-hand sides of Equations (3.92)<sub>2,3</sub>. Consequently,

$$\frac{\partial^2 \bar{u}}{\partial \bar{x}^2} = 0, \quad \frac{\partial^2 \bar{u}}{\partial \bar{x} \partial \bar{y}} + \frac{\partial^2 \bar{v}}{\partial \bar{x}^2} = 0.$$

Integrating these equations together with the continuity equation yields

$$\bar{u} = \bar{x}g(\bar{y}) + h(\bar{y}), \quad \bar{v} = - \int_0^{\bar{y}} g(\xi) d\xi + k(\bar{x}),$$

where  $g, h, k$  are arbitrary functions of their arguments. To determine these, observe that the boundary conditions at the free surface require  $\tau$  to vanish, so that  $\partial \bar{u}/\partial \bar{y} + \partial \bar{v}/\partial \bar{x} = 0$  at  $\bar{y} = 1$ . Moreover, since  $\tau$  is independent of  $\bar{x}$ , so must be  $\partial \bar{u}/\partial \bar{y} + \partial \bar{v}/\partial \bar{x}$  which implies  $g(\bar{y})$  to be a constant,  $g(\bar{y}) = r_0$ .

The boundary conditions at the rockbed, finally, imply  $k = 0$  and

$$\bar{u}_0 = \bar{x}r_0 + h(0), \quad (3.93)$$

where  $\bar{u}_0$  is the sliding velocity at the base. According to the boundary condition (3.68)<sub>1</sub>,  $\bar{u}_0 = \mathcal{C} \sin^m \gamma = \tau_{\text{base}}^m$ , which is constant. On the other hand, the right-hand side of (3.93) is  $\bar{x}$ -dependent. It follows that Nye's solution of extending and compressing flow is inconsistent with the assumption of a stress dependent sliding law, unless, of course, basal shear stress vanishes. This is only the case for ice shelves. Hence, in order to maintain an equation of the form (3.93), stress-dependent sliding must be abandoned. Equation (3.93) is then simply regarded as an equation determining  $\bar{u}_0$ . Proceeding on such a basis we may write  $h(\bar{y}) = l_0 + \bar{h}(\bar{y})$ , where  $l_0 = h(1)$  so that  $\bar{h}(1) = 0$ . Hence,

$$\bar{u} = \bar{x}r_0 + l_0 + \bar{h}(\bar{y}), \quad \bar{v} = -r_0\bar{y}, \quad (3.94)$$

where the two constants  $r_0$  and  $l_0$  are determined from surface measurements on the glacier. The value of  $r_0$  is the longitudinal strain rate  $\partial \bar{u} / \partial \bar{x}$ , which does not vary with depth. The solution also shows that  $\bar{v}$  has the opposite sign of  $r_0$ .

There still remains the determination of  $\bar{h}(\bar{y})$  and of the stress  $\sigma_x$ . Combining Equations (3.92)<sub>3</sub> and (3.94) and integrating the resulting differential equation for  $\bar{h}$ , subject to the boundary condition  $\bar{h}(1) = 0$  yields

$$\bar{h} = -2 \sin \gamma \int_{\bar{y}}^1 \exp(\mathbb{A}\theta) \mathfrak{F}(\tau'_{\text{II}})(1 - \xi) d\xi, \quad (3.95)$$

which can be evaluated as soon as  $\theta$  and  $\tau'_{\text{II}}$  are known. One equation for the evaluation of these can be obtained by evaluating the second stretching tensor invariant

$$\left( \frac{\partial \bar{u}}{\partial \bar{x}} \right)^2 + \left( \frac{\partial \bar{v}}{\partial \bar{y}} \right)^2 + \frac{1}{2} \left( \frac{\partial \bar{u}}{\partial \bar{y}} + \frac{\partial \bar{v}}{\partial \bar{x}} \right)^2,$$

once with the aid of the relations (3.92) and once with (3.94) instead.

Equating the emerging expressions then reveals

$$r_0^2 + e^{2\mathbb{A}\theta} \mathfrak{F}^2(\tau'_{\text{II}}) [\sin^2 \gamma (1 - \bar{y})^2 - \tau'_{\text{II}}] = 0, \quad (3.96)$$

which is a first equation determining the second deviator invariant and the temperature. The second equation is the energy equation (3.92)<sub>4</sub>. The simultaneous solution of the Equations (3.96) and (3.92)<sub>4</sub>, subject to the boundary conditions (3.83), will yield the  $\bar{y}$ -distribution of the temperature  $\theta$  and the deviator invariant  $\tau'_{\text{II}}$  provided  $r_0$  is given. Once these are known, the function  $h$  follows from (3.95) and  $\sigma_x$  from

$$\sigma_x = \pm \{4\tau'_{\text{II}} - 4 \sin^2 \gamma (1 - \bar{y})^2\}^{1/2} - \cos \gamma (1 - \bar{y}) - \bar{p}^{\text{atm}}, \quad (3.97)$$

which is simply the inversion formula of  $\tau'_{\text{II}} = \frac{1}{4}(\sigma_x - \sigma_y)^2 + \tau^2$ .

To solve the above coupled non-linear system of equations one best starts with an estimated temperature distribution over the depth of the plate and solves Equation (3.96) for the distribution of  $\tau'_{II}$ . This first approximation of the deviator invariant then may be used in the evaluation of an improved temperature distribution, and so on. The solution procedure using Equation (3.96) for *constant* temperature is due to Nye [37]. In the evaluation of the stress  $\sigma_x$  two solutions are possible, depending on the two signs in front of the square root sign in (3.97). If the (+) sign applies, the flow is called *extending* flow and  $\sigma_x + \bar{p}^{atm}$  is positive. On the other hand, when the (-) sign applies  $\sigma_x + \bar{p}^{atm}$  is negative throughout and the flow is called *compressing*. Inspection of Equation (3.92)<sub>2</sub> shows that  $r_0$  determines the sign of  $(\sigma_x - \sigma_y)$ . Hence,

$$\sigma_x = 2 \operatorname{sgn} r_0 \{ \tau'_{II} - \sin^2 \gamma (1 - \bar{y})^2 \}^{1/2} - \cos \gamma (1 - \bar{y}) - \bar{p}^{atm}. \quad (3.98)$$

One feature of this solution of extending and compressing flow is that it allows for a non-vanishing surface velocity component  $\bar{v} = -r_0$ . Recalling the boundary conditions (3.75) this necessitates the inclusion of a constant accumulation rate given by  $\bar{a} = r_0$ . Consequently, *the dimensionless longitudinal strain rate equals the dimensionless accumulation rate*. However, it requires  $\bar{a}$  to be constant along the glacier. Very roughly then,  $\bar{a} > 0$  in the upper part of an ice slope and the flow must be extending. Below the snow line,  $\bar{a} < 0$  and the flow will be compressing if the above solutions make sense at all.

The coupled boundary-value problem for velocities and temperature has not been solved yet, and it probably is not very meaningful because basal sliding conditions are unrealistic. However, when decoupling the temperature from the velocity problem and restricting considerations to thermal behavior, qualitative insight into the thermal behavior of an ice sheet may nonetheless be gained. Such approximate solutions of the temperature equation (3.92)<sub>4</sub> alone have been considered by several authors. It is worthwhile to discuss these in some detail. Robin [50] was the first to recognize the importance of heat convection caused by accumulation and induced by the associated transverse velocity field. He observed that, since the deformation rate of ice for a given stress increases with temperature, a small increase in the deformation rate will raise the strain heating and, therefore, the temperature, giving rise to a further increase in the deformation rate. Thus, the above system has positive feedback, and under certain conditions a runaway increase in temperature will result. This is the process of creep instability. Such instabilities have been described and elaborated on by Lliboutry [25], Budd [6], Nye [44], Neave and Savage [35], Boshinskiy and Grigoryan [5], Boshinskiy [4] and Clarke *et al.* [8]. The analysis of Clarke *et al.* is the most recent one and so we restrict attention to discussing their results.

The temperature equation (3.92)<sub>4</sub> alone could be integrated were it not for the stress deviator invariant  $\tau'_{II}$  which is unknown. It was observed above that strain heating is often of little importance; therefore an estimate for it may suffice.

Clark *et al.* consider two cases, namely, (i) a stress distribution as determined in the last subsection ( $\sigma_x = \sigma_y$ ,  $\tau$  increases linearly with depth) and (ii) a stress state in which longitudinal stresses are independent of depth and, furthermore, are very much larger than the remaining normal and shear stresses. Neither case is an exact solution of Equations (3.92); yet when Glen's power law is used, one obtains

case (i):

$$\tilde{\delta}(\tau'_{II})\tau'_{II} = \sin^{n+1} \gamma (1 - \bar{y})^{n+1},$$

case (ii):

$$\tilde{\delta}(\tau'_{II})\tau'_{II} = (\frac{1}{3})^{(n+1)/2} \sigma_L^{n+1},$$

where  $\sigma_L$  is the longitudinal stress. By introducing the above representations into Equation (3.92)<sub>4</sub> and by defining a new dimensionless temperature according to

$$\hat{\vartheta} = \mathbb{A}(1 - \mathbb{Z})\vartheta \quad (3.99)$$

the differential equation for  $\hat{\vartheta}$  becomes

case (i):

$$\frac{d^2\hat{\vartheta}}{d\bar{y}^2} + \varepsilon\bar{y}\frac{d\hat{\vartheta}}{d\bar{y}} + \beta(1 - \bar{y})^{n+1} \exp\left(\frac{\hat{\vartheta}}{1 + \hat{\vartheta}/\alpha}\right) = 0, \quad (3.100)$$

case (ii):

$$\frac{d^2\hat{\vartheta}}{d\bar{y}^2} + \varepsilon\bar{y}\frac{d\hat{\vartheta}}{d\bar{y}} + \tilde{\beta} \exp\left(\frac{\hat{\vartheta}}{1 + \hat{\vartheta}/\alpha}\right) = 0,$$

in which

$$\begin{aligned} \alpha &= \frac{\mathbb{A}(1 - \mathbb{Z})}{\mathbb{Z}}, & \varepsilon &= \frac{r_0}{\mathbb{D}} = \frac{\bar{a}_0}{\mathbb{D}}, \\ \beta &= \frac{2\mathbb{E} \sin^{n+1} \gamma}{\mathbb{A}(1 - \mathbb{Z})}, & \tilde{\beta} &= \frac{2\mathbb{E} \sigma_L^{(n+1)/2}}{\mathbb{A}(1 - \mathbb{Z})}. \end{aligned} \quad (3.101)$$

In the derivation of these formulas, use has also been made of Equation (3.60). Equations (3.100) are identical with those of Clarke *et al.*, who call  $\varepsilon$  an advection parameter and  $\beta$  a stability parameter. They also normalize temperature such that  $T = T_s + T_0\vartheta$ , where  $T_s$  is the surface temperature. This choice makes the surface boundary condition, namely the prescription

of the surface temperature  $T_s$ , particularly simple. It now merely reads  $\hat{\vartheta}(1) = 0$ . The other boundary condition at the base is

$$\begin{aligned}\frac{d\hat{\vartheta}}{dy}(0) &= -A(1-Z)\mathbb{Q}^{\text{geoth}} = -\Phi, \quad \text{when } \hat{\vartheta} < \hat{\vartheta}_M, \\ \hat{\vartheta}(0) &= \hat{\vartheta}_M, \quad \text{when } \hat{\vartheta} = \hat{\vartheta}_M,\end{aligned}\quad (3.102)$$

where  $\hat{\vartheta}_M$  is the temperature at the melting point.

*No strain heating.* Consider the first of the differential equations (3.100) subject to the above boundary conditions. The case  $\varepsilon = 0$  corresponds to the analysis of the previous subsection and will no longer be treated here. When  $\beta = 0$  but  $\varepsilon \neq 0$  strain heating is negligible, but advection is accounted for and the solution reads

$$\vartheta(\bar{y}) = \Phi \int_{\bar{y}}^1 \exp\left(\pm |\varepsilon| \frac{\xi^2}{2}\right) d\xi, \quad (3.103)$$

where the upper and the lower signs apply when  $\varepsilon \gtrless 0$ . For the  $\varepsilon > 0$  the right-hand side of Equation (3.103) can easily be expressed in terms of the error function

$$\text{erf}(x) = \frac{2}{\sqrt{\pi}} \int_0^x \exp(-\xi^2) d\xi; \quad (3.104)$$

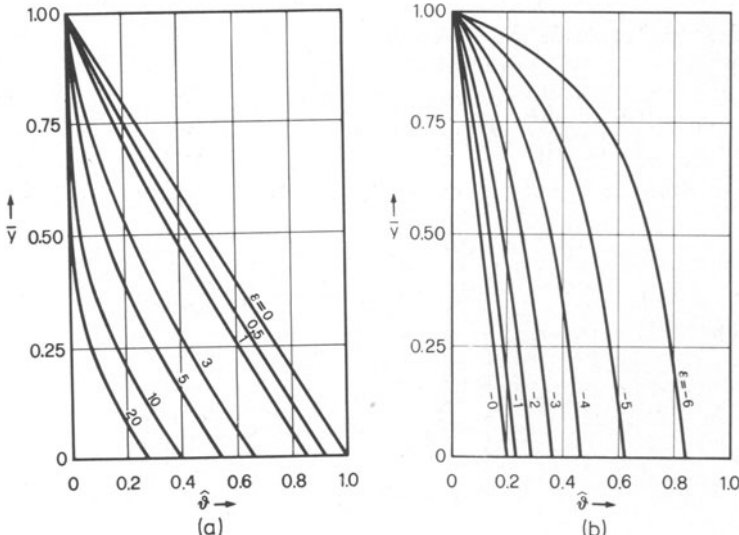


FIG. 3.17. Dimensionless steady-state temperature profiles with no strain heating for (a) various positive values of the advection parameter  $\varepsilon$  (corresponding to accumulation at the surface) and (b) various negative values of  $\varepsilon$  (corresponding to ablation). The geothermal flux parameter  $\Phi$  is taken as unity. For other values the abscissa should be interpreted as  $\hat{\vartheta}/\Phi$ . (From [8].)

for  $\varepsilon < 0$ , a representation of the integral in a higher transcendental function is not possible. The above solutions were obtained by Robin [50] and Lliboutry [25]. Figures 3.17a and 3.17b show the corresponding temperature profiles for the case that  $\Phi = 1$  and for various values of  $\varepsilon$ . Profiles for other values of  $\Phi$  differ by a simple scale factor from those presented. Typical values for a polar ice sheet are  $\bar{a}_0 = \pm 0.05 \text{ m a}^{-1}$  and  $D = 3000 \text{ m}$ ; this together with the values of Table 3.4, p. 163, gives  $\varepsilon = 3.6$  and  $\hat{\vartheta}(0) = 0.63\Phi$ . On the other hand, for the ablation zone of a typical valley glacier  $\bar{a}_0 = -1 \text{ m a}^{-1}$ ,  $D \approx 300 \text{ m}$ , so that  $\varepsilon \approx -7$  and  $\hat{\vartheta}(0) = 5.8\Phi$ . Hence, and as can be seen from Figure 3.17, transverse advection has an important effect on the temperature in glaciers and ice sheets. Accumulation, or downward advection decreases the temperature (when compared with the no-advection case), while ablation, or upward advection increases it. Physically, this is obvious. These results provide sufficient corroboration for our earlier statement that accumulation is the dominant control parameter for the temperature distribution in a grounded ice sheet which must not be neglected. It causes a transverse velocity field to be built up which convects cold downward (accumulation) or heat upward (ablation).

Solutions (3.103) are in fair agreement with measured temperature distributions, as can be seen from Figure 3.18 which displays the measured temperature distribution at Camp Century in Greenland (solid line) and compares it with the theoretical profile as obtained with the aid of Equation (3.103) (dashed). An improved theoretical solution due to Weertman [68] and Zotikov [73] is also shown in Figure 3.18 (pointed curve). It differs from the above theoretical findings by allowing ice to be melted at the base so that the coefficient of the term  $d\hat{\vartheta}/d\bar{y}$  in Equation (3.100) is  $\varepsilon(\bar{y} + W)$  rather than  $\varepsilon\bar{y}$ . Weertman and Zotikov clearly account for basal melting by this addition of the constant  $W$ . Yet when solving the differential equation (3.100)<sub>1</sub>, they

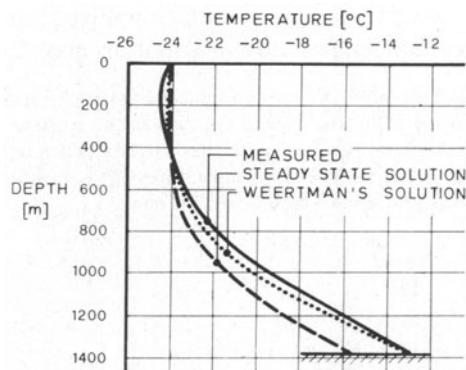


FIG. 3.18. Observed (solid) and theoretical temperature profiles (dashed and pointed), Camp Century, Greenland. (From Weertman [68].)

still prescribe geothermal heat flux rather than melting temperature. This restricts considerations of thermal states in which, at the lower boundary, the pressure melting point is just attained. For a given surface temperature and geothermal heat flux it allows an estimation of ice thickness. On this basis, Zotikov finds that the basal ice may reach the melting point over about half the area of Antarctica.

Figure 3.18 points at a peculiarity of the measured temperature profile not shared by the corresponding theoretical results. What is meant is the decrease of the measured temperature in the uppermost layer with depth and the associated ‘negative’ temperature gradient. This behavior is not shared by the theoretical solutions. Robin [50] has offered an explanation for the occurrence of these negative gradients. It involves longitudinal temperature gradients at the free surface which have been neglected here.\* *Hence, when temperature profiles with inversions are to be modeled, longitudinal convection cannot be neglected and longitudinal temperature variations must be included in the analysis.* This would suggest a model of a strictly parallel sided slab in which stresses are  $\bar{x}$ -independent, but temperature and velocity distributions are not. Such an analysis has been presented by Weertman [68], but he gives even further reasons for the occurrence of temperature inversions, one being time dependent effects. Indeed his dashed curve in Figure 3.18 is only obtained when accumulation rate is about three-quarters of the present measured accumulation rate.

*Strain heating, but no advection.* In Equations (3.100) this case corresponds to the specializations  $\varepsilon = 0$  but  $\beta \neq 0$ , or  $\tilde{\beta} \neq 0$ . When the first of Equations (3.100) is considered, the temperature problem is exactly the same as that of Yuen and Schubert [72] discussed earlier, except that here no velocity distributions across depth are analysed. What differs in the work of Clarke *et al.* [8] as opposed to that of Yuen and Schubert [72] is the presentation of the results. Accordingly, Equation (3.100)<sub>1</sub> with  $\varepsilon = 0$  may have multiple solutions. In other words, to a given surface temperature and geothermal heat flux, more than one temperature distribution may exist, which corres-

\*Robin’s argument is as follows: Consider two material points  $P_1$  and  $P_2$ , see Figure 3.19, which at time  $t$  occupy the free surface and are a distance  $u_s \cdot 1$  apart. After a unit timestep accumulation has buried the two particles and  $P_1$  has moved to a position just below the point where  $P_2$  was before ( $P'_1$ ). Let the (steady) temperatures at the positions  $P_1$ ,  $P_2$  and  $P'_1$  be  $T_1$ ,  $T_2$  and  $T'_1$ , respectively and assume that  $T_1 = T'_1$ . Then

$$T_2 - T'_1 \simeq -\left.\frac{\partial T}{\partial y}\right|_S a = (T_2 - T_1) \simeq \left.\frac{\partial T}{\partial x}\right|_S u_s,$$

or

$$\left.\frac{\partial T}{\partial y}\right|_S \cong -\left.\frac{\partial T}{\partial x}\right|_S \frac{u_s}{a}.$$

For positive longitudinal gradients of the surface temperature, the right-hand side is negative.

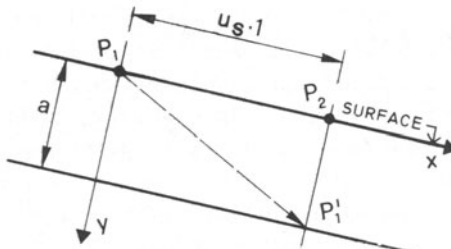


FIG. 3.19. Explaining the occurrence of temperature inversions.

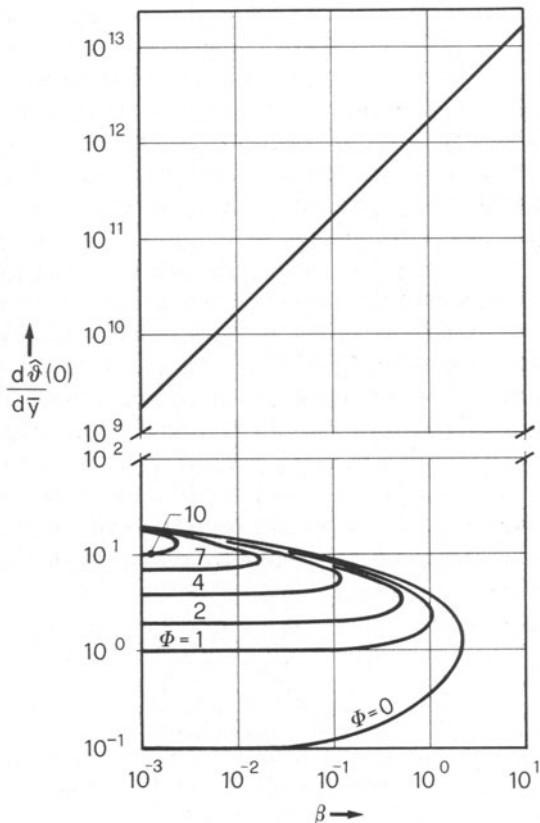


FIG. 3.20. Range of existence of multiple solutions for the heat transfer equation (3.100)<sub>1</sub> for different values of the geothermal flux parameter  $\Phi$ . In this example it is assumed that  $\epsilon = 0$  (no advection) and  $\alpha = 30$  ( $T_s = -30^\circ\text{C}$ ). For a given choice of the stability parameter  $\beta$ , there can be as many as three values of the surface temperature gradient  $d\hat{\vartheta}(0)/d\xi$  which yield solutions of (3.100)<sub>1</sub>. The high temperature solution is the same for all values of  $\Phi$  because internal strain heating overwhelms the geothermal flux contribution. Note the change in the vertical scale. (From [8].)

pounds to particular values of a certain given control variable. Recall that Yuen and Schubert use ice thickness as a control variable to determine the multiplicity of solutions of the temperature equation. Contrary to this, Clarke *et al.* keep the ice thickness fixed and vary instead the surface heat flux. Their control variable is, therefore, atmospheric heat flux. In Figure 3.20 this surface heat flux for which the stated two-point boundary value problem admits a solution is plotted against the parameter  $\beta$ . The individual curves belong to different values of the geothermal heat flux  $\Phi$ . A three-dimensional plot in which  $\Phi$  is the third coordinate would look as shown in Figure 3.21. Notice that for some  $\beta$  there are as many as three solutions for a prescribed value of  $\beta$ . In the limiting case for large  $\beta$ , only one single solution exists, and when  $\beta = 0$  (and  $\varepsilon = 0$ ) it is obvious that Equation (3.100)<sub>1</sub> possesses only one solution. This indicates that for small and for very large values of  $\beta$  there are unique solutions, but for intermediate values of  $\beta$  there must be three solutions. When plotting basal temperature  $\hat{\vartheta}_b$  versus  $\beta$ , the qualitative behavior must therefore be as shown in Figure 3.22. In this figure it is temporarily assumed that the temperature at the base of the slab does not reach the melting point.

Consider now a steady-state temperature profile with a low basal temperature corresponding to a point on segment AB in Figure 3.22. Assume that by some small disturbance this steady state is perturbed such that a new steady state will be reached. This new state will again correspond to a point on the curve ABCEDF, but states on the segment CE are anticipated to be forbidden so that, once the point C is reached, a jump discontinuity will arise to point D. Such a behavior is called critical. An analogous argument applies, when a steady state corresponding to a point on segment DF is perturbed and the basal temperature decreases. Then the curve FDEBA will be traversed. Hence, as is schematically shown in Figure 3.22, the

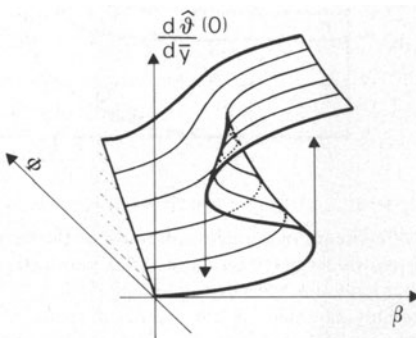


FIG. 3.21. A sketch of the surface  $d\hat{\vartheta}(0)/d\bar{y}$ , the dimensionless surface temperature gradient, plotted as a function of the stability parameter  $\beta$  and the geothermal flux parameter  $\Phi$  for constant advection parameter  $\alpha$ . (From [8].)

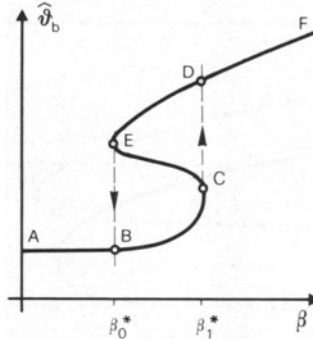


FIG. 3.22. Schematic solution of (3.100) for small  $\Phi$ . As  $\beta$  increases, the basal temperature of an initially cool slab increases along the path ABCDF, while an initially hot slab cools along FDEBA. The temperature changes discontinuously at the critical values  $\beta_0^*$  and  $\beta_1^*$ . The segment EC represents an unstable solution. (From [8].)

steady-state temperature distribution in the slab for  $\beta_0^* < \beta < \beta_1^*$  depends on the initial condition; it is given by the segment BC or ED depending on whether  $\beta$  is initially smaller than  $\beta_0^*$  or larger than  $\beta_1^*$ . Thus, while the temperature of an initially cool slab changes along the path ABCDF, an initially hot slab will cool along the path FDEBA. In both cases there is a finite temperature jump at  $\beta_0^*$  and  $\beta_1^*$ . In mathematical literature, points E and C in Figure 3.22 are referred to as *bifurcation points* (Clarke *et al.* [8]), and the surface as displayed in Figure 3.21 corresponds to the so-called *cusp catastrophe* in catastrophe theory, see [8].

It is clear that melting will affect the above results, and often the upper Branch EDF in Figure 3.22, or part of it, will correspond to molten ice. On the segment ABC, on the other hand, the usual temperature distribution in a glacier or ice sheet which is frozen to its bed is obtained. If  $\beta$  of an initially cold and stable ice mass changes, so that  $\beta > \beta_1^*$ , the temperature will gradually increase until the basal temperature reaches the melting point. This happens before the high temperature state is attained and changes the boundary condition from a constant flux  $d\hat{\theta}/d\bar{y} = -\Phi$  to a constant temperature  $\hat{\theta}_M$ .

The solution of Equation (3.100)<sub>1</sub> with the prescribed basal temperature shows a critical behavior similar to that for the case of the prescribed flux, but this is of little glaciological interest, since the critical value of  $\beta$  can now be reached only after the temperature in the interior of the slab exceeds  $\hat{\theta}_M$ . Thus, instead of critical behavior, the question of interest for the case of a temperate bed is the existence of a stationary state in which the temperature in the slab does not exceed the melting point.

Figure 2.23 illustrates the effect of changes in boundary conditions on

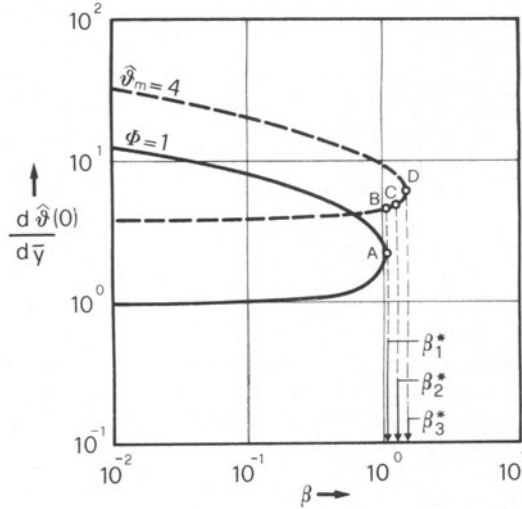


FIG. 3.23. Range of existence of multiple solutions of the heat transfer equation for the case of no advection and two different lower-boundary conditions: frozen base (solid curve) and base at melting point (dashed curve). At the onset of instability (point A) the thermal state cannot switch to the high-temperature state because when B is reached, the basal ice reaches melting point. A further increase of  $\beta$  will move the solution toward a new instability at point D, but this point will not be reached because the basal layer of ice at melting point starts to form at some intermediate point C. (From [8].)

the solutions of Equation (3.100)<sub>1</sub>. When  $\beta$  reaches  $\beta_1^*$ , the thermal state starts to move toward the high-temperature solution. However, it reaches the melting point first (point B). A further increase in  $\beta$  will move the solution toward point D, the critical point for the solution of Equation (3.100)<sub>1</sub> with the basal temperature boundary condition. Before this point can be reached, a layer of basal ice starts to form at melting point. This occurs at some point C corresponding to  $\beta = \beta_1^*$  (where  $\beta_1^* < \beta_2^* < \beta_3^*$ ). (Clarke *et al.* [8].) At this point the above solution breaks down completely and a thermal analysis involving a layer of cold ice lying on top of a layer of temperate ice should be analysed.

*Strain heating and advection.* The above results pertain to parallel-sided slabs in which stress, temperature and velocity fields are independent of the longitudinal coordinate and in which accumulation/ablation effects are set aside. This is the reason why Equation (3.100)<sub>2</sub> has not been considered; it is only meaningful when  $\varepsilon \neq 0$ . It should be noted that when  $\varepsilon \neq 0$ , both Equations (3.100) represent approximations, since strain heating is evaluated with stress distributions that cannot represent solutions of corresponding momentum equations. This should be borne in mind and the results discussed below should be taken with the necessary caution.

The addition of advection normal to the surface does not alter the qualitative results discussed above and the numerical solutions of Equations (3.100), for positive and negative values of  $\varepsilon$  are similar to the results for  $\varepsilon = 0$  shown in Figures 3.20 and 3.21. However, whereas advection does not change results qualitatively, large quantitative changes emerge from its inclusion in the analysis. In particular, the critical value  $\beta_1^*$  strongly depends on the value of  $\varepsilon$ .

Figures 3.24 and 3.25, valid for a frozen bed, show how advection affects the critical value  $\beta_1^*(\bar{\beta}_1^*)$  which is plotted against  $\varepsilon$  for various values of the geothermal heat flux  $\Phi$ .<sup>\*</sup> Also shown are the maximal basal temperatures  $\bar{\beta}_b$  in the low temperature solutions of (3.100), namely the values attained at  $\beta = \beta_1^*$ . These are uniquely determined by  $\varepsilon$  and  $\Phi$ . For example, by selecting in Figure 3.24,  $\varepsilon = -2$  and  $\Phi = 2$ ,  $\beta_1^* = 0.17$  is obtained, and the maximum value of the temperature  $\bar{\beta}_b$  is about 4.3. From both figures it is also seen that the value of  $\beta_1^*(\bar{\beta}_1^*)$  decreases with decreasing  $\varepsilon$ . Conditions favoring bifurcating states are, clearly, large geothermal heat flux for a fixed value of the surface temperature and negative  $\varepsilon$  corresponding to an upward velocity such as would be found in the ablation region of glaciers and ice sheets. It can also be seen from the figures that in many cases, in particular those with strong upward advection, bifurcation cannot occur because this would demand a basal temperature above the melting point.

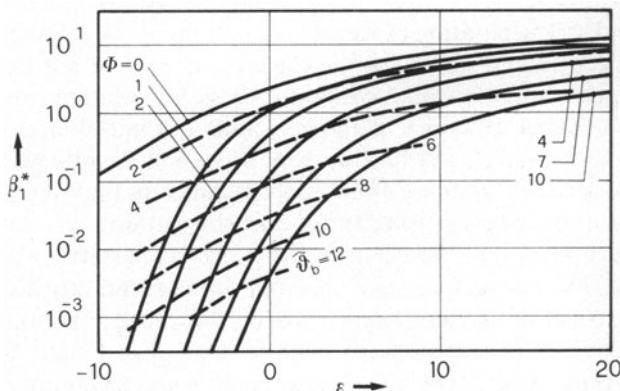


FIG. 3.24. Critical values of the stability parameter  $\beta_1^*$  for various values of the advection parameter and the geothermal parameter  $\Phi$ . Also shown are values of the basal temperature  $\bar{\beta}_b$  at the onset of instability. The stress is assumed to increase linearly with depth, and the base of the ice sheet is frozen to its bed. Positive values correspond to accumulation at the upper surface. For this calculation,  $\alpha = 30$ , a value corresponding to  $T_s = -30^\circ\text{C}$ . (From [8].)

\* $\bar{\beta}_1^*$  applies for the second of Equations (3.100), which is valid for a state of stress when longitudinal stress is dominant.

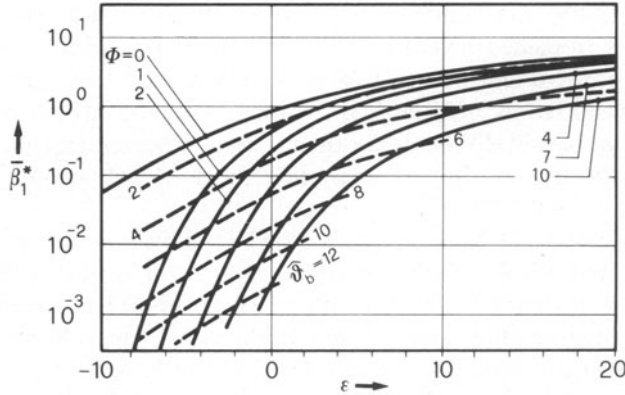


FIG. 3.25. Critical values of the stability parameter  $\beta_1^*$  for various values of the advection parameter and the geothermal parameter  $\Phi$ . Also shown are values of the basal temperature parameter  $\hat{\vartheta}_0$  at the onset of instability. The stress is assumed to be constant with depth, and the ice sheet is taken to be frozen to its base. For this calculation,  $\alpha = 30$ , a value corresponding to  $T_s = -30$  C. (From [8].)

Clarke *et al.* [8] extend the above results by a small perturbation time-dependent stability analysis. On the right-hand side of Equation (3.100)<sub>1</sub> they add a time dependent term  $\partial\hat{\vartheta}/\partial t$  and perturb the steady-state temperature  $\hat{\vartheta}_0$  by writing  $\hat{\vartheta} = \hat{\vartheta}_0 + \tilde{\vartheta}$ . They then deduce a linearized differential equation for  $\tilde{\vartheta}$ , and seek separation of variables solutions,  $\tilde{\vartheta} = \psi_m(\bar{y}) \exp(\lambda_m t)$ . The associated eigenvalue problem for the eigenvalues  $\lambda_m$  is of Sturm–Liouville type, thus eigenvalues are real. Asymptotically stable solutions for  $\tilde{\vartheta}$  require  $\lambda_m < 0$ . For a range of values of the constants  $\epsilon$ ,  $\beta$  and  $\Phi$  appropriate to natural ice, Clarke *et al.* [8] find both positive and negative eigenvalues, indicating possible instabilities. Their analysis indicates that rapid growth of instability is obtained for strong transverse convection and that ablation tends to reduce  $\beta_1^*$ , thereby favoring the onset of creep instability.

*Critique.* The above analysis is incomplete in several aspects. Only the temperature equation is considered in which the effect of strain heating is approximated by selecting a specific simple stress distribution. This stress distribution is not an exact solution of the equilibrium equations; yet multiple-valued solutions for the temperature profile are caused by exactly this approximated term. This raises certain doubts regarding the reliability of the results. In a complete analysis, the temperature and the creep problem would have to be solved simultaneously. Further, the instability analysis should, apart from temperature perturbations, also include velocity perturbations. This was done by Yuen and Schubert [72] and for the cases considered by them they found no instabilities. This brings us to a further critique raised by Fowler [10]. He argues that the stability parameter  $\beta$ , as listed in Equation

(3.101), depends on glacier thickness  $D$  (recall from Table 3.3, that  $\mathbb{E}$  depends on  $D$ , while all other parameters in (3.101) are independent of  $\mathcal{J}_S$ ,  $Q^{\text{geoth}}$  and  $D$ ). We have seen earlier that in a more complete description, the glacier depth would itself be determined from ice dynamics. In the above analysis, the glacier depth was given and conditions for the accumulation rate function consistent with the kinematic surface condition were determined. For the steady state and the stress and temperature distribution to be independent of  $\bar{x}$ , the only possibilities were found to be  $\bar{a} = 0$  and  $\bar{a} = \text{constant}$ .

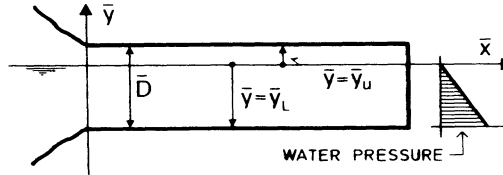
In a more complete approach one should, therefore, use as control variable accumulation and determine the stress, velocity temperature and glacier depth in terms of it. The parameter  $\beta$  would then be expressed in terms of the accumulation rate and, through the solution of the dynamics problem, also possibly of surface temperature and geothermal heat flux. Multiplicity of steady-state solutions should then be examined in terms of accumulation. Fowler gives arguments which indicate that such an approach will most likely preclude multiplicity of solutions for given external input functions. In such a case, the runaway instability as envisaged by Clarke *et al.* and Yuen and Schubert may not occur. Fowler and Larson, in recent works [12a, b], demonstrate that for their model glacier there is indeed no multiplicity of solutions in this case.

One may, alternatively, analyse the mechanical problem rather than the thermal one. This can be done by selecting estimates for the transverse temperature distribution and the distribution of the second stress-deviator invariant. Paterson [48] reports field measurements by Gerrard *et al.* [13], Sharp [55], Mathews [30], and Savage and Paterson [53] which broadly corroborate the findings obtained this way. Improvements will be dealt with in Chapters 4 and 5.

( $\gamma$ ) *Floating ice shelves.* Floating ice shelves are extensions of grounded ice sheets into the ocean. In the Arctic and in Antarctica they are generally several tens or hundreds of kilometers long and, over long distances, very nearly of constant thickness. When frictional effects due to the ocean current are neglected and the shelf is unconfined sidewise, the deformation is planar and the state of stress very nearly uniform over large distances with vanishing shear stress at the ice-water interface.

Previous theoretical studies of ice shelves are, among others, by Weertman [64], Thomas [61, 62, 62a], Shumskiy and Krass [57] and Hutter and Williams [18, 21a]. With the exception of the work of Thomas, the ice shelves are unconfined and planar deformations are assumed.

Consider a floating ice shelf of constant thickness in steady state. Assume that the stresses are uniform with  $\bar{x}$ , but that strains may vary (see Figure 3.26). Except for local regions close to the snout and the hinge, these assumptions are probably reasonable for the flow is driven by the steady

FIG. 3.26. Geometry of an unconfined ice shelf of thickness  $D$ .

flux of ice from grounded ice sheets at the hinge. The thickness of the shelf is maintained by a balance of accumulation from above, melting or freezing from below, and by the flux of the mass in the longitudinal direction. Introducing the coordinate system as shown in Figure 3.26 with the  $\bar{x}$ -axis along the waterline a momentum balance yields  $\tau = 0$ ,  $\sigma_y = \bar{y} - \bar{y}_u - \bar{p}^{\text{atm}}$ , provided that zero drag is assumed. The value for  $\bar{y}_u$  follows by equating  $\sigma_y(\bar{y}_L)$  to the water pressure at the lower boundary of the sheet and yields

$$\bar{y}_u = \frac{\rho_w - \rho}{\rho_w} \bar{D}, \quad \bar{y}_L = - \frac{\rho}{\rho_w} \bar{D}. \quad (3.105)$$

Here  $\bar{D}$  is the dimensionless thickness of the ice sheet. It will become apparent later that the characteristic length  $D$  with which the equations were made dimensionless, should not be chosen to be exactly the shelf thickness but only nearly so, so that  $\bar{D} \neq 1$ . The remaining analysis now parallels that of the extending and compressing flow in the last section, with appropriate adjustments due to a different choice of the coordinate system and the particular value of  $\gamma (=0)$ . For instance, Equation (3.95) implies  $\bar{h} = 0$  so that

$$\bar{u} = r_0 \bar{x} + l_0, \quad \bar{v} = -r_0 (\bar{y} - \bar{y}_u) - \bar{a} \quad (3.106)$$

is the velocity field in the shelf; it satisfies the kinematic boundary condition  $v(\bar{y}_u) = -\bar{a}$ . The two constants  $r_0$  and  $l_0$  characterize the flow completely;  $l_0$  is the velocity at the hinge and can be obtained from velocity or mass flux measurements.  $r_0$  is the longitudinal stretching and can be calculated from a combination of (3.92) and (3.96),

$$\begin{aligned} r_0^2 - \exp(2\mathbb{A}\theta) \mathfrak{F}^2(\tau'_{\text{II}}) \tau'_{\text{II}} &= 0, \\ \mathbb{D} \frac{d^2 \vartheta}{d\bar{y}^2} + [r_0(\bar{y} - \bar{y}_u) + \bar{a}] \frac{d\vartheta}{d\bar{y}} + 2\mathbb{E} \exp(\mathbb{A}\theta) \mathfrak{F}(\tau'_{\text{II}}) \tau'_{\text{II}} &= 0. \end{aligned} \quad (3.107)$$

$\sigma_x$  then follows from the definition of  $\tau'_{\text{II}}$  as

$$\sigma_x = 2 \operatorname{sgn} r_0 \sqrt{\tau'_{\text{II}}} + (\bar{y} - \bar{y}_u) - \bar{p}^{\text{atm}}. \quad (3.108)$$

Finally, the integral of the longitudinal stress  $\sigma_x$  over the height must equal

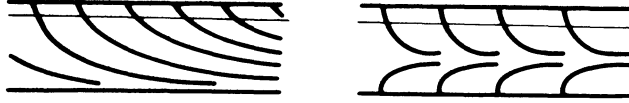


FIG. 3.27. Possible flow lines in an unconfined ice shelf.

the total pressure excited at the tongue end, see Figure 3.26,

$$(2 \operatorname{sgn} r_0) \int_{\bar{y}_u}^{\bar{y}_L} \sqrt{\tau'_{II}} dy = \frac{1}{2} \frac{\rho_w - \rho}{\rho_w} \bar{D}^2 > 0. \quad (3.109)$$

Thus,  $r_0 > 0$ ; the shelf can only spread but cannot creep compressively. This agrees with intuition. Depending upon the values of  $r_0$  and  $\bar{a}$ , two types of flow configurations are possible. In the first case  $\bar{v}$  does not change sign within the shelf and is always negative. Flow lines are as shown in Figure 3.27a; ice particles are convected from the top surface to the ice-water interface. The condition on  $r_0$  that this occurs is  $\bar{v}(\bar{y}_L) < 0$  or  $r_0 \bar{D} - \bar{a} < 0$ . Consequently, thinning due to spreading is smaller than thickening due to accumulation, and shelf thickness is maintained by melting at the ice-water interface. In the other case (see Figure 3.27b),  $\bar{v}$  changes sign within the shelf. Flow lines look like those shown in Figure 3.27b. Ice particles are convected into the ice from above and below, accumulating inside the shelf. In this case,  $r_0 \bar{D} - \bar{a} > 0$ , thinning due to spreading is larger than thickening due to accumulation and shelf thickness is maintained by freezing at the bottom. For  $r_0 \bar{D} = \bar{a}$ , thinning due to spreading and thickening due to accumulation are balanced so that neither freezing nor melting can occur at the ice-water interface. Ice particles are all convected downwards reaching the ice-water interface horizontally. Which of these flow configurations occurs depends on the solution of Equations (3.107)–(3.109), subject to the thermal boundary conditions at the ice-water interface, see Equations (3.72). For the situation at hand they read

$$\begin{aligned} \frac{d\vartheta}{d\bar{y}} &= -Q^{\text{atm}}, \quad \text{or} \quad \vartheta = \vartheta_s, \quad \bar{y} = \bar{y}_u, \\ L(r_0 \bar{D} - \bar{a}) &= \begin{cases} \left. \frac{d\vartheta}{d\bar{y}} \right|_{\vartheta=\vartheta_w}, & \text{if } r_0 \bar{D} - \bar{a} > 0, \\ 0 = N(\vartheta_w - \vartheta) - \frac{d\vartheta}{d\bar{y}}, & \text{if } \vartheta_w < \vartheta < \vartheta_M, \quad \bar{y} = \bar{y}_L, \\ N(\vartheta_w - \vartheta_M) - \left. \frac{d\vartheta}{d\bar{y}} \right|_{\vartheta=\vartheta_M}, & \text{if } r_0 \bar{D} - \bar{a} < 0, \end{cases} \end{aligned} \quad (3.110)$$

Solutions have not yet been constructed and there is little hope that analytical solutions could be found. It is, however, not surprising if the temperature distribution corresponding to the flow configurations of Figures 3.27a, b should differ appreciably. Indeed, in the situation of Figure 3.27a, heat generated by viscous friction is convected from above down to the ice-water interface, where it becomes available for melting. No undue temperature profile should result from this. In the case of Figure 3.27b, all viscous heat is convected into a single layer, there becoming available to raise the temperature, perhaps even as far as to let a layer of the shelf become temperate.

An approximate solution can be constructed as follows: Assume  $\bar{D}$  and the temperature profile to be known from measurements or estimates and restrict considerations to Glen's flow law for which  $\mathfrak{F}(\tau'_{II}) = \tau'^{(n-1)/2}_{II}$ . Equations (3.108) and (3.109) may then be used to determine  $r_0$  by

$$r_0 = \left[ \frac{\bar{y}_u}{\int_{\bar{y}_L}^{\bar{y}_u} \exp(\mathbb{A}\theta/n) d\bar{y}} \right]^n \bar{D}^n. \quad (3.111)$$

This formula is due to Weertman [64]; it allows determination of  $r_0$ , and when stretching is also measured, it may be used to obtain values for  $\mathbb{A}$  and  $n$ . This then constitutes a semi-inverse method to determine the material behavior of naturally-grown ice [61, 62]. With (3.111), the second stress-deviator invariant becomes from (3.107)

$$\tau'_{II} = [r_0^2 \exp(-2\mathbb{A}\theta)]^{1/n}, \quad (3.112)$$

so coefficients of the heat conduction equation (3.107)<sub>2</sub> are approximately known so that a new approximation of the temperature profile can be found by integrating that equation.

An exact integration of the boundary value problem (3.107)–(3.110) has never been attempted and must be very difficult. Hutter and Williams [18, 71a], however, found approximate solutions for the thermal boundary value problem by assuming a reasonable functional relationship for the vertical temperature distribution and solving the free parameter in this functional relation. This trial function should account for the fact that heat is accumulated at the line into which the flow lines converge. Results, of course, will depend somewhat on the choice of the trial function, but with it the complicated thermomechanical problem can be reduced to a much simpler problem by relating thermal conditions in the atmosphere and the ocean to the shelf thickness (see [18]). A linear stability analysis of the steady-state solution [71a] then shows that flow configurations according to Figure 3.27a are thermally stable, while those of Figure 3.27b are unstable. This result is a proven one, but was conjectured by Shumskiy and Krass [57]. For details the reader is referred to the original literature.

#### 4. Concluding Remarks

In this chapter it was shown how generally-accepted views of continuum physics can be used to formulate a rational theory of glacier and ice sheet dynamics. Attention was focused on two-dimensional motions. In the first part of the chapter, the field equations governing the motion and the temperature evolution were derived, including associated boundary conditions that must hold at a free surface, the base, an ice-water interface, and at the melting surface, which is defined as the surface separating cold and temperate ice. A novel feature was introduced into the theory of temperate ice in that a balance equation for the moisture content was derived. The moisture content is thereby defined as the voluminous fraction of the water in the ice, and its amount depends on the frictional heat produced by the deformation of the ice and on the moisture flux (drainage) through the boundaries. Emphasis was laid on a clear derivation of the relevant equations from physical principles.

In the second part of the chapter, the derived equations were subjected to first simple applications, all of which dealt with the deformation and temperature distribution of a strictly parallel-sided (cold) ice slab. Many simple results for this configuration are well known to glaciologists, yet our mathematically more rigorous approach shows that, with only little additional effort, useful additional results can be obtained. We might mention the calculations regarding extending and compressing flow in ice slopes sliding over their bed, the temperature analysis in cold glaciers, and the treatment of ice shelves relating ice thicknesses to the atmospheric climate.

Most calculations in the problems were performed using cold ice as an example. When temperate ice was looked at, only simplified calculations were performed, by assuming that the flow law was independent of the moisture content. Under such conditions the field equations governing the motion and that of the moisture content separate. The motion and the stresses can be determined in a first step delivering the moisture content as an *a posteriori* information. Actually when using Equation (3.15), or its dimensionless equivalent

$$\frac{\partial \bar{w}}{\partial t} + \frac{\partial \bar{w}}{\partial \bar{x}} \bar{u} + \frac{\partial \bar{w}}{\partial \bar{y}} \bar{v} = \mathbb{D}_w \left( \frac{\partial^2 w}{\partial \bar{x}^2} + \frac{\partial^2 \bar{w}}{\partial \bar{y}^2} \right) + 2\mathbb{E}_w \mathfrak{F}(\tau'_{II}) \tau'_{II},$$

in which  $\bar{w}$  is the dimensionless moisture content  $\bar{w} = w/w_0$ , and  $\mathbb{D}_w$  and  $\mathbb{E}_w$  are characteristic numbers given by

$$\mathbb{D}_w = \frac{\nu}{\rho} \frac{\mathfrak{T}}{D^2}, \quad \mathbb{E}_w = \frac{gD}{w_0},$$

as a balance equation for the moisture content, then the calculations performed for cold ice formally carry over to temperate ice, the moisture content

playing the role of the temperature. Boundary conditions at the base and the free surface must prescribe  $\bar{w}$  or its flux. For an impermeable base the flux of  $\bar{w}$  through the base must vanish, and at the free surface the moisture content is prescribed. Very little is known about these boundary conditions from an applied point of view, which is the reason why we have preferred to assume the stress constitutive relationship to be independent of moisture content.

Only the very simplest problems have been analysed above by restricting the geometry to the strictly parallel-sided ice slab and by looking at cold or temperate ice, but not at polythermal ice. The subsequent chapters will show how solutions are constructed when the geometry or the physical situation is more complex. The following chapter will give a first application of such a more general situation.

#### REFERENCES

1. Bellman, R. and R. Kalaba, *Quasilinearization and Non-linear Boundary Value Problems*. Elsevier, New York, 1965.
2. Bird, R. G., N. E. Stewart, and E. N. Leightfoot, *Transport Phenomena*, Wiley, New York, 1965.
3. Björnsson, H., Subglacial water reservoirs, Jökulhlaups and volcanic eruptions, *Jökull*, **25**, 1–11, 1975.
4. Boshinsky, A. N., On unstable internal heating of glaciers (in Russian), *Izv. Akad. Nauk S.S.R. Mekh Zhidk. Gaza*, **5**, 169–172, 1975.
5. Boshinsky, A. N. and S. S. Grigoryan, Possible displacement mechanism in cold glaciers (in Russian), *Izv. Akad. Nauk S.S.R. Mater. Glyatsiologicheskikh Isslet.* **24**, 64–68, 1974.
6. Budd, W. F., A first simple model for periodically self-surging glaciers, *J. Glaciology*, **14**, 3–21, 1975.
7. Budd, W. F., The dynamics of ice masses, *Anare Sci. Reports. Publ.*, **120**, 1–178, 1971.
- 7a. Carslaw, H. S. and J. C. Jeger, *Conduction of Heat in Solids*, 2nd edn., Clarendon Press, Oxford, 1959.
8. Clarke, G. K. C., V. Nitsan and W. S. B. Paterson, Strain heating and creep instability in glaciers and ice sheets, *Rev. Geophys. Space Phys.*, **15**, 235–247, 1977.
9. Fowler, A. C., Glacier dynamics, thesis submitted for the degree of Doctor of Philosophy in the University of Oxford, Corpus Christi College, England, 1977.
10. Fowler, A. C., The existence of multiple steady states in the flow of large ice masses, *J. Glaciology*, **25**, 183–184, 1980.
- 10a. Fowler, A. C., A theoretical treatment of the sliding of glaciers in the absence of cavitation, *Phil. Trans. Royal Soc. London*, **298**, 637–685, 1981.
11. Fowler, A. C. and D. A. Larson, On the flow of polythermal glaciers. I. Model and preliminary analysis, *Proc. Royal Soc. London*, **A363**, 217–242, 1978.
12. Fowler, A. C. and D. A. Larson, On the flow of polythermal glaciers. II. Surface wave analyses, *Proc. Royal Soc. London*, **A370**, 155–171, 1980.
- 12a. Fowler, A. C. and D. A. Larson, Uniqueness of steady state flows of glaciers and ice sheets, *Geophys. J. Royal Astron. Soc.*, **63**, 333–345, 1980.
- 12b. Fowler, A. C. and D. A. Larson, Thermal stability properties of a model of glacier flow, *Geophys. J. Royal Astron. Soc.*, **63**, 347–359, 1980.

13. Gerrard, J. A. F., M. F. Perutz and A. Roch, A measurement of the velocity distribution along a vertical line through a glacier, *Proc. Royal Soc. London*, **A213**, 546–558, 1952.
14. Grigoryan, S. S., M. S. Krass, and P. A. Shumskiy, Mathematical model of a three-dimensional non-isothermal glacier, *J. Glaciology*, **17**, 401–417, 1976.
- 14a. Hutter, K., A mathematical model of polythermal glaciers and ice sheets, *J. Geophys. Astrophys. Fluid Mech.*, **21**, 201–224, 1982.
15. Hutter, K. and V. O. S. Olunloyo, On the distribution of stress and velocity in an ice strip, which is partly sliding over and partly adhering to its bed using a Newtonian viscous approximation, *Proc. Royal Soc. London*, **A373**, 385–403, 1980.
16. Hutter, K. and V. O. S. Olunloyo, Basal stress concentrations due to abrupt changes in boundary conditions. A cause for high till concentration at the bottom of a glacier, *Ann. Glaciology*, **2**, 29–33, 1981.
17. Hutter, K. and U. Spring, Distribution of stresses and velocities in an ice slope with spatially dependent material response. *Festschrift Peter Kasser, Mitteilung der Versuchsanstalt für Wasserbau, Hydrologie und Glaziologie*, **41**, 99–122, 1979.
18. Hutter, K. and F. M. Williams, Theory of floating ice sheets, in *Proc. IUTAM-Symposium on the Mechanics and Physics of Ice*, edited by P. Tryde, Springer Verlag, Berlin, New York, Heidelberg, pp. 147–162, 1979.
19. Iken, A., Measurements of water pressure in moulin as part of movement study of the White Glacier, Axel Heiberg Island 1, Northwest Territories, *Can. J. Glaciology*, **11**, 53–58, 1972.
20. Iken, A., Variations of surface velocities of some Alpine glaciers measured at intervals of a few hours. Comparison with Arctic glaciers, *Zeitschrift für Gletscherkunde und Glaziologie*, **13**, 23–35, 1977.
21. Kamb, B., Sliding motion of glaciers. Theory and observation, *Rev. Geophys. Space Phys.*, **8**, 673–728, 1970.
22. Kamb, B. and E. LaChapelle, Direct observation of the mechanism of glacier sliding over bedrock, *J. Glaciology*, **5**, 159–172, 1964.
23. Kantorovich, L. W. and G. P. Akilov, *Funktionalanalysis in genormten Räumen*. Akademieverlag, Berlin, 1964.
24. Lliboutry, L. A., Une théorie du frottement du glacier sur son lit, *Annales de Géophysique*, **15**, 250–265, 1959.
25. Lliboutry, L. A., *Traité de Glaciologie*, Vol. 1, Masson, Paris, 1964.
26. Lliboutry, L. A., General theory of subglacial cavitation and sliding of temperate glaciers, *J. Glaciology*, **7**, 21–58, 1968.
27. Lliboutry, L. A., Lois de glissement d'un glacier sans cavitations, *Annales de Géophysique*, **31**, 207–226, 1975.
28. Lliboutry, L. A., Physical processes in temperate glaciers, *J. Glaciology*, **16**, 151–158, 1976.
- 28a. Lliboutry, L. A., Local friction laws for glaciers: A critical review and new openings, *J. Glaciology*, **23**, 67–75, 1979.
29. Lliboutry, L. A. and C. Ritz, Ecoulement permanent d'un fluide visqueux non linéaire (corps de Glen) autour d'une sphère parfaitement lisse, *Annales de Géophysique*, **34**, 133–146, 1978.
30. Mathews, W. H., Vertical distribution of velocity in Salmon Glacier, British Columbia, *J. Glaciology*, **3**, 448–454, 1959.
31. Mathews, W. H., Record of two Jökulhlaups, Symposium on the hydrology of glaciers, Cambridge, 7–13 Sept. 1969, International Union of Geodesy and Geophysics, *International Association of Scientific Hydrology, Publ.*, **95**, 99–110, 1973.
32. Mises, R. von, *Mathematical Theory of Compressible Fluid Flow*, Completed by H. Geiringer and G. S. S. Ludford, Academic Press, New York, 1958.

33. Morland, L. W.. Glacier sliding down an inclined wavy bed. *J. Glaciology*. **17**, 447–462. 1976.
34. Morland, L. W.. Glacier sliding down an inclined wavy bed with friction. *J. Glaciology*. **17**, 463–476. 1976.
35. Neave, K. G. and J. C. Savage. Ice-quake on the Athabasca glacier. *J. Geophys. Res.*. **25**, 1351–1362. 1970.
36. Nye, J. F.. The mechanics of glacier flow. *J. Glaciology*. **2**, 82–93. 1952.
37. Nye, J. F.. The distribution of stress and velocity in glaciers and ice sheets. *Proc. Royal Soc. London*. **A239**, 113–133. 1957.
38. Nye, J. F.. The motion of ice sheets and glaciers. *J. Glaciology*. **3**, 493–507. 1959.
39. Nye, J. F.. The response of glaciers and ice sheets to seasonal and climatic changes. *Proc. Royal Soc. London*. **A256**, 559–584. 1960.
40. Nye, J. F.. On the theory of advance and retreat of glaciers. *Geophys. J. Royal Astron. Soc.*. **7**, 431–456. 1963.
41. Nye, J. F.. The response of a glacier to changes in the rate of nourishment and wastage. *Proc. Royal Soc. London*. **A275**, 87–112. 1963.
42. Nye, J. F.. A calculation on the sliding of ice over a wavy surface using a Newtonian viscous approximation. *Proc. Royal Soc. London*. **A311**, 445–467. 1969.
43. Nye, J. F.. Glacier sliding without cavitation in a linear viscous approximation. *Proc. Royal Soc. London*. **A315**, 381–403. 1970.
44. Nye, J. F.. Causes and mechanisms of glacier surges: A discussion. *Can. J. Earth Sci.*. **8**, 306–307. 1971.
45. Nye, J. F.. Water flow in glaciers: Jökulhlaups, tunnels and veins. *J. Glaciology*. **17**, 181–207. 1976.
46. Nye, J. F. and C. F. Frank. Hydrology of the intergranular veins in a temperate glacier. symposium on the hydrology of glaciers, Cambridge. 1969, International Union of Geodesy and Geophysics. *International Association of Scientific Hydrology. Publ.*, **95**, 157–161. 1973.
47. Olunloyo, V. O. S. and K. Hutter. Stress concentrations in an ice slope due to abrupt changes in boundary conditions. (in preparation).
48. Paterson, W. S. B.. *The Physics of Glaciers*. Pergamon Press. Oxford. New York. Toronto. 1969.
49. Poston, T. and I. Stewart. *Catastrophe Theory and Its Applications*. Pitman. London. San Francisco. Melbourne. 1978.
50. Robin, G. de Q.. Ice movement and temperature distribution in glaciers and ice sheets. *J. Glaciology*. **2**, 523–532. 1955.
51. Robin, G. de Q.. Is the basal ice of a temperate glacier at the pressure melting point? *J. Glaciology*. **16**, 183–196. 1976.
52. Roethlisberger, H.. Water pressure in intraglacial and subglacial channels. *J. Glaciology*. **11**, 177–203. 1972.
53. Savage, J. C. and W. S. F. Paterson. Borehole measurements in Athabasca glacier. *J. Geophys. Res.*, **68**, 4521–4536. 1963.
54. Schlichting, H.. *Boundary Layer Theory*. McGraw-Hill. New York. 1968.
55. Sharp, R. P.. Deformation of a vertical bore hole in a piedmont glacier. *J. Glaciology*. **2**, 182–184. 1953.
56. Shreve, R. L.. Movements of water in glaciers. *J. Glaciology*. **11**, 205–214. 1972.
57. Shumskiy, P. A. and M. S. Krass. Mathematical models of ice shelves. *J. Glaciology*. **17**, 419–432. 1976.
58. Spring, U.. Zur Theorie des instationären Wasserabflusses durch intraglaziale Kanäle. Adhandlung zur Erlangung des Titels eines Doktors der Technischen Wissenschaften der Eidgenössischen Technischen Hochschule. Zürich. 1979.

59. Spring, U. and K. Hutter, Conduit flow of a fluid through its solid phase and its application to intraglacial channel flow, *Int. J. Eng. Sci.*, **20**, 327–363, 1982.
60. Spring, U. and K. Hutter, Numerical Studies of Jökulhlaups, *Cold Region Sci. Tech.*, **4**, 227–244, 1981.
- 60a. Szidovszky, F. and S. Yakowitz, *Principles and Procedures of Numerical Analysis*, Plenum Press, New York, London, 1978.
61. Thomas, R. H., The creep of ice shelves: Theory, *J. Glaciology*, **12**, 45–53, 1973.
62. Thomas, R. H., The creep of ice shelves: Interpretation of observed behavior, *J. Glaciology*, **12**, 55–70, 1973.
- 62a. Thomas, R. H., Ice shelves: A review, *J. Glaciology*, **24**, 273–286, 1979.
63. Weertman, J., On the sliding of glaciers, *J. Glaciology*, **3**, 33–38, 1957.
64. Weertman, J., Deformation of floating ice shelves, *J. Glaciology*, **3**, 38–42, 1957.
65. Weertman, J., Mechanism for the formation of inner moraines found near the edge of cold ice caps and ice sheets, *J. Glaciology*, **3**, 965–978, 1961.
66. Weertman, J., The theory of glacier sliding, *J. Glaciology*, **5**, 287–303, 1964.
67. Weertman, J., An examination of the Liboutry theory of glacier sliding, *J. Glaciology*, **6**, 489–494, 1967.
68. Weertman, J., Comparison between measured and theoretical temperature profiles of the Camp Century, Greenland, Boreholes, *J. Geophys. Res.*, **73**, 2691–2700, 1968.
69. Weertman, J., In defense of a simple model of glacier sliding, *J. Geophys. Res.*, **76**, 6485–6487, 1971.
- 69a. Weertman, J., The unsolved general glacier sliding problem, *J. Glaciology*, **23**, 97–115, 1979.
70. Wengfeld, P., Momentum-, heat and mass transfer at the surface of an open channel flow under the influence of the wind, Dissertation, Institut Wasserbau III, Universität Karlsruhe, Germany, 1978.
71. Whitham, G. B., *Linear and Nonlinear Waves*, John Wiley, New York, London, Sydney, Toronto, 1974.
- 71a. Williams, F. M. and K. Hutter, Thermal response of unconfined ice shelves to climate conditions, *Acta Mechanica* (in press).
72. Yuen, D. A. and G. Schubert, The role of shear heating in the dynamics of large ice masses, *J. Glaciology*, **24**, 195–212, 1979.
73. Zotikov, I. A., Bottom melting in the central zone of the ice shield on the antarctic continent and its influence upon the present balance of the ice mass, International Union of Geodesy and Geophysics, *International Association of Scientific Hydrology, Bull.*, **8**, 36–44, 1963.

## **Chapter 4**

# **THERMO-MECHANICAL RESPONSE OF NEARLY PARALLEL-SIDED ICE SLABS SLIDING OVER THEIR BED**

### *1. Motivation*

In Chapter 3, the strictly parallel-sided ice slab was analysed. Solutions to the flow and temperature problem were constructed for which stresses did not vary with the coordinate along the glacier axis. Two solutions were found which satisfied these conditions. In the first, apart from stresses, velocities and temperature are also independent of the coordinate along the ice slab. For this solution to be consistent with the boundary conditions of the general model, both accumulation and ablation had to be neglected. To account for the inclusion of the latter, and for floating ice shelves, in order to properly allow for mass flux from the grounded portion of the ice sheet, the velocity field had to be assumed to vary with the length coordinate. On the basis that stress and temperature are still independent of this coordinate, it was found that the longitudinal velocity components vary linearly along the ice sheet axis, whereas transverse velocities remain independent of the length coordinate and vary linearly with depth. Longitudinal and transverse stretchings are equal and constant in this case, and the constant transverse surface velocity gives the possibility of including a constant accumulation rate. For a grounded ice slab, it was shown that this solution is in violation with a stress-dependent sliding law. For an ice shelf, on the other hand, the solution is meaningful, provided that the drag from the ocean current is neglected; in this case, the flow parameters can be related to the thermal conditions in the atmosphere. It is clear from the above that for ice slabs resting on a rockbed, a more general solution to the flow problem should be sought which is free from the defects mentioned above. This is one reason why one should search for a solution, in which longitudinal stretching effects are consistently taken into account. A second reason is the fact that glaciers and ice sheets are only very nearly parallel-sided. Generally, the rockbed and free surface undulate about a mean plane surface. Rockbed protuberances force the ice to flow around them. Together with the spatially-dependent accumulation rate, they cause (also in the steady state) surface undulations and are thus responsible for the longitudinal stretching effects occurring in ice slopes. It is

evident in these instances that stresses can no longer be independent of the longitudinal coordinate.

The existence of surface undulations on ice caps has been reported by many authors, among them Bourgoin [6], Swithinbank [47], Robin [42, 43], Robinson [46], Budd [8, 10], Clough *et al.* [16] and Mälzer [31]. Observations indicate that the dominant wavelengths of the surface undulations are generally several times the thickness of the ice sheet. One question that arises in this connection is whether the bedrock slope influences the surface profile and, if it does, how much of the undulation amplitude will be transferred to the surface. Several authors have tackled this problem. First attempts were by Bourgoin [6], Nye [35] and Lliboutry [30]. In these early works, the mathematical formulation of longitudinal stretching effects was not yet clearly presented. A consistent description of these effects and their influence on the stress distribution in the ice sheet was initiated by Robin [43]; his analysis aimed at an improvement of the basic shear-stress formula. This formula states that the basal shear stress is proportional to the local thickness and local mean inclination of the surface. Improved derivations of Robin's formula were given by Collins [18] and Nye [40]. However, it was Budd [10, 11, 12] who tried not only to present a systematic derivation of the longitudinal stretching effects on the stress and velocity distribution, but also to describe the effect of bedrock protuberances on the geometry of the free surface. Budd's analysis was critically reviewed by Hutter *et al.* [26], who analysed the entire problem anew. Their results are different from those of Budd because their theory is free from conceptual inconsistencies, some of which are hidden in Budd's analysis. The analysis presented below parallels that of Hutter *et al.* [26].

*On a length scale much shorter than the actual horizontal extension of an ice sheet, but also larger than the local thickness of the sheet, a glacier or ice cap may, without essential loss of accuracy, be assumed to be of nearly constant thickness with (mostly) small variations of the rockbed and the free surface from mean flat surfaces, whose inclinations are the same on this scale (see Figure 4.1). This then suggests a search for a solution to the governing equations derived in Chapter 3 for an ice slab which is only nearly parallel-sided. If bedrock perturbations about a mean flat rockbed possess amplitudes which are small as compared to the thickness of the ice slope, then this suggests the construction of an approximate solution of the governing equations in terms of a perturbation expansion. This is precisely what we shall do.*

The small perturbation analysis may not only be applied to the steady-state response as envisaged when the rockbed undulates about a straight mean bed, but equally also when time-dependent processes are analysed. Time-dependent processes occur whenever accumulation rates and climatic conditions are unsteady. Sudden changes in the accumulation rate may,

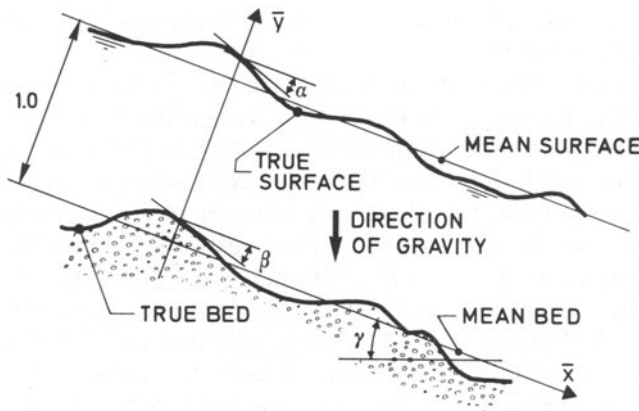


FIG. 4.1. Nearly parallel-sided ice slab. Mean inclination of bed and surface is  $\gamma$ . Actual inclinations of top and bottom surface are  $(\alpha + \gamma)$  and  $(\beta + \gamma)$ . Amplitudes of bottom and surface undulations are assumed to be small.

in particular, induce surface waves. These are the motions of surface bulges travelling down the glacier. Three types of such waves are observed: (1) the slow 'kinematic' waves travelling at speeds which are three to four times as large as the surface speeds, (2) the fast 'seasonal' waves and (3) the 'surges'. The speeds of the latter two are very much larger than those of the former (20 to 150 times the surface speed, see Hodge [23], Meier and Post [32]). Approximate theories have been developed for the kinematic wave theory, (see Nye [36–39]), and for surges, (see Robin [44], Robin and Weertman [45], Budd [13] and Budd and McInnes [14]), yet no satisfactory mathematical model exists for the seasonal and surge-type waves.

The propagation of small-amplitude surface elevations of an otherwise parallel-sided ice slab can systematically be analysed using the small-perturbation theory, and the method will provide information as to the stability of the motion. The analysis will explore the application of a rigorous fluid-stability analysis to glacier-flow dynamics incorporating the rheological non-linearities introduced and used in the previous chapters. It yields surface speeds and wave attenuation with no particular indication of instabilities (see Thompson [49]). The stability analysis, however, paves the road for how in further studies time-dependent processes in glaciers and ice sheets might be analysed.

## 2. The Basic Boundary-value Problem and its Reduction to Linear Form

Consider flow of ice on a slope with small-amplitude undulations. Assume that the ice slab is infinitely large and for the purpose of this section, under *steady-state conditions*. To simplify calculations, assume further that

the entire ice slab is either cold, or temperate, but *not* polythermal. The field equations and boundary conditions for the thermo-mechanical problem under such conditions have been presented in Chapter 3, and the equations were non-dimensionalized there using the slab thickness  $D$  as a reference length, the total overburden pressure as a reference stress, and a time  $\mathfrak{T}$  suggested by the non-linear flow law as a characteristic time. The same quantities can also be used to non-dimensionalize the equations for the problem at hand, but  $D$  must now be interpreted as a mean thickness. The  $\bar{x}$ -axis is taken to be parallel to the mean direction of the top or bottom surface, and the local depth is measured perpendicular to the  $\bar{x}$ -axis (see Figure 4.1). Neither the top nor the bottom surface coincides with the  $\bar{x}$ -axis which only nearly matches the rockbed. Both surfaces are inclined with respect to the  $\bar{x}$ -direction with relative inclination angles which will be denoted by  $\alpha$  and  $\beta$ , respectively. It will be assumed that the deviations of the glacier surface from its mean  $y = D(\bar{y} = 1)$  and of the bottom topography from the line  $\bar{y} = 0$  are small. Denoting the distances of these surfaces from the  $\bar{x}$ -axis by  $\bar{y}_S$  and  $\bar{y}_B$ , respectively, it may therefore be assumed that  $|\bar{y}_B| \ll 1$  and  $|\bar{y}_S - 1| \ll 1$ .

With the coordinate system of Figure 4.1, the field equations and boundary conditions assume the form:

*Field equations* (see Equations (3.62), (3.66)):

$$\begin{aligned} \frac{\partial \sigma_x}{\partial \bar{x}} + \frac{\partial \tau}{\partial \bar{y}} + \sin \gamma &= 0, \\ \frac{\partial \tau}{\partial \bar{x}} + \frac{\partial \sigma_x}{\partial \bar{y}} - \cos \gamma &= 0, \\ \frac{\partial \bar{u}}{\partial \bar{x}} + \frac{\partial \bar{v}}{\partial \bar{y}} &= 0, \\ \frac{\partial \bar{u}}{\partial \bar{x}} = - \frac{\partial \bar{v}}{\partial \bar{y}} &= \frac{1}{2} \exp(\mathbb{A}\theta) \mathfrak{F}(\tau'_{II})(\sigma_x - \sigma_y), \\ \frac{\partial \bar{u}}{\partial \bar{y}} + \frac{\partial \bar{v}}{\partial \bar{x}} &= 2 \exp(\mathbb{A}\theta) \mathfrak{F}(\tau'_{II})\tau, \\ \frac{\partial \vartheta}{\partial \bar{t}} + \frac{\partial \vartheta}{\partial \bar{x}} \bar{u} + \frac{\partial \vartheta}{\partial \bar{y}} \bar{v} &= \mathbb{D} \left( \frac{\partial^2 \vartheta}{\partial \bar{x}^2} + \frac{\partial^2 \vartheta}{\partial \bar{y}^2} \right) + 2\mathbb{E} \mathfrak{F}(\tau'_{II})\tau'_{II}, \end{aligned} \quad (4.1)$$

in which  $\partial \vartheta / \partial \bar{t}$  vanishes in a steady state and where

$$\tau'_{II} = \frac{1}{4}(\sigma_x - \sigma_y)^2 + \tau^2, \quad \theta = \frac{1 - \mathbb{Z}}{1 + \mathbb{Z}\vartheta} \vartheta. \quad (4.2)$$

$\mathbb{A}$ ,  $\mathbb{D}$ ,  $\mathbb{E}$  and  $\mathbb{Z}$  are dimensionless characteristic numbers defined in Table 3.3.

*Boundary conditions :*

At the free surface :  $\bar{y} = \bar{y}_S(\bar{x}, t)$ ,

$$\begin{aligned}\frac{\partial \bar{y}_S}{\partial \bar{t}} + \bar{y}'_S \bar{u} - \bar{v} &= \bar{a}, & \tau y'_S - \sigma_y &= -\bar{p}^{\text{atm}}, \\ \sigma_x \bar{y}'_S - \tau &= -\bar{p}^{\text{atm}} \bar{y}'_S, & \vartheta &= \vartheta_S.\end{aligned}\quad (4.3)$$

Here, the kinematic surface condition (4.3) has been written for general non-steady conditions. In a steady state, the term  $\partial \bar{y}_S / \partial \bar{t}$  has to be set to zero.

At the rockbed :  $\bar{y} = \bar{y}_B(\bar{x})$

$$\begin{aligned}\bar{y}'_B \bar{u} - \bar{v} &= 0, \\ \bar{u} \frac{1}{\sqrt{1 + \bar{y}'_B^2}} + \bar{v} \frac{\bar{y}'_B}{\sqrt{1 + \bar{y}'_B^2}} &= \mathbb{C} \left\{ \tau \frac{1 - \bar{y}'_B^2}{1 + \bar{y}'_B^2} + (\sigma_y - \sigma_x) \frac{\bar{y}'_B}{1 + \bar{y}'_B^2} \right\}^m \\ \frac{\partial \vartheta}{\partial \bar{x}} \bar{y}'_B - \frac{\partial \vartheta}{\partial \bar{y}} &= \mathbb{Q}^{\text{geoth}} \sqrt{1 + \bar{y}'_B^2}, \quad \text{for cold ice only.}\end{aligned}\quad (4.4)$$

Here,  $\bar{y}'_S$  and  $\bar{y}'_B$  are the derivatives of  $\bar{y}_S$  and  $\bar{y}_B$  with respect to the length coordinate,  $\bar{x}$  and all formulas are direct applications of corresponding formulas in Section 2 of Chapter 3.

Let us illustrate the derivation of the second of Equations (4.4). To this end, recall that the sliding law has the form

$$\bar{u}_s = \mathbb{C} \tau_{sn}^m \quad (4.5)$$

where  $s$  and  $n$  indicate at a particular point directions tangential and perpendicular to the rockbed, respectively. Using the transformation laws (see Figure 4.2),

$$\begin{aligned}\bar{u}_s &= \bar{u} \cos \beta - \bar{v} \sin \beta, \\ \tau_{sn} &= \tau (\cos^2 \beta - \sin^2 \beta) - (\sigma_y - \sigma_x) \cos \beta \sin \beta,\end{aligned}\quad (4.6)$$

and the identity  $\bar{y}'_B = -\tan \beta$  a substitution of (4.6) into (4.5) shows that (4.4)<sub>2</sub> is obtained.

Equations (4.1)–(4.4) comprise the boundary-value problem of the thermo-mechanical flow problem appropriate for the internal portion of a glacier or an ice sheet. Similar mathematical analyses have been performed before by Yosida [56] and Budd [11]. The former uses the no-slip condition,  $\mathbb{C} \rightarrow 0$ , thereby restricting considerations to cold ice; the latter assumes perfect sliding,  $\mathbb{C} \rightarrow \infty$ , but this condition is not likely to be appropriate either because it ignores the fact that the flow furthest away from the base always ‘sees’ the latter as a viscous smoothed-out surface.

The boundary-value problem (4.1)–(4.4) is highly non-linear, defies in general, an exact analysis, and must therefore be solved approximately. The key idea is hereby that the glacier surface and the bottom topography do not deviate much from the infinite parallel-sided slab. On this presumption,

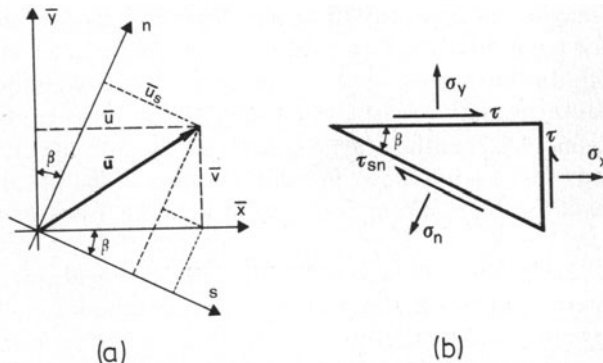


FIG. 4.2. Explaining formulas (4.6). (a) The  $s$  component of the vector  $\bar{u}$  and its connection with the components  $\bar{u}, \bar{v}$  in the  $(\bar{x}, \bar{y})$  system. (b)  $\tau_{sn}$  and  $\sigma_n$  can be expressed in terms of  $\sigma_x, \sigma_y$  and  $\tau$  by 'establishing equilibrium' on a triangular element.

an iterative scheme will be developed which allows an estimation of the influence of the bottom topography and of the steady accumulation or ablation rate on the stress and velocity distribution and on the surface topography. A further assumption is the formal decoupling of the temperature and velocity problem by either restricting considerations to temperate glaciers or by assuming the temperature distribution to be known. The exact procedure will be made precise shortly.

The basic assumption upon which the following regular perturbation approach is based is that amplitudes of the base are small in comparison to the mean ice sheet thickness. Consequently, we may write

$$\bar{y}_S(\bar{x}) = \varepsilon \Lambda(\bar{x}), \quad \text{where } 0 < \varepsilon \ll 1. \quad (4.7)$$

In this equation,  $\Lambda(\bar{x})$  and its derivative  $\Lambda'(\bar{x})$  are functions of order unity. Representation (4.7) suggests a search for the solution to the boundary-value problem (4.1)–(4.4) by means of perturbation expansion, in which the lowest-order problem defines the solution to the stress, velocity and (for cold ice) temperature distribution of the strictly parallel-sided ice slab, in which none of the field variables involved varies with  $\bar{x}$ .\* In other words, the lowest-order solution is the same as that constructed in Section 3b(α) of Chapter 3. Hence, we write

$$(\sigma_x, \sigma_y, \tau, \bar{u}, \bar{y}_S, \vartheta) = \sum_{v=0}^{\infty} \varepsilon^v (\sigma_x^{(v)}, \sigma_y^{(v)}, \tau^{(v)}, \bar{u}^{(v)}, \bar{y}_S^{(v)}, \vartheta^{(v)}), \quad (4.8)$$

$$\bar{v} = \sum_{v=1}^{\infty} \varepsilon^v \bar{v}^{(v)},$$

\*The reader might ask himself here whether a lowest-order solution with non-vanishing longitudinal strain would not also be appropriate. This solution has been ruled out in Chapter 3 on grounds that it is in violation with a stress-dependent sliding law.

in which  $\bar{y}_S^{(0)}$  may be set equal to 1 since the depth is presumed to be determined from the solution of the flow problem over length scales much larger than this depth. In the expansion of the transverse velocity component  $\bar{v}$ , it was further assumed that  $\bar{v} = \mathcal{O}(\varepsilon \bar{u})$ , where  $\mathcal{O}$  is the usual order symbol. The different ordering of  $\bar{v}$  from the other variables is based on the experience of observed speeds, but it also follows from the solution of the strictly parallel-sided slab (Section 3b( $\alpha$ ), Chapter 3) for which the transverse velocity component vanishes.

If the representations (4.8) are substituted into the field equations (4.1) and boundary conditions (4.3) and (4.4), each of these equations will formally involve all powers of  $\varepsilon$ . Most terms will appear as power series of  $\varepsilon$ , and if this is consistently the case for all terms in the equation, terms with equal powers in  $\varepsilon$  may be collected to obtain an entire sequence of equations. For instance, by substituting the expansions for  $\bar{u}$  and  $\bar{v}$  into the continuity equation (4.1)<sub>3</sub> one obtains

$$\frac{\partial \bar{u}^{(0)}}{\partial \bar{x}} + \sum_{v=1}^{\infty} \varepsilon^v \left( \frac{\partial \bar{u}^{(v)}}{\partial \bar{x}} + \frac{\partial \bar{v}^{(v)}}{\partial \bar{y}} \right) = 0,$$

or, since this equation must hold for all orders of  $\varepsilon$

$$\frac{\partial \bar{u}^{(0)}}{\partial \bar{x}} = 0, \quad \frac{\partial \bar{u}^{(1)}}{\partial \bar{x}} + \frac{\partial \bar{v}^{(1)}}{\partial \bar{y}} = 0, \text{ etc.} \quad (4.9)$$

Similarly, all other field equations and boundary conditions are handled, if necessary by expanding the functions of  $\varepsilon$  in a power series of it. What results is a hierarchy of boundary-value problems for the  $v$ th-order field variables which can be solved successively, starting with the zeroth-order equations. For temperate glaciers in which the energy equation (4.1)<sub>6</sub> is replaced by an equation for the moisture content, and to first order the Arrhenius factor may be set equal to unity, the equations for the velocity field separate formally from that for the moisture content. For cold glaciers, the  $v$ th-order velocity and temperature fields are coupled, making an exact solution of the first-order equations very cumbersome. A different solution technique is therefore suggested. The procedure is to expand all variables, except the temperature  $\vartheta$ , in a power series of  $\varepsilon$  and in a first iteration to assume  $\vartheta$  to be determined by the temperature distribution of the strictly parallel-sided slab or known from field measurements or estimates. The perturbation scheme may then be used in the velocity boundary-value problem using this lowest-order temperature distribution as a given function to determine the Arrhenius factor. Once the solution to the stress and velocity boundary-value problem is determined to a certain order of  $\varepsilon$  (in practice, linear terms are sufficient), these velocity and stress fields may be used in the energy equation to determine an improved estimate of the temperature distribution

which, in turn, can be used in the velocity boundary-value problem to obtain an improved velocity and stress field. Often this last step need not be performed.

Replacing (4.8) by

$$\begin{aligned} (\sigma_x, \sigma_y, \tau, \bar{u}, \bar{y}_S) &= \sum_{v=0}^{\infty} \varepsilon^v (\sigma_x^{(v)}, \sigma_y^{(v)}, \tau^{(v)}, \bar{u}^{(v)}, \bar{y}_S^{(v)}), \\ \bar{v} &= \sum_{v=1}^{\infty} \varepsilon^v \bar{v}^{(v)}, \quad \theta = \hat{\theta} \quad (\text{hat for iteration}), \end{aligned} \quad (4.10)$$

substituting these representations into Equations (4.1), expanding all the terms in powers of  $\varepsilon$  and collecting the terms of equal powers in  $\varepsilon$ , the following field equations are obtained:

to zeroth order

$$\begin{aligned} \frac{\partial \sigma_x^{(0)}}{\partial \bar{x}} + \frac{\partial \tau^{(0)}}{\partial \bar{y}} + \sin \gamma &= 0, & \frac{\partial \tau^{(0)}}{\partial \bar{x}} + \frac{\partial \sigma_y^{(0)}}{\partial \bar{y}} - \cos \gamma &= 0, \\ \frac{\partial \bar{u}^{(0)}}{\partial \bar{x}} &= 0, & \sigma_x^{(0)} &= \sigma_y^{(0)}, & \frac{\partial \bar{u}^{(0)}}{\partial \bar{y}} &= 2 \exp(\mathbb{A}\hat{\theta}) \mathfrak{F}(\tau_{II}^{(0)2}) \tau^{(0)}, \\ \frac{\partial \hat{\theta}}{\partial \bar{x}} \bar{u}^{(0)} &= \mathbb{D} \left( \frac{\partial^2 \hat{\theta}}{\partial \bar{x}^2} + \frac{\partial^2 \hat{\theta}}{\partial \bar{y}^2} \right) + 2 \mathbb{E} \mathfrak{F}(\tau^{(0)2}) \tau^{(0)}. \end{aligned} \quad (4.11)$$

to first order

$$\begin{aligned} \frac{\partial \sigma_x^{(1)}}{\partial \bar{x}} + \frac{\partial \tau^{(1)}}{\partial \bar{y}} &= 0, & \frac{\partial \tau^{(1)}}{\partial \bar{x}} + \frac{\partial \sigma_y^{(1)}}{\partial \bar{y}} &= 0, \\ \frac{\partial \bar{u}^{(1)}}{\partial \bar{x}} + \frac{\partial \bar{v}^{(1)}}{\partial \bar{y}} &= 0, \\ \frac{\partial \bar{u}^{(1)}}{\partial \bar{x}} &= \frac{1}{2} [\mathfrak{F}(\tau_{II}^{(0)}) (\sigma_x^{(1)} - \sigma_y^{(1)})] \exp(\mathbb{A}\hat{\theta}), \\ \frac{\partial \bar{u}^{(1)}}{\partial \bar{y}} + \frac{\partial \bar{v}^{(1)}}{\partial \bar{x}} &= 2 [\mathfrak{F}(\tau_{II}^{(0)}) \tau^{(1)} + \mathfrak{F}'(\tau_{II}^{(0)}) \tau^{(0)} \tau_{II}^{(1)}] \exp(\mathbb{A}\hat{\theta}), \end{aligned} \quad (4.12)$$

where

$$\mathfrak{F}'(x) = \frac{d\mathfrak{F}(x)}{dx}, \quad \tau_{II}^{(1)} = 2\tau^{(0)}\tau^{(1)}. \quad (4.13)$$

Notice that there is no first-order temperature equation, this is owing to our proposed solution procedure. On the other hand, higher-order equations could also be deduced. They are of little interest, however.

Once the velocity, stress, and temperature fields to the above problem are determined, an improved temperature distribution is obtained from the equation

$$\frac{\partial \hat{g}}{\partial \bar{x}} \bar{u} + \frac{\partial \hat{g}}{\partial \bar{y}} \bar{v} = \mathbb{D} \left( \frac{\partial^2 \hat{g}}{\partial \bar{x}^2} + \frac{\partial^2 \hat{g}}{\partial \bar{y}^2} \right) + 2\mathbb{E} \exp(\mathbb{A} \hat{g}) \mathfrak{F}(\tau_{II}') \tau_{II}'. \quad (4.14)$$

Notice also that in the boundary value problem for the lowest-order fields, the velocities and stresses are coupled with the temperature field, whereas this is not the case for the first-order problem (4.12). Furthermore, the zeroth-order equations are *non-linear*, whereas the first-order problem is *linear*.

Before presenting the derivation of the boundary conditions, it should be realized that in most practical situations it is advantageous to guess the temperature distribution  $\hat{g}$  rather than to determine it from Equations (4.11) and associated boundary conditions. The reason is that the lowest-order problem will be that of the strictly parallel-sided ice slab with no longitudinal dependencies of the velocities. According to the results of Chapter 3, this problem requires a vanishing accumulation rate and, consequently, cannot account for transverse advection, a term that is crucial for the determination of the transverse temperature distribution; indeed, Equation (4.11)<sub>6</sub> does not contain a transverse advective term.

The derivation of approximate representations of the boundary conditions is based on the idea that the condition valid on the boundary surface is replaced by an appropriate condition on the mean bed and mean surface, respectively. To explain the procedure, consider Equation (4.3)<sub>2</sub>. The velocity components in this equation are those on the surface  $\bar{y} = \bar{y}_S$ , so that

$$\begin{aligned} \bar{u} &= \bar{u}(\bar{x}, \bar{y}_S) = \bar{u}\left(\bar{x}, 1 + \sum_{v=1}^{\infty} \varepsilon^v \bar{y}_S^{(v)}\right) \\ &= \bar{u}(\bar{x}, 1) + \varepsilon \frac{\partial \bar{u}}{\partial \bar{y}} \Big|_{\bar{y}=1} \bar{y}_S^{(1)} + \mathcal{O}(\varepsilon^2) \\ &= \bar{u}^{(0)}(\bar{x}, 1) + \varepsilon \left\{ \bar{u}^{(1)}(\bar{x}, 1) + \frac{\partial \bar{u}^{(0)}}{\partial \bar{y}} \Big|_{\bar{y}=1} \bar{y}_S^{(1)} \right\} + \mathcal{O}(\varepsilon^2). \end{aligned} \quad (4.15)$$

A similar equation must also hold for  $\bar{v}$ . The second line in (4.15) follows by a Taylor series expansion of the function  $\bar{u}$  in the second variable and the last line by substituting the perturbation expansion for  $\bar{u}$ . Substituting expression (4.15) for  $\bar{u}$ , and a similar one for  $\bar{v}$ , into the first of (4.3) and writing  $\bar{y}'_S = \sum_{v=1}^{\infty} \varepsilon^v \bar{y}_S^{(v)}$  yields

$$\begin{aligned} &\varepsilon \{ \bar{u}^{(0)}(\bar{x}, 1) \bar{y}'_S^{(1)} - \bar{v}^{(1)}(\bar{x}, 1) \} + \\ &+ \varepsilon^2 \{ \bar{u}^{(1)}(\bar{x}, 1) \bar{y}'_S^{(1)} + \bar{u}^{(0)}(\bar{x}, 1) \bar{y}'_S^{(2)} - \bar{v}^{(2)}(\bar{x}, 1) \} + \mathcal{O}(\varepsilon^3) = \bar{a}(\bar{x}). \end{aligned} \quad (4.16)$$

All functions in this expression are evaluated *at the mean free surface* and not on the true surface as was originally the case. In other words, the simple relation (4.3)<sub>1</sub>, valid on the complex and unknown geometry, has been replaced by a formally more complex equation on a much simpler geometry, namely  $\bar{y} = 1$ . Equation (4.16), however, is not more complicated than the original one it evolved from, because the left-hand side is a power series in  $\varepsilon$  which must match the term on the right-hand side. Because in our scaling ( $\mathbb{G} = 1$ , see Chapter 3, Section 2),  $\bar{a} = (10^{-2})$ , or smaller, we write

$$\bar{a} = \varepsilon \mathfrak{A}, \quad \mathfrak{A} \leq \mathcal{O}(1). \quad (4.17)$$

Using this ordering in (4.16) and collecting terms of equal powers in  $\varepsilon$ , yields the sequence of boundary conditions

$$\begin{aligned} \bar{u}^{(1)}(\bar{x}, 1)\bar{y}_S^{(0)} - \bar{v}^{(1)}(\bar{x}, 1) &= \mathfrak{A}(\bar{x}), \\ \bar{u}^{(0)}(\bar{x}, 1)\bar{y}_S^{(2)} + \bar{u}^{(1)}(\bar{x}, 1)\bar{y}_S^{(1)} - \bar{v}^{(2)}(\bar{x}, 1) &= 0. \end{aligned} \quad (4.18)$$

Proceeding in this fashion with all the boundary equations stated in Equations (4.3) and (4.4), the following statements are obtained:

*At the upper surface  $\bar{y} = 1$ :*

To zeroth order (taking  $\varepsilon^0$  terms)

$$\left. \begin{aligned} \sigma^{(0)} &= -\bar{p}^{\text{atm}}, & \tau^{(0)} &= 0, \\ \hat{\vartheta} &= \vartheta_S \quad \text{for cold ice.} \end{aligned} \right\} \quad \bar{y} = 1, \quad (4.19)$$

and to first order (taking  $\varepsilon^1$ -terms)

$$\left. \begin{aligned} \frac{d\bar{y}_S^{(1)}}{d\bar{x}} \bar{u}^{(0)} - \bar{v}^{(1)} &= \mathfrak{A}, \\ \sigma_x^{(1)} + \frac{d\sigma_y^{(0)}}{d\bar{y}} \bar{y}_S^{(1)} - 2\tau^{(0)} \frac{d\bar{y}_S^{(1)}}{d\bar{x}} &= 0, \\ \tau^{(1)} + \frac{d\tau^{(0)}}{d\bar{y}} \bar{y}_S^{(1)} &= 0, \end{aligned} \right\} \quad \bar{y} = 1, \quad (4.20)$$

where, in line with our approximation scheme, the thermal boundary condition has been written down for the lowest-order equations only. Higher-order boundary conditions could straightforwardly be derived; they will not be needed below and are deleted for this reason.

*At the lower surface  $\bar{y} = 0$ :*

To zeroth order

$$\bar{u}^{(0)} = \mathbb{C}[\tau^{(0)}]^m, \quad \frac{d\hat{\vartheta}}{d\bar{y}} = -\mathbb{Q}^{\text{geoth}}, \quad \bar{y} = 0, \quad (4.21)$$

and to first order

$$\bar{u}^{(1)} + \frac{d\bar{u}^{(0)}}{d\bar{y}} \Lambda = \mathbb{C}m[\tau^{(0)}]^{m-1} \left( \tau^{(1)} + \frac{d\tau^{(0)}}{d\bar{y}} \Lambda \right), \quad \bar{v}^{(1)} = \bar{u}^{(0)} \Lambda', \quad \bar{y} = 0. \quad (4.22)$$

Here again the thermal-boundary condition has been formulated only for the lowest-order problem. If solutions to the boundary-value problems expressed by Equations (4.11), (4.12), and (4.19)–(4.22) are constructed, an improved estimate of the temperature distribution can be obtained with the aid of Equation (4.14). The corresponding boundary conditions that must fall on  $\bar{\vartheta}$  now follow from relations (4.3)<sub>4</sub> and (4.4)<sub>3</sub> by performing the indicated perturbation expansions up to terms linear in  $\varepsilon$ : This gives

$$\begin{aligned} \hat{\vartheta} + \varepsilon \frac{\partial \hat{\vartheta}}{\partial \bar{y}} \bar{y}_S^{(1)} &= \vartheta_S, \quad \bar{y} = 1, \\ \frac{\partial \hat{\vartheta}}{\partial \bar{y}} - \varepsilon \left\{ \frac{\partial \hat{\vartheta}}{\partial \bar{x}} - \frac{\partial^2 \hat{\vartheta}}{\partial \bar{y}^2} \right\} \Lambda &= -\mathbb{Q}^{\text{geoth}}, \quad \bar{y} = 0. \end{aligned} \quad (4.23)$$

In summary, we thus have to solve the following boundary value problems: to lowest order, Equations (4.11) have to be integrated subject to the boundary conditions (4.19) and (4.21). This boundary value problem is the same as that constructed in Section 3b( $\alpha$ ) of Chapter 3, provided it is assumed that the stress, velocity, and temperature fields in a strictly parallel-sided slab have no  $\bar{x}$ -dependency. We refrain from re-deriving this solution, but will write down the necessary results needed for the construction of the solutions to the higher-order equations. The first-order system of equations is the system (4.12), (4.13) subject to the boundary conditions (4.20) and (4.22). The construction of its solution will concern us in most parts of the remainder of this chapter. This boundary-value problem is a *linear* one, even though the material response is non-linear. This formal linearization is of great advantage and is indeed the beauty of the formal perturbation procedure. Finally, an improved temperature field can be found by solving Equation (4.14) subject to the boundary conditions (4.23).

Before embarking on the solution procedures for these equations it is noteworthy to point out that *the solution of the stress-velocity boundary-value problem depends on the form of the sliding law only at the first order and at higher order levels*. To see this, assume that instead of Equation (4.5) we were to prescribe the  $\bar{x}$ -component of the sliding velocity; the sliding condition at the rockbed would then read

$$\bar{u} = \bar{u}^{\text{given}}(\bar{x}), \quad \bar{v} = \varepsilon \Lambda' \bar{u}^{\text{given}}(\bar{x}), \quad \text{at } \bar{y} = \bar{y}_B(\bar{x}), \quad (4.24)$$

where use has been made of relation (4.7). With the aid of the same pertur-

bation approach as above, the relations (4.24) yield the following hierarchy of sliding conditions for the zeroth-order and first-order velocity problem:

$$\left. \begin{aligned} \bar{u}^{(0)} &= \bar{u}^{\text{given}}, \\ \bar{u}^{(1)} + \frac{d\bar{u}^{(0)}}{d\bar{y}} \Lambda &= 0, \quad \bar{v}^{(1)} = \Lambda' \bar{u}^{\text{given}}, \end{aligned} \right\} \quad \text{at } \bar{y} = 0. \quad (4.25)$$

If these relations are compared with the corresponding sliding conditions (4.21)<sub>1</sub>, and (4.22)<sub>1</sub>, it is seen that the zeroth-order sliding velocities match, if at  $\bar{y} = 0$   $\bar{u}^{\text{given}} = \mathbb{C}(\tau^{(0)})^m$ . In other words, to zeroth order the sliding laws (4.5) and (4.24) are the same. However, when first-order equations are compared, it is no longer possible to bring the equations in coincidence. It follows that differences in the sliding laws will manifest themselves in the stress and velocity distribution of the first-order problem. In view of the fact that applied glaciologists frequently prescribe sliding velocities but do not use a viscous sliding law, a comparison of solutions is illuminating when based on the boundary conditions (4.25) rather than on (4.22).

### 3. The Solution of the Boundary-value Problems

#### (a) Zeroth-order problem

The zeroth-order boundary-value problem as given by the differential equations (4.11) and the boundary conditions (4.19) and (4.21), is that of the strictly parallel-sided slab with zero accumulation. A solution that is consistent with a stress-dependent sliding law is necessarily  $\bar{x}$ -independent. The  $\bar{x}$ -independent stress, velocity, and temperature fields were for such conditions determined in Section 3b(α) of Chapter 3 and stresses and velocities are given by

$$\begin{aligned} \sigma_x^{(0)} &= \sigma_y^{(0)} = -\cos \gamma(1 - \bar{y}) - \bar{p}^{\text{atm}}, \\ \tau^{(0)} &= \sin \gamma(1 - \bar{y}), \\ \bar{u}^{(0)} &= \mathbb{C} \sin^m \gamma + 2 \sin \gamma \int_0^{\bar{y}} \exp(\mathbb{A}\hat{\theta}(\xi)) \mathfrak{F}(\sin^2 \gamma(1 - \xi)^2)(1 - \xi) d\xi, \\ \bar{v}^{(0)} &= 0, \end{aligned} \quad (4.26)$$

where  $\hat{\theta}$  is defined in terms of the temperature  $\hat{\vartheta}$  in Equation (4.2). These variables are assumed to be known, either from field measurements or from an approximate solution of the energy equation. We do not, however, recommend to use for  $\hat{\vartheta}$  the temperature distribution, as it is obtained from an exact solution of the velocity-temperature boundary-value problem of the strictly parallel-sided slab. As illustrated in Chapter 3, the transverse temperature distribution is almost always nearly linear. A more realistic temperature distribution is rather as shown in Figure 3.18 of Chapter 3. An approximate formula for steady-state accumulation is due to Robin [41] and

reads

$$\hat{g}(\bar{y}) = Q^{\text{geoth}} \int_{\bar{y}}^1 \exp\left(-\frac{\bar{a}}{D} \frac{\xi^2}{2}\right) d\xi + \hat{g}_s. \quad (4.27)$$

This formula is useful for a positive and a negative  $\bar{x}$ -independent accumulation rate function  $\bar{a}$ . It should also be noticed that the above temperature distribution is formed with  $\bar{a}$ , a quantity that has entered the perturbation scheme at the higher-order level only. By using the above formula or other formulas involving the accumulation rate function, more accurate low-order solutions can often be obtained than would be possible otherwise. This guarantees a faster convergence of the perturbation procedure.

The solution (4.26) is valid for cold ( $A \neq 0$ ) and temperate ( $A = 0$ ) ice. In ensuing calculation, considerations will mostly be restricted to the latter when

$$\mathfrak{F}(x) = (x^{(n-1)/2} + \mathbb{E})/(1 + \mathbb{E}) \quad (4.28)$$

for which

$$u^{(0)}(y) = C \sin^m \gamma + \frac{1}{1 + \mathbb{E}} \left\{ \frac{2 \sin^n \gamma}{n+1} (1 - (1 - \bar{y})^{n+1}) + \mathbb{E} \sin \gamma (1 - (1 - \bar{y})^2) \right\}, \quad (4.29)$$

with a value of  $\mathbb{E}$  in the order of  $10^{-n}$ ;  $\mathbb{E} = 0$  corresponds to a solution when using Glen's flow law. The contribution of the longitudinal zeroth-order velocity due to gliding has been plotted in Chapter 3 (Figures 3.12 and 3.14) against depth. That analysis has shown that  $\bar{u}^{(0)}$  depends critically on the temperature distribution, but does only depend marginally on the constant  $\mathbb{E}$ , if  $\mathbb{E}$  is sufficiently small, ( $\mathbb{E} < 10^{-n}$ ).

### (b) First-order problem

The first-order boundary-value problem is defined by Equations (4.12), (4.13), (4.20) and (4.22). The construction of its solution is very much simplified by introducing stress and stream functions according to

$$\begin{aligned} \sigma_x^{(1)} &= \frac{\partial^2 \Phi}{\partial \bar{y}^2}, & \sigma_y^{(1)} &= \frac{\partial^2 \Phi}{\partial \bar{x}^2}, & \tau^{(1)} &= -\frac{\partial^2 \Phi}{\partial \bar{x} \partial \bar{y}}, \\ \bar{u}^{(1)} &= \frac{\partial \Psi}{\partial \bar{y}}, & \bar{v}^{(1)} &= -\frac{\partial \Psi}{\partial \bar{x}}. \end{aligned} \quad (4.30)$$

$\Phi$  is called *stress function* and  $\Psi$  *stream function*. With their introduction, the first-order momentum equations (4.12)<sub>1,2</sub> and the continuity equation (4.12)<sub>3</sub> are identically satisfied; the remaining field equations, on the other hand, transform into the system

$$\frac{\partial^2 \Psi}{\partial \bar{x} \partial \bar{y}} = -f(\bar{y}) \left[ \frac{\partial^2 \Phi}{\partial \bar{x}^2} - \frac{\partial^2 \Phi}{\partial \bar{y}^2} \right], \quad \left[ \frac{\partial^2 \Phi}{\partial \bar{x}^2} - \frac{\partial^2 \Psi}{\partial \bar{y}^2} \right] = g(\bar{y}) \frac{\partial^2 \Phi}{\partial \bar{x} \partial \bar{y}}, \quad (4.31)$$

where

$$\begin{aligned} f(\bar{y}) &= \frac{1}{2} \exp(\mathbb{A}\hat{\theta}) \mathfrak{F}(\sin^2 \gamma(1 - \bar{y})^2), \\ g(\bar{y}) &= 2 \exp(\mathbb{A}\hat{\theta}) [\mathfrak{F}(\sin^2 \gamma(1 - \bar{y})^2) + \mathfrak{F}'(\sin^2 \gamma(1 - \bar{y})^2) \sin^2 \gamma(1 - \bar{y})^2]. \end{aligned} \quad (4.32)$$

Equations (4.31) are a second-order system of linear partial differential equations for  $\Phi$  and  $\Psi$  with  $\bar{y}$ -dependent coefficients  $f(\bar{y})$  and  $g(\bar{y})$  (recall that  $\mathfrak{F}$  is treated as a known function of  $\bar{y}$ ). Except for the occurrence of the functions  $f$  and  $g$ , the system shows a nice symmetry in the coupling of the stress and stream functions. It is also interesting to see what form Equations (4.31) reduce to for a *Newtonian* fluid. Such a fluid is temperature insensitive,  $\mathbb{A} = 0$ , with  $\mathfrak{F} = 1$ ,  $f(\bar{y}) = \frac{1}{2}$ ,  $g(\bar{y}) = 2$ . By eliminating either  $\Phi$  or  $\Psi$  in the differential equations (4.31) we then obtain  $\nabla^4 \Phi = 0$ , or  $\nabla^4 \Psi = 0$ . For a Newtonian fluid the stress and stream functions must therefore be *biharmonic*. This is a well known result of slow viscous fluid dynamics, see Batchelor [1], Schlichting [48]. Equations (4.31) and (4.32) are therefore natural generalizations of a slow viscous flow to non-Newtonian behavior (of the restricted class considered here).

The differential equation (4.31) must be complemented by the boundary conditions, Equations (4.20) and (4.22). When expressed in terms of the stress and stream functions they read:

*At the upper surface*  $\bar{y} = 1$ :

$$\left. \begin{array}{l} \frac{\partial \Psi}{\partial \bar{x}} + \bar{u}_s^{(0)} \frac{dy_s^{(1)}}{d\bar{x}} = \mathfrak{U} \\ \frac{\partial^2 \Phi}{\partial \bar{x}^2} + \cos \gamma \bar{y}_s^{(1)} = 0 \\ \frac{\partial^2 \Phi}{\partial \bar{x} \partial \bar{y}} + \sin \gamma \bar{y}_s^{(1)} = 0 \end{array} \right\} \bar{y} = 1, \quad (4.33)$$

where  $\bar{u}_s^{(0)}$  is the zeroth order *surface velocity* which can be evaluated by setting  $\bar{y} = 1$  in (4.26), or, for temperate ice, in (4.29). Both formulas consist of a sliding and a gliding term.

*At the base*  $\bar{y} = 0$ : If (4.22) is used

$$\begin{aligned} \frac{\partial \Psi}{\partial \bar{y}} + \mathbb{C} m \sin^{m-1} \gamma \frac{\partial^2 \Phi}{\partial \bar{x} \partial \bar{y}} &= -\{\Lambda [\mathbb{C} m \sin^m \gamma + 2 \exp(\mathbb{A}\hat{\theta}) \mathfrak{F}(\sin^2 \gamma) \sin \gamma]\}, \\ \frac{\partial \Psi}{\partial \bar{x}} &= -\mathbb{C} \sin^m \gamma \Lambda', \end{aligned} \quad (4.34)$$

but

$$\frac{\partial \Psi}{\partial \bar{y}} = -2 \sin \gamma \mathfrak{F}(\sin^2 \gamma) \Lambda, \quad \frac{\partial \Psi}{\partial \bar{x}} = -\mathbb{C} \sin^m \gamma \Lambda', \quad (4.35)$$

if the relations (4.24) are used. Notice also that the surface topography must be determined along with the stress and velocity fields. This complicates calculations, but it turns out that construction of solutions to the first-order boundary-value problem is simplified if, instead for the function  $\bar{y}_S^{(1)}$ , one searches for

$$\eta_S = \bar{y}_S^{(1)} - \bar{y}_S^a, \quad \text{where } \bar{y}_S^a = \frac{1}{\bar{u}_S^{(0)}} \int_0^{\bar{x}} \mathfrak{A}(\xi) d\xi. \quad (4.36)$$

With the new variable  $\eta_S$  and the known function  $\bar{y}_S^a$ , which may be called the *accumulation-flux function*, the boundary conditions (4.33) read

$$\left. \begin{array}{l} \frac{\partial \Psi}{\partial \bar{x}} + \bar{u}_S^{(0)} \frac{\partial \eta_S}{\partial \bar{x}} = 0, \\ \frac{\partial^2 \Phi}{\partial \bar{x}^2} + \cos \gamma \eta_S = -\cos \gamma \bar{y}_S^a, \\ \frac{\partial^2 \Phi}{\partial \bar{x} \partial \bar{y}} + \sin \gamma \eta_S = -\sin \gamma \bar{y}_S^a. \end{array} \right\} \bar{y} = 1. \quad (4.37)$$

In view of the linearity of the boundary-value problem for  $\Phi$  and  $\Psi$ , it follows that the effects due to steady-state accumulation and due to bedrock undulations can be separated. Indeed, let

$$\Phi = \Phi_{\mathfrak{A}} + \Phi_{\Lambda}, \quad \Psi = \Psi_{\mathfrak{A}} + \Psi_{\Lambda}, \quad \eta_S = \eta_S^{\mathfrak{A}} + \eta^{\Lambda}, \quad (4.38)$$

where the functions carrying the indices  $\Lambda$  and  $\mathfrak{A}$  are, respectively, solutions of the boundary value problem when either accumulation rate is set to zero, or else bottom undulations vanish. The respective terms only enter the boundary conditions, making these homogeneous when the corresponding terms vanish. The sum of solutions with the indices  $\mathfrak{A}$  and  $\Lambda$ , respectively, therefore forms another solution in which now both, accumulation and bedrock undulations, are present. *We may therefore investigate the effect of the accumulation rate and bedrock protuberances independently.*

(a) *Harmonic perturbation from uniform flow for zero accumulation rate.* Let us proceed and construct solutions to the above formulated boundary-value problem for the special case that  $\mathfrak{A} = 0$ . As regards the form of the bed, this is generally known from seismic investigations. If records are sufficiently extended over the range of interest, these bedrock topographies can be periodically extended and subsequently subjected to a harmonic analysis. Fast Fourier transforms with appropriately applied filtering are the vehicle to analyse these bedrock topographies. In the subsequent analysis, therefore, it may be assumed that the rockbed is given by a Fourier series; it even suffices

to consider only one single Fourier component of unit amplitude,

$$\Lambda(\bar{x}) = \cos \omega \bar{x} = \cos\left(\frac{2\pi \bar{x}}{\lambda}\right) \quad (4.39)$$

because, owing to linearity, the solution will be superimposable, and for each Fourier component proportional to the bedrock amplitude. The dimensionless *frequency*  $\omega$  and the dimensionless *wavelength*  $\lambda$  are assumed known from the harmonic analysis of the rockbed.

The bottom topography being prescribed by a trigonometric function, it is only natural to assume that the general solution for the stress and stream functions and for the surface elevation can also be expressed by trigonometric functions, but *shifted* with respect to (4.39), so that

$$\begin{aligned} \Phi &= \Phi_1 \cos \omega \bar{x} + \Phi_2 \sin \omega \bar{x}, \\ \Psi &= \Psi_1 \cos \omega \bar{x} + \Psi_2 \sin \omega \bar{x}, \\ \eta_S &= h_1 \cos \omega \bar{x} + h_2 \sin \omega \bar{x}. \end{aligned} \quad (4.40)$$

The functions

$$\mathcal{F}(\omega) = [h_1^2(\omega) + h_2^2(\omega)]^{1/2}, \quad \varphi(\omega) = \tan^{-1} \frac{h_2(\omega)}{h_1(\omega)} \quad (4.41)$$

will henceforth be called the *transfer* or *filter function* and the *phase shift function*, respectively. The former determines that fraction of the protuberance amplitude that is, at a certain frequency, carried over to the surface. It could also be interpreted as the ratio of the surface to the basal amplitude of the *inclination*.  $\varphi$ , on the other hand, describes the circular angle by which the troughs of the surface undulations lag behind those of the base. Indeed, relation (4.40)<sub>3</sub> may also be written as  $\eta_S = \mathcal{F} \cos(\omega \bar{x} - \varphi)$ . For positive  $\varphi$  the wave troughs of surface undulations are ahead of those of the base, for negative  $\varphi$  they lag behind. It will be shown that  $\varphi < 0$ .

Substituting expressions (4.26) into the differential equations (4.31) will result in a system of *ordinary* differential equations for the unknown functions  $\Phi_1$ ,  $\Phi_2$ ,  $\Psi_1$ , and  $\Psi_2$ . This system is obtained by recognizing that by substitution of (4.40) into (4.31) these equations will transform into statements which are expressible as linear combinations of sine- and cosine-terms which must vanish. Consequently, the coefficients of each of these terms must vanish. This argument leads to the *field equations*

$$\begin{aligned} \frac{d^2\Phi_1}{d\bar{y}^2} &= \frac{\omega}{f(\bar{y})} \frac{d\Psi_2}{d\bar{y}} - \omega^2 \Phi_1, & \frac{d^2\Phi_2}{d\bar{y}^2} &= -\frac{\omega}{f(\bar{y})} \frac{d\Psi_1}{d\bar{y}} - \omega^2 \Phi_2, \\ \frac{d^2\Psi_1}{d\bar{y}^2} &= -\omega g(\bar{y}) \frac{d\Phi_2}{d\bar{y}} - \omega^2 \Psi_1, & \frac{d^2\Psi_2}{d\bar{y}^2} &= \omega g(\bar{y}) \frac{d\Phi_1}{d\bar{y}} - \omega^2 \Psi_2. \end{aligned} \quad (4.42)$$

The boundary conditions, on the other hand, yield the expressions

*At the base  $\bar{y} = 0$ :* When the stress dependent viscous sliding law (4.34) is used,

$$\begin{aligned}\frac{d\Psi_1}{d\bar{y}} + \omega \mathbb{C}m \sin^{m-1} \gamma \frac{d\Phi_2}{d\bar{y}} &= -\{\mathbb{C}m \sin^m \gamma + 2 \exp(\mathbb{A}\hat{\theta})\mathfrak{F}(\sin^2 \gamma) \sin \gamma\} \\ \frac{d\Psi_2}{d\bar{y}} - \omega \mathbb{C}m \sin^{m-1} \gamma \frac{d\Phi_1}{d\bar{y}} &= 0, \\ \Psi_1 &= -\mathbb{C} \sin^m \gamma, \quad \Psi_2 = 0.\end{aligned}\tag{4.43}$$

On the other hand, when (4.35) is used

$$\left. \begin{aligned}\frac{d\Psi_1}{d\bar{y}} &= -2 \sin \gamma \mathfrak{F}(\sin^2 \gamma) \exp(\mathbb{A}\hat{\theta}), & \frac{d\Psi_2}{d\bar{y}} &= 0, \\ \Psi_1 &= -\bar{u}_b^{(0)} = (-\mathbb{C} \sin^m \gamma), & \Psi_2 &= 0.\end{aligned}\right\}\tag{4.44}$$

*At the mean upper surface  $\bar{y} = 1$ :* Here Equations (4.33) yield:

$$\left. \begin{aligned}\omega^2 \Phi_1 - \cos \gamma h_1 &= \omega^2 \Phi_1 + \frac{\cos \gamma}{\bar{u}_S^{(0)}} \Psi_1 = 0, \\ \omega^2 \Phi_2 - \cos \gamma h_2 &= \omega^2 \Phi_2 + \frac{\cos \gamma}{\bar{u}_S^{(0)}} \Psi_2 = 0, \\ \omega \frac{d\Phi_1}{d\bar{y}} - \sin \gamma h_2 &= \omega \frac{d\Phi_1}{d\bar{y}} + \frac{\sin \gamma}{\bar{u}_S^{(0)}} \Psi_2 = 0, \\ \omega \frac{d\Phi_2}{d\bar{y}} + \sin \gamma h_1 &= \omega \frac{d\Phi_2}{d\bar{y}} - \frac{\sin \gamma}{\bar{u}_S^{(0)}} \Psi_1 = 0, \\ h_1 &= -\frac{\Psi_1}{\bar{u}_S^{(0)}}, \quad h_2 = -\frac{\Psi_2}{\bar{u}_S^{(0)}},\end{aligned}\right\}\tag{4.45}$$

where the expressions on the far right of (4.45)<sub>1-4</sub> are obtained by replacing  $h_1$  and  $h_2$  with the aid of (4.45)<sub>5,6</sub>. For a non-Newtonian fluid there is little hope that the above system of ordinary differential equations can be solved analytically. Resort must therefore be made to numerical procedures. Before we embark on these, it is worthwhile to obtain a qualitative understanding of the behavior of the solution of the above boundary-value problem. Such an understanding can be obtained by integrating the system of equations for a linear Newtonian liquid. In this case, an analytical solution can be found with reasonable effort. The solution of this Newtonian flow problem may then be contrasted with earlier treatments of the same problem by Budd [11] and may further be used to check the numerical procedure used for the non-Newtonian fluid.

(β) *Analytic solution for a Newtonian fluid.* It has already been indicated before that for a Newtonian fluid  $f(\bar{y}) = \frac{1}{2}$  and  $g(\bar{y}) = 2$ . Substituting these

representations into the differential equations (4.42), it is not hard to see that the emerging equations must admit solutions of the form  $\exp(s\bar{y})$ ,  $\Psi_i = \alpha_i \exp(s\bar{y})$ ,  $\Psi_i = \beta_i \exp(s\bar{y})$ , ( $i = 1, 2$ ) where  $\alpha_i$  and  $\beta_i$  are constants. When substituting these trial solutions into (4.45), a linear homogeneous system of equations for the coefficients  $\alpha_i$  and  $\beta_i$  ( $i = 1, 2$ ) is obtained. Its characteristic equation can be shown to have the form  $(s^2 - \omega^2)^4 = 0$  with the four-fold roots  $s = \pm\omega$ . Consequently,

$$\begin{aligned} \exp(\omega\bar{y}), & \quad \bar{y} \exp(\omega\bar{y}), & \quad \bar{y}^2 \exp(\omega\bar{y}), & \quad \bar{y}^3 \exp(\omega\bar{y}), \\ \exp(-\omega\bar{y}), & \quad \bar{y} \exp(-\omega\bar{y}), & \quad \bar{y}^2 \exp(-\omega\bar{y}), & \quad \bar{y}^3 \exp(-\omega\bar{y}) \end{aligned} \quad (4.46)$$

are the fundamental solutions of (4.42) but only four of these are independent. To see this, notice that in view of the special form of (4.42) solutions having the factor  $\bar{y}^2$  and  $\bar{y}^3$  cannot arise so that the most general solution has the form

$$\begin{aligned} \Psi_1 &= (a_0 + a_1\bar{y}) \exp(\omega\bar{y}) + (\bar{a}_0 + \bar{a}_1\bar{y}) \exp(-\omega\bar{y}), \\ \Psi_2 &= (b_0 + b_1\bar{y}) \exp(\omega\bar{y}) + (\bar{b}_0 + \bar{b}_1\bar{y}) \exp(-\omega\bar{y}), \\ \Phi_1 &= (b_0 + b_1\bar{y}) \exp(\omega\bar{y}) - (\bar{b}_0 + \bar{b}_1\bar{y}) \exp(-\omega\bar{y}), \\ \Phi_2 &= -(a_0 + a_1\bar{y}) \exp(\omega\bar{y}) + (\bar{a}_0 + \bar{a}_1\bar{y}) \exp(-\omega\bar{y}), \end{aligned} \quad (4.47)$$

When the representations (4.47) are substituted into the boundary conditions (4.43) and (4.45)<sub>1-4</sub> a system of linear equations for the eight unknowns  $a_0, \bar{a}_0, \dots, b_1, \bar{b}_1$  in terms of  $h_1$  and  $h_2$  is obtained. Lengthy, but elementary operations allow the solving of  $a_0, \bar{a}_0, \dots, b_1, \bar{b}_1$  in terms of  $h_1, h_2$  and the basal sliding velocity  $\bar{u} = C \sin \gamma (m = 1)$ . This solution reads:

$$\begin{aligned} a_0 &= -h_1\Omega_1 \sin \gamma - h_2\Omega_2 \cos \gamma - B\Omega_3 \sin \gamma - \frac{1}{2}B\bar{u}(\Omega_4 + 1), \\ \bar{a}_0 &= h_1\Omega_1 \sin \gamma + h_2\Omega_2 \cos \gamma + B\Omega_3 \sin \gamma + \frac{1}{2}B\bar{u}(\Omega_4 - 1), \\ a_1 &= h_1\Omega_5^- \sin \gamma + h_2\Omega_6^- \cos \gamma + 2B\Omega_7^- \sin \gamma + B\bar{u}\omega\Omega_8^-, \\ \bar{a}_1 &= -h_1\Omega_6^+ \sin \gamma + h_2\Omega_5^+ \cos \gamma - 2B \sin \gamma \Omega_8^+ + B\bar{u}\omega\Omega_7^+, \end{aligned} \quad (4.48)$$

and

$$\begin{aligned} \bar{b}_0 &= -b_0 = -h_1\Omega_2 \cos \gamma + h_2\Omega_1 \sin \gamma, \\ b_1 &= -h_1\Omega_6^- \cos \gamma + h_2\Omega_5^- \sin \gamma, \\ \bar{b}_1 &= -h_1\Omega_5^+ \cos \gamma - h_2\Omega_6^+ \sin \gamma, \end{aligned} \quad (4.49)$$

where

$$\begin{aligned} \Omega_1 &= \cosh \omega/(2\omega\Delta), \\ \Omega_2 &= \cosh \omega + \omega \sinh \omega)/(2\omega^2\Delta), \\ \Omega_3 &= \omega/\Delta, \\ \Omega_4 &= (\omega - \cosh \omega \sinh \omega)/\Delta, \\ \Omega_5^\pm &= (\cosh \omega + \omega \exp(\pm \omega))/(2\omega\Delta), \end{aligned} \quad (4.50)$$

(cont.)

$$\Omega_6^\pm = (\cosh \omega - \omega \exp(\pm \omega))/(2\omega\Delta),$$

$$\Omega_7^\pm = (\omega - \exp(\pm \omega) \cosh \omega)/(2\Delta),$$

$$\Omega_8^\pm = (\omega + \exp(\pm \omega) \cosh \omega)/(2\Delta),$$

and

$$\Delta(\omega) = \cosh^2 \omega + \omega^2. \quad (4.51)$$

It is seen that the functions  $\Omega_x$  are all expressible in terms of elementary functions of the frequency of  $\omega$ . The constants of integration,  $a_0, \dots, b_1$ , on the other hand, contain the unknowns  $h_1$  and  $h_2$ . With the aid of equations (4.45)<sub>5,6</sub> which may be written as

$$\Psi_1(1) + (\bar{u} + \sin \gamma)h_1 = 0, \quad \Psi_2(1) + (\bar{u} + \sin \gamma)h_2 = 0, \quad (4.52)$$

the amplitudes  $h_1$  and  $h_2$  can be determined. Indeed, substituting the representations (4.47)<sub>3,4</sub> for  $\Psi_1$  and  $\Psi_2$  into Equations (4.52) and using the results (4.48), (4.49) yields a system of linear equations for  $h_1$  and  $h_2$  in terms of  $\bar{u}$ ,  $\omega$  and  $\gamma$ . Its solution is

$$h_1 = \frac{(4\omega\Omega_1 \sin \gamma + 2\bar{u}\omega^2\Omega_2)(\bar{u} + \sin \gamma(1 + (1/\Delta)))}{D^2(\omega)},$$

$$h_2 = \frac{(4\omega\Omega_1 \sin \gamma + 2\bar{u}\omega^2\Omega_2)(\cos \gamma\Omega_4/\omega^2)}{D^2(\omega)}, \quad (4.53)^*$$

where

$$D^2 = \left\{ \sin \gamma \left( 1 + \frac{1}{\Delta} \right) + \bar{u} \right\}^2 + \cos^2 \gamma \frac{\Omega_4^2}{\omega^4}. \quad (4.54)^*$$

The transfer or filter function  $\mathcal{F}$  and the phase lag angle  $\varphi$  are therefore given by

$$\mathcal{F}(\omega, \gamma, \bar{u}) = \frac{|4\omega\Omega_1 \sin \gamma + 2\bar{u}\omega^2\Omega_2|}{D(\omega)},$$

$$\tan \varphi = \frac{\cos \gamma \Omega_4}{\omega^2 [\sin \gamma(1 + (1/\Delta)) + \bar{u}]}.$$

$$(4.55)^*$$

Two limits are interesting to analyse. First, as  $\omega \rightarrow \infty$ , or  $\lambda \rightarrow 0$ , that is for very small wavelengths,  $\mathcal{F}(\omega, \gamma, \bar{u}) \rightarrow 0$ ,  $\tan \varphi \rightarrow 0$ . Bottom undulations of very small wavelengths are therefore localized disturbances whose effect is limited to a small layer close to the base. This result is an explicit corroboration of earlier statements in Chapter 3 which indicate that small-scale roughnesses of the bed are confined to a boundary layer. Secondly, as

\*The formulas corresponding to (4.53)–(4.55) as listed in [26] are in error.

$\omega \rightarrow 0$ , or as  $\lambda \rightarrow \infty$ , that is for asymptotically large wavelengths

$$\begin{aligned}\mathcal{F}(\omega, \gamma, \bar{u}) &\rightarrow 1 - \frac{\bar{u}^2}{(2 \sin \gamma + \bar{u})^2} < 1, \\ \tan \varphi &\rightarrow -\frac{\frac{5}{6} \cos \gamma}{(2 \sin \gamma + \bar{u})} \omega.\end{aligned}\quad (4.56)$$

It is evident that bottom undulations are not optimally transferred to the surface, even at asymptotically-large wavelengths, unless of course,  $\bar{u} = 0$ . The asymptotic value of the phase lag angle  $\varphi$  (4.56) deserves special considerations. For fixed and finite  $\gamma$  and as  $\omega \rightarrow 0$  we have  $\varphi \rightarrow 0$ , but for  $\omega$  small and fixed and  $\gamma \rightarrow 0$

$$\lim_{\substack{\gamma \rightarrow 0, \\ \omega \text{ small, fixed}}} (\tan \varphi) = \frac{\text{const}}{\gamma}, \quad (4.57)$$

so  $\varphi \rightarrow -(\pi/2)$  in this case. This should be borne in mind, in particular when plots of the transfer function and the phase lag function are interpreted.

Figures 4.3 and 4.4 display the filter function  $\mathcal{F}$  and the phase-lag angle  $\varphi$  for  $\bar{u} = 0$  (results for  $\bar{u} \neq 0$  are qualitatively similar) plotted against wavelength  $\lambda = 2\pi/\omega$  and parameterized for various inclination angles  $\gamma$ . It is seen that the transfer of bottom undulations is small for small wavelengths

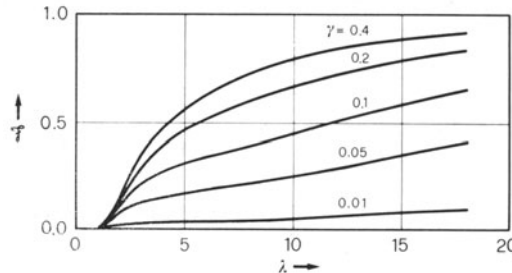


FIG. 4.3. Filter function  $\mathcal{F}$  plotted against dimensionless wave length  $\lambda = 2\pi/\omega$  for a Navier-Stokes liquid and parameterized for various mean inclinations  $\gamma$ . *No slip* at the bottom.

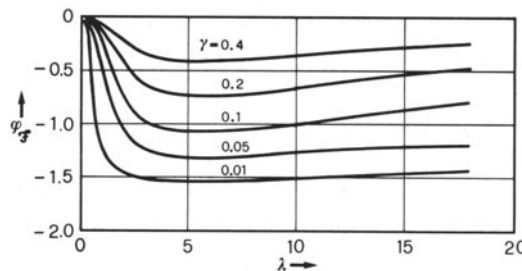


FIG. 4.4. Phase lag angle  $\varphi_F$  for the same situation as in Figure 4.3.

and gets larger for growing wavelengths, reaching the value (4.56) as  $\lambda \rightarrow \infty$ . The phase angle  $\varphi$  (Figure 4.4) is persistently negative; wave troughs of surface undulations thus lag behind those of the base by an angle  $|\varphi|$ . At small wavelengths  $\varphi$  is approximately zero, while at larger wavelengths, it assumes a finite negative value which is fairly independent of  $\lambda$ . In particular, for very small  $\gamma$ ,  $\varphi$  is approximately  $-\pi/2$ , the value predicted by Equation (4.57). The limit (4.56),  $\varphi \rightarrow 0$ , lies outside the range of the figure, but an onset of an approach of the value  $\varphi \rightarrow 0$  as  $\lambda \rightarrow \infty$  can be stipulated from Figure 4.4.

Other results could also be described, e.g., longitudinal stress variations. These will be deferred to a later section. Here, it may suffice to mention that the results of Figure 4.3 suggest a monotone increase of the value of the filter function  $\mathcal{F}$  with increasing wavelength. This contradicts earlier results by Budd [11].

(γ) *Numerical solution for non-linear rheology.* We now return to the general boundary value problem for non-linear rheology and begin with the case

(i) *Sliding velocity prescribed:* The equations to be solved are the differential equations (4.42) and the boundary conditions (4.43) and (4.45). These equations constitute a two-point boundary-value problem. Its numerical solution is probably most easily found by forward shooting starting from  $\bar{y} = 0$ . This implies that the system of second-order differential equations, (4.42), for  $\Phi_i$  and  $\Psi_i$ , should be reduced to a first-order system, which may then be subject to a forward integration routine.

To transform (4.42) to a first-order system of ordinary differential equations we introduce the vector

$$\mathbf{f} = (f_1, \dots, f_8)^T = (\Phi_1, \Phi_2, \Psi_1, \Psi_2, \Phi'_1, \Phi'_2, \Psi'_1, \Psi'_2)^T. \quad (4.58)$$

Its first four components are the stress and stream functions and the remaining four are the derivatives of these with respect to  $\bar{y}$ . In terms of  $\mathbf{f}$  it can readily be shown that Equations (4.42) correspond to the linear vector differential equation

$$\frac{d\mathbf{f}}{d\bar{y}} = \mathbf{A}(\bar{y}) \cdot \mathbf{f}$$

where  $\mathbf{A}$  is given by

$$\mathbf{A} = \left[ \begin{array}{cc|cc|cc} 0 & & 1 & & 1 & \\ -\omega^2 & -\omega^2 & -\omega/f(y) & & & \\ -\omega^2 & -\omega^2 & & -\omega/f(y) & & \\ -\omega^2 & -\omega^2 & & & -\omega g(y) & \\ & & & & & \omega g(y) \end{array} \right]. \quad (4.59b)$$

In terms of the components of the vector  $\mathbf{f}$  the boundary conditions (4.44) and (4.45) read

$$\left. \begin{array}{l} f_3 = -\bar{u}_b^{(0)} (= -C \sin^m \gamma), \\ f_4 = 0, \\ f_7 = -2 \sin \gamma \exp(\mathbb{A}\hat{\theta}) \mathfrak{F}(\sin^2 \gamma), \\ f_8 = 0. \end{array} \right\} \bar{y} = 0 \quad (4.60)$$

and

$$\left. \begin{array}{l} g_1 \equiv -\omega^2 f_1 - \frac{\cos \gamma}{\bar{u}_S^{(0)}} f_3 = 0, \\ g_2 \equiv -\omega^2 f_2 - \frac{\cos \gamma}{\bar{u}_S^{(0)}} f_4 = 0, \\ g_3 \equiv -\omega f_5 - \frac{\sin \gamma}{\bar{u}_S^{(0)}} f_4 = 0, \\ g_4 \equiv \omega f_6 - \frac{\sin \gamma}{\bar{u}_S^{(0)}} f_3 = 0, \end{array} \right\} \bar{y} = 1 \quad (4.61)$$

where  $\bar{u}_S^{(0)} = \bar{u}^{(0)}(\bar{y} = 1)$  is obtained from Equations (4.26) and (4.29). To solve the linear vector differential equation (4.59), subject to the conditions (4.60) and (4.61), it is best to integrate it numerically with a forward integration scheme such as the Runge-Kutta method. Because of the linearity of the problem the principle of superposition can be used. In order to explain the procedure, assume that for  $\bar{y} = 0$  the value of the vector  $\mathbf{f}$  corresponding to the above boundary conditions were known. The components would be given by the expressions (4.60) and by  $f_1 = x_1, f_2 = x_2, f_5 = x_3, f_6 = x_4$ . The solution of the differential equation would then be obtained by straightforward integration, starting at  $\bar{y} = 0$ . Of course the quantities  $x_1, \dots, x_4$  are not known and must be determined, but prompted by the linearity of the problem, the system (4.59) is solved with the following five different initial conditions at  $\bar{y} = 0$

$$\begin{aligned} \mathbf{f}_0^0 &= (0, 0, -C \sin^m \gamma, 0, 0, 0, -2 \sin \gamma \exp(\mathbb{A}\hat{\theta}) \mathfrak{F}(\sin^2 \gamma), 0)^T \\ \mathbf{f}_0^1 &= (1, 0, 0, 0, 0, 0, 0, 0)^T \\ \mathbf{f}_0^2 &= (0, 1, 0, 0, 0, 0, 0, 0)^T \\ \mathbf{f}_0^3 &= (0, 0, 0, 0, 1, 0, 0, 0)^T \\ \mathbf{f}_0^4 &= (0, 0, 0, 0, 0, 1, 0, 0)^T \end{aligned} \quad (4.62)$$

For each of these initial conditions the values of  $g_1, \dots, g_4$  in (4.61) can be evaluated; they will be denoted by  $g_i^j$ , where the lower index  $i = 1, \dots, 4$  denotes the function given in (4.61) and the upper index  $j = 0, \dots, 4$  indicates, for which initial condition the  $g$ -functions have been evaluated. The

correct solution is obtained provided that

$$g_i^0 + \sum_{j=1}^4 g_i^j x_j = 0, \quad (i, j = 1, 2, 3, 4). \quad (4.63)$$

This is a linear system of equations for the unknowns  $x_j$ . The meaning of Equation (4.63) is the following: If the vector differential equation (4.59) were solved using the initial condition  $(\mathbf{f}_0^0 + \sum_j \mathbf{f}_0^j x_j)$  at  $\bar{y} = 0$ , the boundary values  $g_i$  at  $\bar{y} = 1$  would be  $(g_i^0 + \sum_j g_i^j x_j)$  which according to the statements (4.61) must vanish; this is exactly the statement expressed by Equation (4.63). Hence, solving the linear system also solves the given boundary-value problem. Once the unknowns  $x_j$  are determined the solution to the originally posed problem is obtained by superposing the solutions corresponding to the initial conditions  $\mathbf{f}_0^0$  and  $\mathbf{f}_0^j x_j$ ,  $j = 1, \dots, 4$ . In practice, it is advantageous to integrate the system (4.59) once more using the single initial condition

$$\mathbf{f}_0 = (x_1, x_2, -\mathbb{C} \sin^m \gamma, 0, x_3, x_4, -2 \sin \gamma \exp(\mathbb{A}\hat{\theta}) \mathfrak{F}(\sin^2 \gamma), 0)^T.$$

First-order stresses are then obtained by differentiations of  $\mathbf{f}$ , whereas velocity components follow directly from the appropriate components of the vector  $\mathbf{f}$ .

(ii) *Stress-dependent sliding law*: All the forgoing calculations are based on the kinematic boundary conditions (4.35). We have seen that, to zeroth order, this condition is equivalent to (4.34); but when first-order equations are considered, (4.35) and (4.34) differ from each other. It is interesting to investigate in what respect the difference in boundary conditions results in differences in the state of first-order stresses and velocities.

The boundary value problem that must be solved is now Equations (4.31)–(4.34). For the vanishing accumulation rate and harmonic solutions, Equations (4.59) and (4.61) still apply, but the stress-dependent sliding law, when written in terms of the components of the vector  $\mathbf{f}$ , require that

$$\left. \begin{aligned} f_3 &= -\mathbb{C} \sin^m \gamma, & f_4 &= 0, \\ f_7 + \mathcal{X} f_6 &= -m\mathbb{C} \sin^m \gamma - 2 \sin \gamma \exp(\mathbb{A}\hat{\theta}) \mathfrak{F}(\sin^2 \gamma), \\ f_8 - \mathcal{X} f_5 &= 0, \end{aligned} \right\} \bar{y} = 0, \quad (4.64)$$

where

$$\mathcal{X} = m\omega\mathbb{C} \sin^{m-1} \gamma. \quad (4.65)$$

The form of the relations (4.64) suggests to introduce a new vector  $\mathbf{f}'$  by

$$\mathbf{f}' = (\mathbf{f}_1, \dots, \mathbf{f}_8)^T = (f_1, f_2, \dots, f_6, f_7 + \mathcal{X} f_6, f_8 - \mathcal{X} f_5)^T. \quad (4.66)$$

In terms of this new vector the differential equation (4.59) assumes the form

$$\frac{d\mathbf{f}'}{d\bar{y}} = \mathcal{A}(\omega, \bar{y}) \mathbf{f}', \quad (4.67a)$$

where  $\mathcal{A}$  is given by

$$\mathcal{A} = \begin{bmatrix} 0 & 1 & 0 & 0 \\ 0 & 0 & 1 & 0 \\ 0 & 0 & -\mathcal{X} & 1 \\ \mathcal{X} & 0 & 0 & 1 \end{bmatrix} \quad \begin{bmatrix} -\omega^2 & 0 & 0 & 0 \\ 0 & -\omega^2 & 0 & 0 \\ 0 & -\omega^2\mathcal{X} & -\omega^2 & 0 \\ \omega^2\mathcal{X} & 0 & 0 & -\omega^2 \end{bmatrix} \begin{bmatrix} \frac{\omega\mathcal{X}}{f(\bar{y})} & 0 & 0 & \frac{\omega}{f(\bar{y})} \\ 0 & \frac{\omega\mathcal{X}}{f(\bar{y})} & -\frac{\omega}{f(\bar{y})} & 0 \\ 0 & \omega\left(\frac{\mathcal{X}^2}{f(\bar{y})} - g(\bar{y})\right) & -\frac{\omega}{f(\bar{y})} & 0 \\ \omega\left(g(\bar{y}) - \frac{\mathcal{X}^2}{f(\bar{y})}\right) & 0 & 0 & -\frac{\omega\mathcal{X}}{f(\bar{y})} \end{bmatrix} \quad (4.67)$$

Furthermore, in terms of the new vector  $\mathbf{f}$  the boundary conditions read:

At  $\bar{y} = 0$

$$\left. \begin{array}{l} f_3 = -\bar{u}_b^{(0)} (= -C \sin^m \gamma), \quad f_4 = 0, \\ f_7 = -mC \sin^m \gamma - 2 \sin \gamma \exp(A\theta) \mathfrak{F}(\sin^2 \gamma), \quad f_8 = 0 \end{array} \right\} \quad \bar{y} = 0, \quad (4.68)$$

and at  $\bar{y} = 1$ ,

$$\left. \begin{array}{l} g_1 \equiv -\omega^2 f_1 - \frac{\cos \gamma}{\bar{u}_S^{(0)}} f_3 = 0 \\ g_2 \equiv -\omega^2 f_2 - \frac{\cos \gamma}{\bar{u}_S^{(0)}} f_4 = 0 \\ g_3 \equiv -\omega f_5 - \frac{\sin \gamma}{\bar{u}_S^{(0)}} f_4 = 0 \\ g_4 \equiv \omega f_6 - \frac{\sin \gamma}{\bar{u}_S^{(0)}} f_3 = 0 \end{array} \right\} \quad \bar{y} = 1. \quad (4.69)$$

Formally there is no difference between the problem described by Equations (4.67), (4.68) and (4.69) and the previous ones described by (4.59)–(4.61). The same solution technique may therefore be used to integrate the system. There is no need to further elaborate on it, yet it may be mentioned that in an actual computation only the differential equations (4.67) subject to the boundary conditions (4.68), (4.69) must be integrated; for by simply setting  $C$  equal to zero everywhere except where  $\bar{u}_b^{(0)} = C \sin^m \gamma$ , the boundary-value problem for  $\mathbf{f}$  is obtained. The presentation of results will be deferred until Section 3c.

( $\delta$ ) *Effect of a steady accumulation rate.* In the last three subsections accumulation was set to zero but bottom undulations were present. Here, a non-vanishing accumulation rate will be assumed and bottom undulations will be set aside. As was proved above, both effects can be linearly superimposed.

It was mentioned earlier that the zeroth-order solution constructed in Equations (4.26) did not account for the geometric effects of the steady-state accumulation rate. *This limits considerations to length scales which are not asymptotically large as compared to glacier thicknesses.* The effect of the accumulation rate on length scales somewhat larger than glacier thickness may, however, still be analysed.

The boundary-value problem consisting of Equations (4.31), (4.32), (4.33) and (4.34) or (4.35) is now solved by setting  $\Lambda = 0$  and prescribing the accumulation rate. Of particular interest would be solutions when the accumulation rate is constant along the glacier; corresponding solutions are not easily found. For the subsequent analysis it will therefore be assumed that  $\bar{y}_s$  is given in terms of a Fourier cosine series. The long wavelength limit will then approximately describe the behavior for constant accumulation. It then suffices to restrict considerations to the single component

$$\bar{y}_s^a = H \cos \omega x, \quad (4.70)$$

where  $H$  will be chosen such that accumulation amplitudes assume realistic values.\* It goes almost without further explanation that stress and stream functions  $\Phi$  and  $\Psi$  and first-order surface elevation  $\eta_s$  can be represented in the form (4.39). Substitution of these representations into the differential equations (4.31) and into the boundary conditions (4.33), (4.34) or (4.35) will yield the differential equations (4.42) subject to boundary conditions, which are slightly different from those listed in (4.43)–(4.45). Instead of these the new boundary conditions are,

*At the mean base  $\bar{y} = 0$ :* When the stress dependent viscous sliding law is used,

$$\begin{aligned} \Psi_1 &= \Psi_2 = 0, \\ \frac{d\Psi_1}{d\bar{y}} + \omega C m \sin^{m-1} \gamma \frac{d\Phi_2}{d\bar{y}} &= 0, \quad \frac{d\Psi_2}{d\bar{y}} - \omega C m \sin^{m-1} \gamma \frac{d\Phi_1}{d\bar{y}} = 0. \end{aligned} \quad (4.71)$$

On the other hand, when sliding velocity is prescribed

$$\Psi_1 = \Psi_2 = 0, \quad \frac{d\Psi_1}{d\bar{y}} = \frac{d\Psi_2}{d\bar{y}} = 0. \quad (4.72)$$

\*Since bottom undulations are assumed to be zero in the accumulation analysis the perturbation parameter  $\varepsilon$  can be chosen such that in  $\bar{a} = \varepsilon \mathfrak{A}$ ,  $\mathfrak{A}$  becoming of order 1,  $H$  must then be of order 1 as well.

At the mean upper surface  $\bar{y} = 1$ :

$$\begin{aligned}\omega^2 \Phi_1 - \cos \gamma h_1 &= \omega^2 \Phi_1 + \frac{\cos \gamma}{\bar{u}_S^{(0)}} \Psi_1 = \cos \gamma H, \\ \omega^2 \Phi_2 - \cos \gamma h_2 &= \omega^2 \Phi_2 + \frac{\cos \gamma}{\bar{u}_S^{(0)}} \Psi_2 = 0, \\ \omega \frac{d\Phi_1}{dy} - \sin \gamma h_2 &= \omega \frac{d\Phi_1}{dy} + \frac{\sin \gamma}{\bar{u}_S^{(0)}} \Psi_2 = 0, \\ \omega \frac{d\Phi_2}{dy} + \sin \gamma h_1 &= \omega \frac{d\Phi_2}{dy} - \frac{\sin \gamma}{\bar{u}_S^{(0)}} \Psi_1 = -\sin \gamma H, \\ \Psi_1 + \bar{u}_S^{(0)} h_1 &= 0, \\ \Psi_2 + \bar{u}_S^{(0)} h_2 &= 0.\end{aligned}\tag{4.73}$$

Solutions to the boundary-value problem, comprising the equations (4.42), (4.71) or (4.72) and (4.73) can be constructed as it was demonstrated before for the case where the effect of bottom undulations on the stress and velocity distributions was analysed. For instance, for a *Newtonian fluid* the stress and stream functions can again be expressed in the form (4.47), but now the free constants  $a_0, \bar{a}_0, \dots, b_1, \bar{b}_1$  are given by

$$\begin{aligned}a_0 &= -\sin \gamma(h_1 + H)W_1 - \cos \gamma h_2 W_2, \\ \bar{a}_0 &= -a_0, \\ a_1 &= \sin \gamma(h_1 + H)W_3^- + \cos \gamma h_2 W_4^-, \\ \bar{a}_1 &= -\sin \gamma(h_1 + H)W_4^+ + \cos \gamma h_2 W_3^+, \end{aligned}\tag{4.74}$$

and

$$\begin{aligned}b_0 &= \cos \gamma(h_1 + H)W_5 - \sin \gamma h_2 W_6, \\ \bar{b}_0 &= -b_0, \\ b_1 &= -\cos \gamma(h_1 + H)W_4^- + \sin \gamma h_2 W_3^-, \\ \bar{b}_1 &= -\cos \gamma(h_1 + H)W_3^+ - \sin \gamma h_2 W_4^+, \end{aligned}\tag{4.75}$$

where

$$\begin{aligned}W_1 &= \frac{\cosh \omega}{2\omega\Delta}, & W_2 &= \frac{\cosh \omega}{2\omega^2\Delta} + \frac{\sinh \omega}{2\omega\Delta}, & W_3^\pm &= \frac{\cosh \omega}{2\omega\Delta} + \frac{e^{\pm\omega}}{2\Delta}, \\ W_4^\pm &= \frac{\cosh \omega}{2\omega\Delta} - \frac{e^{\pm\omega}}{2\Delta}, & W_5 &= \frac{\cosh \omega}{2\omega\Delta} - \frac{\sinh \omega}{2\omega\Delta},\end{aligned}\tag{4.76}$$

and where  $\Delta$  is defined in Equation (4.51);  $h_1$  and  $h_2$  follow from the equations

$$\frac{h_1}{H} = -1 + \frac{\bar{u} + \sin \gamma}{N}, \quad \frac{h_2}{H} = \frac{\bar{u} + \sin \gamma}{N} \Omega_4 \quad (4.77)$$

in which

$$N = \{\sin \gamma(1 + (1/\Delta)) + \bar{u}\}^2 - \cos \gamma \Omega_4 \frac{\sinh^2 \omega}{\omega^3 \Delta}. \quad (4.78)$$

For the non-Newtonian liquid, on the other hand, the boundary-value problems for  $\Phi_i, \Psi_i$  ( $i = 1, 2$ ) can be expressed in terms of the vectors  $\mathbf{f}$  or  $\mathbf{f}'$  as introduced in Equations (4.58) and (4.66), respectively, but as explained before, only the boundary-value problem for  $\mathbf{f}'$  must be formulated because that for  $\mathbf{f}$  can be obtained from the former by setting  $C = 0$  except where  $\bar{u}_h^{(0)} = C \sin \gamma$ . In terms of  $\mathbf{f}'$  the boundary-value problem reads

$$\begin{aligned} \frac{d\mathbf{f}'}{d\bar{y}} &= \mathcal{A}(\omega, \bar{y})\mathbf{f}', \quad 0 \leq \bar{y} \leq 1, \\ f'_3 &= f'_4 = f'_7 = f'_8 = 0, \quad \bar{y} = 0, \\ g'_1 &= -\cos \gamma H, \quad g'_2 = g'_3 = 0, \quad g'_4 = -\sin \gamma H, \quad \bar{y} = 1. \end{aligned} \quad (4.79)$$

The construction of solutions to these equations follows the approach used in Section 3b ( $\gamma$ ). Consequently, no further explanations are needed. Results will be presented in Section 3c.

(e) *A historical note on a previous approach.* The effect of bedrock protuberances on the stress and velocity distribution and on the shape of the surface geometry has been analysed in the way presented above by Hutter *et al.* [26]; yet there was an earlier analysis by Budd [10, 11, 12] also summarizing earlier work. His analysis is different from ours as he introduces two further assumptions, for which there is no justification. First, he writes the first-order momentum equations in terms of stress deviators  $\sigma_x^{(1)}, \sigma_y^{(1)}, \tau^{(1)}$  and *perturbation pressure*  $\bar{p}$  and assumes the latter to *vanish*. Budd's first-order momentum equations thus read

$$\frac{\partial \sigma_x^{(1)}}{\partial \bar{x}} + \frac{\partial \tau^{(1)}}{\partial \bar{y}} - \frac{\partial \bar{p}}{\partial \bar{x}} = 0, \quad \frac{\partial \tau^{(1)}}{\partial \bar{x}} + \frac{\partial \sigma_y^{(1)}}{\partial \bar{y}} - \frac{\partial \bar{p}}{\partial \bar{y}} = 0,$$

where  $\bar{p} = 0$ . He then introduces the stress function  $\Phi'$  for the deviatoric stress according to which

$$\sigma_x^{(1)} = \frac{\partial^2 \Phi'}{\partial \bar{y}^2}, \quad \sigma_y^{(1)} = \frac{\partial^2 \Phi'}{\partial \bar{x}^2}, \quad \tau^{(1)} = -\frac{\partial^2 \Phi'}{\partial \bar{x} \partial \bar{y}}$$

and uses the continuity equation to deduce the relation<sup>\*</sup>  $\sigma_x^{(1)} + \sigma_y^{(1)} = 0$ , which, when expressed in terms of the stress function  $\Phi$ , yields  $\nabla^2 \Phi = 0$ . Budd's stress function is therefore *harmonic*. The interesting feature of this result is that it does not depend upon the form of the constitutive relationship, provided that the stress deviator is proportional to stretching. When solving the Laplace equation, Budd further assumes that there is perfect slip at the bed. This allows him to impose pure stress boundary conditions at both bounding surfaces, the rockbed and the free surface which makes a direct integration of the stress problem possible. The stress field can therefore be determined for the known geometry of the base and the free surface.

In his second assumption, Budd neglects to properly describe a kinematic surface condition, replacing it by a global mass balance statement. The equation together with the remaining constitutive relation for shear stress then allows the determination of the velocity field and of the surface geometry. It is not appropriate to demonstrate this erroneous solution procedure because this has been done elsewhere (see Hutter *et al.* [26]), but it should be mentioned that rectifications of Budd's analysis were proposed simultaneously and to various degrees of accuracy by Hutter and Legerer [25], Lliboutry (in an oral presentation at the conference on Dynamics of Large Ice Masses, Ottawa, August 1978), Morris [33] and others. Of these approaches, the one presented by Hutter *et al.* [26] is the only one applicable to non-linear rheologies. These last authors also provided numerical proof for the inappropriateness of Budd's assumptions.

(η) *The first-order temperature problem.* Let us return now to the analysis of the first-order problem and complete its formal solution by indicating how longitudinal strain effects might affect the temperature distribution. Prerequisite for the evaluation of this influence is the knowledge of the zeroth and first-order stress and velocity distributions. Once the first-order differential equations for the velocity and stress fields are solved with the lowest order temperature distribution  $\hat{\vartheta}$ , this temperature distribution can be improved by substituting the stress and velocity fields into Equation (4.14). Introducing the zeroth and first-order velocity and stress representations into Equation (4.14) it is straightforward to show that  $\hat{\vartheta}$ , the second approximation of the temperature distribution, must satisfy the equation

$$\frac{\partial \hat{\vartheta}}{\partial \bar{x}}(\bar{u}^{(0)}(\bar{y}) + \varepsilon \bar{u}^{(1)}) + \frac{\partial \hat{\vartheta}}{\partial \bar{y}}\varepsilon \bar{v}^{(1)} - \mathbb{D} \nabla^2 \hat{\vartheta} = \varepsilon \mathbb{E} \left\{ \tau^{(1)} \frac{\partial \bar{u}^{(0)}}{\partial \bar{y}} + \tau^{(0)} \left( \frac{\partial \bar{u}^{(1)}}{\partial \bar{y}} + \frac{\partial \bar{u}^{(1)}}{\partial \bar{x}} \right) \right\}. \quad (4.80)$$

\*Recall that for the constitutive class describing glacier flow stretching and the stress deviator are proportional. Continuity thus immediately implies  $\sigma_x^{(1)} + \sigma_y^{(1)} = 0$ .

The right-hand side of this equation is known as are all the coefficient functions on the left-hand side. However, some of these coefficients are  $\bar{x}$ -dependent; the construction of the general solution is, therefore, rather difficult. The following approximate procedure may be suggested: Let  $\tilde{\vartheta}$  be Robin's steady-state solution (4.27) and assume that it approximates the true temperature distribution reasonably accurately. Presume, moreover that

$$\hat{\vartheta} = \tilde{\vartheta} + \varepsilon \tilde{\vartheta}, \quad (4.81)$$

where  $\varepsilon \tilde{\vartheta}$  is a small correction and  $\varepsilon$  is the perturbation parameter introduced earlier. Introducing the representation (4.81) into Equation (4.80) and neglecting higher-order terms yields as a differential equation for  $\tilde{\vartheta}$

$$\begin{aligned} \mathbb{D}\nabla^2\tilde{\vartheta} + \frac{\partial\tilde{\vartheta}}{\partial\bar{x}}\bar{u}^{(0)} &= -(\mathfrak{A}\bar{y} + \bar{v}^{(1)})\frac{d\tilde{\vartheta}}{d\bar{y}} + \\ &+ \mathbb{E}\left\{\tau^{(1)}\frac{\partial u^{(0)}}{\partial\bar{y}} + t^{(0)}\left(\frac{\partial\bar{u}^{(1)}}{\partial\bar{y}} + \frac{\partial\bar{v}^{(1)}}{\partial\bar{x}}\right)\right\}. \end{aligned} \quad (4.82)$$

In the derivation of this equation, it was assumed that  $\hat{\vartheta}$  satisfies the equation  $-\mathbb{D} d^2\hat{\vartheta}/d\bar{y}^2 = \varepsilon \mathfrak{A}\bar{y} d\hat{\vartheta}/d\bar{y}$ . Expressing the first-order velocity components in terms of the stream function  $\Psi$ , the stress  $\tau^{(1)}$  in terms of the stress function  $\Phi$ , and assuming

$$\begin{aligned} \hat{\vartheta} &= -\frac{\mathfrak{A}}{\mathbb{D}}\left\{\int_{\bar{y}}^1(2\xi - \bar{y})\hat{\vartheta}(\xi)d\xi + (\bar{y} - 1)\int_0^1\hat{\vartheta}(\xi)d\xi\right\} + \\ &+ \vartheta_1 \cos \omega\bar{x} + \vartheta_2 \sin \omega\bar{x}. \end{aligned} \quad (4.83)$$

Equation (4.82) may be transformed into a system of second-order ordinary differential equations in the variable  $\bar{y}$  for the unknown functions  $\vartheta_1$  and  $\vartheta_2$ . This was the reason for introducing in (4.83) the term in curly brackets in the first place. It represents the solution to Equation (4.82) when all terms on the right-hand side vanish except the term involving the derivative  $d\hat{\vartheta}/d\bar{y}$ . Notice also that this term vanishes at  $\bar{y} = 1$  and that its derivative vanishes at  $\bar{y} = 0$ . This should be borne in mind when boundary conditions are derived. Expressing the first velocity components in terms of the stream function  $\Psi$ , the stress  $\tau^{(1)}$  in terms of the stress function  $\Phi$  and assuming harmonic perturbations from uniform flow, as in Equations (4.40), the differential equation (4.82) may be transformed into a system of ordinary differential equations for  $\vartheta_1$  and  $\vartheta_2$  which reads

$$\begin{aligned}
& \mathbb{D} \left[ \frac{d^2 \vartheta_1}{d\bar{y}^2} - \omega^2 \vartheta_1 \right] - \omega \vartheta_2 \bar{u}^{(0)}(\bar{y}) \\
&= -\omega \frac{d\hat{\vartheta}}{d\bar{y}} \Psi_2(\bar{y}) - \mathbb{E} \left\{ \left[ \frac{d^2 \Psi_1}{d\bar{y}^2} + \omega^2 \Psi_1 \right] \tau^{(0)}(\bar{y}) + \omega \frac{d\bar{u}^{(0)}}{d\bar{y}} \frac{d\Phi_2}{d\bar{y}} \right\}, \\
& \mathbb{D} \left[ \frac{d^2 \vartheta_2}{d\bar{y}^2} - \omega^2 \vartheta_2 \right] + \omega \vartheta_1 \bar{u}^{(0)}(\bar{y}) \\
&= \omega \frac{d\hat{\vartheta}}{d\bar{y}} \Psi_1(\bar{y}) - \mathbb{E} \left\{ \left[ \frac{d\Psi_2}{d\bar{y}} + \omega^2 \Psi_2 \right] \tau^{(0)}(\bar{y}) + \omega \frac{d\bar{u}^{(0)}}{d\bar{y}} \frac{d\Phi_1}{d\bar{y}} \right\}.
\end{aligned} \tag{4.84}$$

Notice that the quantities on the right-hand side of these equations are known. Recall further that  $\mathbb{D}$  is small; this might influence the numerical integration procedure for their solution.

The boundary conditions which must fall on  $\vartheta_1$  and  $\vartheta_2$  follow from Equations (4.23) by invoking the representations (4.81) and (4.83). For instance, the boundary condition at  $\bar{y} = 1$  can be written as  $\hat{\vartheta} + \varepsilon\hat{\vartheta} + \varepsilon(d\hat{\vartheta}/d\bar{y})(\eta_s + \bar{y}_s^a) + \mathcal{O}(\varepsilon^2) = \vartheta_s$ , at  $\bar{y} = 1$ . Because Robin's solution for  $\hat{\vartheta}$  satisfies the condition  $\hat{\vartheta}(\bar{y}) = \vartheta_s$  and since  $\hat{\vartheta}$  is given by Equation (4.83), the above relation implies

$$\vartheta_1 \cos \omega \bar{x} + \vartheta_2 \sin \omega \bar{x} + \frac{d\hat{\vartheta}}{d\bar{y}} \Big|_{\bar{y}=1} (\eta_s + \bar{y}_s^a) = 0.$$

The final form of the boundary condition follows now from the harmonic decompositions of  $\eta_s$ , (4.40)<sub>3</sub>, and that for  $\bar{y}_s^a$ , (4.70), and collecting coefficients of  $\cos \omega \bar{x}$  and  $\sin \omega \bar{x}$ . The basal boundary condition (4.23)<sub>2</sub> is also treated in an analogous manner. This yields

$$\begin{aligned}
\frac{d\vartheta_1}{d\bar{y}} &= \frac{\varepsilon \mathfrak{A} H_\Lambda d\hat{\vartheta}}{\mathbb{D}} \Big|_{\bar{y}=0}, \quad \frac{d\hat{\vartheta}_2}{d\bar{y}} = 0, \quad \bar{y} = 0, \\
\vartheta_1 &= -\frac{d\hat{\vartheta}}{d\bar{y}} (h_1 + H_\mathfrak{A}), \quad \vartheta_2 = -\frac{d\hat{\vartheta}}{d\bar{y}} h_2, \quad \bar{y} = 1,
\end{aligned} \tag{4.85}$$

where the quantities on the right-hand sides are known. In the derivation of Equations (4.85), it was also assumed that the geothermal heat flux is constant along  $\bar{x}$ . Moreover,  $H_\Lambda$  and  $H_\mathfrak{A}$  are the amplitudes of the bottom undulation of wavelength  $(\omega/2\pi)$  or of the flux function  $\bar{y}_s^a$  as given in (4.70). The two-point boundary-value problem, therefore, allows the estimation of longitudinal steady-state temperature variations due to both bottom undulations and longitudinal variations of accumulation rate.

With Equations (4.84) and (4.85) the boundary-value problem for the temperature corrections has now been brought to a form from which it can

easily be transformed into a form appropriate for numerical integration. Explicit solutions have not yet been constructed, but Weertman [51], in a different approach, has drawn attention to the fact that measured vertical temperature profiles often show inversions\* which are not predictable without longitudinal variations of velocities and stresses. Such longitudinal variations are assumed above to be due to longitudinal variations of the bottom topography and of the accumulation rate function. Weertman's calculations, which are based on a different approximate solution technique, however, indicate that reasonable inversion profiles may be obtained by including such longitudinal effects. That not all inversive temperature profiles can successfully be predicted must lie in the steady-state assumption invoked above and in the restriction to the small perturbation assumptions.

Finally, we note that this solution technique could also be used in the determination of small longitudinal temperature variations, if the geothermal heat flux  $Q^{\text{geoth}}$  varies along  $\bar{x}$  with small amplitudes about a mean value.

### (c) Numerical results for steady state

In the previous sections, an analysis of the stress, velocity and temperature distribution in a nearly parallel-sided ice slab under steady conditions has been presented; it was assumed that bottom protuberance amplitude are small as compared to the entire thickness of the ice sheet and that these undulations would cause only small amplitude perturbations in the surface geometry and the stress, velocity, and temperature distributions. An approximate solution procedure was proposed in which it was assumed that the velocity and stress fields were only affected by the temperature distribution in the strictly parallel-sided slab. In other words, effects of longitudinal temperature variations are assumed negligible in the determination of longitudinal stress and velocity variations. It is appropriate now to present solutions and to discuss the physical relevance of the results. Before we embark on these, however, a few remarks seem to be in order regarding certain procedures in the construction of numerical solutions.

The analysis has been kept general enough to include the possibility of a variation of the flow law within the constitutive class of stress-strain rate relationships for which stress deviator is proportional to strain rate, see Equations (4.1). When performing the numerical calculations with the 'Glen flow law'  $\mathfrak{F}(\tau'_{II}) = \tau'_{II}^{(n-1)/2}$ , it is found that calculations become singular at the upper surface  $\bar{y} = 1$ . A scrutiny of the cause of this singularity shows that the 'effective viscosity' becomes infinitely large at the upper surface  $\bar{y} = 1$ . To see this, consider the constitutive relation for stress

\*That is, the temperature is not monotone with depth; it drops first, reaches a minimum between the surface and the bottom and then increases reaching the maximum temperature at the base.

$$\bar{\mathbf{D}} = \mathcal{A}(\theta) \bar{\mathfrak{F}}(\tau'_{II}) \boldsymbol{\sigma}, \quad \boldsymbol{\sigma} = \mathfrak{B}(\theta) \mathfrak{G}\left(\frac{D_{II}}{\mathcal{A}}\right) \mathbf{D}, \quad (4.86)$$

The first of these was met throughout, and the second is the inverse relationship of the first when  $\boldsymbol{\sigma}$  is solved in terms of  $\mathbf{D}$ . A straightforward calculation shows that  $\mathfrak{B}(\theta) = \mathcal{A}^{-1}(\theta)$  and  $\mathfrak{G}(x) = 1/\bar{\mathfrak{F}}(h(x))$ , where  $h$  is obtained from the Equation  $\bar{D}_{II} = \mathcal{A}^2(\theta) \bar{\mathfrak{F}}^2(\tau'_{II}) \tau'_{II}$ , when this equation is solved for  $\tau'_{II}$ . For Glen's flow law  $\bar{\mathfrak{F}}(x) = x^{(n-1)/2}$ , so  $\bar{D}_{II} = \mathcal{A}^2(\theta) \tau''_{II}$ ,  $\tau'_{II} = [\bar{D}_{II}/\mathcal{A}^2]^{1/n}$ , or  $h(x) = x^{1/n}$  so that  $\mathfrak{G}(x) = x^{(1-n)/(2n)}$ . It follows that the power flow law may be written as  $\boldsymbol{\sigma} = \mathcal{A}^{-1/n}(\theta) \bar{D}_{II}^{(1-n)/(2n)} \mathbf{D}$ , yielding the viscosity  $\mu = \mathcal{A}^{-1/n} \bar{D}_{II}^{(1-n)/(2n)}$ . Since  $n > 1$ ,  $\mu \rightarrow \infty$  whenever  $\bar{D}_{II} \rightarrow 0$ . Because this occurs at the free surface of the strictly parallel-sided ice slab, singular behavior at the free surface is demonstrated. To avoid this, a constitutive relation having a Newtonian part, e.g.,  $\bar{\mathfrak{F}}(x) = [(x^{(n-1)/2} + k)/(k+1)]$  was introduced, where  $k$  is small. It prevents the viscosity of the main flow from asymptotically approaching infinity near the surface.

The reader should be cautioned that by introducing the parameter  $k$ , two small quantities, namely  $\varepsilon$  and  $k$ , have entered the analysis of the first-order problems. Perturbation methods were used with respect to  $\varepsilon$ , but  $k$  has been treated as an  $\mathcal{O}(1)$  quantity. Our solution therefore, corresponds to the limit analysis  $\varepsilon \rightarrow 0$ ,  $k$  is fixed, finite and bounded away from zero. Clearly, a limit analysis in which the limits  $\varepsilon \rightarrow 0$  and  $k \rightarrow 0$  could be approached simultaneously, would from a mathematical point of view be more satisfactory and certainly more rigorous.

The failure of the solutions to be meaningful near  $\bar{y} = 1$  when  $k = 0$  is expressed mathematically by the fact that these solutions are not uniformly valid over the entire interval  $0 \leq \bar{y} \leq 1$  as  $k$  approaches zero. As long as  $\bar{y}$  is sufficiently distant from  $\bar{y} = 1$ , there is no difficulty with the above perturbation approach, even when  $k = 0$ . Near  $\bar{y} = 1$ , however, a different solution technique would have to be applied, which would guarantee that close to  $\bar{y} = 1$  and in the limit  $\varepsilon \rightarrow 0$ ,  $k \rightarrow 0$  the zeroth-order solution would yield a finite effective viscosity. The reader familiar with the methods of singular perturbations, or matched asymptotic expansions (see Cole [17], Nayfeh [34], van Dyke [20]), will undoubtedly recognize that this mathematically more appropriate approach will include methods of singular perturbations. Matched asymptotic expansions can be excluded because the limit  $k \rightarrow 0$  is not accompanied by a loss of a surface-boundary condition. *Multiple variable expansions* motions, however, render a solution procedure in which singularities as described above can be avoided. The idea would be to expand the dependent variables and  $\bar{y}$  in terms of  $k$ , e.g.,  $\bar{y} = \bar{y}_0 + k \bar{y}_1 + k^2 \bar{y}_2 \dots$ ,  $\bar{u} = \bar{u}^{(0)} + \varepsilon \bar{u}^{(1,0)} + k \bar{u}^{(0,1)} + \dots$  and to exclude the occurrence of secular terms by appropriately selecting the variables  $\bar{y}_1, \bar{y}_2$ , etc. It is apparent that such an analysis is very complicated and, indeed, it has so far not been

performed.\* Our simplified analysis is, however, valid for  $\zeta = \mathcal{O}(1)$ . Since this is not the case numerically, certain quantities may, numerically, not be too reliable, in particular, close to the free surface. Since the viscosity is large only in a small boundary layer close to the free surface, we do not believe that essential inaccuracies are introduced, however.

With the above precautions in mind, the theoretical results derived above were subject to a numerical exploitation using finite difference approximations of the differential equations. Several interesting features can thereby be obtained. We shall discuss the transfer of bottom undulations to the surface topography, describe their influence on the stress and velocity distribution, and shall also look at the influence of the temperature distribution and of the various sliding conditions on these quantities. Our presentation follows in parts Hutter *et al.* [26] and Hutter and Spring [27].

(a) *Transfer of bottom protuberances to the surface.* Let us begin with the presentation of the filter function  $\mathcal{F}$  and the phase angle  $\varphi_{\mathcal{F}}$ . First results for a Newtonian fluid adhering to its bed based on an analytic representation of the solution, were presented in Section 3b. In Figures 4.3 and 4.4, the corresponding results were displayed. The filter function  $\mathcal{F}$  and the phase lag angle  $\varphi_{\mathcal{F}}$  were plotted against a dimensionless wavelength  $\lambda = 2\pi/\omega$  for various mean inclination angles  $\gamma$ . A distinct dependency of the transfer function  $\mathcal{F}$  on this angle was recognized, and a monotonic increase of the transfer function  $\mathcal{F}$  with growing wavelengths was observed. This means that small wavelength protuberances are filtered out, but that large wavelengths are transferred to the surface, even though in an attenuated manner. The plot for the phase angle  $\varphi_{\mathcal{F}}$  (see Figure 4.4) on the other hand, demonstrated a distinct dependency of  $\varphi_{\mathcal{F}}$  on the inclination angle  $\gamma$ . Furthermore, at small wavelengths, the phase lag angle  $\varphi_{\mathcal{F}}$  was very small, but nearly attained a constant value for larger  $\lambda$ 's. It was also shown that for  $\gamma \rightarrow 0$ , and large but finite values of  $\lambda$ ,  $\varphi_{\mathcal{F}}$  approaches the value  $-\pi/2$ .

The above results are different from those of Budd [11] whose transfer function, valid for small  $\gamma$  and for an ice slope perfectly sliding over its bed, behaves as follows: Transfer of bottom undulations to the surface are maximal at a distinct wavelength  $\lambda \sim 3.3$ . For wavelengths smaller and also larger than  $\lambda_{\text{opt}}$ , bottom undulations are less visible at the surface. This fact prompted Budd to conclude that transfer of bottom undulations to the surface must be the cause for the preferred wavelength  $\lambda \sim 3.3$  of the measured surface undulations. That the state of the art is more complicated than predicted by Budd will be demonstrated below. A careful study will have to

\**Note added in proof:* This statement is wrong, as R. E. Johnson and R. M. McMeeking demonstrate in “Near-surface flow in glaciers obeying Glen’s flow law” (T. & A. M. report No. 454, University of Illinois, Urbana–Champaign, 1982) that matched asymptotic expansions allow determination of uniformly valid solutions.

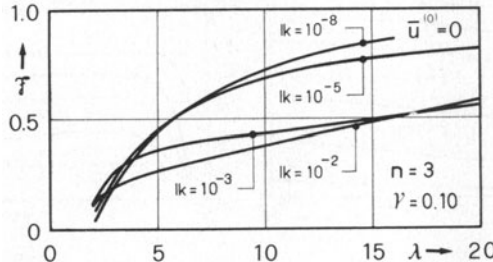


FIG. 4.5. Filter function  $\mathcal{F}$  plotted for  $\gamma = 0.1$  against  $\lambda = 2\pi/\omega$  parameterized for various values of  $k$ . No slip was used as a basal boundary condition.

include variations in material properties, boundary conditions at the base, and the thermal state of the ice.

In a first step, temperature variations and a possible influence of the moisture content will be discarded. The creep function (4.28) will be selected as a non-linear constitutive relation. It follows that  $A = 0$  and, consequently,  $n$  and  $k$  are the only parameters characterizing this material. Figure 4.5 shows a plot of the filter function  $\mathcal{F}$  for a fixed inclination angle  $\gamma = 0.1$ , for  $n = 3$  and for various values of  $k$ . It can be seen that  $\mathcal{F}$  depends significantly on  $k$ , provided that  $k > 10^{-5}$ . This is natural and points to the importance of the quasi-Newtonian behavior of the material response. For when  $k \rightarrow 0$ , the surface is infinitely rigid, suggesting that the smaller  $k$ , the stiffer the surface. Only a finite surface viscosity will allow the latter to deform accordingly. Reasonable values of  $k$  depend on the value of  $n$  (see Chapter 3). For  $n = 2$ ,  $k = \mathcal{O}(10^{-2})$ , for  $n = 3$ ,  $k = \mathcal{O}(10^{-3})$ . This, together with the results of Figure 4.5, indicates that *linear viscosity effects at small stretchings are of real physical importance*.

Figures 4.6a and 4.6c display the filter function  $\mathcal{F}$  as a function of the undulation wavelength  $\lambda$  for no-slip, various mean inclination angles  $\gamma$ , and for a generalized Glen's flow law with  $n = 2$  ( $k = 10^{-2}$ ) and  $n = 3$  ( $k = 10^{-3}$ ), respectively. The figures prove that a wavelength of dominant transfer of the bottom undulations to the surface does not exist in these cases either; they corroborate that  $\mathcal{F}$  grows monotonically with  $\lambda$  and becomes vanishingly small as  $\lambda$  approaches zero. A scrutiny of the Figures 4.3 and 4.6 further shows that the transfer of the bottom undulations to the surface is marginally enhanced with increasing  $n$ . Phase angles  $\varphi_{\mathcal{F}}$  show a distinct dependency on mean inclination  $\gamma$ ; for most wavelengths  $\varphi_{\mathcal{F}}$  is nearly independent of  $\lambda$ , but as  $\lambda$  decreases  $\varphi_{\mathcal{F}} \rightarrow 0$ . This behavior is analogous to that of a Newtonian fluid.

Before we proceed, it should be mentioned that the above results can only be trusted for  $\lambda > 1$ . The reason is a stress singularity that develops at small  $\lambda$  resulting in a failure of the perturbation procedure used to derive

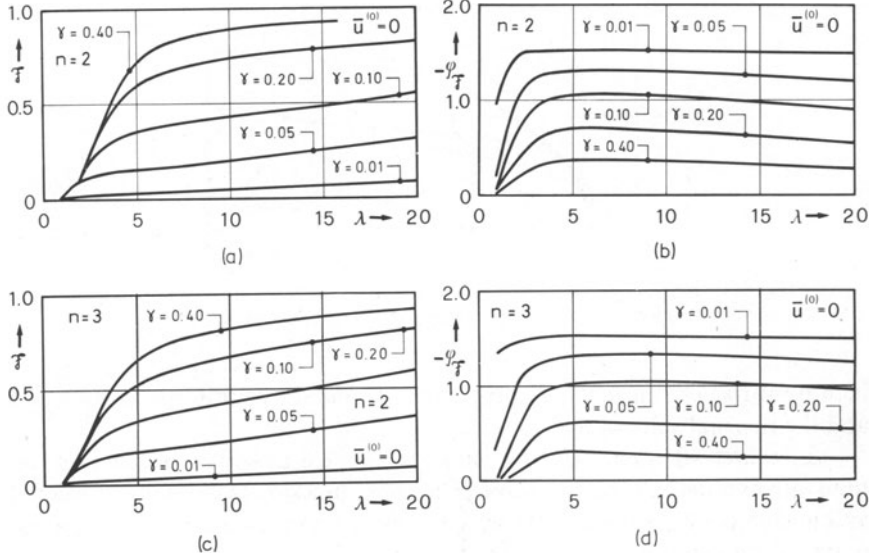


FIG. 4.6. Filter function  $\mathcal{F}$  and phase lag angle  $\varphi_{\mathcal{F}}$  plotted as a function of wavelength  $\lambda = 2\pi/\omega$  and parameterized for various values of the inclination angle  $\gamma$ . Figures 4.6a, b show the results for an exponent  $n = 2$  of the power flow law. Figures 4.6c, d show the corresponding results for  $n = 3$ . The basal boundary condition that is applied is no-slip. The transfer of basal undulations grows with growing wavelength, whereas corresponding phase lag angles are nearly wavelength-independent, yet both functions depend on the inclination angle  $\gamma$ .

the first-order boundary-value problem. We shall come back to this point later, when discussing stresses.

All previous numerical results apply when the no-slip condition at the bottom is used. The general theory has, however, been developed for two different sliding conditions, namely that

- (i) a sliding velocity,  $\bar{u}_s$ , is prescribed and
- (ii) a viscous sliding law  $\bar{u}_s = \mathbb{C}\tau_{sn}^m$  is used, where  $m = (n + 1)/2$ .

Zeroth-order solutions for the boundary-value problem using either one of these boundary conditions are the same, if  $\bar{u}_s^{(0)} = \mathbb{C}(\tau_s^{(0)})^m$ . Differences in the form of the sliding conditions do, therefore, only occur in the first-order correction problem.

An objective means of comparing the two boundary conditions is to present numerical results for particular values of the sliding velocity  $\bar{u}_s$  and to evaluate  $\mathbb{C}$  according to  $\bar{u}_s^{(0)} = \mathbb{C} \sin^m \gamma$  where  $m = (n + 1)/2$ . This guarantees that the lowest-order problems are the same. Figure 4.7 provides an easy

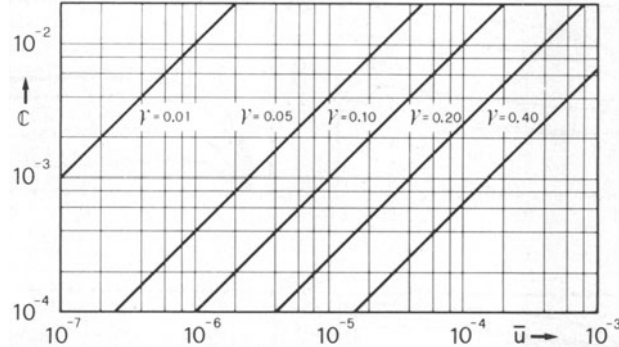


FIG. 4.7. Plot of the sliding velocity  $\bar{u} = C \sin^m \gamma$  for  $m = 2$  as a function of the viscosity coefficient  $C$  and of the inclination angle  $\gamma$ . (From [26].)

calculation of  $C$  from  $\bar{u}_s^{(0)}$  for the case that  $m = 2$ . Calculations were performed for  $\bar{u}_s^{(0)} \leq 5 \times 10^{-3}$ . The upper bound  $\bar{u}_s^{(0)} = 5 \times 10^{-3}$  corresponds to real velocities of 100 to 500 m/a and may thus be regarded as a reasonable maximal non-surging sliding velocity.

Filter functions  $\mathcal{F}$  and phase lag angles  $\varphi_{\mathcal{F}}$  were calculated for various sliding velocities and for both boundary conditions listed above. A selection of results is presented in Figures 4.8 and 4.9. Attention is restricted to the generalized Glen flow law in which  $n = 3$  and  $k = 10^{-3}$ . Figure 4.8 summarizes results when the sliding velocity is prescribed [case (i)]. It is evident that the filter functions do not change essentially in character when compared with those for no-slip. In particular, the transfer of bottom undulations to the surface is very small for small undulation wavelengths. It increases with a growing wavelength and, for large  $\lambda$ , reaches a constant asymptotic value which depends on the inclination angle  $\gamma$ . No distinct wavelength exists for which the transfer would be maximal. [Notice, however, that Figure 4.8b points at an onset of an intermediate maximum of the transfer function for a particular value of  $\gamma$ , yet a more pronounced development of such a maximum could not be observed.] Moreover, with an increasing sliding velocity, the dependency of the filter function on the mean inclination angle  $\gamma$  becomes less and less. An analogous behavior can also be observed for the phase angle which for no-slip and very small sliding velocities shows a distinct dependence on the inclination angle  $\gamma$ , which becomes less and less pronounced as the sliding velocity increases. It can also be seen from Figure 4.8 that for small inclination angles  $\gamma$ ,  $\varphi_{\mathcal{F}}$  is smaller when the sliding velocity is larger.

Figure 4.9 displays the same results, namely the filter function  $\mathcal{F}$  and the phase angle  $\varphi_{\mathcal{F}}$ , but now for the Weertman-type boundary condition. Zeroth-order sliding velocities are the same in Figure 4.9 as those in Figure 4.8 ( $\bar{u}^{(0)} = C \sin^m \gamma$ ; for given  $m = 2$ ,  $\gamma$  and  $\bar{u}^{(0)}$ ,  $C$  was determined in each case to match the conditions of Figure 4.8). As far as the filter function  $\mathcal{F}$  is

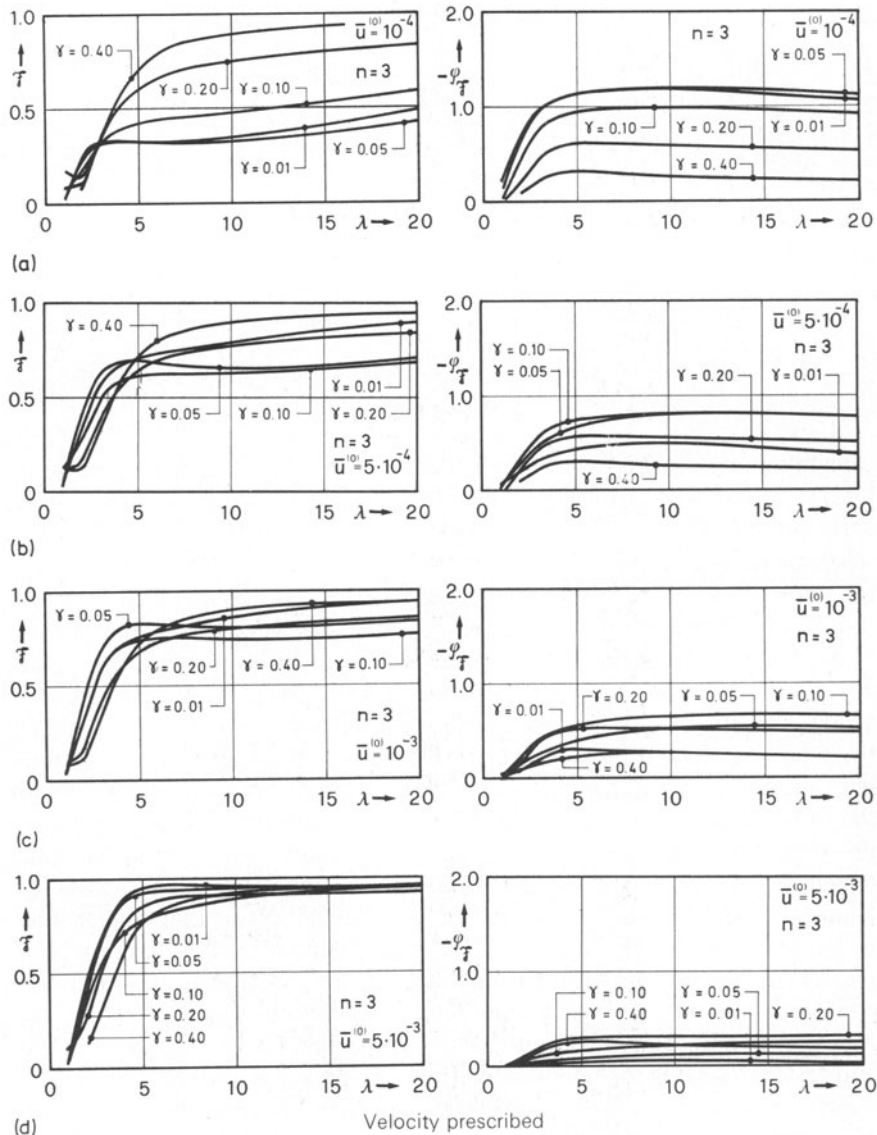


FIG. 4.8. Filter function  $\mathcal{F}$  (left) and phase lag angle  $\varphi_{\dot{\varphi}}$  (right) plotted against wavelength  $\lambda = 2\pi/\omega$  for various inclination angles  $\gamma$ . The curves are valid for a flow law with  $n = 3$  and  $k = 10^{-3}$  and for various values of the sliding velocity in the range  $\bar{u}^{(0)} = 10^{-4}$  to  $\bar{u}^{(0)} = 5 \times 10^{-3}$ . The mechanical boundary condition applied at the base is the *prescribed sliding velocity*. For all calculated sliding velocities filter function  $\mathcal{F}$  grows with wavelength and the dependence of  $\mathcal{F}$  on  $\gamma$  becomes less. A similar result applies for the phase lag angle  $\varphi_{\dot{\varphi}}$ , which is persistently negative. The results should be contrasted with those shown in Figure 4.9.

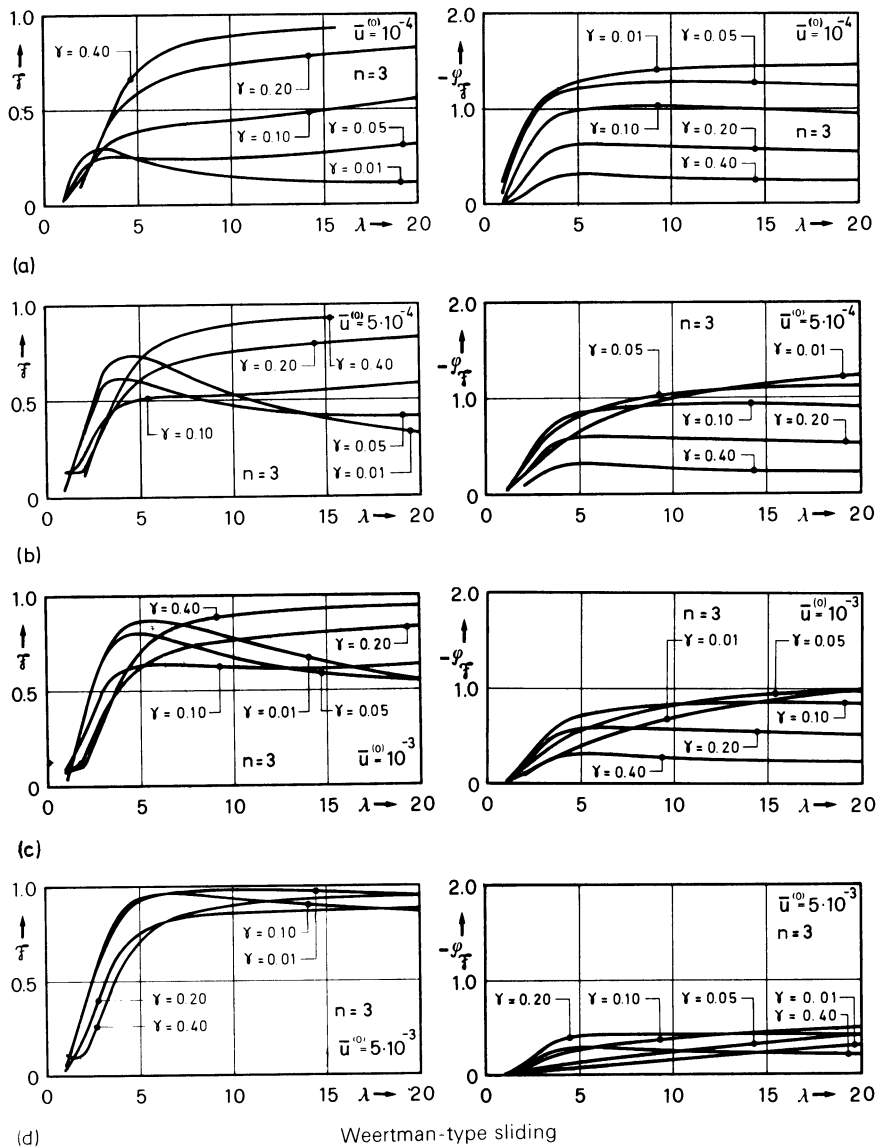


FIG. 4.9. Filter function  $F$  (left) and phase lag angle  $\varphi_F$  (right) plotted against wavelength  $\lambda = 2\pi/\omega$  for various inclination angles  $\gamma$ . The curves are valid for the same conditions as those in Figure 4.8 except that the sliding velocity is not prescribed, but that  $\bar{u}^{(0)}$  is given by  $\bar{u}^{(0)} = C\tau_{sn}^{(m)}$ , where  $m = 2$ . In order to allow comparison with Figure 4.8,  $C$  is chosen such that for a given value of the inclination angle  $\gamma$ ,  $\bar{u}^{(0)}$  assumes the values as indicated in the figures. Notice that under certain conditions, the transfer of bottom undulations to the surface seems to be maximal for a wavelength of the order of  $\lambda = 3 \div 5$ . With a growing sliding velocity, the dependence of  $F$  and  $\varphi_F$  on inclination angle  $\gamma$  becomes less and less. Compare the results with those shown in Figure 4.8.

concerned, the behavior in Figure 4.9 differs considerably from that shown in Figure 4.8. At small sliding velocities, the filter functions show the same characteristic behavior as they do for no-slip. Maximum transfer occurs at large wavelengths. At sliding velocities  $\bar{u}^{(0)} = 5 \times 10^{-4}$  and  $10^{-3}$  and for small mean inclinations  $\gamma \leq 0.05$ , however, a clear maximum exists at wavelengths between  $3 < \lambda < 5$ . For larger values of  $\gamma$  and also for larger sliding velocities than those mentioned above, the filter function  $\mathcal{F}$  grows again monotonically with  $\lambda$  attaining the maximum at large  $\lambda$ . [Incidentally, the numerical calculations did not indicate whether  $\mathcal{F}$  would attain a single maximum only. Indeed, in these cases for which a relative maximum exists, a second maximum of  $\mathcal{F}$  could exist as  $\lambda \rightarrow \infty$ . It has numerically not been detected, however.] Figure 4.9 also contains the results of the phase angle  $\varphi_{\mathcal{F}}$ . The results are not distinctly different from those of Figure 4.8. Hence, no further discussion is needed.

The above results seem to give the correct answer to the original problem tackled by Budd [11], but unlike Budd, who claims that a distinct wavelength for the optimal transfer of bottom undulations always exists for perfect slip, the above analysis indicates that in order for such an optimum to exist, sliding velocities must be right; if they are too low, no clear maximum develops, if they are too high, such a maximum has disappeared again. Moreover, the maximum does not develop for the case that the sliding velocity is prescribed (see Figure 4.8). It thus appears that the cause of a predominant transfer-wavelength is Weertman-type sliding paired with appropriate mean inclination.

The existence of an optimal transfer of bottom undulations to the surface must be a property exclusively attributable to the type of boundary conditions. This remark is important as neither of the two boundary conditions is universally accepted.

All foregoing calculations were performed for ice sheets with spatially independent material properties. For temperate glaciers and ice sheets such conditions are satisfied to a sufficient degree of accuracy, but in cold ice sheets such as Greenland and Antarctica material properties may change drastically with depth. It should therefore be tested to what extent the above analysis remains correct when temperature variations perpendicular to the main flow direction are taken into account.

According to our perturbation procedure, the temperature is treated as a known function. It was already mentioned before that a reasonable first estimate of the temperature distribution can be obtained by balancing transverse heat conduction with transverse heat advection. Such a temperature distribution was proposed by Robin [41]. With the prescribed surface temperature  $\hat{\vartheta} = \hat{\vartheta}_s$  and constant basal heat flux  $d\hat{\vartheta}/d\bar{y}(0) = -Q^{\text{geoth}}$  Robin's solution is given by Equation (4.27). With  $\hat{\vartheta} = (T - T_f)/T_0$  Robin's solution

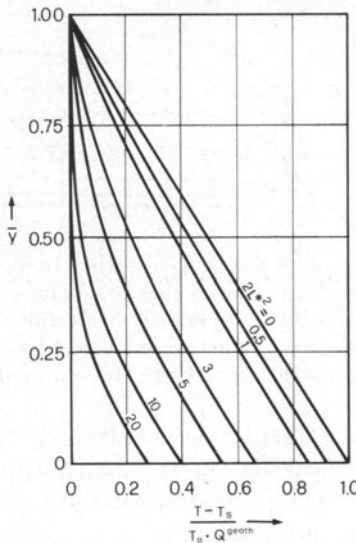


FIG. 4.10. Normalized temperature distribution as a function of depth for various values of the accumulation parameter  $L^* > 0$ . The plot applies only for positive accumulation.

can also be expressed as

$$\frac{T - T_s}{T_0 Q^{\text{geoth}}} = \frac{\sqrt{\pi}}{2} \frac{1}{L^*} (\text{erf}(L^*) - \text{erf}(L^* \bar{y})), \quad (4.87)$$

where

$$L^* = \sqrt{\frac{\bar{a}}{2D}}, \quad \text{erf}(x) = \frac{1}{\sqrt{\pi}} \int_0^x \exp(-t^2) dt. \quad (4.88)$$

This solution is meaningful for  $\bar{a} > 0$  and in the subsequent analysis attention will be restricted to this case.

Figure 4.10 displays  $\bar{y}$  as a function of the variable on the left-hand side of Equation (4.87), the parameter  $L^*$  essentially determining the shape of the temperature profile. Although the temperature profile (4.87) is not consistent with the temperature distribution of the strictly parallel-sided slab, it has a good chance to be fairly accurate, provided one is in a region where accumulation is fairly independent of  $\bar{x}$ .

Zeroth- and first-order velocity distributions were calculated for an ice sheet with a surface temperature 249.15 K and 258.8 K, respectively. Choosing  $L^* = 3.70$  and  $T_0 Q^{\text{geoth}} \sqrt{\pi / L^* T_s} = 1.05$ , formula (4.87) implies a base temperature which is 262 K in the first case and 272.12 K in the second.\*

\*The melting temperature  $T_M = 272.12$  K corresponds to an ice thickness of 1400 m.

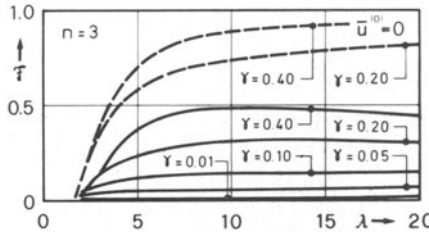


FIG. 4.11. Filter function  $\mathcal{F}$  plotted as a function of wavelength  $\lambda = 2\pi/\omega$  for various inclination angles  $\gamma$ . Curves hold for no-slip at the base and for  $n = 3$  and  $k = 10^{-3}$ . Solid lines belong to an ice sheet with a variable temperature distribution. Dashed lines are for a temperate ice sheet. The transfer of bottom undulations to the surface therefore depends on temperature.

The ice sheet is, therefore, cold throughout, reading the melting temperature in the second case. When calculating the velocity distribution, it is therefore appropriate to apply the no-slip condition in the first case and to implement the viscous sliding law in the second.

Results concerning the filter function  $\mathcal{F}$  are summarized in Figures 4.11 and 4.12. In the former, the filter function  $\mathcal{F}$  is plotted against wavelength  $\lambda$  for various inclination angles  $\gamma$  and the case that the ice remains cold at the base (no-slip boundary condition). For comparison, certain curves are also shown for an ice sheet whose temperature is constant throughout (dashed lines are taken over from Figure 4.6c). It is seen that the filter functions are drastically reduced by the vertical temperature variation, implying that the transfer of bottom undulations to the surface in cold ice cannot, in general, be calculated by neglecting temperature variations. Figure 4.12 summarizes the results for the second case that the basal temperature reaches the melting point. Plots 4.12a and 4.12b apply when the sliding velocity is prescribed; plots 4.12c and 4.12d are valid for a Weertman-type sliding law. It is clearly seen that the behavior of the transfer function strongly depends on the sliding velocity. For  $\bar{u}^{(0)} = 10^{-4}$  filter functions do not show a distinct maximum (although mathematically a wavelength of optimal transfer exists at small inclinations  $\gamma$ ). For  $\bar{u}^{(0)} = 10^{-3}$  on the other hand, there exist rather pronounced maxima for both boundary conditions, but only at small inclination angles. A comparison of figures 4.12b and 4.12d shows, however, that the transfer characteristics are strongly dependent on boundary conditions. For instance, if  $\gamma = 0.05$  the filter functions in Figures 4.12b, d are virtually the same; for  $\gamma = 0.01$  they differ drastically. Comparison with Figures 4.8 and 4.9 further indicates that no relative maximum exists when a sliding velocity is prescribed (Figure 4.8a), whereas such a maximum exists when the temperature varies across the thickness of the sheet (Figure 4.8c). For Weertman-type sliding, a relative maximum exists for both cases (Figures 4.9c and d.).

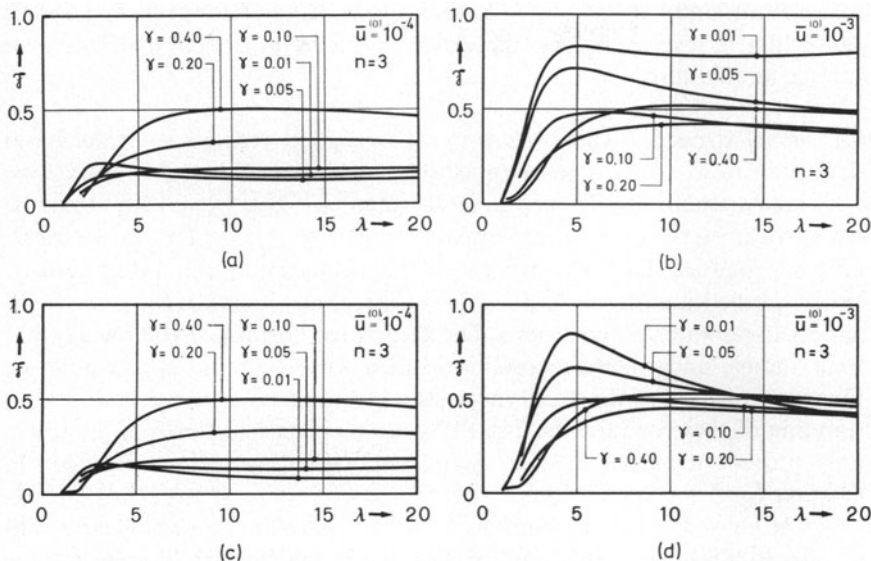


FIG. 4.12. Filter function  $\mathcal{F}$  in a cold ice sheet with variable temperature, as described in the text, reaching the melting point at the base and hence giving rise to the possibility of sliding. Figures 4.12a, b apply when the sliding velocity is prescribed, plots 12c and 12d are valid when a Weertman-type sliding law is used.

The above results may be summarized as follows: *The transfer of bottom undulations to the surface in the ice sheet is generally larger the larger the wavelengths of the bottom undulations. Wavelengths of the order of the ice thickness and smaller are essentially fully filtered out. Under special situations, however, an optimal wavelength  $\lambda$  exists for which transfer is maximum. The existence of this maximum requires the following conditions to be fulfilled: Firstly, the basal boundary condition must be sliding; and, secondly, the mean inclination  $\gamma$  of the bed must be small. These conditions are necessary, but not always sufficient. In a glacier which is temperate throughout and material properties independent of temperature, basal sliding may or may not yield an optimal wavelength for maximal transfer; in cold glaciers which are temperate at the base, such an optimal wavelength may exist when it does not for temperate ice sheets under otherwise identical conditions. Temperature variations, therefore, enhance the possibility of maximum transfer of bottom undulations to the surface. When this optimal wavelength exists, it is between three and five times the ice thickness.*

Frequency analyses of measured surface undulations indicate that on occasion the dominant wavelength lies in the range mentioned above (see the literature mentioned in the introduction to this chapter), indicating

that bottom undulations might be their cause. It may, however, be another cause that is responsible for the existence of the preferred wavelength of surface undulations.

( $\beta$ ) *Basal stresses.* There are at least two good reasons to study basal stresses. Firstly, at the base of an ice sheet of thickness  $D$  and surface slope  $\alpha$  (assumed small), it has been demonstrated (see Nye [35], [40]) that the basal shear stress  $t_{xy}^b$  is approximately given by  $t_{xy}^b = \rho g D \alpha$ . In a strictly parallel-sided ice slab  $\alpha = \gamma$ , where  $\gamma$  is the inclination of the bed or surface. When the bed undulates, so does the surface, and  $\gamma$  denotes the *mean* inclination angle which differs from  $\alpha$ . The shear stress formula involving  $\alpha$  rather than  $\gamma$  must, under certain conditions, then still be a valid approximation. Our investigation of the basal shear stress formula aims at a proper understanding of these conditions. The calculations in this section will, however, only provide a partial answer. A full understanding will be obtained in Chapter 5.

The second reason to study basal stresses is to find possible limitations of the solution procedure, in particular of the perturbation technique used. For instance, tractions normal to the rockbed should be negative, since ice can only sustain negligible tension and tensions are impossible if the ice slides over the bed. It follows from formulas (4.6) and (4.26)<sub>1</sub> that to within  $\mathcal{O}(\varepsilon^2)$  terms the tangential traction  $\tau_{sn}$  equals  $\tau_b$ . Using  $\tau_b^{(0)} = \sin \gamma$  and  $\tau_b^{(1)} = -\partial^2 \Phi / \partial \bar{x} \partial \bar{y}$ , substituting for  $\Phi$  the Fourier representation (4.40) and replacing  $\Phi'_1$  and  $\Phi'_2$  by  $f_5$  and  $f_6$ , respectively, yields for  $\tau_b$

$$\begin{aligned} \frac{\tau_b}{\tau_b^{(0)}} &= 1 + \varepsilon \Theta \cos (\omega x - \varphi_\Theta), \\ \Theta &:= \frac{\omega \sqrt{f_5^2 + f_6^2}}{\sin \gamma}, \quad \tan \varphi_\Theta = \frac{f_5}{-f_6}. \end{aligned} \tag{4.89}$$

Analogously, it can be shown that  $\sigma_y$  at the base is given by

$$\begin{aligned} \left. \frac{\sigma_y}{\sigma_y^{(0)}} \right|_b &= 1 + \varepsilon \Sigma \cos (\omega x - \varphi_\Sigma), \\ \Sigma &:= \frac{\omega^2 \sqrt{f_1^2 + f_2^2}}{\cos \gamma + \bar{p}}, \quad \tan \varphi_\Sigma = \frac{f_2}{f_1}. \end{aligned} \tag{4.90}$$

The stress amplitudes  $\Theta$  and  $\Sigma$  and the phase angles  $\varphi_\Theta$  and  $\varphi_\Sigma$  depend on the wavelength  $\lambda$ , the mean inclination angle  $\gamma$ , the sliding law, and the atmospheric pressure  $\bar{p}$ , but  $\bar{p}$  is negligible in comparison to  $\cos \gamma$ . In order to compare the sliding laws already used, we shall choose in the subsequent comparison, the (zeroth order) sliding velocity and evaluate  $\mathbb{C}$  by means of the formula  $\bar{u}^{(0)} = \mathbb{C} \sin^m \gamma$  with  $m = (n + 1)/2$ .

The functions  $\Theta$  and  $\Sigma$  are indicators for the significance of the effect of longitudinal strains upon the basal shear and for the limitations of the applied mathematical approach therein. In order that the perturbation procedure is a valid one, they must be  $O(1)$ , with one exception, however. It is seen from (4.89) that  $\Theta$  will become large as  $\gamma \rightarrow 0$ . This singularity occurs because of the normalization used in Formula (4.89). It is obvious that for  $\gamma$  small  $\tau_b^{(0)}$  is small and so is  $\varepsilon\tau_b^{(1)}$ , yet  $\tau_b^{(1)}$  is finite. The singularity associated with  $\Theta$  as  $\gamma \rightarrow 0$  is therefore spurious.

Figure 4.13a shows the shear stress amplitude  $\Theta$  plotted against wavelength  $\lambda$  and parameterized for various values of  $\gamma$ . No-slip is assumed to occur at the base and results are presented for the cases that the ice temperature is constant throughout (dashed) or else varies according to formula (4.87) [for numerical values of the surface and basal temperature, see the text immediately below (4.87)]. It is clearly seen that perturbation amplitudes for the basal shear stresses grow with decreasing wavelengths; they are generally larger the smaller  $\gamma$ . This is no surprise and can be traced to the  $\sin \gamma$  term appearing in the denominator of (4.89)<sub>2</sub>. The other singularity of  $\Theta$  as  $\lambda$  becomes small is, however, real. Perturbation stresses become infinitely large as  $\lambda \rightarrow 0$ . It follows, therefore, that the perturbation solution must break down for wavelengths  $\lambda$  of the order of the glacier thickness and smaller. The exact value of  $\lambda$  where this occurs depends very strongly on temperature. Indeed, Figure 4.13a also contains results for a cold glacier with a variable temperature (solid lines). Evidently, first-order basal shear stresses are drastically reduced by transverse temperature variations. Figure 4.13a gives also indications as to the validity of the 'classical' formula  $t_{xy}^b = \rho g D \gamma$ . If the bottom undulations are small ( $\varepsilon \ll 1$ ), first-order corrections may be negligible at large wavelengths, but certainly not for small ones. For cold ice and again  $\varepsilon \ll 1$  the simple formula is generally valid for small

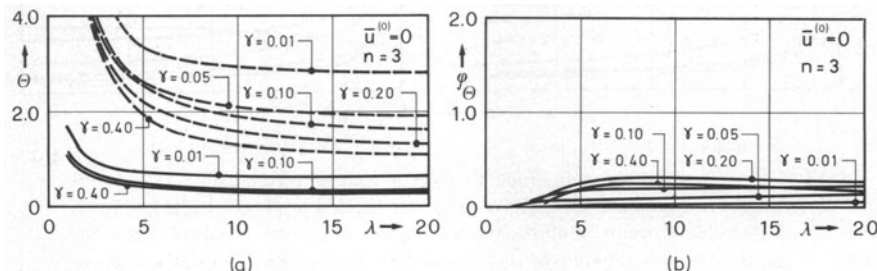


FIG. 4.13. Shear-stress amplitude  $\Theta$  and corresponding phase angle  $\varphi_\Theta$  plotted against wavelength  $\lambda = 2\pi/\omega$  for several inclination angles  $\gamma$ . The exponent in the flow law is  $n = 3$  with  $\varepsilon = 10^{-3}$  and the boundary condition at the base is no slip. Figure 4.13a shows the shear-stress amplitude when the transverse temperature distribution is as described in the text (solid lines) and for temperate ice (dashed). Figure 4.13b displays the phase-lag angle for cold ice.

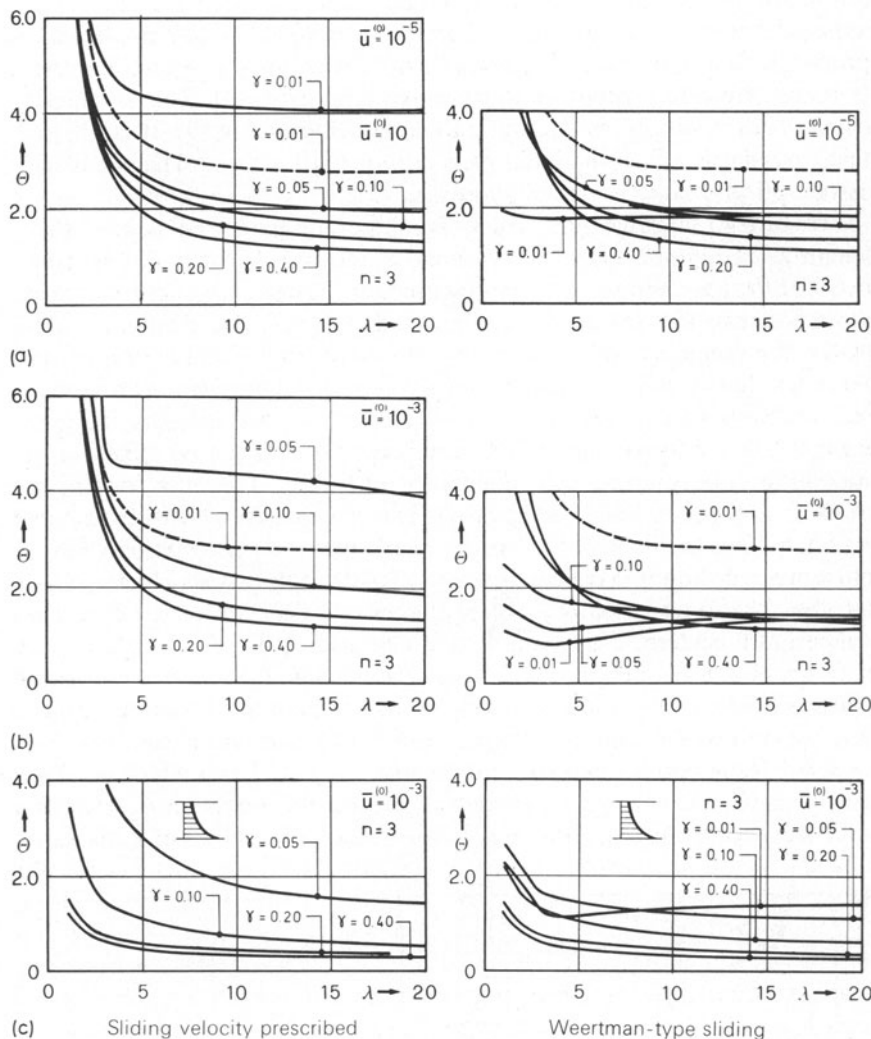


FIG. 4.14. Shear-stress amplitude  $\Theta$  plotted against wavelength  $\lambda = 2\pi/\omega$  for various inclination angles  $\gamma$ . The exponent in the flow law is  $n = 3$ , and  $k = 10^{-3}$ . Basal sliding occurs in all the figures. Figures on the left-hand side show the results when the sliding velocity is prescribed, those on the right give the corresponding results when a Weertman-type sliding law is applied. Figures 4.14a, b hold for temperate ice, Figures 4.14c when temperature varies across depth, as explained in the text following Formula (4.87). For comparison, the dashed lines in Figures 4.14a, b represent results for no-slip at the base. Notice the drastic differences in the results for the two sliding conditions.

wavelengths (down to  $\lambda \lesssim 1$ ) but not for temperate ice, see however, Figure 4.14. Figure 4.13b, which is valid for temperate ice, displays the phase angle  $\varphi_\Theta$ . It is small, in general, and results are insignificantly different for cold ice. Generally,  $\varphi_\Theta$  grows with growing  $\gamma$ , is zero for small  $\lambda$ , and approaches a constant value as  $\lambda$  becomes large.

It is interesting to compare the above results with corresponding results when basal sliding occurs. Figure 4.14 summarizes some of the corresponding results for the shear stress amplitude  $\Theta$ . Figures 4.14a and b show the results for a temperate ice sheet with  $\bar{u}^{(0)} = C \sin^m \gamma = 10^{-5}$  and  $10^{-3}$ , respectively. Figures 4.14c give the results for  $\bar{u}^{(0)} = 10^{-3}$  when the ice is cold and the temperature varies according to Formula (4.87). When compared with Figures 4.13a, the results in Figure 4.14 indicate that first-order basal shear stresses are enhanced by sliding when a sliding velocity is prescribed, but they are attenuated when the viscous sliding law is used. [Compare in Figures 4.14a the curves for  $\gamma = 0.01$ . For no-slip, they are also shown as dashed lines.] In other words, when sliding velocities are prescribed, first-order shear stress amplitudes  $\Theta$  grow faster with a decreasing inclination angle  $\gamma$  than they do for no-slip. When the viscous sliding law is used, the growth of  $\Theta$  with decreasing  $\gamma$  is not as pronounced as for the no-slip boundary condition. Consequently, as  $\lambda$  decreases and  $\Theta$  approaches the singularity (at small wavelengths),  $\Theta$  begins to raise at larger values of  $\lambda$  when a sliding velocity is prescribed than when the viscous sliding law is used. Hence, the domain of wavelengths for which our perturbation approach is valid is considerably larger for Weertman-type sliding than is the case for the other ‘sliding law’. *The correct application of a basal sliding law is therefore very crucial in the evaluation of first-order stresses.* Figures 4.14c, which are valid for  $\bar{u}_s^{(0)} = 10^{-3}$  further demonstrate that the effect of temperature variation on basal shear amounts to a considerable reduction of first-order stresses. Its significance is particularly apparent when the behavior of the curves for small  $\lambda$  is compared with that of Figures 4.14b.

Besides shear, the other significant stress component is  $\sigma_y$ . For no-slip, its first-order amplitudes  $\Sigma$  are plotted in Figure 4.15a for the two cases that the temperature is constant (dashed) and the temperature varies according to Formula (4.87). As expected, the influence of the temperature variation on the stress distribution is substantial. In both cases and for values of  $\lambda$  larger than roughly 5, a weak dependency of  $\Sigma$  on  $\lambda$  is detectable. Only at smaller wavelengths and relatively steep inclination angles  $\gamma$  can a stronger dependency on  $\lambda$  be observed. In particular, for wavelengths  $\lambda \approx 2$  and for all inclination angles  $\gamma$ ,  $\Sigma < 1$ . Yet for large values of  $\gamma$  and as  $\lambda \rightarrow 0$ , an onset of a singularity can be observed. Consequently, the sign of  $\sigma_y$ , for  $\varepsilon < 1$  and for most wavelengths, will be that of  $\sigma_y^{(0)}$  which is negative (pressure). The  $\sigma_y$ -singularity that develops as  $\lambda \rightarrow 0$  accompanies, of course, that of the shear stresses but for no-slip, the  $\tau$ -singularity seems to be more pro-

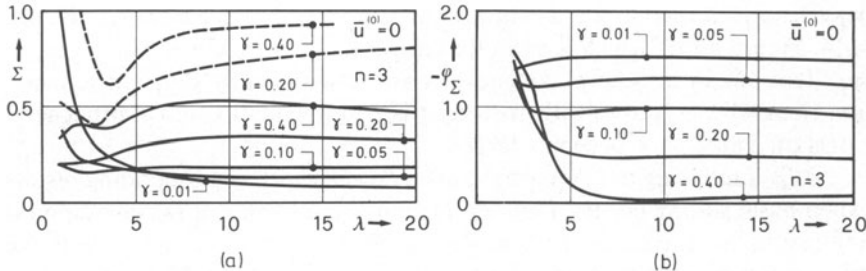


FIG. 4.15. First-order basal normal-stress amplitude  $\Sigma$  (Figure 4.15a) and corresponding phase angle (Figure 4.15b) plotted against wavelength  $\lambda = 2\pi/\omega$  for various values of the inclination angle  $\gamma$ . The flow-law parameters are  $n = 3$  and  $k = 10^{-3}$ . The boundary condition at the base is no-slip. The stress amplitudes are plotted for a temperate ice sheet (dashed) and cold ice (solid lines). Phase-lag angles are plotted only for cold ice because the differences for temperate ice are small.

nounced than that for  $\sigma_y$ . We shall see that this is different when sliding occurs. Figure 4.15b gives a plot for the phase lag angle  $\varphi_\Sigma$  for temperate ice; it is evident that  $\varphi_\Sigma$  chiefly depends on the mean inclination angle  $\gamma$ . In particular, for small values of  $\gamma$ ,  $\varphi_\Sigma$  is close to  $-\pi/2$ . For larger inclinations and for large wavelengths,  $\varphi_\Sigma$  increases and is close to zero, provided that  $\gamma \geq 0.4$ . At wavelengths of the order  $\lambda \sim 5$  and smaller  $\varphi_\Sigma$  depends more strongly on  $\lambda$  and all curves seem to converge to the value  $\varphi_\Sigma = -\pi/2$ . For cold ice, the behavior is qualitatively the same with less pronounced dependences of  $\varphi_\Sigma$  on  $\gamma$ .

Whereas first-order shear stress amplitudes  $\Theta$  react critically to the type of boundary condition applied at the base, this is not so for the normal stresses  $\sigma_y$ : results for  $\Sigma$  are reasonably insensitive to differences in boundary conditions. Figure 4.16 summarizes numerical results of the stress amplitude  $\Sigma$  for both boundary conditions and the same sliding velocities as used in Figure 4.14. The plots prove that with growing sliding velocity  $\bar{u}^{(0)}$ , the dependency of  $\Sigma$  on mean inclination angle  $\gamma$  becomes less and less; moreover, the singular behavior for small wavelengths, observed for the no-slip boundary condition only at large values of  $\gamma$  is now carried over to small  $\gamma$ 's. Astoundingly, at  $\bar{u}^{(0)} = 10^{-3}$  and for Weertman-type sliding (Figure 4.16b, right) no singularity could be observed to develop for  $\gamma = 0.40$ , but they did for  $\gamma < 0.40$ . On the other hand, for  $\bar{u}^{(0)} = 10^{-5}$  it is the other way around. Furthermore, the effect of temperature variation is to reduce  $\Sigma$  substantially (compare Figures 4.16b and c, which show results for  $\bar{u}^{(0)} = 10^{-3}$ ); singularities still develop as wavelengths become small. These singularities are stronger when sliding velocities are prescribed than when Weertman-type sliding is used, but how they develop depends on virtually all variables considered here and must be decided upon a case-by-case basis.

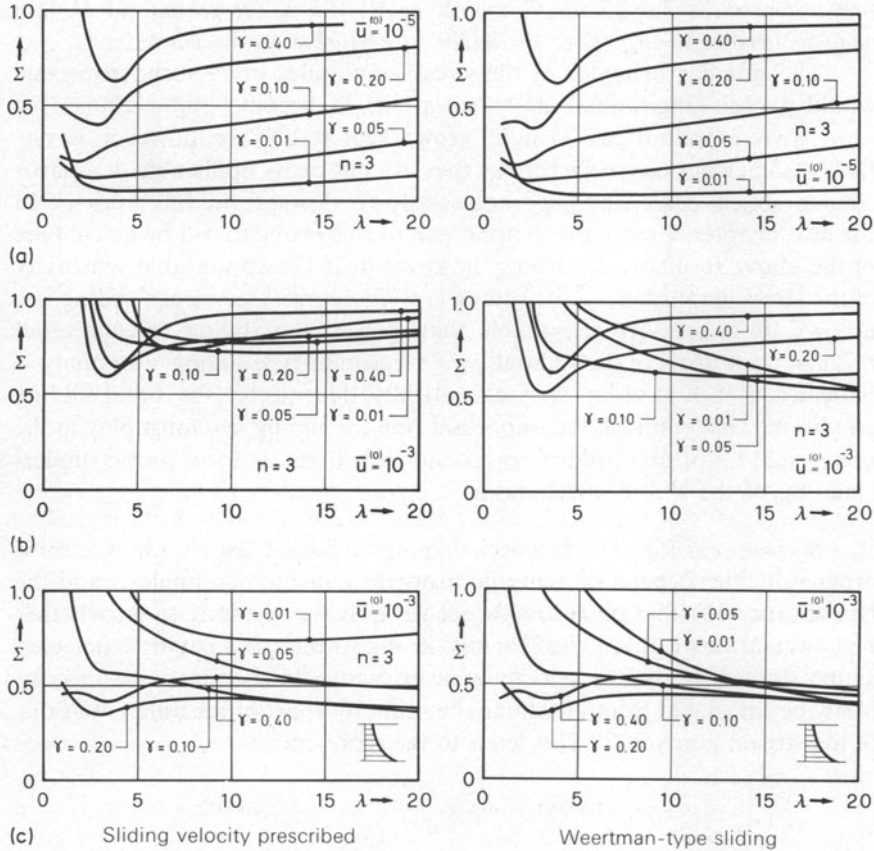


FIG. 4.16. First-order basal normal-stress amplitude  $\Sigma$  for overburden pressure  $\sigma_y$  plotted against wavelength  $\lambda = 2\pi/\omega$  for various values of the inclination angle  $\gamma$ . The flow law parameters are  $n = 3$  and  $k = 10^{-3}$ . The boundary condition at the base is sliding. Figures 4.16a, b hold for temperate ice, whereas Figures 4.16c hold for cold ice and a temperature distribution according to Formula (4.87). In the figures to the left, the sliding velocity is prescribed whereas in the figures on the right, a Weertman-type sliding velocity is applied.

In conclusion, we may summarize our findings as follows: *First-order basal stresses depend strongly on the temperature distribution across the ice sheet, on mean inclination angles  $\gamma$ , on undulation wavelengths  $\lambda$  and on the sliding law. Most significant are the dependencies on the sliding law and temperature. Temperature variation across depth diminishes first-order stress amplitudes. Of the two sliding laws, Weertman-type sliding generally leads to smaller first-order stresses at comparable sliding velocities, implying that the perturbation analysis remains valid for a wider range of wavelengths  $\lambda$  and inclination angles  $\gamma$  than is possible when sliding velocities are prescribed. At smaller wavelengths, generally for  $\lambda < 3$ , but occasionally also for  $\lambda < 1$ ,*

*first-order stress amplitudes  $\Theta$  and  $\Sigma$  grow with a decreasing wavelength and may become so large as to invalidate the perturbation procedure.*

The singular behavior of the stress amplitudes is no surprise, as one would expect longitudinal stress variations to become important as the ratio ‘wave amplitude/wavelength’ grows. Our results are, however, nevertheless somewhat unsatisfactory as they are not easily applicable in a particular practical case. One must necessarily go through the full analysis. In the next chapter, a more direct approach to this problem will be given. One of the above results is disturbing, however. It is the appreciable sensitivity of the stress amplitudes to the sliding law. Of course, the viscous sliding law  $\tilde{u}^{(0)} = C \sin^m \gamma$  is more reasonable than prescribing sliding velocities, yet this fact is no proof of the suitability of Weertman-type sliding. Our analysis indicates that first-order stresses critically depend on the basal sliding condition. This points at the important role the sliding law must play in the determination of first-order stresses and calls urgently for a proper understanding of the sliding mechanism.

( $\gamma$ ) *Surface velocities.* It has been demonstrated in Chapter 3 how zeroth-order velocities depend on material properties, inclination angles  $\gamma$  and the temperature distribution across the ice sheet. It is interesting to see whether bed undulations would be sufficiently strong so that they could be detected at the surface by surface velocity measurements. First-order velocities can easily be calculated from the stream function by appropriate differentiations of the stream function  $\Psi$ . This leads to the representation

$$\left. \frac{\tilde{u}^{(1)}}{\tilde{u}^{(0)}} \right|_{\text{surface}} = U_0 \cos(\omega x - \varphi_{U_0}), \quad \left. \frac{\tilde{v}^{(1)}}{\tilde{u}^{(0)}} \right|_{\text{surface}} = V_0 \cos(\omega x - \varphi_{V_0}),$$

where  $\tilde{u}^{(0)}$  is the zeroth-order surface velocity. Clearly, as was the case for the previous quantities,  $U_0$ ,  $V_0$  and the corresponding phase lag angles  $\varphi_{U_0}$  and  $\varphi_{V_0}$  will depend on basal boundary conditions, temperature distribution, mean inclination angle, and material response. Results will only be shown for the generalized Glen flow law (4.28) with  $n = 3$  and  $k = 10^{-3}$  since for  $n = 2$  ( $k = 10^{-2}$ ) first-order surface velocities behave qualitatively alike and differ quantitatively only marginally. Figures 4.17a, b give plots for  $U_0$ ,  $V_0$ , for both a temperate (dashed) and cold ice sheet at no-slip. A strong dependency of  $U_0$  and  $V_0$  on temperature distribution can be observed, as first-order velocity amplitudes are, by a factor of 2 to 3, smaller for cold ice than they are for temperate ice. Very roughly, the longitudinal velocity amplitudes  $U_0$  grow with a growing wavelength, and they get larger, the smaller the inclination angles  $\gamma$ . For small wavelengths, they tend to zero. Since for small  $\gamma$   $U_0 = O(1)$  it is the bottom protuberance amplitude  $\epsilon$  which indicates whether first-order velocity corrections should be accounted for. First-order transverse velocity amplitudes  $V_0$  are shown in Figure 4.17b;

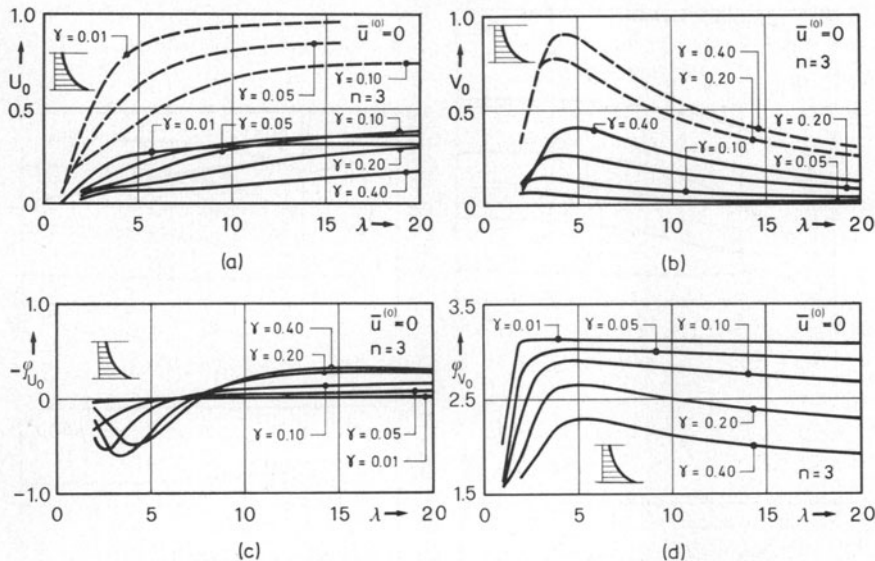


FIG. 4.17. First order amplitudes  $U_0$  and  $V_0$  and corresponding phase lag angles  $\varphi_{U_0}$  and  $\varphi_{V_0}$  for the streamwise and the transverse surface velocity plotted against wavelength  $\lambda = 2\pi/\omega$  for various values of the inclination angle  $\gamma$ . The flow law parameters are  $n = 3$  and  $k = 10^{-3}$ , and the boundary condition at the base is no slip. The solid curves are for cold ice with temperature variation according to Formula (4.87) and as described in the text. Dashed curves are for temperate ice.

accordingly, there exists a distinct wavelength  $\lambda$ , which depends on the mean inclination for which  $V_0$  is a maximum. Moreover,  $V_0$  is  $\mathcal{O}(1)$  for large  $\gamma$  but becomes negligibly small for small  $\gamma$ .

Phase lag angles  $\varphi_{U_0}$  and  $\varphi_{V_0}$  (for cold ice only) are displayed in Figures 4.17c and d.  $\varphi_{U_0}$  undulates, it is positive at moderate wavelengths and negative at larger ones. For small  $\gamma$ ,  $\varphi_{U_0}$  is nearly zero, so that the bottom protuberances and longitudinal surface velocities are nearly in phase in this case. For most wavelengths, on the other hand,  $\varphi_{V_0}$  which is illustrated in Figure 4.17d is fairly independent of the wavelength, but shows a clear dependence on  $\gamma$ . For small inclination angles and  $\lambda \gtrsim 2.5$  bottom protuberances and transverse surface velocities are out of phase.

What are the changes drawn upon the above results when basal sliding is introduced? For longitudinal surface velocity and when basal sliding velocity is prescribed, these changes may be large; but for Weertman-type sliding, they are generally small. Figure 4.18 should provide sufficient corroboration of this statement. It shows the first-order longitudinal surface velocity amplitude  $U_0$  in a temperate ice sheet for various different prescribed basal sliding velocities. These vary between  $10^{-4}$  and  $5 \times 10^{-3}$ , and

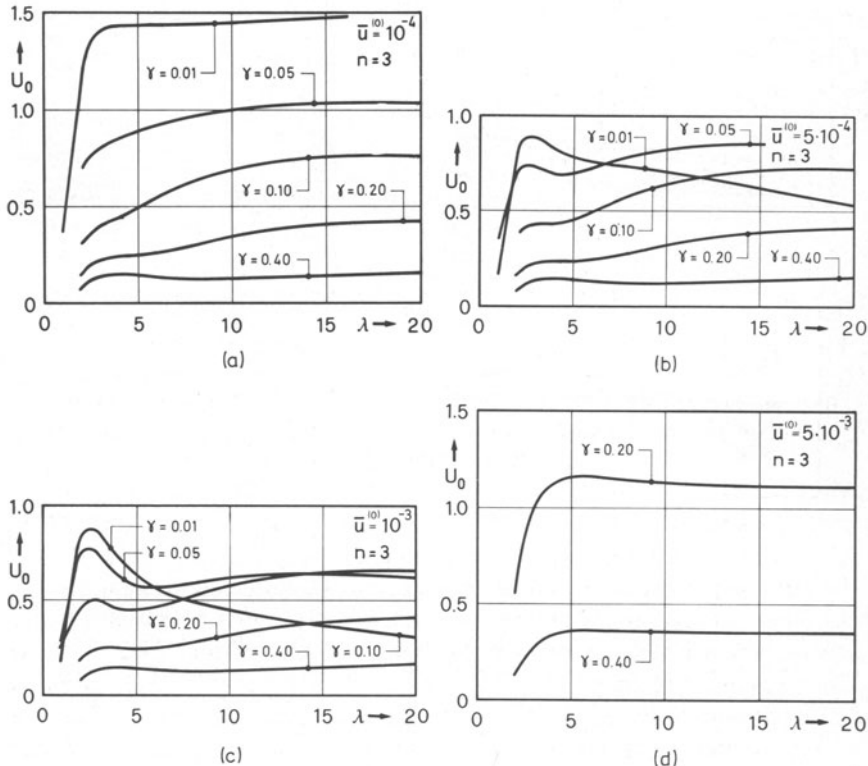


FIG. 4.18. First-order amplitudes  $U_0$  of the streamwise surface velocity plotted against wavelength  $\lambda = 2\pi/\omega$  for various values of the inclination angle  $\gamma$ . The flow law parameters are  $n = 3$  and  $\bar{u}^{(0)} = 10^{-3}$  and basal sliding is permitted. The curves are valid for temperate ice and basal velocities are between  $\bar{u}^{(0)} = 10^{-4}$  and  $5 \times 10^{-3}$ . Basal sliding is prescribed in all four figures. Streamwise velocity is of an oscillatory type and heavily depends on the basal sliding velocity. Results for a Weertman-type sliding law do not show this oscillatory character as results are persistently of the type shown in Figures 4.18b, c.

they grow from Figure 4.18a to d. Results of Figures 4.18a and d are distinctly different from those of Figures 4.18b and c. Evidently an oscillatory-type behavior of the first-order longitudinal velocity seems to occur;  $\bar{u}^{(0)} = 10^{-4}$  and  $\bar{u}^{(0)} = 5 \times 10^{-4}$  are apparently conditions for which the ice sheet reacts critically. For small inclination angles  $U_0$  becomes large. (In Figure 4.18d these curves are not even shown because they lie outside the scale of the figure.) For intermediate velocities  $\bar{u}^{(0)} = 5 \times 10^{-4}$  and  $\bar{u}^{(0)} = 10^{-3}$ , the behavior is drastically different as the motion seems to remain stable under all conditions, which is contrary to the behavior for a Weertman-type condition! For the latter,  $U_0$  remains  $\mathcal{O}(1)$  or smaller for all investigated inclination angles  $0.01 \leq \gamma \leq 0.4$ . When sliding velocities increase, there is a

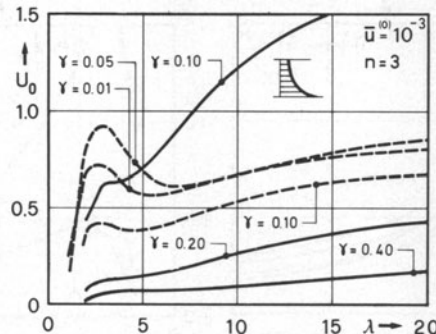


FIG. 4.19. First-order longitudinal surface velocity amplitudes as a function of  $\lambda$  and  $\gamma$ . Shown are the results for  $\bar{u} = 10^{-3}$  and a temperature distribution according to Equation (4.87). As a comparison, results are also shown for constant temperature distributions (dashed). The parameters in the flow law are  $n = 3$ ,  $\bar{u}_s = 10^{-3}$ , and Weertman-type sliding was used.

smooth transition in this case from the behavior for no-slip to that shown in Figure 4.18c, with no indication of an oscillatory type of motion. In fact  $U_0$ -versus- $\lambda$  plots look very much like Figures 4.18b, c.

It thus looks as if an onset of a possible fluid-flow instability would develop according to what boundary conditions are applied at the base. This phenomenon may, when pursued, lead to a possible explanation of the formation of a surge. The problem warrants further study. That the viscous sliding law is not as disappointing in this regard as may be implied from the above can be seen when calculations are repeated for cold ice and when temperature variations are taken into account. Proof for this is given in Figure 4.19 which shows plots of  $U_0$  for Weertman-type sliding,  $\bar{u}_s^{(0)} = 5 \times 10^{-3}$  and both cold (solid lines) and temperate ice (dashed lines). Temperature dependency has evidently led to a certain destabilization of the flow. Whether this will lead to a true fluid flow instability remains to be proved, however.

Interestingly, the transverse surface velocity is insensitive to the form of the boundary conditions at the bottom. But sliding velocity does affect the size and the wavelength behavior of  $V_0$  and its phase. As was already the case for  $U_0$ , temperature variations enhance the values of  $V_0$  and thus contribute also in the transverse velocity undulations to an onset of destabilization of the flow. Figure 4.20 shows a plot of  $V_0$  for temperate (Figure 4.20a) and cold ice (Figure 4.20b).

The above findings can, perhaps, be summarized as follows: *First-order corrections of surface velocities due to small bed undulations react critically to basal boundary conditions and to transverse temperature variations. For no-slip at the bed the first-order surface velocity amplitudes  $U_0$  and  $V_0$  are  $\mathcal{O}(1)$  and temperature variation leads to a reduction by a factor of two to*

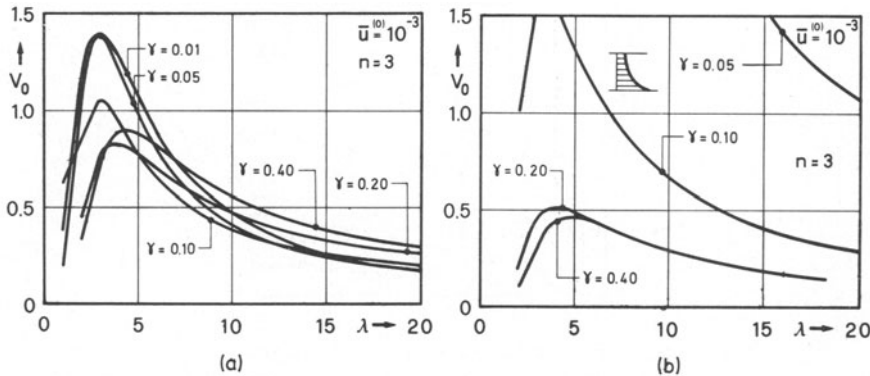


FIG. 4.20. First-order amplitude  $V_0$  for the transverse surface velocity plotted against wavelength  $\lambda = 2\pi/\omega$  for various values of the inclination angle  $\gamma$ . The flow law parameters are  $n = 3$  and  $\bar{u} = 10^{-3}$  and Weertman-type sliding is applied. The results in Figure 4.20a hold for temperate ice, those in Figure 4.20b for cold ice and a temperature distribution as given by Formula (4.87) and described in the text.

three. When sliding occurs,  $U_0$  and  $V_0$  behave according to the sliding law applied; for temperate ice and Weertman-type sliding  $U_0$  and  $V_0$  are of  $\mathcal{O}(1)$  but when sliding velocities are prescribed,  $U_0$  and  $V_0$  may become large depending on the mean inclination and sliding velocity. Sliding and temperature variations together generally destabilize\* the flow. In other words, for both sliding laws temperature variations generally enhance  $U_0$  and  $V_0$ . Large sliding velocities and small inclination angles  $\gamma$  will generally lead to very large values of  $U_0$  and  $V_0$ , occasionally invalidating the perturbation scheme. This points at the importance of a fluid flow instability analysis of surface waves travelling down glacier for the conditions that have demonstrated considerable growth of surface velocity amplitudes. A first attempt to such a stability analysis will be made in Section 5.

(δ) *Effect of a steady accumulation rate.* In Section 3b (δ) it was shown in what sense a steady but spatially-variable accumulation rate can be accounted for; it was further indicated how explicit analytical solutions could be constructed. Calculations were performed for a sinusoidal variation of the accumulation rate function. This harmonic variation can be regarded as one particular term in a general Fourier development. We thus choose

$$\mathfrak{A} = -A_0 \sin \omega \bar{x}, \quad \text{where } A_0 = \omega \bar{u}_S^{(0)}.$$

It then follows from (4.36)<sub>2</sub> that  $\bar{y}_S^a = H \cos \omega \bar{x}$  with  $H = 1$ . The real ampli-

\*The word 'destabilization' should be taken with care in this context. It does not mean here that the fluid flow must necessarily become unstable. It simply means that velocities become large. Stability or instability of the flow has still to be proved.

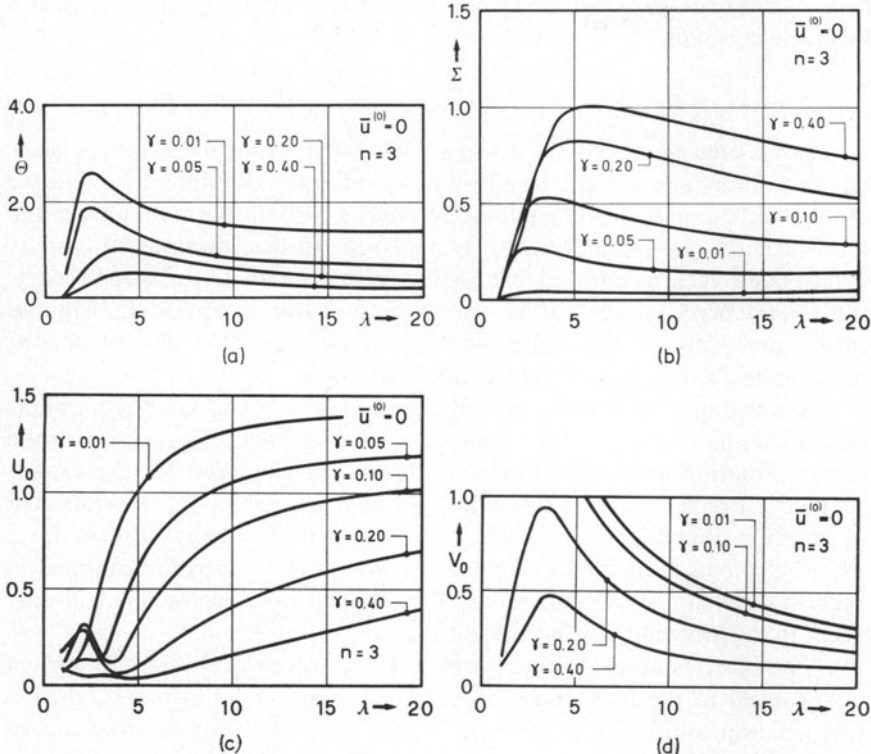


FIG. 4.21. First-order stress and surface-velocity amplitudes for accumulation with amplitude  $A_0 = \omega \bar{u}_S^{(0)}$  plotted against wavelength  $\lambda = 2\pi/\omega$  for various values of the inclination angle  $\gamma$ . The flow law parameters are  $n = 3$  and  $k = 10^{-3}$ , and calculations have been performed for no-slip at the base and for temperate ice.

tude  $H_{\text{real}}$  can be obtained from real accumulation amplitudes  $A_{\text{real}}$  according to

$$H_{\text{real}} = \frac{A_{\text{real}} \lambda}{2\pi \bar{u}_S^{(0)}}.$$

Depending upon the values of  $A_{\text{real}}$ , the wavelengths (which are of the order of  $10^0$ – $10^2$ ) and the zeroth-order surface velocities,  $H_{\text{real}}$  may assume values as large as  $\mathcal{O}(1)$ . Calculations for  $H = 1$  thus lead to realistic results. Figure 4.21 displays first-order amplitudes for basal stresses and surface velocities. Calculations were performed for no-slip and constant temperature. These results demonstrate that the effect of the accumulation rate on both basal stresses and surface velocities may be sufficiently large to have a non-negligible effect on these quantities. This is particularly so when accumula-

tion is large over large distances and surface velocities are small. This should be borne in mind.

#### 4. Remarks on Response to a Time-dependent Accumulation Rate

In the preceding analysis, it was assumed that the ice sheet or the glacier is under time-independent steady-state conditions. To find the influence of the rockbed on the surface geometry such an assumption is no restriction, but when the accumulation rate is analysed, surface motions cannot be investigated. It turns out that, within the realm of small perturbation theory, the time-dependent analysis is only slightly more complicated than the steady problems; in particular, no further non-linearities are introduced by including a time-dependent accumulation rate.

A scrutiny of the governing field equations (4.1) and boundary conditions (4.3) and (4.4) shows that time derivatives explicitly occur only in the energy equation and in the kinematic boundary condition for the surface geometry. For temperate glaciers and for cold glaciers under the restricted assumption that the temperature distribution is negligibly affected by a time-dependent accumulation rate, the approximate procedure outlined in Section 3 remains essentially valid, since explicit time derivatives will only occur in the kinematic surface condition.

The basic boundary-value problem to be solved in this case is system (4.1) subject to the boundary conditions (4.3) and (4.4). Assuming, then, a perturbation solution of the form (4.10), in which the temperature is steady, an approach identical to that presented in Section 2 will lead to the same zeroth-order boundary-value problem as before. This zeroth-order problem is time-independent, and its solution is given in Section 3a. The first-order boundary value problem, on the other hand, yields as field equations the relations (4.12), which subsequently were simplified by introducing stress and stream functions. The boundary conditions at the lower surface also remain the same as do those on the free surface, except for the kinematic boundary condition (4.20)<sub>1</sub>, which now contains a time-dependent term. Summarizing, the first-order stress-velocity boundary value problem is described by the differential equations (4.31), (4.32), the boundary conditions at the base (4.34) or (4.35) and those at the mean free surface (4.33), except that Equation (4.33)<sub>1</sub> is to be replaced by

$$\frac{\partial \bar{y}_S^{(0)}}{\partial \bar{t}} + \bar{u}^{(0)} \frac{\partial \bar{y}_S^{(1)}}{\partial \bar{x}} + \frac{\partial \Psi}{\partial \bar{x}} = \mathfrak{A}(\bar{x}, \bar{t}). \quad (4.91)$$

There are various solution techniques that can be used to solve the boundary-value problem. A harmonic analysis, in which the accumulation rate function is expanded in a double Fourier series with the terms

$$\mathfrak{A}(\bar{x}, \bar{t}) = H \cos(\omega_x \bar{x}) \cos(\omega_t \bar{t}) \quad (4.92)$$

may be appropriate to study periodic processes in space and time. The expansions (4.92) have the further advantage that the integration methods used and tested in Section 3 may be applied. The functions  $\Phi$ ,  $\Psi$  and  $y_S^{(1)}$  are now developed in the form (compare Equations 4.40))

$$\begin{aligned}\Phi = & \{\Phi_1^1 \cos \omega_x \bar{x} + \Phi_2^1 \sin \omega_x \bar{x}\} \cos \omega_t \bar{t} + \\ & + \{\Phi_1^2 \cos \omega_x \bar{x} + \Phi_2^2 \sin \omega_x \bar{x}\} \sin \omega_t \bar{t},\end{aligned}\quad (4.93)$$

with similar expressions for  $\Psi$  and  $y_S^{(1)}$  where  $\Phi_i^j$  ( $i, j = 1, 2$ ) are functions of the variable  $\bar{y}$  only. Proceeding as in Section 3, a two-point boundary-value problem for the coefficient functions  $\Phi_i^j$ , etc. can then be deduced which is entirely analogous to that formulated in Section 3. We shall not demonstrate its derivation here, mainly because explicit calculations based on this system of equations have not been conducted so far. This points at the possibility of further research. On the other hand, such calculations are rather cumbersome and call for a simpler method of determination of stress and velocity for time-dependent processes. Such a simplified analysis can, indeed, be performed, but it hinges on the further assumption that wavelengths of undulations at the base and free surface are large when compared with the thickness of the ice. This is the so-called *shallow ice approximation* which we shall consider in more detail in Chapter 5.

A variant of the above procedure can be developed for the problem of surface waves travelling down glacier. Such surface waves have been treated earlier by Nye using the theory of kinematic waves. Lick [28] and Bind-schadler [5] incorporate large amplitudes for surface elevation. Hutter [24], on the other hand, and Fowler and Larson [22] use the shallow ice approximation to derive two different models for long-wavelength surface elevations. The equations in Section 3 may, however, also be used in yet another model of propagation of surface waves. Such a model essentially corresponds to that of Thompson [49] and is valid for undulation wavelengths of the order of the ice thickness and larger. The following section will give a brief outline of his work.

### 5. Surface-wave Stability Analysis

Many glaciers exhibit short-term flow irregularities. These fluctuations are caused by either sudden changes in the accumulation rate or non-uniformities in the shearing motion in the ice which may be caused by the formation of crevasses or sudden changes in water pressure due to the release of trapped water. Such stress irregularities initiate surface wave. The propagation of such waves has been observed and recorded in the field. For instance, Lliboutry [30] reports changes of mean surface elevation of Mer de Glace in France, and Finsterwalder [21] on the Glacier de Bosson.

Ordinarily, speeds of surface bulges down glacier are in the order of two

to four times the surface-particle speed, yet some glaciers may frequently *surge*. Surging speeds are very much higher than speeds when glacier is in its intermittent phase of relative quietness. This period may last several tens of years. During surge, which ordinarily lasts one to two years, the glacier advances several hundreds of meters, and the fast motion of the ice that is required to produce this advance leads to a high-density of crevass formation. The onset of the surge is still not understood and thus unpredictable, as is a physical explanation of the phenomenon as such.

Nevertheless, there are currently three different explanations offered to explain the origin of glacier surging, namely (i) that the surge arises as a result of wide-spread lubrication of the glacier along its base from a thickening water film (Weertman [50], Robin and Weertman [45], Budd and McInnes [14]), (ii) that a softening of basal ice from geothermal heat flux could allow surging in subpolar glaciers (Robin [44], Clarke [15]), and (iii) that changes in longitudinal stress gradients might allow a change from compressive to extending flow [Robin [44]]. According to Thompson [49], none of these theories adequately explain the erratic behavior of surging glaciers. He favors the idea that a surge might be an inherent flow instability so that at least the onset of the surge, but not the phenomenon itself, should be predictable from a fluid flow stability analysis.

Classical stability analyses of Newtonian viscous fluids (Lin [29], Yih [54]) aim at a description of the laminar-turbulent transition phenomenon. Inertial effects play an important role thereby; all the more they are chiefly responsible for fluid instabilities. Inertial forces in glaciers being negligibly small, any natural flow instability must be expected, due primarily to the non-linearity in the flow law, and must arise from a change in the stress state which alters the ‘effective viscosity profile’ in a destabilizing sense. It will be seen that small amplitude surface waves are linearly stable under the restricted assumptions that the temperature is constant across depth and there is no-slip at the bedrock. This does not imply that fluid instability analysis would, in general, fail to explain the onset of surge-type phenomena; nor does the analysis become meaningless because of this failure. Rather, it is designed to produce guidelines for further, more complicated or more realistic problems.

In methodology, the analysis proceeds along the classical approaches of the stability of viscous fluids down an inclined plane (see for example, Benney [4], Benjamin [3], Yih [52, 53, 55] and Craik and Smith [19]).

#### *(a) The eigenvalue problem*

To develop the linearized stability equations, we start from the time-dependent boundary-value problem stated in Sections 3 and 4 [these are Equations (4.31)–(4.35) with the kinematic boundary condition (4.33), as replaced by (4.91)]. These equations hold for the perturbation flow about

the steady strictly parallel-sided slab with no bottom undulations, and unknown field quantities are the perturbation stress and stream functions and the surface elevation. We assume plane wave solutions of the form

$$\begin{aligned}\Phi &= \hat{\Phi}(\bar{y})\delta \exp(i\alpha(\bar{x} - c\bar{t})), \\ \Psi &= \hat{\Psi}(\bar{y})\delta \exp(i\alpha(\bar{x} - c\bar{t})), \\ \bar{y}_S^{(i)} &= \delta \exp(i\alpha(\bar{x} - c\bar{t})),\end{aligned}\quad (4.94)$$

where  $\delta$  is the maximum amplitude of the surface elevation, small compared to unity, and  $\alpha$  is the *dimensionless wavenumber*  $2\pi/\lambda$ .<sup>\*</sup> For large perturbation wavelengths  $\lambda$ ,  $\alpha$  will be small and hence  $\partial\bar{y}_S^{(i)}/\partial\bar{x}$  will also be small. The complex quantity  $c = c_r + ic_i$  is called *phase speed*. Its real part  $c_r$  is the speed at which a single wavelet propagates in the  $\bar{x}$  direction; the imaginary part  $c_i$  is a measure of the growth or decay of the disturbance with time. Attenuation or amplification occurs according to whether  $\alpha c_i$  is negative or positive.

Substituting the representations (4.94) into the mentioned equations with a zero accumulation rate results in the eigenvalue problem for the eigenvalue  $c$ . The corresponding equations are:

*Field equations:*

$$\begin{aligned}i\alpha\hat{\Psi}' &= f(\bar{y})[\alpha^2\hat{\Phi} + \hat{\Phi}''], \\ i\alpha\hat{\Phi}' &= -\frac{1}{g(\bar{y})}[\alpha^2\hat{\Psi} + \hat{\Psi}''],\end{aligned}\quad (4.95)$$

where primes denote derivatives with respect to  $\bar{y}$ .

*Boundary conditions:* At  $\bar{y} = 0$ : When the viscous sliding law is used:

$$\hat{\Psi}' - i\alpha Cm \sin^{m-1} \gamma \hat{\Phi}' = 0, \quad \hat{\Psi} = 0, \quad \text{at } \bar{y} = 0. \quad (4.96a)$$

and when sliding velocities are prescribed

$$\hat{\Psi}' = \hat{\Psi} = 0, \quad \text{at } \bar{y} = 0. \quad (4.96b)$$

At  $\bar{y} = 1$ :

$$(c - 1)\hat{\Psi} - \bar{u}_S^{(0)} = 0, \quad -\alpha^2\hat{\Phi} + \cos \gamma = 0, \quad -i\alpha\hat{\Phi} - \sin \gamma = 0. \quad (4.97)$$

Notice that the surface-wave amplitude  $\delta$  has disappeared from the boundary-value problem (4.95)–(4.97). This is so because  $\delta$  was introduced in (4.94) as a common factor which has cancelled out in Equations (4.95)–(4.97). This implies that trivial solutions are excluded, and it led to the inhomogeneous boundary conditions (4.97) which otherwise would be homogeneous, as are the remaining equations (4.95) (4.96). This approach makes the surface-wave amplitude the undetermined parameter of the eigenvalue problem (4.95)–(4.97). The complex valued functions  $\hat{\Phi}$  and  $\hat{\Psi}$  are determined from the above

\*We write  $\delta$  instead of  $\varepsilon$  to differentiate this case from that treated previously; yet  $\delta$  plays the same role as  $\varepsilon$  did in the previous analysis.

equations by integrating Equations (4.95) subject to the boundary conditions (4.96) and (4.97). In general, since the Equations (4.95) are two second-order differential equations, but there are five boundary conditions in (4.96) and (4.97), the boundary-value problem possesses no solution unless, of course,  $c$  assumes for a given wavenumber  $\alpha$  a particular specific value. This value of  $c$  is called the eigenvalue and the functions  $\hat{\Phi}$  and  $\hat{\Psi}$  corresponding to it are called the *eigenfunctions* of the problem.

The integration of the differential equations (4.95) has to be performed for both the real and imaginary parts of  $\hat{\Phi}$  and  $\hat{\Psi}$ ; Equations (4.95) therefore, constitute four real equations of second order. It is not difficult to see that these equations are coupled and must therefore simultaneously be integrated. It turns out, on the other hand, that real and imaginary parts separate when the differential Equations (4.95) are reduced to a fourth-order equation in only one unknown. Selecting the stream function  $\hat{\Psi}$  as a basic variable, this fourth-order equation reads

$$a_5(\bar{y})\hat{\Psi}^{IV} + a_4(\bar{y})\hat{\Psi}''' + a_3(\bar{y})\hat{\Psi}'' + a_2(\bar{y})\hat{\Psi}' + a_1(\bar{y})\hat{\Psi} = 0. \quad (4.98)$$

where the coefficients  $a(\bar{y})$  are given by the expressions:

$$\begin{aligned} a_5(\bar{y}) &= g^2, \\ a_4(\bar{y}) &= -(g^2)' = -2g'g, \\ a_3(\bar{y}) &= \alpha^2 \left( 2 - \frac{g}{f} \right) g^2 + (2g'^2 - g''g), \\ a_2(\bar{y}) &= \alpha^2 \left( \frac{g^3 f'}{f^2} - 2g'g \right), \\ a_1(\bar{y}) &= \alpha^4 g^2 + \alpha^2 (2g'^2 - gg''). \end{aligned} \quad (4.99)$$

Because all coefficients in Equation (4.98) are real, the differential equations for the real and imaginary parts of  $\hat{\Psi}$  are the same equations. Furthermore, for a Newtonian fluid,  $g = 2$ ,  $f = \frac{1}{2}$ , (4.98) reduced to

$$\hat{\Psi}^{IV} - 2\alpha^2 \hat{\Psi}'' + \alpha^4 \hat{\Psi} = 0, \quad (4.100)$$

which could equally also be obtained from the equation  $\nabla^4 \Psi = 0$  by substituting the representation (4.94)<sub>2</sub>.\*

The boundary conditions that must fall on  $\hat{\Psi}$  are obtained from Equations (4.96) and (4.97) upon elimination of  $\hat{\Phi}$ . These read:

*At  $\bar{y} = 0$ :* For the viscous sliding law

$$mC \sin^{m-1} \gamma \hat{\Psi}'' + g \hat{\Psi}' = 0, \quad \hat{\Psi} = 0, \quad (4.101a)$$

\*Incidentally, the equation corresponding to (4.100) in the stability analysis of viscous Newtonian fluids is the so-called Orr–Sommerfeld equation. It reduces to (4.100) when neglecting terms corresponding to inertial forces, see Lin [29].

but

$$\hat{\Psi}' = \hat{\Psi} = 0 \quad (4.101b)$$

when sliding velocities are prescribed.

At  $\bar{y} = 1$ :

$$(c - 1)\hat{\Psi} - \bar{u}_S^{(0)} = 0, \\ \frac{g'}{g^2}\hat{\Psi} + \left(\frac{1}{f} - \frac{1}{g}\right)\hat{\Psi}' + \frac{g'}{x^2 g^2}\hat{\Psi}'' - \frac{1}{x^2 g}\hat{\Psi}''' + \frac{i}{x}\cos\gamma = 0, \quad (4.102) \\ \frac{g'}{g^2}\hat{\Psi} + \left(\frac{1}{f} - \frac{1}{g}\right)\hat{\Psi}' + \frac{g'}{x^2 g^2}\hat{\Psi}'' - \frac{1}{x^2 g}\hat{\Psi}''' - \sin\gamma = 0.$$

These equations may easily be decomposed into real and imaginary parts. When this is done, it is seen that the coupling of the functions  $\hat{\Psi}_r$  and  $\hat{\Psi}_i$  only occurs at the mean free surface  $\bar{y} = 1$ . This fact may constructively be used in the determination of the eigenfunctions  $\hat{\Psi}_r$  and  $\hat{\Psi}_i$ .

In general, four different complementary solutions must be derived from Equation (4.98), and the general solution  $\hat{\Psi}(\bar{y})$  is obtained as the linear combination

$$\hat{\Psi}(\bar{y}) = \sum_{j=1}^4 k_j \hat{\Psi}^{(j)}(\bar{y}) \quad (4.103)$$

of the four independent solutions. Once these four independent solutions are determined over the range  $0 \leq \bar{y} \leq 1$ , the constants  $k_j$  are found from a substitution of expression (4.103) into (4.101) and (4.102). What results from such a substitution is a linear system of five equations with complex coefficients for the five unknowns  $c$  and  $k_j$ . Because the eigenvalue  $c$  occurs only in one equation, the constants  $k_j$  are sought first using Equations (4.101) and (4.102)<sub>2,3</sub>. The eigenvalue  $c$  follows then from Equation (4.102)<sub>1</sub> as an *a posteriori* information.

We turn now to the determination of the solutions  $\hat{\Psi}^{(j)}$  from Equation (4.98). To this end, Equation (4.98) is transformed to a first-order system by introducing the four-dimensional vector

$$\boldsymbol{\psi} = (\hat{\Psi}, g(0)\hat{\Psi}' + mC \sin^{m-1} \gamma \hat{\Psi}'', \hat{\Psi}'', \hat{\Psi}''')^T \\ = (\psi_1, \psi_2, \psi_3, \psi_4)^T \quad (4.104)$$

It is straightforward, then, to show that (4.98) corresponds to the vector differential equation

$$\frac{d\boldsymbol{\psi}}{d\bar{y}} = \mathcal{A}(\bar{y})\boldsymbol{\psi} \quad (4.105)$$

where the  $4 \times 4$  matrix  $\mathcal{A}$  is given by

$$\mathcal{A} = \begin{bmatrix} 0 & \frac{1}{g(0)} & -\frac{m\mathcal{C} \sin^{m-1} \gamma}{g(0)} & 0 \\ 0 & 0 & g(0) & m\mathcal{C} \sin^{m-1} \gamma \\ 0 & 0 & 0 & 1 \\ -\frac{a_1}{a_5} & \frac{-a_2}{g(0)a_5} & \frac{1}{a_5} \left( \frac{m\mathcal{C} \sin^{m-1} \gamma}{g(0)} a_2 - a_3 \right) & -\frac{a_4}{a_5} \end{bmatrix}. \quad (4.106)$$

The vector differential equation (4.105) is solved as an initial value problem for the four linearly-independent orthogonal vectors

$$\mathbf{f}_{(0)}^{(j)} = \begin{bmatrix} 1 \\ 0 \\ 0 \\ 0 \end{bmatrix}, \quad \begin{bmatrix} 0 \\ 1 \\ 0 \\ 0 \end{bmatrix}, \quad \begin{bmatrix} 0 \\ 0 \\ 1 \\ 0 \end{bmatrix}, \quad \begin{bmatrix} 0 \\ 0 \\ 0 \\ 1 \end{bmatrix} \quad (4.107)$$

The solutions corresponding to these four different initial vectors will be denoted by  $\mathbf{f}^{(j)}$ . The general solution is a linear combination of these,

$$\mathbf{f} = \sum_{j=1}^4 k_j \mathbf{f}_{(0)}^{(j)} \quad (4.108)$$

and the first component  $f_1$  corresponds to Equation (4.103). Notice that not all of the eigenfunctions  $\mathbf{f}^{(j)}$  must be determined, since only those which satisfy the boundary conditions at  $\bar{y} = 0$  are relevant to our problem. The last two vectors in (4.107) do satisfy the boundary conditions. In fact, the vector  $\mathbf{f}$  has been selected in (4.104) in this way in order to make the satisfaction of the condition (4.101) more direct. Notice further that both sliding laws (4.101a) and (4.101b) are included in the above formulation (4.107) by simply assigning  $\mathcal{C}$  the appropriate values\* ( $\mathcal{C} = 0$  for boundary condition (4.101)). The eigenvalue problem can therefore be solved by determining  $\mathbf{f}$  from a linear combination of  $\mathbf{f}^{(3)}$  and  $\mathbf{f}^{(4)}$  only.<sup>†</sup>

$$\mathbf{f} = k_3 \mathbf{f}^{(3)} + k_4 \mathbf{f}^{(4)} \quad (4.109)$$

The complex constants  $k_3$  and  $k_4$  are then determined by writing the boundary conditions (4.102) in terms of the components of the vector  $\mathbf{f}$  and substituting (4.109) into the emerging equations. This yields a system of two

\*Observe, however, that in the evaluation of the zeroth order surface velocity  $\bar{u}_S^{(0)}$  in the boundary condition (4.102)  $\mathcal{C}$  should not be set to zero if the basal sliding velocity is expressed by it. See, e.g., formula (4.27).

<sup>†</sup>Notice that  $\mathbf{f}^{(3)}$  and  $\mathbf{f}^{(4)}$  are real valued functions, but that  $k_3$  and  $k_4$  are complex.

complex (four real) linear equations for the unknowns  $k_3$  and  $k_4$ . Once they are determined, the eigenvalue  $c$  follows from Equation (4.102)<sub>1</sub> as

$$c = \frac{\bar{u}_S^{(0)}}{\mathcal{f}_1(1)} + 1,$$

where  $\mathcal{f}_1(1)$  is the value of the first component of the vector  $\mathcal{f}$  evaluated at  $\bar{y} = 1$ .

The above integration scheme follows essentially Thompson's work [49] who has focused attention on the restricted case when there is no sliding at the bed. He states that for this restricted class of motions the above integration scheme would be ideal were it not for one additional difficulty. Because of the numerical values of the coefficients in the differential equation (4.98) one of the complementary functions  $\mathcal{f}^{(j)}$  will dominate the other over the integration range such that although analytically the solutions  $\mathcal{f}^{(3)}$  and  $\mathcal{f}^{(4)}$  are linearly independent, numerically they will appear as linearly dependent. Since our formulation of the problem differs from that of Thompson only by a different non-dimensionalization of the equations, such difficulties are expected also to occur here. It is thus necessary to ensure that the two solution vectors remain orthogonal throughout the integration. Thompson presents an alternative determination of the function value of  $\mathcal{f}$  at  $\bar{y} = 1$  which follows a scheme developed by Bellman and Kalaba, (see [2], pp. 98–103.) For a detailed discussion, we must refer the reader to the literature.\*

### (b) Discussion of results

Thompson's analysis of the above problem is more restrictive than the formulation described above, because he focuses attention on glaciers which adhere to the bed yet do not show a temperature-dependency of the flow law. His analysis is more general than our presentation in that he, in a preliminary analysis, includes acceleration terms in the momentum equations but we do not. For a Newtonian fluid with a fixed viscosity that changes exponentially with depth, he reports results to the effect that inertial effects would have to be very much larger than they ordinarily are in glaciers if they were to have any significant influence on the stability of the glacier flow. In that analysis, the effective viscosity of the glacier in its unperturbed state is approximated by a fixed exponential profile. Identical perturbations are imposed, but the viscosity is not allowed to respond to changes in the strain rate. Hence, this problem isolates the effect of inertial forces arising from perturbation. Thus *instabilities in glaciers will not arise from inertial terms* and they are safely negligible as already done in the above presentation of

\*The most recent work appears to be: Lord, M. E., Scott, M. R. and Watts, H. R., *Computation of Eigenvalues/Eigenfunctions for Two-Point Boundary Value Problems*, App. Nonlinear Analysis, Academic Press, New York, 1979.

the analysis. Potential flow instabilities in glaciers must therefore arise from this interaction of the material non-linearity with the perturbed flow conditions of the glacier.

Inspection of the governing equations shows that the eigenvalue  $c$  depends on the following parameters:

- (i) The physical state of the unperturbed ice, that is the temperature distribution with depth and the flow law.
- (ii) Angle of inclination  $\gamma$  of the unperturbed ice slope.
- (iii) The sliding law describing the roughness of the bed.
- (iv) The wavenumber  $\alpha$  or wavelength  $\lambda$  of the surface elevations.

Of these, item (i) needs further explanation. When performing the numerical calculations and using Glen's flow law,  $\mathfrak{F}(\tau'_{II}) = \tau'^{(n-1)/2}_{II}$  then it is found that calculations become singular close to the upper surface  $\bar{y} = 1$ . A scrutiny of the cause of this singularity shows that effective viscosities at the surface become infinitely large. The same phenomenon has already been discussed in Section 3c, and it has been explained there that introducing the small parameter  $k$  in Equation (4.28) prevents the viscosity of the main flow from asymptotically approaching infinity near the surface, which would preclude either growth or decay of any infinitesimal surface perturbation.

With the necessary precaution suggested by the above remarks, we now proceed to the discussion of results. Thompson [49] restricts considerations to uniform temperature distributions, no slip at the base and inclination angles  $\gamma$  appropriate for glaciers. His analysis is based on the flow law  $\sigma' = \mathfrak{B}(\bar{D}_{II} + \delta)^{(1-n)/(2n)} \mathbf{D} = \text{constant}$ , corresponding to the polynomial creep law  $\bar{\mathbf{D}} = \mathcal{A}(\tau'^{(n-1)/2}_{II} + 1)/(1 + k)\sigma'$  with the correspondences  $\mathfrak{B} = 1/\mathcal{A}$  and  $k \simeq \delta^{(n-1)/n}$ , if both,  $\mathfrak{B}$  and  $\delta$  are small. For values of  $k$  or  $\delta$  which are  $\mathcal{O}(1)$ , the two constitutive relationships cannot simply be related; the two constitutive relations are then different.

Since the value of  $\delta$  (or  $k$ ) is not reliably known, it is worthwhile extending  $\delta$  beyond the range indicated purely from a computation of data. Thompson thus varied  $\delta$  over a wide range – much broader than needed to avoid the singularity in the effective viscosity at the free surface. Calculations were performed for  $10^{-3} \leq \delta \leq 10$  and for  $n = 4.5$ ,  $\mathfrak{B} = 1.62 \text{ bar } a^{1/n}$ , within a range of dimensionless wavenumbers from 0 to 10. *His results show that over the entire range of mean inclinations, the imaginary part of  $c, c_i$ , is negative, and hence the flow is stable.* He plotted the decay rate as a function of wavenumber  $\alpha$ . The results indicate (see Figures 4.22, 4.23, 4.24) that  $|xc_i|$  increases as the wavenumber increases from zero. It reaches a maximum at values of the wavenumber  $\alpha$  in the order of 1 to 3 and decays in an apparently asymptotic fashion, possibly reaching the value zero as  $\alpha \rightarrow \infty$ . Surface waves seem to be more stable for small bedrock inclinations than for large ones, but no sign changes have been observed for  $xc_i$ .

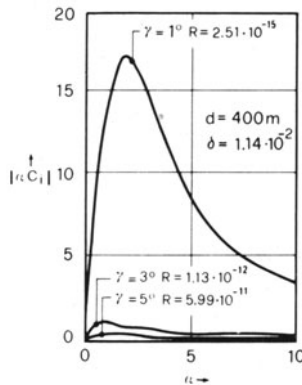


FIG. 4.22. Decay-rate magnitude versus perturbation wavenumber for models of constant thickness  $d = 400$  m and material parameter  $\delta = 1.14 \times 10^{-2} \text{ a}^{-1}$  but with variations in slope  $\gamma$  (from [49]).

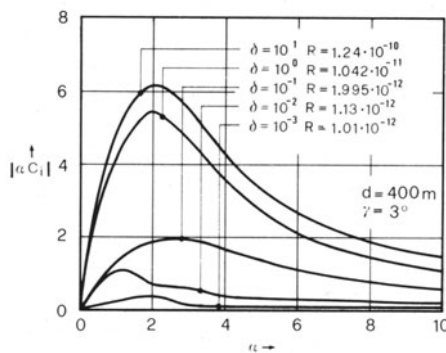


FIG. 4.23. Decay-rate magnitude versus perturbation wavenumber for models of constant thickness  $d = 400$  m and slope  $\gamma = 3^\circ$  but with variations in material parameter  $\delta$ , related to the viscosity (from [49]).

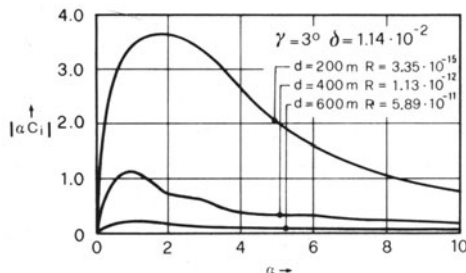


FIG. 4.24. Decay-rate magnitude versus perturbation wavenumber for models of constant slope  $\gamma = 3^\circ$  and material parameter  $\delta = 1.14 \times 10^{-2} \text{ a}^{-1}$  but with variations in thickness  $d$  (from [49]).

Unfortunately, Thompson has not extended his numerical analysis to include variations in the material non-linearities. For instance, it would be illuminating to see the results for different values of the exponent  $n$  and the constant  $\mathfrak{B}$ , and other non-linear constitutive relationships. Furthermore, temperature should be varied across the thickness of the ice sheet and various sliding conditions, including different proposals for the sliding law, should be tested. Consequently, the fact that the flow is stable over the whole range of  $k$  is not conclusive proof that instabilities arising from material non-linearities or differences in boundary conditions cannot occur in glaciers. A variation of the parameters that are incorporated in our analysis is necessary to answer this question completely.

### *6. Final Remarks*

In this chapter, first-order stresses, velocities (and temperatures) in a nearly parallel-sided ice slope have been analysed. The formulation of the fundamental governing equations was performed on the basis of the mathematical glacier model developed in Chapter 3. In the approximate solution technique, efficient use was made of regular perturbation methods by assuming that longitudinal bottom undulations, surface perturbations, and stress and velocity variations are small enough to justify the introduction of the amplitude of one of these as a perturbation parameter. The perturbation method was applied to mainly analyse the steady response of the ice slab and to study the stability of an ice sheet to small surface perturbations. It should have amply indicated that resort must be made to extensive numerical techniques if problems with some practical interest are to be solved.

Although a rather large number of important physical problems arising in ice sheets are discussed above, further applications and extensions of the calculations are possible. For instance, small longitudinal variations in the geothermal heat flux could be analysed. Such variations could, in steady state, result in longitudinal temperature variations, which in turn would (through the Arrhenius factor) lead to longitudinal variations of the mechanical response of the ice. If a stability analysis of surface waves were performed under such conditions, it could be tested whether longitudinal temperature variations would result in potential flow instabilities.

A large number of parameter variations further needs to be made to properly understand the physical response of an ice sheet. For instance, since the steady-state analysis shows that the first-order flow depends critically on the sliding law, a study should be undertaken giving information on how flow conditions respond to various reasonable sliding laws. Such a study would fruitfully enlighten the basic understanding of sliding and its significance for the flow response of the glacier. Such an analysis is, in particular, needed in a stability study.

Finally, the reader's attention should be drawn to the mathematical singularities which arose in our solution procedure, when Glen's flow law was used. The difficulties were overcome by introducing a finite viscosity law, i.e., by introducing a stress-strain rate curve with a finite tangent at zero strain rate. It was shown that by introducing a finite viscosity law, effective viscosities at the upper free surface did not become infinite, so that the analysis could be performed without leading into numerical instabilities. The applied solution technique, however, fails for a constitutive response of the stress deviator of the structure of Glen's flow. An analysis which could be extended to such a constitutive law would have to make use of the methods of matched asymptotic expansions. This should at least be done for a typical problem of the class presented above. Detailed calculations are to be expected to be very complicated, but such an analysis would confirm or disprove whether the approach used above and applied for  $k = \mathcal{O}(10^{-3})$  yields correct numerical values for the interested physical quantities.

The complexity of the analysis, on the other hand, calls for an alternative approach to some of the above problems which allows a simpler calculation of the field variables involved. Such a simplified analysis is indeed possible under rather mild further restrictions which often hold in glaciers and ice sheets. This analysis will be performed in the next chapter.

#### REFERENCES

1. Batchelor, G. K., *An Introduction to Fluid Mechanics*. Cambridge University Press. 1967.
2. Bellman, R. E. and R. E. Kalaba, *Quasilinearization and Nonlinear Boundary Value Problems*, Elsevier, New York, 1965.
3. Benjamin, T. B., Wave formation in laminar flow down an inclined plane, *J. Fluid. Mech.*, **2**, 554–574, 1957.
4. Benney, D. J., Long waves on liquid films, *J. Math. Phys.*, **45**, 150–155, 1966.
5. Bindschadler, R. A., A time-dependent model of temperate glacier flow and its application to predict changes in the surge-type variegated glacier during its quiescent phase. PhD Thesis, University of Washington, 1978.
6. Bourgois, J. P., Quelques caractères analytiques de la surface et du socle de l'inlandis groenlandais, *Ann. Géophys.*, **12**, 75–83, 1956.
7. Budd, W. F., Glaciological studies in the region of Wilkes. Eastern Antarctica. 1961 ANARE Scientific Reports, Ser. A (IV), *Glaciology, Publ.* No. 88, 1966.
8. Budd, W. F., The longitudinal velocity profile of large ice masses, International Union of Geodesy and Geophysics, International Association of Scientific Hydrology, General Assembly of Bern, 25. Sep.–7. Oct. 1967 (Commission of Snow and Ice). Reports and Discussions, *International Association of Scientific Hydrology, Publ.*, **79**, 58–77, 1968.
9. Budd, W. F., The dynamics of ice masses, ANARE Scientific Reports, Ser. A (IV). *Glaciology Publ.* No. 108, 1969.
10. Budd, W. F., The longitudinal stress and strain rate gradients in ice masses. *J. Glaciology*, **9**, 19–27, 1970.
11. Budd, W. F., Ice flow over bedrock perturbations. *J. Glaciology*, **9**, 29–47, 1970.
12. Budd, W. F., Stress variations with ice flow over undulations. *J. Glaciology*, **10**, 177–195, 1971.

13. Budd, W. F.. A first simple model for periodically self-surging glaciers. *J. Glaciology*. **14**, 3–21, 1975.
14. Budd, W. F. and B. J. McInnes. Modelling periodically surging glaciers, *Science*, **186**, 925–927, 1974.
15. Clarke, G. K. C.. Thermal regulation of glacier surging. *J. Glaciology*. **16**, 231–250, 1976.
16. Clough, J. W., C. R. Bentley, and C. K. Porter. Ice thickness investigations on SPQTILT III. *Antarctic J. U. S.*, **3**, 96–97, 1968.
17. Cole, J. D.. *Perturbation Methods in Applied Mathematics*. Blaisdell. Waltham, Mass., Toronto, London, 1968.
18. Collins, L. F.. On the use of the equilibrium equations and flow law in relating the surface and bed topography of glaciers and ice sheets. *J. Glaciology*. **7**, 199–204, 1968.
19. Craik, A. D. D. and F. I. P. Smith. The stability of free surface flows with viscosity stratification. *J. Fluid Mech.*, **34**, 393–406, 1968.
20. Van Dyke, M.. *Perturbation Methods in Fluid Mechanics*. The Parabolic Press. Stanford, California, 1975.
21. Finsterwalder, S.. Die Theorie der Gletscherschwankungen. *Zeitschrift für Gletscherkunde*. **2**, 81–103, 1907.
22. Fowler, A. C. and D. A. Larson. On the flow of polythermal glaciers. II: Surface wave analysis, *Proc. Royal Soc. London*. **A370**, 155–171, 1980.
23. Hodge, S. M.. Variations in the sliding of temperate glaciers. *J. Glaciology*. **13**, 349–369, 1974.
24. Hutter, K.. Time dependent surface elevation of an ice slope. *J. Glaciology*. **25**, 247–266, 1980.
25. Hutter, K. and F. Legerer. First-order stresses and deformations in glaciers and ice sheets. Abstract. *J. Glaciology*. **24**, 481–82, 1979.
26. Hutter, K., F. Legerer, and U. Spring. First-order stresses and deformations in glaciers and ice sheets. *J. Glaciology*. **27**, 227–270, 1981.
27. Hutter, K. and U. Spring. Distribution of stresses and velocities in an ice slope with spatially dependent material response. *Festschrift Prof. Kasser. Mitteilung der Versuchsanstalt für Wasserbau, Hydrologie und Glaziologie*, Zürich, Nr. 41, pp. 99–122, 1979.
28. Lick, W.. The propagation of disturbances on glaciers. *J. Geophys. Res.* **75**, 2189–2197, 1970.
29. Lin, C. C.. *The Theory of Hydrodynamic Stability*. Cambridge University Press. London, 1966.
30. Liboutry, L. A.. La dynamique de la Mer de Glace et la vague de 1891–95 d’après les mesures de Joseph Vallot, Association Internationale d’Hydrologie Scientifique. Symposium de Chamonix (1958) Physique du mouvement de la glace. *International Association of Scientific Hydrology, Publ.*, **47**, 125–138, 1958.
31. Mälzer, H.. Das Nivellment über das grönlandische Inlandeis der Internationalen Glaziologischen Grönland-Expedition 1959. *Meddelelser om Grönland*. Bd. 173, 1964.
32. Meier, M. F. and A. Post. What are glacier surges? *Can. J. Earth Sci.*, **6**, 807–816, 1969.
33. Morris, E. M.. The flow of ice treated as a Newtonian viscous liquid around a cylindrical obstacle near the bed of a glacier. *J. Glaciology*. **23**, 117–129, 1979.
34. Nayfeh, A. H.. *Perturbation Methods*. John Wiley. New York, London, Sydney, Toronto, 1973.
35. Nye, J. F.. The motion of ice sheets and glaciers. *J. Glaciology*. **3**, 493–507, 1959.
36. Nye, J. F.. The response of glaciers and ice sheets to seasonal and climatic changes. *Proc. Royal Soc. London*. **A256**, 559–584, 1960.
37. Nye, J. F.. On the theory of advance and retreat of glaciers. *Geophys. J. Royal Astron. Soc.*, **7**, 431–456, 1960.
38. Nye, J. F.. The response of a glacier to changes in the rate of nourishment and wastage. *Proc. Royal Soc. London*. **A275**, 87–112, 1963.

39. Nye, J. F.. The frequency response of glaciers. *J. Glaciology*, **5**, 567–587, 1965.
40. Nye, J. F.. The effect of longitudinal stress on the shear stress at the base of an ice sheet. *J. Glaciology*, **8**, 207–213, 1969.
41. Robin, G. de Q.. Ice movement and temperature distribution in glaciers and ice sheets. *J. Glaciology*, **2**, 523–532, 1955.
42. Robin, G. de Q.. Glaciology III: Seismic shooting and related investigations. Norwegian-British-Swedish Antarctic Expedition, 1949–1952. *Scientific Results*, **5**, 1958.
43. Robin, G. de Q.. Surface topography of ice sheets. *Nature*, **215**, 1029–1032, 1967.
44. Robin, G. de Q.. Initiation of glacier surges. *Can. J. Earth Sci.*, **6**, 916–926, 1969.
45. Robin, G. de Q. and J. Weertman. Cyclic surging glaciers. *J. Glaciology*, **12**, 3–18, 1973.
46. Robinson, E. S.. On the relationship of ice-surface topography to bed topography on the south polar plateau. *J. Glaciology*, **6**, 43–54, 1966.
47. Swithinbank, C. W. M.. Glaciology I: The morphology of the inland ice sheet and nunatak areas of Western Dronning Mond Land. The regime of the ice sheet of Western Dronning Mond Land as shown by stake measurements. Norwegian-British-Swedish Antarctic Expedition 1949–52. *Scientific Results*, **3D**, 97–117, 1959; **3E**, 121–144, 1959.
48. Schlichting, H., *Boundary Layer Theory*, translated by J. Kestin, McGraw-Hill, New York, 1968.
49. Thompson, D. E.. Stability of glaciers and ice sheets against flow perturbations. *J. Glaciology*, **24**, 427–441, 1979.
50. Weertman, J.. Water lubrication mechanism of glacier surges. *Can. J. Earth Sci.*, **6**, 915–939, 1969.
51. Weertman, J.. Comparison between measured and theoretical temperature profiles of the Camp Century, Greenland, borehole. *J. Geophys. Res.*, **73**, 2691–2700, 1968.
52. Yih, C. S.. Stability of parallel laminar flow with a free surface. *Proc. 2nd U.S. Congress of Applied Mechanics*. American Soc. Mechanical Engineers, New York, pp. 623–628, 1955.
53. Yih, C. S.. Stability of liquid flow down an inclined plane. *Phys. Fluids*, **6**, 321–334, 1963.
54. Yih, C. S., *Dynamics of Nonhomogeneous Fluids*, Macmillan, New York, 1965.
55. Yih, C. S.. Instability due to viscosity stratification. *J. Fluid Mech.*, **27**, 337–352, 1967.
56. Yosida, Z.. Internal stress and viscous flow of snow covers on sloping ground surfaces (In Japanese). *Low Temperature Science, Ser. A*, **22**, 83–127, 1964.

## **Chapter 5**

# **THE APPLICATION OF THE SHALLOW-ICE APPROXIMATION**

### *1. Background and Previous Work*

In the previous chapter, the nearly parallel-sided ice slab was thoroughly analysed; in particular, its steady-state response was treated, and it was shown how small-amplitude bottom protuberances affect surface topography, basal stresses and surface velocities. Attention was restricted to plane motion and to ice slabs for which the mean bed and mean surface were plane and strictly parallel so that the mean ice thickness was constant. In reality, this is only approximately correct as it is well known that ice-sheet thicknesses may vary from up to 3000 m inland or more to zero thickness at the snout. On length scales which are comparable with the extension of the ice sheet, the assumption of small variations about a parallel-sided ice slab is thus unrealistic. On the other hand, calculations, as those performed in Chapter 4, must be limited to length scales for which ice-sheet thicknesses do not deviate appreciably from a layer with a constant thickness.

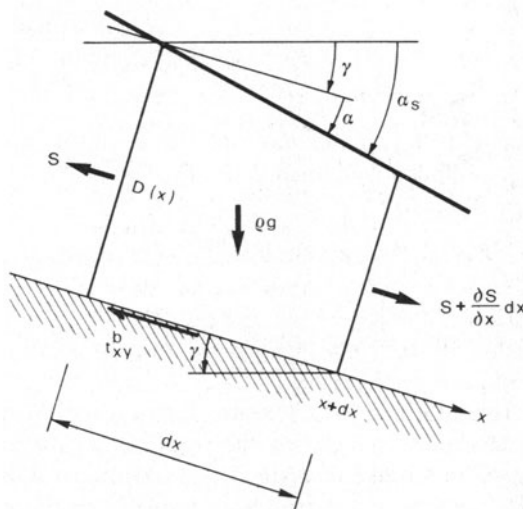
When analysing glaciers and ice sheets on length scales over which ice thicknesses may vary appreciably, a different approach should be taken, in which the solution for the strictly parallel-sided slab plays no explicit role. Incidentally, such an approach is also desirable for the situation dealt with in Chapter 4, if the analysis describing the ice flow problem turns out to be less involved and, perhaps, amenable to instant exploitation on a programmable calculator. Of course, a simpler analysis than that performed in Chapter 4 will necessarily be based on a relatively strong assumption. This assumption may be called the *shallow ice approximation*. It limits attention to the physical processes in which important length scales in the longitudinal direction are large, as compared to those in the transverse direction. For glaciers and ice sheets, flow variations are usually looked at on length scales of several ice thicknesses; only rarely, and then for special investigations, are short-range stress and velocity variations of interest. This is, for instance, the case when stresses and velocities are analysed in the neighborhood of crevasses, the snout region, or close to a ridge. In a shallow ice approximation, such rapid changes of stress and velocity must be looked at to be ‘smeared over’. On the

other hand, it is largely true that the topography of the smoothed-out base and of the surface does not change appreciably over length scales which are comparable to the *local* thickness of the ice making the shallow ice approximation a rather weak one, as long as one delimits attention to positions far from the snout where such assumptions are no longer justified.

Historically, the introduction of the shallow ice approximation into ice-flow dynamics is very recent. The interest in longitudinal strain-rate variations grew from discrepancies that evolved when one was trying to use the formula for basal shear to obtain ice thicknesses by measuring surface inclinations. To explain the situation, consider a longitudinal increment of an ice sheet whose top and bottom surface angles differ from each other by the angle  $\alpha$ . We do not assume  $\gamma$  to be small, but to make the subsequent equilibrium equations approximately valid, the angle  $\alpha$  must be assumed small, see Figure 5.1. A balance of forces in the direction of  $x$  gives

$$t_x^{by} = \rho g \sin \gamma D - \rho g D \cos \gamma \frac{dD}{dx} = \rho g D (\sin \gamma + \cos \gamma \tan \alpha). \quad (5.1)$$

The first term is the contribution from the weight and the second is the change of the longitudinal force  $\partial S/\partial x$ .  $S$  itself can be obtained from an integration over the ice thickness of the longitudinal stresses which, in a



$$S = - \int_0^{D(x)} \rho g \cos \gamma (D-y) dy + \int_0^{D(x)} (t_{xx} - t_{yy}) dy$$

FIG. 5.1. Explaining the derivation of the stress formula for basal shear.

strictly parallel-sided slab, are given by  $t_{xx} = -\rho g \cos \gamma(D - y)$ , the small contribution from atmospheric pressure being neglected in this formula. (Recall that in a strictly parallel-sided slab  $t_{xx} = t_{yy}$ .) When restricting bottom slopes to small angles, formula (5.1) goes over into

$$t_{xy}^b = \rho g D(\gamma + \alpha) = \rho g D \alpha_s, \quad (5.2)$$

where  $\alpha_s$  is the surface slope. This formula has been derived by Nye [26, 29] and has already been mentioned. Very roughly, ice may be regarded as a plastic material with a yield stress of approximately 1 bar. Setting the basal shear stress equal to this yield stress and measuring the surface inclinations  $\alpha_s$  will allow us to determine ice thicknesses. Alternatively, when measuring ice thicknesses and surface inclinations, basal shear stresses can be calculated and information can be gained as to whether the assumption of plastic flow is reasonably satisfied. Qualitatively formula (5.2) has been found to be in good agreement with observations; the quantitative differences, however, call for improvements. To find the root for these improvements, the reader may recall that in deriving Equation (5.1) it was assumed that the longitudinal stress  $t_{xx}$  is given by the formula valid in a strictly parallel-sided slab in which none of the field variables vary with the length coordinate, see Chapter 3, Section 3c. When the stresses vary along  $x$ ,  $t_{yy}$  is still given by the formula  $t_{yy} = -\rho g \cos \gamma(D - y)$ , but  $t_{xx}$  must be evaluated from the deformation, see Chapter 3, Section 3d. This suggests

$$S = \int_0^{D(x)} [t_{yy} + (t_{xx} - t_{yy})] dy = -\rho g \cos \gamma \frac{D^2(x)}{2} + \int_0^{D(x)} (t_{xx} - t_{yy}) dy.$$

Recalling further that for plane motion, the deviator stress is given by  $t'_{xx} = 1/2(t_{xx} - t_{yy})$ , an improved formula for (5.1) is

$$\begin{aligned} t_{xy}^b &= \rho g D(\sin \gamma + \cos \gamma \tan \alpha) + 2 \frac{d}{dx} \int_0^{D(x)} t'_{xx} dy = \\ &= \rho g D(\sin \gamma + \cos \gamma \tan \alpha) + \frac{dF}{dx}. \end{aligned} \quad (5.3)$$

Here  $F$  is the ‘longitudinal force’ taking longitudinal stress (strain rate) variations into account. Previous to the rigorous derivations of formulas like (5.3), the importance of the term  $dF/dx$  was pointed out by Orowan [30]; and the formula had been used by Lliboutry [21] in the analysis of data of the Mer de Glace. The equation was further used by Shumskiy [35–37], Robin [34] and Budd [3, 4]. Satisfactory treatments of its derivation were given by Collins [10], Nye [29] and Budd [5]. A derivation from basic

principles using the shallow ice approximation is as recent as 1981 and due to Hutter [16].\*

Before we proceed to construct the longitudinal force, let us pause and explain what role formula (5.3) plays in applied glaciology. Basically, it has been used in the following different contexts:

- (i). Given measured ice thicknesses, the accumulation rate, and an assumed flow law, the steady-state longitudinal strain rates, stresses, and surface slopes are calculated, Robin [34].
- (ii) Given measured longitudinal surface strain rates and ice surface and rockbed topographies, the flow parameters of a postulated flow law can be calculated.

Towards the above ends, the longitudinal force  $F$  must be related to a flow law. Since  $F$  is the integrated deviator stress  $t'_{xx}$ , this is possible in an averaged sense. The procedure of most authors is to formulate this constitutive relation approximately by introducing various *ad hoc* assumptions. One such assumption is the *observational* fact that  $t^b_{xy}$  can be replaced by  $\rho g D \bar{\alpha}_S$  where  $\bar{\alpha}_S$  is the mean surface inclination of the top surface *averaged over roughly ten to twenty ice thicknesses*. Another one is to write  $F$  in terms of surface strain rate  $\dot{\varepsilon}_x|_S$ . The postulate is, e.g. (see Budd [3]),

$$F = DB(\dot{\varepsilon}_x|_S)^{1/n}, \quad \dot{\varepsilon}_x > 0, \quad (5.4)$$

where  $D$  is the ice-sheet thickness and  $B$  and  $n$  are two parameters. With these assumptions, and for small surface inclinations, relation (5.3) assumes the form

$$\frac{d}{dx}(DB\dot{\varepsilon}_x|_S)^{1/n} = \rho g D(\bar{\alpha}_S - \alpha_S), \quad (5.5)$$

which is suitable to solve the problems stated above.

It is obvious that the above derivation is unsatisfactory in many respects as it contains a series of *ad hoc* assumptions. Indeed, it will be shown that most of these are dispensable at moderate costs of increased complexity. It should also be noticed that a basal shear-stress formula cannot be of interest in its own right. The ultimate goal in an ice sheet analysis is either to determine the velocity distribution when the ice sheet geometry and the constitutive response is given, or else, for given ice-sheet geometry and measured velocities, to determine the free parameters in a postulated constitutive relationship. Ideally, given the accumulation rate as a function

\*Rational derivations in which no use is made of integrals over ice thickness are also by Morland and Johnson [24] and Fowler [12], but the analysis of these authors emphasizes different aspects of the theory.

of position and time we should be able to determine not only the velocity and stress distribution, but also the geometry. It will be shown that this is possible mathematically, but the solutions of the corresponding boundary-value problem are complex. Steady-state analyses have been conducted by Morland and Johnson [23, 24], time dependent processes, including the prediction of ice sheet or glacier advance, have not been systematically analysed, except for some particular aspects, such as the propagation of surface and seasonal waves on glaciers, (see Fowler and Larson [13] and Fowler [12]).

## 2. Derivation of the Basal Shear-stress Formula by Integrating the Momentum Equations over Ice Thickness

### (a) Derivation

Consider the slow plane flow of a viscous medium down a slope. In what follows we shall work with the non-dimensional variables already introduced in Chapters 3 and 4. Let  $(\bar{x}, \bar{y})$  be a dimensionless Cartesian coordinate system;  $\bar{x}$  is down glacier approximately in the direction of the mean bed inclination, but this is not a necessity. A perfect legitimate choice for the  $\bar{x}$ -axis is also horizontal.  $\bar{y}$  is normal to  $\bar{x}$  (see Figure 5.2). Further, let,  $\gamma$ ,  $\alpha$ , and  $\beta$  be the inclination angles of the  $\bar{x}$ -axis relative to the horizontal direction and the slopes of the free surface and the bed relative to the  $\bar{x}$ -direction, respectively.  $\gamma$  is fixed, but  $\alpha$  and  $\beta$  may vary along the respective surfaces; these angles are further defined such that

$$\tan \alpha = - \frac{\partial \bar{y}_S}{\partial \bar{x}}, \quad \tan \beta = - \frac{d \bar{y}_B}{d \bar{x}}, \quad (5.6)$$

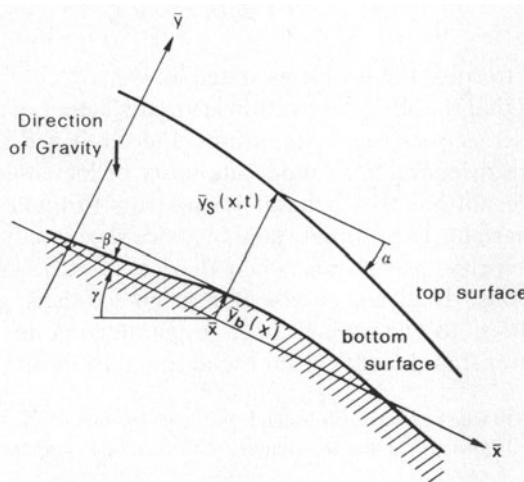


FIG. 5.2. Geometry and definitions of ice sheet.

where  $\bar{y} = \bar{y}_S(\bar{x}, \bar{t})$  and  $\bar{y} = \bar{y}_B(\bar{x})$  are the equations of the surface and bed topographies. Later on, certain assumptions regarding  $\alpha$ ,  $\beta$  and  $\gamma$  will be invoked but, for the time being, they are completely arbitrary so long as  $\bar{y}_B$  and  $\bar{y}_S$  define unique non-intersecting curves. Notice also that the ice slab need not be nearly parallel-sided, as was the case in Chapter 4. This more general situation necessitates a clear definition of the reference length  $D$  with which the equations to be presented below are non-dimensionalized. In what follows, it will tacitly be assumed that  $D$  is a representative *mean thickness* of the ice sheet considered. The actual dimensionless thickness will then be denoted by  $\bar{D}$ , which will assume values slightly larger and slightly smaller than unity.

In what follows, it will suffice to write down the equilibrium equations and boundary conditions of tangential stress at the top and bottom surfaces. These equations are

$$\frac{\partial \sigma_x}{\partial \bar{x}} + \frac{\partial \tau}{\partial \bar{y}} + \sin \gamma = 0, \quad \frac{\partial \tau}{\partial \bar{x}} + \frac{\partial \sigma_y}{\partial \bar{y}} - \cos \gamma = 0. \quad (5.7)$$

and  $(\sigma_x - \sigma_y) \sin \alpha \cos \alpha - \tau (\sin^2 \alpha - \cos^2 \alpha) = 0$ , at  $\bar{y} = \bar{y}_S(\bar{x}, \bar{t})$ ,  $\tau_b = (\sigma_x - \sigma_y) \sin \beta \cos \beta + \tau (\cos^2 \beta - \sin^2 \beta)$ , at  $\bar{y} = \bar{y}_B(\bar{x})$ ,

in which  $\tau_b$  is defined as in Figure 5.1 (in which it corresponds to  $t_{xy}^b$ ) and the notation is as in previous chapters. All remaining calculations in this section make use of transformations of the above equations. Our aim is to use Equations (5.7) and boundary conditions of stress at the free surface and the base (5.8) to derive an equation similar to that of (5.3). The derivation should thereby involve as few simplifying assumptions as possible so that longitudinal strain-rate effects can be clearly isolated. The analysis is outlined below and the result is given as Equation (5.16), to which readers not interested in the analytical details are advised to pass on to.

Differentiating (5.7)<sub>1</sub> with respect to  $\bar{y}$  and (5.7)<sub>2</sub> with respect to  $\bar{x}$ , subtracting the emerging equations, and then integrating the resulting equation between  $\bar{y}$  and  $\bar{y}_S$  yields

$$\frac{\partial(\sigma_x - \sigma_y)}{\partial \bar{x}} = -\sin \gamma - \frac{\partial \tau}{\partial \bar{y}} - \left. \frac{\partial \sigma_y}{\partial \bar{x}} \right|_{\bar{y}_S} - \int_{\bar{y}}^{\bar{y}_S} \frac{\partial^2 \tau}{\partial \bar{x}^2} d\bar{y} \quad (5.9)$$

and, after a further integration between  $\bar{y} = \bar{y}_B$  and  $\bar{y} = \bar{y}_S$ ,

$$\begin{aligned} \frac{d}{dx} \int_{\bar{y}_B}^{\bar{y}_S} (\sigma_x - \sigma_y) d\bar{y} &= -(\sigma_x - \sigma_y)|_{\bar{y}_S} \tan \alpha + (\sigma_x - \sigma_y)|_{\bar{y}_B} \tan \beta - \\ &- \sin \gamma \bar{D} - \left. \frac{\partial \sigma_y}{\partial \bar{x}} \right|_{\bar{y}_S} \bar{D} - \tau|_{\bar{y}_S} + \tau|_{\bar{y}_B} - \int_{\bar{y}_B}^{\bar{y}_S} \int_{\bar{y}_B}^{\bar{y}} \frac{\partial^2 \tau}{\partial \bar{x}^2} d\bar{y}' d\bar{y}. \end{aligned} \quad (5.10)$$

in which Leibnitz' rule for interchanging integration and differentiation has been used. This equation possesses all the ingredients to lead to a generalization of (5.3) because its term on the left-hand side is twice the dimensionless term  $d\bar{F}/d\bar{x}$ . Noticing further that, in view of the boundary condition (5.8),

$$\begin{aligned} (\sigma_x - \sigma_y)|_{\bar{y}_B} \tan \beta &= \frac{\tau_b}{\cos^2 \beta} - \tau|_{\bar{y}_B} (1 - \tan^2 \beta), \\ (\sigma_x - \sigma_y)|_{\bar{y}_S} \tan \alpha &= -\tau|_{\bar{y}_S} (1 - \tan^2 \alpha), \end{aligned} \quad (5.11)$$

an alternative form of (5.10) is

$$\begin{aligned} \frac{d\bar{F}}{d\bar{x}} &= \frac{d}{d\bar{x}} \int_{\bar{y}_B}^{\bar{y}_S} (\sigma_x - \sigma_y) d\bar{y} = -\sin \gamma \bar{D} - \left. \frac{\partial \sigma_y}{\partial \bar{x}} \right|_{\bar{y}_S} \bar{D} - \tau|_{\bar{y}_S} \tan^2 \alpha + \\ &\quad + \tau|_{\bar{y}_B} \tan^2 \beta + \frac{\tau_b}{\cos^2 \beta} - \int_{\bar{y}_B}^{\bar{y}_S} \int_{\bar{y}_B}^{\bar{y}} \frac{\partial^2 \tau}{\partial \bar{x}^2} d\bar{y}' d\bar{y}. \end{aligned} \quad (5.12)$$

In the limit  $\alpha \rightarrow 0, \beta \rightarrow 0$ , and when neglecting the last term on the right-hand side, this formula reduces to

$$\tau_b = \sin \gamma \bar{D} + \left. \frac{\partial \sigma_y}{\partial \bar{x}} \right|_{\bar{y}_S} \bar{D} + \frac{d\bar{F}}{d\bar{x}},$$

which would agree with (5.3) if  $\partial \sigma_y / \partial \bar{x}|_{\bar{y}_S} = \cos(\gamma)\alpha$ . Consider, therefore, this term; by regarding  $\sigma_y$  and  $\tau$  as functions of  $\bar{s}$  and  $\bar{y}$  rather than  $\bar{x}$  and  $\bar{y}$  (see Figure 5.3) it follows that

$$\left. \frac{\hat{\partial}(\sigma_y \tau)}{\hat{\partial} \bar{x}} \right|_{\bar{y}_S} = \frac{\hat{\partial}(\sigma_y \tau)}{\hat{\partial} \bar{s}} \frac{1}{\cos \alpha} + \frac{\hat{\partial}(\sigma_y \tau)}{\hat{\partial} \bar{y}} \tan \alpha, \quad (5.13)$$

in which (5.6) was used. From this and a repeated application of (5.7), we may then deduce

$$\begin{aligned} \left. \frac{\partial \sigma_y}{\partial \bar{x}} \right|_{\bar{y}_S} &\stackrel{(5.7)}{=} \left. \frac{\hat{\partial} \sigma_y}{\hat{\partial} \bar{s}} \right. \frac{1}{\cos \alpha} - \left[ \left. \frac{\partial \tau}{\partial \bar{x}} \right. - \cos \gamma \right] \tan \alpha \\ &\stackrel{(5.13)}{=} \left. \frac{\hat{\partial} \sigma_y}{\hat{\partial} \bar{s}} \right. \frac{1}{\cos \alpha} - \left[ \left. \frac{\partial \tau}{\partial \bar{s}} \right. \frac{1}{\cos \alpha} + \left. \frac{\partial \tau}{\partial \bar{y}} \right. \tan \alpha - \cos \gamma \right] \tan \alpha \\ &\stackrel{(5.7)}{=} \cos \gamma \tan \alpha - \left. \frac{\partial \sigma_x}{\partial \bar{x}} \right|_{\bar{y}_S} \tan^2 \alpha - \sin \gamma \tan^2 \alpha - \left. \frac{\partial \tau}{\partial \bar{s}} \right|_{\bar{y}_S} \frac{\sin \alpha}{\cos^2 \alpha} + \left. \frac{\partial \sigma_y}{\partial \bar{s}} \right|_{\bar{y}_S} \frac{1}{\cos \alpha}. \end{aligned} \quad (5.14)$$

In a final step, the longitudinal surface stress  $\sigma_l$  and the atmospheric pressure  $p^{\text{atm}}$  are introduced according to

$$\left. \begin{aligned} \sigma_y &= -\bar{p}^{\text{atm}} \cos^2 \alpha + \sigma_l \sin^2 \alpha \\ \tau &= \frac{1}{2}(\sigma_l + \bar{p}^{\text{atm}}) \sin \alpha \end{aligned} \right\} \quad \text{at } \bar{y} = \bar{y}_S.$$

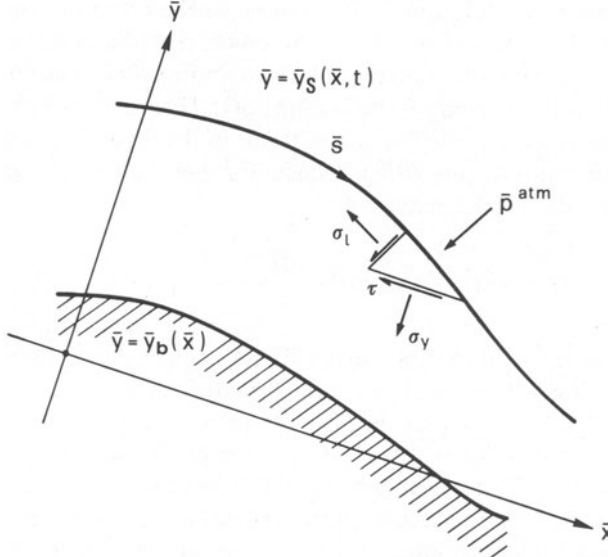


FIG. 5.3. At the free surface, the stress components  $\sigma_y, \tau$  can be assumed to be functions of arc-length  $\bar{s}$  and  $\bar{y}$  rather than  $\bar{x}$  and  $\bar{y}$ . Analogously it is more natural to introduce surface-stress components parallel and perpendicular to the free surface. These are the longitudinal stress and the atmospheric pressure  $\bar{p}^{\text{atm}}$ .

From this, by supposing  $\bar{p}^{\text{atm}}$  to be position-independent, it follows that

$$\begin{aligned}\frac{\partial \sigma_y}{\partial \bar{s}} &= \frac{\partial \sigma_l}{\partial \bar{s}} \sin^2 \alpha + (\sigma_l + \bar{p}^{\text{atm}}) \sin 2\alpha \frac{d\alpha}{d\bar{s}}, \\ \frac{\partial \tau}{\partial \bar{s}} &= \frac{d}{d\bar{s}} [\frac{1}{2}(\sigma_l + \bar{p}^{\text{atm}})] \sin 2\alpha + (\sigma_l + \bar{p}^{\text{atm}}) \cos 2\alpha \frac{d\alpha}{d\bar{s}}.\end{aligned}\quad (5.15)$$

Substituting these expressions into (5.14) and the resulting equation into (5.12), finally gives

$$\begin{aligned}\frac{d\bar{F}}{d\bar{x}} &= -(\sin \gamma + \cos \gamma \tan \alpha) \bar{D} + \frac{\tau_b}{\cos^2 \beta} - \int_{\bar{y}_B}^{\bar{y}_S} \int_{\bar{y}}^{\bar{y}_S} \frac{\partial^2 \tau}{\partial \bar{x}^2} d\bar{y} d\bar{y} + \\ &+ \left[ \frac{\partial \sigma_x}{\partial \bar{x}} \Big|_{\bar{y}_S} \bar{D} + \sin \gamma \bar{D} - \tau \Big|_{\bar{y}_S} \right] \tan^2 \alpha + \\ &+ \frac{d}{d\bar{s}} [\frac{1}{2}(\sigma_l + \bar{p}^{\text{atm}})] \frac{\sin 2\alpha \sin \alpha}{\cos^2 \alpha} \bar{D} - \frac{\partial \sigma_l}{\partial \bar{s}} \frac{\sin^2 \alpha}{\cos \alpha} \bar{D} + \\ &+ (\sigma_l + \bar{p}^{\text{atm}}) \bar{D} \left[ \frac{\sin \alpha \cos 2\alpha}{\cos^2 \alpha} \frac{d\alpha}{d\bar{s}} - \frac{\sin 2\alpha}{\cos \alpha} \frac{d\alpha}{d\bar{s}} \right] + \\ &+ \tau \Big|_{\bar{y}_B} \tan^2 \beta.\end{aligned}\quad (5.16)$$

This equation is exact; it applies for arbitrary orientations of the  $\bar{x}$ -axis and of the top and bottom surfaces. The terms on the right-hand side are arranged according to their orders of magnitudes as  $\alpha$  and/or  $\beta$  become small. Indeed, in the limit  $\alpha \rightarrow 0$ , the terms in the first line of (5.17) are  $\mathcal{O}(1)$  or  $\mathcal{O}(\alpha)$  and those in the second and third line  $\mathcal{O}(\alpha^2)$ . The terms in the fourth line are  $\mathcal{O}(\alpha(d\alpha/d\bar{s}))$  and those in the fifth line  $\mathcal{O}(\beta^2)$ . Hence, for *small*  $\alpha$  and  $\beta$  (but still finite slopes  $\gamma$ ), Equation (5.16) reduces to

$$\tau_b = (\sin \gamma + \cos \gamma \alpha) \bar{D} + \frac{d\bar{F}}{d\bar{x}} + \int_{\bar{y}_B}^{\bar{y}_S} \int_y^{\bar{y}_S} \frac{\partial^2 \tau}{\partial \bar{x}^2} d\bar{y}' dy' d\bar{y}, \quad (5.17)$$

provided that terms of  $\mathcal{O}(\alpha^2, \beta^2, \alpha(d\alpha/d\bar{s}))$  are neglected. Notice that relation (5.17) is the dimensionless analogue of Equation (5.3). As in the latter, the slope angle  $\beta$  does not enter, but here terms  $\mathcal{O}(\beta)$  are taken into account, whereas in Equation (5.3)  $\beta$  was set to zero at the outset. A comparison further shows that (5.3) can only be valid if (i) relative slope angles are small, and (ii) the last double-integral term on the right-hand side of (5.17) is negligibly small. The conditions for this to be valid will be formulated later. For future reference, we would once more clearly state the conditions under which formula (5.17) is valid. These are:

- (1) The inclination angle  $\alpha$  of the surface relative to the mean inclination  $\gamma$  must be small;
- (2) The inclination angle  $\beta$  of the bed relative to the mean inclination  $\gamma$  must be small;
- (3) The surface inclination angle  $\alpha$  must be a slowly varying function of  $\bar{s}$ :  $d\alpha/d\bar{s} \ll 1$ .

Clearly, other representations of (5.16) could also be obtained by selecting special values for  $\alpha, \beta$  and  $\gamma$ . These will not be given here. Suffice it then to state that the above derivation of Equation (5.17) follows Budd [5] and that earlier derivations of the same equation are by Collins [10] and Nye [29].

*(b) The use of the basal shear-stress formula in applied glaciology*

To demonstrate the use of Formula (5.17) let us mention that it has thus far been used for  $\gamma$  small only. Then with  $(\alpha + \gamma) = \alpha_s$  it reduces to

$$\tau_b = \bar{D}\alpha_s + \frac{d\bar{F}}{d\bar{x}} + T, \quad (5.18)$$

where  $T$  is the last term on the right-hand side of (5.17). An estimate for it must be found. To this end, Leibnitz' rule is used twice to transform  $T$  into

the following form:

$$\begin{aligned} T \equiv & \int_{\bar{y}_B}^{\bar{y}_S} \int_{\bar{y}}^{\bar{y}_S} \frac{\partial^2 \tau}{\partial \bar{x}^2} d\bar{y}' d\bar{y} = \frac{d^2}{d\bar{x}^2} \int_{\bar{y}_B}^{\bar{y}_S} \tau d\bar{y}' d\bar{y} + \frac{d\bar{y}_B}{d\bar{x}} \int_{\bar{y}_B}^{\bar{y}_S} \tau d\bar{y} - \\ & - \left[ \frac{\partial}{\partial \bar{x}} \int_{\bar{y}}^{\bar{y}_S} \tau d\bar{y} \right]_{\bar{y}_S} \frac{\partial \bar{y}_S}{\partial \bar{x}} + \left[ \frac{\partial}{\partial \bar{x}} \int_{\bar{y}}^{\bar{y}_S} \tau d\bar{y} \right]_{\bar{y}_B} \frac{d\bar{y}_B}{d\bar{x}} - \\ & - \frac{d}{d\bar{x}} \left[ \frac{\partial \tau}{\partial \bar{x}} \Big|_{\bar{y}_S} \frac{\partial \bar{y}_B}{\partial \bar{x}} \right] \bar{D} - \frac{\partial \tau}{\partial \bar{x}} \Big|_{\bar{y}_S} \frac{\partial \bar{y}_S}{\partial \bar{x}} \bar{D}. \end{aligned} \quad (5.19)$$

Because (5.18) is valid for small  $\alpha$ ,  $\beta$  and  $\gamma$ , only the terms which are linear in these quantities must be retained in this formula. Since approximately  $\tau = \alpha_s [\bar{y}_S - \bar{y}]$  all terms in (5.19) involving  $\partial \bar{y}_S / \partial \bar{x}$  and  $d\bar{y}_B / d\bar{x}$  may thus be omitted because they would be quadratic in  $\alpha_s$  and  $\beta$ . The right-hand side of (5.19) may thus be replaced by its first term, which with  $\tau = \alpha_s \bar{D}$ , where  $\bar{D} = \bar{y}_S - \bar{y}_B$ , reduces to  $d^2 [\alpha_s \bar{D}^3 / 6] / d\bar{x}^2$ . To evaluate this term, consider a flat bed and a harmonic undulation of the thickness function  $\bar{D}$ ,

$$\bar{D} = \bar{D}_0 - \bar{\alpha}_s \bar{x} + A \cos \left( \frac{2\pi}{\lambda} \bar{x} \right); \quad (5.20)$$

then because of a flat base ( $\gamma = 0$ ,  $\alpha = \alpha_s$ )

$$\alpha_s = \bar{\alpha}_s + \frac{2\pi}{\lambda} A \sin \left( \frac{2\pi}{\lambda} \bar{x} \right), \quad (5.21)$$

where  $\bar{\alpha}_s$  is a mean surface inclination and  $A$  is an amplitude of the sinusoidal undulation.  $\bar{\alpha}_s$  must be small to be consistent with our basic assumption that  $\alpha_s$  is small. The wavelength  $\lambda$ , on the other hand, must be large in order that (5.21) conforms with the assumption that  $\alpha_s$  and  $d\alpha_s / d\bar{x}$  are small; in fact (5.21) suggests that  $\lambda > 2\pi$ . Hence to linear orders in  $\alpha_s$  we may write

$$T \cong \frac{1}{6} \frac{d^2 \alpha_s}{d\bar{x}^2} \bar{D}^3 = \frac{\bar{D}^3}{6} \left( \frac{2\pi}{\lambda} \right)^2 (\alpha_s - \bar{\alpha}_s). \quad (5.22)$$

This is the desired approximation for  $T$ . Since  $\bar{D} \simeq \mathcal{O}(1)$ ,  $T$  becomes comparable with the remaining terms in Equation (5.18) provided that  $\lambda \gtrsim \sqrt{\frac{2}{3}}\pi \simeq 1.7$ . Wavelengths for which the validity of the assumption that  $d\alpha / d\bar{x}$  is small is doubtful. Strictly speaking, therefore, formula (5.18) is valid only for wavelengths which are long in comparison to the ice-sheet thickness ( $\lambda \gg 6.3$ , say) for which case  $T$  is negligible. If we now write

$$\bar{F} = \int_{\bar{y}_B}^{\bar{y}_S} (\sigma_x - \sigma_y) d\bar{y} = 2 \int_{\bar{y}_B}^{\bar{y}_S} \sigma'_x d\bar{y} = 2\bar{D}\bar{\sigma}'_x,$$

a thickness average  $\bar{\sigma}'_x$  of the longitudinal stress deviator  $\sigma'_x$  is introduced. It is a common postulate in applied glaciology to relate  $\bar{\sigma}'_x$  with longitudinal surface strains  $\dot{\varepsilon}_x^S$  according to

$$\dot{\varepsilon}_x^S = \mathcal{A} \bar{\sigma}'_x^n \quad \text{or} \quad \bar{\sigma}'_x = \left( \frac{1}{\mathcal{A}} \right)^{1/n} |\dot{\varepsilon}_x^S|^{(1-n)/n} \dot{\varepsilon}_x^S,$$

where  $\mathcal{A}$  and  $n$  are phenomenological constants,  $\mathcal{A}$  possibly being a representative temperature average.  $\bar{F}$  may then be represented as

$$\bar{F} = 2\bar{D} \left( \frac{1}{\mathcal{A}} \right)^{1/n} |\dot{\varepsilon}_x^S|^{(1-n)/n} \dot{\varepsilon}_x^S. \quad (5.23)$$

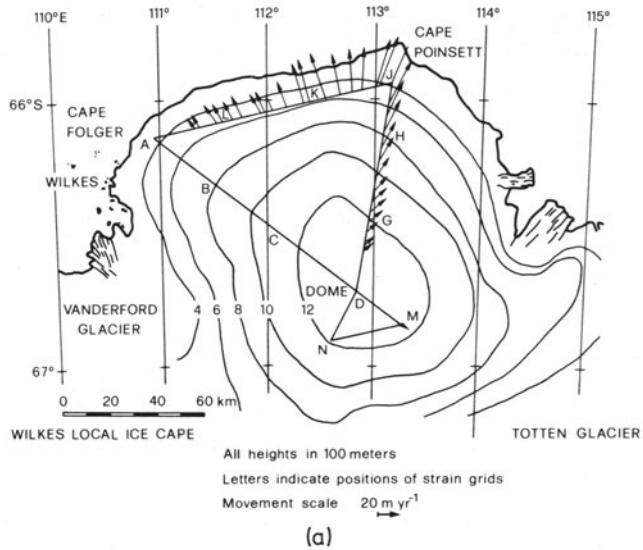
On a long wavelength scale, Equation (5.18) therefore assumes the form\*

$$\frac{d}{dx} \left[ \bar{D} \left( \frac{1}{\mathcal{A}} \right)^{1/n} |\dot{\varepsilon}_x^S|^{(1-n)/n} \dot{\varepsilon}_x^S \right] = -\frac{1}{2} [\bar{D}(\alpha_s - \bar{f})]. \quad (5.24)$$

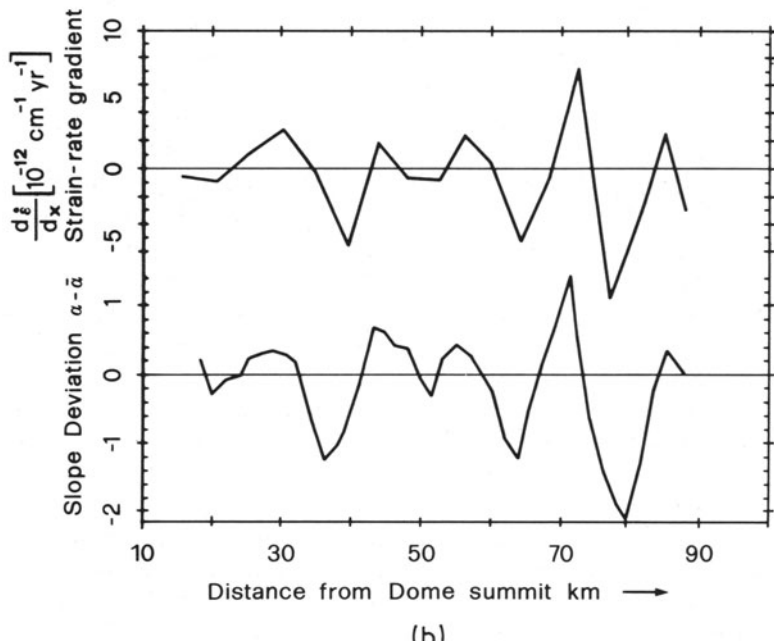
where  $\bar{f} = \tau_b/\bar{D}$ . If surface inclinations  $\alpha_s$  are measured and a rule is found how to evaluate  $\bar{f}$ , Equation (5.24) may be used to determine  $\mathcal{A}$  and  $n$  by measuring surface-strain rates  $\dot{\varepsilon}_x^S$  and their longitudinal derivatives. This is expertly done by Budd [4]. To find the rule for  $\bar{f}$ , consider a region where  $\bar{D}$  is constant;  $d\dot{\varepsilon}_x^S/d\bar{x}$  may be plotted versus distance and the same may be done for the quantity  $(\alpha_s - \bar{\alpha}_s)$ , where  $\bar{\alpha}_s$  is an average of  $\alpha_s$  over a representative length. Observationally, it is found that the functions  $d\dot{\varepsilon}_x^S/d\bar{x}$  and  $(\alpha_s - \bar{\alpha}_s)$  are best correlated if  $\bar{\alpha}_s$  is an average extending over lengths 20 times the thickness  $\bar{D}$ . Proof for this is provided by Figure 5.4. It shows for the Wilkes local ice cap in Antarctica the above two functions along the line Dome D–Cape Poinsett plotted against the distance from Dome D. It follows that, in Equation (5.24), we should set  $\bar{f} = \bar{\alpha}_s$ , where  $\bar{\alpha}_s$  is an average of the surface inclination angle  $\alpha_s$  over roughly 20 times the local thickness. For such a choice (5.24) does then indeed provide a reliable equation to be used to solve the two basic problems stated in the Introduction. Measuring  $\alpha_s$ ,  $\bar{D}$ ,  $\dot{\varepsilon}_x^S$  and determining the mean  $\bar{\alpha}_s$  allows the evaluation of  $n$  and  $\mathcal{A}$ . This has been done by Budd [4] who also gives further results. A further application is given by Robin [34].

The above procedure may be appealing to the practitioner but, mathematically, it is most unsatisfactory for various reasons. Firstly, the application of Equation (5.24) is limited to situations where surface and bottom inclination angles are small and where surface inclination angles are slowly varying functions of  $\bar{x}$ . With such drastic limitations of the basic theory, it is almost compelling that a more rigorous determination of the ice-flow solution

\*Budd [5] includes the term  $T$  and states that it becomes important at wavelengths  $\lambda \sim 3.6$  and smaller. Yet, assuming  $\alpha_s$  to be slowly varying (which is necessary for (5.18) to be correct)  $\lambda$  cannot become  $\mathcal{O}(1)$ . Equation (5.18) only makes sense when  $\lambda$  is large.



(a)



(b)

FIG. 5.4 (a) The Wilkes local ice cap showing movement vectors calculated from the differences between tellurometer traverses carried out in 1965 and 1966. (b) For the traverse line Dome-Poinsett of Figure 5.4a, the longitudinal strain rate gradient is plotted from the differences in tellurometer measurements over distances of about 5 km. Below are plotted the deviations in average slopes  $\alpha$  measured at 1.6 km intervals along the line (smoothed with a running mean of 5 km) from the smoothed slope  $\bar{\alpha}$  over 16 km. (From [3].)

would be possible. Secondly, the introduction of the representation  $\bar{f} = \bar{\alpha}_s$  is basically observational and cannot be rigorously justified. Finally, the introduction of the constitutive relationship is *ad hoc* and, in particular, the establishment of a constitutive equation relating the longitudinal surface-strain rate and the average stress-deviator constitutes a most unpleasant feature of the formulation. In the next section a more rigorous and satisfactory mathematical approach will be taken, which will turn out to be valid under less stringent conditions than is the case for Equation (5.24).

### 3. Solution of the Ice-flow Problem using the Shallow-ice Approximation

The ultimate goal of the theoretical developments in this section is to either mathematically predict the velocity and stress distribution in a plane flow problem when temperature distribution and the material properties of the ice are known, or else, to solve an inverse problem, namely to measure certain kinematic quantities, say surface velocities, longitudinal strain rates, and temperature distribution, etc., and to use these data to obtain information about the material properties.

#### (a) Governing equations

To achieve this goal, the procedure is essentially the same as in the previous chapters. The differential equations and boundary conditions governing the plane motion of ice must be formulated and integrated for the geometry depicted in Figure 5.2.

In dimensionless coordinates, the field equations for stresses and velocities are [see (4.1), (4.2)]

$$\begin{aligned} \frac{\partial \bar{u}}{\partial \bar{x}} + \frac{\partial \bar{v}}{\partial \bar{y}} &= 0, & \frac{\partial \sigma_x}{\partial \bar{x}} + \frac{\partial \tau}{\partial \bar{y}} + \sin \gamma &= 0, \\ \frac{\partial \bar{u}}{\partial \bar{x}} &= \frac{1}{2} \mathbb{G} \tilde{\mathfrak{F}}(\tau'_{II}, \hat{\theta})(\sigma_x - \sigma_y), & \frac{\partial \tau}{\partial \bar{x}} + \frac{\partial \sigma_y}{\partial \bar{y}} - \cos \gamma &= 0, \\ \frac{\partial \bar{u}}{\partial \bar{y}} + \frac{\partial \bar{v}}{\partial \bar{x}} &= 2 \mathbb{G} \tilde{\mathfrak{F}}(\tau'_{II}, \hat{\theta})\tau, \end{aligned} \quad (5.25)$$

where

$$\tau'_{II} = \frac{1}{4}(\sigma_x - \sigma_y)^2 + \tau^2, \quad \tilde{\mathfrak{F}}(\tau'_{II}, \hat{\theta}) = \exp(\mathbb{A}\theta) \mathfrak{F}(\tau'_{II}), \quad \theta = \frac{(1 - \mathbb{Z})\hat{\theta}}{1 + \mathbb{Z}\hat{\theta}} \quad (5.26)$$

and the boundary conditions, at the base  $\bar{y} = \bar{y}_B(\bar{x})$  [see (4.4)(4.6)]

$$\bar{v} = \frac{d\bar{y}_B}{d\bar{x}} \bar{u}, \quad \bar{u} \cos \beta + \bar{v} \sin \beta = \mathbb{C} \{ \tau(\cos^2 \beta - \sin^2 \beta) + (\sigma_x - \sigma_y) \sin \beta \cos \beta \}^m \quad (5.27)$$

and at the top surface  $\bar{y} = \bar{y}_s(\bar{x}, \bar{t})$  [see (4.3)]

$$\left. \begin{aligned} \frac{\partial \bar{y}_s}{\partial \bar{t}} + \frac{\partial \bar{y}_s}{\partial \bar{x}} \bar{u} - \bar{v} &= \bar{a} \\ \sigma_x \sin^2 \alpha + \sigma_y \cos^2 \alpha + \tau \sin 2\alpha &= -\bar{p}^{\text{atm}}, \\ \tau &= \frac{1}{2}(\sigma_y - \sigma_x) \tan 2\alpha. \end{aligned} \right\} \quad \text{at } \bar{y} = \bar{y}_s(\bar{x}, \bar{t}). \quad (5.28)$$

In the above,  $\tilde{\mathfrak{F}}(\cdot)$  is the creep response function,  $\mathbb{A}$  the Arrhenius factor and  $\hat{\vartheta}$  the dimensionless temperature, assumed to be known as a function of position, and  $\mathbb{Z} \ll 1$  is a constant. The constant  $\mathbb{G}$  was set equal to unity in previous normalizations. With the exception of steep glaciers, this resulted in magnitudes for the dimensionless longitudinal velocity in the order of  $10^{-2}$  or smaller, but did not cause any substantial difficulties when solutions of the governing equations were constructed. For most parts of this chapter we shall normalize equations again by taking  $\mathbb{G} = 1$ , but in Section 5  $\mathbb{G}$  will first be left arbitrary and subsequently determined by applying order of magnitude arguments.

Equations (5.25) represent the balance of momentum, the continuity equation and the constitutive equation relating strain rate and stress deviator. Equation (5.27)<sub>1</sub> states that the flow at the base must be tangential to this base and (5.27)<sub>2</sub> is the viscous sliding law  $u_s = \mathbb{C}\tau_b^m$ , where  $u_s$  is the component of the velocity at the base tangential to it, and  $\tau_b$  is the basal shear traction. In the boundary conditions (5.28) for the top surface, the first equation represents the kinematic surface condition, whereas the remaining two are expressions of the continuity of stress.

In the above presentation of field equations and boundary conditions, attention has been limited to the boundary-value problem of stress and velocity. As was basically the case in Chapter 4, temperature is treated as a known function of space and time, which is determined from field measurements or approximate solutions of the energy equation. When stresses and velocities for the approximate temperature profile are determined it is possible to improve on this temperature profile. The respective boundary-value problem follows from Equations (4.1)–(4.4) and reads

$$\begin{aligned} \frac{\partial \hat{\vartheta}}{\partial \bar{t}} + \frac{\partial \hat{\vartheta}}{\partial \bar{x}} \bar{u} + \frac{\partial \hat{\vartheta}}{\partial \bar{y}} \bar{v} &= \mathbb{D} \nabla^2 \hat{\vartheta} + \frac{\mathbb{E}}{2} \tilde{\mathfrak{F}}(\tau_{II}', \hat{\vartheta}) \tau_{II}', \\ \hat{\vartheta} &= \vartheta_s, \quad \text{at } \bar{y} = \bar{y}_s(\bar{x}, \bar{t}), \\ \frac{\partial \hat{\vartheta}}{\partial \bar{x}} \sin \beta - \frac{\partial \hat{\vartheta}}{\partial \bar{y}} \cos \beta &= \mathbb{Q}^{\text{geoth}}, \quad \text{at } \bar{y} = \bar{y}_B(\bar{x}). \end{aligned} \quad (5.29)$$

In this set of equations the surface geometry, the stress and velocity fields, the surface temperature  $\vartheta_s$  and the geothermal heat flux are prescribed or known from the solution of (5.25)–(5.28). The boundary-value problem

(5.29) then serves to obtain an improved estimate for the temperature field which, in turn, may again be used to obtain an improved iterate of the stress-velocity boundary-value problem. It is our belief that this last step need not be pursued.

Henceforth, approximate solutions to the above boundary-value problems will be sought. These are based on a perturbation expansion procedure in which the *shallow ice approximation* is naturally incorporated. This approximation will now be discussed.

### (b) Shallow-ice approximation

A function  $f(\bar{x})$  defined in  $\bar{x}_0 \leq \bar{x} \leq \bar{x}_1$  is called *slowly varying* in  $\bar{x}$ , if the absolute value of its gradient remains small in the domain of its definition; in other words,  $|df/d\bar{x}| \ll 1$ , for  $\bar{x}_0 \leq \bar{x} \leq \bar{x}_1$ . This in turn implies that function values change appreciably only over distances which are large as compared to unity. A transformation of the independent variable is therefore suggested with the property that in terms of this new, independent variable, the gradients will be  $\mathcal{O}(1)$ . To give an example, (see Figure 5.5), let  $f(\bar{x}) = \cos(2\pi\bar{x}/\lambda)$ , where  $\lambda$  is supposed to be large. Then  $|df/d\bar{x}| = (2\pi/\lambda)|\cos(2\pi\bar{x}/\lambda)|$  is necessarily small. Introducing the new variable  $\xi = 2\pi\bar{x}/\lambda$ , one has  $f(\xi) = \cos \xi$ ; it follows that  $|df/d\xi| = |\sin \xi|$  is  $\mathcal{O}(1)$ , in fact it assumes the value 1 for  $\xi = \pi/2$ . More intuitively the graph of  $f(\xi)$  is *squeezed* relative to that of  $f(\bar{x})$ , or alternatively the graph of  $f(\bar{x})$  is *stretched* as compared to that of  $f(\xi)$ . For this reason, the transformation  $\xi \rightarrow \bar{x}$ , is generally called a *stretching transformation*.

Prompted by the observationally-established fact that surface and smoothed-out base undulations are generally slowly varying, we now incorporate a statement to that effect into the boundary-value problem (5.25)–(5.29). Since the geometry of the ice slope is slowly varying, we introduce a stretching transformation

$$\xi = \mu\bar{x}, \quad \eta = \bar{y}, \quad (5.30)$$

in which the stretching parameter  $\mu$  is a small quantity  $0 < \mu \ll 1$ .  $\mu$  must be

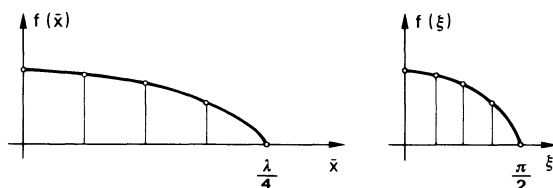


Fig. 5.5 Explaining the introduction of stretched coordinates.

determined for any particular ice sheet. A reasonable definition is

$$\mu = \frac{\text{mean thickness of ice sheet}}{\text{typical wavelength of surface undulations}}.$$

Another one would be  $\mu = D/L$  where  $D$  is a mean thickness and  $L$  a representative length of the sheet. For the Wilkes ice cap in Antarctica (see Budd [4]), this yields an order of magnitude of  $\mu \lesssim 0.05$ .

A slowly varying geometry must lead to a corresponding ordering of the field variables. Indeed, it is to be expected that transverse velocities  $\bar{v}$  are much smaller than longitudinal velocities  $\bar{u}$ . It is therefore natural to scale velocities according to

$$U = \bar{u}, \quad V = \frac{1}{\mu} \bar{v}. \quad (5.31)$$

Finally, time is scaled according to

$$\tau = \mu \bar{\tau}; \quad (5.32)$$

this last scaling will be explained later.

The scalings (5.30)–(5.32) may now be introduced into the governing equations (5.25)–(5.28). If that is done, it can readily be shown that the boundary-value problem for  $U$ ,  $V$ ,  $\sigma_x$ ,  $\sigma_y$ ,  $\tau$  and  $\bar{y}_s$  assumes the form:

*Field equations :*

$$\begin{aligned} \frac{\partial U}{\partial \xi} + \frac{\partial V}{\partial \eta} &= 0, & \mu \frac{\partial \sigma_x}{\partial \xi} + \frac{\partial \tau}{\partial \eta} + \sin \gamma &= 0, \\ \mu \frac{\partial U}{\partial \xi} &= \frac{1}{2} \tilde{\mathfrak{F}}(\tau'_H, \hat{\theta})(\sigma_x - \sigma_y), & \mu \frac{\partial \tau}{\partial \xi} + \frac{\partial \sigma_y}{\partial \eta} - \cos \gamma &= 0, \\ \frac{\partial U}{\partial \eta} + \mu^2 \frac{\partial V}{\partial \xi} &= 2 \tilde{\mathfrak{F}}(\tau'_H, \hat{\theta})\tau, \end{aligned} \quad (5.33)$$

where  $\mathbb{G}$  has been set equal to 1.

*Boundary conditions :*

$$\left. \begin{aligned} U \left[ 1 - \mu^2 \left( \frac{d\bar{y}_B}{d\xi} \right)^2 \right] &= \zeta \mathbb{C} \left( \frac{1}{1 + \mu^2 (d\bar{y}_B/d\xi)^2} \right)^{(2m-1)/2} \times \\ &\times \left\{ \zeta \left[ \left( 1 - \mu^2 \left( \frac{d\bar{y}_B}{d\xi} \right)^2 \right) \tau - \mu \frac{d\bar{y}_B}{d\xi} (\sigma_x - \sigma_y) \right] \right\}^m, \\ V &= U \frac{d\bar{y}_B}{d\xi}, \quad \zeta = \text{sgn} \left( U - \mu^2 \frac{d\bar{y}_B}{d\xi} V \right), \end{aligned} \right\} \quad \eta = \bar{y}_B(\xi) \quad (5.34)$$

$$\left. \begin{aligned} \frac{\partial \bar{y}_s}{\partial t} + \frac{\partial \bar{y}_s}{\partial \xi} U - V &= \frac{\bar{a}}{\mu}, \\ (\sigma_x - \sigma_y) \left( 1 + \mu^2 \frac{\partial \bar{y}_s}{\partial \xi} \right) - (\sigma_x - \sigma_y) \left( 1 - \mu^2 \frac{\partial \bar{y}_s}{\partial \xi} \right) - \\ - 4\tau\mu \frac{\partial \bar{y}_s}{\partial \xi} &= -2\bar{p}_{\text{atm}} \left[ 1 + \mu^2 \left( \frac{\partial \bar{y}_s}{\partial \xi} \right)^2 \right], \\ \tau \left[ 1 - \mu^2 \left( \frac{\partial \bar{y}_s}{\partial \xi} \right)^2 \right] + \mu(\sigma_x - \sigma_y) \frac{\partial \bar{y}_s}{\partial \xi} &= 0, \end{aligned} \right\} \quad \eta = \bar{y}_s(\xi, t) \quad (5.35)$$

where for further applications  $\bar{a} = \mu \mathfrak{A}$ .

In these equations only the boundary conditions need further explanations. To derive (5.34) and (5.35) use has been made of relations (5.6) and  $\sin \alpha, \cos \alpha, \sin \beta$  and  $\cos \beta$  have been expressed in terms of  $\partial \bar{y}_s / \partial \xi$  and  $d\bar{y}_B / d\xi$ , respectively. The form of Equation (5.35)<sub>1</sub> also indicates why time was scaled according to Equation (5.32). Equations (5.28)<sub>1</sub> and (5.35)<sub>1</sub> are formally identical, a fact which was only achieved through the scaling (5.32). The preservation of the form of the equation is desired because it guarantees that the stretched equation exhibits the same properties as the original equation. Since the kinematic surface condition is the only equation where explicit time dependencies enter this is especially important for the determination of the surface geometry. In fact, only when both time and space derivatives are kept under scalings such as the ones above, can it be ascertained that surface wave propagations may be predicted by Equation (5.35)<sub>1</sub>. To see

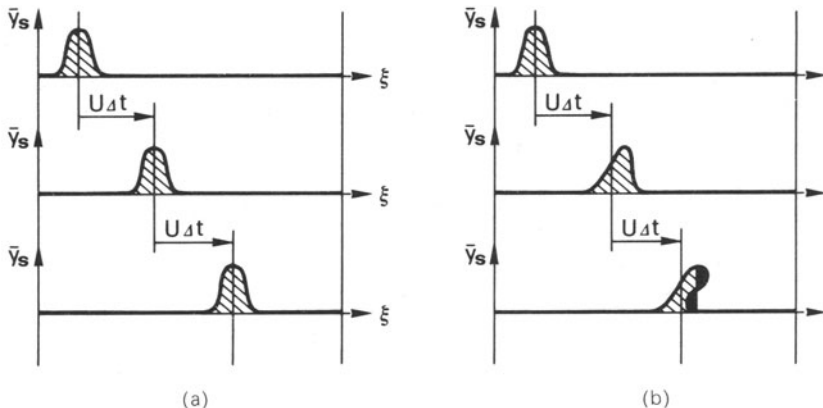


FIG. 5.6. Qualitative behavior of the kinematic surface condition (5.35)<sub>1</sub> to time-dependent perturbations when  $\bar{a} = 0$  and  $V = 0$ . Figure 5.6a illustrates the linear cases, Figure 5.6b the non-linear response. Bulges may deform in this latter case and waves may break, giving rise to shock formation.

this notice that for  $\bar{a} = 0$ ,  $V = 0$  and  $U = U(\bar{y}_S)$ , the simple forward wave equation, (see Whitham [48]), emerges from (5.35)<sub>1</sub>, namely  $\partial\bar{y}_S/\partial\ell + U(\bar{y}_S)\partial\bar{y}_S/\partial\xi = 0$ , with the solution  $\bar{y}_S = F(\xi - U(\bar{y}_S)\ell)$ , where  $F$  is any differentiable function, given by the initial distribution  $\bar{y}_S(\xi, 0)$ . For  $U$  constant, the equation is linear and a surface bulge propagates with constant speed  $U$  and is undistorted to the right, see Figure 5.6a. In the non-linear case,  $U = U(\bar{y}_S)$ , the wave speed depends on amplitude and, consequently, waves may deform. For monotone increasing  $U(\bar{y}_S)$ , wave speeds at crests are faster than at neutral positions giving rise to an oversteepening of the surface elevation which eventually leads to breaking waves and thus shock formation, see Figure 5.6b. Hence the kinematic surface equation is capable of describing a wealth of physical phenomena whose prediction should be maintained in the scaled equations. This is the true reason for the scaling (5.32).

Finally, in subsequent calculations, an expression for the basal shear stress  $\tau_b$  will be needed. When formula (5.8)<sub>2</sub> is expressed in the new coordinates  $\xi$  and  $\eta$  it becomes

$$\tau_b = \tau \left[ 1 - 2\mu^2 \left( \frac{d\bar{y}_B}{d\xi} \right)^2 \right] - (\sigma_x - \sigma_y)\mu \frac{d\bar{y}_B}{d\xi} + \mathcal{O}(\mu^3). \quad (5.36)$$

By formulating the boundary-value problem in the stretched variables, a small parameter has entered the governing equations. This suggests seeking an approximate solution of the basic boundary-value problem in terms of powers of the stretching parameter  $\mu$ . The introduction of the scaled variables  $\xi$ ,  $\ell$ ,  $V$  together with the implementation of the suggested perturbation expansion is called the *shallow ice approximation*. It was introduced into ice-flow problems by Hutter [16] and in a slightly different form by Fowler and Larson [13].\*

The same transformations can also be performed with Equations (5.29). When this is done, the following form of the temperature boundary-value problem is obtained:

$$\begin{aligned} \frac{\partial \hat{\vartheta}}{\partial \ell} + U \frac{\partial \hat{\vartheta}}{\partial \xi} + V \frac{\partial \hat{\vartheta}}{\partial \eta} &= \mu^{-1} \left[ \mathbb{D} \frac{\partial^2 \hat{\vartheta}}{\partial \eta^2} + \frac{1}{2} \mathbb{E} \tilde{\mathfrak{F}}(\tau'_{II}, \hat{\vartheta}) \tau'_{II} + \mu^2 \mathbb{D} \frac{\partial^2 \hat{\vartheta}}{\partial \xi^2} \right], \\ \hat{\vartheta} &= \vartheta_S, \quad \text{at } \bar{y} = \bar{y}_S(\xi, \ell), \\ \frac{\partial \hat{\vartheta}}{\partial \eta} - \mu^2 \frac{\partial \hat{\vartheta}}{\partial \xi} \frac{d\bar{y}_B}{d\xi} &= -\mathbb{Q}^{\text{geoth}} \left[ 1 + \frac{1}{2} \mu^2 \left( \frac{d\bar{y}_B}{d\xi} \right)^2 \right], \quad \text{at } \bar{y} = \bar{y}_B(\xi). \end{aligned} \quad (5.37)$$

\*The stretching transformation (5.30)–(5.32) and a corresponding perturbation expansion of the stretched equations is widely used in many branches of fluid mechanics. Friedrichs [14] and Keller [20] have introduced them to derive the shallow water equations, see Stoker [39]. A summary of research on surface water waves based on these transformations is given by Wehausen and Laitone [47]. Benney [1] uses them in a theory of liquid films.

In this boundary-value problem for  $\hat{\vartheta}$ , the time rate of temperature change is balanced by longitudinal and transverse advection, transverse conduction, and dissipation, whereas the longitudinal conduction is, of higher order, small. The reader may recall that with the exception of the longitudinal advective terms, this was exactly the situation dealt with in Chapters 3 and 4. There it was also mentioned that longitudinal advective terms must be included if temperature profiles with inversions are to be properly predicted. This was tacitly assumed by previous authors, for instance Weertman [46], and thus provides one possible *a posteriori* justification for the shallow-ice approximation introduced above.

(c) *Construction of the perturbation solution*

In what follows in the remainder of this section, we shall set the kinematic surface equation (5.35)<sub>1</sub> aside and assume that both surface equation  $\eta = \bar{y}_S(\xi, \tau)$  and equation of the base  $\eta = \bar{y}_B(\xi)$  be given prescribed functions of position and/or time. What remains of the original boundary-value problem is then the determination of the stress and velocity distribution for known geometry.

Solutions to the Equations (5.33)–(5.35) are being sought in terms of the perturbation expansion

$$(\sigma_x, \sigma_y, \tau, U, V) = \sum_{j=0}^{\infty} \mu^j (\sigma_x^{(j)}, \sigma_y^{(j)}, \tau^{(j)}, U^{(j)}, V^{(j)}).$$

Substituting these expansions into the governing Equations (5.33)–(5.35) will result in a hierarchy of boundary-value problems for the  $j$ th-order quantities, which can be solved in a consecutive order. The zeroth-order equations are obtained by simply deleting from Equations (5.33)–(5.35) all terms involving the factor  $\mu$ . This yields the differential equations

$$\begin{aligned} \frac{\partial \tau^{(0)}}{\partial \eta} &= -\sin \gamma, & \frac{\partial \sigma_y^{(0)}}{\partial \eta} &= \cos \gamma, & \sigma_x^{(0)} &= \sigma_y^{(0)}, \\ \frac{\partial U^{(0)}}{\partial \xi} + \frac{\partial V^{(0)}}{\partial \eta} &= 0, & \frac{\partial U^{(0)}}{\partial \eta} &= 2\tilde{\mathcal{F}}(\tau^{(0)2}, \hat{\vartheta})\tau^{(0)} \end{aligned} \quad (5.38)$$

subject to the boundary conditions

$$\begin{aligned} U^{(0)} &= C[\tau^{(0)}]^m, & V^{(0)} &= U^{(0)} \frac{d\bar{y}_B}{d\xi} \quad \text{at } \eta = \bar{y}_B(\xi), \\ \sigma_y^{(0)} &= -\bar{p}^{\text{atm}}, & \tau^{(0)} &= 0, \quad \text{at } \eta = \bar{y}_S(\xi, \tau). \end{aligned} \quad (5.39)$$

The stress equations in (5.38) can immediately be integrated since sufficient boundary conditions are prescribed to determine the ‘constants’ of integra-

tion; consequently,

$$\begin{aligned}\tau^{(0)}(\xi, \eta, \ell) &= \sin \gamma [\bar{y}_s(\xi, \ell) - \eta] \\ \sigma_x^{(0)}(\xi, \eta, \ell) &= \sigma_y^{(0)}(\xi, \eta, \ell) = \cos \gamma [\eta - \bar{y}_s(\xi, \ell)] - \bar{p}^{\text{atm}}.\end{aligned}\quad (5.40)$$

Having determined  $\tau^{(0)}$ , its value can be substituted into the creep response function  $\tilde{\mathfrak{F}}(\tau^{(0)2})$  of (5.38)<sub>5</sub> and into the boundary condition (5.39)<sub>1</sub>. A simple quadrature then determines the longitudinal velocity  $U^{(0)}$  in which the 'constant' of integration is determined using Equation (5.39)<sub>1</sub>. The result of this integration is

$$U^{(0)}(\xi, \eta, \ell) = \mathbb{C} \sin^m \gamma \bar{D} + 2 \int_{\bar{y}_B(\xi)}^{\eta} \tilde{\mathfrak{F}}(\mathcal{X}^2(\eta'), \hat{\mathcal{G}}(\eta')) \mathcal{X}(\eta') d\eta' \quad (5.41)$$

where

$$\begin{aligned}\bar{D} &\equiv \bar{y}_s(\xi, \ell) - y_B(\xi), \\ \mathcal{X} &= \mathcal{X}(\xi, \eta, \ell) \equiv \sin \gamma (\bar{y}_s(\xi, \ell) - \eta)\end{aligned}$$

are the local dimensionless glacier thicknesses and the zeroth-order shear stress. Notice also that in the variables  $\mathcal{X}$  and  $\hat{\mathcal{G}}$  of the integrand function  $\tilde{\mathfrak{F}}$ , only the variable to be integrated over has been made explicit, although both quantities are functions of three variables, namely  $\xi$ ,  $\eta$  and  $\ell$ . Henceforth this abbreviated notation will be consistently used and the reader is advised to bear this in mind.

The representation (5.41) may now be used in the continuity Equation (5.38)<sub>4</sub>; a further integration of the resulting equation with respect to  $\eta$  in combination with the boundary condition (5.39) will finally determine the transverse velocity component  $V^{(0)}$ . The pertinent calculations are not presented but the result is as follows.\*

$$\begin{aligned}V^{(0)}(\xi, \eta, \ell) &= -2 \frac{\partial \bar{y}_s}{\partial \xi} \int_{\bar{y}_B}^{\eta} [\sin \gamma \tilde{\mathfrak{F}}(\mathcal{X}^2(\eta''), \hat{\mathcal{G}}(\eta'')) + \\ &\quad + 2 \sin^3 \gamma (\bar{y}_s - \eta'')^2 \tilde{\mathfrak{F}}_x(\mathcal{X}^2(\eta''), \hat{\mathcal{G}}(\eta''))] d\eta'' - \\ &\quad - 2 \int_{\bar{y}_B}^{\eta} d\eta' \int_{\bar{y}_B}^{\eta''} \tilde{\mathfrak{F}}_g(\mathcal{X}^2(\eta''), \hat{\mathcal{G}}(\eta'')) \sin \gamma (\bar{y}_s - \eta'') \frac{\partial \hat{\mathcal{G}}(\eta'')}{\partial \xi} d\eta'' + \\ &\quad + 2 \frac{d\bar{y}_B}{d\xi} \tilde{\mathfrak{F}}(\mathcal{X}^2(\bar{y}_B), \hat{\mathcal{G}}(\bar{y}_B)) \sin \gamma \bar{D}(\eta - \bar{y}_B) - \\ &\quad - m \sin^m \gamma \frac{\partial}{\partial \xi} (\mathbb{C} \bar{D}^m)(\eta - \bar{y}_B) + \mathbb{C} \sin^m \gamma \bar{D}^m \frac{d\bar{y}_B}{d\xi}.\end{aligned}\quad (5.42)$$

Here,  $\tilde{\mathfrak{F}}_x$  and  $\tilde{\mathfrak{F}}_g$  denote the derivatives of  $\tilde{\mathfrak{F}}$  with respect to the first and

\*Hutter in [16] neglected the term involving  $\tilde{\mathfrak{F}}_g$ . This amounts to assuming  $\hat{\mathcal{G}} = \hat{\mathcal{G}}(\eta)$ .

second arguments. Equations (5.40)–(5.42) comprise the complete solution provided that the free surface and the base geometry are prescribed functions of position and time. Notice that  $U^{(0)}$  varies essentially with  $\bar{y}_B$  and, on the free surface, with  $\bar{y}_S$ . No dependence on gradients  $\partial\bar{y}_S/\partial\xi$ ,  $d\bar{y}_B/d\xi$  occurs. Such dependencies, however, enter the expression for  $V^{(0)}$ .

What has been achieved by this zeroth-order solution? An approximation of the stress and velocity distribution in the entire ice sheet has been obtained. With the feature that stress and longitudinal velocity are calculated as if the ice strip were strictly parallel-sided with no changes in the longitudinal direction. To lowest order, the shallow ice approximation is therefore equivalent to the assumption of a strictly parallel-sided ice slab in which no fields vary with  $\bar{x}$ . But unlike the exact solution to the latter problem, the shallow-ice approximation also yields a non-vanishing transverse velocity field. The solution is such that for a given creep response function  $\tilde{\mathfrak{F}}$ , temperature distribution and geometry, at most quadratures are needed to obtain zeroth-order stress and velocity components. This is a big step forward when compared with the procedure using the basal shear-stress formula in Section 2. The method allows us to account for viscous sliding at the bed and for an arbitrary transverse variation of material properties but, as can be seen, is not yet general enough if the zeroth-order basal shear stress is calculated:

$$\tau_b^{(0)} = \tau^{(0)} = \sin \gamma \bar{D}(\xi, \eta, \ell).$$

This result is not sufficiently accurate, but may be regarded as a first term of an expansion such as, e.g., (5.16). The next step is, therefore, to proceed to higher-order equations. Collecting terms linear in  $\mu$  results in the following boundary-value problem for first-order stresses and velocities:

$$\begin{aligned} \frac{\partial \tau^{(1)}}{\partial \eta} &= \cos \gamma \frac{\partial \bar{y}_S}{\partial \xi}, & \frac{\partial \sigma_y^{(1)}}{\partial \eta} &= -\sin \gamma \frac{\partial \bar{y}_S}{\partial \xi}, \\ \sigma_x^{(1)} &= \sigma_y^{(1)} + \frac{2}{\tilde{\mathfrak{F}}(\tau^{(0)}, \hat{\mathfrak{G}})} \frac{\partial U^{(0)}}{\partial \xi}, \\ \frac{\partial U^{(0)}}{\partial \xi} + \frac{\partial V^{(1)}}{\partial \eta} &= 0, & \frac{\partial U^{(1)}}{\partial \eta} &= 2\tilde{\mathfrak{F}}(\tau^{(0)}, \hat{\mathfrak{G}})\tau^{(1)} \end{aligned} \quad (5.43)$$

and

$$\begin{aligned} U^{(1)} &= \mathbb{C}m[\tau^{(0)}]^{m-1}\tau^{(1)}, & V^{(1)} &= U^{(1)} \frac{d\bar{y}_B}{d\xi}, \quad \text{at } \eta = \bar{y}_B(\xi), \\ \sigma_y^{(1)} &= -2\tau^{(0)} \frac{\partial \bar{y}_S}{\partial \xi} = 0, & \tau^{(1)} &= 0, \quad \text{at } \eta = \bar{y}_S(\xi, \ell). \end{aligned} \quad (5.44)$$

In these equations, all zeroth-order quantities are known. Integration is

again straightforward if somewhat tedious. In a first step, the stresses are determined by integrating (5.43)<sub>1,2</sub> subject to the boundary conditions (5.44)<sub>3,4</sub>. The result is

$$\begin{aligned}\tau^{(1)}(\xi, \eta, \ell) &= \cos \gamma(\eta - \bar{y}_S(\xi, \ell)) \frac{\partial \bar{y}_S}{\partial \xi}(\xi, \ell), \\ \sigma_y^{(1)}(\xi, \eta, \ell) &= -\sin \gamma(\eta - \bar{y}_S(\xi, \ell)) \frac{\partial \bar{y}_S}{\partial \xi}(\xi, \ell), \\ \sigma_x^{(1)}(\xi, \eta, \ell) &= -\sin \gamma(\eta - \bar{y}_S(\xi, \ell)) \frac{\partial \bar{y}_S}{\partial \xi}(\xi, \ell) \\ &\quad + \frac{2}{\tilde{\mathfrak{F}}(\mathcal{X}^2(\eta), \hat{\mathfrak{G}}(\eta))} \frac{\partial U^{(0)}}{\partial \xi}(\xi, \eta, \ell)\end{aligned}\tag{5.45}$$

and the reader may check that (5.43) and (5.44)<sub>3,4</sub> are satisfied. The representations for the stresses  $\tau^{(1)}$  and  $\sigma_y^{(1)}$  are regular under all reasonable physical situations, but first-order longitudinal stresses  $\sigma_x^{(1)}$  may become infinitely large at the free surface if  $\tilde{\mathfrak{F}}(0, \hat{\mathfrak{G}})$  should vanish. For Glen's flow law, this is indeed the case, but when the more general law

$$\tilde{\mathfrak{F}}(x, \hat{\mathfrak{G}}) = \exp(\mathbb{A}\theta) \frac{x^{(n-1)/2} + \mathbb{I}}{1 + \mathbb{I}},$$

is used, which exhibits Newtonian behavior at small stretching,  $\tilde{\mathfrak{F}}(0, \hat{\mathfrak{G}}) \neq 0$ , and  $\sigma_x^{(1)}$  remains finite. Of course, in order for the perturbation analysis to remain valid  $\sigma_x^{(1)}$  must not become large. In view of formula (5.45)<sub>3</sub>, this implies that  $\partial U^{(0)}/\partial \xi \sim \mathbb{L} \lesssim 10^{-3}$ . This is usually the case. Nevertheless, the singular behavior points at a limitation of the above perturbation procedure. Rectification will involve the methods of matched asymptotic expansions in which boundary-layer solutions are developed, see e.g. Cole [7].

There remains the integration of Equations (5.43)<sub>4,5</sub>. In a first step,  $U^{(1)}$  is determined by substituting  $\tau^{(1)}$  and  $\tau^{(0)}$  as given in (5.40)<sub>1</sub> and (5.45), respectively, and integrating the resulting equation subject to the boundary condition (5.44)<sub>1</sub>. This process yields

$$\begin{aligned}U^{(1)}(\xi, \eta, \ell) &= 2 \cos \gamma \frac{\partial \bar{y}_S}{\partial \xi} \int_{\bar{y}_B}^{\eta} \tilde{\mathfrak{F}}(\mathcal{X}^2(\eta'), \hat{\mathfrak{G}}(\xi, \eta', \ell)) (\eta' - \bar{y}_S) d\eta' - \\ &\quad - \mathbb{C}m \sin^{m-1} \gamma \tilde{D}^m \cos \gamma \frac{\partial \bar{y}_S}{\partial \xi}.\end{aligned}\tag{5.46}$$

This result for  $U^{(1)}$  may now be used in the first-order continuity equation, and a subsequent integration subject to the boundary condition (5.44)<sub>2</sub> will give an explicit expression for the first-order transverse velocity  $V^{(1)}$ . The

result of the straightforward calculation is

$$\begin{aligned}
 V^{(1)} = & + 2 \cos \gamma \left( \frac{\partial \bar{y}_S}{\partial \xi} \right)^2 \int_{\bar{y}_B}^{\eta} d\eta' \int_{\bar{y}_B}^{\eta'} \{ 2 \tilde{\mathfrak{F}}_x(\mathcal{X}^2(\eta''), \hat{\mathfrak{H}}(\eta'')) \sin^2 \gamma (\eta'' - \bar{y}_S)^2 + \right. \\
 & + \tilde{\mathfrak{F}}(\mathcal{X}^2(\eta''), \hat{\mathfrak{H}}(\eta'')) \} d\eta'' - \\
 & - 2 \cos \gamma \frac{\partial^2 \bar{y}_S}{\partial \xi^2} \int_{\bar{y}_B}^{\eta} d\eta' \int_{\bar{y}_B}^{\eta'} (\eta'' - \bar{y}_S) \tilde{\mathfrak{F}}(\mathcal{X}^2(\eta''), \hat{\mathfrak{H}}(\eta'')) d\eta'' - \\
 & - 2 \cos \gamma \frac{\partial \bar{y}_S}{\partial \xi} \int_{\bar{y}_B}^{\eta} d\eta' \int_{\bar{y}_B}^{\eta'} (\eta'' - \bar{y}_S) \tilde{\mathfrak{F}}_g(\mathcal{X}^2(\eta''), \hat{\mathfrak{H}}(\eta'')) \frac{\partial \hat{\mathfrak{H}}(\eta'')}{\partial \xi} d\eta'' - \\
 & - 2 \cos \gamma \frac{\partial \bar{y}_S}{\partial \xi} \frac{d\bar{y}_B}{d\xi} \tilde{\mathfrak{F}}(\mathcal{X}^2(\bar{y}_B), \hat{\mathfrak{H}}(\bar{y}_B)) \bar{D}(\eta - \bar{y}_B) + \\
 & \left. + m \cdot \sin^{m-1} \gamma \cos \gamma \left[ \frac{\partial}{\partial \xi} \left( \mathbb{C} \bar{D}^m \frac{\partial \bar{y}_S}{\partial \xi} \right) (\eta - \bar{y}_B) - \mathbb{C} \bar{D} \frac{\partial \bar{y}_S}{\partial \xi} \frac{d\bar{y}_B}{d\xi} \right] \right]. \tag{5.47}
 \end{aligned}$$

$\tilde{\mathfrak{F}}_x$  and  $\tilde{\mathfrak{F}}_g$  are again the partial derivatives of  $\tilde{\mathfrak{F}}$  with respect to the first and second arguments, respectively. Notice that  $\tilde{\mathfrak{F}}_g$  will vanish for a temperate glacier. Observe also that for actual calculations, the two-fold integrals can be reduced to single integrals by means of the formula

$$\int_{\bar{y}_B(\xi)}^{\eta} d\eta' \int_{\bar{y}_B(\xi)}^{\eta'} f(\eta'') d\eta'' = \int_{\bar{y}_B(\xi)}^{\eta} (\eta - \eta') f(\eta') d\eta'. \tag{5.48}$$

Here  $f(\cdot)$  stands for either one of the innermost integrand functions in (5.47). The Equations (5.45)–(5.47) furnish first-order corrections to the lowest-order velocity and stress solutions. Finally, notice that both  $U^{(1)}$  and  $V^{(1)}$  are regular as  $\xi \rightarrow 0$ , but that the integrand function in  $V^{(1)}$  involving  $\tilde{\mathfrak{F}}_x$  may become singular in this case. The singularity only arises for  $1 < n < 3$  and is integrable.

Let us pause for a moment and point at the importance of the results at this level. A means to test them is to evaluate the basal shear stress to within terms linear in  $\mu$ . This yields

$$\begin{aligned}
 \tau_b &= \tau^{(0)} + \mu \left[ \tau^{(1)} - (\sigma_x^{(0)} - \sigma_y^{(0)}) \frac{d\bar{y}_B}{d\xi} \right] = \tau^{(0)} + \mu \tau^{(1)} \\
 &= \left( \sin \gamma - \mu \cos \gamma \frac{\partial \bar{y}_S}{\partial \xi} \right) \bar{D} = \left( \sin \gamma - \cos \gamma \frac{\partial \bar{y}_S}{\partial \bar{x}} \right) \bar{D} \\
 &= (\sin \gamma + \cos \gamma \alpha) \bar{D}.
 \end{aligned} \tag{5.49}$$

Here the transformation (5.29)<sub>1</sub> has been used, and  $\partial \bar{y}_S / \partial \xi$  has been replaced by  $-\alpha$  which is in line with the basic assumption that  $\bar{y}_S$  is slowly varying in  $\bar{x}$ . The result (5.49) agrees with the first term on the right-hand side of (5.17), and it reduces to  $\tau_b = \bar{D} \alpha_S$ , where  $\alpha_S = \alpha + \gamma$  is the local surface inclination,

when the latter is small. To within first-order terms, the basal shear stress is, therefore, proportional to the local inclination  $\alpha_s$  and to the respective depth; this agrees with the familiar result derived in the introduction to this Chapter by a physically more-appealing and more-direct approach; the above mathematical approach arrives at the same result on the basis of a more rigorous footing as it clearly speaks out the conditions of validity of relation (5.49) (and of previous results). *These conditions are that the bounding surfaces  $\bar{y} = \bar{y}_S(\bar{x}, \ell)$  and  $\bar{y} = \bar{y}_B(\bar{x})$  be slowly varying functions of  $\bar{x}$ .* These are more stringent than the conditions of validity for Equation (5.16), a relationship that has never been used in its utmost generality. In fact, the basal shear-stress formula has in applied glaciology only been used under the restrictive conditions that  $\alpha, \beta, \gamma$  and  $d\alpha/d\bar{x}$  are small. The shallow ice approximation is slightly weaker than this. The results derived by using it must, therefore, be equivalent to those of Section 2. All the more, the shallow ice approximation provides us with a wealth of additional results. In fact, the entire stress and velocity distributions are derived. They can be calculated provided that the geometry of the sheet, the material properties of ice, and the basal sliding law are known. Of these results, the formulas for the longitudinal velocity (5.41) and (5.46) are probably the most useful ones, as they allow evaluation of the corresponding surface velocity. To be sure, and in *unstretched coordinates*

$$\begin{aligned}\bar{u}_s = & C \{ \sin^m \gamma + m \sin^{m-1} \gamma \cos \gamma \alpha \} \bar{D}^m + \\ & + 2(\sin \gamma - \cos \gamma \alpha) \int_{\bar{y}_B(\bar{x})}^{\bar{y}_S(\bar{x}, \bar{\eta})} \tilde{\mathfrak{F}}(\sin^2 \gamma (\bar{y}_S - \eta)^2, \hat{\mathcal{G}}(\xi, \eta, \ell))(\eta - \bar{y}_S) d\eta,\end{aligned}\quad (5.50)$$

where  $\alpha \simeq -d\bar{y}_S/d\bar{x}$ . This formula contains one single quadrature for a well-behaved integrand function and can be exploited on any programmable pocket calculator.

In practical work, the use of (5.50) lies in a comparison of measured surface velocities with the numerical results obtained from (5.50) or, in solving an inverse problem, namely in the use of (5.50) to obtain creep response functions  $\tilde{\mathfrak{F}}$  from measured surface velocities and (perhaps) their longitudinal gradients. The formula can also be used to obtain information about basal sliding.

For the reader new to the field of glaciology, the shallow-ice approximation undoubtedly constitutes an improvement over the basal shear-stress formula, but applied glaciologists may, perhaps, question the reliability of the results because the basal shear-stress formula (5.49), including first-order terms, does not include longitudinal stress-gradient effects, whereas these effects have to be included when the basal shear-stress formulas (5.17) or (5.18) are used to derive an expression relating strain rates and basal shear. The answer is that the shear stress happens to be a variable, which

responds very weakly to small changes in glacier geometry, whereas normal stresses and velocity components do more vividly. A corroboration for this statement will be given shortly. On the other hand, any formula derived from the above zeroth- and first-order theory is at last subject to verification with field data. Prompted by the above statement, we now proceed to constructing second-order terms. A full second-order solution is, however, very cumbersome to obtain, but second-order basal shear stresses may still be calculated with reasonable effort. The corresponding differential equations and boundary conditions are obtained by substituting the perturbation expansions for stress and velocity in terms of  $\mu$  into Equations (5.33)–(5.35) and collecting terms of order  $\mu^2$ . The pertinent differential equations and boundary conditions for  $\tau^{(2)}$  read

$$\begin{aligned}\frac{\partial \tau^{(2)}}{\partial \eta} &= -\frac{\partial \sigma_x^{(1)}}{\partial \xi}, \quad 0 \leq \eta \leq \bar{y}_S, \\ \tau^{(2)} &= (\sigma_x^{(1)} - \sigma_y^{(1)}) \frac{\partial \bar{y}_S}{\partial \xi}, \quad \text{at } \eta = \bar{y}_S(\xi, \ell)\end{aligned}\quad (5.51)$$

and integration yields

$$\begin{aligned}\tau^{(2)} &= \sin \gamma \left\{ \frac{\partial^2 \bar{y}_S}{\partial \xi^2} \left[ \left( \bar{y}_S^2 - \frac{\bar{y}_S^2}{2} \right) - \left( \bar{y}_S \eta - \frac{\eta^2}{2} \right) \right] + \left( \frac{\partial \bar{y}_S}{\partial \xi} \right)^2 (\bar{y}_S - \eta) \right\} + \\ &+ \frac{2}{\tilde{\mathfrak{F}}(0, \hat{\mathfrak{g}}(\eta))} \frac{\partial U^{(0)}}{\partial \xi} \frac{\partial \bar{y}_S}{\partial \xi} + 2 \int_{\eta}^{\bar{y}_S} \frac{\bar{\eta} (\partial^2 U^{(0)} / \partial \xi^2) d\bar{\eta}}{\tilde{\mathfrak{F}}(\mathcal{X}(\bar{\eta})^2, \hat{\mathfrak{g}}(\bar{\eta}))} - \\ &- 4 \sin^2 \gamma \frac{\partial \bar{y}_S}{\partial \xi} \int_{\eta}^{\bar{y}_S} \frac{(\bar{y}_S - \eta) (\partial U^{(0)} / \partial \xi) \tilde{\mathfrak{F}}_x(\mathcal{X}(\bar{\eta})^2, \hat{\mathfrak{g}}(\bar{\eta})) d\bar{\eta}}{(\tilde{\mathfrak{F}}(\mathcal{X}(\bar{\eta})^2, \hat{\mathfrak{g}}(\bar{\eta})))^2} - \\ &- 2 \int_{\eta}^{\bar{y}_S} \frac{\tilde{\mathfrak{F}}_g(\mathcal{X}(\bar{\eta})^2, \hat{\mathfrak{g}}(\bar{\eta}))}{(\tilde{\mathfrak{F}}(\mathcal{X}(\bar{\eta})^2, \hat{\mathfrak{g}}(\bar{\eta})))^2} \frac{\partial U^{(0)}}{\partial \xi} \frac{\partial \hat{\mathfrak{g}}(\bar{\eta})}{\partial \xi} s\bar{\eta}.\end{aligned}\quad (5.52)$$

It is seen that second-order shear stresses depend on the first- and second-order gradients  $\partial U^{(0)} / \partial \xi$  and  $\partial^2 U^{(0)} / \partial \xi^2$  of the zeroth-order velocity field. These can be calculated from Equation (5.41) and the resulting expressions can be substituted into the above relations (5.52). The analysis is too complex to be presented here, but it can be shown that  $\tau^{(2)}$  may then be written as follows:

$$\begin{aligned}\tau^{(2)}(\xi, \eta, \ell) &= T_1 \frac{\partial \bar{y}_S}{\partial \xi} - T_2 \frac{d \bar{y}_B}{d \xi} + T_3 \frac{\partial^2 \bar{y}_S}{\partial \xi^2} - T_4 \frac{d^2 \bar{y}_B}{d \xi^2} + \\ &+ T_5 \left( \frac{d \bar{y}_S}{d \xi} \right)^2 + T_6 \frac{\partial \bar{y}_S}{\partial \xi} \frac{d \bar{y}_B}{d \xi} + T_7 \left( \frac{d \bar{y}_B}{d \xi} \right)^2\end{aligned}\quad (5.53)$$

where  $T_i = T_i(\xi, \eta, \bar{y}_S, \bar{y}_B)$ , ( $i = 1, 2, \dots, 7$ ) and where the independent variables in  $\bar{y}$  and  $\bar{y}_B$  have been omitted. For the reader's benefit, explicit formulas for the functions  $T_i$  ( $i = 1, 2, \dots, 7$ ) are collected in an Appendix at the end of the book. A glance at this shows that only quadratures are needed in the evaluation of  $T_i$ . These can even be performed explicitly when a possible temperature-dependence of the creep-response function  $\tilde{\mathfrak{F}}$  is discarded. Such explicit calculations have also been performed by Hutter [16].

It is interesting to see now how the formula for basal shear stress looks like when terms up to second order are included. The basic formula is (5.36), which to second order reads

$$\tau_b = \tau^{(0)} + \mu\tau^{(1)} - \mu^2 \left[ (\sigma_x^{(1)} - \sigma_y^{(1)}) \frac{d\bar{y}_B}{d\xi} + 2\tau^{(0)} \left( \frac{d\bar{y}_B}{d\xi} \right)^2 - \tau^{(2)} \right].$$

With the formulas (5.40) and (5.33) it can be written as

$$\begin{aligned} \tau_b = & \left[ \sin \gamma - \mu \frac{\partial \bar{y}_S}{\partial \xi} \cos \gamma \right] (\bar{y}_S - \bar{y}_B) + \\ & + \mu^2 \left\{ T_1 \frac{\partial \bar{y}_S}{\partial \xi} - T_2 \frac{d\bar{y}_B}{d\xi} + T_3 \frac{\partial^2 \bar{y}_S}{\partial \xi^2} - T_4 \frac{d^2 \bar{y}_B}{d\xi^2} + T_5 \left( \frac{\partial \bar{y}_S}{\partial \xi} \right)^2 + \right. \\ & \left. + \left[ T_6 - \frac{2U_{11}^{(0)}}{\tilde{\mathfrak{F}}(\sin^2 \gamma (\bar{y}_S - \bar{y}_B)^2, \hat{\vartheta})} \right] \frac{\partial \bar{y}_S}{\partial \xi} \frac{\partial \bar{y}_B}{\partial \xi} + \right. \\ & \left. + \left[ T_7 + 2 \sin \gamma (\bar{y}_S - \bar{y}_B) + \frac{2U_{21}^{(0)}}{\tilde{\mathfrak{F}}(\sin^2 \gamma (\bar{y}_S - \bar{y}_B)^2, \hat{\vartheta})} \right] \left( \frac{\partial \bar{y}_B}{\partial \xi} \right)^2 \right\} \end{aligned} \quad (5.54)$$

where  $U_{11}^{(0)}$  and  $U_{21}^{(0)}$  are defined by

$$\frac{\partial U^{(0)}}{\partial \xi} = U_{11}^{(0)} \frac{\partial \bar{y}_S}{\partial \xi} - U_{21}^{(0)} \frac{d\bar{y}_B}{d\xi} \quad (5.55)$$

and are explicitly evaluated in the Appendix. It is an almost trivial matter to see how the various terms in (5.54) have to be interpreted. The terms on the first line have already been seen to lead to the classical formula  $\tau_b = \tilde{D}\alpha_S$  where  $\alpha_S$  is the surface inclination angle. Hence, the remaining terms arising on the right-hand side must correspond to the longitudinal strain effects on basal shear. Since formula (5.54) is valid under the same conditions as Equation (5.18), it follows that

$$\frac{d\bar{F}}{d\bar{x}} + \int_{\bar{y}_B}^{\bar{y}_S} \int_{\bar{y}}^{\bar{y}_S} \frac{\partial^2 \tau}{\partial \bar{x}^2} d\bar{y}' d\bar{y} = \mu^2 \{ \cdot \},$$

where the curly brackets stand for the corresponding bracketed term in (5.54).

The usefulness of formula (5.54) is limited, unless of course, one is

directly interested in basal shear stresses. However, in conjunction with Formula (5.24), Equation (5.54) could be used to test the observational fact that basal shear  $\tau_b \simeq \bar{D}\bar{\alpha}_s$ , where  $\bar{\alpha}_s$  is a suitable average of the surface inclination. Equation (5.54) might then give information on what lengths these averages would have to be evaluated and whether Budd's [5] observation in the Wilkes ice cap that averages extend over roughly 20 times the ice thickness, is a universal statement or an accidental one.

#### (d) Results

To obtain quantitative information regarding the behavior of the ice sheet and, in particular, its velocity distribution, the various integrals in the zeroth- and first-order velocity components were executed for the case that no temperature dependence was involved. This situation corresponds to a *temperate glacier* or ice sheet in which the influence of the moisture content is discarded and amounts to setting the Arrhenius factor  $\mathbb{A}$  to zero. Hence,

$$\tilde{\mathfrak{F}} = \mathfrak{F}(\mathcal{X}^2) = \frac{\mathcal{X}^{2(n-1/2)} + \dots}{1 + \dots}, \quad \mathcal{X}^2 = \sin^2 \gamma (\bar{y}_s - \eta)^2. \quad (5.56)$$

The evaluation of the velocity components (5.41), (5.42), (5.46) and (5.47) is relatively straightforward, and one obtains

$$\begin{aligned} U^{(0)}(\xi, \eta, \gamma) &= \mathbb{C} \sin^m \gamma \bar{D}^m + \frac{\sin^n \gamma}{(n+1)(1+\dots)} [\bar{D}^{n+1} - (\bar{y}_s - \eta)^{n+1}] + \\ &\quad + \frac{\sin \gamma}{1+\dots} [\bar{D}^2 - (\bar{y}_s - \eta)^2], \\ U^{(1)}(\xi, \eta, \gamma) &= -\mathbb{C} m \cos \gamma \sin^{m-1} \gamma \bar{D}^m \frac{\partial \bar{y}_s}{\partial \xi} + \\ &\quad + 2 \cos \gamma \left[ \frac{\sin^{n-1}}{(n+1)(1+\dots)} (\bar{D}^{n+1} - (\bar{y}_s - \eta)^{n+1}) + \right. \\ &\quad \left. + \frac{\sin \gamma}{2(1+\dots)} (\bar{D}^2 - (\bar{y}_s - \eta)^2) \right] \frac{\partial \bar{y}_s}{\partial \xi}, \\ V^{(0)}(\xi, \eta, \gamma) &= \mathbb{C} \sin^m \gamma \bar{D}^m \frac{d\bar{y}_B}{d\xi} - \sin^m \gamma \frac{\partial}{\partial \xi} (\mathbb{C} \bar{D}^m) (\eta - \bar{y}_B) + \\ &\quad + 2 \sin \gamma \bar{D} (\eta - \bar{y}_B) \frac{d\bar{y}_B}{d\xi} \frac{\sin^{n-1} \gamma \bar{D}^{n-1} + \dots}{1 + \dots} - \\ &\quad - 2 \frac{\partial \bar{y}_s}{\partial \xi} \left\{ \frac{\sin^n \gamma}{1 + \dots} \left[ \bar{D}^n (\eta - \bar{y}_B) - \frac{1}{n+1} (\bar{D}^{n+1} - (\bar{y}_s - \eta)^{n+1}) \right] + \right. \\ &\quad \left. + \frac{1}{2(1+\dots)} \sin \gamma (\eta - \bar{y}_B)^2 \right\}, \end{aligned} \quad (5.58)$$

$$\begin{aligned}
V^{(1)}(\xi, \eta, t) = & \sin^{m-1} \gamma \cos \gamma m \frac{\partial \bar{y}_S}{\partial \xi} \left[ \frac{\partial}{\partial \xi} (\mathbb{C} \bar{D}^m)(\eta - \bar{y}_B) - \mathbb{C} \bar{D}^m \frac{d \bar{y}_B}{d \xi} \right] - \\
& - 2 \cos \gamma \frac{\partial \bar{y}_S}{\partial \xi} \frac{d \bar{y}_B}{d \xi} \bar{D}(\eta - \bar{y}_B) \frac{\sin^{n-1} \gamma \bar{D}^{n-1}}{1 + \bar{z}} + \\
& + 2 \cos \gamma \left( \frac{\partial \bar{y}_S}{\partial \xi} \right)^2 V_1^{(1)} - 2 \cos \gamma \frac{\partial^2 \bar{y}_S}{\partial \xi^2} V_2^{(1)},
\end{aligned}$$

where

$$\begin{aligned}
V_1^{(1)} = & \frac{\sin^{n-1} \gamma}{1 + \bar{z}} \left\{ \bar{D}^n (\eta - \bar{y}_B) - \frac{1}{n+1} (\bar{D}^{n+1} - (\bar{y}_S - \eta)^{n+1}) \right\} + \frac{\bar{z}}{2(1 + \bar{z})} (\eta - \bar{y}_B)^2 \\
V_2^{(1)} = & \frac{1}{1 + \bar{z}} \left\{ \frac{\sin^{n-1}}{n+1} \left[ \frac{1}{n+2} (\bar{D}^{n+2} - (\bar{y}_S - \eta)^{n+2}) - \bar{D}^{n+1} (\eta - \bar{y}_B) \right] + \right. \\
& \left. + \frac{\bar{z}}{2} [\frac{1}{3} (\bar{D}^3 - (\bar{y}_S - \eta)^3) - \bar{D}^2 (\eta - \bar{y}_B)] \right\} - \\
& - \frac{1}{2} \mathbb{C} m \sin^{m-1} \gamma \bar{D}^m (\eta - \bar{y}_B).
\end{aligned} \tag{5.59}$$

All these expressions are regular as long as  $\bar{y}_S$  and its derivative remain regular. This is true also in the limit  $\bar{z} \rightarrow 0$ . This fact warrants special attention as the integrand functions for  $V^{(1)}$  in Equation (5.47) can easily be shown to be singular when the limit  $\bar{z} \rightarrow 0$  is considered. The singularity is integrable and disappears after integration. It should also be noticed that the formula for the lowest longitudinal velocity  $U^{(0)}$  is identical with that of the strictly parallel-sided slab.

To obtain quantitative information regarding the order of magnitude and the distribution of velocities, a temperate ice sheet was analysed whose bottom and top surfaces were varied according to the expressions

$$\begin{aligned}
\bar{y}_S(\xi) &= \bar{y}_1(\xi) + \varepsilon \cos(2\pi\xi), \quad \varepsilon \ll 1, \\
\bar{y}_B(\xi) &= \varepsilon_B \cos(2\pi\xi), \quad \varepsilon_B \ll 1,
\end{aligned} \tag{5.60}$$

where

$$\bar{y}_1(\xi) = [1 - (\kappa \xi)^{(n+1)/n}]^{n/2(n+1)}, \quad 0 < \kappa < 1, \tag{5.61}$$

in which  $n$  is the exponent in Glen's flow law. As is evident from Equations (5.60), the bottom ice bedrock interface oscillates sinusoidally with an amplitude  $\varepsilon_B \ll 1$  and with wavelength  $\lambda = 1$ . Written in physical variables Equation (5.60)<sub>2</sub> reads

$$y_B(x) = \varepsilon_B D \cos \left( 2\pi \mu \frac{x}{D} \right) = \varepsilon_B D \cos \left( 2\pi \frac{x}{l} \right), \tag{5.62}$$

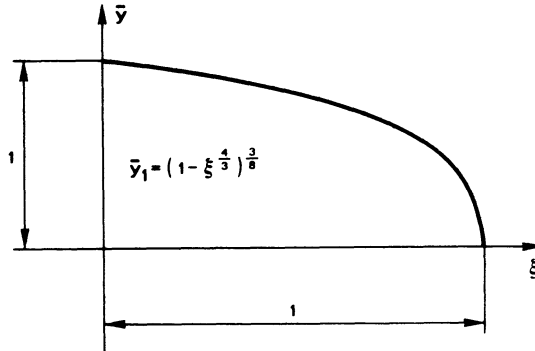


FIG. 5.7. The surface profile of an ice sheet as given by formula (5.63) plotted for  $n = 3$ .

in which  $D$  and  $l$  are the maximum thickness of the ice sheet and the wavelength of the bottom undulation, respectively and  $\mu = D/l$  is the ratio of the two. The oscillating part of Equation (5.60)<sub>1</sub> must be interpreted in an analogous fashion. The stretching parameter  $\mu$  is thus built with the ice thickness and the undulation wavelength. Expression (5.61) for  $\bar{y}_1(\xi)$ , on the other hand, corresponds to

$$y_1(x) = D \left[ 1 - \left( \frac{x}{L} \right)^{(n+1)/n} \right]^{n/2(n+1)}, \quad (5.63)$$

in which  $L$  is the half length of the ice sheet, see Figure 5.7. For brevity,  $\bar{y}_1(\xi)$  will be called *equilibrium surface*. Comparison of the expressions on the right-hand sides of Equations (5.61) and (5.63) yields  $\kappa = l/L$ . The parameter  $\kappa$  therefore gives the number of undulation wavelengths of the sinusoidal oscillation that occur on the entire length of the sheet shown in Figure 5.7.

Relations (5.60) and (5.61) may not be realistic in an actual situation, but they give an indication of the order of magnitude and distribution of the velocity field. For  $\bar{y}_1(\xi)$  is close to the top geometry of a steady-state ice sheet, and the sinusoidal term may be regarded as a particular term of a Fourier-cosine decomposition of the difference  $\bar{y}_{\text{real}} - \bar{y}_1$ . Varying  $\epsilon$ ,  $\epsilon_B$  and  $\kappa$  thus will give a reasonably realistic picture of the zeroth- and first-order velocity distributions. Furthermore, longitudinal strain-rate effects on basal shear can be analysed by using the above expressions for bottom and top surface geometry in calculations of second-order stress effects. In this regard  $\mathcal{O}(\mu^2)$  corrections of the basal shear stresses are interesting to analyse. It may, consequently be convenient to write Equation (5.54) in the form

$$\frac{\tau_b}{\tau^{(0)}} = 1 - \mu \frac{\tau_b^{(1)}}{\tau^{(0)}} + \mu^2 \frac{\tau_b^{(2)}}{\tau^{(0)}} + \dots, \quad (5.64)$$

where  $\tau_b^{(1)}$  and  $\tau_b^{(2)}$  are the coefficients in Equation (5.54) of the terms which

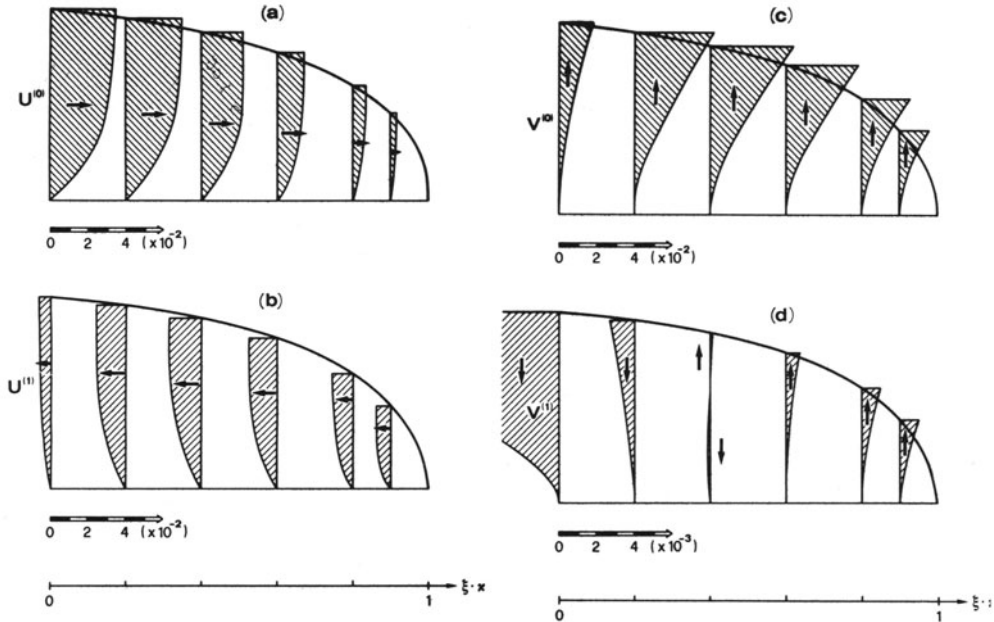


FIG. 5.8. Zeroth- and first-order velocity profiles at various positions along the glacier. A temperature-independent creep law and no basal slip are assumed. The mean inclination of the base is  $\gamma = 0.1$  and  $n = 3$ ,  $k = 10^{-3}$ . Velocity profiles are shown at  $\kappa\xi = (10^{-2}, 0.2, 0.4, 0.6, 0.8, 0.9)$ . For an interpretation of the velocity profile, see the text. The indicated scales apply for the dimensionless velocities.

are linear and quadratic in the parameter  $\mu$ , respectively. Calculations were performed for no-slip and a Weertman-type sliding law by varying the coefficient  $C$ . A selection of results is given below.

Figures 5.8, 5.9 and 5.10 show cross-sectional distributions of the velocity components  $U_0$ ,  $U_1$ ,  $V_0$  and  $V_1$  at several positions of the ice sheet. These are the stretched variables, and real variables are obtained by executing the inverse transformation. This has not been done here because it involves the stretching parameter  $\mu$  whose value depends on the actual situation. Figures 5.8 to 5.10 hold for an ice sheet with a flat but inclined mean bottom and surface topography according to formula (5.63). As far as the velocity distribution is concerned, results are qualitatively not much different when the small undulations about this profile are analysed. Notice further that  $V^{(1)}$  at  $\xi \approx 0$  in Figure 5.8 is much larger in value than for  $\xi \neq 0$ . This happens in all cases where the profile (5.63) is used and so the  $V^{(1)}$ -profile at  $\xi \approx 0$  is not shown in the other figures. The reason is that  $V^{(1)}$  involves second-order derivatives  $\partial^2 \bar{y}_S / \partial \xi^2$  which, for the selected profile  $y_1(\xi)$ , have a singularity at  $\xi = 0$ . This is merely a mathematical peculiarity of the selected profile  $\bar{y}_1(\xi)$

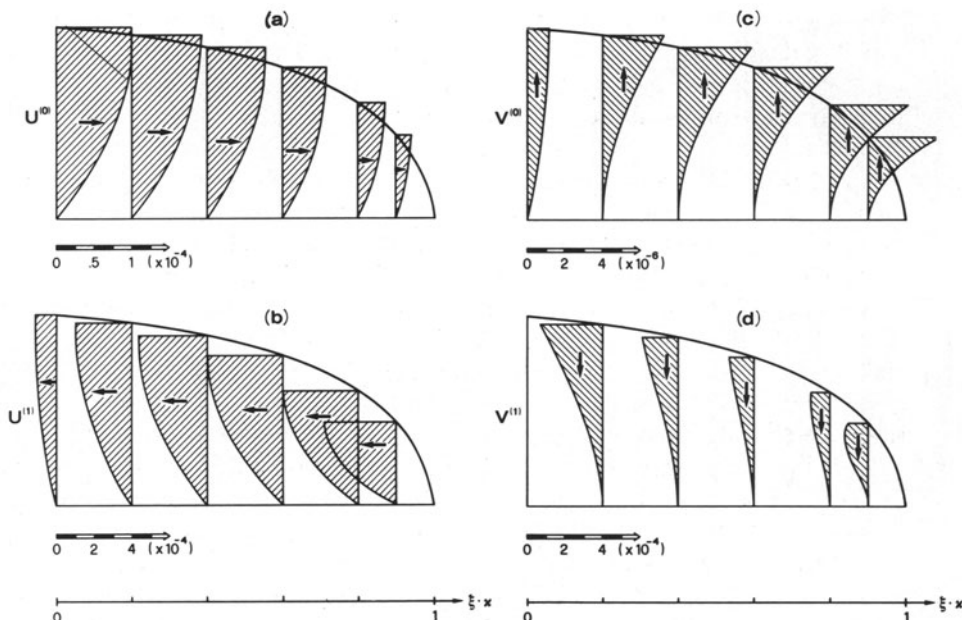


FIG. 5.9. The same as Figure 5.8, but now for a mean inclination  $\gamma = 0.01$ , thus a very flat bed. Velocities are two orders of magnitudes smaller.

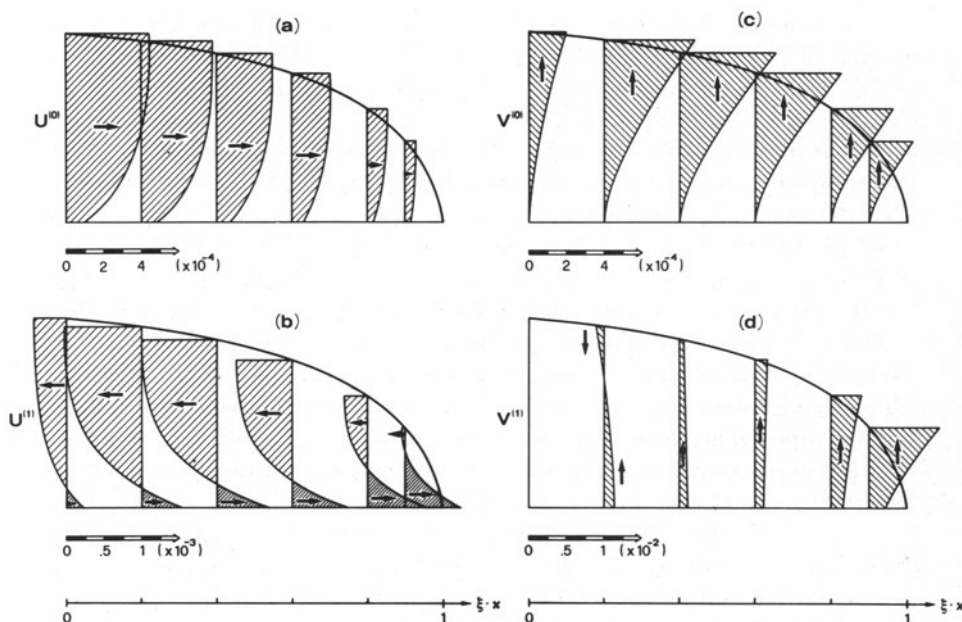


FIG. 5.10. The same as Figure 5.8, but now for temperate ice and basal sliding with a sliding coefficient  $C = 10^{-2}$ . All other details are the same as in Figure 5.8.

and has no physical meaning. It indicates that when using pointwise-given surface geometries care should be observed with the selection of the mathematical representation of the smoothed-out surface. Polynomial representations such as splines are most likely to be more appropriate than closed formulas.

In Figure 5.8 velocity profiles are displayed when the mean inclination angle is  $\gamma = 0.1$ ; this corresponds to a fairly steep glacier. No slip at the base is assumed,  $C = 0$ , and  $n = 3$ ,  $\kappa = 10^{-3}$ . It is seen that the zeroth- and first-order longitudinal velocity components  $U^{(0)}$  and  $U^{(1)}$  are of the same order of magnitude ( $10^{-2}$ ) but have opposite signs. The lowest-order transverse velocity,  $V^{(0)}$  is of equal magnitude but first-order transverse velocities are smaller except at  $\kappa\xi = 10^{-2}$ , this is so because this cross-section is close to  $\xi = 0$  where  $d^2y_1(\xi)/d\xi^2 \rightarrow \infty$ . In subsequent figures  $V^{(1)}$  at  $\kappa\xi = 10^{-2}$  will therefore no longer be displayed. Transverse velocities are mostly positive, whence upwards, except for  $V^{(1)}$  and in the interior of the sheet, yet total transverse velocities,  $(V^{(0)} + \mu V^{(1)})$ , remain positive [except, perhaps very close to  $\xi = 0$  where the model breaks down anyhow]. At the surface  $\bar{y}_1(\xi)$ , the velocity vectors point uniformly out of the ice indicating that the entire portion of the shown ice mass is subject to ablation. If the given ice geometry corresponds to a steady-state equilibrium profile, the results would allow calculation of the ablation rate by the use of Equation (5.35). It follows that the sheet would have to be continued beyond the point  $\xi = 0$ .

In Figure 5.9, the same quantities as those presented in Figure 5.8 are displayed, but now for small bed inclinations,  $\gamma = 0.01$ . It is seen that  $|U^{(1)}| \approx |U^{(0)}|$  and  $|V^{(1)}| \geq |V^{(0)}|$ , implying that the demonstrated perturbation expansion has probably reached its limit of validity for it can no longer necessarily be ascertained that  $|\mu V^{(1)}| \ll |V^{(0)}|$ . This calls for a different scaling procedure when  $\gamma$  is small. It will be introduced in the next section. Nevertheless, it is our belief that orders of magnitude for the velocity components are correct down to approximately  $\gamma \gtrsim 0.01$ .

To give quantitative information regarding the effect of sliding calculations have also been performed for ice sliding over its rockbed. The results for  $C = 10^{-2}$  and  $\gamma = 0.1$  are shown in Figure 5.10. For the given value of  $C$ , the sliding velocities are of comparable magnitude with the creep velocities. Qualitatively, the results are not much different from those without sliding, and no unusual behavior develops as long as  $C$  is not too large. Figure 5.10b, however, indicates the importance of the first-order corrections in longitudinal velocities. This should be borne in mind.

With a detailed picture of the velocity distribution being determined, the most important entities of glaciological interest are known. Since basal shear stress plays an important role in common glaciological arguments, a selection of results will also be given for these. Zeroth- and first-order shear stresses yield the classical shear-stress formula, see Equation (5.49); second-order

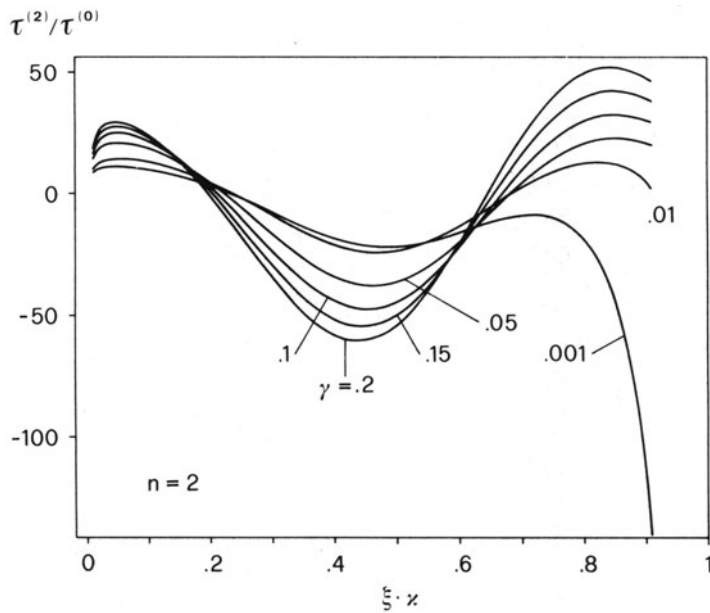


FIG. 5.11. Second-order stress corrections  $\tau^{(2)}/\tau^{(0)}$  according to Equation (5.64) for basal shear stresses plotted against  $\kappa\xi$  for temperate ice and no-slip and for a sinusoidal bed undulation with amplitude  $\varepsilon_B = 0.1$  and a wavelength agreeing with the semi-length of the ice sheet,  $\kappa = 1$ . The various curves apply for inclination angles  $0.001 \leq \gamma \leq 0.2$  and the creep law with  $n = 2$  ( $k = 10^{-2}$ ) is used. (From [16].)

shear-stress corrections will therefore yield longitudinal strain effects. To estimate these effects it suffices to present results for  $\tau^{(2)}/\tau^{(0)}$ , the third term save the factor  $\mu^2$  on the right-hand side of Equation (5.64). A detailed investigation of these effects is given by Hutter [16]. Here we focus attention on summarizing his results. Accordingly, second-order shear-stress corrections depend strongly on the flow law parameter  $n$ , mean bed inclination  $\gamma$  and both surface and bed undulations. The values obtained for basal shear stress when such bed undulations are present, may completely overshadow corresponding values without such undulations. An example indicating the strong dependence on  $n$ ,  $\gamma$ , and undulation strength is shown in Figures 5.11 and 5.12. The former displays  $\tau^{(2)}/\tau^{(0)}$  at the base for  $n = 2$ ,  $k = 10^{-2}$ , a selection of values of the inclination angle  $\gamma$ , and a sinusoidal bed undulation with  $\kappa = 1$  and  $\varepsilon_B = 0.1$ . This means that the undulation amplitude is 10% of the maximum thickness of the sheet and that its period has the same length as the equilibrium profile displayed in Figure 5.7. The same results are shown in Figure 5.12 for  $n = 3$ ,  $k = 10^{-3}$ . It is clearly seen that the order of magnitude of the second-order shear-stress corrections depends on the value of  $n$ .

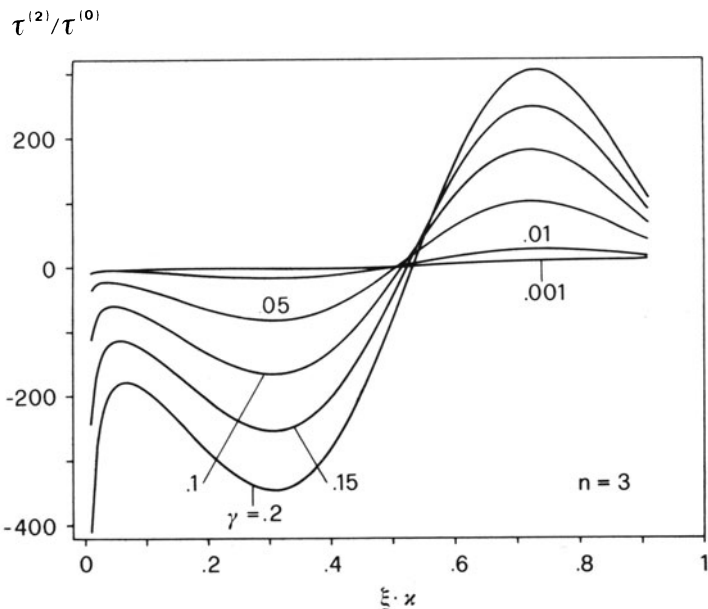


FIG. 5.12. Same as Figure 5.11, but the flow law is now characterized by  $n = 3$  ( $\kappa = 10^{-3}$ ). Notice the substantial differences of orders of magnitudes for  $\tau^{(2)}/\tau^{(0)}$  when compared with those of Figure 5.11, indicating the importance of the flow law. (From [16]).

Their variation largely reflects the sinusoidally assumed bed profile, although the non-periodicity still indicates a dominant influence of the equilibrium surface profile  $\bar{y}_1(\xi)$ . This influence becomes less for shorter undulation wavelengths.

In conclusion, it should be said that the numerical calculations, upon which Figures 5.8 to 5.12 are based, are for ice in which the influence of the temperature on the stress and velocity distribution was ignored. Calculations for zero- and first-order velocity components can equally be performed when the spatial temperature distribution is prescribed. It is expected that the results will not change qualitatively; but quantitative changes must be expected, particularly in the distribution of stresses.

#### (e) Temperature field

All the above calculations pertain to stress and velocity distribution. Let us also indicate how these solutions can be used in obtaining an improved temperature distribution. The relevant equations are Equations (5.37). Depending on the order of accuracy, different improved temperature fields  $\hat{\theta}$  can be obtained and several approximate solution procedures for the governing equations are possible. Here we restrict attention to a solution

approach in which  $\hat{\vartheta}$  is determined by iteration. The strategy is to substitute the perturbation series for the velocity and stress fields into Equations (5.37) and to truncate these at a certain level of the perturbation parameter  $\mu$ . As seen from Equation (5.37)<sub>1</sub>, the small parameter  $\mu$  appears with a negative power at the right-hand side. However, since both  $\mathbb{E}$  and  $\mathbb{D}$  are small  $\mu^{-1} \mathbb{E}$  and  $\mu^{-1} \mathbb{D}$  are of order unity or smaller. Neglecting longitudinal conduction, in other words to within  $\mathcal{O}(\mu)$  terms, Equation (5.37)<sub>1</sub> becomes

$$\frac{\partial \hat{\vartheta}}{\partial \ell} + (V^{(0)} + \mu V^{(1)}) \frac{\partial \hat{\vartheta}}{\partial \eta} - \frac{\mathbb{D}}{\mu} \frac{\partial^2 \hat{\vartheta}}{\partial \eta^2} + (U^{(0)} + U^{(1)}) \frac{\partial \hat{\vartheta}}{\partial \xi} = \frac{\mathbb{E}}{2\mu} \tilde{\mathfrak{F}}(\tau_{II}', \hat{\vartheta}) \tau_{II}' \quad (5.65)$$

in which

$$\tau_{II}' = (\tau^{(0)} + \mu \tau^{(1)})^2 \cong \tau^{(0)2} + 2\mu \tau^{(0)} \tau^{(1)}. \quad (5.66)$$

From the above, the solution procedure is now easily recognizable, if one observes that the transverse variation of temperature is more physically pronounced than the longitudinal variation. We now *postulate* that this is so, even in the stretched coordinates. In other words, of the terms on the left-hand side of Equation (5.65) the last term is of lesser importance than the first three. If ignored, the complexity of the problem reduces by one dimension. If, furthermore, the term on the right-hand side of Equation (5.65) is omitted, the temperature equation formally linearizes. It is known, however, from the discussion of the determination of the temperature profile in strictly parallel-sided ice slabs (Chapter 3) that exclusion of strain heating may lead to a loss in certain solutions. All these considerations suggest the determination of the temperature distribution by the following procedure: Let  $\{\vartheta^{(v)}\}$  be a sequence of temperature fields and let  $\vartheta^{(v)}$  be the solution of the initial boundary value problem

$$\begin{aligned} & \frac{\partial \vartheta^{(v)}}{\partial \ell} + V^{(0)} \frac{\partial \vartheta^{(v)}}{\partial \eta} - \mu^{-1} \mathbb{D} \frac{\partial^2 \vartheta^{(v)}}{\partial \eta^2} - \frac{\mathbb{E}}{2\mu} \tilde{\mathfrak{F}}(\tau_{II}', \vartheta^{(v)}) = f(\vartheta^{(v-1)}), \\ & \vartheta^{(v)} = \vartheta_S, \quad \text{at } \bar{y} = \bar{y}_S(\xi, \ell), \\ & \frac{\partial \vartheta^{(v)}}{\partial \eta} = -\mathbb{Q}^{\text{geoth}} \left[ 1 + \frac{\mu^2}{2} \left( \frac{d\bar{y}_B}{d\xi} \right)^2 \right] + \mu^2 \frac{d\bar{y}_B}{d\xi} \frac{\partial \vartheta^{(v-1)}}{\partial \xi}, \quad \text{at } \bar{y} = \bar{y}_B(\xi), \\ & \vartheta^{(v)} = \vartheta_0(\xi, \eta), \quad \text{for } \ell = 0, \end{aligned} \quad (5.67)$$

with

$$f(\vartheta) = - \left[ (U^{(0)} + \mu U^{(1)}) \frac{\partial \vartheta}{\partial \xi} + V^{(1)} \frac{\partial \vartheta}{\partial \eta} \right]. \quad (5.68)$$

This system of equations represents nothing else than Equation (5.37) in which  $\vartheta$  is iterated such that  $\xi$ -derivatives and  $\mathcal{O}(\mu)$  terms in Equation (5.65)

are treated as known from previous iterates. [As a matter of rigor, it should also be mentioned that the last term on the left-hand side of Equation (5.67)<sub>1</sub> contains an  $\mathcal{O}(\mu^2)$  term, as can be seen from (5.66). By expanding this term equally in powers of  $\mu$ , this portion could be incorporated into the function  $f$  on the right-hand side. *This is not advisable*, however, because derivatives of  $\hat{\vartheta}$  would arise which are singular when a power flow law is used.]

Two variations of strategy are possible to solve the initial boundary-value problem (5.67), namely either to regard  $V^{(0)}$ ,  $V^{(1)}$  and  $\tau^{(0)}$ ,  $\tau^{(1)}$  as determined with the temperature estimate  $\hat{\vartheta}$  or by also iterating on the stress and velocity fields. This latter approach is more accurate and  $V^{(0)}, \dots, V^{(1)}, \tau^{(0)}, \tau^{(1)}$  are then functions of  $\vartheta^{(v-1)}$ .

The two-point boundary-value problem (5.67) for  $\vartheta^{(v)}$  is non-linear, the non-linearity arising from the last term on the left-hand side of Equation (5.67)<sub>1</sub>. Inclusion of this term is regarded as important for the reasons already mentioned above. The iteration on the index  $v$  is commenced by setting  $v = 0$  and neglecting all terms with a negative index. Hence, for  $v = 0$  the term  $f(\vartheta^{(v-1)})$  must be omitted. The corresponding boundary-value problem is believed to have incorporated all essential features of cold ice sheets. Indeed, the boundary-value problem for  $v = 0$  is formally identical with that of the strictly parallel-sided slab if the corresponding expression for  $V^{(0)}$  is substituted (see Chapter 3, page 166). Moreover, the dependence of the solution on the distribution of  $V^{(0)}$  and on viscous dissipation is generally weak so that a determination of  $V^{(0)}$  and  $\tau^{(0)}$  from rough temperature profiles will most likely have only marginal influence on the distribution of  $\vartheta^{(0)}$ . This implies that only a few iterates will be necessary to determine a reasonable estimate for the final temperature distribution.

Explicitly the procedure is as follows: Assuming the bottom and top surfaces to be known as functions of  $\xi$  and  $\ell$ , a rough estimate of the temperature distribution  $\hat{\vartheta}$  is selected, where  $\hat{\vartheta}$  is, in general, a function of  $\xi$ ,  $\eta$  and  $\ell$ . One possibility of obtaining this estimate is to approximately select for  $V^{(0)}$  the expression that is obtained for temperate ice and to determine  $\hat{\vartheta}$  from the initial boundary-value problem

$$\begin{aligned} \frac{\partial \hat{\vartheta}}{\partial \ell} + V^{(0)} \frac{\partial \hat{\vartheta}}{\partial \eta} - \mu^{-1} \mathbb{D} \frac{\partial^2 \hat{\vartheta}}{\partial \eta^2} - \frac{\mathbb{E}}{2\mu} \bar{F}(\tau^{(0)}, \hat{\vartheta}) &= 0, \\ \hat{\vartheta} = \vartheta_s, \quad \text{at } \bar{y} = \bar{y}_s(\xi, \ell), \\ \frac{\partial \hat{\vartheta}}{\partial \eta} = -\mathbb{Q}^{\text{geoth}}, \quad \text{at } \bar{y} = \bar{y}_B(\xi, \ell), \\ \hat{\vartheta} = \hat{\vartheta}_0(\xi, \eta), \quad \text{at } \ell = 0. \end{aligned} \tag{5.69}$$

In these equations,  $\tau^{(0)} = \sin \gamma (\bar{y}_s - \eta)$  and  $V^{(0)}$  is given by the expression on the right-hand side of Equation (5.58)<sub>1</sub>. Both quantities are functions of  $\xi$ ,  $\eta$

and  $\ell$ , whereby  $\xi$  may be regarded as a parameter. At this stage we are not concerned with the presentation of solution procedures to these equations. Various approaches are possible and we must refer the reader to the respective literature on numerical analysis; see Szidarovszky and Yakowitz [40], Bulirsch and Stoer [7] and other treatises on numerical analysis.

Once the temperature field  $\vartheta$  is known from (5.69), Equations (5.67) and (5.68) can be attacked. In a first step,  $U^{(0)}, \dots, V^{(1)}$  are calculated using (5.41), (5.42), (5.46) and (5.47). With the values of these the temperature iterates can be determined from the initial boundary value problem (5.67) and (5.68). It is to be noticed that the same numerical routine that must be developed for the solution of Equations (5.69) can also be used in the solution of these equations.

#### 4. Theoretical Steady-state Profiles

In the preceding analysis of the stress, velocity, and temperature distribution, no use was made of the kinematic surface equations (5.28)<sub>1</sub> or (5.28)<sub>2</sub>. Indeed, one could pretend that the free surface, and the base, where prescribed functions of position which were determined by other means. Under such conditions, one could solve the problems for the stress and velocity fields by a series of quadratures. This separation of the stress, velocity, and temperature problems inside the body and that of the geometry of the free surface, which must be determined via the kinematic surface condition, is evidently due to the *shallow-ice approximation*. It is to be expected that the equation for the surface geometry will emerge when, in a second step, the kinematic surface condition is analysed. This will be demonstrated in this section.

##### (a) Earlier theories and their limitations

We shall confine attention to plane motion and to ice sheets in steady state resting on a *horizontal* bed, see Figure 5.13.\* The  $x$ -axis will be taken as horizontal,  $y$  is vertical, and the top surface is assumed to be slowly varying in  $x$ . Ice thicknesses will be measured as  $d(x)$  with  $D$  being the maximum thickness in the middle of the symmetric ice sheet.

Theoretical models to predict the surface geometry of an ice sheet are by Orowan [30], Nye [27], Vialov [41] and Bodvarsson [2]. Orowan considers the case of a perfectly plastic ice sheet. The basal shear stress therefore equals  $t_{xy}^b \simeq 1$  bar. If, furthermore, the ice sheet in Figure 5.13 is regarded to be approximately parallel-sided, overburden pressure and longitudinal stress  $t_{xx}$  must be equal. From a force balance at the illustrated portion of the ice sheet, it therefore follows that

$$S(x) = \frac{\rho g d^2(x)}{2} = t_{xy}^b(L - x). \quad (5.70)$$

\*In this subsection  $(x, y)$  is the physical space.

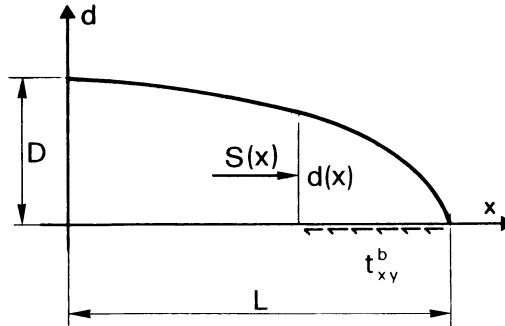


FIG. 5.13. Ice sheet with semi-length  $L$  and maximal thickness  $D$ . Thickness at an arbitrary position  $x$  is  $d(x)$ . Basal shear stress is  $t_{xy}^b$  and normal force is  $S(x)$ .

Substituting  $x = 0$  allows the evaluation of the maximum thickness, and (5.70) becomes

$$\left(\frac{d(x)}{D}\right)^2 = 1 - \frac{x}{L}, \quad D^2 = \frac{2t_{xy}^b L}{\rho g}, \quad (5.71)$$

which is the equation of a parabola.

Clearly, the assumption of a perfectly plastic response is too crude an approximation. Nye [27] has, therefore, offered an improved derivation. He starts from a Weertman-type sliding law

$$u_b = \mathcal{C}(t_{xy}^b)^m$$

and uses the classical formula for basal shear,  $t_{xy}^b = -\rho g d d'$ , where  $d'$  is the change of  $d$  with  $x$ . So far, no approximation is introduced that would not be consistent with the shallow ice approximation. However, when replacing the flux function  $s(x)$  of mass flux by the product of  $u_b$  with the local thickness, Nye assumes  $u$  to be constant across the depth. Such an assumption is tantamount to attributing the entire motion to sliding rather than gliding. The volume flux at  $x$  through a cross-section is thus given by  $d u_b$ , and in steady state it must be balanced by the flux function  $\int_0^x a(\xi) d\xi$ . Hence

$$s(x) = \int_0^x a(\xi) d\xi = d u_b = d \mathcal{C} [-\rho g d d']^m, \quad (5.72)$$

which is a differential equation for  $d$ . Integration yields

$$\frac{m}{2m+1} d^{(2m+1)/m} + k = -\frac{1}{\rho g \mathcal{C}^{1/m}} \int_0^x (s(\xi))^{1/m} d\xi, \quad s(x) > 0. \quad (5.73)$$

The constant of integration,  $k$  can be determined from the condition that  $d(x = L) = 0$ . If, furthermore,  $d(x = 0) = D$  is introduced, the solution to

Equation (5.72) assumes the form

$$\left(\frac{d}{D}\right)^{(2m+1)/m} + \frac{\int_0^x s(\xi)^{1/m} d\xi}{\int_0^L s(\xi)^{1/m} d\xi} = 1. \quad (5.74)$$

where

$$\frac{m}{2m+1} D^{(2m+1)/m} = \frac{a^{1/m}}{\rho g C^{1/m}} \int_0^L s(\xi)^{1/m} d\xi.$$

Nye [27] assumes that  $s$  varies linearly with  $x$ , which corresponds to a constant accumulation rate function, and then obtains

$$\left(\frac{d}{D}\right)^{(2m+1)/m} + \left(\frac{x}{L}\right)^{(m+1)/m} = 1. \quad (5.74a)$$

This agrees with Orowan's result (5.71) provided that  $m \rightarrow \infty$ . For  $m = 2$ ,  $(d/D)^{4/2} + (x/L)^{3/2} = 1$  is obtained. Vialov [41] and Bodvarsson [2] have introduced different postulates yielding essentially the same results. They start from the approximate shear-stress formula  $t_{xy} = -\rho g(d-y)d'$  and further presume that all deformation is simple shear, so that  $\partial u/\partial y = 2At_{xy}^n$ . Combining these, integrating over ice thickness, and assuming that the ice is not sliding over bedrock, it is easily shown that the flux  $\int_0^d u(y) dy$  is given by

$$\int_0^d u(y) dy = Kd^{n+2}(-d')^n$$

in which  $K$  is a constant. Equating this to  $s(x) = \int_0^x a(\xi) d\xi$  and integrating in the same way as before yields

$$\left(\frac{d}{D}\right)^{2(n+1)/n} - \frac{\int_0^x a(\xi)^{1/n} d\xi}{\int_0^L a(\xi)^{1/n} d\xi} = 1, \quad (5.75)$$

a formula of which the structure is the same as that of Equation (5.74). If  $s$  varies linearly with  $x$ , one obtains

$$\left(\frac{d}{D}\right)^{2(n+1)/n} - \left(\frac{x}{L}\right)^{(n+1)/n} = 1. \quad (5.75a)$$

The representations expressed by Formulas (5.74a) and (5.75a) may be called *hyper-ellipses*. They are characterized by an equation of the form

$$\left(\frac{d}{D}\right)^\alpha + \left(\frac{x}{L}\right)^\beta = 1 \quad (5.76)$$

and are valid in this form, provided that  $a = \text{constant}$ . In other words, mass is not balanced, which is in violation with steady-state conditions. For accumulation and ablation in conformity with mass balance, the flux function

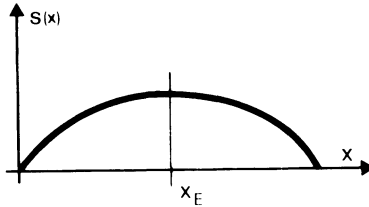


FIG. 5.14. Distribution of the mass flux function  $s(x) = \int_0^x a(\xi) d\xi$  along the ice sheet.

must be as shown in Figure 5.14. It reaches its maximum at the accumulation/ablation equilibrium point  $x_E$ . If the accumulation and ablation zones are of the same length and the function is symmetric about  $x_E$ , a reasonable choice is

$$s(x) = k^m \frac{x}{L} \left(1 - \frac{x}{L}\right).$$

Consequently,

$$\int_0^x (s(\xi))^{1/m} d\xi = k \int_0^x \left(\frac{\xi}{L}\right)^{1/m} \left(1 - \frac{\xi}{L}\right)^{1/m} d\xi.$$

With the transformation of the integration variable

$$\xi = \frac{L}{2}(\cos \varphi + 1), \quad d\xi = -\frac{L}{2} \sin \varphi d\varphi$$

may be written as

$$\int_0^x s(\xi) d\xi = \frac{kL}{2} \left(\frac{1}{2}\right)^{1/m} \int_{\cos^{-1}(2x/L)-1}^{\pi} \sin^{((2/m)+1)} \varphi d\varphi.$$

It is hardly worthwhile exploiting this formula for general  $m$ , but for  $m \rightarrow \infty$  and  $m = 2$ , explicit expressions are relatively easily obtained. For  $m \rightarrow \infty$  the equation of the surface geometry again becomes Equation (5.71), implying that *for an ideally plastic material the surface geometry is independent of the distribution of the accumulation rate function*. This statement is independent of the form of the flux function, as can be seen when the limit  $m \rightarrow \infty$  is taken in Formula (5.74). For  $m = 2$  one obtains instead

$$\left(\frac{d}{D}\right)^{5/2} = \frac{1}{\pi} \left\{ \cos^{-1} \left( \frac{2x}{L} - 1 \right) + \frac{1}{2} \sin \left( 2 \cos^{-1} \left( \frac{2x}{L} - 1 \right) \right) \right\}, \quad (5.77)$$

which is quite different in form from the hyper-ellipse obtained previously.

In Figure 5.15a, the surface geometries, as obtained with the aid of Formulas (5.71), (5.74) and (5.77) for  $m = 2$  are plotted and compared with

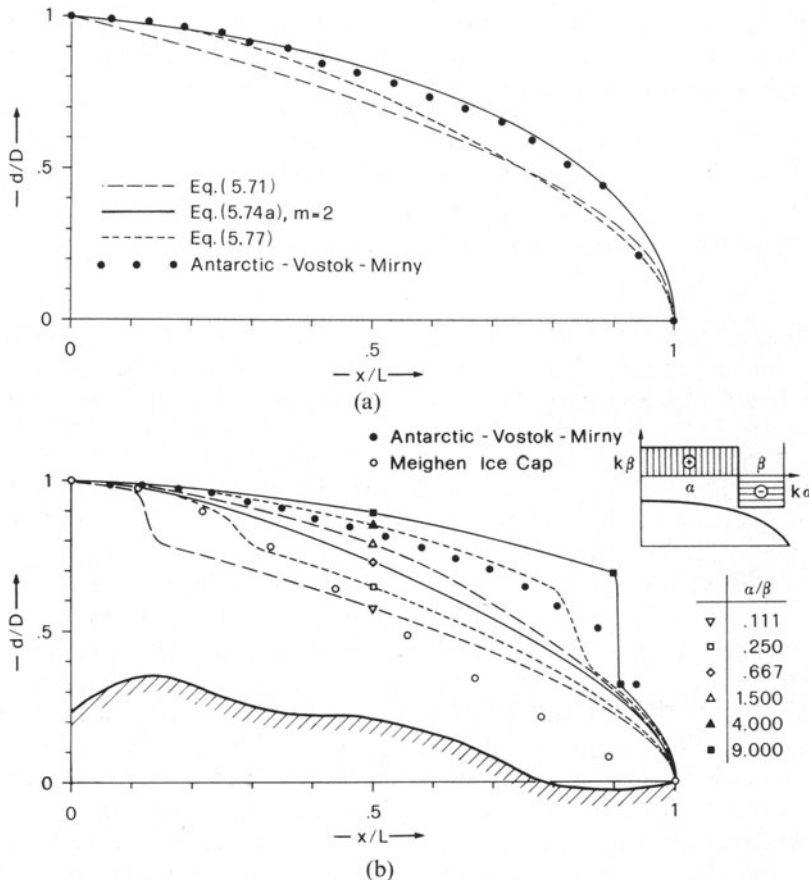


FIG. 5.15. (a) Surface profiles as obtained with Equations (5.71), (5.74a) and (5.77) compared with measured surface points for Antarctic-Vostok-Mirny. (From [32].) (b) Surface profiles as obtained with Equation (5.78), compared observed data from Antarctic-Vostok-Mirny and with the Meighen Ice Cap. (From [32] with additions.)

measured values of the surface geometry for Antarctic-Vostok-Mirny. The profile based on constant accumulation fits the data most satisfactorily. This is in line with the common understanding that surface ablation in Antarctica is small and most loss of mass is due to calving, see Paterson [32].

In order to investigate how the accumulation rate function affects the surface geometry a theoretical model was analysed for which the flux function is given by

$$s(x) = \begin{cases} k\beta x, & 0 \leq x \leq \alpha, \\ k\alpha(L - x), & \alpha \leq x \leq L = (\alpha + \beta). \end{cases}$$

This flux function vanishes at the glacier head and snout and thus satisfies the conditions of a steady-state ice sheet. With the aid of formula (5.74) it is straightforward to show that the surface geometry is given by

$$\left(\frac{d}{D}\right)^{(2m+1)/m} = 1 - \left\{ \begin{array}{ll} \frac{2^{(m+1)/m}}{1 + (\alpha/\beta)^{1/m}} \left(\frac{x}{L}\right)^{(m+1)/m}, & 0 \leq x \leq \alpha, \\ \frac{1 + (\alpha/\beta)^{1/m} [1 - (2(1-x/L))^{(m+1)/m}]}{1 + (\alpha/\beta)^{1/m}}, & \alpha \leq x \leq L. \end{array} \right\} \quad (5.78)$$

A similar solution was also given by Paterson [31]. The ratio  $\alpha/\beta$  describes the location of the accumulation-ablation equilibrium point; for  $\alpha/\beta = 1$  this equilibrium point lies midway between the head and the snout.  $\alpha/\beta < 1$  corresponds to a glacier for which the accumulation zone is smaller than the ablation zone; for  $\alpha/\beta > 1$  it is reverse. The results are displayed in Figure 5.15b. They indicate that depending on the distribution of the accumulation-rate function along the ice sheet axis many different profiles of the surface geometry are possible. This suggests that an adequate corroboration of Equation (5.74) is only possible by correlating the accumulation rate (or its flux function) with the surface geometry. It is now obvious that the surprisingly good coincidence of the surface geometry based on Equation (5.74), with that of the Antarctic-Vostok-Mirny data must be because the ablation zone is much smaller than the accumulation zone. On the other hand, for valley glaciers and smaller ice caps, the measured points may not be matchable with a curve based on the above formulae. This is the case, e.g., for the Meighen Ice Cap, see Figure 5.15b. In the ablation zone, measured surface points are far below any of the theoretical profiles, indicating that effects of bottom topography and unsteady flow conditions probably account for the difference.

It should also be observed that *in all above formulae the center height D is related to the semi-length L*. This can most easily be seen from (5.71)<sub>2</sub>, but equally holds also for the other models. It follows that apart from material properties, either the center height D, or the semi-length L, or the ratio D/L, must be fixed to complete the solution. This is a disadvantage. Moreover, formulas like (5.76) have a vertical tangent at the margin, therefore, violating the shear stress formula in a neighborhood close to this margin. And, finally, close to the center, pure shear cannot be a realistic approximation for the stress state either. It is seen that this simple approach of determining the surface geometry is too restrictive and should be replaced by a more general method. Nevertheless, Paterson [32] states that

such theoretical profiles are often used in reconstructions of past ice sheets based on the evidence of their extent provided by moraines [Paterson [31], Sugden [38]]. Such reconstructions are made, for example, to estimate the amount of isostatic depression or the change in world sea level produced by the former ice sheets in Europe and North America.

If past accumulation/ablation rates can be estimated and if the extent of the ice sheets are known, the ice sheet height and its approximate geometry can be calculated and estimates for mass balances be given.

Before we proceed to present a rational model of a steady-state ice surface, mention should be made of further studies which also include additional effects. Weertman [42], for instance, showed that taking longitudinal stress into account made the profile in the central region somewhat flatter than those previously derived. Nye [28], on the other hand, gives an analysis of the margin zone based on the assumption that ice behaves as an ideally plastic body. Weertman [43], moreover, considers the fact that the bed can deflect under the weight of the ice. He calculates this isostatic bed depression on the basis of a highly-viscous model and finds that the bedrock will depress by the amount  $d(\rho_i/\rho_r)$ , where  $d$  is as above, the height of the free surface about the horizontal line connecting the edges and  $\rho_i$  and  $\rho_r$  are the mass densities of ice and rock, respectively. In a further work, he estimates the effect of water at the bed [44], and calculates a corresponding reduction of the basal shear stress. He finds reduction in these of up to a factor of 2–4 resulting in substantial spreading. In all these works the ice sheet is considered symmetric about its summit point, and the accumulation rates are assumed to be the same on either side of the ice sheet. Weertman considers the differences in these in his work on the position of ice divides and ice centres on ice sheets [45]. The ice divide is obviously displaced towards the side with a higher accumulation.

All these analyses give careful consideration to mass balance but little to momentum balance or constitutive relations. These are only slightly improved in the numerical models of ice-sheet changes by Mahaffy [22] and Budd and Jenssen [6]. Improvement is therefore vital.

*(b) Surface profiles determined by using the shallow-ice approximation*

The above rather simple-minded calculations can be improved and stripped from the many simplifying assumptions. In fact, it is to be expected that the surface geometry will depend on material properties, on bottom geometry, on temperature distribution within the ice, on accumulation/ablation rate, and on sliding law. Most of these were not properly taken into account above. Yet, the calculations based on the shallow-ice approximation have shown that a fairly rigorous approach to the determination of surface geometry is possible, even when processes are time-dependent. In this section, corroboration for this statement will be given. To this end, recall that in the boundary-value problem (5.33)–(5.35) the kinematic surface condition (5.35)<sub>1</sub> has not been used so far. By exploring it, the equation of surface geometry is obtained.

In this chapter, attention will be focused on *steady-state conditions* (time-dependent processes will be analysed in Chapter 6). Under such

limited conditions, Equation (5.35)<sub>1</sub> reads

$$\frac{d\bar{y}_S}{d\xi} U - V = \frac{\bar{a}}{\mu} = \mathfrak{A}, \quad \text{at } \eta = \bar{y}_S(\xi), \quad (5.79)$$

in which all variables have already been defined. This equation can be transformed into the form of a total differential by use of the continuity equation

$$\frac{\partial U}{\partial \xi} + \frac{\partial V}{\partial \eta} = 0$$

and the kinematic boundary condition

$$V = U \frac{d\bar{y}_B}{d\xi}, \quad \text{at } \eta = \bar{y}_B(\xi). \quad (5.80)$$

Integrating the continuity equation with respect to  $\eta$  from  $\eta = \bar{y}_B$  to  $\eta = \bar{y}_S$ , yields

$$\int_{\bar{y}_B}^{\bar{y}_S} \frac{\partial U(\xi, \eta)}{\partial \xi} d\eta + V(\bar{y}_S) - V(\bar{y}_B) = 0,$$

or when interchanging differentiation and integration with Leibnitz' rule,

$$\frac{d}{d\xi} \int_{\bar{y}_B}^{\bar{y}_S} U(\xi, \eta) d\eta + V(\bar{y}_S) - U(\bar{y}_S) \frac{d\bar{y}_S}{d\xi} = 0,$$

where use has been of Equation (5.80). Combining this equation and (5.79) finally yields

$$\frac{d}{d\xi} \left[ \int_{\bar{y}_B}^{\bar{y}_S} U(\xi, \eta) d\eta - s(\xi) \right] = 0, \quad (5.81)$$

where  $s(\xi)$  may be called the *flux function* and is given by

$$s(\xi) = \int_{\xi_M^-}^{\xi} \mathfrak{A}(\bar{\xi}) d\bar{\xi}. \quad (5.82)$$

In (5.81) and (5.82)  $\mathfrak{A}$  and also  $s$  are functions of  $\xi$  only. A dependence on  $\bar{y}_S$  is ignored here. This makes ensuing integration procedures easier than would be otherwise. Also,  $\xi_M^-$  denotes the position of the left margin. Notice that in a steady state the total addition of mass to the glacier must be zero; hence  $s(\xi_M^\pm) = 0$  at the left and right margins. Equation (5.81) is in the form of a total differential and integration can be performed by inspection, provided the distribution of the longitudinal velocity component is sufficiently regular and the flux function  $s(\xi)$  is known. The former is given by relations (5.41) and (5.46), which for ease of reference will be repeated here. The latter is supposed

to be given by field observations. Explicitly the velocity  $U$  reads

$$U = U^{(0)} + \mu U^{(1)} + \mathcal{O}(\mu^2)$$

with

$$\begin{aligned} U(y)^{(0)} &= \mathbb{C} \sin^m \gamma \bar{D}^m + 2 \int_{\bar{y}_B}^{\bar{y}} \tilde{\mathfrak{F}}(\sin^2 \gamma (\bar{y}_S - \eta)^2, \hat{\beta}) \sin \gamma (\bar{y}_S - \eta) d\eta, \\ U(y)^{(1)} &= - \mathbb{C} m \sin^{m-1} \gamma \bar{D}^m \cos \gamma \frac{\partial \bar{y}_S}{\partial \xi} + \\ &\quad + 2 \cos \gamma \frac{\partial \bar{y}_S}{\partial \xi} \int_{\bar{y}_B}^{\bar{y}} \tilde{\mathfrak{F}}(\sin^2 \gamma (\bar{y}_S - \eta)^2, \hat{\beta})(\eta - \bar{y}_S) d\eta. \end{aligned} \quad (5.83)$$

From these expressions it is seen that when  $\mathcal{O}(\mu)$  terms are ignored, the differential equation (5.81) is of first order. In this case, integration is possible by inspection; whence follows

$$\int_{\bar{y}_B}^{\bar{y}_S} U^{(0)}(\xi, \eta) d\eta - s(\xi) = k,$$

from which  $\bar{y}_S$  can be determined implicitly once  $k$  is known. This constant of integration follows from the conditions at the right or left margin, for which  $s(\xi_M^\pm) = 0$  and  $\bar{y}_S(\xi_M^\pm) = \bar{y}_B(\xi)$ . Consequently, provided  $U^{(0)}(\xi_M^\pm)$  is bounded,  $k = 0$  and

$$\int_{\bar{y}_B}^{\bar{y}_S} U^{(0)}(\xi, \eta) d\eta = s(\xi). \quad (5.84)$$

This is the equation for the geometry of the sheet. In the general case of cold ice, an evaluation of  $\bar{y}_S$  as a function of position  $\xi$  depends on the temperature profile, so integration must be performed with an estimated  $\bar{y}_S$ , and the determination of  $\bar{y}_S$  is iterative. For temperate ice or cold ice in which the influence of the temperature on the flow law is neglected, Formula (5.57) may be used to obtain as equations for  $\bar{y}_S$  the following equivalent forms:

$$\mathbb{C} \sin^m \gamma \bar{D}^{m+1} + \frac{\sin^n \gamma}{(n+1)(1+\kappa)} \bar{D}^{n+2} + \frac{2\kappa \sin \gamma}{3(1+\kappa)} \bar{D}^3 = s(\xi) \quad (5.85)$$

or

$$\left\{ (m+1)\mathbb{C} \sin^m \gamma \bar{D}^m + \frac{n+2 \sin^n \gamma}{n+1} \bar{D}^{n+1} + \frac{2\kappa \sin \gamma}{1+\kappa} \bar{D}^2 \right\} \frac{d\bar{D}}{d\xi} = \mathfrak{A}(\xi).$$

In connection with these formulas, several facts are worthwhile being mentioned. Firstly, the basic variable in Equations (5.85) is  $\bar{D} = (\bar{y}_S - \bar{y}_B)$ , the *total glacier thickness*. To lowest order, therefore, the bedrock profile is merely

superimposed on the surface profile, or differently stated, the bedrock profile is fully transferred to the surface. Secondly, Equations (5.85) are two different statements of the same physical content.\* In the first,  $s(\xi)$  with  $s(\xi_M^\pm) = 0$  is known and  $\bar{D}$  must be obtained as the solution of a non-linear equation. When numerically solving this equation for  $\bar{D}$ , non-linear root-finder techniques such as Newton's or Müller's method must be used (see Bulirsch [7]). Equation (5.85)<sub>2</sub> is obtained from (5.85)<sub>1</sub> by differentiation and a first-order differential equation results. This can be solved by forward or backward integration since the initial condition  $\bar{D}(\xi_M^\pm) = 0$  is known at either margin. The second boundary condition at the other end will then be automatically satisfied because of the total differential form of the differential equation. Numerically it can serve as a test of the accuracy of the integration routine. Nevertheless, the start of the integration procedure is difficult since for  $C(\xi_M^\pm) = \mathcal{O}(1)$  and  $\mathfrak{A}(\xi_M^\pm) \neq 0$  by inspection of (5.85)<sub>2</sub>,  $d\bar{D}/d\xi \rightarrow \infty$  as  $\xi \rightarrow \xi_M^\pm$ . Hence, to start the integration at  $\xi = \xi_M^-$  we set

$$\bar{D} = k_d^{(1)} |\xi - \xi_M^\pm|^\delta [1 + \mathcal{O}(|\xi - \xi_M^\pm|)], \quad (5.86)$$

where  $k_d^{(1)}$  and  $\delta$  are determined by substituting (5.86) into (5.85)<sub>2</sub>. Results depend on the behavior of  $\mathfrak{A}(\xi)$  close to the margin and on the magnitudes of the exponents  $m$  and  $n$ . When  $n > m$  and when  $\mathfrak{A}(\xi) = \mathfrak{A}_v |\xi - \xi_M^\pm|^v + \mathcal{O}(|\xi - \xi_M^\pm|^{v+1})$  then

$$k_d^{(1)} = \left\{ \frac{|\mathfrak{A}_v|(n+1)(n+2)(1+\gamma)}{(n+3)(v+1)\sin^n \gamma} \right\}^\delta, \quad \delta = \frac{v+1}{n+2}. \quad (5.87)$$

For  $\delta < 1$ , Equation (5.85) is singular at the margin and so gradients  $d\bar{D}/d\xi$  may become large as  $\xi = \xi_M^\pm$  is approached. Only when the accumulation rate vanishes, as  $|\xi - \xi_M^-|^v$  with  $v \geq n+1$ , is  $d\bar{D}/d\xi(\xi_M^-)$  bounded. This is the exception. Hence, the assumptions of small variations of the ice sheet thickness for which  $\bar{D}$  and its  $\xi$ -derivative remain bounded, must break down close to the margin, and the solution (5.85) becomes invalid. Away from this region, the solution (5.85) makes sense and can be determined. It is to be seen whether including  $\mathcal{O}(\mu)$ -terms in the original equation (5.81) will yield an uniformly-valid solution independent of how the accumulation rate behaves close to the margin.

The above discussion hinges on the explicit assumption that  $C(\xi_M^\pm) = \mathcal{O}(1)$ . Since  $C$  may vary with  $\xi$ , there is a possibility with some practicability in which the slope of  $\bar{D}$  remains finite as  $\xi \rightarrow \xi_M^\pm$ . If  $C = C_M |\xi - \xi_M^\pm|^{-\beta}$  and  $\mathfrak{A}(\xi) = \mathfrak{A}_v |\xi - \xi_M^\pm|^v$  as  $\xi \rightarrow \xi_M^\pm$ , then  $d\bar{D}/d\xi$  is bounded, and its behavior is  $\bar{D} = k_d^{(2)} |\xi - \xi_M^\pm|$  as  $\xi \rightarrow \xi_M^\pm$  provided that  $\beta = m - v$ . In fact, an analysis analogous to that leading to Equations (5.86) and (5.87) yields, provided the

\*Actually, (5.85)<sub>2</sub> is more general than (5.85)<sub>1</sub> as  $\mathfrak{A}$  may also depend on  $\bar{D}$ .

lower margin is ablating,

$$\begin{aligned}\mathbb{C} &= \mathbb{C}_M^\pm |\xi - \xi_M^\pm|^{v-m} [1 + \mathcal{O}(|\xi - \xi_M^\pm|)], \\ \bar{D} &= \left\{ \frac{a_v \operatorname{sgn}(\xi - \xi_M^\pm)}{(m+1)\mathbb{C}_M \sin^m \gamma} \right\}^{1/(m+1)} |\xi - \xi_M^\pm| + \mathcal{O}(|\xi - \xi_M^\pm|^2).\end{aligned}\quad (5.88)$$

Hence the slope depends upon whether and how the glacier is ablating at the margin. Since under normal circumstances the accumulation rate does not vanish at the edge, the margin slope of  $\bar{D}$  is bounded only for a friction law with a coefficient that is singular like  $|\xi - \xi_M|^{-m}(v=0)$ . In other words, viscous sliding goes over into perfect slip, and the transition to this perfect slip is as indicated by the singularity. The reduction in sliding is sufficient to change the velocity field at the snout. This can easily be seen from formulas (5.83). They indicate that when  $\mathbb{C}$  is finite at the edge, then zeroth- and first-order velocities vanish. However, when  $\mathbb{C}$  and, hence  $\bar{D}$ , vary according to relations (5.88), then snout velocities may be non-zero. For  $U^{(0)}$  one may use (5.88) to obtain

$$U^{(0)}(\xi_M^\pm) = \mathbb{C}_M^\pm \sin^m \gamma \left\{ \frac{|\mathfrak{A}_v|}{(m+1)\mathbb{C}_M^- \sin^m \gamma} \right\}^{m/(m+1)} (\xi - \xi_M^\pm)^v. \quad (5.89)$$

When the glacier is ablating at the margin, then  $v=0$  and  $U^{(0)}(\xi_M^-)$  is given by the coefficient on the right-hand side of (5.89). This offers the possibility of determining  $\mathbb{C}_M^\pm$  by field observations. Measuring margin velocities and ablation rates will provide an estimate for  $\mathbb{C}_M^\pm$ .

Similar behavior must also be expected when cold ice is looked at. It then follows from Equations (5.83) and (5.84) that thickness is governed by the equation

$$\mathbb{C} \sin^m \gamma \bar{D}^{m+1} + 2 \sin \gamma \int_{\bar{y}_B}^{\bar{y}_S} (\bar{y} - \eta)^2 \tilde{\mathfrak{F}}(\sin^2 \gamma (\bar{y}_S - \eta)^2, \hat{\theta}) d\eta = s(\xi)$$

which can only be written as an equation for  $\bar{D}$  alone, when  $\hat{\theta} = \hat{\theta}(\bar{y}_S - \eta, \xi)$ . In that case

$$\mathbb{C} \sin^m \gamma \bar{D}^{m+1} + 2 \sin \gamma \int_0^{\bar{D}} \bar{y}^2 \tilde{\mathfrak{F}}(\sin^2 \gamma \bar{y}^2, \hat{\theta}(\bar{y}, \xi)) d\bar{y} = s(\xi), \quad (5.90a)$$

or after differentiation

$$\begin{aligned}&\{\mathbb{C}(m+1) \sin^m \gamma \bar{D}^m + 2\bar{D}^2 \sin \gamma \tilde{\mathfrak{F}}(\sin^2 \gamma \bar{D}^2, \hat{\theta}(\bar{D}, \xi))\} \frac{d\bar{D}}{d\xi} + \\ &+ 2 \sin \gamma \int_0^{\bar{D}} \bar{y}^2 \tilde{\mathfrak{F}}_y(\sin^2 \gamma \bar{y}^2, \hat{\theta}(\bar{y}, \xi)) \frac{\partial \hat{\theta}}{\partial \xi}(\bar{y}, \xi) d\bar{y} = \mathfrak{A}(\xi), \\ &\bar{D}(\xi_M^\pm) = 0.\end{aligned}\quad (5.90b)$$

Equations (5.90) correspond to Equations (5.85) and are valid for an arbitrary creep response function  $\tilde{\mathcal{F}}$ . They demonstrate that the total ice thickness is composed of a sliding term and a contribution due to deformation and, hence, material properties. Because  $\tilde{\mathcal{F}}(0, \hat{\mathcal{G}}) = 0$  the differential equation for  $\bar{D}$  is singular, unless the accumulation rate vanishes smoothly enough at the margin and/or the sliding coefficient becomes infinitely large as  $\xi \rightarrow \xi_M^\pm$ . The preceding analysis goes through in this case implying that for  $\delta = 1$  the snout velocity is again given by relations (5.88) and (5.89). Hence, except in these instances, the solution is valid only in an outer region far distant from the margin and integration of the first-order equation must be commenced with a local solution akin to that explained in Equations (5.86) and (5.87).

It is also interesting to observe that with a general temperature distribution function  $\hat{\mathcal{G}} = \hat{\mathcal{G}}(\xi, \eta)$ , a relationship for  $\bar{D}$  alone, such as (5.90), can no longer be derived. In that case the equation for the surface geometry will involve  $\bar{y}_S$ ,  $\bar{y}_B$  and  $(\bar{y}_S - \bar{y}_B)$  separately. It follows that for a general temperature function  $\hat{\mathcal{G}}$ , the bottom profile is not just superimposed on the surface that would correspond to a flat base. Corresponding solutions for the profile geometry are, theoretically, no more difficult to obtain however, even though the algebra will be more complex.

Finally, it should be noticed that according to Equation (5.83)<sub>1</sub>,  $U^{(0)}$  cannot change signs. This restricts mean slope angles  $\gamma$  to being fairly large as there can be no ice divide in this case. The upper margin is always identifiable with the head, while the lower edge is the snout. *For small mean bed slope angles, the shallow ice approximation is therefore unsuitable, and new coordinate stretchings must be found for which a change of sign in the longitudinal velocity is possible.* This will be studied in the next section.

Consider now the *first-order theory* in which  $\mathcal{O}(\mu)$  terms are kept but those of  $\mathcal{O}(\mu^2)$  and higher are omitted. Equation (5.83)<sub>2</sub> then indicates that (5.81) is a second-order equation for  $\bar{y}_S(\xi)$ . Thus, apart from the previous boundary conditions  $\bar{y}_S(\xi_M^\pm) = \bar{y}_B(\xi_M^\pm)$ , the derivative  $d\bar{y}_S/d\xi$  (or  $d\bar{D}/d\xi$ ) must be prescribed at the margin. At present it is not clear, however, what condition this could be. To investigate this, Equation (5.81) is integrated to yield

$$\int_{\bar{y}_B}^{\bar{y}_S} [U^{(0)}(\xi, \eta) + \mu U^{(1)}(\xi, \eta)] d\eta - s(\xi) = k, \quad (5.91)$$

in which  $k$  is a constant of integration. For temperate ice the velocities are given by Equations (5.57); whence direct integration is possible which leads to

$$2\mu \cos \gamma \frac{d\bar{D}}{d\xi} \left\{ \frac{\sin^{n-1} \gamma}{(n+2)(1+\gamma)} \bar{D}^{n+2} + \frac{k}{3(1+\gamma)} \bar{D}^3 - \frac{C}{2} \sin^{m-1} \gamma \bar{D}^{m+1} \right\} +$$

$$\begin{aligned}
& + \mathbb{C} \sin^m \gamma \bar{D}^{m+1} + \frac{\sin^n \gamma}{(n+2)(1+\bar{\zeta})} \bar{D}^{n+2} + \frac{2\zeta \sin \gamma}{3(1+\bar{\zeta})} \bar{D}^3 + \\
& + 2\mu \cos \gamma \frac{d\bar{y}_B}{d\xi} \left\{ \frac{\sin^{n-1} \gamma}{(n+2)(1+\bar{\zeta})} \bar{D}^{n+2} + \frac{\zeta}{3(1+\bar{\zeta})} \bar{D}^3 - \frac{\mathbb{C}}{2} \sin^{m-1} \gamma \bar{D}^{m+1} \right\} \\
& = s(\xi) + k
\end{aligned} \tag{5.92}$$

Notice that the coefficient of the term involving  $d\bar{D}/d\xi$  vanishes as  $\bar{D} \rightarrow 0$ ; Equation (5.92) is therefore singular. Assume now that  $\bar{D}$  vanishes at the margin. In particular, suppose that near the margin the following expansions hold :

$$\begin{aligned}
\mathbb{C} &= \mathbb{C}_M^\pm |\xi - \xi_M^\pm|^{-\beta}, \\
\bar{D} &= k_d^{(2)} |\xi - \xi_M^\pm|^\delta [1 + \mathcal{O}(|\xi - \xi_M^\pm|)], \\
s &= \frac{\mathfrak{A}_v}{(v+1)} (\xi - \xi_M^\pm)^{v+1}
\end{aligned} \tag{5.93}$$

with integer values for  $v$ ; the exponents  $\beta$  and  $v$  and the coefficients  $\mathbb{C}_M^\pm$  and  $\mathfrak{A}_v$  are assumed to be prescribed;  $\delta$  and  $k_d^{(2)}$  and the constant of integration  $k$  must be determined. When this is done, the initial conditions for Equation (5.92) are known, since Equation (5.93), determines  $\bar{D}$  and its derivative in the immediate neighborhood of  $\xi = \xi_M^\pm$ . The exponents  $\beta$ ,  $\delta$  and  $v$  may have any value but are most likely positive. A negative  $\delta$  corresponds to a cliff and  $v = -1$  could model a calving mechanism. Cliffs and calving will be excluded in the following analysis. When the power representations (5.93) are substituted into the differential equation (5.92), the orders of the various terms are (only the exponents of  $|\xi - \xi_M|$  are listed) :

$$\overbrace{\begin{array}{ccc} [(n+3)\delta - 1] & 4\delta - 1 & [(m+2)\delta - 1 - \beta] \\ [(m+1)\delta - \beta] & (n+2)\delta & 3\delta \\ (n+2)\delta & 3\delta & [(m+1)\delta - \beta] \end{array}}^{\text{LHS}} \quad \overbrace{\begin{array}{c} (v+1) \\ 0 \end{array}}^{\text{RHS}} \tag{5.94}$$

Since exponents on the LHS (left-hand side) of Equation (5.92) must match those on the RHS (right-hand side), it follows that the nine entries of the left part of list (5.94) will obey certain restrictive conditions. In principle, there are two possibilities, namely that all entries are positive; this implies  $k = 0$  in Equation (5.92). The other possibility is that at least one entry will vanish; then  $k \neq 0$ . We exclude this latter case and therefore assume that all the exponents in the left of list (5.94) are positive. Of necessity then

$$k = 0 \text{ (by matching } \mathfrak{A}|\xi - \xi_M|^0\text{).} \tag{5.95}$$

TABLE 5.1. Values for the exponents of the terms on the LHS of (5.92) when  $\delta$  is given by the values in the left column.

$\exp_{\delta =}$	$[(m+3)\delta - 1]$	$[(n+2)\delta]$	$4\delta - 1$	$3\delta$	$[(m+1)\delta - \beta]$	$[(m+2)v - 1 - \beta]$
$\frac{v+2}{n+3}$	$v+1$	$\frac{(n+2)(v+2)}{n+3}$	$\frac{4(v+2)}{n+3} - 1$	$\frac{3(v+2)}{n+3}$	$\frac{(m+1)(v+2) - \beta(n+3)}{n+3}$	$\frac{(m+2)(v+2) - (1+\beta)(n+3)}{n+3}$
$\frac{v+1}{n+2}$	$\frac{n+3}{n+2}(v+1) - 1$	$v+1$	$\frac{4(v+1)}{n+2} - 1$	$\frac{3(v+1)}{n+2}$	$\frac{(m+1)(v+1) - \beta(n+1)}{n+2}$	$\frac{(m+2)(v+2) - (1+\beta)(n+2)}{n+2}$
$\frac{v+2}{4}$	$\frac{(n+3)(v+2) - 4}{4}$	$\frac{(n+2)(v+2)}{4}$	$v+1$	$\frac{3(v+2)}{4}$	$\frac{(m+1)(v+2) - 4\beta}{4}$	$\frac{(m+2)(v+2) - 4(1+\beta)}{4}$
$\frac{v+1}{3}$	$\frac{(n+3)(v+1) - 3}{3}$	$\frac{(n+2)(v+1)}{3}$	$\frac{4(v+1)}{3}$	$v+1$	$\frac{(m+1)(v+1) - 3\beta}{3}$	$\frac{(m+2)(v+1) - 3(1+\beta)}{3}$
$\frac{v+1+\beta}{m+1}$	$\frac{(n+3)(v+1+\beta) - (m+1)}{m+1}$	$\frac{(n+2)(v+1+\beta)}{m+1}$	$\frac{4(v+1+\beta) - m - 1}{m+1}$	$\frac{3(v+1+\beta)}{m+1}$	$v+1$	$\frac{(m+2)(v+1+\beta) - (1+\beta)(m+1)}{m+1}$
$\frac{v+2+\beta}{m+2}$	$\frac{(n+3)(v+1+\beta) - (m+2)}{m+2}$	$\frac{(n+2)(v+2+\beta)}{m+2}$	$\frac{4(v+2+\beta)}{m+2} - 1$	$\frac{3(v+2+\beta)}{m+2}$	$\frac{(m+1)(v+2+\beta) - \beta(m+2)}{m+2}$	$v+1$

The coefficient  $k_d^{(2)}$  and the exponent  $\delta$  are determined by matching the dominant term(s) on the LHS with  $s(\xi)$  on the RHS. There are six possibilities, namely

$$\delta = \left\{ \frac{v+2}{n+3}, \frac{v+1}{n+2}, \frac{v+2}{4}, \frac{v+1}{3}, \frac{v+1+\beta}{m+1}, \frac{v+2+\beta}{m+2} \right\}, \quad (5.96)$$

and these are obtained by equating any one of the exponents in the LHS of list (5.94) to  $(v+1)$ . However, only those values of  $\delta$  are admissible for which the remaining five exponents in (5.94) are larger than or equal to that from which  $\delta$  has been selected. Hence, 24 possibilities must be checked which are listed in Table 5.1. In this table only those values of  $\delta$  are admissible where the off-diagonal elements are larger than or equal to  $(v+1)$ . A general analysis would require a cumbersome distinction of cases and so we restrict attention to the most practical cases when

- (i)  $v = 0, \quad \beta = 0$  (bounded  $\mathbb{C}$ , zero margin velocity),
- (ii)  $v = 0, \quad \beta = m$  (singular  $\mathbb{C}$ , finite snout velocity),
- (iii)  $v = \text{arb.}, \quad \delta = 1$  (wedge type snout).

Results are then as follows:

*Case (i):* A careful inspection of Table 5.1 shows that for values of  $m$  and  $n$  larger than 1, only rows 3 and 6 are compatible with the conditions stated above; in particular, row 3 applies, when  $m \geq 2$  and row 6 applies, when  $m \leq 2$  and  $n \geq 2m + 1$ . The restrictions imposed on  $n$  and  $m$  for row 6 are unlikely to be realistic since usually  $m \sim (n+1)/2$ . Hence, case (i) only applies for  $m \geq 2$  (and  $n \geq 3$ ). It follows that

$$\beta = v = 0, \quad \Rightarrow m \geq 2, \quad \delta = \frac{1}{2}, \quad k = 0, \quad (5.97a)$$

and

$$k_d^{(2)} = \begin{cases} \left[ \frac{\operatorname{sgn}(\xi - \xi_M^\pm) \mathfrak{A}_0}{2 \cos \gamma \left[ \frac{\mathbb{K}}{3(1+\mathbb{K})} - \frac{\mathbb{C}}{2} \sin^{m-1} \gamma \right]} \right]^{1/4}, & \text{if } m = 2, \\ \left[ \frac{\operatorname{sgn}(\xi - \xi_M^\pm)(1+\mathbb{K}) \mathfrak{A}_0}{2 \cos \gamma} \right]^{1/4}, & \text{if } m > 2. \end{cases} \quad (5.97b)$$

This implies that the geometry of the snout depends on the Newtonian part of the response function and, when  $m = 2$ , also on the sliding coefficient. Moreover,  $\mathfrak{A}_0$  must have the same sign as  $(\xi - \xi_M^\pm)$ ; integration is therefore usually from the lower margin (snout) to the upper margin (head).

The results (5.97) are somewhat disturbing as for bounded  $\mathbb{C}$  and  $\mathfrak{A}$ , at a regular margin, solutions of the differential equation only exist when

$m \geq 2$ . This means that in this case the differential equation (5.92) cannot be solved for  $m \leq 2$  by starting from the snout (or head), but only by commencing the integration from a position  $\xi_s$  a certain distance away from the snout. The thickness  $\bar{D}$  and the slope  $d\bar{D}/d\xi$  at  $\xi_s$  must be known either from field measurements or from a separate investigation of the flow region close to the snout. These two quantities will then fix the constant  $k$  in Equation (5.92) and integration can be commenced up-glacier to the head, where first derivatives are again expected to become large so that integration should be interrupted before the head is reached.

*Case (ii):* In view of these results it is realistic to *abandon regular behavior* for  $C$  and to *postulate a nonzero snout velocity*. Careful analysis of Table 5.1 reveals that for  $v = 0$ ,  $\beta = m$  only rows 5 and 6 have entries all of which are larger or equal to 1. Matching exponents yields for both

$$\beta = m, \quad v = 0 \quad \Rightarrow \delta = 1, \quad k = 0 \quad (5.98)$$

and, by substitution of these into Equations (5.93) and the emerging representations into (5.92)

$$k_d^{(2)} = \left\{ \frac{\mathfrak{A}_0 + C_M^\pm \mu \cos \gamma \sin^{m-1} \gamma (k_d^{(2)})^{m+1} \left[ \frac{d\bar{y}_B}{d\xi} + \operatorname{sgn}(\xi - \xi_M^\pm) k_d^{(2)} \right]}{C_M^\pm \sin^m \gamma} \right\}^{1/(m+1)} \quad (5.99)$$

Notice that  $\delta = 1$ . Hence  $d\bar{D}/d\xi$  is finite at the margin which is wedge-type. With  $\beta = m$  and  $\delta = 1$  margin velocities are bounded and *non-zero* and given by

$$\begin{aligned} U_s &= (U^{(0)} + \mu U^{(1)})_{\xi=\xi_M^\pm} \\ &= C_M^\pm \sin^{m-1} \gamma \left[ \sin \gamma - \mu m \cos \gamma \frac{d\bar{y}_B}{d\xi} \right] - \\ &\quad - C_M^\pm \sin^{m-1} \gamma \cos \gamma \mu m \operatorname{sgn}(\xi - \xi_M^\pm) k_d^{(2)}. \end{aligned} \quad (5.100)$$

Measuring the margin velocity  $U_s$  thus gives a means of determining  $C_M$ . Equations (5.99) and (5.100) must, however, be solved iteratively. A first estimate is obtained by ignoring the  $\mu$ -order terms, and improved estimates are obtained by iterating these. This is the reason for writing Equations (5.99) and (5.100) in this way.

*Case (iii):* Selecting  $\beta$  so as to obtain a non-zero but finite margin velocity has led to regular snout geometry. It is thus interesting to test whether the reverse is also correct. To this end we set  $\delta = 1$ , assume wedge-type margins, and seek the conditions for which Equation (5.92) will admit solutions of the form (5.93). The method of analysis proceeds as follows: All rows of Table 5.1 are checked for conditions of admissibility, namely

whether two or more entries could be found that would match the exponents of the terms on the right-hand side of Equation (5.92). A total of 24 cases must be distinguished, but many are unrealistic because they either require an unrealistic power law exponent  $n$ , or yield infinite margin velocities, and therefore are abandoned. The results of the analysis may be summarized as follows: For  $v = 0$  the only possibility of regular snout conditions is that expressed by Equations (5.98)–(5.100). From a practical point of view, this is the most important case as most margins are ablating. For  $v \neq 0$ ,  $\delta = 1$  is a possible power-law solution, but it requires a distinct value for the exponent  $\beta$ . For instance,  $v = 1$  implies  $\beta = m - 1$ , leading to a singular sliding law, yet still zero snout velocities. Several possibilities can be differentiated for  $v = 2$ , some even requiring a negative value for  $\beta$ , which would correspond to  $C = 0$  at the margin. In other words, whereas the ice is sliding over its bed in the interior of the glacier, it would adhere to the bed at the snout. This points to the importance of the behavior of the accumulation-ablation rate at the snout; if it vanishes sufficiently fast, regular snout geometries with finite slope may exist, even for a glacier frozen to the base at the snout.

In practice, the most prevailing situation is ablation at the snout, for which the requiring finite margin velocity implies regular snout behavior and vice versa. Integration of the differential Equation (5.92) is then executed by implementing the power laws (5.93) at the lower margin with coefficients and exponents as listed in Equations (5.98)–(5.100). These representations allow the calculation of  $\bar{D}$  and its first derivative at a position which is slightly off the margin, thereby providing the initial conditions for the subsequent forward integration of Equation (5.29).

The above analysis can only partly be extended to cold glaciers, since in these the ice adheres to the bed, implying  $C = 0$  throughout. In lieu of Equation (5.92), the differential equation for  $\bar{y}_S$  is obtained by substituting (5.83) into (5.81). One obtains

$$\begin{aligned} 2 \left[ \sin \gamma - \mu \cos \gamma \frac{d\bar{y}_S}{d\xi} \right] I(\bar{y}_S, \bar{y}_B) + \\ + C \sin^{m-1} \gamma \bar{D}^{m+1} \left[ \sin \gamma - \mu m \cos \gamma \frac{d\bar{y}_S}{d\xi} \right] = s + k, \end{aligned} \quad (5.101)$$

in which

$$I(\bar{y}_S, \bar{y}_B) = \int_{\bar{y}_B}^{\bar{y}_S} (\bar{y}_S - y)^2 \tilde{\mathfrak{F}}(\sin^2 \gamma (\bar{y}_S - y)^2, \hat{\mathfrak{H}}(\xi, y)) dy. \quad (5.102)$$

Equation (5.101) is a first-order differential equation for  $\bar{y}_S$ ; it cannot be transformed into an equation for  $\bar{D}$  unless  $\hat{\mathfrak{J}} = \hat{\mathfrak{H}}(\xi, \bar{y}_S - \bar{y})$ . When  $C = 0$  throughout, since  $\tilde{\mathfrak{F}}(0, \hat{\mathfrak{J}}) = 0$ , the equation is singular; a snout analysis must again be performed with representations of the form (5.93). The details depend on the behavior of  $\tilde{\mathfrak{F}}$  close to the snout.

In order to have regular behavior of the surface at the snout, it may be advantageous to presume that the ice is sliding over its bed at the snout with a friction coefficient that is infinitely large at the margin and drops off as one moves away from it. Requiring a finite snout velocity will then determine the exponent  $\beta$  in Equation (5.93)<sub>2</sub>, and an analysis of the differential equation (5.101) close to the margin will provide the value of the exponent  $\delta$  in (5.93)<sub>1</sub>. Details of the calculations will again depend upon the behavior of  $\tilde{\gamma}$  close to the margin. However, when assuming  $\tilde{\gamma}$  to be temperature-independent at the snout (temperate ice at the snout), the previous analysis goes through so that Equations (5.98)–(5.100) can be used to calculate the initial conditions at a position which is a small distance up-glacier from the snout. The corresponding analysis has not been performed so far.

It would be interesting to see whether the equations of the zeroth- or first-order shallow-ice approximation would lead to realistic steady-state surface profiles. The theory is more general than the steady-state theories summarized in the last sections, as it includes the variation of the bottom topography and *allows a proper account of local material behavior*. Its shortcomings are that longitudinal velocities cannot change signs. The application of the equations are therefore restricted to relatively steep glaciers or portions of an ice sheet where there is no *ice divide*. The reason for a failure to predict changes in the sign of the longitudinal velocity lies in the scalings of the shallow ice approximation. A different scaling, due to Morland and Johnson [24], is possible allowing for spreading in all directions. This will be demonstrated in the next section.

##### 5. An Alternative Scaling – a Proper Analysis of Dynamics of Ice Sheets with Ice Divides

The alternative scaling referred to above has been suggested by Morland and Johnson [23, 24] in a series of papers dealing with the steady motion of ice sheets. They study plane motion and, therefore, consider situations identical to those treated above, but also extend their ideas to axisymmetric ice sheets (see Johnson [17–19]), thereby providing an approximate analysis for the central part of a dome-like ice sheet or a cirque glacier. Attention is, however, limited to temperature-independent creep-response functions, an assumption that is somewhat unrealistic for ice sheets; yet this is no disadvantage as the physically important features will be more transparent, and the analysis may pave the route to further extensions. Moreover, they assume accumulation/ablation to be depending on the height of the free surface above a horizontal reference level rather than on position  $\xi$ . This is an essential generalization because the values of  $a$  will depend on the solution of the problem, which could affect steady-state geometry of the

surface profile. Mathematically, it implies that the flux function  $s$  cannot be defined and, consequently, a first integral of the governing differential equation can no longer be obtained by inspection (compare Equation (5.81)). Finally, they introduce a basal drainage function accounting for mass loss at the ice-bedrock interface, yet disregard this effect in the numerical treatment of the examples shown.

In order to introduce Morland and Johnson's approach, we shall ignore below the temperature-dependence of the creep-response function. In previous calculations, the boundary-value problem expressed by Equations (5.25)–(5.28) was solved by selecting  $\mathbb{G} = 1$ . According to the discussion in Chapter 3, Section 3a, this choice leads to non-dimensional velocities which are not of  $\mathcal{O}(1)$  but  $\mathcal{O}(10^{-2})$  or smaller. Only for steep glaciers can we expect to obtain  $\mathcal{O}(1)$ -longitudinal velocities for  $\mathbb{G} = \mathcal{O}(1)$ . One may, however, select  $\mathbb{G}$  such that dimensionless longitudinal velocities are of  $\mathcal{O}(1)$ , as are the dimensionless stresses  $\sigma_x$  and  $\sigma_y$ . Indeed, the proper approach will be to select scaling factors for stretchings and stresses such that in a real flow, dimensionless stretchings and stresses will be of order unity. This process will then determine the characteristic number  $\mathbb{G}$ . Order-of-magnitude considerations show that for most, if not all, realistic cases  $\mathbb{G}$  is large. One could, therefore be tempted to search for a solution of the governing equations in the asymptotic limit as  $\mathbb{G} \rightarrow \infty$ . Equations (5.25) and (5.28)<sub>2</sub> would then imply\*

$$\begin{aligned}\sigma_x &= \sigma_y = \cos \gamma (\bar{y} - \bar{y}_S) - \bar{p}^{\text{atm}}, \tau = 0, (\bar{u}, \bar{v}) = \text{const.} \\ \bar{y}_S &= \text{const.} + \begin{cases} \bar{x} \tan \gamma, & \gamma = \mathcal{O}(1), \\ 0, & \gamma \ll \mathcal{O}(1). \end{cases}\end{aligned}\quad (5.103)$$

The  $\gamma = \mathcal{O}(1)$  solution is a static ice reservoir with the horizontal surface resting against a steep embankment, and the  $\gamma \ll \mathcal{O}(1)$  solution is a slab of uniform depth on a bed with a small mean inclination. Neither case is a leading approximation to a global solution with an upper and lower margin. It is therefore necessary to scale the longitudinal coordinate  $\bar{x}$  by a small factor  $\varepsilon$  so that the shear-stress gradient enters the lowest-order momentum balance.

Let us now present the key steps in Morland and Johnson's analysis. Their stretching transformation is

\*This result is obtained as follows: From Equations (5.25)<sub>2,3</sub> one concludes that  $\sigma_x \equiv \sigma_y$  and  $\tau \equiv 0$ . Using this result in Equation (5.25)<sub>5</sub>, together with the second boundary condition (5.28),  $\sigma_y = -\bar{p}^{\text{atm}}$ , leads to the result stated in Equation (5.103)<sub>1</sub>. The above results now imply that  $\bar{u}$  and  $\bar{v}$  cannot depend on  $\bar{x}$  and  $\bar{y}$  and therefore must be spatially independent. From the time-independent kinematic surface condition (5.28)<sub>1</sub>, it then follows that accumulation must be constant. From Equation (5.25)<sub>4</sub> and the representation (5.103)<sub>1</sub>, a differential equation for  $d\bar{y}_S/d\bar{x}$  is obtained of which the solution is given by the last of Equations (5.103).

$$\xi = \varepsilon \bar{x}, \quad \tilde{U} = \varepsilon \bar{u}, \quad \tilde{V} = \bar{v}, \quad (5.104a)$$

and will be referred to as the MJ-transformation. It is different from the shallow ice approximation which reads

$$\xi = \varepsilon \bar{x}, \quad \ell = \varepsilon \bar{t}, \quad U = \bar{u}, \quad V = \frac{1}{\varepsilon} \bar{v}. \quad (5.104b)$$

The two different transformations warrant the following remarks. They differ essentially in the scaled velocities  $\bar{u}$ ,  $\bar{v}$ :

$$(\bar{u}, \bar{v})_{\text{MJ}} = \varepsilon (\bar{u}, \bar{v})_{\text{shallow ice}} \quad (5.104c)$$

Requiring  $(U, V)$  to be  $\mathcal{O}(1)$  apparently means that in the shallow ice approximation velocities are scaled with a characteristic *longitudinal* velocity, whence  $\bar{u} = \mathcal{O}(1)$  but  $\bar{v} = \mathcal{O}(\varepsilon)$ , so that  $U = \bar{u}$ ,  $V = \bar{v}/\varepsilon$ . In the MJ-transformation velocities are scaled such that  $\bar{v} = \mathcal{O}(1)$  implying that  $\bar{u}$  is large. Hence, here one must have  $\tilde{V} = \bar{v}$ , but  $\tilde{U} = \varepsilon \bar{u}$ . Clearly, the two scalings will result in two different values for the dimensionless number  $\mathbb{G}$ , denoted by  $\mathbb{G}_{\text{MJ}}$  and  $\mathbb{G}$ , respectively, and it is clear from formulas (5.105) below that for  $U = \tilde{U}$ ,  $V = \tilde{V}$  one has  $\mathbb{G}_{\text{MJ}} = \mathbb{G}/\varepsilon$ .\*

From the kinematic surface condition it can also be seen why a scaling of the time is needed in the shallow-ice approximation, but not in the MJ-approach. This equation remains form-invariant only when the transformations are executed according to Equations (5.104). Indeed, the scaled equation reads,

for (5.104a):

$$\frac{\partial \bar{y}_s}{\partial \bar{t}} + \tilde{U} \frac{\partial \bar{y}_s}{\partial \xi} - \tilde{V} = \bar{a}_{\text{MJ}} = \mathfrak{A},$$

for (5.104b):

$$\frac{\partial \bar{y}_s}{\partial t} + U \frac{\partial \bar{y}_s}{\partial \xi} - V = \frac{\bar{a}}{\varepsilon} = \mathfrak{A}.$$

The difference in the orders of magnitude for accumulation stems again from the two different non-dimensionalizations. Clearly, since  $\bar{a}_{\text{MJ}} = \mathcal{O}(\tilde{V}) = \mathcal{O}(1)$ , one necessarily has  $\bar{a} = \mathcal{O}(\varepsilon)$ , since  $\bar{a} = \mathcal{O}(\bar{v})$ .

Substituting Equations (5.104) into the field equations (5.25) and boundary conditions (5.27) and (5.28) yields:

*For the field equations [compare Equations (5.25)]*

\*The reader may profit from a further glance at the scaling procedure explained in Chapter 3, see pages 149–151, and Table 3.1.

$$\begin{aligned}
& \varepsilon \frac{\partial \sigma_x}{\partial \xi} + \frac{\partial \tau}{\partial \bar{y}} + \sin \gamma = 0, \\
& \varepsilon \frac{\partial \tau}{\partial \xi} + \frac{\partial \sigma_y}{\partial \bar{y}} - \cos \gamma = 0, \\
& \frac{\partial U}{\partial \xi} + \frac{\partial V}{\partial \bar{y}} = 0, \quad \frac{\partial \tilde{U}}{\partial \xi} + \frac{\partial \tilde{V}}{\partial \bar{y}} = 0, \\
& \varepsilon \frac{\partial U}{\partial \xi} = \frac{1}{2} \bar{\mathbb{G}} \mathfrak{F}(\tau'_{II})(\sigma_x - \sigma_y), \quad \frac{\partial \tilde{U}}{\partial \xi} = \frac{1}{2} \bar{\mathbb{G}}_{MJ} \mathfrak{F}(\tau'_{II})(\sigma_x - \sigma_y), \\
& \frac{\partial U}{\partial \bar{y}} + \varepsilon^2 \frac{\partial V}{\partial \xi} = 2 \bar{\mathbb{G}} \mathfrak{F}(\tau'_{II})\tau, \quad \frac{\partial \tilde{U}}{\partial \bar{y}} + \varepsilon^2 \frac{\partial \tilde{V}}{\partial \xi} = 2 \bar{\mathbb{G}}_{MJ} \varepsilon \mathfrak{F}(\tau'_{II})\tau,
\end{aligned} \tag{5.105}$$

where  $\tau'_{II} = \frac{1}{4}(\sigma_x - \sigma_y)^2 + \tau^2$ . Here, the equations are listed for both scalings. Also,  $\bar{\mathbb{G}}_{MJ} = \bar{\mathbb{G}}/\varepsilon$ , and  $\bar{\mathbb{G}} = \mathbb{G} \exp(\mathbb{A}\theta)$  has been introduced because our interest is in a temperature-independent model at an arbitrary temperature. Variations of  $\bar{\mathbb{G}}$  due to this temperature dependence are in the order of a factor from 1 to 10.

*For the top boundary conditions [compare Equations (5.28)]*

$$\left. \begin{aligned}
& (\sigma_x + \sigma_y)(1 + \varepsilon^2 \bar{y}'_S^2) - (\sigma_x - \sigma_y)(1 - \varepsilon \bar{y}'_S^2), \\
& - 4\varepsilon \bar{y}'_S \tau = - 2\bar{p}^{atm}(1 + \varepsilon \bar{y}'_S), \\
& \varepsilon(\sigma_x - \sigma_y)\bar{y}'_S + (1 - \varepsilon^2 \bar{y}'_S^2)\tau = 0, \\
& \frac{\partial \bar{y}_S}{\partial \ell} + U \frac{\partial \bar{y}_S}{\partial \xi} - V = \frac{\bar{a}(z)}{\varepsilon} = \mathfrak{A}, z = \bar{y}_S \cos \gamma - \frac{1}{\varepsilon} \xi \sin \gamma,
\end{aligned} \right\} \text{at } \bar{y} = \bar{y}_S(\xi, \ell), \tag{5.106}$$

in which  $z$  denotes the vertical coordinate which is related to  $\bar{y}_S$  and  $\bar{x} = \varepsilon^{-1}\xi$  by an orthogonal transformation.

*For the basal boundary condition [compare Equations (5.27)]. With  $\zeta = \operatorname{sgn}(U - \varepsilon^2 V \bar{y}'_B)$*

$$\left. \begin{aligned}
& V = U \bar{y}'_B, \\
& U(1 - \varepsilon^2 \bar{y}'_B^2) = \zeta \mathbb{C} \left( \frac{1}{1 + \varepsilon^2 \bar{y}'_B^2} \right)^{(2m-1)/2} \times \\
& \quad \times \{ \zeta [(1 - \varepsilon^2 \bar{y}'_B^2)\tau - \varepsilon \bar{y}'_B(\sigma_x - \sigma_y)] \}^m,
\end{aligned} \right\} \text{at } \bar{y} = \bar{y}_B(\xi). \tag{5.107}$$

Here  $\bar{y}'_S$  and  $\bar{y}'_B$  denote the derivatives of  $\bar{y}_S$  and  $\bar{y}_B$  with respect to  $\xi$ .  $\zeta$  has

been introduced since the tangential velocity, and hence the shear traction, may change sign.

The MJ-transformations achieve a similar goal, as the shallow ice transformations did before: a small parameter,  $\varepsilon$ , is introduced which can be related to the other generally large parameter of the problem,  $\bar{G}$  or  $\bar{G}_{MJ}$ . Such a relation must emerge from an ordering argument in Equations (5.105). To this end, two cases will be distinguished, namely (i)  $\gamma \gg \mathcal{O}(\varepsilon) \sim \mathcal{O}(1)$ , steep glacier, and (ii)  $\gamma = \mathcal{O}(\varepsilon)$ , or  $\gamma = 0$ , ice sheet.

*Case (i):* Lowest-order transverse shear-stress gradients, and therefore shear stresses, are  $\mathcal{O}(1)$  and will balance gravity, while longitudinal stress gradients are small. This means that the last two terms on the left-hand side of Equation (5.105)<sub>1</sub> will balance each other. Since, moreover, the transverse gradients of the longitudinal velocity  $\partial U / \partial \bar{y}$  are essentially given by the shear stresses, the dominant term on the left-hand side of Equation (5.105)<sub>5</sub> will have to balance the right-hand side, suggesting that

$$\bar{G} = \mathcal{O}(1) \Rightarrow \bar{G} = 1, \quad \bar{G}_{MJ} = \mathcal{O}(\varepsilon^{-1}) \quad (5.108)$$

Substituting this value for  $\bar{G}$  into Equations (5.105) yields a set of equations which contains only one single small parameter, namely  $\varepsilon$ . This set is exactly the same as Equations (5.33) with  $\mu$  replaced by  $\varepsilon$ . Similarly, Equations (5.106) and (5.107) are formally identical with the corresponding boundary conditions of the shallow ice approximation, Equations (5.34) and (5.35). Hence, with this identification, *perturbation solutions based on the MJ-transformation must yield identical results with those based on the shallow ice approximation*.

*Case (ii):* When the inclination angle  $\gamma$  is small, either zero (horizontal longitudinal coordinate) or of order  $\varepsilon$ , it follows from Equation (5.105)<sub>1</sub> that the transverse shear-stress gradients must balance the longitudinal pressure gradients ( $\sigma_x$  is composed of pressure and  $\sigma'_x$ , the normal stress deviator in the  $\bar{x}$ -direction). An order of magnitude for  $\tau$  must be found to balance these two terms. This can be obtained from the last of Equations (5.105). Since its left-hand side is  $\mathcal{O}(1)$  and because  $\mathfrak{F}(\tau'_{II}) = \mathcal{O}(1)$  for a finite viscosity law but  $\mathcal{O}(\tau^{n-1})$  for Glen's flow law, we must have  $\bar{G}t^n = \mathcal{O}(1) \rightarrow \tau = \mathcal{O}(\bar{G}^{-1/n})$ . Using this order-of-magnitude relationship in Equations (5.105)<sub>1</sub> yields  $(\bar{G})^{-1/n} = \varepsilon$ , or\*

$$\bar{G} = \varepsilon^{-n}, \quad \bar{G}_{MJ} = \varepsilon^{-(n+1)}, \quad (5.109)$$

a relationship which is valid for all  $n \geq 1$ . This is the scaling for small or zero

\*More precisely,  $\bar{G} = \varepsilon^{-n}$  for a power law with exponent  $n$  and  $\bar{G} = \varepsilon^{-1}$  for a finite viscosity law.

bed inclinations. Upon substitution into (5.105) it is seen that  $\tau$  must be  $\mathcal{O}(\varepsilon)$ , whereas  $\sigma_x - \sigma_y$  is  $\mathcal{O}(\varepsilon^{n+1})$ , and  $(\sigma_x + \sigma_y) \sim \bar{p}$ , the pressure, is  $\mathcal{O}(1)$ . Hence, the following chain of inequalities must hold:  $|\sigma_x - \sigma_y| \ll |\tau| \ll |\sigma_x + \sigma_y|$ .

The above calculations do not resemble any similarity with the non-dimensionalization of Morland and Johnson [23, 24], and indeed these authors proceed along much different and probably less transparent lines. It can, however, be shown (calculations are long) that there is a one-to-one correspondence between the above scalings (5.108) and (5.109) and theirs. Below, solution procedures for the two cases will be discussed.

(a) *Finite-bed inclination [case (i)]*

We now set  $\bar{\mathbb{G}} = 1$  in Equations (5.105) and seek a perturbation solution of the boundary-value problem (5.105)–(5.107) of the form  $\sigma = \sum_{j=0}^{\infty} \varepsilon^j \sigma^{(j)}$  etc., but shall restrict attention to the lowest-order solutions only. Incidentally, this case has already been treated in Section 4, but the analysis is pursued here because Morland and Johnson make the accumulation rate depend on the geographical elevation and further presume the friction coefficient  $\mathbb{C}$  to depend on the overburden depth rather than position.

The momentum Equations (5.105)<sub>1,2</sub> and (5.105)<sub>4</sub> can be integrated to the lowest order, when the boundary conditions (5.106) are invoked. This yields

$$\tau^{(0)} = \sin \gamma (\bar{y}_S - \bar{y}), \quad \sigma_x^{(0)} = \sigma_y^{(0)} = -\cos \gamma (\bar{y}_S - \bar{y}) - \bar{p}^{\text{atm}}, \quad (5.110)$$

in agreement with Equations (5.40). Since  $\tau^{(0)}$  has always the sign of  $\gamma$ , the sliding velocity at the base does not change sign and *there is no ice divide*. We shall restrict attention to  $\gamma > 0$  and may therefore delete the variable  $\zeta$  in the sliding law (5.106)<sub>2</sub>. Substituting the results (5.110) into the fifth of Equations (5.105) yields to lowest order

$$\begin{aligned} \frac{\partial U^{(0)}}{\partial \bar{y}} &= 2\mathfrak{F}(\sin^2 \gamma (\bar{y}_S - \bar{y})^2) \sin \gamma (\bar{y}_S - \bar{y}), \\ &= g(\sin \gamma (\bar{y}_S - \bar{y})). \end{aligned} \quad (5.111)$$

We shall also use the definitions

$$g_1(t) = \int_0^t g(\xi) d\xi, \quad g_2(t) = \int_0^t g_1(\xi) d\xi = \int_0^t (t - \xi) g(\xi) d\xi. \quad (5.112)$$

Integrating Equation (5.111), subject to the basal boundary conditions, would result in Equation (5.41), but Morland and Johnson write their result in the form of function  $g(\cdot)$  and thus obtain

$$U^{(0)} = \mathbb{C} \sin^m \gamma \bar{D}^m + \operatorname{cosec} \gamma [g_1(\sin \gamma \bar{D}) - g_1(\sin \gamma (\bar{y}_S - \bar{y}))], \quad (5.113)$$

where  $\bar{D} = (\bar{y} - \bar{y}_B)$ . The next step in the determination of the surface profile is to use the equation

$$\frac{d}{d\xi} \int_{\bar{y}_B}^{\bar{y}_S} U(\xi, \bar{y}) d\bar{y} = \mathfrak{A}(z), \quad (5.114)$$

which can be obtained from the kinematic surface Equation (5.106)<sub>3</sub> and the continuity Equation (5.105)<sub>3</sub> in a similar way Equation (5.81) was derived. To the lowest order,  $U$  is replaced by  $U^{(0)}$  and  $z$  by  $\varepsilon^{-1}\xi \sin \gamma$ , see Equation (5.106)<sub>3</sub>, so using (5.113) in Equation (5.114) yields

$$\begin{aligned} \frac{d}{d\xi} & \left\{ \mathbb{C} \sin^m \gamma \bar{D}^{m+1} + \operatorname{cosec} \gamma \bar{D} g_1(\sin \gamma \bar{D}) - \operatorname{cosec}^2 \gamma g_2(\sin \gamma \bar{D}) \right\} \\ &= \left\{ \mathbb{C}(m+1) \sin^m \gamma \bar{D}^m \left[ 1 + \frac{\mathbb{C}'}{\mathbb{C}(m+1)} \bar{D} \right] + \bar{D} g(\sin \gamma \bar{D}) \right\} \frac{d\bar{D}}{d\xi} \\ &= \mathfrak{A} \left( \frac{1}{\varepsilon} \xi \sin \gamma \right) = \mathfrak{A}^*(\xi), \end{aligned} \quad (5.115)$$

subject to the end conditions

$$\bar{D}(\xi_M^-) = 0 \quad \text{and} \quad \bar{D}(\xi_M^+) = 0, \quad (5.116)$$

where  $\xi_M^\pm$  denotes the margin positions. Equation (5.115) is a first-order differential equation for the ice thickness  $\bar{D}$  as a function of position. One end condition suffices for the determination of its solution. The second condition (5.116), therefore, determines the range  $(\xi_M^+ - \xi_M^-)$ , but this is pre-determined by the zero mass-flux condition

$$\int_{\xi_M^-}^{\xi_M^+} \mathfrak{A}^*(\xi) d\xi = 0. \quad (5.117)$$

This result warrants further remarks. First, it imposes restrictions on the friction function  $\mathbb{C}(\bar{D})$ , since Equation (5.115) must have perfect differential form; explicitly, as  $\bar{D} \rightarrow 0$ ,  $\mathbb{C} \sim \mathbb{C}_M^* \bar{D}^{-\beta}$  with  $\beta < (m+1)$ , but the requirement of finite snout velocity implies the stronger condition  $\beta \leq m$ . Second, recall that accumulation was assumed to depend on the height of the free surface above a horizontal reference plane. Equation (5.115) indicates that to the lowest-order, the accumulation rate depends on the longitudinal coordinate  $\xi$  only. In other words, the true accumulation is replaced by that at the mean bed. The function  $\mathfrak{A}^*(\xi)$  is therefore known independently of the solution of the differential equation. *The initial value problem (5.115), (5.116) is the same as the lowest-order problem of Section 4, and so must be the implications.*

Subsequent analysis then parallels that of Section 4. Morland and Johnson presume  $\mathbb{C}(\bar{D})$  to be a function of the local glacier thickness and

require regular snout behavior. They write

$$\begin{aligned}\bar{D} &= k_d^{(1)} |\xi - \xi_M^\pm|, \\ \mathbb{C} = \mathbb{C}_M^* \bar{D}^{-\beta} &= \mathbb{C}_M^* (k_d^{(1)})^{-\beta} |\xi - \xi_M^\pm|^{-\beta} = \mathbb{C}_M |\xi - \xi_M^\pm|^{-\beta},\end{aligned}\quad \left. \right\} \quad (5.118)$$

determine  $\beta$  and  $k_d^{(1)}$ , appropriate for regular margin behavior and obtain  $\beta = m$ , and

$$k_d^{(1)} = \frac{\mathfrak{A}^*(\xi_M) \operatorname{sgn}(\xi - \xi_M^\pm)}{\mathbb{C}_M^* \sin^m \gamma(m+1)} = \left\{ \frac{\mathfrak{A}(\xi_M^\pm \operatorname{sgn}(\xi - \xi_M^\pm))}{\mathbb{C}_M \sin^m \gamma(m+1)} \right\}^{1/(m+1)}, \quad (5.119)$$

in agreement with Equation (5.88). The leading order analysis now proceeds exactly as indicated in Section 4. For this reason, no further details are provided and the reader is referred to that analysis.

(b) *Small-bed inclination [case (ii)]*

In this case,  $\bar{\mathbb{G}}$  and  $\varepsilon$  are related by Equation (5.109), implying that Equations (5.105)<sub>4,5</sub> become

$$\varepsilon^{(n+1)} \frac{\partial U}{\partial \xi} = \frac{1}{2} \mathfrak{F}(\tau'_{II})(\sigma_x - \sigma_y), \quad \varepsilon^n \frac{\partial U}{\partial \bar{y}} + \varepsilon^{n+2} \frac{\partial V}{\partial \xi} = 2 \mathfrak{F}(\tau'_{II})\tau, \quad (5.120)$$

where  $n = 1$  for the finite viscosity law. The first of these implies to lead order  $\sigma_x^{(0)} = \sigma_y^{(0)}$ , and Equation (5.105)<sub>2</sub> together with (5.106)<sub>1</sub>, yields

$$\sigma_x^{(0)} = \sigma_y^{(0)} = -\cos \gamma (\bar{y}_S - \bar{y}) - \bar{p}^{\text{atm}}, \quad (5.121)$$

which agrees with the second of Equations (5.110), but the shear stress now follows from Equation (5.105)<sub>1</sub> by considering all three terms, namely

$$\frac{\partial \tau^{(0)}}{\partial \bar{y}} = \varepsilon \cos \gamma \frac{d\bar{y}_S}{d\xi} - \sin \gamma. \quad (5.122)$$

We now write  $\gamma = \varepsilon \gamma_0$  with  $\gamma_0 = \mathcal{O}(1)$  and approximate  $\cos \gamma \simeq 1$ ,  $\sin \gamma \simeq \varepsilon \gamma_0$ . Integration of Equation (5.122) subject to the surface-boundary condition (5.106)<sub>2</sub>,  $\tau^{(0)} = 0$ , then gives

$$\tau^{(0)}(\bar{y}) = \zeta^2 \varepsilon \left( \gamma_0 - \frac{d\bar{y}_S}{d\xi} \right) (\bar{y}_S - \bar{y}), \quad \zeta = \operatorname{sgn} \left( \gamma_0 - \frac{d\bar{y}_S}{d\xi} \right). \quad (5.123)$$

Thus, to lowest order the famous shear-stress formula is obtained, according to which  $\tau^{(0)} = \bar{D}\alpha$ , where  $\alpha$  is the inclination of the free surface relative to the horizontal plane. Equation (5.123) further corroborates our earlier statement that  $\tau$  is  $\mathcal{O}(\varepsilon)$ , and it indicates that  $\tau^{(0)}$  may change sign at position  $\xi = \xi_d$  where

$$\frac{d\bar{y}_S}{d\xi} = \gamma_0. \quad (5.124)$$

Clearly,  $U_b^{(0)} = 0$  at the base at  $\xi = \xi_d$ , since  $\tau^{(0)}$  vanishes, and it will be shown later on that  $U^{(0)} \equiv 0$  at  $\xi = \xi_d$  which is therefore an *ice divide* – there is no

flow across  $\xi = \xi_d$ . Equation (5.124) physically expresses that ice divides are where the surface is horizontal. When Equation (5.123) is substituted into the second of Equation (5.120), one obtains,

$$\begin{aligned} \frac{\partial U^{(0)}}{\partial \bar{y}} &= \varepsilon^{-n} 2 \mathfrak{F} \left[ \varepsilon^2 \left( \gamma_0 - \frac{d\bar{y}_S}{d\xi} \right)^2 (\bar{y}_S - \bar{y})^2 \right] \varepsilon \zeta^2 \left( \gamma_0 - \frac{d\bar{y}_S}{d\xi} \right) (\bar{y}_S - \bar{y}) \\ &= \varepsilon^{-n} \zeta g \left[ \zeta \varepsilon \left( \gamma_0 - \frac{d\bar{y}_S}{d\xi} \right) (\bar{y}_S - \bar{y}) \right] \\ &= \zeta \hat{g} \left[ \zeta \left( \gamma_0 - \frac{d\bar{y}_S}{d\xi} \right) (\bar{y}_S - \bar{y}) \right]. \end{aligned} \quad (5.125)$$

It should be noticed here that although the small parameter  $\varepsilon$  occurs explicitly in this formula, the right-hand side is of  $\mathcal{O}(1)$ , since for Glen's power law  $g \sim \mathcal{O}(\varepsilon^n)$  and for a finite viscosity creep response  $g \sim \mathcal{O}(\varepsilon)$ , but the exponent must also be set equal to  $n = 1$ . Integrating (5.125), subject to the basal boundary condition (5.107), yields

$$\begin{aligned} U^{(0)} &= \zeta \mathbb{C} [\zeta \varepsilon (\gamma_0 - \bar{y}'_S) (\bar{y}_S - \bar{y}_B)]^m + \\ &\quad + \zeta \frac{\hat{g}_1 [(\gamma_0 - \bar{y}'_S) (\bar{y}_S - \bar{y}_B)] - \hat{g}_1 [(\gamma_0 - \bar{y}'_S) (\bar{y}_S - \bar{y})]}{|\gamma_0 - \bar{y}'_S|}, \end{aligned} \quad (5.126)$$

where  $\hat{g}_1$  (and later on  $\hat{g}_2$ ) are defined in a similar way to which  $g_i$  were in Equation (5.112). Now since  $\hat{g}(t) > 0$  for  $t > 0$  we have  $\hat{g}_1 > 0$  for  $t > 0$ . Furthermore,  $\hat{g}_1(0) = 0$  so that  $U^{(0)} = 0$  at  $\xi = \xi_d(\gamma_0 = \bar{y})$  and  $U^{(0)} \gtrless 0$  for  $(\gamma_0 - \bar{y}'_S) \gtrless 0$ . This confirms that  $\xi = \xi_d$  is an ice divide.

Finally, substituting expression (5.126) into Equation (5.114) with  $\mathfrak{A}(z) = \mathfrak{A}(\bar{y}_S - \gamma_0 \xi)$  gives the differential equation

$$\begin{aligned} \frac{d}{d\xi} \{ \zeta \mathbb{C} [\zeta (\gamma_0 - \bar{y}'_S) (\bar{y}_S - \bar{y}_B)]^m (\bar{y}_S - \bar{y}_B) + \\ + \zeta (\bar{y}_S - \bar{y}_B)^2 \Omega [\zeta (\gamma_0 - \bar{y}'_S) (\bar{y}_S - \bar{y}_B)] \} = \mathfrak{A}(\bar{y}_S - \gamma_0 \xi), \end{aligned} \quad (5.127)$$

where

$$\Omega(t) = \frac{\hat{g}_1(t)}{t} - \frac{\hat{g}_2(t)}{t^2} \sim \Omega_0 t^n, \quad \text{as } t \rightarrow 0. \quad (5.128)$$

To evaluate the function  $\Omega$  we go back to Equation (5.125) where  $\hat{g}(t)$  is defined. Accordingly,  $\Omega$  depends on the material response function  $\mathfrak{F}$ . Morland and Johnson use Glen's flow law and the polynomial representation of Colbeck and Evans [8] and write as a constitutive equation relating stress deviator  $\mathbf{t}'$  and stretching tensor  $\mathbf{D}$

$$\hat{\mathbf{D}} = \omega(\hat{\mathbf{t}}_{II}') \hat{\mathbf{t}}, \quad \hat{\mathbf{D}} = \frac{\mathbf{D}}{\mathcal{A}(T)d_0}, \quad \hat{\mathbf{t}}' = \frac{\mathbf{t}'}{\sigma_0}. \quad (5.129)$$

$\mathcal{A}(T)$  is a temperature-dependent rate factor,  $\sigma_0$  a reference stress and  $d_0$  reference stretching chosen as

$$\sigma_0 = 10^5 \text{ Pa}, \quad d_0 = 3 \times 10^7 \text{ s}^{-1}, \quad \mathcal{A} = 0.1 \quad (5.130)$$

appropriate for temperatures in the range 250 K to 273.15 K. Morland and Johnson's material response functions  $\omega$  corresponds to the function  $\mathfrak{F}$  in our non-dimensionalization and they choose

(i) for Glen's flow law

$$\omega(\hat{t}'_{II}) = 1.5 k (3\hat{t}'_{II})^{(n-1)/2}, \quad k = 0.17, n = 1.3 \rightarrow 7, \quad (5.131)$$

$n$  depending on the stress range over which the response is approximated by this law,

(ii) for the polynomial representation of Colbeck and Evans [8]

$$\begin{aligned} \omega(\hat{t}'_{II}) &= 1.5(C_0 + 3C_1\hat{t}'_{II} + 9C_2\hat{t}'_{II}^2), \\ C_0 &= 0.21, \quad C_1 = 0.14, \quad C_2 = 0.055. \end{aligned} \quad (5.132)$$

There is a one-to one correspondence between  $\omega$  and  $\mathfrak{F}$ , which is rather lengthy to determine, because the non-dimensionalizations used in this book and those of Morland and Johnson are different. The relation is

$$\left. \begin{aligned} \omega\left(\frac{\tau'_{II}}{s^2}\right) &= s\delta \frac{\bar{\mathfrak{G}}}{\varepsilon} \mathfrak{F}(\tau'_{II}) \\ s &= \frac{\sigma_0}{\rho g D_0}, \quad \delta = \frac{a_m}{\mathcal{A} d_0 D} \end{aligned} \right\} \quad (5.133)$$

with

The dimensionless parameters  $s$  and  $\delta$  involve the scalings (5.130) and  $D$  and  $a_m$  which are a representative glacier depth and a characteristic accumulation rate used in our scalings, see Chapter 3, pages 148–154.

Using the relations (5.129)–(5.133) in (5.125) it can be demonstrated that

$$\hat{g}(t) = \begin{cases} 3^{(n+1)/2} k t^n, & (\text{Glen}) \\ 3C_0 t, & (\text{Colbeck and Evans}) \end{cases} \quad (5.134)$$

and whence upon integration

$$\Omega(t) = \begin{cases} \frac{3^{(n+1)/2} k}{n+2} t^{n+2}, & (\text{Glen}) \\ \frac{C_0}{2} t^2, & (\text{Colbeck and Evans}) \end{cases} \quad (5.135)$$

The differential Equation (5.127) is second order in  $\bar{y}_S$ , but unlike the corresponding equation with a finite bed inclination it cannot be expressed simply as an equation for the thickness  $\bar{D} = (\bar{y}_S - \bar{y}_B)$  for  $(\gamma_0 - \bar{y}'_S)$  enters

the equation rather than  $(\bar{y}'_B - \bar{y}'_S)$  which would be necessary for an equation in glacier thickness alone. So the bed profile is not simply superimposed on a corresponding flat-bed surface profile. Incidentally, Equation (5.127) exhibits similar features to those already discussed for the finite bed inclination case. For instance, to ensure zero mass flux,  $\int_{\xi_M}^{\xi_M} \mathfrak{A} d\xi = 0$ , the sliding coefficient  $C$ , assumed to depend on  $\bar{D}$ , must behave as  $C \sim C_M^* \bar{D}^\phi$  with  $0 \leq \phi \leq m+1$  as  $\bar{D} \rightarrow 0$  and, in order to guarantee a finite margin velocity, one must have  $0 \leq \phi \leq m$ . The differential equation is again singular at the margins, unless  $C$  has the proper behavior there. To avoid such a singularity, since  $\Omega(0) = 0$ ,  $C$  must have the proper behavior to achieve this. Results will depend on the margin behavior of the accumulation function. We shall restrict considerations to finite non-zero  $\mathfrak{A}_M$ . It then follows from Equation (5.127) that  $C = C_M^* \bar{D}^{-m}$ , as  $\bar{D} \rightarrow 0$ , where  $C_M^*$ ,  $\gamma_0$ ,  $\bar{y}'_S^m$  and  $\bar{y}'_B^M$  satisfy the relation

$$\frac{d}{d\xi} \{ \zeta C_M^* (\zeta (\gamma_0 - \bar{y}'_S^M)^m (\bar{y}_S - \bar{y}_B)) \} = \mathfrak{A}_M, \quad \text{as } \bar{D} \rightarrow 0, \quad (5.136)$$

or

$$\zeta C_M^* (\zeta (\gamma_0 - \bar{y}'_S^M))^m (\bar{y}'_S - \bar{y}'_B^M) = \mathfrak{A}_M, \quad \text{as } \bar{D} \rightarrow 0.$$

The term involving  $\Omega$  does not contribute to this relation, since it vanishes like  $\bar{D}^{n+2}$  as  $\bar{D} \rightarrow 0$ . Equation (5.136) is very important, as it relates margin accumulation with the slope  $\bar{y}'_S^M$  and with  $C_M^*$ ,  $\gamma_0$  and  $\bar{y}'_B^M$ . A horizontal margin surface  $\gamma_0 = \bar{y}'_S^M$ , or a surface tangential to the bed,  $\bar{y}'_S^M = \bar{y}'_B^M$ , imply  $\mathfrak{A}_M = 0$ , and vanishing  $\mathfrak{A}_M$  implies one of these situations. In general

$$\mathfrak{A}_M \geq 0 \Leftrightarrow (\gamma_0 - \bar{y}'_S^M)(\bar{y}'_S^M - \bar{y}'_B^M) \geq 0$$

and  $\bar{y}'_S^M - \bar{y}'_B^M \geq 0$  at the left and right margin, respectively.

Equation (5.136) attains a physically more transparent form if the margin velocity is calculated. It follows from Equation (5.126), since  $\hat{g}_1(t)/t$  vanishes as  $t \rightarrow 0$ , that

$$U^{(0)}(\xi_M) = U_M^{(0)} = \zeta C_M^* [\zeta (\gamma_0 - \bar{y}'_S^M)]^m \quad (5.137)$$

Thus,

$$U_M^{(0)}(\bar{y}'_S^M - \bar{y}'_B^M) = \mathfrak{A}_M. \quad (5.138)$$

Accordingly, a *vanishing margin velocity or a surface tangential to the bed* imply  $\mathfrak{A}_M = 0$ , and a horizontal surface implies a vanishing margin velocity.

The second-order differential Equation (5.127) must be solved, subject to two conditions at one margin, namely by prescribing  $\bar{y}'_S^M = \bar{y}'_B^M$  and  $\bar{y}'_S^M$ . A value for the latter follows by measuring the margin accumulation, velocity, and bottom slope, yet Equation (5.138) has only a solution when  $U_M^{(0)} \neq 0$ : For  $U_M^{(0)} = 0$ , Equation (5.137) implies either  $C_M^* = 0$  or  $\gamma_0 = \bar{y}'_S^M$ . In this latter case,  $C_M^*$  cannot be determined by snout observations. We conclude that in order to be able to prescribe the initial data for the integration of the

differential equation (5.127), which lead to a finite margin slope, the sliding coefficient must be singular as  $C = C_M^* \bar{D}^{-m}$  as  $\bar{D} \rightarrow 0$  and the margin velocities must be non-vanishing. Under these restrictive conditions the surface slope at the margin follows from Equation (5.138) by measuring  $\mathfrak{A}_M$  and  $U_M^{(0)}$  and the coefficient  $C_M^*$  is determined from Equation (5.137). The slope  $\bar{y}'_S^M$  and the coefficient  $C_M^*$  are thereby uniquely determined. For positive  $U_M^{(0)}$  and positive  $\mathfrak{A}_M$ ,  $\zeta > 0$  and  $\gamma_0 > \bar{y}'_S^M$ ,  $\bar{y}'_S^M > \bar{y}'_B^M$ . Hence  $\gamma_0 > \bar{y}'_S^M > \bar{y}'_B^M$ ; that is, the ice slopes below the horizontal from either margin. Other possibilities can be analysed in a similar fashion. The essential property is that these initial conditions are obtained in *unique* fashion when  $U_M^{(0)}$  and  $\mathfrak{A}_M$  are regarded as input parameters in Equations (5.137) and (5.138). Morland and Johnson do not regard  $U^{(0)}$  as the input but take  $C_M^*$  as given and disregard relation (5.137). They then solve Equation (5.136) for  $\bar{y}'_S^M$  for a linear sliding law ( $m = 1$ ) and demonstrate that in the above-mentioned situation of positive  $U_M^{(0)}$  and positive  $\mathfrak{A}_M$  there are two solutions for  $\bar{y}'_S^M$ . They are unable to rule out one of these solutions as being unphysical. Our analysis shows that by regarding  $U_M^{(0)}$  as the input parameter rather than  $C_M^*$ , unique initial conditions are obtained.

The above considerations hinge on the assumption that  $U^{(0)} \neq 0$  at the margin. When  $U^{(0)} = 0$  and  $C = C_M^* \bar{D}^{-m}$  as  $\bar{D} \rightarrow 0$  then the margin slopes are horizontal, but there is no possibility of determining a numerical value for  $C_M^*$ . Perhaps considering next-order equations will provide a means of determining  $C_M^*$ . At present we discard this case, as it is the exception, anyhow.

It remains to consider the behavior at the ice divide  $\xi = \xi_d$  where  $\gamma_0 = \bar{y}'_S^{(0)}$  and  $\bar{y}_S = \bar{y}_S^d$ . With

$$\left. \begin{aligned} \mathfrak{A}(\bar{y}_S - \gamma \cdot \xi) &\sim \mathfrak{A}_d(1 + \mathfrak{A}_1 \bar{z}) + \mathcal{O}(\bar{z}^2), \\ \bar{z} &= \bar{y}_S^d - \bar{y}_S - \gamma_0(\xi_d - \xi), \end{aligned} \right\} \quad (5.139)$$

the essential behavior of the differential Equation (5.127) as  $\bar{y}'_S \rightarrow \gamma_0$  and  $\bar{z} \rightarrow 0$  can be written as

$$\begin{aligned} \frac{d\bar{z}}{d\xi} \frac{d}{d\bar{z}} &\left\{ \zeta C_d \bar{D}^{m+1} [\zeta(\gamma_0 - \bar{y}'_S)]^m + \right. \\ &\left. + \zeta \bar{D}^{n+2} \Omega_0 [\zeta(\gamma_0 - \bar{y}'_S)]^n \right\} = \mathfrak{A}_d(1 + \mathfrak{A}_1 \bar{z}) + \mathcal{O}(\bar{z}^2), \end{aligned} \quad (5.140)$$

or

$$\begin{aligned} \zeta(\gamma_0 - \bar{y}'_S) \frac{d}{d\bar{z}} &[\zeta(\gamma_0 - \bar{y}'_S)]^l \\ &= \frac{l}{l+1} \frac{d}{d\bar{z}} [\zeta(\gamma_0 - \bar{y}'_S)]^{l+1} = c_l \mathfrak{A}_d(1 + \mathfrak{A}_1 \bar{z}) + \mathcal{O}(\bar{z}^2), \end{aligned} \quad (5.141)$$

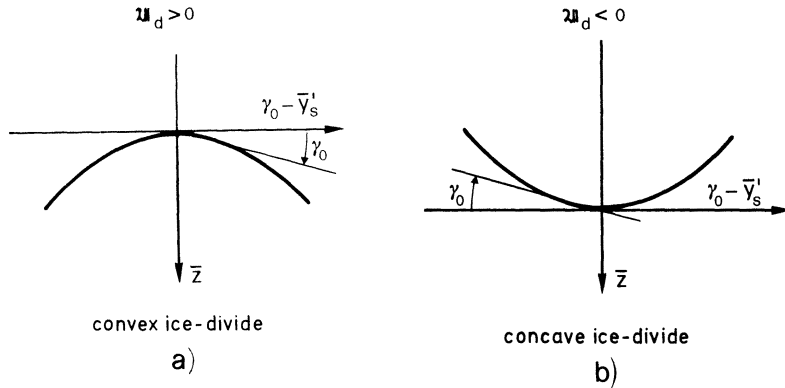


FIG. 5.16. A local form of surface profile for a convex and concave ice divide.

where  $l = \min(m, n)$  and

$$C_l^{-1} = \begin{cases} \mathbb{C}_d \bar{D}^{m+1} > 0, & l = m, \\ \bar{D}^{m+1} \Omega_0 > 0, & l = n. \end{cases} \quad (5.142)$$

Integrating (5.138) subject to the condition  $\bar{y}'_S = \gamma_0$  at  $\bar{z} = 0$  reveals

$$\zeta(\gamma_0 - \bar{y}'_S) = \left\{ \frac{c_l(l+1)\mathfrak{A}_d \bar{z}}{l} \right\}^{1/(l+1)} \left\{ 1 + \frac{\mathfrak{A}_1}{2(l+1)} \bar{z} + \mathcal{O}(\bar{z}^2) \right\}, \quad (5.143)$$

The term on the left-hand side is always positive; so must be the first term in curly brackets on the right-hand side. Thus  $\mathfrak{A}_d \bar{z} > 0$  implying that there must be an accumulation at a convex ice divide and ablation at a concave ice divide, see Figure 5.16.

### (c) Illustrations

Calculations of steady-state surface geometry have been performed by Morland and Johnson for small bed inclinations. In these, the dependence of the surface profile on the accumulation function, the basal friction law, and the material creep response of ice were tested. It was found that direction of integration is crucial in the determination of the desired surface geometry. We first discuss results obtained with a flat horizontal bottom. In this case, integration is commenced at the margin with the initial conditions

$$\bar{y}_S = 0, \quad \frac{d\bar{y}_S}{d\xi} = \left( \frac{|\mathfrak{A}_M|}{\mathbb{C}_M^*} \right)^{1/(m+1)}, \quad \tilde{\zeta} = \xi_M - \xi,$$

see Equation (5.136), which is only meaningful for  $\mathfrak{A}_M < 0$ . Integration is

then carried out into the glacier until  $\bar{y}'_S = 0$ , which defines the ice divide  $\xi = \xi_d$ . For the details of the integration procedure, we refer the reader to Morland and Johnson [23].

(i) *Flat horizontal bed.* For a comparison between laws with different exponents  $n$ , all results are expressed in terms of the same dimensionless horizontal coordinate  $\xi^*$  belonging to  $n = 1$ . Hence  $\bar{x} = \varepsilon^{-1}\xi = \varepsilon^{*-1}\xi^*$ , or

$$\xi^* = \frac{\varepsilon^*}{\varepsilon} \xi = \theta^{[(n-1)/2(n+1)]} \xi, \quad (5.144)$$

where  $\theta$  given below. Morland and Johnson base their calculations on the values

$$\sigma_0 = 10^5 \text{ Pa}, \quad d_S = 3.10^7 \text{ s}, \quad \mathcal{A} = 0.1, \quad a_m = 3.10^{-9} \text{ m s}^{-1},$$

and then obtain, since in their scaling  $\varepsilon = \delta(\delta/s)^{-[n/(n+1)]}$

$$\frac{\varepsilon^*}{\varepsilon} = \frac{(\delta/s)^{-1/2}}{(\delta/s)^{-(n/(n+1))}} = \theta^{(n-1)/2(n+1)}, \quad \theta = \frac{s}{\delta} = \frac{\rho g a_m}{\mathcal{A} d_0 \sigma_0} = 0.09. \quad (5.145)$$

The real magnitude of  $\varepsilon$  follows from values of  $\delta$  as defined in (5.130).

In a first set of calculations tests were conducted to see whether the simple theoretical models of Section 4a would in any way reasonably predict steady-state profiles based on this more general theory. The following representations for the accumulation function and for the sliding law were tested:

$$\left. \begin{aligned} \mathfrak{A}(\bar{y}_S) &= -Q_0 + (1 + Q_0)\bar{y}_S, \\ \bar{\Lambda}(\bar{y}_S) &= \lambda_0 \bar{y}_S, \end{aligned} \right\} \quad (5.146a)$$

or

$$\left. \begin{aligned} \mathfrak{A}(\bar{y}_S) &= -Q_0 + (1 + Q_0)(1 - \exp(-s\bar{y}_S)), \\ \bar{\Lambda}(\bar{y}_S) &= \frac{\lambda_0}{r}(1 - \exp(-r\bar{y}_S)), \end{aligned} \right\} \quad (5.146b)$$

where

$$\mathbb{C} = [\theta^{[(n-1)(m+1)/2m(n+1)]} \bar{\Lambda}]^{-m} \rightarrow \mathbb{C}^* = \lambda_0^{-m} \theta^{[(n-1)(m+1)/2(n+1)]} \quad (5.146c)$$

Both laws (5.146a, b) correspond to a finite margin slope, but the exponential forms with large  $s$  and  $r$  imply small gradients  $\mathfrak{A}'$  and  $\Lambda'$  for  $\bar{y}_S$  of order unity. To compare the profiles based on Equations (5.146) with those of Nye, Equation (5.74a), this latter equation is written in dimensionless form as

$$\left( \frac{\bar{y}_S^d}{\bar{y}_S^d} \right)^{(2m+1)/m} + \left( \frac{\xi}{\xi_M} \right)^{(m+1)/m} = 1. \quad (5.147a)$$

The thickness  $\bar{y}_S^d$  at the ice divide and the semi-length  $\xi_M$  are easily obtained

from the dimensionless form of the second Equation (5.74) as

$$\bar{y}_S^{(2m+1)/m} = \frac{2m+1}{m+1} \frac{1}{C(1)^{1/m}} \xi_M^{(m+1)/m}, \quad (5.147b)$$

$C(1) = C_M^*$  being a constant sliding coefficient\* corresponding to the coefficient (5.146c) when  $\bar{y}_S = 1$ . Nye also sets  $m = \frac{1}{2}(n+1)$ . By choosing  $\bar{y}_S^d$  in Equations (5.147a) as the central height determined by the preceding solution, Equations (5.147) provide a means of comparing the steady profiles and  $\xi_M$  of Equation (5.147b) with those of the leading order solutions of the more rigorous theory. For this comparison, recall that Nye's solution is based on a constant accumulation function and constant sliding coefficient; the exponential representations (5.146) with large  $s$  and  $r$  thus correspond better with Nye's constant  $\mathfrak{A}$  and  $C$  approximation than the linear functions (5.146a). Figure 5.17 summarizes some computational results. A case  $s = r = 5$  is shown together with an example using the linear and exponential forms both with  $\lambda_0 = Q_0 = 1$ , comparing Nye's profiles given by Equations (5.147) with the corresponding complete small-slope solution. In all the demonstrated cases the semi-length of the Nye-solution is much smaller than the corresponding length of the complete solution. This proves that the constitutive response term  $\Omega$  in (5.127) (neglected in the Nye-solution)

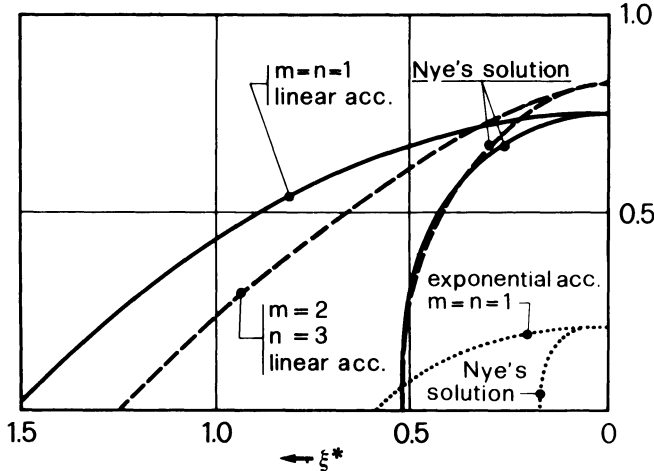


FIG. 5.17. Comparison of slope profile for Glen's law with Nye's profile for  $\lambda_0 = Q_0 = 1$ ; from [23]. . . . .  $m = 1, n = 1$ , and exponential  $\lambda$  and  $Q$ ,  $s = r = 5$ ; —  $m = 1, n = 1$ , and linear  $\lambda$  and  $Q$ ; - - -  $m = 2, n = 3$ , and linear  $\lambda$  and  $Q$ .

\*This choice of  $C(1)$  is somewhat arbitrary. Except for the margin region, values for  $C$  do not vary appreciably, so that a value for  $C$  representative for the middle portion of the ice sheet is regarded as representative.

cannot be ignored, but the examples in Figure 5.17 also illustrate the entirely different profiles obtained with the further assumption of constant (or exponential)  $\mathfrak{U}$  and  $C$ .

Having demonstrated the importance of material response, Morland and Johnson proceed to show how the choice of constitutive law affects the solution. They compare results obtained with Glen's power law (5.128) with  $n = 1$  and  $n = 3$  and the Colbeck and Evans polynomial law (5.129). They vary the linear laws (5.146a) with  $\lambda_0, Q_0$  having values between 1 and 10, and find that semi-lengths and heights of ice divides obtained with Glen's power law and Colbeck and Evans's polynomial law differ by 22% at most, with the differences being very small for small values of  $\lambda_0$ . Figure 5.18 displays the relative differences in semi-lengths  $(\Delta \xi_M^*/\xi_M)_{\max}$ , and in heights of ice divides,  $(\Delta y_S^d/y_S^d)_{\max}$ , in percent obtained with the three different mentioned constitutive laws. It can be seen that these differences grow with growing  $\lambda_0$ , and the greatest differences arise in  $\xi_M^*$ . This is plausible for, as one would expect, with increasing bottom friction the constitutive term in Equation (5.127) becomes more influential, so that the greatest differences occur for the largest values of  $\lambda_0$ . In comparison to this, the variations of  $Q_0$  have less influence. Figure 5.18 summarizes Morland and Johnson's results. In view of this, subsequent illustrations will be based on the polynomial law (5.129), which eliminates the parameter  $n$ .

Next we investigate how sensitive surface profiles react to variations in accumulation rate and sliding properties. The linear laws (5.143a) will be adopted, and  $(\lambda_0, Q_0, m)$  will be varied. The results are summarized in

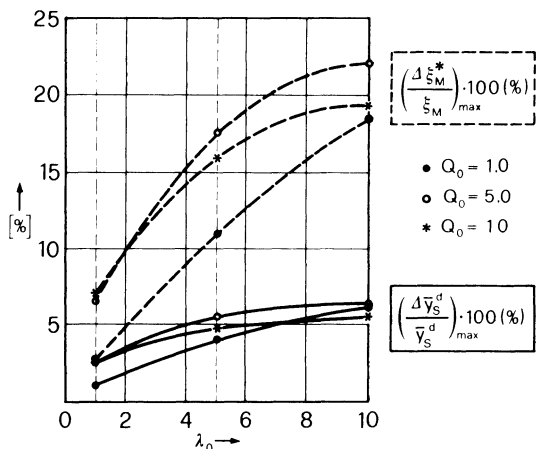


FIG. 5.18. Maximal relative differences of the semi-length and the height of ice divides, in percent, for linear accumulation  $\mathfrak{U}(\bar{y}_S)$  and linear sliding law ( $m = 1$ ) between solutions obtained with the Colbeck and Evans polynomial law and Glen's power law for  $n = 1$  and  $n = 3$ .

Figures 5.19. These show, on the left, the surface geometry for various values of  $(\lambda_0, Q_0, m)$  taking the set  $(1, 1, 1)$  as a reference. Increasing  $Q_0$  and leaving  $\lambda_0$  and  $m$  fixed decreases  $\xi_M^*$  and increases  $\bar{y}_s^d$ . In other words, the ablation at the margin decreases the length and, simultaneously, the large accumulation close to the center increases the center height, (see Figure 5.19a, left). Correspondingly, the sliding velocities are increased (Figure 5.19a, right). Increasing  $\lambda_0$  (Figure 5.19b) and leaving  $m$  and  $Q_0$  fixed significantly decreases  $\xi_M^*$ , but makes little difference to  $\bar{y}_s^d$ . The increased bottom friction thus decreases the horizontal spread. The longitudinal velocities are little changed and remain nearly the same when based on the 'natural' coordinate  $\xi^*/\xi_M^*$  (Figure 5.19b, right). Similarly, increasing  $m$  and leaving  $Q_0$  and  $\lambda_0$

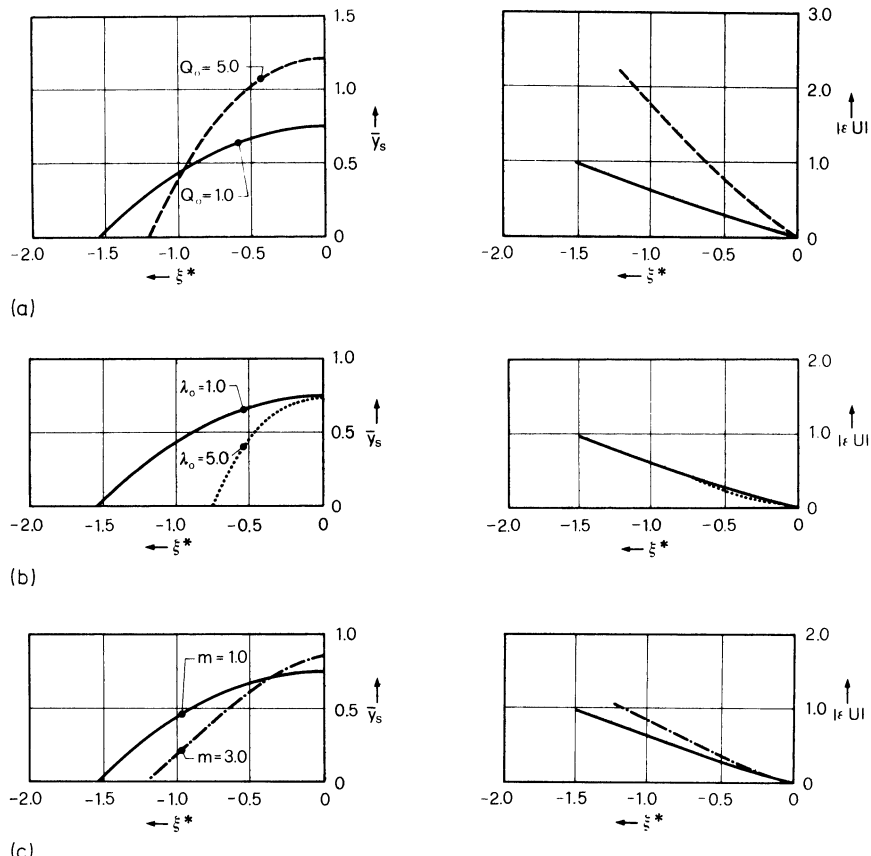


FIG. 5.19. Comparison of profile (left) and basal velocities (right) for Colbeck and Evans law with linear  $\Lambda$  and  $\Omega$ . The lines correspond to particular values of  $(\lambda_0, Q_0, m)$ :  $\text{---} = (1, 1, 1)$ ,  $\text{----} = (1, 5, 1)$ ,  $\dots = (5, 1, 1)$ ,  $\cdots \cdots = (1, 1, 3)$ . (From [23] with changes.)

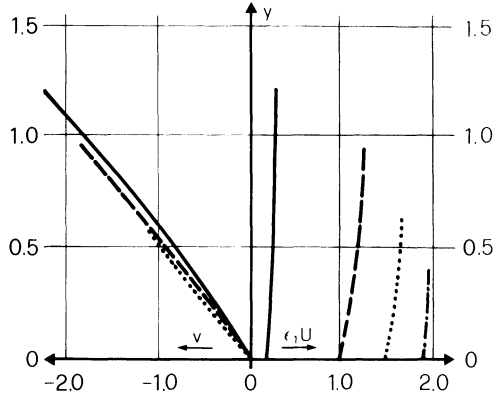


FIG. 5.20. Horizontal and vertical velocity distribution with height for linear  $\lambda$  and  $Q^*$  with  $\lambda_0 = 1$ ,  $Q_0 = 5$ ,  $m = 1$ , at positions, (i)  $\xi^* = -0.13$  — — —, (ii)  $\xi = -0.63$  — — —, (iii)  $\xi^* = -0.87$  · · · · ·, (iv)  $\xi = -1.04$  - - - - -. (From [24].)

fixed, decreases  $\xi_M^*$  and increases  $\bar{y}_S^d$ , (Figure 5.19c). A comparison of longitudinal margin velocities (Figure 5.19, right) shows that ablation strongly influences margin velocities.

Finally, Figure 5.20 shows horizontal and vertical velocity distributions with height at various distances from the center for the case  $(\lambda_0, Q_0, m) = (1, 1, 1)$ . Transverse velocity components are nearly linear in height while longitudinal ones show only a weak vertical gradient. Sliding overrides gliding in this case. However, it does not follow that  $\partial U / \partial \bar{y}$  is small, so the contribution of this term to the shear stretching and, hence, to the  $\Omega$ -term in Equation (5.127) is not negligible.

(ii) *Inclined flat bed.* The previous calculations were performed for a flat bed and for various flow laws and accumulation functions. We now focus attention on the study of the dependence of surface geometry on bottom topography. As a response function, the Colbeck and Evans polynomial law will be used with  $\theta = 0.09$  [consequently  $n = 1$ ,  $\alpha = 0$ ] and the bottom sliding law will be used in the form  $\bar{\Lambda} = \lambda_0 \bar{y}_S$ , with  $\lambda_0 = 1$ ,  $m = 1$ , or equivalently  $C = C_M^* y_S^{-1}$ ,  $C_M^* = 1$ . With accumulation taken as linear in height, we have

$$\mathfrak{A} = -Q_0 + Q_1 \bar{z}, \quad Q_1 = (1 + Q_0). \quad (5.148)$$

$Q_0 > 0$  represents ablation at  $\bar{z} = 0$  and, in turn, implies a unique slope at the margin  $\bar{z} = 0$ .

Choosing a horizontal coordinate system, we may set  $\gamma_0 = 0$  so that  $\bar{z} = \bar{y}_S$ ; the relation  $\bar{y}_B = -\gamma_1 \xi$ ,  $\gamma_1 = \text{constant}$  describes a flat bed at an angle of inclination  $\varepsilon \gamma_1$ . If  $\gamma_1 \geq 0$ ,  $\xi = 0$  is the upper (lower) margin. All profiles will be referred to this coordinate system.\* Morland and Johnson

\*The text which follows parallels closely that of Morland and Johnson [24].

[24] constructed solutions for  $\gamma_1$  in the range 0 (horizontal bed) and 5 for various values of  $Q_0$ , integrating the profile equation (5.127) from the upper margin  $\xi = 0$ . Initial conditions are obtained from Equation (5.133) as

$$\bar{y}'_S(0) = \frac{1}{2} \{ -\gamma_1 + \sqrt{\gamma_1^2 + 4Q_0^2} \}$$

in which only the positive root is physically meaningful.

Further computations have been made for accumulation functions which differ from the linear laws (5.148). In all cases with ablation at the upper margin,  $Q_0 > 0$ , the surface first rises into an accumulation zone, but finally approaches a horizontal one, not returning to the receding bed at a finite span.

Thus the solution approaches that of an ice reservoir with a horizontal surface over which there is uniform accumulation, balanced by decreasing horizontal outflow over increasing depth, illustrated in Figure 5.21. When  $Q_0 < 0$  in Equation (5.148), the upper margin  $\xi = 0$  ( $\bar{z} = 0$ ) is accumulating. Unless margin velocities are prescribed, Equation (5.133) implies two initial (negative) slopes:

$$\bar{y}'_S(0) = \frac{1}{2} \{ \pm \sqrt{\gamma_1^2 - 4Q_0} \}, \quad Q_0 < \frac{\gamma_1}{4}$$

both of which are compatible with the bed slope  $\gamma$ . As indicated in Figure 5.21, the surface slope increases to zero (a concave ice divide) where the surface has dropped to an ablation level.

It appears that reservoir solutions are obtained when integration is performed starting from the upper margin. To avoid this reservoir solution, calculations were repeated for  $\gamma_1 < 0$  and in the range  $0 < -\gamma_1 < 5$ , so

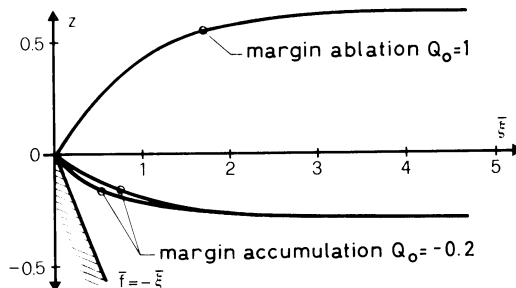


FIG. 5.21. When integration is commenced at the upper margin with margin accumulation or ablation, the solution approaches that of an ice reservoir with a horizontal surface over which there is uniform accumulation, balanced by decreasing horizontal outflow over increasing depth. The plot holds for  $\gamma_1 = 1$ . With margin accumulation two solutions are possible differing in the margin velocities. (From [24].)

that the starting point  $\xi = 0$  is the lower margin, at which there is ablation  $Q_0 > 0$ . In all cases treated, the surface rises to an ice divide at an accumulation level, at which mass balance is attained, and then descends towards the rising bed, but while  $\bar{y}'_S$  remains order unity, it is found that  $-\bar{y}''_S$  increases dramatically as the upper margin is approached. This is in violation with the assumption of bounded slope  $\bar{y}'_S$ , and implies that a global solution with small slope at the upper margin is not possible. Now, we have already seen that the solution with a small slope at the upper margin approaches an unbounded reservoir. Further, for  $\gamma_1 = 0$  the profile is symmetric and again a uniformly-valid solution is obtained. For  $\gamma_1 \neq 0$ , a portion of the upper part of the ice sheet cannot be obtained by solving the lead-order equation (5.127). The solution must be terminated before the upper margin is reached. In fact, Morland and Johnson report contradictory results. Accordingly, for small values of  $-\gamma_1$  ( $-\gamma_1 < 0.1$ ) calculations indicate that the solution of Equation (5.127) remains meaningful for  $\xi$ 's, which are reasonably close to the upper margin, but with increasing  $-\gamma_1$  a contradictory situation of no ablation beyond the ice-divide is reached. Such a case is illustrated in Figure 5.22 for  $\gamma_1 = -0.5$ ,  $Q_0 = 1$  and  $Q_1 = 2$  with the zone of large negative  $\bar{y}''_S$  indicated by dashed lines.

Since mass balance is attained at the ice divide, zero net flux must also be attained in the upper zone beyond the divide. With a rising bed and an accumulation function increasing with height, this requires the surface to steepen in order to reduce the accumulation at the upper levels and to increase the ablation zone. Provided that the rising bed does not eliminate this zone too quickly, this is possible without violating the conditions of mass balance. In either case a valid solution close to the upper margin will require surface slopes of order unity or larger. The perturbation procedure outlined above will become invalid and, presumably, the full equations must be solved in a region around the upper margin which should be matched with the (outer) solution presented above. There is a possibility that this boundary-layer solution could make the outer solution invalid, but this is

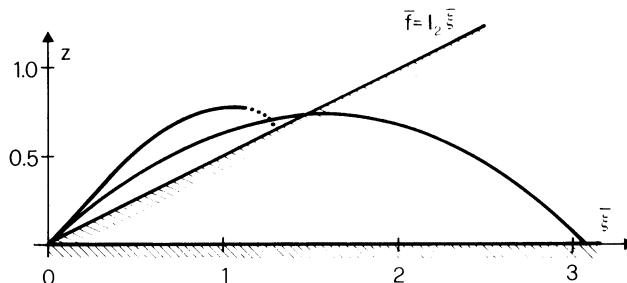


FIG. 5.22. Surface profile for horizontal and inclined flat beds with  $Q_0 = 1$ ,  $Q_1 = 2$ . (From [24].)

unlikely, since the small-slope solution is uniquely determined by the initial conditions at the lower margin so that the boundary layer must be passive.

The reason that the small-slope solution is not uniformly valid for the entire ice sheet, including the zone of the upper margin, is the particular form of the accumulation function. Different accumulation functions in which  $\mathfrak{A}$  may also depend on  $\bar{y}'_S$  (or higher derivatives) and on  $\xi$ , may well lead to uniformly-valid lead-order solutions. Morland and Johnson [24], choose as an example

$$\mathfrak{A}(\bar{z}, \bar{y}'_S) = -Q_0 + Q_1 \bar{z} \bar{y}'_S, \quad Q_0 > 0, Q_1 > 0.$$

Since accumulation is required at a convex ice divide where  $\bar{y}'_S = 0$ , the above form of  $\mathfrak{A}$  implies that an ice divide cannot occur. Other, perhaps more realistic variants of accumulation functions are possible. The above form should illustrate how sensibly the profile reacts to the form of the accumulation function.

(iii) *Topography on a horizontal mean bed.* For a flat bed, the ice-divide height and position are uniquely determined by the small-slope solution of Equation (5.127) by integration from the margin with prescribed  $\bar{y}_S = 0$  and  $\bar{y}'_S$ ; the surface profile is symmetric and the same center height is reached by integration from either margin. Suppose the bed is perturbed at one side of the ice divide only, then the height of the ice divide reached by integrating from the margin at this side is perturbed from the ice-divide height attained by integration over the flat bed side. Provided that the bed profile induces leading-order changes in the profile geometry we may thus anticipate that the small-slope solution of Equation (5.127), starting from either margin, will again lead to a large curvature near the far margin. Morland and Johnson report this to occur in all calculated cases. They present explicit solutions in a single case of sinusoidal bed perturbation and find the large curvature effects near the far margin. Further, profile perturbations do not seem to provide a clear indication of the transmission of undulating topography to the surface. No results are presented with integration performed from the other margin, but it is stipulated that these will now yield large curvature effects at the first margin.

These results seem to suggest that for a bed undulating about a mean flat bed, the small-slope margin is not known in advance, leaving a certain arbitrariness in the determination of the profile geometry. Moreover, bed perturbations which are symmetric about positions of ice divides will always give rise to small-slope margin behavior. A case is illustrated in Figure 5.23. It shows the solution for a flat bed,  $\bar{y}'_S$ , and the corresponding solution when the isostasy relation is used for a bed of highly viscous fluid (Weertman, 1973)

$$\bar{y}_B(\xi) = -\frac{\rho_i}{\rho_b - \rho_i} \bar{y}_S(\xi) \cong -\frac{1}{2} \bar{y}_S(\xi),$$

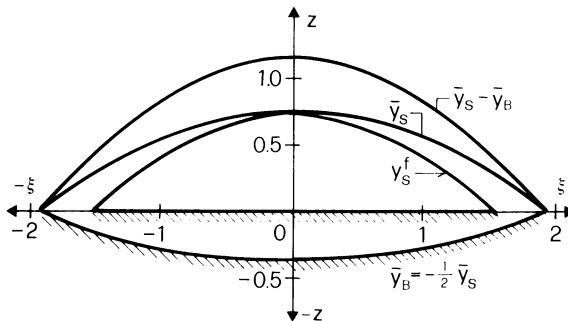


FIG. 5.23. Comparison of the flat bed profile  $\eta_f$ , the isostatic profile  $\eta$ , and the thickness  $\eta - f$ . (From [24].)

where  $\rho_i, \rho_b$  are the ice and bed densities. As illustrated by Figure 5.23, the spread of the ice sheet increases with the deforming bed.

The far-margin problem indicated above calls for the need of further investigations. Inclusion of higher-order terms may well lead to equations which exhibit dispersive and/or diffusive properties and may thus regularize the equations in regions where they now enjoy singular features.

Finally, we mention that Johnson [17–19] has also analysed axisymmetric ice sheets with the same methods outlined above. Qualitatively, no new features are found, however. For the quantitative details we refer the reader to his papers.

In conclusion it may be stated that the evaluation of glacier- or ice-sheet geometry from accumulation data is still not fully possible, even when firm knowledge about the constitutive response and the temperature distribution within the ice is available. Finite lower margin solutions require the ice to slide without friction over its bed at the lower margin and thus limit the applicability of the theory to a particular margin behavior. There are polythermal glaciers which are temperate in their upper parts and cold in their lower parts; they have a snout that adheres to the bed leading to a zero snout velocity. For these cases, the profile solution based on Equations (5.115) or (5.127) is valid only in a region far distant from the margins, and the initial conditions for the solution of the differential equation must be determined by matching this outer solution with the margin solution of the full equations. A complete analysis of the profile geometry will have to include the analysis of the snout and the head. Only when these are solved, are we able to predict steady-state surface geometries for the entire spectrum of practical boundary conditions.

#### REFERENCES

1. Benney, D. J., Long waves in liquid films, *J. Math. Phys.*, **45**, 150–155, 1966.
2. Bodvarsson, G., On the flow of ice-sheets and glaciers, *Jökull*, **5**, 1–8, 1955.

3. Budd, W. F.. The longitudinal velocity profile of large ice masses. International Union of Geodesy and Geophysics. International Association of Scientific Hydrology. General Assembly of Bern, 25 Sept.–7 Oct., 1967 (Commission of Snow and Ice). Reports and Discussions, *International Association of Scientific Hydrology, Publ.*, **79**, 58–77, 1968.
4. Budd, W. F., The dynamics of ice masses. *ANARE Scientific Reports, Ser. A(IV), Glaciology, Publ.*, **108**, 1969.
5. Budd, W. F.. The longitudinal stress and strain-rate gradients in ice masses. *J. Glaciology*, **9**, 19–27, 1970.
6. Budd, W. F. and D. Jenssen. Numerical modelling of glacier systems. Union Géodesique et géophysique Internationale. Association Internationale d'Hydrologie Scientifique. Symposium neiges et glaces. Actes du colloque de Moscow. *International Association of Scientific Hydrology, Publ.*, **104**, 257–291, 1975.
7. Bulirsch, R. and J. Stoer. *Einführung in die Numerische Mathematik. I. II.* Springer-Verlag, Berlin, 1976/78.
8. Colbeck, S. C. and R. J. Evans. A flow law for temperate glaciers. *J. Glaciology*, **12**, 71–86, 1964.
9. Cole, J. D.. *Perturbation Methods in Applied Mathematics*. Blaisdell, Waltham, Mass., 1968.
10. Collins, I. F.. On the use of the equilibrium equations and flow law in relating surface and bed topography of glaciers and ice sheets. *J. Glaciology*, **7**, 199–204, 1968.
11. Fowler, A. C. and D. A. Larson. On the flow of polythermal glaciers: I. Model and preliminary analysis. *Proc. Royal Soc. London, A363*, 217–242, 1978.
12. Fowler, A. C.. Waves on glaciers. *J. Fluid Mech.*, **120**, 283–321, 1982.
13. Fowler, A. C. and D. A. Larson. On the flow of polythermal glaciers: II. Surface wave analysis. *Proc. Royal Soc. London, A370*, 155–171, 1980.
14. Friedrichs, K. O.. Water waves on shallow sloping beach. *Comm. Appl. Math.*, **1**, 109–134, 1948.
15. Hutter, K.. Time dependent surface elevation of an ice slope. *J. Glaciology*, **25**, 247–266, 1980.
16. Hutter, K.. The effect of longitudinal strain on the shear stress of an ice sheet. In defense of using stretched coordinates. *J. Glaciology*, **27**, 39–56, 1981.
17. Hutter, K.. Surface waves in a non-Newtonian incompressible liquid film. *Z. Angew Math. Phys.*, **30**, 1017–1022, 1979.
18. Johnson, I. R.. The steady profile of an axisymmetric ice sheet. *J. Glaciology*, **25**, 25–37, 1981.
19. Johnson, I. R.. Steady Ice sheet flow, a thesis submitted to the University of East Anglia in application for the degree of Doctor of Philosophy, pp. 135, 1981.
20. Keller, J. B.. The solitary wave and periodic waves in shallow water. *Comm. Appl. Math.*, **1**, 323–339, 1948.
21. Lliboutry, L. A.. La dynamique de la Mer de Glace et la vague de 1891–95 d'après les mesures de Joseph Vallot. Union Géodésique et Géophysique Internationale. Association Internationale d'Hydrologie Scientifique. Symposium de Chamonix (1958). Physique du mouvement de la glace. *International Association for Scientific Hydrology, Publ.*, **47**, 125–138, 1958.
22. Mahaffy, M. W.. A three-dimensional numerical model of ice sheets: Tests on the Barnes Ice Cap. North-west Territories. *J. Geophys. Res.*, **81**, 1059–1066, 1976.
23. Morland, L. W. and I. R. Johnson. Steady motion of ice sheets. *J. Glaciology*, **25**, 229–246, 1980.
24. Morland, L. W. and I. R. Johnson. Effects of bed inclination and topography on steady ice sheets. *J. Glaciology*, **25**, 225–246, 1980.
25. Nye, J. F.. A comparison between the theoretical and the measured long profile of the Unteraar glacier. *J. Glaciology*, **2**, 103–107, 1952.

26. Nye, J. F., A method of calculating the thickness of the ice sheets. *Nature*, **169**, 529–530, 1952.
27. Nye, J. F., The motion of ice sheets and glaciers. *J. Glaciology*, **3**, 493–506, 1959.
28. Nye, J. F., Plasticity solution for a glacier snout. *J. Glaciology*, **6**, 695–715, 1967.
29. Nye, J. F., The effect of longitudinal stress on the shear stress at the base of an ice sheet. *J. Glaciology*, **8**, 207–213, 1969.
30. Orowan, E., The flow of ice and other solids. *J. Glaciology*, **1**, 231–240, 1949.
31. Paterson, W. S. B., Laurentide ice sheet: Estimated volumes during Late Wisconsin. *Rev. Geophys. Space Phys.*, **10**, 885–917, 1972.
32. Paterson, W. S. B., Ice sheets and ice shelves. In: *Dynamics of Snow and Ice Masses*, edited by S. C. Colbeck. Academic Press, New York, 1980.
33. Paterson, W. S. B., *The Physics of Glaciers*. Pergamon Press, Oxford, New York, Toronto, Sydney, Braunschweig, 1972.
34. Robin, G. de Q., Surface topography of ice sheets. *Nature*, **215**, 1029–1032, 1967.
35. Shumskiy, P. A., On the theory of glacier motion. International Union of Geodesy and Geophysics. International Association of Scientific Hydrology. General Assembly of Helsinki 25.7.–6.8.1960, *International Association of Scientific Hydrology, Publ.*, **55**, 142–149, 1961.
36. Shumskiy, P. A., On the theory of glacier variations. *Bull., Int. Assoc. Sci. Hydrol.*, **8**, 45–56, 1963.
37. Shumskiy, P. A., The distribution of stress, velocity and temperature in glaciers, in *Physics of Snow and Ice*, edited by H. Oura. International Conference on Low Temperature Science 1966. Proceedings. Vol. 1, pp. 371–384, 1967.
38. Sugden, D. E., Reconstruction of the morphology dynamics and thermal characteristics of the Laurentide Ice Sheet at its maximum. *Arct. Alp. Res.*, **9**, 21–47, 1972.
39. Stoker, J. J., *Water Waves, the Mathematical Theory with Applications*. Interscience Publishers, New York, 1957.
40. Szidarowski, F. and S. Yakowitz, *Principles and Procedures of Numerical Analysis*. Plenum Press, New York, London, 1978.
41. Vialov, S. S., *Regularities of Ice Deformation*. International Union of Geodesy and Geophysics. International Association of Scientific Hydrology. Symposium of Chamonix, 1958. Physics of the movement of the ice, *International Association of Scientific Hydrology, Publ.*, **47**, 383–391, 1958.
42. Weertman, J., Equilibrium profile of ice caps. *J. Glaciology*, **3**, 953–964, 1961.
43. Weertman, J., Rate of growth or shrinkage of nonequilibrium ice sheets. *J. Glaciology*, **5**, 145–158, 1964.
44. Weertman, J., Effect of a basal water layer on the dimensions of ice sheets. *J. Glaciology*, **6**, 191–207, 1966.
45. Weertman, J., Position of ice-divides and ice centers on ice sheets. *J. Glaciology*, **12**, 353–360, 1973.
46. Weertman, J., Comparison between measured and theoretical temperature profiles of the Camp Century, Greenland, borehole. *J. Geophys. Res.*, **73**, 2691–2700, 1968.
47. Wehausen, J. V. and E. V. Laitone, Surface waves, in *Handbuch der Physik*, edited by S. Flügge, Vol. 4. Fluid Dynamics III, pp. 446–758, 1960.
48. Whitham, G. B., *Linear and Non-linear Waves*. John Wiley, New York, 1974.

## **Chapter 6**

### **THE RESPONSE OF A GLACIER OR AN ICE SHEET TO SEASONAL AND CLIMATIC CHANGES**

#### *1. Statement of the Problem*

In the preceding chapters, attention was focused on the development of a mathematical model of glacier flow and on first flow applications under plane motion. Except for the surface-wave stability analysis in a parallel-sided ice strip in Chapter 4, most questions were concerned with the response of a glacier and ice sheet to *steady-state conditions*, or at least conditions close to such a steady state.

The climate glaciers and ice sheets are exposed to is, however, changing continuously, with apparently random fluctuations, from season to season. Superimposed on these are definite long-range changes, which have manifested themselves by repeated growths and retreats of the Arctic and Antarctic ice sheets and glaciers during the Pleistocene. Glaciers are very sensitive to changes in climatic variations, and indeed the latter cause them to advance or retreat repeatedly. To understand the mechanism of the advance and retreat, we need to know how a glacier responds to such changes. The present chapter is an attempt to throw some light on the physics and mathematics of this problem.

The effect of a climatic change to a glacier or an ice sheet can consist of:

- (i) a change in accumulation of glacier mass at the surface or the base,
- (ii) a change of the energy flux from the atmosphere through the surface into the glacier,
- (iii) a change in geothermal heat flux,

or a combination of all. It follows that the description in its utmost generality must be difficult. It is clear, moreover, that a change in energy flux must, in general, result in a change of temperature distribution, except in a temperate glacier, where all energy input is transformed into melting of ice.

A change in accumulation may be attributed to a change in precipitation or a change of melting rate due to energy input or both. The increase in the resulting water content may then increase the sliding velocity. Alternatively, an increase in the temperature distribution changes the material

response of the glacier ice. This, in turn, then results in a different deformation state which eventually changes the gliding mechanism. In this chapter, both sliding and gliding effects, will be assumed to remain constant under climatic changes. *Strictly*, this means that the glacier under consideration is kept at constant energy input from the surfaces and that the accumulation rate is the only significant mechanism to account for such changes. More accurately, such changes are attributed solely to additions and subtractions of mass.

Physically, the description of the response of a glacier to mass changes is fairly straightforward, in particular when approached with the procedures and results of Chapter 5 in mind. Indeed, upon introducing the shallow ice approximation, or more generally the Morland–Johnson stretching of the horizontal coordinate, it was demonstrated in Chapter 5 that the problem for the stress and velocity distribution separates from that of surface geometry. On the one hand, this fact was used to derive stress and velocity distributions in glaciers and ice sheets under plane motion, when the temperature distribution and the geometry is given. On the other hand, it was used to determine the surface geometry when, in turn, the stress and velocity distribution is prescribed. The two problems are, of course, interdependent, and solutions to both should be sought simultaneously. This makes the problem a complicated one and calls for simplification.

Such a simplified theory exists. It restricts attention to the balance law of mass. The neglect of the momentum equation and of the energy balance guarantees that the emerging theory is mathematically simple, but it must be bought at the expense of the introduction of an additional phenomenological statement about the behavior of the glacier as a whole. This phenomenological law can be shown to form a rudimentary momentum balance and the success or failure of the emerging theory hinges upon a reasonable choice of this law.

What results mathematically is a set of equations which belongs into the category of *kinematic waves*, the theory of which was developed by Lighthill and Whitham [19, 20].\* The kinematic wave theory bears its name from the fact that no dynamical equations (momentum equations) are used in the derivation of its governing equations. It has its applications in flood waves on rivers, road traffic flow and group-velocity phenomena. Of course, the neglect of the dynamical equations brings with it a relatively crude physical picture, but in return the mathematics are not unsurmountable.

Because in the kinematic wave theory, one limits attention to a global mass balance and incorporates momentum balance through a constitutive statement, the theory can be developed for valley glaciers with curved axis as well as for ice sheets under plane motion. In this regard, the theory of kine-

\*For a fairly recent review of the kinematic wave theory, see the paper by Kluwick [16].

matic waves embraces the limited two-dimensional theory of plane motion treated so far. On the other hand, it is more special than previous formulations since it treats momentum balance only globally by a rough constitutive statement and, therefore, can not include many of the pertinent features that can be incorporated by a more rigorous treatment.

In the subsequent analysis, we shall first present the kinematic wave theory and will apply it to the response of a glacier to climatic changes. Naturally, this problem can be viewed in two different ways. Firstly, one may ask how a glacier reacts to its climate. This point of view will aim at answers as to the advance and retreat of a glacier snout. Conversely, one may look at the inverse problem, namely to infer from advance and retreat measurements information regarding changes in the accumulation rate. With the aid of the kinematic wave theory and with the presumption that the latter describes the physical processes correctly, such questions can be answered in a fairly satisfactory fashion. A more detailed analysis, however, requires a formulation in which momentum balance is properly taken care of. Such an analysis will be given in the second part of this chapter. It will not only provide indications about the limitations of the kinematic wave theory, but will also pave the way to generalizations of the latter.

The phenomena of surface bulges travelling down-glacier have been observed by numerous scientists. First descriptions were by Marchi [25] and Finsterwalder [10] and their observations and descriptions were later rediscovered by Weertman [43] and Nye [32]. These studies, as well as the careful descriptions of the motion of surface bulges of Mer de Glace (France) by Lliboutry [21], the Glacier des Bossons (France) by Finsterwalder [10], and the Nisqually Glacier (U.S.A.) by Meier and Johnson [26] preceded the adaption to glaciers of the theory of kinematic waves, which was set forth by Lighthill and Whitham [20, 21]. This adaption is largely due to Nye [31 to 35], but he limits attention to small perturbations around a steady state. A first non-linear analysis, including large deformation, is due to Lick [18] and another more recent one is by Bindschadler [1]. General treatments applying these equations aim at validity proofs of the derived equations or at extensions which incorporate the multidimensionality of ice sheets and valley glaciers. Such studies are by Rasmussen and Campell [38], who derive the two-dimensional version of the kinematic wave theory and, e.g., by Langdon and Raymond [17, 37], Bindschadler *et al.* [2, 3] and Budd [4] who all complement the basic one-dimensional formulation with fudge-factors to account for the various subtle phenomena not described by the original equations.

One of the least understood phenomena is the glacier *surge*, i.e., a sudden (and repeated) substantial increase of flow velocities by a factor of 20 up to 150. Surges are of a relaxation type in that they are characterized by a long relatively quiet phase of 30 to 50 years where velocities are small followed

by a short phase of one to two years where velocities are high and generally accompanied with a substantial advance of the glacier snout. Various *ad hoc* explanations have been suggested “involving changes in the mechanical properties of ice (Jonas and Müller [15], Nielson [29]), non-unique thickness profiles caused by longitudinal stress gradients (Robin [39]), wave propagation effects (Palmer [36]), and basal or internal temperature variations (with time) (Clarke [6] *et al.* [7], Thompson [41], Yuen and Schubert [46]) or position (Schytt [40]),” see Raymond [37]. Most of these in one form or another, make use of the kinematic wave equations. Studies of surface waves travelling down-glacier which make use of the *full* dynamical equations are scarce; they are needed, however, because they enable us to base the kinematic wave theory on a more rigorous footing and allow us to delimit its range of applicability. Such a study is by Fowler and Larson [12]. Similar formulations could be obtained from the formulations of Chapter 5 by simply including time-dependent processes, as shown by Hutter [13] and Morland and Johnson [27, 28].\*

## 2. Development of the Kinematic Wave Theory

### (a) Full non-linear theory<sup>†</sup>

Consider a glacier or ice sheet of constant density. Let  $a$  denote the addition of thickness per unit time, which henceforth will be called accumulation rate. In general,  $a$  is a function of time and position. Suppose that there is a steady rate of accumulation  $a_0$  which is only a function of position. Corresponding to  $a_0$  there is a certain steady-state configuration of the glacier. Its surface will be called *datum-surface*. If the glacier is infinitely wide, it may be replaced by a strip of unit width and the coordinate  $x$  may be defined on the datum line which runs down-glacier. For a valley glacier, an exact definition of the coordinate is more difficult (see Figure 6.1). In Figure 6.1a is shown a top view of a glacier in its datum state with its boundary lines at the valley sides. To construct the  $x$  coordinate in this case, consider a point on one of its boundaries and draw from it the shortest connection to the opposite boundary line. The union of all the midpoints of these shortest distances will then define a line on the datum surface, which we shall choose as the  $x$  coordinate. Its positive direction will be down-glacier. The *cross-section* of the glacier at a point  $x$  is then a plane, which cuts the coordinate  $x$  at right angles. An element of such a valley glacier is given in Figure 6.1b, and the

\*I have seen a preprint of a paper by Fowler [11] on ‘Waves on glaciers’ in which the propagation of disturbances is mathematically treated allowing for a very general form of the basal friction law. In this paper, Fowler gives a *possible* explanation for all three types of waves occurring on glaciers, namely surface waves, surges, and seasonal waves.

<sup>†</sup> Until further noticed, the following developments will be made in physical space. Quantities will thus *not* be nondimensionalized.

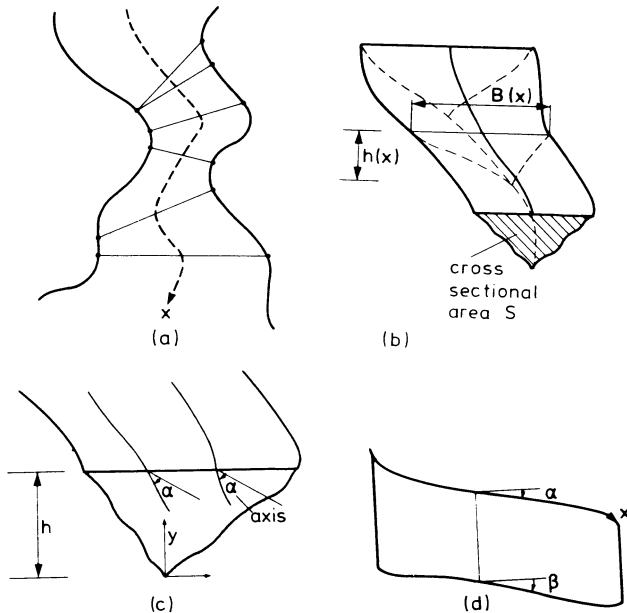


FIG. 6.1. A valley glacier in its datum state: (a) top view with construction of the  $x$  coordinate, (b) a glacier element cut out of the glacier with cross sectional areas, (c) definition of  $h$  and (d) vertical area through  $x$ -axis and projection of Thalweg onto it.

glacier runs from  $x = 0$  to  $x = L$ . Assume, moreover, that the datum surface is nearly flat, that the intersection of the glacier surface with the cross-sectional area is horizontal and that the curvature effects of the  $x$ -line are negligibly small. The balance of mass to be formulated below will be valid under more general conditions, but the geometric relation and the phenomenological assumptions introduced are only correct when these assumptions are invoked. In an infinitely wide glacier, these assumptions are superfluous of course, because they are satisfied *per se*.

Basic to the present treatment is that the glacier is regarded as a one-dimensional continuum which, on such a global view, moves in the direction of  $x$ . In the general case, when the glacier is not in the datum state, accumulation is a function of position and time. Let us define by  $a(x, t)$  the average accumulation over the width  $B(x, t)$  of the glacier, measured perpendicular to the surface of the datum glacier at  $x$ . Let, further,  $S(x, t)$  be the area of the cross-section and  $Q(x, t)$  be the discharge, that is, the volume of ice passing through the cross-sectional area per unit time. Conservation of mass for a glacier element of length  $dx$  then requires that

$$\frac{\partial Q}{\partial x} + \frac{\partial S}{\partial t} = Ba(x, t). \quad (6.1)$$

This equation, of course, is based on the assumption of constant density. In the datum state it reduces to

$$\frac{dQ_0}{dx} = B_0 a_0(x). \quad (6.2)$$

Next, denote by  $y$  the coordinate in the cross-section perpendicular to  $x$  which is measured positively upwards from the lowest point of the cross-section, and let  $h(x, t)$  be the actual depth (see Figure 6.1c). Then

$$S = S(x, t) = \hat{S}(x, h(x, t)) = \int_0^{h(x, t)} \hat{B}(x; y) dy, \quad (6.3)$$

where  $B = B(x, t) = \hat{B}(x, h(x, t))$ . These are geometric relations; they determine the cross-sectional area and the width as functions of the actual height. Substituting (6.3) into Equation (6.1) reveals an equation for  $Q$  and  $h$ , namely,

$$\frac{\partial Q}{\partial x} + \left( \frac{\partial \hat{S}}{\partial h} \right) \frac{\partial h}{\partial t} = Ba,$$

or in view of (6.3),  $\partial \hat{S} / \partial h = \hat{B}[x, h(x, t)]$ ,

$$\frac{\partial Q}{\partial x} + B \frac{\partial h}{\partial t} = Ba. \quad (6.4)$$

Solutions to Equation (6.4) cannot be determined unless some assumption regarding the flow process in the glacier is made. Such an equation must relate  $Q(x, t)$  to the remaining quantities appearing in Equation (6.4). In what follows, we shall not be concerned with the most general constitutive relationship that can be established for  $Q$  but shall limit our attention to a restricted class that will lead to an acceptable physical description of the problem at hand. Such an assumption is

$$Q = \hat{Q}(h(x, t), \alpha(x, t)), \quad (6.5)$$

where  $\alpha$  denotes the surface inclination angle averaged over the local width of the glacier. (In Chapter 5 this angle was denoted by  $\alpha_s$ .) This angle is positive, as indicated in Figure 6.1c. The phenomenological relation (6.5) is not the simplest one by which Equation (6.4) may be complemented. In fact, a simpler expression is

$$Q = \hat{Q}(h(x, t)); \quad (6.6)$$

it would transform (6.4) into a single first-order partial differential equation for  $h$ ,

$$\frac{\partial h}{\partial t} + \mathfrak{C}(h, x) \frac{\partial h}{\partial x} = a(x, t) \quad (6.7a)$$

with

$$\mathfrak{C}(h, x) = \frac{1}{\hat{B}(x, h)} \hat{Q}'(h). \quad (6.7b)$$

It is this equation that is known in fluid dynamics as the kinematic wave equation (see Lighthill and Whitham [19, 20] and Whitham [44]). We shall return to it in a later section.

Notice that Equations (6.1) and (6.5) are still not closed because they contain the variable  $\alpha$  which is a new unknown. A relation for it can be obtained with the aid of Figure 6.1d. It shows the datum line and the projection of the *Thalweg* onto a vertical surface through the  $x$ -axis. Denoting the angle of inclination of the Thalweg with respect to the horizontal by  $\beta(x)$ , the figure suggests that

$$\frac{\partial h}{\partial x} = \tan(\beta - \alpha) \cong \beta - \alpha, \quad (6.8)$$

where the small-angle approximation is always justified. This equation now closes the system.

The phenomenological law (6.5), the geometric relation (6.8), and the mass balance law (6.1) mathematically describe the response of a glacier to changes in accumulation. Before we proceed, we summarize the equations:

Balance of mass,

$$\frac{\partial Q}{\partial x} + B \frac{\partial h}{\partial t} = Ba. \quad (6.9)$$

Phenomenological law,

$$Q = \hat{Q}(h(x, t), \alpha(x, t)). \quad (6.10)$$

Geometric relations,

$$\frac{\partial h}{\partial x} \tan(\beta - \alpha) \cong \beta - \alpha, \quad B(x, t) = \hat{B}(x, h(x, t)). \quad (6.11)$$

Given the functions  $\hat{Q}(h, \alpha)$ ,  $\hat{B}(x, h)$  and  $a(x, t)$ , the union of Equations (6.9) to (6.11) together with the appropriate boundary and initial conditions allows the determination of  $Q$ ,  $h$  and  $\alpha$  as functions of  $x$  and  $t$ .

When the constitutive relation (6.10) is substituted into Equation (6.9) and the angle  $\alpha$  is eliminated from the resulting equation, a single partial differential equation for  $h$  is obtained. This equation reads

$$\frac{\partial h}{\partial t} + C \frac{\partial h}{\partial x} - D \frac{\partial^2 h}{\partial x^2} = a - D \frac{d\beta}{dx}, \quad (6.12a)$$

in which

$$\begin{aligned} C &:= \frac{\partial \hat{Q}}{\partial h} \frac{1}{\hat{B}} = \hat{C}\left(x, h, \beta - \frac{\partial h}{\partial x}\right), \\ D &:= \frac{\partial \hat{Q}}{\partial \alpha} \frac{1}{\hat{B}} = \hat{D}\left(x, h, \beta - \frac{\partial h}{\partial x}\right). \end{aligned} \quad (6.12b)$$

Evidently, Equation (6.12a) is non-linear (but of quasilinear form) since the coefficients  $C$  and  $D$  are functions of both the unknown  $h$  and its derivative  $\partial h / \partial x$ .

There is another second-order partial differential equation, which the relations (6.9) to (6.11) can be reduced to. To obtain it, observe that Equations (6.10) and (6.11) imply

$$\frac{\partial \hat{Q}}{\partial h} \frac{\partial h}{\partial t} = \frac{\partial Q}{\partial t} + \frac{\partial \hat{Q}}{\partial x} \frac{\partial^2 h}{\partial x \partial t} = \frac{\partial Q}{\partial t} + \frac{\partial \hat{Q}}{\partial x} \left( \frac{\partial a}{\partial x} - \frac{\partial}{\partial x} \left( \frac{\partial Q}{\partial x} \frac{1}{B} \right) \right)$$

or

$$\frac{\partial \hat{Q}}{\partial h} \frac{\partial h}{\partial t} = \frac{\partial Q}{\partial t} - \frac{\partial \hat{Q}}{\partial x} \frac{\partial}{\partial x} \left( \frac{\partial Q}{\partial x} \frac{1}{B} \right) + \frac{\partial \hat{Q}}{\partial x} \frac{\partial a}{\partial x}. \quad (6.13)$$

Multiplying both sides of (6.9) with  $C$  and using (6.13) yields

$$\frac{\partial Q}{\partial t} + \left( C + \frac{D}{B} \frac{\partial B}{\partial x} \right) \frac{\partial Q}{\partial x} - D \frac{\partial^2 Q}{\partial x^2} = B \left( aC - D \frac{\partial a}{\partial x} \right). \quad (6.14a)$$

In this equation,  $B$ ,  $D$  and  $C$  must not be given by (6.12b), because in that form they are functions of  $h$  and  $\partial h / \partial x$ . They cannot be expressed in terms of  $Q$  and its derivatives unless (6.10), regarded as a differential equation for  $h$ , can be integrated to yield  $h(x, t) = \hat{h}(Q(x, t), \beta(x))$ . Substituting this into (6.12b), we obtain

$$\left. \begin{aligned} C &= \tilde{C}\left(x, Q(x, t), \frac{\partial Q}{\partial x}(x, t), \beta(x), \frac{d\beta}{dx}\right), \\ D &= \tilde{D}\left(x, Q(x, t), \frac{\partial Q}{\partial x}(x, t), \beta(x), \frac{d\beta}{dx}\right). \end{aligned} \right\} \quad (6.14b)$$

It is obvious that if the functions (6.14b) are not directly available, their determination must be difficult. We conclude that in this non-linear case the formulation (6.12) is mathematically more direct and easier.

To gain some insight into the structure of Equations (6.12) and (6.14) note that only one of them need be discussed because their form is similar. To this end, assume that the non-linearities are weak so that a perturbation scheme may be used in a first approximation. This perturbation approach is discussed in the next subsection.

(b) *Perturbation expansion – linear theory*

We now rewrite (6.9)–(6.11) in terms of perturbations from the datum state. We identify them by the suffix 1 and thus write

$$\begin{aligned} Q &= Q_0(x) + Q_1(x, t), & a &= a_0(x) + a_1(x, t), \\ h &= h_0(x) + h_1(x, t), & B &= B_0(x) + B_1(x, t), \\ \alpha &= \alpha_0(x) + \alpha_1(x, t). \end{aligned} \quad (6.15)$$

Substituting these relations into the governing Equations (6.9)–(6.11), observing that  $|Q_1/Q_0| \ll 1$ ,  $|h_1/h_0| \ll 1$ ,  $|a_1/a_0| \ll 1$  and  $|B_1/B_0| \ll 1$ , neglecting all non-linear terms, and noticing that the zeroth-order quantities describe the datum state and must, therefore, satisfy the steady-state equations, the following equations are obtained:

$$\begin{aligned} \frac{\partial Q_1}{\partial x} + B_0 \frac{\partial h_1}{\partial t} &= B_0 a_1 + B_1 a_0, \\ Q_1 &= B_0 C_0 h_1 - B_0 D_0 \frac{\partial h_1}{\partial x}. \end{aligned} \quad (6.16)$$

In these equations, the coefficients  $B_0$ ,  $C_0$ , and  $D_0$  may be regarded as known, given functions of the coordinate  $x$ . Moreover, in writing down (6.16), use has been made of (6.12b) and  $\alpha_1$  has been replaced by  $-\partial h_1/\partial x$ .

It is not difficult to see that by eliminating  $Q_1$  from Equations (6.16), a second-order partial differential equation for  $h_1$  is obtained. In this reduction it should, however, be observed that  $B_1$  may be expressed in terms of  $h_1$  by considering Equation (6.11)<sub>2</sub>, which yields

$$B_1 = \frac{\partial \hat{B}}{\partial h}(x, h_0(x))h_1 \equiv e_0(x)h_1. \quad (6.17)$$

In valley glaciers,  $B_1$  is generally small and negligible except close to the snout. Nye [31, 32] neglects  $B_1$  in comparison to the remaining terms. Lliboutry [22, 23], on the other hand, has drawn attention to the importance of the term (6.17) close to the snout ‘because such a term may restore stability.’ It will become apparent below that there is little, if any, justification for this statement. With the relation (6.17), the differential equations (6.16) can be shown to reduce to

$$\begin{aligned} \frac{\partial h_1}{\partial t} + \left( C'_0 + \frac{B'_0}{B_0} C_0 - \frac{e_0 a_0}{B_0} \right) h_1 + \\ + \left( C_0 - D'_0 - D_0 \frac{B'_0}{B_0} \right) \frac{\partial h_1}{\partial x} - D_0 \frac{\partial^2 h_1}{\partial x^2} &= a_1, \end{aligned} \quad (6.18a)$$

or

$$\begin{aligned} \frac{\partial Q_1}{\partial t} + \left( C_0 + D_0 \frac{B'_0}{B_0} - \frac{e_0 a_0}{B_0 D_0} \right) \frac{\partial Q_1}{\partial x} - D_0 \frac{\partial^2 Q_1}{\partial x^2} - \\ - D_0 e_0 \left( \frac{B'_0}{B_0} a_0 + \frac{a_0 C_0}{D_0} - \frac{a_0^2 e_0}{B_0} - \frac{(e_0 a_0)'}{e_0} \right) h_1 \\ = \left( B_0 C_0 - \frac{e_0 a_0}{D_0} \right) a_1 - B_0 D_0 \frac{\partial a_1}{\partial x}. \end{aligned} \quad (6.18b)$$

As mentioned previously, the coefficients in these differential equations are treated as known functions of  $x$ ; also, primes denote derivatives with respect to  $x$ . Notice further that the equation for  $Q_1$  still contains a term linear in  $h_1$ . A complete reduction to a single second-order operator for  $Q_0$  is only achieved when  $e_0 \equiv 0$ , when the term (6.17) introduced by Lliboutry is usually neglected. [A full reduction of the Equation (6.18b) would result in a third-order partial differential equation.\*] In that case, Equations (6.18a, b) are mathematically equivalent.<sup>†</sup> Finally, we remark that Nye [32] in his original derivation, apart from omitting  $e_0$  also neglected the term  $B'_0(x)$ , thereby restricting attention essentially to the infinitely wide ice sheet. For this case (6.18) becomes ( $q_1 = Q_1$  per unit width,  $B_0 = 1$ )

$$\begin{aligned} \frac{\partial h_1}{\partial t} + C_0 h_1 + (C_0 - D'_0) \frac{\partial h_1}{\partial x} - D_0 \frac{\partial^2 h_1}{\partial x^2} = a_1, \\ \frac{\partial q_1}{\partial t} + C_0 \frac{\partial q_1}{\partial x} - D_1 \frac{\partial^2 q_1}{\partial x^2} = C_0 a_1 - D_0 \frac{\partial a_1}{\partial x}. \end{aligned} \quad (6.19)$$

### (c) An estimate for the coefficients $C$ and $D$

Essentially, there remain three problems before the kinematic wave equations can be integrated. Firstly, estimates for the coefficient functions  $C_0$ ,  $D_0$  (and  $e_0$ ) must be found; secondly, boundary conditions and, lastly, initial conditions must be prescribed. In this section, we shall be concerned with the estimation of the coefficients.

The determination of the coefficients  $C_0$ ,  $D_0$  and  $e_0$  amounts to the formulation of a phenomenological relationship for  $Q$  or  $q$ . To this end,

\*To derive it, solve Equation (6.18b) for  $h_1$  and substitute the resulting expression into the second Equation (6.16). In so doing, an equation will result containing a  $(\partial^3 Q_1 / \partial x^3)$ -term. This is rather unfortunate since it implies an additional integration condition lost through differentiation.

<sup>†</sup> Then Equation (6.18a) may also be written as

$$\frac{\partial h_1}{\partial t} + \frac{1}{B_0} \frac{\partial}{\partial x} \left[ B_0 C_0 h_1 - B_0 D_0 \frac{\partial h_1}{\partial x} \right] = a_1. \quad (6.20)$$

consider a strictly parallel-sided slab of temperate ice. Its motion consists of sliding and gliding and has been determined in Chapter 3. In particular, a formula for discharge was derived in Equation (3.88). Except for notation this formula reads

$$q = Fh^{n+2} \sin^n \alpha + Gh^{m+1} \sin^m \alpha \equiv \hat{q}(h, \alpha). \quad (6.21)$$

A similar formula also holds for the surface velocity (see Equation (3.88)). It reads

$$u_s = \frac{n+2}{n+1} Fh^{n+1} \sin^n \alpha + Gh^m \sin^m \alpha = u_d + u_b. \quad (6.22)$$

In the above,  $F$  and  $G$  are constants,  $n = 3$  or  $4$  and  $m = \frac{1}{2}(n+1)$ . The first term on the right-hand side of (6.21) is the contribution to the total discharge due to differential motion. This part depends on the material response and has been written down for Glen's flow law. The second term, on the other hand, is the contribution due to sliding assuming a Weertman-type sliding law. Definition (6.12b) of the coefficients  $C_0$  and  $D_0$  implies

$$\begin{aligned} C_0 &= \left( \frac{\partial q}{\partial h} \right)_0 = (n+2) \left( \frac{q_d}{h} \right)_0 + (m+1) \left( \frac{q_b}{h} \right)_0 \\ &= (n+1)u_d + (m+1)u_b, \end{aligned} \quad (6.23)$$

where  $u_b$  and  $u_d$  are the mean speeds due to deformation (gliding) and sliding, respectively.

A better variable than  $u$  is the surface speed  $u_s$  because it is more readily observable. It follows from (6.22) that (6.23) may also be written as

$$C_0 = (n+1)(u_s - u_b) + (m+1)u_b. \quad (6.24)$$

Equation (6.24) may be used to find the upper and lower limits for speed  $C_0$ . If the glacier is sealed to its base,  $u_b = 0$  and

$$C_0 = (n+1)u_s \quad (\text{no sliding}).$$

On the other hand, if the motion consists of entirely sliding, then  $u_b = u_s$ , so that

$$C_0 = (m+1)u_s \quad (\text{no sliding}).$$

Generally, we have to expect both mechanisms so that

$$(m+1)u_s \leq C_0 \leq (n+1)u_s,$$

or since  $m \approx 2$ ,  $n = 3$  to  $4$

$$3u_s \leq C_0 \leq 5u_s. \quad (6.25)$$

Measuring the surface speed of a glacier thus allows us to obtain a rough picture of the order of magnitude of  $C_0$ .

As regards values for  $D_0$  we obtain from its definition and equations (6.21) and (6.22)

$$D_0 = \left\{ \frac{n(n+1)}{n+2} (u_s - u_b) + mu_b \right\} h_0 \cot \alpha_0. \quad (6.26)$$

If the glacier is sealed at the bed

$$\begin{aligned} D_0 &= \frac{n(n+1)}{n+2} u_s h_0 \cot \alpha_0 \\ &\simeq \frac{4 \times 5}{6} u_s h_0 \cot \alpha_0 \simeq 3.3 u_s h_0 \cot \alpha_0 \quad (\text{no sliding}). \end{aligned}$$

Alternatively, if all motion is due to gliding only,

$$D_0 \simeq mu_s h_0 \cot \alpha_0 = 2u_s h_0 \cot \alpha_0.$$

Consequently, since the real motion consists of gliding and sliding,

$$2u_s h_0 \cot \alpha_0 \leq D_0 \leq 3.3 u_s h_0 \cot \alpha_0. \quad (6.27)$$

The above considerations are based on the gliding and sliding mechanism of an infinitely long strip under its own weight and assume that no longitudinal strain rate is present. If strong longitudinal strain rates are present, the index  $n$  in the power law of Glen's creep formula is  $n = 1$ .<sup>\*</sup> Under these circumstances, we must replace (6.25) and (6.27) by

$$2u_s \leq C_0 \leq 5u_s, \quad \frac{2}{3}u_s h_0 \cot \alpha_0 \leq D_0 \leq 3.3 u_s h_0 \cot \alpha_0, \quad (6.28)$$

where the limit values have been obtained by choosing for  $n$  the appropriate value between 1 and 4. Notice also that the dependency of  $D_0$  on  $\cot \alpha$  suggests a strong diffusion influence for ice sheets and a weaker one for steep valley glaciers.

The above discussion on the order of magnitude of  $C_0$  and  $D_0$  does not apply to the extreme end of the glacier, the snout, and here, the whole picture is much less clear. Temperate glaciers have wedge-shaped snouts as indicated in Figure 6.2 with wedge angles  $\theta$  between 0 and  $15^\circ$  or somewhat more. No adequate theory exists to date for the flow of ice in the neighborhood of the snout, where Equation (6.21) breaks down. The above formulas cannot even give a rough picture of the flow because (6.21) predicts that

$$u_0 = \left( \frac{q}{h} \right)_0 \rightarrow 0 \quad (\text{at the snout}).$$

<sup>\*</sup>This can be seen as follows: For large longitudinal stresses  $t_{xx} \gg t_{yy}$ ,  $t_{xx} \gg t_{xy}$ , the stress deviator invariant  $t'_{II} = \frac{1}{4}(t_{xx} - t_{yy})^2 + t_{xy}^2 \simeq \frac{1}{4}t_{xx}^2$  depends approximately only on the longitudinal stress. It follows that shear strain and shear stress are linearly related with a constant of proportionality which depends on  $t_{xx}$  only.

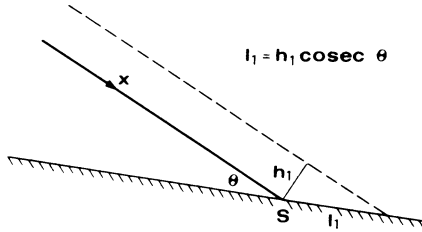


FIG. 6.2. Wedge-shaped glacier snout. An increase of the thickness  $h_1$  at the snout results in an advance of the glacier by an amount  $l_1$ .

This contradicts observations. A better estimate of the situation can be obtained from the definition of  $C_0$  as follows:

$$C_0 := \left( \frac{\partial q}{\partial h} \right)_0 = \left( \frac{\partial(uh)}{\partial h} \right)_0 = u_0 + h_0 \left( \frac{\partial u}{\partial h} \right)_0$$

and since  $h_0 = 0$  at the snout,

$$C_0 = u_0 \quad (\text{at the snout}). \quad (6.29)$$

Alternatively,

$$D_0 := \left( \frac{\partial q}{\partial \alpha} \right)_0 = \left( \frac{\partial(hu)}{\partial \alpha} \right)_0 = h_0 \left( \frac{\partial u}{\partial \alpha} \right)_0 = 0,$$

and hence

$$D_0 = 0 \quad (\text{at the snout}). \quad (6.30)$$

These results should be compared with (6.28). As a consequence,  $C_0$  and  $D_0$  are comparatively small at the snout, but  $D_0$  vanishes, while  $C_0$  is finite.

Finally, we would like to state that in a real glacier, roughly,  $C_0$  monotonically increases down-glacier from the head to midglacier, and then decreases down to a value  $u_0$  at the snout. Hence, again roughly,  $dC_0/dx$  is positive in the upper part of the glacier, but becomes negative in its lower part. The motion in the upper part is extensional, but compressive in the lower part. As we shall see, this is important.

There remains the determination of an estimate for  $e_0(x)$ . As mentioned earlier,  $e_0 \approx 0$  over most part of the glacier. Moreover, Equation (6.17) suggests that  $e_0$  should be larger than zero. For a valley with vertical side walls  $\partial \hat{B}/\partial h = 0$  and so  $e_0 = 0$ , for side walls with small slopes  $e_0$  may be very large. This may be the case close to the snout, however, as we shall see below,  $C_0 - e_0$  should remain positive everywhere for purely mathematical reasons, posing an upper bound on  $e_0$  equal to  $C_0$ .

Lliboutry, in reference [23], gives further indications of how the coefficients  $C_0$  and  $D_0$  may be estimated.

(d) *Boundary and initial conditions*

In what follows we shall assume the glacier to extend from  $x = 0$  to  $x = L$  and shall select  $t \geq 0$ . To solve any one of the differential equations (6.18) in  $0 \leq x \leq L$  and  $t \geq 0$  boundary and initial conditions must be known. As for the former, two boundary conditions are necessary: one at the head, the other at the snout of the glacier. Incidentally, the equations are of second order in  $x$  because of the occurrence of the coefficient  $D_0$ , which accounts for diffusion. Hence, there is a difference in the number of boundary conditions between the full problem, including diffusion and the reduced one in which the latter is neglected. This should be borne in mind.

The glacier head will be identified with  $x = 0$  and the snout with  $x = L$ . At the head there is no discharge through the top cross-section. Consequently,

$$\left. \begin{aligned} Q_1 &= 0, \quad \text{at } x = 0 \quad (\text{valley glacier}), \\ \text{or} \\ q_1 &= 0, \quad \text{at } x = 0 \quad (\text{infinitely wide glacier}). \end{aligned} \right\} \quad (6.31)$$

The proper boundary condition that must be imposed at the snout  $x = L$  is not immediately obvious, since no particular physical restriction seems to be placed on the glacier at the place. However, since  $D_0 = 0$  at the snout (see Equation (6.30)), the differential equation involving  $h_1$  or  $Q_1$  is *singular* at the snout. This suggests enforcing a regularity condition of the solution as an appropriate boundary condition, and indeed it seems to be also physically reasonable to require the perturbation height  $h_1$  to remain finite as  $x$  approaches  $L$ . Consequently, we impose the condition

$$h_1 = \text{finite}, \quad \text{for } x = L. \quad (6.32)$$

By constructing a power-series solution near  $x = L$  to the steady-state Equations (6.16), it is not difficult to demonstrate that condition (6.32) implies that *wedge-shaped snouts remain wedge-shaped*. This appears to be in agreement with observations as the transition from a wedge to a cliff is rather the exception.

As initial condition we may either prescribe  $h_1(x, 0)$  or  $Q_1(x, 0)$ ,

$$h_1(x, 0) = h_1^0(x) \quad \text{or} \quad Q_1(x, 0) = Q_1^0(x). \quad (6.33)$$

The formulation of the initial-boundary-value problem is now complete.

### 3. Theoretical Solutions for a Model Glacier

The differential Equations (6.18) or (6.19) together with the boundary and initial conditions prescribed above will now be integrated for specific analytically given coefficient functions  $C_0, D_0$  and  $e_0$ . Attention shall be limited here to plane motions in an infinitely wide ice sheet so that  $B_0 \equiv 1$ .

Occasionally the coefficient function  $e_0(x)$  shall be taken as the zero function, though, this will not be assumed throughout.

(a) *Solutions neglecting diffusion*

Consider Equation (6.18b) in the limit

$$D_0 \rightarrow 0 \quad \text{and} \quad \frac{e_0}{D_0} \equiv f_0 = \text{finite}. \quad (6.34)$$

Physically, this limit corresponds to the situation that diffusion is negligible. With  $q_1/B_0 = Q_1$  and  $B'_0 = 0$ , Equation (6.18b) then reads

$$\frac{\partial q_1}{\partial t} + (C_0 - f_0) \frac{\partial q_1}{\partial x} = (C_0 - f_0 a_0) a_1, \quad 0 \leq x \leq L. \quad (6.35)$$

In contrast with (6.18), this equation contains only first-order spatial derivatives, and this implies that a boundary condition must be prescribed at only one end. The condition at the head seems to be the more natural one. Let Equation (6.35) therefore be subject to the following initial and boundary conditions

$$q_1(x, 0) = 0, \quad q_1(0, t) = 0. \quad (6.36)$$

Under these restrictions, the initial-boundary-value problem (6.35), (6.36) is most easily solved by the method of characteristics, see Finsterwalder [9], Whitham [44], its characteristic form being

$$\begin{aligned} \frac{dx}{dt} &= (C_0(x) - f_0(x)), & \frac{dq_1}{dt} &= (C_0 - f_0 a_0) a_1, \\ q_1(x_0, 0) &= 0, & x &= x_0, t = 0, \\ q_1(0, t) &= 0, & x &= 0, t > 0, \end{aligned} \quad (6.37)$$

where  $x_0 \in [0, L]$  is the characteristic parameter. For the reader not familiar with the method of characteristics, Equations (6.37) can be motivated as follows: The left-hand side of Equation (6.37)<sub>2</sub> may be interpreted as the total derivative of  $q_1$  following a motion with velocity  $dx/dt = (C_0 - f_0)$ . This consideration determines the first two of Equations (6.37) and the remaining equations are then the initial and boundary conditions already listed as Equations (6.36). Integration now proceeds according to the functional form of the accumulation function  $a_1$ . Since  $C_0$  and  $f_0$  depend on  $x$  only, a first integral follows from (6.37)<sub>1</sub> and is

$$t = \int_{x_0}^x \frac{d\bar{x}}{C_0 - f_0}. \quad (6.38)$$

It determines a relationship between  $x$  and  $t$  and may be used to eliminate the variable  $t$  from  $a_1(x, t)$  which now becomes a function of  $x$  alone. From

a combination of the first two Equations (6.37)  $dq_1/dx$  can be determined; a subsequent integration then yields  $q_1$ . For constant  $a_1$  one obtains

$$q_1 = a_1 \int_{x_0}^x \frac{C_0 - f_0 a_0}{C_0 - f_0} d\bar{x}. \quad (6.39)$$

Integrability of the above integrals preassumed, Equations (6.38) and (6.39) together comprise the complete solution in parametric form. In order to gain some physical insight into the solution, let  $a_0 = 1$ . Equation (6.38) is then explicitly integrable. Let further (see Figure 6.3)

$$\begin{aligned} \text{Case (i): } C_0 - f_0 &= \begin{cases} \varepsilon x, & 0 \leq x \leq \frac{1}{2} \\ \varepsilon(1-x), & \frac{1}{2} \leq x \leq 1 \end{cases} \quad (f_0 = 0) \\ \text{Case (ii): } C_0 - f_0 &= \varepsilon [k^2 - (x-k)^2], \quad k = \frac{1}{2}(1-\delta), \quad |\delta| \ll 1. \\ C_0 + f_0 &= \varepsilon [\bar{k}^2 - (x-\bar{k})^2], \quad \bar{k} = \frac{1}{2}(1+\delta), \end{aligned} \quad (6.40)$$

The first of these cases is due to Nye [32]. It models  $C'_0$  as a discontinuous function of  $x$ ; indeed  $C'_0 > 0$ , for  $0 \leq x < \frac{1}{2}$ , where the glacier motion is extensional; on the other hand,  $C'_0 < 0$  for  $\frac{1}{2} < x \leq 1$  where the motion is compressive. This is a fairly reasonable choice and takes account of the fact that glacier flow is largely extensional in the upper, accumulating zone and compressive in the lower ablating zone. Case (ii) models this phenomenon in a continuous fashion, but has also incorporated the possibility that  $C_0 - f_0$  may become negative close to the snout ( $\delta > 0$ ), while  $C_0$  is strictly positive.

The performance of the integrations for the two cases proceeds now as follows:

*Case (i):* From (6.39) one straightaway obtains

$$q_1 = a_1(x - x_0); \quad (6.41)$$

the integration in (6.38) however, depends on the position of  $x_0 \in [0, 1]$ . Clearly,

$$t = \left\{ \begin{array}{l} \int_{x_0}^x \frac{d\bar{x}}{\varepsilon \bar{x}} = \frac{1}{\varepsilon} \ln \left( \frac{x}{x_0} \right), \quad 0 \leq x_0 \leq \frac{1}{2}, \quad 0 \leq x \leq \frac{1}{2}, \\ \int_{x_0}^{1/2} \frac{d\bar{x}}{\varepsilon \bar{x}} + \int_{1/2}^x \frac{d\bar{x}}{\varepsilon(1-\bar{x})} = \frac{1}{\varepsilon} \ln \left( \frac{1}{4x_0(1-x)} \right), \end{array} \right. \quad (\text{I})$$

$$0 \leq x_0 \leq \frac{1}{2}, \quad \frac{1}{2} \leq x \leq 1 \quad (\text{II})$$

$$\left\{ \begin{array}{l} \int_{x_0}^x \frac{d\bar{x}}{\varepsilon(1-\bar{x})} = \frac{1}{\varepsilon} \ln \left( \frac{1-x_0}{1-x} \right), \quad \frac{1}{2} \leq x_0 \leq 1, \quad \frac{1}{2} \leq x \leq 1 \end{array} \right. \quad (\text{III})$$

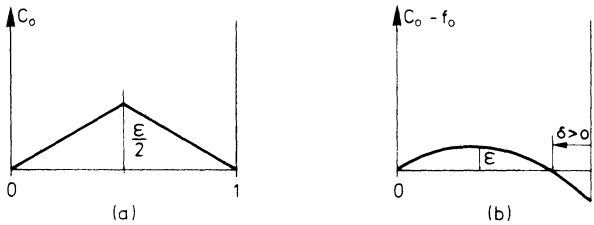


FIG. 6.3. Distribution of  $C_0 - f_0$  along the glacier for two theoretical models:  
(a) for a 'roof-shaped' velocity distribution and (b) for a parabolic velocity distribution.

or alternatively,

$$\begin{aligned} x &= x_0 e^{\varepsilon t}, \quad 0 \leq x_0 \leq \frac{1}{2}, \quad 0 \leq x \leq \frac{1}{2} & (I), \\ 4x_0(1-x) &= e^{-\varepsilon t}, \quad 0 \leq x_0 \leq \frac{1}{2}, \quad \frac{1}{2} \leq x \leq 1 & (II), \\ (1-x) &= (1-x_0)e^{-\varepsilon t}, \quad \frac{1}{2} \leq x_0 \leq 1, \quad \frac{1}{2} \leq x \leq 1 & (III). \end{aligned} \quad (6.42)$$

These  $(x, t)$ -curves have been plotted in Figure 6.4a for various selected values of the parameter  $x_0 \in [0, 1]$ , the domains of applicability of the different formulas being indicated by I, II and III, respectively. The final step in the construction of the solution is the elimination of the parameter  $x_0$  between Equations (6.41) and (6.42). When this is done and the relation  $h_1 = q_1/C_0$  is used (see Equation (6.16)<sub>2</sub> in the limit  $D_0 \rightarrow 0$ ), the following relations are obtained:

$$h_1(x, t) = \begin{cases} \frac{a_1}{\varepsilon}(1 - e^{-\varepsilon t}) & (I), \\ \frac{a_1}{\varepsilon} \left( \frac{x}{1-x} - \frac{1}{4(1-x)^2} e^{-\varepsilon t} \right) & (II), \\ \frac{a_1}{\varepsilon}(e^{\varepsilon t} - 1) & (III). \end{cases} \quad (6.43)$$

Evidently, the solution in regions I and II is asymptotically stable as  $h_1$  remains finite when  $t$  becomes infinitely large. In region III, however,  $h_1$  grows exponentially with time; in other words, the disturbance  $h_1$  increases in an unstable manner. Notice further that in regions I and III,  $h_1$  increases uniformly in  $x$ , whereas in region II this growth is  $x$ -dependent. Moreover, as  $t \rightarrow 0$ , region II is negligibly small and  $h_1$  grows at the rate  $a_1$  for all  $x$ .\* On the other hand, as  $t$  becomes large, region III becomes smaller and smaller so that asymptotically as  $t \rightarrow \infty$ , the solution is given by the cor-

\*Indeed, as  $t \rightarrow 0$ ,  $h_1 \rightarrow a_1$ .

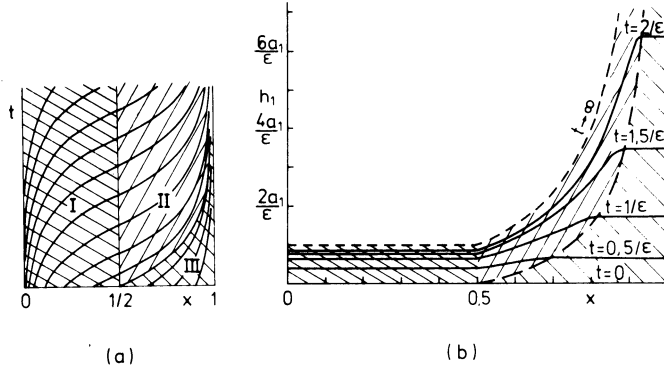


FIG. 6.4. (a) Wave paths in the  $(x, t)$  plane for an idealized glacier, case (i). (b) The increase in thickness  $h_1$  in an idealized glacier at various times after a sudden uniform increase in the rate of accumulation. The upper part responds stably; the lower part, unstably, until the kinematic wave from  $X = 1/2$  arrives. (Redrawn from [31].)

responding expressions of (6.43) in regions I and II, namely

$$h_1^\infty \equiv h_1(x, \infty) = \begin{cases} \frac{a_1}{\epsilon}, & 0 \leq x \leq \frac{1}{2}, \\ \frac{a_1}{\epsilon} \frac{x}{1-x}, & \frac{1}{2} \leq x < 1, \end{cases} \quad \text{as } t \rightarrow \infty. \quad (6.44)$$

As can be seen from this formula,  $h_1^\infty$  is infinitely large at the snout  $x = 1$ . This does not only invalidate the calculations because the small perturbation assumption is no longer satisfied, but the result expresses the fact that for finite  $t$  any  $h_1$  below  $x = \frac{1}{2}$  grows exponentially until the kinematic wave generated initially at  $x = \frac{1}{2}$  reaches it. The cause for the singularity is that the functions  $C_0(x)$  and  $f_0$  vanish at the end of the glacier. As we have seen in (6.29), the assumption  $C_0 = 0$  is unrealistic, and we may terminate the solutions at a point  $x < 1$ . On the other hand, setting  $f_0 = 0$  is not realistic either. But from formulas (6.38)–(6.40) it follows that the above analysis of Case (i) remains valid for  $f_0 \neq 0$ , if  $C_0$  is merely replaced by  $C_0 - f_0$ . This implies that the singularity may still exist if  $C_0 - f_0 = 0$  at  $x = 1$ . Case (ii) in Equations (6.40) has been designed in order to gain more insight into the structure of the solution. It consists of a function  $(C_0 - f_0)$  which shows all essentials of Case (i) but, and depending on the choice of  $\delta$ , Case (ii) allows  $(C_0 - f_0)$  in  $[0, 1]$  to be either strictly positive ( $\delta < 0$ ) or change sign ( $\delta > 0$ ), while at the same time  $C_0$  is positive.

*Case (ii):* The first integration of (6.39) is again straightforward and yields

$$q_1 = a_1(x - x_0). \quad (6.45)$$

Equation (6.38), on the other hand, can be written as

$$t = \frac{1}{\varepsilon k^2} \int_{x_0}^x \frac{dx}{1 - \left(\frac{\bar{x}}{k} - 1\right)^2} = \frac{1}{2\varepsilon k} \ln\left(\frac{x}{x_0} \cdot \frac{2k - x_0}{2k - x}\right)$$

or

$$x_0 = \frac{2kx}{x + (2k - x) \exp(2\varepsilon kt)}. \quad (6.46)$$

Since  $C_0(x)$  was chosen to be continuously differentiable in this case, the characteristics are given by this formula for all  $x \in [0, 1]$ . Elimination of  $x_0$  between (6.45) and (6.46) finally yields

$$q_1 = a_1 x \left\{ 1 - \frac{2k}{x + (2k - x) \exp(2\varepsilon kt)} \right\}. \quad (6.47)$$

This is regular for all  $x \in [0, 1]$  and all times  $t \geq 0$  provided  $k > 0.5$ . Then,

$$\frac{q_1}{C_0} = h_1 = \frac{a_1 x \{ 1 - 2k/[x + (2k - x) \exp(2\varepsilon kt)] \}}{\varepsilon [\delta^2 + x(1 - x)]} \quad (6.48)$$

also remains finite. This, clearly, brings out the conditions of regularity. It is not because  $f_0 \neq 0$  has been introduced, but that  $(C_0 - f_0)$  is strictly

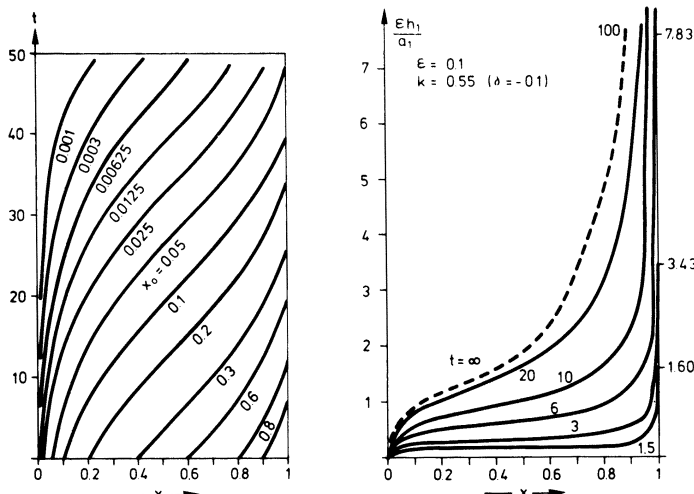


FIG. 6.5. (a) Wave paths in the  $(x, t)$  plane for the idealized glacier, case (ii). (b) The increase in thickness  $h_1$  in the idealized glacier (case (ii)) at various times after a sudden uniform increase in rate of accumulation. The entire glacier responds stably, but in the upper part the increase in height is relatively small, whereas with  $x$  approaching unity, thickness grows assuming a finite maximum at the snout.

positive. The characteristic speed leads to regular representation for the flux, when  $(C_0 - f_0)$  is of one sign and when  $C_0 - f_0$  never vanishes. The results are plotted in Figure 6.5, which shows the wave paths in the  $(x, t)$ -plane (Figure 6.5a) and the increase in glacier thickness  $\varepsilon h_1/a_1$  at various times after a sudden uniform increase of the accumulation rate (Figure 6.5b). Notice that wave heights remain finite as  $x \rightarrow 1$ . Calculations were performed for  $a = 0.1$  and  $k = 0.55$  ( $\delta = -0.1$ ), and results indicate that the new steady-state profile (shown dashed in Figure 6.5b) is non-uniform and typically as shown in Figure 6.4. Qualitatively however, surface profiles depend strongly on the value of  $k$ . This can be seen from Figure 6.6 which shows time evolutions of thickness  $h_1$  for finite times and for the values  $k = 0.55$  and  $k = 0.505$ , respectively. Not only becomes the function  $h_1(x, t)$  more uneven for  $k$  approaching 0.5, but the behavior at the snout is more and more singular. It is now also understandable, why inclusion of  $f_0$  cannot be interpreted as a mechanism to restore stability. The crucial variable according to which  $h_1$  at the snout remains finite is  $(C_0 - f_0)$  which must be positive. A non-vanishing  $f_0$  raises the probability for  $(C_0 - f_0)$  to become negative. Hence the inclusion of  $f_0$  in the theory is a destabilizing rather than stabilizing effect.

The calculations performed with the inclusion of diffusive terms will show that diffusion is the mechanism that achieves a real stabilization of the snout behavior.\*

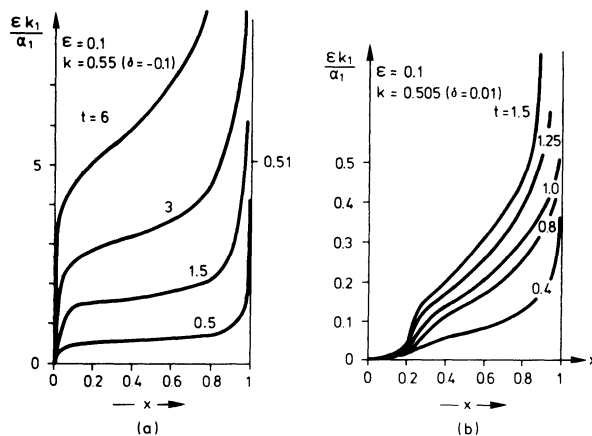


FIG. 6.6. Increase in thickness  $h_1$  for the idealized glacier (case (ii)). The distribution of  $h_1$  strongly depends on the behavior of the characteristic speed  $(C_0 - f_0)$ . The smaller this variable is at the snout, the larger will be the increase in glacier height and therefore the glacier advance at the snout. This is why the distribution of  $h_1$  is less even in Figure 6.6b than Figure 6.6a.

\*It is, perhaps, worthwhile to point out that the occurrence of a possible infinite growth of the glacier thickness at the snout is a property of the *linear* equations. Had we kept the non-linear equations and linearized equations accordingly, such singular behavior could have been avoided, see Fowler and Larson [12] and Section 5a(*y*), where the correct linearization is shown.

(b) *Theoretical solutions for a diffusive model*

(α) *Coefficient functions of the special model.* Having recognized that not  $f_0$  but  $C_0 - f_0$  is responsible for a possible singularity, we shall subsequently require  $C_0$  to be strictly positive and set  $f_0 = 0$ .

To construct solutions to Equations (6.19), a special model is now adopted in which the functions  $C_0(x)$  and  $D_0(x)$  have simple polynomial forms. Consistent with the requirements put forward above, the following polynomial expressions shall be chosen:

$$C_0(x) = \frac{x}{\sigma} \left(1 - \frac{x}{l}\right), \quad D_0(x) = \frac{Ex^2}{\sigma} \left(1 - \delta - \frac{x}{l}\right). \quad (6.49)$$

These functions are sketched in Figure 6.7. In the datum state, the glacier runs from  $x = 0$  to  $x = l(1 - \delta) = L$ .  $E$ , which is dimensionless and  $\sigma$ , which is a time, are constants, as is  $\delta$ , which is a dimensionless small constant.  $l$  is a length, related to the length of the glacier,  $L$ , by the relation  $l(1 - \delta) = L$ .

Perhaps a justification for the selection of the above functions is in order. The function  $C_0$  is strictly positive, except at the head where it vanishes;  $C'_0 > 0$  for the upper portion of the glacier and  $C'_0 < 0$  for the lower one. This is in line with the previous choice. Moreover  $C_0 > 0$  at the snout; this is mandatory in view of the discussion above. The diffusivity function  $D_0(x)$  must be positive and vanish at the snout. Otherwise, no specific requirements regarding its distribution are necessary. Because the non-diffusive models have shown a considerable growth of  $h_1$  in the lower portion of the glacier, its influence should be large in this zone and small in the upper region. The cubic in (6.49) models this qualitatively correctly.

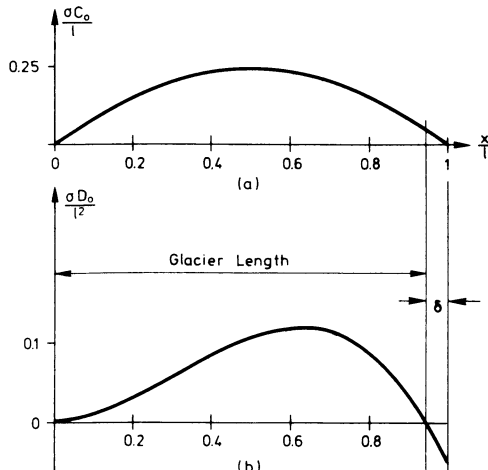


FIG. 6.7. Distribution of characteristic speed  $C_0$  (a), and diffusivity  $D_0$  (b), along the glacier axis for a model glacier characterized by Equations (6.49); parameters are  $E = 1$  and  $\delta = 0.05$ .

To obtain *numerical values* for  $\sigma$ ,  $\delta$  and  $E$  we proceed as follows:  
Note first that

$$C_0 \left( \frac{l}{2} \right) = C_0^{\max} = \frac{l}{4\sigma} \rightarrow \sigma = \frac{l}{4C_0^{\max}}.$$

On the other hand, we have the estimates (6.28). It is thus reasonable to set  $C_0 = 4u_{S_0}$  so that  $\sigma = l/(16u_{S_0})$ . Thus, for example, if  $l = 10$  km,  $u_{S_0} = 100$  ma<sup>-1</sup>, then  $\sigma = 6$  a. An estimate for  $E$  may be obtained from (6.49)<sub>2</sub> by assuming  $\delta \approx 0$  and evaluating  $D_0$  at  $x = l/2$ :  $D_0(l/2) = EI^2/(8\sigma)$ , a reasonable value of which may be suggested by (6.27) by choosing  $D_0(l/2) = 3 \cot \alpha_0$ . Hence

$$E \approx \frac{24 \sigma u_{S_0} h_0 \cot \alpha_0}{l^2} = \frac{3}{2} \left( \frac{h_0}{l} \right) \cot \alpha_0,$$

where  $h_0$  and  $\alpha_0$  are the thickness and the slope at  $x = l/2$ . With  $h_0 = 250$  m,  $\alpha_0 = 4 \times 10^{-2}$ ,  $l = 10$  km we obtain  $E \approx 0.9$ .

The small dimensionless number  $\delta$  may be estimated as follows: It was shown that at the snout  $C_0 = u_0$ , but in the middle of the glacier,  $C_0^{\max} \approx 4 u_0$ . Hence, from (6.49)

$$C_0(L) = \frac{l\delta}{\sigma} (1 - \delta) \approx \frac{l\delta}{\sigma} = 16 u_{S_0} \delta$$

so that

$$\delta \approx \frac{C_0(L)}{16 u_{S_0}} = \frac{u_{S_0}}{16 u_{S_0}} \approx 0.006.$$

These figures are simply illustrative, and no one glacier can be taken as typical of all, but very roughly we may take

$$\sigma \approx 5 \text{ to } 10 \text{ a}, \quad \delta \approx 0.01, \quad E \approx 1. \quad (6.50)$$

$L$  (or  $l$ ) and  $\sigma$  denote a characteristic length and a characteristic time with the aid of which the governing Equations (6.19) can be normalized. Introducing then a new dimensionless time  $\tau$  and a dimensionless length coordinate  $\xi$  according to

$$\tau = \frac{t}{\sigma}, \quad \xi = \frac{x}{l} \quad (6.51a)$$

and non-dimensionalizing  $h_1$  with a representative characteristic length  $H$ ,  $h_1$ ,  $q_1$  and  $a_1$  can be written as

$$h_1^* = \frac{h_1}{H}, \quad a_1^* = \frac{a_1 \sigma}{H}, \quad q_1^* = q_1 H \frac{l}{\sigma}. \quad (6.51b)$$

Equations (6.19) then become

$$\begin{aligned} \frac{\partial h_1^*}{\partial \tau} + C_0^* h_1^* + (C_0^* - D_0^*) \frac{\partial h_1^*}{\partial \xi} - D_0^* \frac{\partial^2 h_1^*}{\partial \xi^2} &= a_1^*, \\ \frac{\partial q_1^*}{\partial \tau} + C_0^* \frac{\partial q_1^*}{\partial \xi} - D_0^* \frac{\partial^2 q_1^*}{\partial \xi^2} &= C_0^* a_1^* - D_0^* \frac{\partial a_1^*}{\partial \xi}, \end{aligned} \quad (6.52)$$

where the coefficient functions  $C_0^*$  and  $D_0^*$  are now given by

$$C_0^*(\xi) = \xi(1 - \xi), \quad D_0^*(\xi) = E\xi^2(1 - \delta - \xi), \quad (6.53)$$

the prime indicating differentiation with respect to  $\xi$ . Incidentally, in the subsequent analysis, we shall drop the asterisk as there is little possibility of confusion.

(β) *Solution for a step function.* It is possible to derive the solution to Equations (6.52), (6.53) if the accumulation rate is an arbitrary function of position and time. The method of integration could then be illustrated using a special example. We find the opposite approach more suitable and shall first investigate the glacier response when  $a_1$  is uniform in  $\xi$  and a step function in time:

$$a_1(\tau) = \begin{cases} 0, & \tau < 0, \\ A, & \tau \geq 0. \end{cases} \quad (6.54)$$

Equations (6.52) with coefficients (6.53) shall be solved subject to the initial and boundary conditions

$$\left. \begin{aligned} q_1(\xi, 0) &= h_1(\xi, 0) = 0, \quad 0 \leq \xi \leq 1 - \delta, \\ q_1(0, \tau) &= 0 \quad \text{or} \quad \lim_{\xi \rightarrow 0} \left[ \xi(1 - \xi)h_1 - E\xi^2(1 - \delta - \xi) \frac{\partial h_1}{\partial \xi} \right] = 0 \\ h_1(1 - \delta, \tau) &= \text{finite} \end{aligned} \right\} \quad 0 < \tau < 1. \quad (6.55)$$

(i) *The final steady state.* We denote the solutions belonging to this case by  $h_1^\infty$  and  $q_1^\infty$ . Setting  $\partial/\partial\tau = 0$  in (6.52) leads to

$$\frac{d}{d\xi} \left\{ E\xi^2(1 - \delta - \xi) \frac{dh_1^\infty}{d\xi} - \xi(1 - \xi)h_1^\infty \right\} = -A, \quad (6.56)$$

so that

$$E\xi(1 - \delta - \xi) \frac{dh_1^\infty}{d\xi} - (1 - \xi)h_1^\infty = -A. \quad (6.57)$$

The constant of integration vanishes in view of the boundary condition at  $\xi = 0$ . Solutions to this equation are not easily found unless the parameter

$E$  assumes special values. For  $E = 0$  which corresponds to the neglect of diffusion, we simply obtain

$$h_1^\infty = \frac{A}{1 - \xi} \quad (E = 0, \text{ no diffusion}). \quad (6.58)$$

For  $0 < E \leq 1$ , an analytic solution might be sought in terms of power series; thus we choose

$$h_1^\infty = \sum_{n=0}^{\infty} H_n \xi^n. \quad (6.59)$$

If convergent, this representation guarantees that the boundary conditions at  $\xi = 0$  and  $\xi = 1 - \delta$  are satisfied. Indeed, if  $h_1^\infty$  is bounded in  $[0, 1 - \delta]$ , then  $q_1(\xi = 0) = 0$  (see Equation (6.16)) and  $h_1^\infty$  at  $\xi = 1 - \delta$  is finite.

Substituting this trial solution into the differential equation (6.57) for  $h_1^\infty$  yields the recurrence relations

$$H_0 = A, \quad H_n = -\frac{1 - (n - 1)E}{[nE(1 - \delta) - 1]} H_{n-1}, \quad n \geq 1,$$

which can also be written as

$$H_n = \frac{\prod_{j=0}^{n-1} (1 - jE)}{\prod_{j=0}^n [1 - j(1 - \delta)E]} A, \quad n \geq 1, \quad (6.60)$$

so that

$$\frac{h_1^\infty}{A} = \sum_{n=1}^{\infty} \frac{\prod_{j=0}^{n-1} (1 - jE)}{\prod_{j=0}^n [1 - j(1 - \delta)E]} \xi^n + 1. \quad (6.61)$$

It is trivial to see that, whenever  $E = 1/k$ , where  $k$  is an integer, the summation in (6.61) terminates. This was observed by Lliboutry [23] who restricted attention to this case. The solution (6.61) is, however, valid for all  $E \in (0, 1]$  as we shall soon see. Special polynomial solutions read

$$\frac{h_1^\infty}{A} = \begin{cases} \left(1 + \frac{\xi}{\delta}\right), & E = 1, \\ 1 + \frac{2}{1 + \delta} \xi + \frac{1}{\delta(1 + \delta)} \xi^2, & E = 1/2, \\ 1 + \frac{3}{2 + \delta} \xi + \frac{6}{(2 + \delta)(1 + 2\delta)} \xi^2 + \frac{2}{\delta(2 + \delta)(1 + 2\delta)} \xi^3, & E = 1/3. \end{cases} \quad (6.62)$$

In all these cases, in fact for all  $E$

$$\frac{h_1^\infty}{A} = \frac{1}{\delta}, \quad \text{for } \xi = 1 - \delta, \quad (6.63)$$

as can easily be seen from (6.57). To find the radius of convergence for the power series expansion (6.61) we form the quotient

$$\begin{aligned} Q &= \lim_{n \rightarrow \infty} \left| \frac{H_n}{H_{n-1}} \right| = \lim_{n \rightarrow \infty} \left| \frac{\prod_{j=1}^n (1-jE) \prod_{j=1}^n (1-j(1-\delta)E)}{\prod_{j=1}^{n+1} (1-j(1-\delta)E) \prod_{j=1}^{n-1} (1-jE)} \right| \\ &= \lim_{n \rightarrow \infty} \frac{|1-nE|}{|1-n(1-\delta)E|} |\xi| = \frac{E|\xi|}{|1-\delta|E}, \end{aligned} \quad (6.64)$$

or if  $E \neq 0$ ,

$$Q = \frac{|\xi|}{|1-\delta|},$$

which must be less than 1; so (6.61) is a convergent series as long as  $|\xi| < (1-\delta)$ . We have thus found a solution to the general Equation (6.57) for a limited set of values for the diffusion constant  $E$ . Nye did not construct the solution (6.64) except for  $E = 0$  and  $E = 1$ . He used a numerical scheme to integrate (6.57) starting from  $\xi = 1 - \delta$  and then plotted  $h_1^\infty/A$  as a function of  $\xi$ . Lliboutry [23], on the other hand, recognized the polynomial solution for  $E = 1/k$ , where  $k$  is an integer. Figure 6.8 shows a plot for  $h_1^\infty/A$  as a function of  $\xi$  as was essentially given by Nye.

There are several striking features that we can observe. Firstly, all curves pass through one point: at  $\xi = 1 - \delta$ , the snout,  $h_1^\infty/A$  has the value  $1/\delta$  irrespective of what value  $E$  might assume. Since  $E$  measures the importance of diffusion, it follows that the rise in thickness at the snout can be predicted correctly with a diffusionless theory. Secondly, the value of  $E$  plays a marked role at all glacier positions except at the head and the snout. In particular, the curve  $E = 1$ , which is roughly representative for our model glacier, and that for  $E = 0$  differ substantially. This implies that diffusion may not be neglected in general. Since for  $\xi = 1 - \delta$ ,  $h_1^\infty = A/\delta$  for all  $E$ , the

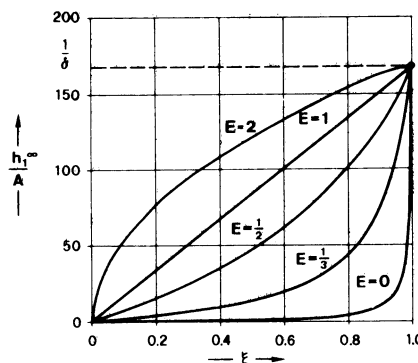


FIG. 6.8. Steady-state profile  $h_1^\infty : \xi$ , after a sudden uniform increase  $A$  in rate of accumulation.  $\delta = 0.006$ . (Redrawn from [32].)

ultimate advance of a glacier due to a sudden uniform increase may be given as

$$l_1 = \frac{A}{\delta} \operatorname{cosec} \theta.$$

Exact solutions to Equation (6.57) for  $E > 1$  have not been found so far.

(ii) *The time-dependent response.* Let us next examine the transient response of the model glacier and thus return to Equations (6.52). In view of the successful approach to the steady-state behavior, we try the separation of the variables solution (boundary conditions are again automatically satisfied by this choice)

$$h_1 = \sum_{n=0}^{\infty} H_n(\tau) \xi^n \quad (6.65)$$

and obtain after substitution into (6.52)<sub>1</sub> the following ordinary differential equations for the coefficient functions  $H_n(t)$ :

$$L_n H_n = S_n A \quad (n = 0, 1, 2 \dots), \quad (6.66)$$

where

$$L_n = \prod_{j=0}^n \left( \frac{d}{d\tau} + r_j \right), \quad r_j = (j+1)[1 - jE(1-\delta)], \quad (6.67)$$

$$S_n = \prod_{j=0}^n s_j, \quad s_0 = 1, \quad s_j = (j+1)[1 - (j-1)E], \quad j > 1, \quad (6.68)$$

subject to the initial conditions

$$\prod_{k=j}^n \left( \frac{d}{d\tau} + r_k \right) H_n(0) = 0, \quad k = 1, 2, \dots, n. \quad (6.69)$$

This formulation is due to Lliboutry [23] and it is easily seen that in the steady-state limit the steady problem analysed above emerges.

It should also be noticed that the product  $S_n$  vanishes whenever  $E = 1/(j-1)$ , for any  $j \leq n$ . For such a case, the differential equation (6.66) is homogeneous, subject to homogeneous initial conditions. Its solution is then  $H_n(x) \equiv 0$ ; and this must be true for all  $j \leq n$ . This implies that the system (6.66) terminates whenever  $E = 1/k$ , where  $k$  is an integer. Representation (6.65) reduces in this case to a polynomial in  $\xi$  with time-dependent coefficients. It will be demonstrated below that this polynomial representation is the only case for which (6.65) is meaningful.

A solution to the initial boundary value problem (6.66)–(6.69) is probably most easily found by Laplace transforms. These are defined as

$$\bar{f}(\omega) = \int_0^\infty f(\tau) e^{-\omega\tau} d\tau, \quad f(\tau) = \frac{1}{2\pi i} \int_{\gamma-i\infty}^{\gamma+i\infty} \bar{f}(\omega) e^{\omega\tau} d\omega,$$

where the second formula is the inversion formula in which integration is along the Bromwich contour. It is not difficult to show that (6.66) and (6.69) become in the transformed domain

$$\bar{H}_n = \frac{S_n}{\omega \prod_{j=0}^n (\omega + r_j)} A, \quad (6.70a)$$

so that inversion gives

$$H_n = \frac{AS_n}{2\pi i} \int_{\gamma-i\infty}^{\gamma+i\infty} \frac{e^{\omega\tau} d\omega}{\omega \prod_{j=0}^n (\omega + r_j)}. \quad (6.70b)$$

For physically reasonable values of  $E$  and  $\delta$  the values of  $r_j$  ( $j = 0, 1, \dots, n$ ) are all positive and distinct. The poles of (6.70b) lie in this case on the negative real  $\omega$ -axis and are simple, see Figure 6.9. Integration can be performed by applying the residue theorem. This procedure yields

$$H_n = A \prod_{j=0}^n S_n \left\{ \frac{1}{\prod_{j=0}^n r_j} + \sum_{j=0}^n \frac{A_j^n}{r_j} e^{-r_j\tau} \right\}, \quad (6.71)$$

where

$$A_j^n = \left\{ \prod_{l=0, l \neq j}^n (r_l - r_j) \right\}^{-1}, \quad A_0^0 = 1 \quad (6.72)$$

as the response of the glacier to a Heaviside pulse in accumulation rate of magnitude  $A$ . With the definitions (6.67), (6.68) and (6.72) one obtains for

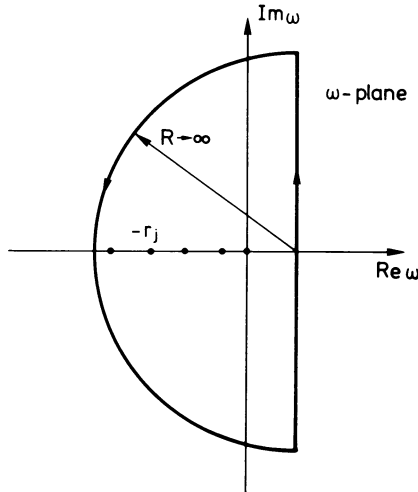


FIG. 6.9. Bromwich contour and location of residues for the evaluation of the integral (6.70b).

the auxiliary quantities

$$\begin{aligned}
 S_0 &= 1, & S_1 &= 2, & S_2 &= 3(1 - E), \\
 r_0 &= 1, & r_1 &= 2[1 - E(1 - \delta)], & r_2 &= 3[1 - 2E(1 - \delta)], \\
 A_0^0 &= 1, & A_0^1 &= -A_1^1 = \frac{1}{1 - 2E(1 - \delta)}, \\
 A_0^2 &= \frac{1}{2[1 - 2E(1 - \delta)][1 - 3E(1 - \delta)]}, \\
 A_1^2 &= \frac{-1}{[1 - 2E(1 - \delta)][1 - 4E(1 - \delta)]}, \\
 A_2^2 &= \frac{1}{2[1 - 3E(1 - \delta)][1 - 4E(1 - \delta)]}
 \end{aligned} \tag{6.73}$$

and consequently for the first three functions  $H_0$ ,  $H_1$  and  $H_2$

$$\begin{aligned}
 H_0 &= A(1 - e^{-\tau}), \\
 H_1 &= A \left\{ \frac{1}{1 - E(1 - \delta)} - \frac{2e^{-\tau}}{1 - 2E(1 - \delta)} - \frac{e^{-2[1 - E(1 - \delta)]\tau}}{[1 - E(1 - \delta)][1 - 2E(1 - \delta)]} \right\}, \\
 H_2 &= \frac{A(1 - E)}{2[1 - 2E(1 - \delta)]} \left\{ \frac{1}{[1 - E(1 - \delta)]} + \frac{3e^{-\tau}}{[1 - 3E(1 - \delta)]} - \right. \\
 &\quad \left. - \frac{3e^{-2[1 - E(1 - \delta)]\tau}}{[1 - E(1 - \delta)][1 - 4E(1 - \delta)]} + \frac{e^{-3[1 - 2E(1 - \delta)]\tau}}{[1 - 3E(1 - \delta)][1 - 4E(1 - \delta)]} \right\}.
 \end{aligned} \tag{6.74}$$

As a special case, consider  $E = 1$ . Then  $H_2 \equiv 0$ , and from (6.66) and (6.68), it immediately follows that  $H_n = 0$ , for all  $n > 2$ . Hence, in this case, the transient solution for  $h_1$  becomes

$$\frac{h_1(\xi, \tau)}{A} = (1 - e^{-\tau}) + \left\{ \frac{1}{\delta} + \frac{2}{1 - 2\delta} e^{-\tau} - \frac{1}{\delta(1 - 2\delta)} e^{-2\delta\tau} \right\} \xi. \tag{6.75}$$

This is the solution as obtained by Nye. As  $\tau$  becomes infinitely large, it must and does reduce to the steady-state solution derived previously. Several interesting features can be extracted from the above construction of the general solution. As already mentioned before, if  $E = 1/k$ , where  $k$  is an integer, (6.65) is a polynomial in  $\xi$  with time-dependent coefficients. As a function of time, Equation (6.75), which is the complete solution for (6.65) when  $E = 1$ , contains two characteristic time scales. One scale is  $\tau_0 = 1$ , the other is  $\tau_1 = 1/2\delta$ . It is large as compared to unity. This second time scale occurs only when diffusion is taken into account. On the other hand,

the solution for  $E = \frac{1}{2}$  and, more generally, that for  $E = 1/n$  contains several time scales which can easily be read off from (6.71):

$$\tau_j = \frac{1}{r_j} = \frac{1}{(1+j)[1-jE(1-\delta)]}, \quad (j = 0, 1, \dots, n). \quad (6.76)$$

If  $E = 1/n$ , then  $\tau_n$  is much larger than  $\tau_0, \tau_1, \dots, \tau_{n-1}$ , which are all  $\mathcal{O}(1)$ . Hence, in this case too, there is a distinct large time scale. On the other hand, if  $E \neq 1/k$ , where  $k$  is an integer, an infinite number of terms arises in (6.65). But in this case, (6.65) cannot possibly represent a solution, because an infinite number of exponentials  $\exp(-\tau/\tau_j)$  would occur, with  $\tau_j$  as given in (6.76). To a given  $E$  there would, then, always be a corresponding  $j$ , namely

$$j \geq \frac{1}{E(1-\delta)}, \left( E \neq \frac{1}{\text{integer}} \right)$$

for which  $\tau_j$  would be negative. This would result in a term exponentially growing in time, thereby destroying the convergence of the series (6.65).

Solutions for other values than  $E = 1/k$ , ( $k = 1, 2, \dots$ ) have not been found so far.

It is instructive to plot  $h_1/A$  at  $\xi = 1 - \delta$  as a function of time  $\tau$ . A reasonable figure for  $E$  for a real glacier is  $E = 1$  and smaller. Since  $E$  characterizes the importance of diffusion, we shall compare results for  $E = 1$  and  $E = 0$ . Mathematical expressions for the former can be obtained from Equation (6.75); those for  $E = 0$  from Equation (6.48) by setting  $k = \frac{1}{2}$  and  $\delta = 0$ , the results being\*

$$\frac{h_1}{A}(\xi = 1 - \delta) = \begin{cases} \frac{1 - e^{-\tau}}{\delta(1 - e^{-\tau}) + e^{-\tau}}, & (E = 0), \\ \frac{1}{\delta} + \frac{e^{-\tau}}{1 - 2\delta} - \frac{(1 - \delta)e^{-2\delta\tau}}{\delta(1 - 2\delta)}, & (E = 1). \end{cases} \quad (6.77)$$

These two functions show a remarkably different behavior in time, although both tend in the limit  $\tau \rightarrow \infty$  to the same value  $1/\delta$ . Since the thickening at  $\xi = 0$  is  $h_1 = A$ , the eventual thickening of the snout is  $1/\delta$  times larger than that of the head. Figure 6.10, in which the results (6.77) are plotted along with those for  $E = \frac{1}{2}$  brings about very clearly the importance of diffusion, as the solution for  $E = 1$  contains two time scales, whereas in that for  $E = 0$  only one such scale occurs. The relaxation times are 1 and  $1/2\delta$ , respectively, the second being very much larger than the first, implying that the response to a change in the accumulation rate is much slower with diffusion than without. Since

\*Equation (6.48) is not non-dimensionalized. We must therefore formally replace  $(x, a_1, \varepsilon, t)$  by  $(\xi, A, 1, \tau)$ .

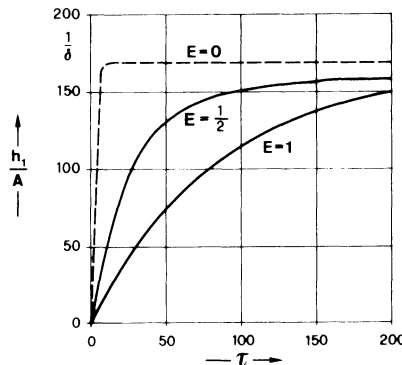


FIG. 6.10. Response  $h_1$  at the datum position of the snout for a step function of accumulation rate of magnitude  $A$ . The curve  $E = 0$  corresponds to the diffusionless case  $D_0 = 0$ . (Redrawn from [32].)

in our non-dimensionalized coordinates the time unit is approximately 5–10 years ( $\sigma \simeq 6$  years) and  $\delta \simeq 10^{-2}$  the slow relaxation time  $\sigma/2\delta \simeq 10^3$  is large, implying that an accumulation change in a human's lifetime may not have reached steady state for a thousand years. Responsible for this is diffusion. The long-time constant for  $E = 1$  has the practical significance that the glacier continues to respond to a climatic change for many hundreds of years after it has happened, which is quite contrary to the behavior when  $E = 0$ . Nye in an appendix of reference [32] provides support for this statement as he presents approximate calculations aiming at a proof that the large relaxation time also exists if only  $E \neq 0$ . His solution is reasonable for  $E$  close to 1. One could, therefore, be tempted to assume that shorter relaxation times could be obtained by lowering the constant  $E$ . This is, indeed, corroborated by the additional curve shown for  $E = \frac{1}{2}$ . Relaxation to the new steady state is somewhat faster than for  $E = 1$ , but to achieve an appreciable reduction,  $E$  would have to be considerably lower than 1. Lliboutry mentions that  $E = \frac{1}{4}$  is a reasonable value for Glacier de Saint Sorlin. An appreciable change of the long relaxation time is, however, not achieved thereby, as can easily be checked by using Equation (6.76). Nevertheless, authors on the subject frequently state that observations do not seem to support these results. Lliboutry [23] shares this view as he states that, "... the time lag in real glaciers should be a score of years, instead of several centuries. Actually the lag observed ... seems to be never longer than 10 years." In this writer's opinion, the discrepancy between theory and observation arises because observational evidence is applied to the wrong theoretical model. In the theoretical model treated above, the accumulation-rate function is position independent, whereas observed accumulation and ablation rates are always position-dependent. They cause the surface to bulge out. The motion of these bulges down-glacier takes place at a speed which is roughly four times

the speed of surface ice particles – of the order of several hundred meters a year. It is then indeed just a score of years until such a surface bulge will have reached the snout. One may then say that using a position-independent accumulation-rate function may be an unrealistic model for the described observational situation. On the other hand, long-term global climatic changes should be described by position-independent rather than position-dependent accumulation-rate functions.

(γ) *General solution for uniform accumulation rate*

(i) *Solution by integral techniques.* In this Section the differential equation (6.52) with coefficient functions (6.53), in which  $E = 1/k$ ,  $k = 1, 2, \dots$ , will be solved when the accumulation rate  $a_1(\xi, \tau)$  is uniform in  $\xi$ , but arbitrary in time  $\tau$ .

Prompted by the success of the polynomial solution (6.65) for the case that  $a_1(\tau)$  is given by the Heaviside function we try again with

$$h_1 = \sum_{k=0}^n H_k(\tau) \xi^k, \quad E = \frac{1}{m}, \quad (m = 1, \dots, n). \quad (6.78)$$

The differential equation that  $H_k$  must satisfy is then

$$L_k H_k = S_k a_1(\tau), \quad (6.79)$$

where the operator  $L_k$  and the quantity  $S_k$  are defined in Equations (6.67) and (6.68). Laplace transforms are again the appropriate vehicle to solve Equation (6.79), subject to the initial conditions (6.69). Instead of (6.70) one then obtains

$$\bar{H}_k(\omega) = \frac{S_k}{\prod_{j=0}^k (\omega + r_j)} \bar{a}_1(\omega) = S_k \sum_{j=0}^k \frac{A_j^k \bar{a}_1(\omega)}{\omega + r_j}. \quad (6.80)$$

Here, the expression to the far right of (6.80) has been obtained by using partial fraction, and assuming that all  $r_j$ 's are distinct. Inversion of Equation (6.80) is best performed by a term-by-term inversion of the expression to the far right, using the Laplace convolution theorem. This yields

$$H_k(\tau) = S_k \sum_{j=0}^k \frac{A_j^k}{r_j} (1 - e^{-r_j \tau}) \langle a_1(\tau) \rangle_j, \quad (6.81)$$

with

$$\langle a_1(\tau) \rangle_j \equiv \frac{r_j}{1 - e - r_j \tau} \int_0^\tau a_1(\tau') e^{r_j(\tau' - \tau)} d\tau'. \quad (6.82)$$

Here  $\langle a_1 \rangle_j$  is the time average of  $a_1$  weighted with  $e^{r_j \tau}$ . Substituting (6.81) into (6.78) yields the full solution for  $h_1(\xi, \tau)$ . Observe that the time dependency of  $h_1(\xi, \tau)$  appears in formula (6.81) in a remarkably simple form, because it is essentially given by a series of weighted time averages.

Consider a particular example and construct the exact solution for  $E = 1$  and  $E = \frac{1}{2}$ . Using the auxiliary quantities (6.73), Equations (6.81) and (6.82) yields

$$\begin{aligned} H_0 &= (1 - e^{-\tau}) \langle a_1 \rangle_0, \\ H_1 &= \frac{2}{1 - 2E(1 - \delta)} \left\{ (1 - e^{-\tau}) \langle a_1 \rangle_0 - \frac{1 - e^{-2[1-E(1-\delta)]\tau}}{2[1-E(1-\delta)]} \langle a_1 \rangle_1 \right\}, \\ H_2 &= \frac{3(1-E)}{2[1-2E(1-\delta)]} \left\{ \frac{1-e^{-\tau}}{1-3E(1-\delta)} \langle a_1 \rangle_0 - \right. \\ &\quad \left. - \frac{1-e^{-2[1-E(1-\delta)]\tau}}{[1-E(1-\delta)][1-4E(1-\delta)]} \langle a_1 \rangle_1 + \right. \\ &\quad \left. + \frac{1-e^{-3[1-2E(1-\delta)]\tau}}{3[1-3E(1-\delta)][1-4E(1-\delta)]} \langle a_1 \rangle_2 \right\}. \end{aligned} \quad (6.83)$$

When these expressions are substituted into Equation (6.78) an exact solution for  $E = 1$  and  $E = \frac{1}{2}$  will be obtained. The decaying exponentials may then be neglected for asymptotically large times. It is interesting to look at this asymptotic behavior more closely. For  $E = 1$  and  $E = \frac{1}{2}$  one obtains from Equations (6.83) and (6.78)

$$\begin{aligned} h_1(\xi, \tau) &\sim \langle a_1 \rangle_0 - \frac{2\xi}{1-2\delta} \left[ \langle a_1 \rangle_0 - \frac{1}{2\delta} \langle a_1 \rangle_1 \right] \quad (E = 1), \\ h_1(\xi, \tau) &\sim \langle a_1 \rangle_0 - \frac{2\xi}{\delta} \left[ \langle a_1 \rangle_0 - \frac{\langle a_1 \rangle_1}{1+\delta} \right] + \\ &\quad + \frac{3\xi}{4\delta} \left[ -\frac{2}{1-3\delta} \langle a_1 \rangle_0 + \frac{2}{(1+\delta)(1-2\delta)} \langle a_1 \rangle_1 + \right. \\ &\quad \left. + \frac{2}{3(1-3\delta)(1-2\delta)} \langle a_1 \rangle_2 \right] \quad (E = 1/2) \end{aligned} \quad (6.84)$$

or when evaluated at the snout  $\xi = 1 - \delta$ , and taking only the dominant terms in  $\delta$ ,

$$\begin{aligned} h_1(1-\delta, \tau) &\sim -\langle a_1 \rangle_0 + \frac{1}{\delta} \langle a_1 \rangle_1 + \langle a_1 \rangle_1 + \mathcal{O}(\delta) \quad (E = 1), \\ h_1(1-\delta, \tau) &\sim -\frac{7}{2\delta} \langle a_1 \rangle_0 + \left( \frac{7}{2\delta} - 4 \right) \langle a_1 \rangle_1 + \\ &\quad + \left( \frac{1}{2\delta} + 2 \right) \langle a_1 \rangle_2 + \mathcal{O}(\delta) \quad (E = 1/2). \end{aligned} \quad (6.85)$$

Multiplication of these with  $\text{cosec } \theta$  (see Figure 6.2) yields the asymptotic advance of the glacier. As an example, consider the Dirac-pulse accumulation

at  $\tau = 0$ ,  $a_1 = \Delta(\tau)$  (we write  $\Delta$  in order to avoid confusion with  $\delta$ , which has already been used). It then follows from (6.82) that  $\langle \Delta(\tau) \rangle_j = e^{(-r_j\tau)}$  and from (6.85)

$$\begin{aligned} h_1(1 - \delta, \tau) &\sim \frac{1}{\delta} e^{-r_1\tau} = \frac{1}{\delta} e^{-2\delta\tau} + \mathcal{O}(1) \quad (E = 1), \\ h_1(1 - \delta, \tau) &\sim \frac{1}{2\delta} e^{-r_2\tau} = \frac{1}{2\delta} e^{-3\delta\tau} + \mathcal{O}(1) \quad (E = 1/2), \end{aligned} \quad (6.86)$$

where terms of order  $\delta^0 = 1$  have been neglected and only terms with the largest relaxation time have been taken into account. The physical meaning of these equations is that, asymptotically, the glacier responds with a very large relaxation time reaching the final state at a very slow rate. In other words, a spatially-uniform change in climate will have an effect on a time scale of the order of  $\sigma/\delta$  where  $\sigma = 6-10$  years. For  $E = 1$  and arbitrary  $a_1$ , these inferences can also be drawn from relations (6.85)<sub>1</sub>, because if  $\langle a_1 \rangle_0$  and  $\langle a_1 \rangle_1$  are comparable then the term involving  $\langle a_1 \rangle_1$  is dominant. Similar, though somewhat less conclusive are the results when  $E = 1/2$ .

More surprising than this is the fact how  $\partial h_1 / \partial \tau$  depends on  $\langle a_1 \rangle_j$ . Intuitively, one would expect that only the recent past would contribute to  $\partial h_1 / \partial \tau$ . This is easily seen not to be true, if (6.84)<sub>1</sub> is differentiated with respect to time. This gives for  $E = 1$

$$\frac{\partial h_1}{\partial \tau}(\xi, \tau) \sim \frac{\partial \langle a_1 \rangle_0}{\partial \tau} - \frac{2\xi}{1-2\delta} \left\{ \frac{\partial \langle a_1 \rangle_0}{\partial \tau} - \frac{1}{2\delta} \frac{\partial \langle a_1 \rangle_1}{\partial \tau} \right\},$$

or, since (6.82) implies  $\partial \langle a_1 \rangle_j / \partial \tau \sim r_j(a_1 - \langle a_1 \rangle_j)$  as  $\tau \rightarrow \infty$ ,

$$\left. \begin{aligned} \frac{\partial h_1}{\partial \tau}(\xi, \tau) &\sim a_1(\tau) - \langle a_1(\tau) \rangle_0 - \frac{2\xi}{1-2\delta} [-\langle a_1(\tau) \rangle_0 + \langle a_1(\tau) \rangle_1], \\ \frac{\partial h_1(1-\delta, \tau)}{\partial \tau} &\sim a_1(\tau) + \langle a_1(\tau) \rangle_0 - 2\langle a_1(\tau) \rangle_1 \\ &= (a_1(\tau) - \langle a_1(\tau) \rangle_1) + (\langle a_1(\tau) \rangle_0 - \langle a_1(\tau) \rangle_1). \end{aligned} \right\} \quad (6.87)$$

This tells us that the rate of advance,  $\partial h_1 / \partial \tau$  depends largely on the long time average. Hence to determine  $\partial h_1 / \partial \tau$  asymptotically, the entire long-range history of  $a_1(\tau)$  must be known. This is in a way very unfortunate, because it states that in order to predict the time evolution of the glacier snout measurements that last much longer than one human's life must be considered.

(ii) *Frequency response.* In the preceding subsection, the influence of a sudden change in accumulation rate was analysed. When the accumulation rate function is periodic in time, but still position-independent, then a Fourier decomposition might be used to write  $a_1 = \sum_{n=1}^{\infty} A_n e^{i\omega_n \tau}$  where  $A_n$  are the Fourier coefficients and  $\omega_n$  the corresponding frequencies.

It suffices to analyse a single Fourier component, whence one can write

$$a_1 = A_\omega e^{i\omega\tau}, \quad h_1 = H(\xi) e^{i\omega\tau}. \quad (6.88)$$

Equation (6.52)<sub>1</sub> then transforms into the ordinary differential equation

$$\frac{d}{d\xi} \left[ C_0(\xi)H - D_0(\xi) \frac{dH}{d\xi} \right] + i\omega H = A_\omega \quad (6.89)$$

subject to the boundary conditions

$$H(0) = 0, \quad H(1 - \delta) = \text{finite}. \quad (6.90)$$

Solutions to (6.89) and (6.90) are sought in the form

$$H(\xi) = \sum_{k=1}^{\infty} H_k \xi^k, \quad (6.91)$$

in which  $H_k$  can be shown to have the form

$$H_0 = \frac{A_\omega}{1 + i\omega}, \quad (6.92)$$

$$H_k = \frac{(k+1)!(1-E)^{k-1}}{\prod_{j=1}^k \{(j+1)[1-E(1-\delta)] + i\omega\}} H_0, \quad k \geq 1.$$

As is seen from these formulas, if  $E = 1$ ,  $H_k = 0$  for all  $k \geq 2$ . Surprisingly, the sum (6.91) does not terminate for any value of  $E$  other than  $E = 1$ . Convergence follows from the quotient criterion:

$$\lim_{n \rightarrow \infty} \left| \frac{H_{n+1}}{H_n} \right| = \lim_{n \rightarrow \infty} \left| \frac{(n+2)(1-E)}{(n+2)(1-E(1-\delta)) + i\omega} \right| \rightarrow \frac{1}{|1 + (E\delta)/(1-E)|}.$$

For the series (6.91) to be convergent in the interval  $0 \leq \xi \leq 1$  it is thus necessary that  $E < 1$ . This result is not surprising; nevertheless, it is interesting insofar as a solution has been found which is valid for all  $E \in [0, 1]$ . This was not so when direct integration was used. There,  $E$  had to be limited to  $E = 1/k$  where  $k$  is an integer. It is also interesting to observe that the only polynomial solution of (6.91) is for  $E = 1$  in which case  $H(\xi)$  is linear in  $\xi$ , namely

$$H(\xi) = \frac{A_\omega}{(1+i\omega)(2\delta+i\omega)} [2(\xi + \delta) + i\omega] \quad (E = 1). \quad (6.93)$$

At the snout  $\xi = (1 - \delta)$ , it becomes

$$H(\xi = 1 - \delta) = \frac{A_\omega (2 + i\omega)}{(1 + i\omega)(2\delta + i\omega)} = |H|_\omega e^{-i\phi_\omega} \quad (E = 1), \quad (6.94)$$

where the modulus  $|H|_\omega$  and the phase angle  $\phi_\omega$  are given by

$$|H|_\omega = A_\omega \sqrt{\frac{4 + \omega^2}{(1 + \omega^2)(4\delta^2 + \omega^2)}}, \quad \tan \phi_\omega = \frac{\omega(2(1 + \delta) + \omega^2)}{4\delta - \omega^2(1 - 2\delta)} \quad (E = 1). \quad (6.95)$$

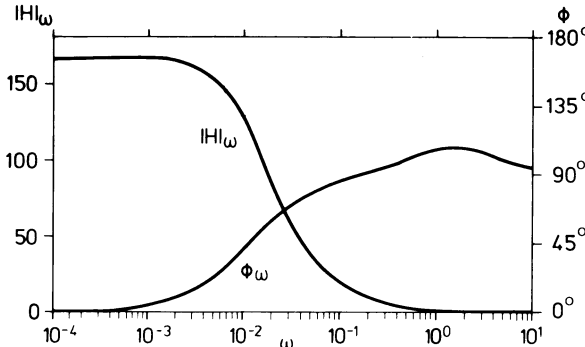


FIG. 6.11.  $|H|_\omega$  and  $\phi_\omega$  plotted against a dimensionless frequency for the case  $E = 1$ . Notice that frequencies  $\omega \geq 10^1$  may be filtered away.

In the above,  $0 < \phi_\omega < \pi$ , so  $\phi_\omega$  is the phase lag of  $h_1$  on  $A_\omega$ .  $|H|_\omega$  and  $\phi_\omega$  are shown in Figure 6.11 plotted against the frequency  $\omega$  on a logarithmic scale, taking  $\delta = 0.006$ . At very low frequencies, the modulus is frequency independent and large. At frequencies  $\omega$  larger than  $10^1$ ,  $|H|_\omega$  virtually vanishes so that in any time response all frequencies larger than  $10^1$  may safely be filtered out. The transition domain is roughly  $10^{-3} \leq \omega \leq 1$ . At low frequencies  $a_1$  and  $h_1$  are in phase. At  $\omega \simeq 10^{-3}$   $\phi_\omega$  grows, reaches a maximum of about  $115^\circ$  and approaches  $90^\circ$  as  $\omega$  becomes large. At large frequencies  $h_1$  lags behind  $a_1$  by  $90^\circ$ . For values of  $E$  other than  $E = 1$  modulus  $|H|_\omega$  and phase lag angle  $\phi_\omega$  have not been plotted so far. This is, however, a simple matter as the solution for  $0 < E < 1$  is explicitly known.

Results like those shown in Figure 6.11 will allow the construction of the response of our model glacier to any spatially uniform time-periodic accumulation rate function. The solution will be a summation over all Fourier components,

$$h_1(\xi, \tau) = \sum_{j=1}^{\infty} \left\{ \sum_{k=1}^{\infty} (H_k^{(\omega_j)} \xi^k) e^{i\omega_j \tau} \right\}, \quad (6.96)$$

where  $H_k^{(\omega_j)}$  for each  $\omega_j$  is given by Equations (6.92). Similarly,  $H$  evaluated at the snout can be written as

$$H(\xi = 1 - \delta) = \sum_{j=1}^{\infty} |H|_{\omega_j} e^{-i\phi_{\omega_j}}, \quad (6.97)$$

where the moduli  $|H|_{\omega_j}$  and the phase lag angles  $\phi_{\omega_j}$  can be obtained from a plot analogous to that shown in Figure 6.11. (Alternatively, the explicit algebraic expressions might be used to evaluate them.)

(d) *The inverse problem – calculation of climate from variations of the snout.* In all preceding calculations, the accumulation rate  $a_1$  was a prescribed

function of position and time and the perturbation in height  $h_1$  was searched for. It was found that in order to be able to determine the asymptotic behavior of the height  $h_1$ , the entire history of  $a_1$  had to be known. Now we invert the problem, that is, we assume that  $h_1$  is known as a function of position and time. Our aim is in determining the 'climate'  $a_1$  that has caused this variation in height. Of course, if  $h_1$  would be known, both as a function of position and time, a direct substitution into Equation (6.52) would determine  $a_1$  as a function of position and time. Generally, one has no access to the functional relationship of  $h_1$  at all places in the glacier. The reason is that measurements for variations in height are extremely difficult except at the snout whose position can directly be related to  $h_1$ . On the basis of such limited knowledge, we therefore assume  $a_1$  to be uniform and may then restrict our considerations to the snout region.

Consider the model glacier with  $E = 1$ . The general solution of  $h_1$  for a given  $a_1$  as  $\tau \rightarrow \infty$  is then

$$h_1(\xi, \tau) \sim \langle a_1(\tau) \rangle_0 - \frac{2\xi}{1-2\delta} \left[ \langle a_1(\tau) \rangle_0 - \frac{1}{\delta} \langle a_1(\tau) \rangle_1 \right]. \quad (6.98)$$

The time-rate of this expression has been determined in Equation (6.87):

$$\frac{\partial h_1(\xi, \tau)}{\partial \tau} \sim a_1(\tau) - \langle a_1(\tau) \rangle_0 - \frac{2\xi}{1-2\delta} [-\langle a_1(\tau) \rangle_0 + \langle a_1(\tau) \rangle_1] \quad (6.99)$$

and the second time derivative is

$$\begin{aligned} \frac{\partial^2 h_1(\xi, \tau)}{\partial \tau^2} \sim & \dot{a}_1(\tau) - a_1(\tau) + \langle a_1(\tau) \rangle_0 - \\ & - \frac{2\xi}{1-2\delta} [(2\delta-1)a_1(\tau) + \langle a_1(\tau) \rangle_0 - 2\delta \langle a_1(\tau) \rangle_1]. \end{aligned} \quad (6.100)$$

Equations (6.98)–(6.100) are three equations involving  $h_1$ , its first and second time derivatives,  $a_1$ ,  $\dot{a}_1$  and the averages  $\langle a_1 \rangle_0$  and  $\langle a_1 \rangle_1$ . Eliminating the latter two gives a differential equation for  $a_1$  which when written down for  $\xi = 1 - \delta$  becomes

$$\dot{a}_1 + 2a_1 = \ddot{h}_1 + (1+2\delta)\dot{h}_1 + 2\delta h_1 = f(\tau), \text{ say.}$$

With the initial condition  $a_1(0) = 0$  its solution is

$$a_1(\tau) = e^{-2\tau} \int_0^\tau e^{2\tau'} (\ddot{h}_1 + (1+2\delta)\dot{h}_1 + 2\delta h_1) d\tau',$$

or upon integration by parts in appropriate terms

$$a_1(\tau) = \dot{h}_1(\tau) - (1-2\delta)h_1(\tau) + (1-\delta)\langle h_1(\tau) \rangle_0 - e^{-2\tau}(2\delta h_1(0) + \dot{h}_1(0)), \quad (6.101)$$

where

$$\langle h_1(\tau) \rangle_0 = \frac{2}{1 - e^{-2\tau}} \int_0^\tau h_1(\tau') e^{2(\tau' - \tau)} d\tau' \xrightarrow{\tau \rightarrow \infty} 2 \int_0^\tau h_1(\tau') e^{2(\tau' - \tau)} d\tau'. \quad (6.102)$$

The last term in (6.101) describes the influence of the initial condition. Asymptotically this term is negligibly small, whence  $\delta \ll 1$ , (6.102) may be approximated as

$$a_1(\tau) \sim \dot{h}_1(\tau) - h_1(\tau) + \langle h_1(\tau) \rangle_0. \quad (6.103)$$

Thus  $a_1(\tau)$  is determined by the height  $h_1$ , its time rate of change  $\dot{h}_1$  and its history  $\langle h_1 \rangle_0$ . However, because the exponential in (6.102) has the relaxation time  $\tau = 0.5$ , the values of  $h_1$  at the distant past play only a very minor role. In other words, the memory of  $a_1$  to the distant past of  $h_1$  fades exponentially with a relaxation time of 0.5 units of time. This is just a few years, when expressed in terms of  $\sigma$ .

This result is interesting, because it tells us that a record of the glacier snout during the recent past will accurately determine the accumulation rate. Hence, measuring positions of a glacier snout for only a few years will determine the accumulation rate. This is remarkably different from the previous results. To determine the present value of  $h_1$ , the history of  $a_1$  over many hundred years had to be known. This may also be stated in the following way: Whereas the memory of the glacier to changes in the accumulation rate is very long and may last for several hundred years, the memory of the accumulation rate as a function of  $h_1$  is very short. From a practical point of view, this means that there is only little hope that the advance and retreat of a glacier to climatic changes can be determined by measuring the accumulation rates continuously. On the other hand, recording the position of the snout for a few years allows us to estimate the accumulation rate quite accurately. This argument neglects spatial variations which lead to surface bulges travelling down glacier that may yield snout movement of a short duration.

#### 4. General Treatment for an Arbitrary Valley Glacier

So far, treatment of the response of a glacier to seasonal and climatic changes has been restricted to a model glacier. No attempt was made to demonstrate how an arbitrary glacier or ice sheet could be handled. Furthermore, attention was restricted to a spatially-uniform accumulation-rate function. In order to apply the theory to real glaciers, several techniques will now be discussed that may be used in an integration approach of the governing equations. To this end, let us go back to the basic linearized equations (6.16) which read

$$\frac{\partial Q_1}{\partial x} + B_0 \frac{\partial h_1}{\partial t} = B_0 a_1, \quad Q_1 = B_0 C_0 h_1 - B_0 D_0 \frac{\partial h_1}{\partial x}. \quad (6.104)$$

Boundary and initial conditions these equations are subject to are

$$Q_1(x = 0) = 0, \quad h_1(x = L) = \text{finite}, \quad h_1(t = 0) = 0. \quad (6.105)$$

$Q_1$  is the perturbation discharge,  $h_1$ , as before, the perturbation of the height,  $B_0$  is the width and  $C_0$  and  $D_0$  are the same coefficients as before,  $C_0$  being a speed,  $D_0$  a diffusivity. When writing down Equation (6.104)<sub>1</sub> a change in width with height was neglected. This, strictly, requires the perturbations to be small.

The system (6.104) with known coefficient functions  $C_0$  and  $D_0$  is singular as  $C_0$  and  $D_0$  both vanish at the head and  $D_0$  vanishes at the snout. This fact will require special attention in the treatment of boundary conditions (6.105). Notice further that the Equations (6.104) and (6.105) are not non-dimensionalized as they will now be applied to a real glacier.

Several integration methods suggest themselves as solution procedures of the initial-boundary-value problem (6.104) and (6.105). Among these, mention might be made of the following possibilities:

- (i) Fourier analysis in time: This works when time series of accumulation-rate functions are sufficiently long and initial conditions sufficiently far distant in the past to become irrelevant. Equations (6.104) and (6.105) are then transformed into a boundary-value problem in frequency domain.
- (ii) Direct integration techniques might be applied by either constructing the Green's function corresponding to the initial-boundary-value problem, or else by discretizing in  $x$ -space and using forward integration in time. This is probably the most efficient technique, but has never been used.

(a) *Fourier analysis in time*

The system (6.104) is driven by the accumulation rate function  $a_1(x, t)$ , which will be assumed to be separable in the form

$$a_1(x, t) = \sum_{v=1}^{\infty} X_v(x) \mathcal{A}_v e^{i\Omega_v t}.$$

$X_v$  is the  $v$ th amplitude function, and  $\mathcal{A}_v$  a reference amplitude;  $\Omega_v$  is the  $v$ th frequency. It has been capitalized to contrast it with the dimensionless frequency that was used before and was denoted by  $\omega$  ( $\Omega = \omega/\sigma$ ). In view of the linearity of the system, (6.104) and (6.105), attention may be restricted to one single Fourier component only. The index  $v$  may then be deleted and we may write

$$\begin{aligned} a_1(x, t) &= X(x) \mathcal{A} e^{i\Omega t}. \\ h_1(x, t) &= \mathcal{H}(x, \Omega) e^{i\Omega t}, \\ Q_1(x, t) &= \mathcal{Q}(x, \Omega) e^{i\Omega t}. \end{aligned} \quad (6.106)$$

$\mathcal{H}$  and  $\mathcal{Q}$  are the complex-valued response functions and must satisfy the differential equations

$$\frac{d\mathcal{Q}}{dx} + i\Omega B_0 \mathcal{H} = B_0 X \mathcal{A}, \quad \mathcal{Q} = B_0 C_0 \mathcal{H} - B_0 D_0 \frac{d\mathcal{H}}{dx}, \quad (6.107)$$

subject to the boundary conditions

$$\mathcal{Q}(0) = 0, \quad \mathcal{H}(L) = \text{finite}. \quad (6.108)$$

Our goal is to solve the boundary-value problem (6.107) and (6.108). A computer adapted method will be discussed in the next section. Here we demonstrate how solutions can be obtained if  $\Omega$  is either very small or else very large.

(x) *Low-frequency response.* If the frequency in Equations (6.107) is sufficiently low, we may seek a solution in terms of a Taylor series expansion

$$\mathcal{H}(x, \Omega) = \mathcal{A}(\Omega) \sum_{p=0}^{\infty} \mu_p(x) (i\Omega)^p. \quad (6.109)$$

Here,  $\mu_p(x)$  are the coefficient functions to be determined. The series (6.109) is assumed to converge sufficiently fast so that it may be truncated at a finite number of terms. Substituting (6.109) into (6.107)<sub>1</sub> gives a first-order differential equation, which can easily be integrated subject to the boundary condition  $\mathcal{Q}(0) = 0$ , yielding an expression for  $\mathcal{Q}(x)$ . Another expression for  $\mathcal{Q}$  can be obtained from (6.107)<sub>2</sub> and (6.109). Equating the resulting relations and comparing coefficients of equal powers in  $(i\Omega)$ , finally yields the recursive differential equations

$$D_0 \frac{d\mu_j}{dx} - C_0 \mu_j = \frac{1}{B_0} \int_0^x B_0 \mu_{j-1} d\xi, \quad j = 0, 1, 2 \dots \quad (6.110)$$

in which  $\mu_{-1} \equiv -X(x)$  is known. Given an appropriate boundary condition at  $x = 0$  or  $x = L$ ,  $\mu_j$  may therefore be determined in an iterative procedure. In order to be able to actually perform the integration, a boundary condition at either the glacier head or glacier snout must be known. The boundary condition at the head is  $\mathcal{Q}(0) = 0$ , but it has been used already in the determination of (6.110). Hence, the integrations in (6.110) must be carried out backwards, from the snout to the head, and the boundary condition is to be applied at the snout. It is readily obtained from Equations (6.110) themselves if it is remembered that  $D_0(L) = 0$ , so that all Equations (6.110) are singular. Hence, for regular  $\mu_j$ , (6.110) at  $x = L$  implies

$$\mu_j(L) = \frac{-1}{B_0 C_0} \Big|_L \int_0^L B_0 \mu_{j-1} d\xi = \mu_j^{(0)}. \quad (6.111)$$

On the assumption that  $\mu_{j-1}(x)$  has been determined, integration for  $\mu_j(x)$  proceeds as follows: In a first step, standard integration routine is used to evaluate

$$f_j(x) = \frac{1}{B_0(x)} \int_0^x B_0(\xi) \mu_{j-1}(\xi) d\xi, \quad 0 \leq x \leq L \quad (j = 0, 1, \dots). \quad (6.112)$$

This will yield both the driving function for the differential equation governing  $\mu_j(x)$  and the boundary condition for it. In a second step, the variable transformation  $y = L - x$  will transform Equations (6.110) to

$$\frac{d\mu_j}{dy} = -\frac{C_0(y)}{D_0(y)} \mu_j - \frac{f_j(y)}{D_0(y)} = F(\mu_j, y), \quad \mu_j(y=0) = \mu_j^{(0)} \quad (j = 0, 1, \dots). \quad (6.113)$$

To integrate this differential equation, the method of integrating factors does not work. A standard integration routine should therefore be used with appropriate modification, since the equation is singular at  $y = 0$  (remember  $D_0(y=0) = 0$ ). Backward differencing of (6.113) near  $y = 0$  yields

$$\mu_j(\Delta y) = \left\{ \mu_j^{(0)} - \frac{f_j(\Delta y)}{D_0(\Delta y)/\Delta y} \right\} \Big/ \left\{ 1 + \frac{C_0(\Delta y)}{D_0(\Delta y)/\Delta y} \right\}.$$

This formula now allows determination of  $\mu_j$  a small distance  $\Delta y$  from the boundary, where all coefficients of (6.113) are regular. Integration can, thus, be proceeded with a standard integration routine.

We could, if we so desired, test our approach using the model glacier of Section 3. Alternatively for  $X = 1$  exact solutions for  $E = 1/k$ ,  $k = 1, 2, \dots$  were found in the previous section. The function that corresponds to  $\mathcal{H}$  was called  $H$  there. For  $E = 1$  the solution is given in (6.94)\*, and it is obvious that the low-frequency solution of this subsection must agree with that obtained there, if the latter is expanded in terms of a Taylor series expansion of  $i\omega$ . From these considerations, we can easily find an estimate of the convergence of the series (6.109). When (6.94) is expanded in terms of  $i\omega$ , a Taylor series of  $(2\delta + i\omega)^{-1}$  must be used, which obviously is only convergent if

$$\omega < 2\delta \quad \text{or} \quad \Omega < 2\delta/\sigma. \quad (6.114)$$

For  $\sigma \sim 10a$ ,  $\delta = 0.01$  we obtain  $\Omega < 2 \times 10^{-3}$  which is extremely small.

The key idea, how the range of convergence could be substantially widened, is brought by the form of Equation (6.94) itself. Its numerator contains only the term  $(2 + i\omega)$  whose reciprocal can also be expanded in a Taylor series, the radius of convergence of which is much larger, namely of the order  $2/\sigma$ . This is a factor of  $10^2$  larger than (6.114). Consequently, we

\*(6.94) reads

$$H(1 - \delta) = \mathcal{H}(1 - \delta) = \frac{A(2 + i\omega)}{(1 + i\omega)(2\delta + i\omega)}.$$

rather look for a series expansion of  $\mathcal{A}(\Omega)/\mathcal{H}(x, \Omega)$  than  $\mathcal{H}(x, \Omega)/\mathcal{A}(\Omega)$  as was done in (6.109). Such an expansion may be written as

$$\frac{\mathcal{A}(\Omega)}{\mathcal{H}(x, \Omega)} = \sum_{p=0}^{\infty} \lambda_p(x) (i\Omega)^p, \quad (6.115)$$

so that

$$\left\{ \sum_{p=0}^{\infty} \mu_p(x) (i\Omega)^p \right\} \left\{ \sum_{q=0}^{\infty} \lambda_q(i\Omega)^q \right\} = 1,$$

or

$$\sum_{m=0}^{\infty} \sum_{p=0}^m \mu_p(x) \lambda_{m-p}(x) (i\Omega)^m = 1,$$

from which we obtain

$$\lambda_0 \mu_0 = 1, \quad \sum_{p=0}^m \mu_p(x) \lambda_{m-p}(x) (i\Omega)^m = 0. \quad (6.116)$$

If the  $\mu_j$ 's,  $j = 1, 2, \dots$  are known, Equation (6.116) allows determination of the  $\lambda$ 's in succession from the  $\mu$ 's. When  $\mathcal{H}$  is determined from (6.115), the radius of convergence is about a hundred times larger than for (6.109). The reader may show this using the example of our model glacier.

(β) *High-frequency response.* For high frequencies, an *asymptotic representation* of the form

$$\mathcal{H}(x, \Omega) = \mathcal{A}(\Omega) \sum_{p=0}^{\infty} v_p(x) (i\Omega)^{-p} \quad (6.117)$$

may be the appropriate procedure to determine the solutions to (6.107). By substituting (6.117) into (6.107) two different expressions for  $d\mathcal{L}/dx$  may be obtained from a comparison of which the following recurrence relations are obtained:

$$\begin{aligned} B_0 v_0(x) &= 0, & X - v_1(x) &= 0, \\ v_{j+1}(x) &= -\frac{1}{B_0} \frac{d}{dx} \left( B_0 C_0 v_j(x) - B_0 D_0 \frac{dv_j(x)}{dx} \right). \end{aligned} \quad (6.118)$$

No integration is needed to solve them. This is interesting because it means that physically the high-frequency response is independent of boundary conditions.

Of course, the above high-frequency response and the convergence properties of the respective series can again be tested using our special model of Section 3. Indeed the high-frequency approximation here must produce the

same solution as is obtained when Equation (6.94) is expanded in terms of  $1/i\omega$ . We leave the proof as an exercise to the reader and restrict ourselves here to an estimate of the radius of convergence. To this end, we write (6.94) as

$$H(1 - \delta) = A \frac{(1 + 2/(i\omega))}{(1 + 1/(i\omega))(1 + 2\delta/(i\omega))i\omega} \quad (6.119)$$

and obtain as range of convergence

$$\omega > 1 \quad \text{or} \quad \Omega > 1/\sigma. \quad (6.120)$$

This result is remarkable because we have already found a low-frequency series expansion, namely (6.115), which converges in our model glacier for  $\Omega < 2/\sigma$  and have just shown that (6.117) converges for  $\Omega > 1/\sigma$ . The two domains of convergence overlap and thus a numerical scheme has been found which covers the entire frequency spectrum. It requires determination of the functions  $\mu_j$  by a forward integration, the evaluation of the associated functions  $\lambda_j$ , and that of the functions  $v_j$ . *The evaluation is independent of frequency.*

(γ) *Use of the results.* It has just been observed that a frequency analysis need not be performed for the determination of the functions  $\mu_j$ ,  $\lambda_j$  and  $v_j$ . This is a great advantage as these functions depend only on the spatial part of the accumulation rate  $X$ , on  $B_0$ ,  $C_0$  and  $D_0$  and can be determined once and for all if a particular glacier is given and  $X$  is prescribed. However, the spatial distribution function  $X$  may be frequency dependent. If it is not, in other words, if  $a_1(x, t) = X(x)\Theta(t) = X(x)\sum_q \mathcal{A}_q e^{i\Omega_q t}$  the above frequency analysis offers an interesting approach to analyse snout advance and retreat data. To see this, consider a low frequency  $\Omega_q$ . The response of the glacier to an accumulation rate of this frequency is then given by (6.115), or

$$\Theta_q \equiv \mathcal{A}(\Omega_q) e^{i\Omega_q t} = \mathcal{H}(x, \Omega_q) e^{i\Omega_q t} \sum_{p=0}^{\infty} \lambda_p(i\Omega_q)^p. \quad (6.121)$$

The left-hand side of this expression is the  $q$ th Fourier component of the function  $\Theta(t)$  introduced above. The right-hand side may be written as  $\sum_{p=0}^{\infty} \lambda_p(x) d^p H_q / dt^p$ , (where  $d^0 H_q / dt^0 \equiv H_q$ ). Clearly,  $H_q$  is the  $q$ th Fourier component of  $h_1$ . Hence, we may write

$$\Theta_q = \sum_{p=0}^{\infty} \lambda_p(x) \frac{d^p H_q}{dt^p}. \quad (6.122)$$

Summation over all  $q$ , thereby observing that  $\lambda_p$  does not depend on frequency, yields

$$\Theta(t) = \sum_{q=0}^{\infty} \sum_{p=0}^{\infty} \lambda_p \frac{d^p H_q}{dt^p} = \sum_{p=0}^{\infty} \lambda_p \frac{d^p}{dt^p} \sum_{q=0}^{\infty} H_q = \sum_{p=0}^{\infty} \lambda_p \frac{d^p h_1}{dt^p}. \quad (6.123)$$

An analogous argument, but now used with the series (6.109), gives

$$h_1(x, t) = \sum_{p=0}^{\infty} \mu_p(x) \frac{d^p \Theta(t)}{dt^p}. \quad (6.124)$$

In these formulas, the definitions  $h_1 \equiv d^0 h_1 / dt^0$  and  $\Theta \equiv d^0 \Theta / dt^0$  are applied.

The results (6.123) and (6.124) are interesting insofar as they provide the answers to inverse problems. For instance, if we have continuously measured the motion of the snout of the glacier, (6.123) delivers its climate. Equation (6.124) solves the inverse problem. This result is of lesser practical importance. Of course, since (6.123) and (6.124) are correct only for low frequencies, the high frequencies of the data must be filtered out before they are used in (6.123) and (6.124). This is a disadvantage and makes the method difficult to handle. An example how to apply the method is given by Nye [34].

The boundary-value problem (6.108) can also be solved by direct integration, valid for all frequencies. Because of its linearity the ‘initial value approach’ is advantageous. In this approach system (6.107) is solved twice by subjecting it to the end conditions

$$\begin{aligned} \mathcal{H}^{(1)}(L) &= (1.0), & \mathcal{Q}^{(1)}(L) &= B_0(L)C_0(L)\mathcal{H}^{(1)}(L), \\ \mathcal{H}^{(2)}(L) &= (0.1), & \mathcal{Q}^{(2)}(L) &= B_0(L)C_0(L)\mathcal{H}^{(2)}(L) \end{aligned}$$

and, for each, by integrating backwards,  $\mathcal{Q}(x = 0)$  can be calculated. The corresponding values shall be denoted by  $\mathcal{Q}^{(1)}(0)$  and  $\mathcal{Q}^{(2)}(0)$ , respectively. Because of the linearity of the system, one may then write  $\mathcal{Q}(0) = \alpha + \beta\mathcal{H}(L)$  where  $\alpha$  and  $\beta$  can be evaluated, when the two initial conditions are substituted. Imposing the boundary condition  $\mathcal{Q}(0) = 0$  gives  $0 = \alpha + \beta\mathcal{H}(L)$  which, finally, yields a value for  $\mathcal{H}(L)$  appropriate to satisfy both boundary conditions (6.108). This integration procedure, which is standard in numerical analysis, see [45], has been used by Nye [35] and Untersteiner and Nye [42] to predict the climatic response of actual glaciers.

### (b) Direct integration methods

The conceivably best approach to numerically treat the initial boundary value problem (6.104) and (6.105) is to discretize the system in  $x$  and to integrate the emerging first-order system in time. In numerical analysis this is called the *method of line*, see Szidarovskiy and Yakowitz [45]. We start from the two-point boundary value problem

$$\frac{\partial h_1}{\partial t} + \frac{1}{B_0} \frac{\partial}{\partial x} \left[ B_0 C_0 h_1 - B_0 D_0 \frac{\partial h_1}{\partial x} \right] = a_1(x, t), \quad (6.125)$$

$h_1(0, t)$  and  $h_1(L, t)$  are finite,

$$h_1(x, 0) = 0.$$

To implement the discretization the interval  $0 \leq x \leq L$  is divided into a series of  $(N + 1)$  subintervals separated by the points  $x_j$  ( $j = 0, 1, \dots, N + 1$ ). The unknown function  $h_1(x)$  is then replaced by the discretized unknowns  $h_1(x_j) = y_j$  where  $y_0 = h(x_0) = h(0)$  and  $y_{N+1} = h_1(x_{N+1}) = h(L)$  are treated as known from the boundary conditions. How they are determined will be shown in a moment. Spatial derivatives of  $h_1$  at the inner points  $x_1, \dots, x_N$  will be replaced by finite difference approximations. Defining then the vectors

$$\mathbf{y} \equiv (y_1, y_2, \dots, y_N)^T, \quad \mathbf{a} \equiv (a_1(x_1, t), a_1(x_2, t), \dots, a_1(x_N, t))^T. \quad (6.126)$$

it is easy to see that Equation (6.125)<sub>1</sub> can be written as the vector differential equation

$$\dot{\mathbf{y}}(t) = \mathbf{A}\mathbf{y} + \mathbf{y}_B + \mathbf{a}(t) = \mathbf{f}(\mathbf{y}, t), \quad \mathbf{y}(0) = \mathbf{0}, \quad (6.127)$$

where  $\mathbf{A}$  is a  $N \times N$ -matrix and  $\mathbf{y}_B$  a vector involving the boundary perturbations  $h_0 = y_0$ ,  $h(L) = y_{N+1}$ . Equations (6.127) would form an initial-value problem if  $\mathbf{y}_B$  were known.

It remains thus to show that the boundary conditions (6.127)<sub>2</sub> can be implemented in this finite difference approximation. To investigate the boundary behavior of  $h_1(x)$  near  $x = 0$ , let us write

$$\left. \begin{array}{l} B_0(x) = B_1 + \mathcal{O}(x), \quad B_1 > 0, \\ C_0(x) = C_1 x + \mathcal{O}(x^2), \quad C_1 > 0, \\ D_0(x) = d_1 x^2 + \mathcal{O}(x^3), \quad d_1 > 0, \\ a_1(x, t) = a_1^I(t) + \mathcal{O}(x), \end{array} \right\} \quad 0 \leq x \ll L$$

and search for a power series solution

$$h_1(x, t) = y_0(t) + \mathcal{O}(x), \quad 0 \leq x \leq L.$$

Substituting the above representations into the differential Equation (6.125) and collecting all terms of order  $x^0$  yields

$$\dot{y}_0 + C_1 y_0 = a_1^I(t), \quad y_0(0) = 0 \quad (6.128)$$

as a differential equation and initial condition for  $y_0$ , whose solution is

$$y_0(t) = \int_0^t a_1^I(\tau) e^{-C_1(t-\tau)} d\tau; \quad (6.129)$$

given the function  $a_1^I(\tau)$  this determines  $h_1(x=0) = y_0(t)$  and guarantees, furthermore, that  $y_0$  remains bounded, as it must.

To find the boundary condition at  $x = L$ , a similar approach is taken. First we write the differential equation in terms of the variable  $\bar{x} = L - x$

and write again

$$\left. \begin{aligned} B_0(\bar{x}) &= B_{\text{II}} + \mathcal{O}(\bar{x}), & B_{\text{II}} > 0, \\ C_0(\bar{x}) &= C_{\text{II}} + C'_{\text{II}}\bar{x} + \mathcal{O}(\bar{x}^2), & C_{\text{II}} > 0, \\ D_0(\bar{x}) &= d_{\text{II}}\bar{x} + \mathcal{O}(\bar{x}^2), & d_{\text{II}} > 0, \\ a_1(\bar{x}) &= a_1^{\text{II}} + \mathcal{O}(\bar{x}) \end{aligned} \right\} \quad 0 \leq \bar{x} \ll L.$$

A solution bounded for  $\bar{x}$  near 0 is again sought in the form of a power series

$$h_1(\bar{x}, t) = y_{N+1}(t) + y'_{N+1}(t)\bar{x} + \mathcal{O}(\bar{x}^2), \quad 0 \leq \bar{x} \ll L \quad (6.130)$$

and it can again be shown that by substituting the above representation into the differential Equation (6.125) that  $y_{N+1}$  must obey the initial-value problem

$$\begin{aligned} \dot{y}_{N+1}(t) - C'_{\text{II}}y_{N+1}(t) - [C_{\text{II}} + d_{\text{II}}]y'_{N+1}(t) &= a_1^{\text{II}}(t), \\ \dot{y}_{N+1}(0) &= 0. \end{aligned}$$

This equation cannot be integrated because  $y'_{N+1}(t)$  is unknown. However, since

$$y_N(t) \simeq y_{N+1}(t) + y'_{N+1}(t)(x_{N+1} - x_N)$$

we also have

$$\begin{aligned} \dot{y}_{N+1} &= C'_{\text{II}}y_{N+1}(t) + \frac{C_{\text{II}} + d_{\text{II}}}{x_{N+1} - x_N}(y_N(t) - y_{N+1}(t)) + a_1^{\text{II}}(t), \\ y_{N+1}(0) &= 0. \end{aligned} \quad (6.131)$$

It is now obvious how to incorporate the boundary conditions. We augment the system (6.127) by Equations (6.128) and (6.131). With the vectors

$$\begin{aligned} \mathbf{z} &= (y_0, y_1, \dots, y_N, y_{N+1})^T, \\ \mathbf{a} &= (a_1(x_0, t), a_1(x_1, t), \dots, a_1(x_N, t), a_1(x_{N+1}, t))^T \end{aligned}$$

equations (6.127), (6.128) and (6.131) may be written in the form

$$\dot{\mathbf{z}} = \mathbf{A}_1 \mathbf{z} + \mathbf{a}(t), \quad \mathbf{z}(0) = \mathbf{0},$$

where  $\mathbf{A}_1$  is an  $(N+2) \times (N+2)$ -matrix. Boundary conditions are incorporated in this system. A standard Runge-Kutta integration routine will yield the solution for any given function  $a_1(x, t)$ .

Another integration method (see Nye [35]) makes use of Green's function technique. It offers no advantage when compared with the above scheme for which reason a detailed discussion will be omitted.

##### 5. Derivation of the Surface-wave Equation from First Principles – Non-linear Theory

In the analysis of the preceding sections we dealt exclusively with the application of the kinematic wave theory to the glacier as a whole. The non-

linear equations, which were obtained from a mass balance, a geometric relationship, and a constitutive-type relationship for mass flux, were subsequently linearized, and the linearized equations were then solved with various analytic and numerical solution procedures. No effort was made to justify the derived equations and neither was there any particular attempt to derive the basic equations from a rational formulation based on the conservation laws of mass and momentum and the associated kinematic and dynamic boundary conditions at the base and the surface. In the remainder of this chapter we shall, therefore, deal with the following two general questions.

- (i) Do the linear equations derived above by any means realistically describe waves on glaciers, or should they be replaced by non-linear equations?
- (ii) Is the concept of kinematic wave theory an accurate one to describe waves on glaciers, or must it be replaced by a different one?

The answers to these questions depend, in a way, on the accuracy with which one attempts to describe the physical phenomenon of *waves on glaciers*. It will be demonstrated that the concept of kinematic waves is, in many respects, a useful one, but that momentum balance must be treated more carefully in order to arrive at an evolution equation which accurately predicts surface profiles.

In the ensuing analysis, attention will be limited to plane motion as an example. More complicated three-dimensional cases must be deferred until this is fully understood.

In principle, the derivation of the non-linear surface wave equation in plane motion for a glacier or ice sheet is simple. It follows from the application of the field equations and boundary conditions used in Chapters 3 to 5. In Chapter 5, it was demonstrated that a substantial reduction in mathematical complexity is obtained by introducing the concept of *slow variation*. This led to the shallow-ice approximation and the Morland–Johnson transformations. Both achieve the same goal, namely to separate the determination of the stresses and velocities from those of the surface profile. The procedure to achieve this is the following:

A stretching of coordinates is introduced on the basis of the slow variation of basal topography and surface profile. The small parameter of this stretching transformation enters the field equations and boundary conditions and can, in general, be related to another parameter left free in the field equations. Two cases must be distinguished, namely  $\mathcal{O}(1)$ -mean-bed-inclination and small mean-bed-inclination. It can be shown that in a *steady state* the two cases are easily distinguishable. In the  $\mathcal{O}(1)$ -case ice flows in one direction only, thus preventing ice divides, in the other, ice divides are possible. These are where the surface slopes horizontally, implying that with  $\mathcal{O}(1)$ -mean inclination surface slopes retain their sign. Below we shall mainly discuss the case where ice flow is in one direction only.

(a) *Surface waves in the shallow-ice approximation*

In what follows, the reader is supposed to be familiar with Sections 3 to 5 of Chapter 5, as the subsequent treatment will closely follow the developments outlined there.

Consider plane flow. The dimensionless field equations and boundary conditions for non-dimensional stresses and velocities are then given by Equations (5.25)–(5.28). The geometry is depicted in Figure 6.12. In these equations, the temperature field is assumed to be known from estimates. An improvement of it can be determined from the boundary-value problem (5.29) after the determination of a first iterate of the stress/velocity/surface problem. With the aid of the shallow ice approximation

$$U = \bar{u}, \quad V = \frac{1}{\mu} \bar{v}, \quad \ell = \frac{1}{\mu} \bar{t}, \quad \xi = \mu \bar{x}, \quad \eta = \bar{y}, \quad (6.132)$$

in which  $\mu \ll 1$  is the small parameter, the perturbation solutions to the stress and velocity fields can soon be found. In the construction of these solutions no use is made of the kinematic surface condition, which is an evolution equation for the free surface and can be solved provided that the velocity field is known as a function of the surface coordinate. This goal is exactly achieved using the perturbation scheme of the shallow ice approximation. Consequently, substitution of the expressions for the velocity into the kinematic surface condition will result in a differential equation for the surface coordinate. In the ensuing analysis, it will be shown how this equation can be derived. For this demonstration, not all field equations and boundary conditions are needed as the velocity field is known. The following statements,

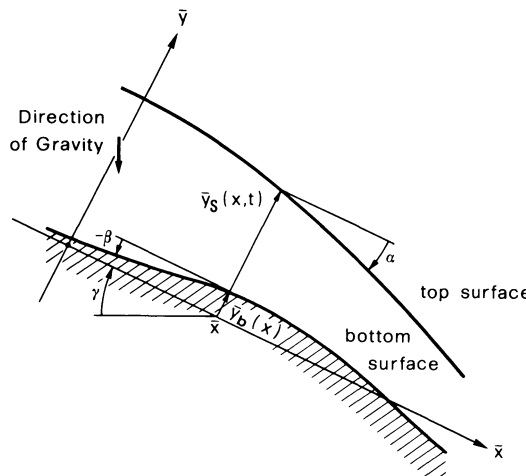


FIG. 6.12. Geometry and definitions of the ice sheet.

written in the variables of the shallow ice transformation, suffice (see Section 3 of Chapter 5).\*

*Continuity Equation:*

$$\frac{\partial U}{\partial \xi} + \frac{\partial V}{\partial \eta} = 0. \quad (6.133)$$

*Kinematic Surface Conditions:*

$$\begin{aligned} V &= U \frac{d\bar{y}_B}{d\xi}, \quad \text{at } \eta = \bar{y}_B(\xi), \\ \frac{\partial \bar{y}_S}{\partial t} + \frac{\partial \bar{y}_S}{\partial \xi} U - V &= \mathfrak{U}, \quad \text{at } \eta = \bar{y}_S(\xi, t), \end{aligned} \quad (6.134)$$

which are already listed as Equations (5.33)–(5.35). Although written in the stretched variables, the perturbation parameter  $\mu$  does not explicitly occur. However,  $U$  and  $V$  are known in terms of a perturbation series of the parameter  $\mu$ , an approximate expression for  $U$  being given in (5.83).

Integrating the continuity equation with respect to  $\eta$  from  $\eta = \bar{y}_B$  to  $\eta = \bar{y}_S$  yields

$$\int_{\bar{y}_B}^{\bar{y}_S} \frac{\partial U}{\partial \xi} dy + V(\bar{y}_S) - V(\bar{y}_B) = 0,$$

or when interchanging differentiation and integration with Leibnitz' rule and using the first of the kinematic surface conditions (6.134),

$$\frac{\partial}{\partial \xi} \int_{\bar{y}_B}^{\bar{y}_S} U(\xi, y, t) dy + V(\bar{y}_S) - U(\bar{y}_S) \frac{\partial \bar{y}_S}{\partial \xi} = 0. \quad (6.135)$$

Adding Equations (6.134)<sub>2</sub> and (6.135) yields the desired relation, namely

$$\frac{\partial \bar{y}_S}{\partial t} + \frac{\partial Q}{\partial \xi} = \mathfrak{U}, \quad Q \equiv \int_{\bar{y}_B}^{\bar{y}_S} U(\xi, \eta, t) d\eta. \quad (6.136)$$

Introducing the variables

$$\bar{D} = \bar{y}_S - \bar{y}_B, \quad z = \bar{y}_S - \eta, \quad (6.137)$$

the above equations may also be written as

$$\frac{\partial \bar{D}}{\partial t} + \frac{\partial Q}{\partial \xi} = \mathfrak{U}, \quad Q = \int_0^{\bar{D}} U(\xi, z, t) dz. \quad (6.138)$$

$Q$  is called the flux function and Equations (6.136)<sub>1</sub> and (6.138)<sub>1</sub> are formally

\*The non-linear analysis of surface-wave propagation is due to Fowler and Larson [12]. This treatment relies heavily upon their work.

identical with the *kinematic wave equation* listed in (6.1). It is seen that (6.136) or (6.138) describe the surface profile as a function of position and time, provided that the accumulation rate function  $\mathfrak{A}$  and the flux function  $Q$  are prescribed functions of  $\xi$ ,  $t$  and  $\bar{y}_S$  (and its derivatives). Complemented by appropriate boundary and initial conditions, Equations (6.136) or (6.138) will then allow the determination of the surface profile.

There is an alternative formulation using the *generalized streamfunction*  $\Psi$  defined by

$$\Psi(\xi, \eta, t) \equiv \int_{\bar{y}_B}^{\eta} U(\xi, \sigma, t) d\sigma + \frac{\partial}{\partial t} \int_{\xi_M(t)}^{\xi} \bar{D}(\sigma, t) d\sigma, \quad (6.139a)$$

in which  $\xi_M(t)$  denotes the left margin. Notice that the first term on the right-hand side of (6.139a) is known, whereas the second term is unknown. Thus the problem consists here of expressing the kinematic surface condition in terms of  $\Psi$ . Before we demonstrate this, we mention that the velocity components  $U$  and  $V$  and the stream function  $\Psi$  are related by

$$\begin{aligned} U &= \frac{\partial}{\partial \eta} \left[ \Psi - \frac{\partial}{\partial t} \int_{\xi_M(t)}^{\xi} \bar{D}(\sigma, t) d\sigma \right] = \frac{\partial \psi}{\partial \eta}, \\ V &= -\frac{\partial}{\partial \xi} \left[ \Psi - \frac{\partial}{\partial t} \int_{\xi_M(t)}^{\xi} \bar{D}(\sigma, t) d\sigma \right] = -\frac{\partial \psi}{\partial \xi} \end{aligned} \quad (6.140)$$

and thus automatically satisfy the continuity equation. [The proof of (6.140) is straightforward.] Hence the term in brackets in Equations (6.140) may be interpreted as a stream function  $\psi$ . When  $U$  and  $V$  are known functions of position and time the differential equations  $U = (\partial \psi / \partial \eta)$ ,  $V = -(\partial \psi / \partial \xi)$  may be integrated to obtain  $\psi$ . When this is performed it is easily seen that

$$\psi = \int_{\bar{y}_B}^{\eta} U(\xi, \sigma, t) d\sigma. \quad (6.141)$$

Combining this with (6.136)<sub>2</sub>, it is seen that  $\psi(\bar{y}_S, \bar{y}_B, t) = Q$ . Evaluating the stream function at the free surface therefore gives the flux. On the other hand, this may also be expressed in the form

$$\Psi(\xi, \bar{y}_S, t) = Q + \frac{\partial}{\partial t} \int_{\xi_M(t)}^{\xi} \bar{D}(\sigma, t) d\sigma. \quad (6.139b)$$

This representation of  $Q$  is useful in the derivation of boundary conditions that apply at the snout region.

Equation (6.139b) implies at  $\eta = \bar{y}_S(\xi, t)$ :

$$\frac{d}{d\xi} \Psi(\xi, \bar{y}_S(\xi, t), t) = \frac{\partial Q}{\partial \xi} + \frac{\partial \bar{D}}{\partial t} = \mathfrak{A}. \quad (6.142a)$$

In view of the indeterminacy of  $\Psi$  one may, without loss of generality, set  $\Psi(\xi_M(\ell), y, \ell) \equiv 0$ , so that a further integration of the above equation with respect to  $\xi$  leads to

$$\Psi(\xi, \bar{y}_S(\xi, \ell), \ell) = \int_{\xi_M^-(\ell)}^{\xi} \mathfrak{U}(\sigma) d\sigma, \quad (6.142b)$$

or

$$Q + \frac{\partial}{\partial \ell} \int_{\xi_M^-(\ell)}^{\xi} \bar{D}(\sigma, \ell) d\sigma = \int_{\xi_M^-(\ell)}^{\xi} \mathfrak{U}(\sigma) d\sigma.$$

Moreover, at  $\eta = \bar{y}_B(\xi)$ :

$$\Psi(\xi, \bar{y}_B(\xi), \ell) = \frac{\partial}{\partial \ell} \int_{\xi_M^-(\ell)}^{\xi} \bar{D}(\sigma, \ell) d\sigma. \quad (6.143)$$

Equation (6.142a) is the kinematic surface condition and corresponds to (6.138), but is now expressed in terms of  $\Psi$ , whereas (6.143) corresponds to the basal boundary condition. To see this, consider the first of Equations (6.134) and use (6.140) to express the tangency condition of the velocity vector at the base in terms of  $\Psi$ . This yields

$$\left. \frac{\partial \Psi}{\partial \eta} \right|_{\eta=\bar{y}_B} = \frac{d\bar{y}_B}{d\xi} + \frac{\partial \Psi}{\partial \xi} - \frac{\partial}{\partial \xi} \left[ \frac{\partial}{\partial \ell} \int_{\xi_M^-(\ell)}^{\xi} \bar{D}(\sigma, \ell) d\sigma \right] = 0,$$

or

$$\frac{d}{d\xi} \Psi(\xi, \bar{y}_B(\xi), \ell) = \frac{d}{d\xi} \left[ \frac{\partial}{\partial \ell} \int_{\xi_M^-(\ell)}^{\xi} \bar{D}(\sigma, \ell) d\sigma \right].$$

A further integration with respect to  $\xi$  from  $\xi_M^-(\ell)$  to  $\xi$  now suffices to obtain (6.143).

(a) *Integration by the methods of characteristics.* Solutions of Equations (6.136)<sub>1</sub>, (6.138) or (6.142a) can be determined if an explicit expression for  $Q$  in terms of  $\bar{y}_S$  and  $\bar{y}_B$  or  $\bar{D}$  is found. This is easy because  $U$  is known. For temperate ice, expressions for it are given in (5.57), for cold ice corresponding expressions are listed in (5.83). In order not to complicate the ensuing calculations, however, let us assume that the model glacier under consideration is temperate. Let us further restrict attention to lowest-order representations, that is to say, let  $U$  approximately equal  $U^{(0)}$ , where  $U^{(0)}$  is the first term in the shallow ice approximation. In this case  $U^{(0)}$  is given by (5.57)<sub>1</sub>. In view of (6.143) we therefore obtain

$$\begin{aligned}\psi^{(0)} &= \mathbb{C} \sin^m \gamma \bar{D}^m (\eta - \bar{y}_B) + \frac{\sin^n \gamma}{(n+1)(1+\kappa)} \times \\ &\quad \times \left[ \frac{n+1}{n+2} \bar{D}^{n+2} - \bar{D}^{n+1} (\bar{y}_S - \eta) + \frac{(\bar{y}_S - \eta)^{n+2}}{n+2} \right] + \\ &\quad + \frac{\kappa \sin \gamma}{1+\kappa} \left[ \frac{2}{3} \bar{D}^3 - \bar{D}^2 (\bar{y}_S - \eta) + \frac{(\bar{y}_S - \eta)^3}{3} \right].\end{aligned}\quad (6.144)$$

$$Q^{(0)} = \mathbb{C} \sin^m \gamma \bar{D}^{m+1} + \frac{\sin^n \gamma}{(n+2)(1+\kappa)} \bar{D}^{n+2} + \frac{2\kappa \sin \gamma}{3(1+\kappa)} \bar{D}^3,$$

$$\Psi^{(0)} = \psi^{(0)} + \frac{\hat{c}}{\hat{c}\ell} \int_{\xi_M(\ell)}^{\xi} \bar{D}(\sigma, \ell) d\sigma,$$

the superscript (0) indicating lowest-order approximations. With the aid of (6.144), Equation (6.142a) becomes

$$\frac{\partial \bar{D}}{\partial \ell} + \mathfrak{C}(\bar{D}) \frac{\partial \bar{D}}{\partial \xi} = \mathfrak{A}, \quad (6.145)$$

in which

$$\mathfrak{C}(\bar{D}) = \frac{dQ^{(0)}}{d\bar{D}} = (m+1)\mathbb{C} \sin^m \gamma \bar{D}^m + \frac{\sin^n \gamma}{1+\kappa} \bar{D}^{n+1} + \frac{2\kappa \sin \gamma}{1+\kappa} \bar{D}^2. \quad (6.146)$$

Equation (6.145) governs the evolution of the glacier thickness. For steady state, it agrees with Equation (5.85).

A boundary condition for (6.145) is obtained by substituting the results (6.144) in (6.142b)<sub>2</sub>, yielding

$$Q^{(0)} + \frac{\partial}{\partial \ell} \int_{\xi_M(\ell)}^{\xi} \bar{D}(\sigma, \ell) d\sigma = \int_{\xi_M(\ell)}^{\xi} \mathfrak{A} d\sigma \quad (6.147)$$

with  $Q^{(0)}$  given by (6.144)<sub>2</sub>. Consider now the limit  $\xi \rightarrow \xi_M^-(\ell)$ . This limit has already been carefully looked at in Chapter 5 when the steady-state analysis was treated. It was found there that finite margin surface slopes are only obtained when the sliding coefficient  $\mathbb{C}$  becomes singular as  $\xi \rightarrow \xi_M^-$ .

Assuming  $\mathfrak{A}$ ,  $\bar{D}$  and  $\partial \bar{D} / \partial \ell$  to be bounded as  $\xi = \xi_M^-$  is approached, the evaluation of (6.147) at  $\xi = \xi_M^-$  gives

$$\lim_{\xi \rightarrow \xi_M^-} \left\{ Q^{(0)} + \int_{\xi_M^-}^{\xi} \frac{\partial \bar{D}}{\partial \ell} d\sigma - \bar{D}(\xi_M^-, \ell) \dot{\xi}_M^- - \int_{\xi_M^-}^{\xi} \mathfrak{A} d\sigma \right\} = 0,$$

or

$$\lim_{\xi \rightarrow \xi_M^-} Q^{(0)} - \bar{D}(\xi_M^-, \ell) \dot{\xi}_M^- = 0. \quad (6.148)$$

This relation is only meaningful when  $\xi$  approaches  $\xi_M^-$  from above for otherwise (6.147) does not hold. Hence, (6.148) can only hold for  $\dot{\xi}_M^- > 0$ . When  $\dot{\xi}_M^- < 0$  one simply has  $\bar{D} = 0$ . Consequently, a complete boundary condition for (6.145) is

$$\begin{aligned}\bar{D}(\xi_M^-, \ell) \dot{\xi}_M^- &= \lim_{\xi \rightarrow \xi_M^-} Q^{(0)}, \quad \text{for } \dot{\xi}_M^- > 0, \\ \bar{D}(\xi_M^-, \ell) &= 0, \quad \text{for } \dot{\xi}_M^- \leq 0.\end{aligned}\quad (6.149)$$

(This boundary condition applies for general  $Q$  although it is presented here for  $Q^{(0)}$  only.) Depending on how  $C$  behaves near  $\xi = \xi_M^-$ , the right-hand side of (6.149)<sub>1</sub> assumes different forms. Indeed, with the aid of (6.144)<sub>2</sub> it is easy to show that for  $\dot{\xi}_M^-(\ell) > 0$

$$\left. \begin{aligned}\bar{D}(\xi_M^-, \ell) &= \left[ \frac{n+2}{\sin^n \gamma} \dot{\xi}_M^-(\ell) \right]^{1/(1+n)}, \quad \text{for } C = 0, k = 0, \\ \text{but} \quad C_M^* \sin^m \gamma \bar{D} &= \bar{D} \dot{\xi}_M^-, \quad \text{for } C = C_M^* \bar{D}^{-m}, \text{ as } \xi \rightarrow \xi_M^-. \end{aligned}\right\} \quad (6.150)$$

In steady state, the choice  $C = C_M^* \bar{D}^{-m}$  near the margin resulted in a finite slope at an ablating margin. In the dynamic case Equation (6.150)<sub>2</sub> can be satisfied by either setting  $\bar{D} \neq 0$ ,  $\dot{\xi}_M^- = C_M^* \sin^m \gamma$ , or else  $\bar{D} = 0$ . The former is physically unrealistic. For a finite surface slope at the margin, we thus require as a boundary condition in this case  $(\bar{D}(\xi_M^-(\ell))) = 0$ , for  $\dot{\xi}_M^- \gtrless 0$ .

To complete the initial-boundary-value problem an initial condition must be prescribed; this is

$$\bar{D}(\xi, 0) = H(\xi), \quad \xi_M^-(0) \leq \xi \leq \xi_M^+(0), \quad (6.151)$$

where  $H(\xi)$  is a known function of position. The initial-boundary-value problem posed by Equations (6.145), (6.146), (6.149) and (6.151) is to be solved for non-negative  $\bar{D}$  in regions where  $\xi > \xi_M^-$  and  $\ell \geq 0$ . Identifying the margin  $\xi = \xi_M^-(\ell)$  with the head, the snout position  $\xi_M^+(\ell)$  is then defined as the smallest value of  $\xi > \xi_M^-(\ell)$  such that  $\bar{D}(\xi, \ell) = 0$ .

In order to simplify the study of solutions to the initial-value problem posed above, it will be assumed that  $\mathfrak{A}$  is  $\xi$ -dependent only and  $\dot{\xi}_M^-$  does not depend on time. The more general case can then be handled analogously without difficulties. The initial-boundary-value problem for  $\bar{D}$  thus reads

$$\begin{aligned}\frac{\partial \bar{D}}{\partial \ell} + \mathfrak{C}(\bar{D}) \frac{\partial \bar{D}}{\partial \xi} &= \mathfrak{A}(\xi), \\ \bar{D}(\xi_M^-, \ell) &= 0, \quad \bar{D}(\xi, 0) = H(\xi),\end{aligned}\quad (6.152)$$

in which  $\mathfrak{C}(\bar{D})$  is defined in Equation (6.146). To solve (6.152), the method

of characteristics is chosen. Accordingly, we write (6.152) in the form

$$\begin{aligned}\frac{d\xi}{dt} &= \mathfrak{C}(\bar{D}), & \frac{\partial \bar{D}}{\partial t} &= \mathfrak{U}(\xi), \\ \bar{D}(\xi_M^-, t) &= 0, & t &\geq 0, \\ \bar{D}(\xi_0, 0) &= H(\xi_0), & \xi_M^- \leq \xi_0 \leq \xi_M^+, \end{aligned}\quad (6.153)$$

where  $\xi_0$  is the *characteristic parameter*.

The quantity  $\mathfrak{C}(\bar{D})$  is the surface-wave speed, that is the speed at which ice thickness disturbances propagate. It may be contrasted with the surface particle speed  $U_s$  and the basal sliding velocity  $U_b$ ,

$$\left. \begin{aligned} U_s &= \frac{\partial \Psi}{\partial \eta} \Big|_{\eta=\bar{y}_s} = \mathfrak{C} \sin^m \gamma \bar{D}^m + \frac{\sin^n \gamma}{(n+1)(1+\mathbb{k})} \bar{D}^{n+1} + \frac{\mathbb{k} \sin \gamma}{1+\mathbb{k}} \bar{D}^2, \\ U_b &= \frac{\partial \Psi}{\partial \eta} \Big|_{\eta=\bar{y}_b} = \mathfrak{C} \sin^m \gamma \bar{D}^m, \end{aligned} \right\} \quad (6.154)$$

obtained from (6.144). Combining (6.154) and (6.146) we obtain

$$\mathfrak{C} = (m+1)U_b + (n+1)(U_s - U_b) + \frac{(1-n)\mathbb{k}}{1+\mathbb{k}} \sin \gamma \bar{D}^2. \quad (6.155)$$

For realistic values of  $n$ , the last term is negative. In general, it is also small, so that

$$\mathfrak{C} \lesssim (m+1)U_b + (n+1)(U_s - U_b).$$

This is the same result obtained earlier in Equation (6.24) where it was derived in a less rigorous manner. As before, it follows with  $m = (n+1)/2$  and  $n \approx 3$  to 4 that  $\mathfrak{C}$  is about 3 to 5 times the particle surface speed, which is in good agreement with field observation as long as *no seasonal or surge-type waves* are considered.

Combining (6.153)<sub>1</sub> and (6.153)<sub>2</sub> it is seen that

$$\frac{d\bar{D}}{dt} = \frac{d\bar{D}}{d\xi} \frac{d\xi}{dt} = \frac{d\bar{D}}{d\xi} \mathfrak{C}(\bar{D}) = \mathfrak{U}(\xi),$$

or in view of (6.146)

$$\frac{dQ^{(0)}}{d\bar{D}} \frac{d\bar{D}}{d\xi} = \frac{dQ^{(0)}}{d\xi} = \mathfrak{U}(\xi), \quad (6.156)$$

which can immediately be integrated. (Notice that this would not be possible if  $\mathfrak{U}$  should depend on time.) Therefore with  $s(\xi) = \int_{\xi_M^-}^{\xi} \mathfrak{U}(\sigma) d\sigma$ , which is called the *accumulation flux function*

$$Q^{(0)}(\bar{D}) = s(\xi) - s_1(\xi_0), \quad (6.157)$$

where  $s_1$  depends on the characteristic parameter  $\xi_0$ . It may be determined by noticing that for  $\ell = 0$ ,  $\xi = \xi_0$  and  $\bar{D} = H$ , so that  $s_1$  is defined by the relation

$$Q^{(0)}(H(\xi_0)) = s(\xi_0) - s_1(\xi_0). \quad (6.158)$$

This equation allows a unique determination of  $s_1(\xi_0)$  so that, henceforth,  $s_1(\xi_0)$  is treated as a known function. Equations (6.157) and (6.158) together define the glacier thickness as a function of  $\xi$  and  $\xi_0$ ,  $\bar{D} = \bar{D}(\xi, \xi_0)$ . This function must be unique at least for times  $\ell < \ell^*$  where  $\ell^*$  is fixed, the reason being that  $\bar{D} = H$  is unique at  $\ell = 0$  so that continuity also requires this uniqueness for some time onwards. Substituting  $\bar{D} = \bar{D}(\xi, \xi_0)$  into (6.153)<sub>1</sub>, the emerging differential equation can be solved, and one obtains

$$\ell = \hat{\ell}(\xi, \xi_0) = \int_{\xi_0}^{\xi} \frac{d\sigma}{\mathfrak{C}(\bar{D}(\sigma, \xi_0))}, \quad \text{for } \ell \leq \ell^*, \quad (6.159)$$

provided the integration can be performed. This completes the construction of the formal solution. Relations (6.157) to (6.159) define  $\bar{D}(\xi, \ell)$  implicitly. In a first step we choose  $\xi_0$  in the interval  $\xi_M^- \leq \xi_0 \leq \xi_M^+$  and use (6.157), (6.158) to find  $\bar{D}(\sigma, \xi_0)$  for  $\sigma < \xi$ . Equation (6.159) then provides the time  $\ell$  at which  $\bar{D}$  attains the value  $\bar{D}(\xi, \xi_0)$ . Equations (6.157)–(6.159) are called a characteristic solution and the  $(\xi, \ell)$ -curves defined for each value of  $\xi_0$  are called *characteristics*.

It is interesting to demonstrate that the initial-boundary-value problem (6.152) does not permit a solution when  $\mathfrak{A} = \mathfrak{A}(\ell)$ . To see this, let

$$X = \int_{\xi_M^-}^{\xi} \frac{d\sigma}{\mathfrak{C}(\bar{D}(\sigma))}$$

be a new spatial-variable. It transforms the differential equation (6.152)<sub>1</sub> to

$$\frac{\partial \bar{D}}{\partial \ell} + \frac{\partial \bar{D}}{\partial X} = \mathfrak{A}(\ell)$$

which admits the solution

$$\bar{D} = \phi(X - \ell) + \int_0^\ell \mathfrak{A}(\ell') d\ell',$$

where  $\phi$  is a differentiable function which can be implicitly obtained from the initial condition (6.152)<sub>3</sub>:

$$\bar{D}(\xi, 0) = H(\xi) = \phi(\xi) = \phi \left[ \int_{\xi_M^-}^{\xi} \frac{d\sigma}{\mathfrak{C}(H(\sigma))} \right].$$

On the other hand, the boundary conditions (6.152)<sub>2</sub> imply

$$\phi(-\ell) = - \int_0^\ell \mathfrak{A}(\ell') d\ell'.$$

The last two expressions contradict each other since both  $H$  and  $\mathfrak{A}$  can arbitrarily be assigned.

A generalization of (6.152) must therefore directly assume  $\mathfrak{A}$  to depend on position *and* time.

In order to illustrate the general nature of the characteristic solution, consider the special case where  $C = 0$  (no sliding) and  $k = 0$  (power flow law). In this case an explicit formula for  $\bar{D}(\xi, \xi_0)$  can be given as (6.144)<sub>2</sub> and (6.157) imply

$$\bar{D}(\xi, \xi_0) = \left[ \frac{n+2}{\sin^n \gamma} (s(\xi) - s_1(\xi_0)) \right]^{1/(n+2)}. \quad (6.160)$$

Consequently,

$$\ell = \hat{\ell}(\xi, \xi_0) = \int_{\xi_0}^{\xi} \frac{d\sigma}{\sin \gamma^{[n(n+1)]/(n+2)} [(n+2)(s(\sigma) - s_1(\xi_0))]^{(n+1)/(n+2)}}, \quad (6.161)$$

in which  $s_1(\xi_0)$  is regarded as known from (6.158).

For a steady-state ice flow we have  $\bar{D} = H$  for all time so that agreement of (6.157) with (6.158) implies  $s_1 \equiv 0$ . Thickness  $\bar{D}$ , governed by (6.160), has infinite slopes at the head and the snout in this case, since  $s$  vanishes there. Further, along any characteristic (where  $\xi_0$  is constant) (6.161) with  $s_1 \equiv 0$  implies, since  $s \geq 0$ , that as  $\ell$  is increased  $\xi$  increases until  $\xi = \xi_M^+$  where  $\bar{D}$  vanishes and the characteristic slope  $d\ell/d\xi = +\infty$ . The characteristic curves therefore have a similar shape to those shown in Figure 6.5. The time afforded for a disturbance initially at  $\xi = \xi_0$  to reach the snout  $\xi = \xi_M^+$  is finite or infinite depending on whether  $s^{-(n+1)/(n+2)}$  is integrable or not. The former is generally true because the ablation rate at the snout is typically finite.

In the *general case* when  $s_1(\xi_0) \neq 0$ , Equations (6.160), (6.161) together with (6.158) provide an implicit solution, uniquely determining  $\bar{D}(\xi, \ell)$  as long as two characteristic curves belonging to two different values of  $\xi_0$  do not intersect. At such a point to the given pair  $(\xi, \ell)$ , there are at least two values of  $\xi_0$ , and consequently the function  $\xi_0(\xi, \ell)$  ceases to be single-valued. The formal solution (6.160), (6.161) is therefore valid in regions where the function  $\xi_0(\xi, \ell)$  is single-valued. In such regions this solution looks qualitatively very much the same as in the steady-state situation (see Figure (6.5)) as  $\ell$  increases with  $\xi$  until a  $(\xi, \ell)$ -point is reached where  $\xi_0(\xi, \ell)$  ceases to be

single valued or  $s(\xi) = s_1(\xi_0)$ . At points where this latter condition is valid, (6.160) implies  $\tilde{D} = 0$ ;  $s(\xi) = s_1(\xi_0)$  thus marks the glacier snout position, where the characteristics terminate.

This discussion indicates how the position of the snout can be found from the above equation in the  $(\xi, \ell)$ -region where  $\xi_0(\xi, \ell)$  is single-valued. In the special case for which (6.160) and (6.161) are valid, the snout position  $\xi = \xi_M^+$  is governed by the equations

$$\begin{aligned} s(\xi_M^+) &= s_1(\xi_0), \\ \ell &= \int_{\xi_0}^{\xi_M^+} \frac{d\sigma}{\sin^{-[n(n+1)]/(n+2)} [(n+1)[s(\sigma) - s_1(\xi_0)]]^{(n+1)/(n+2)}}, \end{aligned} \quad (6.162)$$

which define  $\xi_M^+(\ell)$  implicitly. For each  $\xi_0$  (6.162)<sub>1</sub> determines the position of the snout whereas (6.162)<sub>2</sub> gives the time when this position is attained. This time is finite provided that  $[s(\xi) - s_1(\xi_0)]^{-(n+1)/(n+2)}$  is integrable in any neighbourhood of  $\xi_M^+$ . This will be assumed.

The above solutions are valid as long as neighboring characteristics do not intersect or are the same as long as  $\xi_0(\xi, \ell)$  is single-valued. This might only be the case for part of the domain  $\xi_M^- \leq \xi \leq \xi_M^+, \ell \geq 0$ . Conditions are therefore needed which indicate, firstly, in which domains of the characteristic parameter  $\xi_0$ , the above representations comprise the complete solution for all time and, secondly, how solutions are continued when  $\xi_0(\xi, \ell)$  ceases to be single valued.

The answer to the first question is as follows: *Equations (6.160) to (6.162) provide a complete solution if and only if  $ds_1/d\xi_0 \leq 0$ .* This statement is only valid for the limited situation that  $C \equiv 0$  and  $k = 0$ . For glaciers allowing sliding and flow laws other than the power law, the above statement has not been proved. The proof is given by Fowler and Larson [12]. In general,  $ds_1/d\xi_0$  can be positive for some points  $\xi_0$  in the interval  $[\xi_M^-, \xi_M^+]$  and, so for these characteristic parameters, the solution (6.160) to (6.161) will hold only as long as  $\ell \leq \ell^* < \infty$ .

The next problem is therefore to find the  $(\xi, \ell)$ -points where solutions break down. To find this condition we remark that (6.161) defines  $\ell$  as a function of  $\xi$  and  $\xi_0$ . A graph of this function may look as shown in Figure 6.13a. Its inverse function  $\xi_0 = \hat{\xi}_0(\xi, \ell)$  is the mirror picture reflected at the  $45^\circ$ -line. This function is shown in Figure 6.13b. Its region of multi-valuedness is marked by the two vertical lines which are tangent to the function. They mark the points where  $\hat{\xi}_0 = \hat{\xi}_0(\xi, \ell)$  has infinite slope. These are the points in Figure 6.13a where  $\hat{\ell}(\xi, \xi_0)$  has horizontal slopes. Hence characteristics intersect, where

$$\ell = \hat{\ell}(\xi, \xi_0), \quad \frac{\partial \hat{\ell}(\xi, \xi_0)}{\partial \xi_0} = 0. \quad (6.163)$$

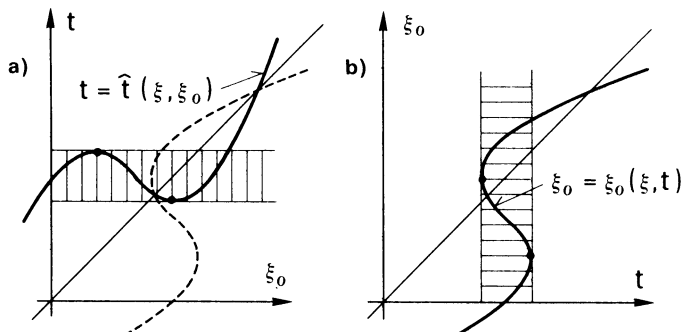


FIG. 6.13. Explaining conditions (6.163) which mark the points where characteristics intersect. (a) portrays the function  $\hat{\eta}(\xi, \xi_0)$  for a fixed value of  $\xi$ . In (b) the mirror picture about the  $45^\circ$ -line is shown. The graph of  $\xi = \hat{\xi}_0(\xi, t)$  is multi-valued in the dashed region also shown in (a).

The two equations define curves  $t^* = \hat{t}^*(\xi)$  where (6.160)–(6.162) cease to hold. On these curves, which are called *shocks* the characteristics intersect or merge, so that (6.163) also determines the envelope of intersecting characteristics. Such a situation is shown in Figure 6.14, in which shocks have the form of a cusp. We are thus led to conclude that the ‘continuous’ solutions (6.160)–(6.162) hold for all those times  $t < t^*$  for which shocks are not crossed. On the curves  $t^* = \hat{t}^*(\xi) - \varepsilon$ ,  $\varepsilon \rightarrow 0$ , any variable  $f$  assumes the value  $f^-$ . The further problem is how to evaluate  $f$  on the other side of the shock, that is to find  $f^+$  at  $t^* = \hat{t}^*(\xi) + \varepsilon$ ,  $\varepsilon \rightarrow 0$ , and moreover, to find an extension of the solution for times  $t > t^*$ .

The problem of evaluating the conditions at the shock cannot stem from any of the above statements, say Equation (6.138), as differentiability is assumed which cannot hold, since  $\bar{D}$  must jump at the shock. *The shock condition must therefore be derived from an integrated statement.* This can only be found from a physical argument. This argument is the conservation

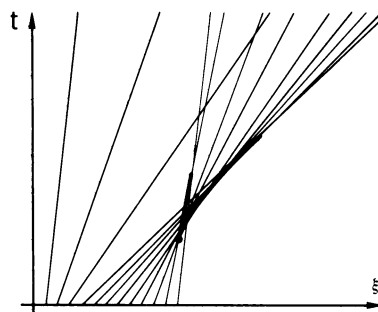


FIG. 6.14. An example of intersecting characteristics leading to a ‘cusp’.

law of mass formulated for the glacier as a whole and reads

$$\frac{\partial}{\partial \ell} \int_{\xi_1}^{\xi_2} \bar{D} d\xi - [Q^{(0)}(\xi_2) - Q^{(0)}(\xi_1)] = \int_{\xi_1}^{\xi_2} \mathfrak{A} d\xi \quad (6.164)$$

where  $\xi_1$  and  $\xi_2$  are two arbitrary fixed positions of which the corresponding interval includes the shock position  $\xi_d(\ell^*)$ , if a shock should exist. The first term on the left is the rate of change of volume between the fixed positions  $\xi_1$ ,  $\xi_2$  the term in brackets represents the excess of volume flux out of the control-volume through the cross-sections at  $\xi_1$  and  $\xi_2$ . The term on the right-hand side is the addition of volume on the surface by accumulation. If  $\bar{D}$ ,  $Q^{(0)}$  and  $\mathfrak{A}$  are differentiable in  $(\xi_1, \xi_2)$  then (6.164) implies

$$\int_{\xi_1}^{\xi_2} \left( \frac{\partial \bar{D}}{\partial \ell} + \frac{\partial Q^{(0)}}{\partial \xi} - \mathfrak{A} \right) d\xi = 0,$$

or, since  $\xi_1$  and  $\xi_2$  are arbitrary,

$$\frac{\partial \bar{D}}{\partial \ell} + \frac{\partial Q^{(0)}}{\partial \xi} = \mathfrak{A}.$$

This agrees with (6.138). Equation (6.164) is therefore the physically meaningful extension when shock-discontinuities are present. In this case it implies

$$\begin{aligned} \frac{\partial}{\partial \ell} \int_{\xi_1}^{\xi_2} \bar{D} d\xi &= \frac{\partial}{\partial \ell} \int_{\xi_1}^{\xi_d^-} \bar{D} d\xi + \frac{\partial}{\partial \ell} \int_{\xi_d}^{\xi_2} \bar{D} d\xi \\ &= \int_{\xi_1}^{\xi_d^-} \frac{\partial \bar{D}}{\partial \ell} d\xi + \bar{D}(\xi_d^-) \frac{d\xi_d^-}{d\ell} + \int_{\xi_d^+}^{\xi_2} \frac{\partial \bar{D}}{\partial \ell} d\xi - \bar{D}(\xi_d^+) \frac{d\xi_d^+}{d\ell}. \end{aligned}$$

Notice that  $\xi_d^- = \xi_d^+$  but that  $\bar{D}(\xi_d^-)$  may differ from  $\bar{D}(\xi_d^+)$ . When jump discontinuities in  $\bar{D}$  are present, (6.164) reads therefore

$$\int_{\xi_1}^{\xi_2} \frac{\partial \bar{D}}{\partial \ell} d\xi + [\bar{D}(\xi_d^+) - \bar{D}(\xi_d^-)] \frac{d\xi_d}{d\ell} - Q^{(0)}(\xi_2) + Q^{(0)}(\xi_1) = \int_{\xi_1}^{\xi_2} \mathfrak{A} d\xi,$$

where  $[\bar{D}(\xi_d)] = \bar{D}(\xi_d^+) - \bar{D}(\xi_d^-)$  is the jump of the quantity  $\bar{D}$  across the shock. Setting  $\xi_1 = \xi_2 = \xi_d$  in the above formula finally yields

$$\frac{d\xi_d}{d\ell} = \frac{[Q^{(0)}(\xi_d)]}{[\bar{D}(\xi_d)]}, \quad \text{at } \ell = \ell^*, \quad (6.165)$$

which relates the velocity of the shock to the jumps of  $Q^{(0)}$  and  $\bar{D}$ . For our simple example ( $C = k = 0$ ) (6.165) implies

$$\frac{d\xi_d}{d\ell} = \frac{\sin^n \gamma}{n+2} \frac{[\bar{D}^{n+2}(\xi_d)]}{[\bar{D}(\xi_d)]}, \quad \text{at } \ell = \ell^*.$$

Conditions of the ice flow ahead of the shock are usually known as they often correspond to steady conditions. Those behind the shock can be calculated from the continuous solution. The right-hand side of (6.165) is therefore known, so (6.165) yields the shock velocity and, by integration, its position. In general, the extended solution to the initial-value problem (6.152) for  $\ell > \ell^*$  is very complex and will often involve multiple shocks. These solutions must generally be treated on a case-by-case basis. There exists an extensive literature on these problems (i.e., the books by Courant and Friedrichs [8] and by Whitham [44]).

We may summarize as follows: The non-linear analysis of disturbance propagation at the glacier surface for a glacier with a stationary snout position requires, to lowest order, the solution of the initial-boundary-value problem (6.152). Its characteristic solution is given by formulae (6.157) to (6.159) for all  $(\xi, \ell)$ -points where this solution is uniquely defined. The  $(\xi, \ell)$ -curves, where this uniqueness ceases to exist, can be calculated from (6.163), marking the position of shocks of which the velocities are given by (6.165). For the reader's benefit, these equations are collected below in one place:

*Unique Smooth Solution:*

$$Q^{(0)}(\bar{D}(\xi)) = s(\xi) - s_1(\xi_0), \quad (6.157)$$

$$Q^{(0)}(H(\xi_0)) = s(\xi_0) - s_1(\xi_0), \quad \left. \right\} \ell < \ell^*. \quad (6.158)$$

$$\ell = \hat{\ell}(\xi, \xi_0) = \int_{\xi_0}^{\xi} \frac{d\sigma}{\mathfrak{C}(\bar{D}(\sigma, \xi_0))}, \quad \left. \right\} \quad (6.159)$$

*Shock solution:*

$$\ell^* = \hat{\ell}(\xi, \xi_0) \quad \text{and} \quad \left. \frac{\partial \hat{\ell}}{\partial \xi_0} = 0, \right\} \ell = \ell^*. \quad (6.163)$$

$$\left. \frac{d\xi_d}{d\ell} = \frac{[Q^{(0)}(\xi_d)]}{[\bar{D}(\xi_d)]} \right\} \quad (6.165)$$

These formulae hold for an arbitrary flux function  $Q^{(0)}$  as long as  $Q^{(0)}$  depends only on  $\bar{D}$  (and not derivatives of it). Provided that the single-valued solution applies at the snout, its position is described by  $Q^{(0)} = 0$  and hence by the equations

$$s(\xi_M^+) = s_1(\xi_0), \quad \ell = \hat{\ell}(\xi_M^+, \xi_0). \quad (6.166)$$

Setting  $\xi_0 = \xi_M^-$  marks the time  $\ell_F$  by which all initial disturbances have reached the glacier snout, and the ice flow is steady for all subsequent times.

Before we proceed with the presentation of an example, we would like to point out once more that the above formulation holds for arbitrary flux functions but that the developments were illustrated using a temperature-independent power flow law and assuming no slip at the base. When the material properties are position-dependent through a known temperature-variation, it was shown in Chapter 5 that  $Q^{(0)}$  is given by (see (5.90))

$$Q^{(0)} = \mathbb{C} \sin^m \gamma \bar{D}^{m+1}(\xi) + 2 \sin \gamma \int_0^{\bar{D}} \bar{y}^2 \tilde{\mathfrak{F}}(\sin^2 \gamma \bar{y}^2, \hat{\mathfrak{A}}(\bar{y}, \xi)) d\bar{y}, \quad (6.167)$$

where  $\tilde{\mathfrak{F}}(\cdot)$  is the creep response function and  $\hat{\mathfrak{A}}(\cdot)$  the known temperature distribution. The first term is the contribution to  $Q^{(0)}$  by a Weertman-type sliding law and could be replaced by a well-behaved single-valued function  $f(\bar{D})$ . In general, the integration in (6.167) cannot be performed explicitly so that the construction of the solution must be carried out numerically. This is a very difficult task and has so far not been undertaken.

(β) *An illustrative example.* In order to elucidate the nature of the characteristic solutions to (6.152) when shocks are present, consider the initial value problem (6.152) with special initial data. It will be assumed that the glacier is in steady state for all time  $t < 0$ . At  $t = 0$  it is supposed that ice mass is suddenly added between  $\xi_1$  and  $\xi_2$ . This addition of ice mass may physically correspond to the deposition of ice after the surge of a tributary glacier. We shall again restrict attention to the simplest possible model, ignoring sliding and assuming a power flow law. The model is due to Fowler and Larson [12].

A sudden change in ice thickness about a steady state can be modelled for instance by choosing

$$s_1(\xi_0) = \begin{cases} -c, & \text{for } \xi_1 < \xi_0 < \xi_2, \\ 0, & \text{otherwise,} \end{cases} \quad (6.168)$$

where  $c$  is constant; with the aid of (6.158) this could be expressed in terms of a discontinuous addition of glacier thickness, as shown in Figure 6.15.

To construct the characteristic diagram in this case we observe that  $\bar{D}$  is initially discontinuous at  $\xi_1$  and  $\xi_2$  so that shocks can in principle emanate from both points. To make it plausible that a shock only forms at  $\xi_2$ , we argue as follows: consider the initial value problem (6.152) for  $\mathfrak{U}(\xi) = 0$  and a discontinuous initial distribution of  $\bar{D}$  along  $\xi$ . In particular, let

$$H(\xi, t) = \begin{cases} H_1, & \text{a constant, for } \xi < \xi_1, \\ H_2 > H_1, & \text{a constant, for } \xi > \xi_1. \end{cases} \quad (6.169)$$

This initial distribution of the glacier thickness is realistic close to  $\xi = \xi_1$ . The jump in  $\bar{D}$  is  $H_2 - H_1$ , see Figure 6.16a. Let further  $\mathbb{C}(\bar{D})$  be monotonically increasing in  $\bar{D}$ ; this implies  $\mathbb{C}'(\bar{D}) > 0$  and is valid for  $\mathbb{C}$  given by

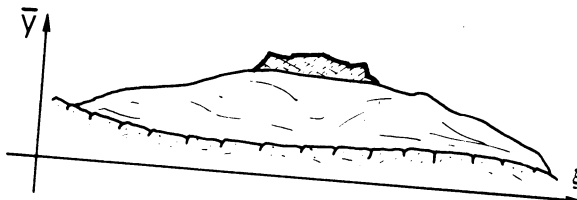


FIG. 6.15. Glacier in its steady state to which, at  $t = 0$ , a large ice mass is suddenly deposited between  $\xi_1$  and  $\xi_2$ .

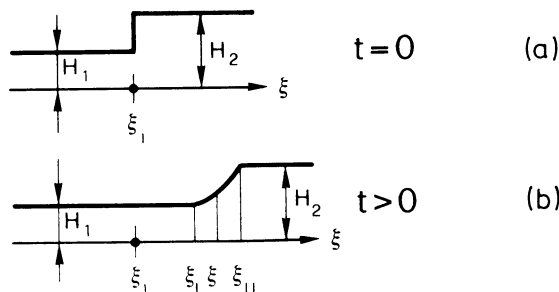


FIG. 6.16. A discontinuous glacier profile in which the glacier depth increases down glacier smoothes out with growing time when  $\mathfrak{C}'(\bar{D}) > 0$ .

(6.146). As a result at 'high altitudes' a wave travels faster than at low altitudes, which must lead to a smoothing of an initially discontinuous profile, Figure 6.16b. The corresponding motion therefore can be justly termed *expanding*. As seen from (6.153)<sub>1,2</sub>, the characteristics have constant slope  $1/\mathfrak{C}(H_1)$  for  $\xi < \xi_1$  and  $1/\mathfrak{C}(H_2)$  for  $\xi > \xi_1$ ; for  $\mathfrak{C}' > 0$  these are larger for  $\xi < \xi_1$  than for  $\xi > \xi_1$ , so that a fan, as portrayed in Figure 6.17a, is obtained. It remains to fill the fan. To this end, on the right leg of the cone, the slope of the characteristics is  $1/\mathfrak{C}(H_2)$ , whereas on the left leg it is larger with value

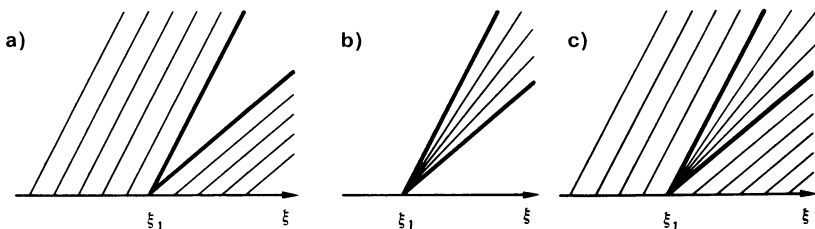


FIG. 6.17. Characteristics corresponding to the motion of an initial jump in glacier depth as shown in Figure 6.16. (a) displays the characteristics in the regions where the glacier depth is  $H_1$  and  $H_2$ , respectively, (b) gives the expansion fan solution which corresponds to the region  $\xi_L < \xi < \xi_U$  in Figure 6.16b, (c) combines the two.

$1/\mathfrak{C}(H_1)$  given by the characteristics to the left of  $\xi = \xi_1$ . An obvious guess for a continuous solution is the construction of characteristics as shown by the fan-type transition indicated in Figure 6.17b. The characteristic slopes of this solution have the form  $1/\mathfrak{C}(\bar{D})$  where  $\bar{D}$  may assume any value between  $\bar{D} = H_1$  and  $\bar{D} = H_2$ . Hence, the complete solution for  $\bar{D}$  is (compare Figure 6.16c)

$$\bar{D} = \begin{cases} H_1, & \xi < \xi_L = \xi_1 + \mathfrak{C}(H_1)/ \\ s, & \xi_L < \xi = \xi_1 + \mathfrak{C}(s)/ < \xi_U \\ H_2, & \xi > \xi_U = \xi_1 + \mathfrak{C}(H_2)/ \end{cases} \quad H_1 < s < H_2. \quad (6.170)$$

The reader may easily show that the differential equation, initial and boundary conditions are identically satisfied by this solution.

The above analysis shows the existence of a continuous solution, but this does not yet exclude a shock solution at  $\xi_1$  when  $\mathfrak{C}' > 0$ . Such a discontinuous solution indeed exists but a stability analysis of an assumed shock solution would prove the instability of this shock-solution, that is small perturbations would change the flow into something quite different – the expansion fan explained and obtained in (6.166). Another method to exclude the shock at  $\xi_1$  and to make the solution unique, is to apply a thermodynamic argument and to require that entropy can only grow. This also excludes the shock solution. These questions are too delicate to be treated here; the reader is referred to the literature, see Courant and Friedrichs [8] and Whitham [44].

An identical argument as used for the situation near  $\xi = \xi_1$  can now also be applied near  $\xi = \xi_2$ , however, for initial conditions in which  $H_1 > H_2$ . One is easily convinced that a shock must form in this situation, since the characteristics now intersect ‘within the cone’.

Having shown that shocks can only form from  $\xi_2$  and solutions emanating from  $\xi_1$  take on the form of an expansion fan, it will now be made plausible that the characteristic diagram must have the typical form shown in Figure 6.18. The characteristics which begin on  $\xi_M^- \xi_1$  and those between  $\xi_2 \xi_M^+(0)$  are steady ones for which  $s_1 \equiv 0$ . For a smooth function  $s(\xi)$ , no steady-shock can exist. All characteristics emanating from  $\xi_M^- \xi_1$  are thus given by (6.159), and this solution is valid for all time. The ‘lowest’ such steady-state characteristic is denoted by  $\xi_1 A$ ,  $A$  being the point where this characteristic reaches the steady snout (assuming this time is finite). Similarly, characteristics emanating from  $\xi_2 \xi_M^+(0)$  are also steady, but they terminate either along the shock  $\xi_2 D$  or at the snout  $\xi_M^+(0) D$ . They are also given by (6.159), and the shock position is obtained from (6.163).

Let  $C$  indicate the position where the shock terminates. In Figure 6.18, this position marks the greatest advance of the glacier snout, but in principle one could have  $\xi_C < \xi_M^+(0)$ . We now prove that only  $\xi_C > \xi_M^+(0)$  is possible. To this end, assume that  $C$  lies in  $\xi < \xi_M^+(0)$ . Then at this point  $\xi_2 C$  must

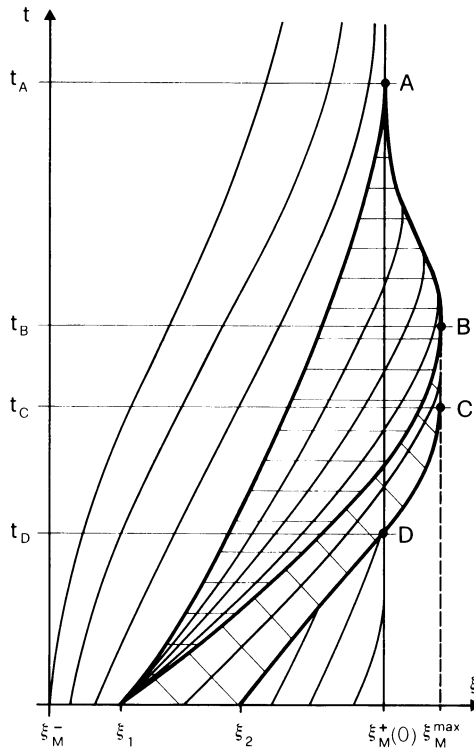


FIG. 6.18. Characteristics for the propagation of surface bulge due to a deposition of a large mass of ice between  $\xi_1$  and  $\xi_2$ . Characteristics emanating from  $\xi_M^- \xi_1$  and  $\xi_2 \xi_M^+(0)$  are steady, those coming from  $\xi_1 \xi_2$  contribute to the advance and retreat of the model glacier. The motion in the neighbourhood of  $\xi_1$  is steady, characteristics have the typical form of an expansion fan. At  $\xi_2$  a shock is formed. It terminates at  $C$ . The advancement of the snout is described by  $DC$ . Advancement starts at the time  $t_D$ . The glacier reaches its largest extent at  $t_C$ , stays there until  $t_B$ , when the glacier commences to retreat and resides at its steady state at  $t_A$ , from [12].

be tangential to two characteristics, one coming from  $\xi_1 \xi_2$ , the other coming from  $\xi_2 \xi_M^+(0)$ , see Figure 6.19. The glacier thickness  $\bar{D}$  must be continuous at  $C$ , since the shock terminates, and hence both merging characteristics are steady there, one emanating from  $\xi_M^- \xi_1$  the other from  $\xi_2 \xi_M^+(0)$ . But distinct steady-state characteristics can never intersect, as  $s(\xi)$  was assumed to be smooth (thus no steady shocks exist), and so we are forced to conclude that  $C$  can actually lie only in  $\xi > \xi_M^+(0)$ . *Initially present shocks of the type considered here must therefore always lead to a temporary advance of the snout.*

Another interesting result is obtained when the velocity of the shock at the snout is evaluated. This is obtained from (6.165) by recognizing that

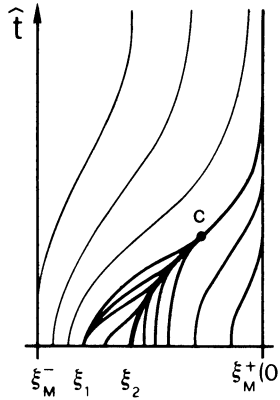


FIG. 6.19. A hypothetical portrayal of characteristics that could develop when the shock emanating from  $\xi_2$  does not reach the snout.

along  $DC \bar{D}(\xi_d^+) = 0$  and  $Q^{(0)}(\xi_d^+) = 0$ , so that

$$\frac{d\xi_d}{d\ell} = \frac{Q^{(0)}(\xi_d^-(\ell), \ell)}{\bar{D}(\xi_d^-(\ell), \ell)} = \frac{\sin^n \gamma}{n+1} \bar{D}^{n+1}(\xi_d^-(\ell), \ell), \quad (6.171)$$

where the expression to the far right holds for  $Q^{(0)}$  as listed in (6.144)<sub>2</sub> when  $C = 0$  and  $k = 0$ . On comparing (6.169) with (6.154), it is seen that (when there is a shock at the snout)

$$\frac{d\xi_d/d\ell}{U_s} = \frac{n+1}{n+2} \approx \frac{4}{5};$$

the rate of advance of the snout is about  $\frac{4}{5}$ th of the local surface speed. This result is due to Fowler and Larson [12] and they quote that their prediction should be capable of field verification, unless altered by the effects of diffusion and seasonal variations. On the other hand, Equation (6.171) forms a differential equation for the snout position as a function of time. The shock terminates at the snout at the point  $C$  implying that  $d\xi_d/d\ell = 0$ . Hence  $\xi_2 C$  at  $\xi = \xi_C$  is tangential to a vertical line.

Consider now the unsteady characteristics emanating from  $\xi_1 \xi_2$ . Two types can be differentiated, the expansion fan at  $\xi_1$  and the characteristics emanating from  $\xi_1 \xi_2$ . We denote by  $B$  the point where the characteristic emanating from  $\xi_1$  meets  $\xi_2 DCA$ . On this curve the  $DCA$  part marks the transient snout position. All characteristics emanating from  $\xi_1 \xi_2$  are given by Equations (6.157)–(6.159) in which  $s_1 = -c$ . They terminate at the snout of which the position is given by (6.166). For our simple example (see, e.g. (6.161)) these equations read

$$s(\xi_M^+) = -c, \\ \ell = \int_{\xi_0}^{\xi_M^+} \frac{d\xi}{\sin \gamma^{[n(n+1)]/(n+2)} [(n+2)(s(\xi) - s_1(\xi_0))]^{(n+1)/(n+2)}}, \quad (6.172)$$

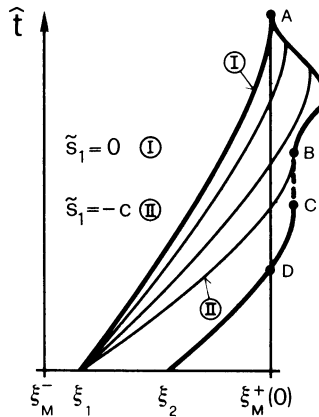


FIG. 6.20. A hypothetical sketch of the characteristics within the expansion fan and position of the snout for the case that the snout within this fan is both advancing and retreating.

and these imply  $d\ell/d\xi_M^+ = \infty$ . It follows that  $CB$  is vertical, as portrayed in Figure 6.18 (this result hinges on the simple form of the glacier model and does not hold in general). On the other hand, characteristics emanating from  $\xi_1$  and arriving at  $BA$  can be obtained as follows: at the point  $\xi_1$ ,  $s_1$  jumps from the value  $-c$  to 0. The expansion fan is therefore obtained by continuously changing the value of  $s_1$  from  $-c$  (yielding  $\xi_1$ ,  $B$ ) to 0 (yielding  $\xi_1$ ,  $A$ ) denoted by ① and ② in Figure 6.20. If we parameterize the characteristics within the expansion fan by  $\tilde{s}_1$ , where  $-c < \tilde{s}_1 < 0$ , so that the  $\tilde{s}_1$ -characteristic is the curve where  $Q^{(0)}(\bar{D}(\xi)) = s(\xi) - \tilde{s}_1$ , then Equations (6.157)–(6.159) and (6.166) with  $\xi_0$  and  $s_1$  replaced by  $\xi_1$  and  $\tilde{s}_1$  completely describe the solution along these characteristics. In particular, the snout is retreating in time along  $BA$ . This can be seen as follows: First, notice that  $\tilde{s}_1$  increases monotonically as the expansion fan is traversed in an anti-clockwise manner, and  $s$  is monotonically decreasing in  $\xi$  for  $\xi > \xi_M^+(0)$  (the glacier is ablating in the snout zone). Second, at the snout one must have  $s(\xi_M^+(\ell)) = \tilde{s}_1$ . If within the expansion fan the snout would advance for some time as indicated in Figure 6.20, then  $\tilde{s}_1$  viewed as a function of  $\xi_M^+(\ell)$  would be multivalued whereas  $s$  is single valued. Either for the advancing or for the retreating portion of the snout  $s(\xi_M^+(\ell))$  could not equal  $\tilde{s}_1$ . We conclude that  $BA$  must be the retreating portion of the snout, as portrayed in Figure 6.18, and so  $C$  indeed marks the maximum advance. The equation for the position of this maximum is really deduced by recognizing that  $C$  marks the end of the shock as well as the snout position for the unsteady characteristics emanating from  $\xi_2^-$ . Hence  $Q^{(0)}(\xi_M^{\max}) = 0$ , because there can be no jump in  $\bar{D}$  and  $s_1 = +c$  so that from (6.157)

$$s(\xi_M^{\max}) + c = 0, \quad (6.173)$$

defining  $\xi_M^{\max}$  implicitly. If  $c$  is small,  $s$  deviates only slightly from its steady-state distribution so that  $s(\xi_M^{\max}) \approx -\mathfrak{A}_S(\xi_M^{\max} - \xi_M^+(0))$ , where  $\mathfrak{A}_S$  is the steady-state ablation rate at the snout. Hence,

$$\xi_M^{\max} - \xi_M^+(0) \approx \frac{c}{\mathfrak{A}_S}, \quad (6.174)$$

which provides an estimate for the maximum advance. Denoting dimensional quantities by superscript  $D$  and re-introducing dimensional variables, (6.174) can be shown to lead to

$$\Delta x^{\max} = U \frac{c^D}{\mathfrak{A}_S^D},$$

where  $U$  is a typical longitudinal velocity. If, for example  $U = 100 \text{ m a}^{-1}$ ,  $c^D = 10 \text{ m}$ ,  $\mathfrak{A}_S^D = 5 \text{ m a}^{-1}$  then  $\Delta x^{\max} = 200 \text{ m}$ . A sudden addition of 10 m of ice somewhere on the glacier will thus result in an eventual advance of the snout in the order of 200 m. This result is independent of the length  $\xi_2 - \xi_1$  of the initial disturbance. On the other hand, the duration at which the snout stays at its maximum advance (the distance  $BC$ ) will strongly depend on  $\xi_2 - \xi_1$ : In general, the larger the distance  $\xi_2 - \xi_1$  is, the longer will the snout dwell at its maximal advance before retreating. This time can be easily calculated from (6.159). It is

$$\ell_{BC} = \int_{\xi_1}^{\xi_M^{\max}} \frac{d\sigma}{\mathfrak{C}(\bar{D}(\sigma, \xi_1))} - \int_{\xi_2}^{\xi_M^{\max}} \frac{d\sigma}{\mathfrak{C}(\bar{D}(\sigma, \xi_2))}.$$

(y) *A remark on linearization.* The full analysis of the non-linear problem treated above is rather complex so that one may justly ask whether an approximate linear analysis is possible. This linear analysis should then give a connection with Nye's linearized procedure in Sections 2 and 3. It was shown there that small perturbations eventually decay to zero, but not uniformly in the length coordinate, as may be seen from Figure 6.4b. In Nye's words, "the lower parts thicken unstably until a kinematic wave arrives to restore stability".

We now propose a linearization procedure in which this instability does not arise. This linearization analysis is due to Fowler and Larson [12]. Let us start with the equation

$$\frac{\partial \bar{D}}{\partial \tau} + \mathfrak{C}(\bar{D}) \frac{\partial \bar{D}}{\partial \xi} = \mathfrak{A}, \quad \bar{D}(\xi) = H(\xi), \quad \text{on } \tau = 0, \quad (6.175)$$

and suppose that  $\bar{D}$  suffers only small perturbations. This assumes that  $\mathfrak{A}$  is small. A straightforward linearization of (6.175)<sub>1</sub> is obtained if  $\mathfrak{C}(\bar{D})$  is replaced by its value in steady state. Hence, we now replace (6.175) by

$$\frac{\partial \bar{D}}{\partial \tau} + \mathfrak{C}(\bar{D}_0) \frac{\partial \bar{D}}{\partial \xi} = \mathfrak{A}(\xi), \quad \bar{D}(\xi) = H(\xi), \quad \text{on } \tau = 0, \quad (6.176)$$

in which  $\mathfrak{C}(\bar{D}_0)$  is obtained from the steady-state solution

$$\frac{dQ^{(0)}(\bar{D}_0)}{d\xi} = \mathfrak{A}(\xi) \rightarrow Q^{(0)}(\bar{D}_0) = s(\xi), \quad (6.177)$$

which was analysed in detail in Chapter 5.

To solve (6.176), let

$$\zeta = \int_{\xi_0}^{\xi} \frac{d\sigma}{\mathfrak{C}(\bar{D}_0(\sigma))}, \quad f(\zeta) = \bar{D}_0(\xi); \quad (6.178)$$

with these, and (6.176) we have

$$\begin{aligned} \frac{\partial \bar{D}}{\partial \xi} &= \frac{\partial \bar{D}}{\partial \zeta} \frac{d\zeta}{d\xi} = \frac{1}{\mathfrak{C}(\bar{D}_0)} \frac{\partial \bar{D}}{\partial \zeta}, \\ \mathfrak{A}(\xi) &= \frac{ds}{d\xi} = \frac{dQ^{(0)}}{d\bar{D}_0} \frac{d\bar{D}_0}{d\xi} \frac{1}{\mathfrak{C}(\bar{D}_0)} = f'(\zeta), \end{aligned}$$

so that the initial value problem (6.176) becomes

$$\frac{\partial \bar{D}}{\partial \ell} + \frac{\partial \bar{D}}{\partial \zeta} = f'(\zeta) \quad \bar{D}(\zeta) = H(\zeta), \quad \text{on } \ell = 0. \quad (6.179)$$

The general solution of the differential equation is  $\bar{D} = f(\zeta) + \phi(\zeta - \ell)$ , where  $\phi$  is any differentiable function. Incorporating the initial conditions (6.179)<sub>2</sub> then determines  $\phi$ . Hence,

$$\bar{D} = \bar{D}_0(\zeta) + \phi(\zeta - \ell), \quad \phi(\zeta) = H(\zeta) - \bar{D}_0(\zeta) \quad (6.180)$$

is the complete solution.  $\phi(\zeta)$  as the initial perturbation in glacier depth is small by assumption. Since depth perturbations at  $\ell > 0$  are also given by  $\phi$  – an initial disturbance at  $\zeta$  is merely shifted to  $(\zeta(\zeta) - \ell)$  – glacier thickness can never become large. This is different from Nye's result, and the differences can be traced back to the differences in linearizations. There is, however, one limitation in that the results can only be correct as long as no shocks develop. Fowler and Larson [12] show, using the smallness assumption on  $s(\xi)$ , that shocks are likely to develop only close to the snout. To the exclusion of these small regions, the above linearization is therefore useful (and rigorous).

So far, only steady accumulation rates were treated. The above linearized analysis can, of course, also be used when small time-dependent perturbations of the accumulation rate about steady state are introduced. One may then write

$$\mathfrak{A}(\xi, \ell) = \mathfrak{A}_0(\xi) + \mathfrak{A}_1(\xi, \ell)$$

where  $\mathfrak{A}_0(\xi)$  is the steady accumulation-rate function and  $\mathfrak{A}_1$  a small time-

dependent perturbation. Fowler and Larson [12] show that the typical non-dimensional frequencies of  $\mathfrak{A}_1$  must be large in order for the linearized analysis to be applicable. In other words, typical periods of  $\mathfrak{A}_1$  should be short. Otherwise the non-linear analysis must be applied. This raises queries as to whether inferences drawn from the linearized formulation of Sections 2 and 3 are correct at all.

( $\delta$ ) *Effects of diffusion.* The calculations presented above restricted considerations to the case when velocity profiles were approximated by the lowest-order expressions in the perturbation parameter  $\mu$  of the shallow ice approximation. The basic equation (6.136),

$$\frac{\partial \bar{y}_S}{\partial \ell} + \frac{\partial Q}{\partial \xi} = \mathfrak{A}, \quad Q = \int_{\bar{y}_B}^{\bar{y}_S} U(\xi, z, \ell) dz \quad (6.138)$$

is, however, generally valid. It is interesting to see what effects emerge, when results of the shallow-ice approximation are carried up to and including first-order terms in the shallow ice parameter. Previously,  $Q$  was only a function of  $\bar{D}$ . However, when higher-order terms are included,  $Q$  may also depend on derivatives of  $\bar{D}$  with respect to  $\xi$ . To within the linear terms in  $\mu$ , such expressions have been derived in Chapter 5 and the respective formulae are given in Equations (5.101) and (5.102). Explicitly they read

$$Q\left(\bar{y}_S, \bar{y}_B, \frac{\partial \bar{y}_S}{\partial \xi}\right) = 2 \left[ \sin \gamma - \mu \cos \gamma \frac{\partial \bar{y}_S}{\partial \xi} \right] I(\bar{y}_S, \bar{y}_B) + \\ + \mathfrak{C} \sin^{m-1} \gamma (\bar{y}_S - \bar{y}_B)^{m+1} \left[ \sin \gamma - \mu m \cos \gamma \frac{\partial \bar{y}_S}{\partial \xi} \right], \quad (6.181)$$

in which

$$I(\bar{y}_S, \bar{y}_B) = \int_{\bar{y}_B}^{\bar{y}_S} (\bar{y}_S - y)^2 \bar{\mathcal{F}}(\sin^2 \gamma (\bar{y}_S - y)^2, \hat{\mathcal{G}}(\xi, y)) dy. \quad (6.182)$$

This representation of  $Q$  applies for both temperate and cold ice, and whether there is basal sliding or not. Using the chain rule of differentiation in (6.138) gives

$$\frac{\partial \bar{y}_S}{\partial \ell} + \mathfrak{C} \frac{\partial \bar{y}_S}{\partial \xi} - \mathfrak{D} \frac{\partial^2 \bar{y}_S}{\partial \xi^2} + \mathfrak{E} \frac{\partial \bar{y}_S}{\partial \xi} \frac{\partial \bar{y}_B}{\partial \xi} = \mathfrak{A}, \quad (6.183a)$$

with

$$\mathfrak{C} = \frac{\partial Q}{\partial \bar{y}_S} = 2 \left[ \sin \gamma - \mu \cos \gamma \frac{\partial \bar{y}_S}{\partial \xi} \right] \frac{\partial I}{\partial \bar{y}_S} + \\ + \mathfrak{C} \sin^{m-1} \gamma (m+1) (\bar{y}_S - \bar{y}_B)^m \left[ \sin \gamma - \mu \cos \gamma \frac{\partial \bar{y}_S}{\partial \xi} \right],$$

$$\mathfrak{D} = -\frac{\partial Q}{\partial(\partial \bar{y}_S / \partial \xi)} = \mu [2 \cos \gamma I(\bar{y}_S, \bar{y}_B) - \mathbb{C} m \cos \gamma \sin^{m-1} \gamma (\bar{y}_S - \bar{y}_B)^{m+1}],$$

$$\begin{aligned} \mathfrak{E} = \frac{\partial Q}{\partial \bar{y}_B} &= 2 \left[ \sin \gamma - \mu \cos \gamma \frac{\partial \bar{y}_S}{\partial \xi} \right] \frac{\partial I}{\partial \bar{y}_B} - \mathbb{C} \sin^{m-1} \gamma (m+1) (\bar{y}_S - \bar{y}_B)^m \times \\ &\quad \times \left[ \sin \gamma - \mu m \cos \gamma \frac{\partial \bar{y}_S}{\partial \xi} \right]. \end{aligned} \quad (6.183b)$$

Here,  $\mathbb{C}$  is a wave speed, as before,  $\mathfrak{D}$  a diffusivity and  $\mathfrak{E}$  has no special name. An easy calculation shows that for temperate ice  $I$  is a function of the difference  $\bar{D} = \bar{y}_S - \bar{y}_B$ . This was the reason why our earlier treatment involved the glacier thickness as a basic variable rather than  $\bar{y}_S$ . Equations (6.183) make it clear that this simple superposition of basal geometry on the surface profile of the flat base no longer holds when  $\mathcal{O}(\mu)$ -terms are included.

In order to elucidate the inferences that can be drawn from (6.183), let us assume a flat bed  $\bar{y}_B \equiv 0$ . Equation (6.183a) is then a *convection-diffusion equation*. The diffusivity  $\mathfrak{D}$  is positive over most of the glacier, since  $I > 0$  when  $\bar{y}_S \neq \bar{y}_B$ , and so the first term in the defining equation of  $\mathfrak{D}$  generally overrides the second term. Diffusion affords a smoothening process, and so we expect that the shock solutions found above should, in fact, be smoothed out and made continuous. This is true with the possible exception of the snout region where the glacier depth and the diffusion coefficient  $\mathfrak{D}$  vanish simultaneously.

In order to demonstrate that diffusion will smooth out shocks, let us consider an ice strip with a flat base ( $\bar{y}_B \equiv 0$ ) and a surface which initially is at  $\bar{D} = H_1$  for  $\xi < 0$  and at  $\bar{D} = H_2$  for  $\xi > 0$  with  $H_2 < H_1$ . At time  $t = 0$  we thus have a discontinuity in glacier depth at  $\xi = 0$ . We are interested in how this initial shock will develop for  $t > 0$ , when the convection-diffusion equation (6.183) applies. At infinity, we hold  $\bar{D}$  fixed at its initial value so that  $\bar{D} = H_1$  as  $\xi \rightarrow -\infty$  and  $\bar{D} = H_2$  as  $\xi \rightarrow \infty$ . We expect the initial discontinuity to propagate at an unknown speed  $V$  so that the ‘similarity’ transformation

$$Z = \frac{1}{\mu}(\xi - Vt) \quad (6.184)$$

is suggested,  $V$  being an unknown velocity. The purpose of introducing (6.184) is to transform (6.184) into an ordinary differential equation. Clearly,  $Z = 0$  marks the position of the ‘shock’ and  $V$  is its speed. Using (6.184) in (6.183a) yields

$$(\mathbb{C} - V) \frac{d\bar{D}}{dZ} - \frac{\mathfrak{D}}{\mu} \frac{d^2\bar{D}}{dZ^2} = \mu \mathfrak{U}, \quad (6.185)$$

of which the coefficient of the second term is  $\mathcal{O}(1)$ , since  $\mathfrak{D}$  is  $\mathcal{O}(\mu)$ . Noticing that

$$\mathfrak{C} = \frac{\partial \hat{Q}}{\partial Z}, \quad \frac{\mathfrak{D}}{\mu} = -\frac{\partial \hat{Q}}{\partial (\partial \bar{D}/\partial Z)},$$

(6.185) implies to lowest order in  $\mu$

$$V \frac{d\bar{D}}{dZ} - \frac{d\hat{Q}}{dZ} = 0,$$

or after an integration

$$V \bar{D} - Q = K, \quad (6.186)$$

subject to the boundary conditions  $\bar{D} = H_1, H_2$  for  $Z \rightarrow \mp \infty$ . Hence  $K = VH_1 - Q(H_1) = VH_2 - Q(H_2)$  from which the shock speed can be calculated

$$V = \frac{Q(H_1) - Q(H_2)}{H_1 - H_2} = \frac{[Q]}{[H]}, \quad (6.187)$$

in agreement with (6.165). A further integration of (6.186) would then allow us to find the detailed shock structure as  $Z$  is varied between  $-\infty$  and  $\infty$ . With  $Q$  having the form  $Q = Q_\alpha - Q_\beta(d\bar{D}/dZ)$  a further integral of (6.186) is

$$Z = \int_0^{\bar{D}} \frac{Q_\beta d\bar{D}}{K + Q_\alpha - V\bar{D}}. \quad (6.188)$$

Better qualitative insight can, however, be gained when a variant of (6.183a) is looked at, namely

$$\frac{\partial \bar{D}}{\partial \ell} - \mathfrak{D} \frac{\partial^2 \bar{D}}{\partial \xi^2} = 0,$$

with constant diffusivity. Its solution

$$\bar{D} = H_1 + \frac{H_2 - H_1}{\sqrt{\pi}} \int_{-\infty}^{\xi \sqrt{4(\mathfrak{D}\mu)\ell}} \exp(-\sigma^2) d\sigma$$

represents a smoothed-out step approaching of values  $H_{1,2}$  as  $\xi \rightarrow \pm \infty$ , see Figure 6.21. The width of the step is proportional to  $(4\mathfrak{D}/\mu\ell)^{1/2}$ , thus growing in time so that *the significance of diffusion diminishes with time*.

It was pointed out in Chapter 5 when analysing the steady-state profile that under usual circumstances, Equation (6.138) gives profiles with infinite slopes at the margin, even when  $\mathcal{O}(\mu)$ -terms are included in the calculations. To have finite margin slopes requires the sliding coefficient  $\mathfrak{C}$  to become singular as the margin is approached. Irrespective of whether  $\mathfrak{C}$  is bounded or singular at the snout, local solutions to the differential equation could be

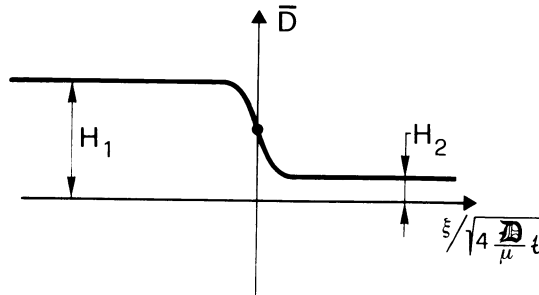


FIG. 6.21. Spreading of an initial jump in glacier thickness for the linear diffusion model.

found near the margin by postulating a solution having the structure of a power law. Requiring  $\bar{D} = 0$  at the snout was sufficient to find such a local solution and no new boundary condition had to be formulated. As noted by Fowler and Larson [12], *for unsteady problems*,

It is still not clear as to what constitutes a proper set of spatial boundary conditions for ... [see (6.183)]. Moving boundary problems for parabolic equations such as ... [see (6.183)] typically involve the prescription of *three* spatial boundary conditions (i.e., two to augment an equation which has second-order spatial derivatives and one to describe the moving boundary) and there seem to be only two natural ones, namely the conditions at the snout [see (6.149)], and the head, where  $\bar{y}_S = \bar{y}_B$ . It is, however known that many boundary-value problems for parabolic equations with diffusion coefficients which degenerate (i.e., become zero) on part of the boundary are properly posed and admit unique solutions only, if less than the 'usual' amount of boundary data is prescribed.

Fowler and Larson then conjecture that two boundary conditions suffice, but they give no clue as to why they arrive at their conjecture. There may even be reasons against such a conjecture, for even more disturbing is the fact that when increasing the number of terms in the shallow ice approximation by including  $\mathcal{O}(\mu^2)$  and  $\mathcal{O}(\mu^3)$  terms etc., the surface profile will be governed by equations of higher and higher order so that more and more complex boundary conditions are to be expected. For an example the reader is referred to Hutter [13], and Section c in this chapter.

It is seen that the calculation of unsteady surface profiles on glaciers based on a non-linear theory is incomplete and requires further study before predictions of snout movement can be made.

#### (b) Remarks regarding time-dependent surface profiles in ice sheets

In this section we briefly touch upon the procedure that should be followed when time-dependent processes in the ice sheets resting on a bed with a small slope are analysed. We cannot present any results, as this is an entirely new field, which so far has been left untouched by any theoretical analysis.

To start with, recall that in the steady-state analysis of Chapter 5, two separate cases were differentiated according to whether the mean bed inclination is of order unity or small. One case was treated above, the steady-state analysis of the second case is given in Section 5 of Chapter 5. The governing equation is still (6.136) and all that is needed is an expression for the longitudinal velocity  $U$  or the flux term  $Q$ . To lowest order in the perturbation parameter  $Q$  is given by [see (5.127)]

$$\begin{aligned} Q = \zeta C & \left[ \zeta \left( \gamma_0 - \frac{\partial \bar{y}_S}{\partial \xi} \right) (\bar{y}_S - \bar{y}_B) \right]^m (\bar{y}_S - \bar{y}_B) + \\ & + \zeta (\bar{y}_S - \bar{y}_B) \Omega \left[ \zeta \left( \gamma_0 - \frac{\partial \bar{y}_S}{\partial \xi} \right) (\bar{y}_S - \bar{y}_B) \right], \end{aligned} \quad (6.189)$$

where

$$\zeta = \operatorname{sgn} \left( \gamma_0 - \frac{\partial \bar{y}_S}{\partial \xi} \right),$$

$$\Omega[x] = \frac{g_1(x)}{x} - \frac{g_2(x)}{x^2},$$

and

$$\begin{aligned} g_1(x) &= \int_0^x g(\sigma) d\sigma, \quad g_2(x) = \int_0^x g_1(\sigma) d\sigma, \\ g(x) &= \varepsilon^{-n} \zeta \mathfrak{F}[\varepsilon^2 x^2] x, \end{aligned}$$

$\mathfrak{F}$  being the creep response function at constant temperature and  $\varepsilon$  a small parameter. Substituting the above representation for  $Q$  into (6.136) gives a non-linear convection-diffusion equation with a structure which is very much the same as (6.183). Similar inferences must therefore be drawn. In particular, presently nothing is known about associated boundary conditions. In steady state, analysis of the differential equation showed that the emerging differential equation is singular at the margin, since the surface slope grows indefinitely as the margin position is approached, unless the basal sliding law is singular so as to make the margin slopes finite. In view of the boundary condition (6.149), which was derived for the shallow ice approximation, we expect boundary conditions for the unsteady motion to differ from those of the steady-state situation. The application of (6.189) will therefore have to await the derivation of the boundary conditions and the proof that the emerging initial-boundary-value problem is physically and mathematically sound.

### (c) Long waves in an infinite ice slab – Is accounting for diffusion enough?

The purpose of the non-linear analysis of surface-wave propagation was to show that the original approach of Nye which led to a linearized diffusion

equation could be based on a rational footing. Indeed, for glaciers with no ice divides, the application of the shallow ice approximation resulted to first order in a non-linear diffusion equation. No explicit solutions, except a brief analysis of the shock structure, were presented, the difficulty being that the boundary conditions of the unsteady ice flow problem with moving margins are still not clearly understood. The physical significance of diffusion is without question and has already been made clear in the linear theory by Nye (compare Section 3). Unanswered is whether derivatives of  $\bar{y}_s$  of higher order than 2 could arise and how significant these derivatives would be.

To answer these questions, let us consider an ice slab which in steady state is strictly parallel-sided. This slab is assumed to undergo small amplitude long wavelength perturbations in surface elevation. By treating such an infinite geometry, difficulties with boundary conditions do not arise because the boundaries are at infinity. Further, the surface profile undulates about a constant mean thickness which may, without loss of generality, be taken as the reference depth. Lengths can thus be made dimensionless with this depth so that  $\bar{y}_s = 1 + \gamma$ , where  $\gamma$  is the surface elevation assumed to be small. This smallness implies that the velocity and stress distributions will deviate only slightly from the corresponding steady-state profile, so that a perturbation expansion in the surface elevation amplitude is suggested.

(a) *Basic equations* In non-dimensional variables, the governing field equations are

$$\left. \begin{aligned} \frac{\partial \bar{u}}{\partial \bar{x}} + \frac{\partial \bar{v}}{\partial \bar{y}} &= 0, \\ \frac{\partial \sigma_x}{\partial \bar{x}} + \frac{\partial \tau}{\partial \bar{y}} + \sin \gamma &= 0, \\ \frac{\partial \tau}{\partial \bar{x}} + \frac{\partial \sigma_y}{\partial \bar{y}} - \cos \gamma &= 0, \\ \frac{\partial \bar{u}}{\partial \bar{x}} &= \frac{1}{2} \tilde{\mathfrak{F}}(\tau'^2)(\sigma_x - \sigma_y), \\ \frac{\partial \bar{u}}{\partial \bar{y}} + \frac{\partial \bar{v}}{\partial \bar{x}} &= 2 \tilde{\mathfrak{F}}(\tau'^2)\tau, \\ \tau'^2 &= \frac{1}{4}(\sigma_x - \sigma_y)^2 + \tau^2, \end{aligned} \right\} \quad (6.190)$$

where  $\gamma$  is the slope angle, and  $\bar{u}, \bar{v}$  are the dimensionless velocity components in the  $\bar{x}$ - and  $\bar{y}$ -directions, respectively, and  $\tilde{\mathfrak{F}}$  is the creep response function which, in general, may also depend on temperature. Here we focus attention on temperate ice. Equations (6.190) are solved subject to the boundary

conditions,

$$\bar{u} = \mathbb{C}\tau^m, \quad \bar{v} = 0, \quad \text{at } \bar{y} = 0, \quad (6.191)$$

and

$$\left. \begin{aligned} \frac{\partial \bar{y}_S}{\partial \bar{t}} + \frac{\partial \bar{y}_S}{\partial \bar{x}} \bar{u} - \bar{v} &= \bar{a} \\ \sigma_x \sin^2 \alpha + \sigma_y \cos^2 \alpha + \tau \sin 2\alpha &= -\bar{p} \\ \tau - \frac{1}{2}(\sigma_y - \sigma_x) \tan 2\alpha &= 0 \end{aligned} \right\} \quad \text{at } \bar{y} = \bar{y}_S(\bar{x}, \bar{t}), \quad (6.192)$$

in which  $\alpha = -\partial \bar{y}_S / \partial \bar{x}$ .

A steady solution of (6.190)–(6.192), henceforth denoted by a circumflex and valid for the vanishing steady accumulation rate, is (see Chapter 3)

$$\begin{aligned} \hat{\tau} &= \sin \gamma(1 - \bar{y}), \\ \hat{\sigma}_x = \hat{\sigma}_y &= -\cos \gamma(1 - \bar{y}) - \bar{p}, \\ \hat{u} &= 2 \int_0^{\bar{y}} \tilde{\mathfrak{F}}(\sin^2 \gamma(1 - y)^2) \sin \gamma(1 - y) dy + \mathbb{C} \sin^m \gamma, \\ \hat{v} &= 0, \quad \bar{y}_S = 1, \quad \hat{\alpha} = 0, \end{aligned} \quad (6.193)$$

provided that the accumulation rate vanishes. In actual glaciers this condition is satisfied only at the snowline. Yet on length scales over which glacier depths do not appreciably vary, the ensuing analysis is still reasonable, and conclusions are likely to be qualitatively correct.

Consider fluctuations on the motion (6.193); denote these by tildes so that  $u = \hat{u} + \tilde{u}$ . The governing equations can now be separated for the two parts. We shall perform this separation under the assumption that the steady-state stresses are large in comparison to the stresses set up by the transient motion. The perturbation equations can then be linearized with respect to the stresses. When also introducing the stretching transformation of the shallow ice approximation,

$$\xi = \mu \bar{x}, \quad \eta = \bar{y}, \quad U = \tilde{u}, \quad V = \frac{1}{\mu} \tilde{v}, \quad \ell = \frac{1}{\mu} \bar{t},$$

the governing field equations and boundary conditions for the quantities carrying a tilde are

$$\begin{aligned} \mu \frac{\partial \tilde{\sigma}_x}{\partial \xi} + \frac{\partial \tilde{\tau}}{\partial \eta} &= 0, \quad \mu \frac{\partial \tilde{\tau}}{\partial \xi} + \frac{\partial \tilde{\sigma}_y}{\partial \eta} = 0, \quad \frac{\partial U}{\partial \xi} + \frac{\partial V}{\partial \eta} = 0, \\ \mu \frac{\partial U}{\partial \xi} &= \frac{1}{2} \tilde{\mathfrak{F}}(\tilde{\tau}'^2)(\tilde{\sigma}_x - \tilde{\sigma}_y), \\ \frac{\partial U}{\partial \eta} + \mu^2 \frac{\partial V}{\partial \xi} &= 2\tilde{\mathfrak{F}}(\tilde{\tau}'^2)\tilde{\tau} + 2\tilde{\mathfrak{F}}'(\tau'^2)\tilde{\tau}\tau'^2, \end{aligned} \quad (6.194)$$

$$U = m\mathbb{C} \hat{\tau}^{m-1} \tilde{\tau}, \quad V = 0, \quad \text{at } \eta = 0, \quad (6.195)$$

and

$$\begin{aligned} \frac{\partial \mathcal{Y}}{\partial \xi} + (\hat{\mu} + U) \frac{\partial \mathcal{Y}}{\partial \xi} - V &= \frac{\bar{a}}{\mu} = \mathfrak{A}, \\ \hat{\sigma}_y + \hat{\sigma}_y - 2\mu(\tilde{\tau} + \hat{\tau}) \frac{\partial \mathcal{Y}}{\partial \xi} + \mu^2(\hat{\sigma}_x + \hat{\sigma}_x - \hat{\sigma}_y - \hat{\sigma}_y) \left( \frac{\partial \mathcal{Y}}{\partial \xi} \right)^2 \\ &= -\bar{p} + \mathcal{O}(\mu^3), \quad \text{at } \eta = 1 + \mathcal{Y}, \\ \tilde{\tau} - \mu(\hat{\sigma}_x - \hat{\sigma}_y) \frac{\partial \mathcal{Y}}{\partial \xi} + \hat{\tau} + \mathcal{O}(\mu^3) &= 0, \end{aligned} \quad (6.196)$$

in which  $\mathfrak{Y}'$  is the derivative of  $\mathfrak{Y}$  with respect to its argument and where

$$\begin{aligned} \hat{\tau}_{II}^{'} &= \frac{1}{4}(\hat{\sigma}_x - \hat{\sigma}_y)^2 + \hat{\tau}^2 = \hat{\tau}^2, \\ \hat{\tau}_{II}^2 &= 2\left[\frac{1}{4}(\hat{\sigma}_x - \hat{\sigma}_y)(\hat{\sigma}_x - \hat{\sigma}_y) + \hat{\tau}\hat{\tau}\right] = 2\hat{\tau}\hat{\tau}. \end{aligned} \quad (6.197)$$

So far the stretching parameter  $\mu$  has been left unspecified. It must be chosen as the ratio of a typical transverse to a longitudinal length scale. These lengths are a representative glacier depth and the wavelength of a typical surface wave. These are assumed to be long and so approximate solutions to Equations (6.194)–(6.197) can be sought for small  $\mu$ . Further, Equations (6.194)<sub>4,5</sub> have been linearized with respect to stresses, but boundary conditions were left arbitrary and could be linearized on the basis that  $\mathcal{Y}$  is small. Solutions will be sought in the form

$$(\hat{\sigma}_x, \hat{\sigma}_y, \tilde{\tau}, U, V) = \sum_{v=0}^{\infty} \mu^v (\sigma_x^{(v)}, \dots, V^{(v)}). \quad (6.198)$$

The expansions (6.198) are substituted into (6.194)–(6.197) and the emerging expressions are expressed as power series of  $\mu$ . Collecting terms of like orders of  $\mu$  will then result in a hierarchy of initial-boundary-value problems. The procedure is the same as outlined and explained in the previous two chapters and so our presentation will be brief.

(β) *Construction of perturbation solutions.* When the terms of  $\mathcal{O}(1)$  are collected, one obtains the differential equations

$$\begin{aligned} \frac{\partial^{(0)}}{\partial \eta} \tau &= 0, & \frac{\partial^{(0)}}{\partial \eta} \sigma_y &= 0, & \sigma_x^{(0)} &= \sigma_y^{(0)}, & \frac{\partial^{(0)}}{\partial \xi} u + \frac{\partial^{(0)}}{\partial \eta} v &= 0, \\ \frac{\partial^{(0)}}{\partial \eta} u &= 2[\mathfrak{F}(\sin^2 \gamma(1-\eta)^2) + 2\mathfrak{F}'(\sin^2 \gamma(1-\eta)^2)\sin^2 \gamma(1-\eta)^2]^{(0)} \tau \end{aligned} \quad (6.199)$$

subject to the boundary conditions

$$\overset{(0)}{u} = m\mathbb{C} \sin^{m-1} \gamma \overset{(0)}{\tau}, \quad \overset{(0)}{v} = 0, \quad \text{at } \eta = 0 \quad (6.200)$$

and

$$\left. \begin{aligned} \overset{(0)}{\sigma}_y &= \cos \gamma (1 - \bar{y}_S), & \overset{(0)}{\tau} &= -\sin \gamma (1 - \bar{y}_S), \\ \frac{\partial \bar{y}_S}{\partial \xi} + \frac{\partial \bar{y}_S}{\partial \xi} \left\{ 2 \int_0^{\bar{y}_S} \mathfrak{F}(\sin^2 \gamma (1-y)^2) \sin \gamma (1-y) dy + \right. \\ &\left. + \mathbb{C} \sin^m \gamma + \overset{(0)}{u} \right\} - \overset{(0)}{v} &= \mathfrak{A}, \end{aligned} \right\} \text{ at } \eta = \bar{y}_S(\xi, \ell). \quad (6.201)$$

These equations can easily be integrated. Indeed, in a first step the zero-order stresses are determined by using  $(6.199)_{1,2,3}$  and the boundary conditions  $(6.201)_{1,2}$ . The resulting expressions are then substituted into the last of Equations  $(6.199)$  which subsequently allows integration of the emerging equation governing  $\overset{(0)}{u}$ , subject to the boundary condition  $(6.200)_1$ . This result for  $\overset{(0)}{u}$  may then be used in the continuity equation  $(6.199)_4$  to obtain an integrable expression for  $\overset{(0)}{v}$  subject to the boundary condition  $(6.200)_2$ . When  $\mathfrak{F}(x)$  is given by

$$\mathfrak{F}(x) = \frac{x^{(n-1)/2} + \mathbb{k}}{1 + \mathbb{k}} \quad (6.202)$$

this process gives

$$\begin{aligned} \overset{(0)}{\tau} &= -\sin \gamma (1 - \bar{y}_S), & \overset{(0)}{\sigma}_y &= \cos \gamma (1 - \bar{y}_S), & \overset{(0)}{\sigma}_x &= \overset{(0)}{\sigma}_y, \\ \overset{(0)}{u} &= (\bar{y}_S - 1) \left\{ \frac{2 \sin \gamma}{1 + \mathbb{k}} \left[ \mathbb{k}\eta + n \int_0^\eta f(y) dy \right] + m\mathbb{C} \sin^m \gamma \right\}, \\ \overset{(0)}{v} &= -\frac{\partial \bar{y}_S}{\partial \xi} \left\{ \frac{2 \sin \gamma}{1 + \mathbb{k}} \left[ \frac{\mathbb{k}}{2} \eta^2 + n \int_0^\eta \int_0^{\eta'} f(y) dy d\eta' \right] + m\mathbb{C} \sin^m \gamma \eta \right\}, \end{aligned} \quad (6.203a)$$

where

$$\begin{aligned} f(y) &= [\sin \gamma (1-y)]^{n-1}, \\ \int_0^\eta f(y) dy &= \frac{1}{n} \sin^{n-1} \gamma (1 - (1-\eta)^n), \\ \int_0^\eta \int_0^{\eta'} f(y) dy d\eta' &= \frac{\sin^{n-1} \gamma}{n(n+1)} ((n+1)\eta + (1-\eta)^{n+1} - 1). \end{aligned} \quad (6.203b)$$

So far all equations (6.199)–(6.201) are exploited with the sole exception of the kinematic surface condition (6.201)<sub>3</sub>. From our experience with non-linear surface waves earlier in this section, it is quite clear what one has to expect as the result. The simple wave equation

$$\frac{\partial \bar{y}_s}{\partial t} + \mathfrak{C}(\bar{y}_s) \frac{\partial \bar{y}_s}{\partial \xi} = \mathfrak{A}$$

with

$$\begin{aligned} \mathfrak{C} = & \frac{2 \sin^n \gamma}{1 + \mathbb{k}} [(1 - \bar{y}_s)^{n+1} + (2\bar{y}_s - 1)] + \\ & + \frac{2\mathbb{k} \sin \gamma}{1 + \mathbb{k}} \bar{y}_s^2 + \mathbb{C}m \sin^m \gamma \left( 2\bar{y}_s - 1 + \frac{1}{m} \right) \end{aligned} \quad (6.204)$$

is obtained. The analysis must therefore be carried further to include higher-order terms in the perturbation parameter  $\mu$ .

Bearing in mind the results (6.203) the first-order boundary-value problem can easily be obtained from (6.194)–(6.197) by collecting terms of  $\mathcal{O}(\mu)$ . What is obtained reads as follows:

$$\begin{aligned} \frac{\partial^{(1)} \tau}{\partial \eta} &= - \frac{\partial^{(0)} \sigma_x}{\partial \xi} = \cos \gamma \frac{\partial \bar{y}_s}{\partial \xi}, \\ \frac{\partial^{(1)} \sigma_y}{\partial \eta} &= \frac{\partial^{(0)} \tau}{\partial \xi} = - \sin \gamma \frac{\partial \bar{y}_s}{\partial \xi}, \\ \frac{\partial^{(0)} u}{\partial \xi} &= \frac{1}{2} \mathfrak{F}(\sin^2 \gamma (1 - \eta)^2) (\sigma_x^{(1)} - \sigma_y^{(1)}), \\ \frac{\partial^{(1)} u}{\partial \eta} &= 2\mathfrak{F}(\sin^2 \gamma (1 - \eta)^2) \tau^{(1)} + 2\mathfrak{F}'(\sin^2 \gamma (1 - \eta)^2) \sin^2 \gamma (1 - \eta)^2 \tau^{(1)}, \\ \frac{\partial^{(1)} u}{\partial \xi} + \frac{\partial^{(1)} v}{\partial \eta} &= 0, \end{aligned} \quad (6.205)$$

subject to the boundary conditions

$$u^{(1)} = - \mathbb{C}m \sin^{m-1} \gamma \tau^{(1)}, \quad v^{(1)} = 0, \quad \text{at } \eta = 0, \quad (6.206)$$

and

$$\tau^{(1)} = 0, \quad \sigma_y^{(1)} = 0, \quad \text{at } \eta = \bar{y}_s. \quad (6.207)$$

Again, this boundary-value problem can straightforwardly be solved. The procedure is to first integrate (6.205)<sub>1,2</sub>; in the second step the stress  $\sigma_y^{(1)}$  and the velocity field  $u^{(1)}$ , obtained earlier, are substituted in (6.205)<sub>3</sub> to

obtain an expression for  $\sigma_x^{(1)}$ . Then,  $u^{(1)}$  is calculated by integrating (6.205)<sub>4</sub> subject to the boundary condition (6.206)<sub>1</sub> and last, the continuity equation (6.205)<sub>5</sub> is used together with the boundary condition on  $v^{(1)}$ , (6.206)<sub>2</sub>. For the flow law (6.202) this process yields

$$\begin{aligned} \tau^{(1)} &= \cos \gamma \frac{\partial \bar{y}_S}{\partial \xi} (\eta - \bar{y}_S), & \sigma_y^{(1)} &= -\sin \gamma \frac{\partial \bar{y}_S}{\partial \xi} (\eta - \bar{y}_S), \\ \sigma_x^{(1)} &= \frac{\partial \bar{y}_S}{\partial \xi} \left\{ \sin \gamma (\bar{y}_S - \eta) + \frac{4 \sin \gamma}{f(\eta) + k} \left[ k \eta + \sin^{n-1} \gamma (1 - (1 - \eta)^n) \right] + \right. \\ &\quad \left. + C m \frac{2(1 + k)}{f(\eta) + k} \sin^m \gamma \right\}, \\ u^{(1)} &= U_{11}^{(1)}(\eta, \bar{y}_S) \frac{\partial \bar{y}_S}{\partial \xi}, \\ v^{(1)} &= -V_{11}^{(1)}(\eta, \bar{y}_S) \frac{\partial^2 \bar{y}_S}{\partial \xi^2} + V_{12}^{(1)}(\eta, \bar{y}_S) \left( \frac{\partial \bar{y}_S}{\partial \xi} \right)^2, \end{aligned} \quad (6.208)$$

in which

$$\begin{aligned} U_{11}^{(1)}(\eta, \bar{y}_S) &= \cos \gamma \left\{ \frac{2}{1 + k} \left[ k \left( \frac{\eta^2}{2} - \eta \bar{y}_S \right) + \right. \right. \\ &\quad + \sin^{n-1} \gamma (1 - \eta)^n \left( \bar{y}_S - \eta - \frac{1 - \eta}{n + 1} \right) + \\ &\quad \left. \left. + \sin^{n-1} \gamma \left( \frac{1}{n + 1} - \bar{y}_S \right) - C m \sin^{m-1} \gamma \bar{y}_S \right\}, \right. \\ V_{11}^{(1)}(\eta, \bar{y}_S) &= \cos \gamma \left\{ \frac{2}{1 + k} \left[ k \left( \frac{\eta^3}{6} - \frac{\eta^2 \bar{y}_S}{2} \right) + \right. \right. \\ &\quad + \frac{\sin^{n-1} \gamma}{n + 1} \left[ \left( \bar{y}_S - \frac{1}{n + 1} \right) (1 - (1 - \eta)^{n+1}) - \right. \\ &\quad \left. \left. - \left( 1 - \frac{1}{n + 1} \right) \left( \frac{1 - (1 - \eta)^{n+2}}{n + 2} - \eta (1 - \eta)^{n+1} \right) \right] + \right. \\ &\quad \left. + \sin^{n-1} \gamma \left( \frac{1}{n + 1} - \bar{y}_S \right) \eta \right] - m C \sin^{m-1} \gamma \bar{y}_S \eta \right\}, \\ V_{12}^{(1)}(\eta, \bar{y}_S) &= \cos \gamma \left\{ \frac{2}{1 + k} \left[ k \frac{\eta^2}{2} - \frac{\sin^{n-1} \gamma}{n + 1} (1 - (1 - \eta)^{n+1}) + \sin^{n-1} \gamma \eta \right] + \right. \\ &\quad \left. + C m \sin^{m-1} \gamma \eta \right\}. \end{aligned} \quad (6.209)$$

It should be noticed that for  $k = 0$ , the longitudinal stress  $\sigma_x^{(1)}$  is singular at  $\eta = 1$ , since  $f(1) = 0$ , according to (6.203)<sub>1</sub>. We shall say more about this singularity in a moment. If the zeroth-order solution (6.203) and the first-order solution (6.208) and (6.209) are combined, i.e.  $U = \bar{u}^{(0)} + \mu \bar{u}^{(1)}$  and the results are substituted into the kinematic surface equation, the convection diffusion equation is obtained. Hence, in order to answer our original question whether terms other than diffusion play a significant role in the surface wave equation, one must proceed to include  $\mathcal{O}(\mu^2)$ -terms. Explicit calculations become unwieldy in this case. For this reason, ensuing calculations will be restricted to the absolute necessary minimum.

The differential equation and boundary condition for the second-order shear stress  $\tau^{(2)}$  follow from (6.194)<sub>1</sub> and (6.196)<sub>3</sub> by collecting  $\mathcal{O}(\mu^2)$ -terms. They are

$$\begin{aligned} \frac{\partial \tau^{(2)}}{\partial \eta} &= -\frac{\partial \sigma_x^{(1)}}{\partial \xi}, \\ \tau^{(2)}(\eta = \bar{y}_S) &= (\sigma_y^{(1)} - \sigma_x^{(1)}) \frac{\partial \bar{y}_S}{\partial \xi}, \end{aligned} \quad (6.210)$$

The right-hand sides are known functions in view of (6.208)<sub>2,3</sub> and thus integration can be performed explicitly. The result is

$$\tau^{(2)} = -T_{11}^{(2)}(\eta, \bar{y}_S) \left( \frac{\partial \bar{y}_S}{\partial \xi} \right)^2 - T_{12}^{(2)}(\eta, \bar{y}_S) \frac{\partial^2 \bar{y}_S}{\partial \xi^2}, \quad (6.211)$$

in which

$$\begin{aligned} T_{11}^{(2)}(\eta, \bar{y}_S) &= \left\{ \sin \gamma (\eta - \bar{y}_S) + \frac{4 \sin \gamma}{f(\bar{y}_S) + k} [k \bar{y}_S + \sin^{n-1} \gamma (1 - (1 - \bar{y}_S)^n)] + \right. \\ &\quad \left. + \frac{2(1+k)}{f(\bar{y}_S) + k} C_m \sin^m \gamma \right\} \end{aligned}$$

$$T_{12}^{(2)}(\eta, \bar{y}_S) = A [G_n(x)(1 - \bar{y}_S) - G_n(x)] + \quad (6.212)$$

$$\begin{aligned} &+ \sin \gamma \left\{ \left[ \left( \eta \bar{y}_S - \frac{\eta^2}{2} \right) - \left( \bar{y}_S^2 - \frac{\bar{y}_S^2}{2} \right) \right] - \right. \\ &\quad \left. - 2 \left[ (1 - (1 - \eta)^2) - (1 - (1 - \bar{y}_S)^2) \right] \right\} \end{aligned}$$

and

$$\begin{aligned} x &= \sin \gamma / \kappa^{1/(n-1)}, \\ A &\equiv 4(\sin^{n-1} \gamma \kappa^{(2-n)/(n-1)} + \kappa^{1/(n-1)}) + 2(1+\kappa)Cm \sin^{m-1} \gamma \kappa^{(2-n)/(n-1)}, \\ G_n(x) &= \int_0^x \frac{d\sigma}{\sigma^{n-1} + 1} = \begin{cases} \ln(x+1), & \text{for } n=2, \\ \tan^{-1}(x), & \text{for } n=3, \end{cases} \end{aligned} \quad (6.213)$$

appropriate for  $n=2, 3$  only.

Beyond this point calculations are very complicated, but it suffices to derive expressions for the velocity components  $\overset{(2)}{u}$  and  $\overset{(2)}{v}$ . The differential equations follow from  $(6.194)_{3,5}$  as

$$\begin{aligned} \frac{\partial \overset{(2)}{u}}{\partial \eta} &= -\frac{\partial \overset{(1)}{v}}{\partial \xi} + 2[\mathfrak{F}(x^2) + \mathfrak{F}'(x^2)x] \overset{(2)}{\tau} = \frac{2}{1+\kappa}(\kappa + nx^{n-1}) \overset{(2)}{\tau}, \\ \frac{\partial \overset{(2)}{u}}{\partial \xi} + \frac{\partial \overset{(2)}{v}}{\partial \eta} &= 0, \quad \text{with } x = \sin \gamma(1-\eta), \end{aligned} \quad (6.214)$$

subject to the boundary conditions

$$\overset{(2)}{u} = -Cm \sin^{(m-1)} \gamma \overset{(2)}{\tau}, \quad \overset{(2)}{v} = 0, \quad \text{at } \eta = 0. \quad (6.215)$$

Since  $\overset{(2)}{\tau}$  is known from (6.211) and (6.212), it is possible to find expressions for the velocity components  $\overset{(2)}{u}$  and  $\overset{(2)}{v}$  by mere quadratures, namely

$$\begin{aligned} \overset{(2)}{u} &= U_{11}^{(2)}(\eta, \bar{y}_S) \frac{\partial^2 \bar{y}_S}{\partial \xi^2} - U_{12}^{(2)}(\eta, \bar{y}_S) \left( \frac{\partial \bar{y}_S}{\partial \xi} \right)^2, \\ \overset{(2)}{v} &= -V_{11}^{(2)}(\eta, \bar{y}_S) \frac{\partial^3 \bar{y}_S}{\partial \xi^3} - V_{12}^{(2)}(\eta, \bar{y}_S) \frac{\partial^2 \bar{y}_S}{\partial \xi^2} \frac{\partial \bar{y}_S}{\partial \xi} - V_{13}^{(2)}(\eta, \bar{y}_S) \left( \frac{\partial \bar{y}_S}{\partial \xi} \right)^3 \end{aligned} \quad (6.216)$$

with

$$\begin{aligned} U_{11}^{(2)} &= C_m \sin^{m-1} \gamma T_{12}^{(2)}(0, \bar{y}_S) + \\ &\quad + \frac{2}{1+\kappa} \int_0^\eta [\kappa + (\sin \gamma(1-\sigma))^{n-1}] T_{12}^{(2)}(\sigma, \bar{y}_S) d\sigma, \\ U_{12}^{(2)} &= -Cm \sin^{m-1} \gamma T_{11}^{(2)}(0, \bar{y}_S) - \\ &\quad - \frac{2}{1+\kappa} \int_0^\eta [\kappa + (\sin \gamma(1-\sigma))^{n-1}] T_{11}^{(2)}(\sigma, \bar{y}_S) d\sigma, \end{aligned}$$

$$\begin{aligned} {}^{(2)}V_{11}(\eta, \bar{y}_S) &= \int_0^\eta {}^{(2)}U_{11}(\sigma, \bar{y}_S) d\sigma, \\ {}^{(2)}V_{12}(\eta, \bar{y}_S) &= \int_0^\eta \left\{ \frac{\partial {}^{(2)}U_{11}(\sigma, \bar{y}_S)}{\partial \bar{y}_S} - 2 {}^{(2)}U_{12}(\sigma, \bar{y}_S) \right\} d\sigma, \\ {}^{(2)}V_{13}(\eta, \bar{y}_S) &= \int_0^\eta \frac{\partial {}^{(2)}U_{12}(\sigma, \bar{y}_S)}{\partial \bar{y}_S} d\sigma. \end{aligned} \quad (6.217)$$

The selection of the sign in  $(6.217)_{1,2}$  is such that under usual circumstances  ${}^{(2)}U_{11}$  and  ${}^{(2)}U_{12}$  will be positive.

Before we proceed, let us pause for a moment and look at the derived formulae more closely. First, it was observed in connection with the stress formulae (6.208) that for a power flow law ( $\kappa = 0$ )  ${}^{(1)}\sigma_x$  will become infinitely large at the free surface, since  $f = 0$  there. Because of our approximation procedure, in which small surface elevations were assumed this singularity occurs at  $\eta = 1$  rather than at  $\eta = \bar{y}_S$ . However, this does not change the fact that higher-order stress corrections become infinitely large. A similar behavior arises in the second-order shear stress  ${}^{(2)}\tau$ , see (6.212). These singularities enter into the integrals of the relations (6.217) but for a power law fluid such as Glen's flow law, the singularities are integrable so that  ${}^{(2)}u$  and  ${}^{(2)}v$  remain bounded in this case. Nevertheless, the singularities cause numerical difficulties and this is one reason why the power flow law was replaced by the more general law involving the constant  $\kappa$ . It causes the singularities to disappear. However, for small values of  $\kappa$ ,  ${}^{(1)}\sigma_x$  and  ${}^{(2)}\tau$  may still become large so that the perturbation technique applied here is, strictly speaking, invalid. The difficulty with the power flow law is a mathematical rather than a physical one, which is connected to the proposed perturbation procedure. It would, therefore, be appropriate to search for a mathematical procedure which remains regular as  $\kappa \rightarrow 0$ . Such a procedure would have to be sought using matched asymptotic expansions, but has not been attacked so far. Some of the numerical values of the results presented below will therefore have to be taken with some reservation.

With these cautious remarks in mind, we now proceed and evaluate  $U$  and  $V$  at the surface

$$U = {}^{(0)}u + \mu {}^{(1)}u + \mu^2 {}^{(2)}u + \dots, \quad V = {}^{(0)}v + \mu {}^{(1)}v + \mu^2 {}^{(2)}v + \dots, \quad (6.218)$$

where the ordered quantities are given in (6.203), (6.208) and (6.216). Upon substitution into the kinematic surface equation  $(6.196)_3$ , the following

differential equation is obtained :

$$\begin{aligned} \frac{\partial \bar{y}_S}{\partial \xi} + \mathfrak{C} \frac{\partial \bar{y}_S}{\partial \xi} - \mu \left[ \mathfrak{D} \frac{\partial^2 \bar{y}_S}{\partial \xi^2} + \mathfrak{E} \left( \frac{\partial \bar{y}_S}{\partial \xi} \right)^2 \right] - \\ - \mu^2 \left[ \mathfrak{F} \frac{\partial^3 \bar{y}_S}{\partial \xi^3} + \mathfrak{G} \frac{\partial^2 \bar{y}_S}{\partial \xi^2} \frac{\partial \bar{y}_S}{\partial \xi} + \mathfrak{H} \left( \frac{\partial \bar{y}_S}{\partial \xi} \right)^3 \right] + \\ + \mathfrak{C}(\mu^3) = \frac{\bar{a}}{\mu} \end{aligned} \quad (6.219)$$

where  $\mathfrak{C}$  is given in (6.204) and

$$\begin{aligned} \mathfrak{D}(\bar{y}_S) &\equiv - \overset{(1)}{V}_{11}(\bar{y}_S, \bar{y}_S), \\ \mathfrak{E}(\bar{y}_S) &\equiv \overset{(1)}{V}_{12}(\bar{y}_S, \bar{y}_S) - \overset{(1)}{U}_{11}(\bar{y}_S, \bar{y}_S), \\ \mathfrak{F}(\bar{y}_S) &\equiv - \overset{(2)}{V}_{11}(\bar{y}_S, \bar{y}_S), \\ \mathfrak{G}(\bar{y}_S) &\equiv - \overset{(2)}{U}_{11}(\bar{y}_S, \bar{y}_S) - \overset{(2)}{V}_{12}(\bar{y}_S, \bar{y}_S), \\ \mathfrak{H}(\bar{y}_S) &\equiv \overset{(2)}{U}_{12}(\bar{y}_S, \bar{y}_S) - \overset{(2)}{V}_{13}(\bar{y}_S, \bar{y}_S). \end{aligned} \quad (6.220)$$

All these quantities can be calculated, in principle, but the corresponding algebra is unwieldy and becomes unjustifiably involved to be presented explicitly.

Equation (6.219) is the relation we were looking for because it includes more than just second order derivatives which are typical for diffusion. Nonetheless, (6.219) is too complex to allow us to extract analytical solutions, yet some insight might be gained for special cases. To this end we write  $\bar{y}_S = 1 + \delta\eta$  in which  $\eta$  is  $\mathcal{O}(1)$  but  $\delta \ll 1$  (since  $\eta$  no longer appears we may use this symbol with this new meaning). Then

$$\begin{aligned} \frac{\partial \eta}{\partial \tau} + \mathfrak{C}(1 + \delta\eta) \frac{\partial \eta}{\partial \xi} - \mu \left[ \mathfrak{D}(1 + \delta\eta) \frac{\partial^2 \eta}{\partial \xi^2} + \delta \mathfrak{E}(1 + \delta\eta) \left( \frac{\partial \eta}{\partial \xi} \right)^2 \right] - \\ - \mu^2 \left[ \mathfrak{F}(1 + \delta\eta) \frac{\partial^3 \eta}{\partial \xi^3} + \delta \mathfrak{G}(1 + \delta\eta) \frac{\partial^2 \eta}{\partial \xi^2} \frac{\partial \eta}{\partial \xi} + \delta^2 \mathfrak{H}(1 + \delta\eta) \left( \frac{\partial \eta}{\partial \xi} \right)^3 \right] = \frac{\bar{a}}{\delta \mu}. \end{aligned} \quad (6.221)$$

Here, the parameter  $\delta$  represents a typical surface elevation above the undisturbed level  $\bar{y}_S = 1$ . According to the perturbation procedure, it cannot be larger than  $\mathcal{O}(\mu)$  but could be smaller. Furthermore, (6.221) gives indications on the size of  $\bar{a}$  for which the equation makes sense. Clearly,  $\bar{a}$  should not be larger than  $\mathcal{O}(\mu\delta)$ . This condition is well satisfied for real glaciers and ice sheets. In what follows we shall set  $\bar{a} = \mu\delta\mathfrak{A}$  with  $\mathfrak{A} = \mathcal{O}(1)$ . With such limitations, Equation (6.221) may be expressed in powers of  $\delta$ . To zeroth

order, the linear long-wave theory emerges for which

$$\frac{\partial \eta}{\partial \tau} + \mathfrak{C}(1) \frac{\partial \eta}{\partial \xi} - \mu \mathfrak{D}(1) \frac{\partial^2 \eta}{\partial \xi^2} - \mu^2 \mathfrak{F}(1) \frac{\partial^3 \eta}{\partial \xi^3} = \mathfrak{A}. \quad (6.222a)$$

To first order in  $\delta$  we find

$$\begin{aligned} & \frac{\partial \eta}{\partial \tau} + \mathfrak{C}(1) \frac{\partial \eta}{\partial \xi} - \mu \mathfrak{D}(1) \frac{\partial^2 \eta}{\partial \xi^2} - \mu^2 \mathfrak{F}(1) \frac{\partial^3 \eta}{\partial \xi^3} + \\ & + \delta \left\{ \mathfrak{C}'(1) \eta \frac{\partial \eta}{\partial \xi} - \mu \left[ \mathfrak{D}'(1) \eta \frac{\partial^2 \eta}{\partial \xi^2} + \mathfrak{E}(1) \left( \frac{\partial \eta}{\partial \xi} \right)^2 \right] - \right. \\ & \left. - \mu^2 \left[ \mathfrak{F}'(1) \eta \frac{\partial^3 \eta}{\partial \xi^3} + \mathfrak{G}(1) \frac{\partial^2 \eta}{\partial \xi^2} \frac{\partial \eta}{\partial \xi} \right] \right\} = \mathfrak{A}. \end{aligned} \quad (6.222b)$$

This equation has the form suitable for further analysis. Nothing can be inferred about the size of the various coefficients involved. In particular, they need not be  $\mathcal{O}(1)$  as they follow from the integrations that must be performed to evaluate them.

Our aim here is not a full exploitation of Equation (6.222b), as we are merely interested in a first-order extension of the kinematic wave theory. We shall therefore *assume* that terms of order  $\mathcal{O}(\mu\delta)$  and  $\mathcal{O}(\mu^2\delta)$  are negligible as compared to the other terms so that we shall now be dealing with the equation

$$\frac{\partial \eta}{\partial \tau} + \mathfrak{C}(1) \frac{\partial \eta}{\partial \xi} - \mu \mathfrak{D}(1) \frac{\partial^2 \eta}{\partial \xi^2} - \mu^2 \mathfrak{F}(1) \frac{\partial^3 \eta}{\partial \xi^3} + \delta \mathfrak{C}'(1) \eta \frac{\partial \eta}{\partial \xi} = \mathfrak{A}. \quad (6.223)$$

In this equation,  $\mathfrak{C}$  and  $\mathfrak{D}$  are, as above, a wave speed and a diffusivity. The term involving the third spatial derivative is attributed to *dispersion* and the last non-linear term is of a convective nature. The equation combines two well-known equations of the wave literature, namely the *Korteweg-de Vries equation* and the *Burgers equation*. When dispersion is ignored, the Burgers equations emerges, when the non-linear term is neglected the Korteweg–de Vries equation obtains. Solution techniques for these equations are well understood and discussed, for instance, by Whitham [44]. Coefficients are constant, since small perturbations about the steady state of a strictly parallel-sided ice slab are analysed.

Clarity about which terms of Equation (6.223) must be considered is obtained if the magnitude of the various coefficient functions is determined. First indications follow, if no slip is assumed,  $\mathfrak{C} = 0$ , and Glen's flow law is used,  $k = 0$ , for which  $\mathfrak{C}$  and  $\mathfrak{D}$  are still well defined. Equations (6.204), (6.209) and (6.220) then show that

$$\frac{\mathfrak{C}(1)}{\sin \gamma} = 2, \quad \frac{\mathfrak{C}'(1)}{\mathfrak{C}(1)} = 2, \quad \frac{\mathfrak{D}(1)}{\mathfrak{C}(1)} = \frac{d}{2} \cotan \gamma$$

with  $d = (\frac{1}{3}, \frac{1}{2}, \frac{3}{5})$  for  $n = 1, 2, 3$ . Hence, provided the last two terms on the left-hand side turn out to be negligible and as long as the inclination angles  $\gamma$  are not small, the simple forward wave equation is a good model for the prediction of surface waves on glaciers. For small inclination angles, on the other hand,  $\cot \gamma$  becomes large and diffusion is no longer negligible. In the discussion below this will be assumed, even when glaciers are moderately steep.

Because Equation (6.223) has constant coefficients, it can best be studied when it is subject to the Galilean transformation

$$X = \frac{\xi - \mathfrak{C}t}{(\mu \mathfrak{D})^{1/2}}, \quad T = \bar{t}.$$

Then, because

$$\frac{\partial}{\partial t} = \frac{\partial}{\partial T} - \frac{\mathfrak{C}}{(\mu \mathfrak{D})^{1/2}} \frac{\partial}{\partial X},$$

it assumes the form

$$\frac{\partial \eta}{\partial T} - \frac{\partial^2 \eta}{\partial X^2} - \left( \frac{\delta}{\mu^{1/2} \mathfrak{D}^{1/2}(1)} \right) \eta \frac{\partial \eta}{\partial X} - \left( \mu^{1/2} \frac{\mathfrak{F}(1)}{\mathfrak{D}(1)^{3/2}} \right) \frac{\partial^3 \eta}{\partial X^3} = \mathfrak{A}. \quad (6.224)$$

The first two terms on the left-hand side correspond to the theory accounting for diffusion. The third term represents a non-linear convection, whereas the last term corresponds to dispersion. The significance of these latter two terms depends upon the order of magnitude of the coefficients. To calculate these only the evaluation of  $\mathfrak{F}(1)$ ,  $\mathfrak{D}(1)$  and  $\mathfrak{C}'(1)$  is necessary. Expressions for these can be obtained from (6.204), (6.217) and (6.220).

(γ) *Numerical results.* The calculations performed above remain rather theoretical and are of little help for real glaciological problems as long as no numerical values for the various coefficients of the surface-wave equation are available. Since our model treats surface waves on a plane parallel-sided slab, it will be of value for a glacier in the regions far from its head or its snout.

Several effects are built into the model:

- (i) finite inclination of the ice slab,
- (ii) sliding of the ice over its bed,
- (iii) generalization of the power flow law.

It is interesting to see how these effects influence the coefficients in the basic governing equations, but it is hardly worthwhile presenting explicit calculations that are involved in the evaluation of the coefficient functions. These calculations were performed by Hutter, and explicit formulae for the coefficients of (6.224) are given in [13]. Here we simply discuss the results.

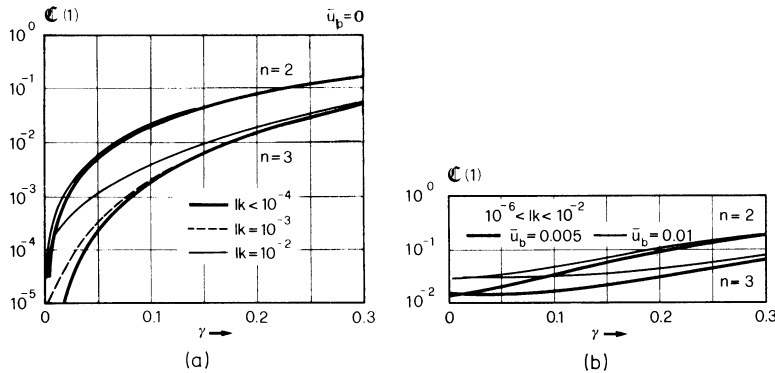


FIG. 6.22. (a) Surface-wave velocity  $C(1)$  as a function of the inclination angle  $\gamma$  parameterized for  $n = 2, 3$  and various values of  $k$  in the generalized Glen flow law. No slip of the glacier at the bed. (b) Same as (a), but for the case when sliding occurs. The sliding law is  $\bar{u}_b = C\tau^m$ , and has been used for  $m = 2$ . The thick lines are for  $\bar{u}_b = 0.005$ , the thin lines for  $\bar{u}_b = 0.01$ . (From [13].)

In the original coordinates  $\xi$  and  $\ell$  the corresponding equation contains two constants,  $C(1)$  and  $D(1)$ , which are now incorporated in the variable  $X$ . In Figure 6.22 and 6.23 these two coefficients are plotted against the inclination angle  $\gamma$ . Curves are shown for two values, namely  $n = 2$  and  $n = 3$ , of the exponent in the power flow law. Furthermore, they are parameterized for different values of the coefficient  $k$  in the more general law (6.202). Figure 6.22a and 6.23a hold for an ice slope adhering to its bed. In Figures 6.22b and 6.23b, two sliding velocities have been introduced, namely  $\bar{u}_b = 0.005$  and  $\bar{u}_b = 0.01$ . (Notice that this corresponds to a sliding parameter  $C = \bar{u}_b / \sin^m \gamma$ ; hence, keeping  $\bar{u}_b$  fixed means that  $C$  changes with  $\gamma$ . Calculations were per-

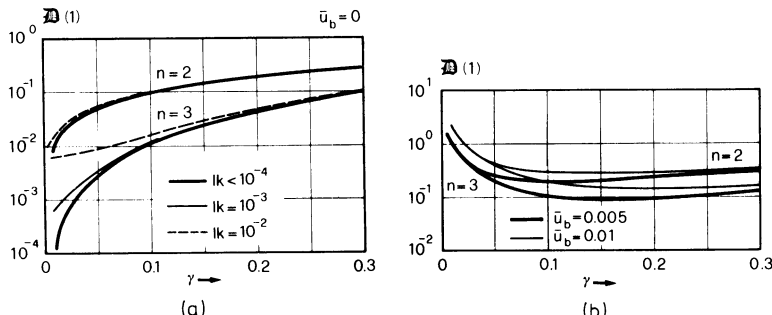


FIG. 6.23. (a) Diffusion parameter  $D(1)$  as a function of the inclination angle  $\gamma$  parameterized for  $n = 2, 3$  and for various values of  $k$  in the generalized Glen flow law. No slip of the glacier at the bed. (b) Same as (a), but for the case when sliding occurs. The sliding law is  $\bar{u}_b = C\tau^m$ ,  $m = 2$ . (From [13].)

formed for  $m = 2$ .) It is seen that the generalization of the power-flow law has little effect on the numerical values of  $\mathfrak{C}$  and  $\mathfrak{D}$ . This is no surprise after all, because the expressions for  $\mathfrak{C}$  and  $\mathfrak{D}$  show no singularity when  $k = 0$ . The dependence on the inclination angle  $\gamma$ , the exponent  $n$ , and on the sliding velocity are more important. To find the range of importance of diffusion we write Equation (6.223) with respect to the variables

$$\bar{\xi} = \xi / \mathfrak{C}(1), \ell$$

and the find to first order in  $\mu$

$$\frac{\partial \eta}{\partial \tau} + \frac{\partial \eta}{\partial \bar{\xi}} - \mu \frac{\mathfrak{D}(1) \partial^2 \eta}{\mathfrak{C}(1) \partial \bar{\xi}^2} + \mathcal{O}(\mu^2) = \mathfrak{A}.$$

For the power-flow law and when the ice adheres to the bed, it is shown that  $\mathfrak{D}(1)/\mathfrak{C}(1) \propto \cot \gamma$ . For small angles (in reality, for most glaciers) diffusion is therefore important. Whether this fact also persists when sliding over the bed is allowed for, can easily be inferred from Figures 6.22b and 6.23b. Accordingly,  $\mathfrak{D}(1)/\mathfrak{C}(1)$  grows monotonically with decreasing  $\gamma$ . Numerical calculations indicate that with sufficient accuracy one may set  $\mathfrak{D}(1)/\mathfrak{C}(1) = 0.6 \cot \gamma$ . Hence, even when sliding occurs, diffusion remains significant at all occurring inclination angles.

Diffusion being significant, we shall henceforth and irrespective of what value the wavelength parameter  $\mu$  may have, use  $X$  and  $T$  as independent variables. With their use, significance of dispersion and 'convection' follows from numerical values of  $\mathfrak{C}'(1)/\sqrt{\mathfrak{D}(1)}$ ,  $\mathfrak{F}(1)/\mathfrak{D}(1)^{3/2}$ .

In Figure 6.24 the first of these parameters is plotted as a function of  $\gamma$ , parameterized for different values of  $k$ . In Figure 6.24a the no-slip condition has been applied, whereas Figure 6.24b shows the corresponding results,

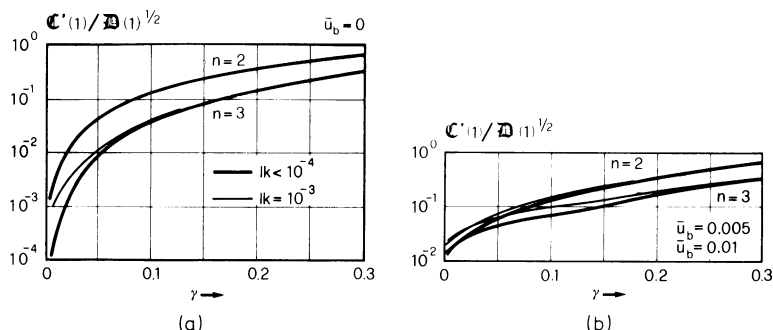


FIG. 6.24. (a)  $\mathfrak{C}'(1)/\mathfrak{D}(1)^{1/2}$  as a function of the inclination angle  $\gamma$  parameterized for  $n = 2, 3$  and various values of  $k$  in the generalized Glen flow law. No slip of the glacier at the bed. (b) Same as (a), but for the case when sliding occurs. The sliding law is  $\bar{u}_b = \mathfrak{C}\tau^m$ ,  $m = 2$ . (From [13].)

including sliding. Generally, sliding enhances the value of  $\mathfrak{F}(1)/\sqrt{\mathfrak{D}(1)}$  at small inclinations, but has practically no influence on it at larger inclinations  $\gamma$ . Since, for most inclinations  $\gamma$  occurring in practice  $|\mathfrak{F}(1)/\sqrt{\mathfrak{D}(1)}| = \mathcal{O}(10^{-1})$  we conclude that *the non-linear term  $\eta(\partial\eta/\partial X)$  in equation (6.224) need not be taken into account except, perhaps, in steep and hanging glaciers* for which the last term on the left-hand side of (6.224) may be of the same order as the usual diffusion parameters.

The significance of dispersion can be estimated from Figures 6.25a, b, c. Unlike the functions of the previous graphs, the value of  $\mathfrak{F}(1)/\mathfrak{D}(1)^{3/2}$  strongly depends on the parameter  $k$  in the flow law. The reason, clearly, is that  $\mathfrak{F}(1) \rightarrow \infty$  as  $k \rightarrow 0$ . For a glacier adhering to its bed  $\mathfrak{F}(1)/\mathfrak{D}(1)^{3/2}$  grows with growing  $\gamma$  and is, except for very small angles  $\gamma$ , of the order of  $10^0$ – $10^3$ . When sliding takes place  $\mathfrak{F}(1)/\mathfrak{D}(1)^{3/2}$  also increases as  $\gamma \rightarrow 0$ . Here we may uniformly say that  $\mathfrak{F}(1)/\mathfrak{D}(1)^{3/2}$  is large. Its value also depends rather critically on the value of the coefficient  $n$ . We conclude that *under no circumstances is it allowed to neglect the dispersion term* because, under usual situations,

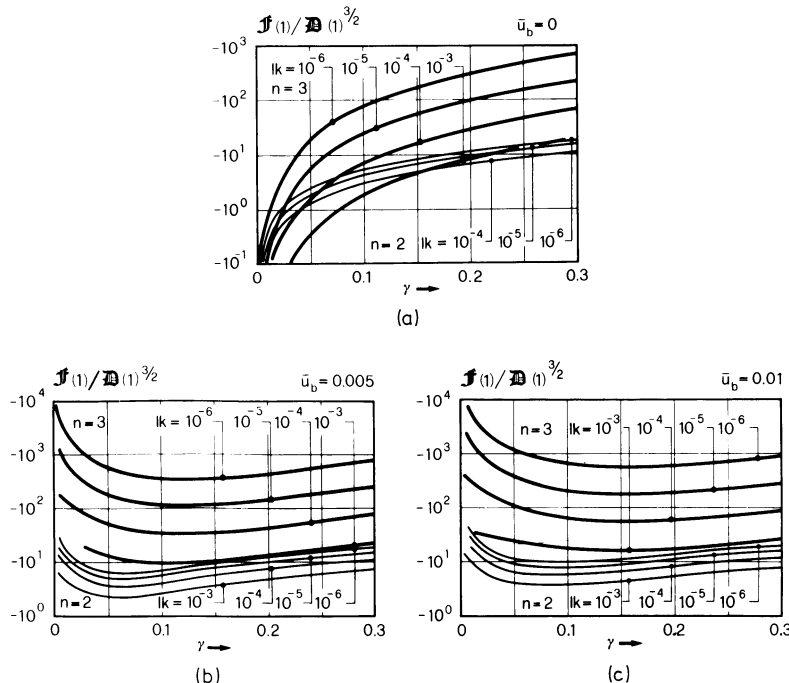


FIG. 6.25. (a) Dispersion parameter  $\mathfrak{F}(1)/\mathfrak{D}(1)^{3/2}$  plotted against the inclination angle  $\gamma$  parameterized for  $n = 2, 3$  and various values of  $k$ . No slip of the glacier at the bed. (b) Same as (a), but for a sliding velocity  $\bar{u}_b = 0.005$ . The sliding law is  $\bar{u}_b = C\tau^m$ ,  $m = 2$ . (c) Same as (a), but for a sliding velocity  $\bar{u}_b = 0.01$ . The sliding law is  $\bar{u}_b = C\tau^m$ ,  $m = 2$ . (From [13].)

its coefficient is of the order of  $10^0$  and larger. The dispersion coefficient may even exceed the value  $10^0$  by several orders of magnitude. Consequently, dispersion in glaciers may very well be of greater significance than is diffusion.

We thus see that the wave equation describing perturbations of surface profiles include terms which go beyond diffusion. It is a disadvantage that this result is obtained by an approximation procedure which becomes singular when the creep response function  $\mathfrak{F}(x)$  has an infinite slope at  $x = 0$ . Nevertheless, the above calculations indicate that the present status of the theory of surface waves is by no means satisfactory, and this is so for several different reasons. It appears that accounting for diffusion is not enough, and even if it were, it is still not clear what boundary conditions should be imposed at the margins in an unsteady surface-wave problem in which diffusion is taken into account. Any useful reliable application of the surface-wave problem ought to await the proper result of these questions.

### 6. Concluding Remarks

In this chapter time-dependent processes on model glaciers were analysed with the aim of understanding the physics and mathematics underlying the basic problem. In the first part, glaciers were treated as a whole; their response to climatic changes was described by treating the flow as being unidirectional. By applying balance of mass to the glacier as a whole along the preferred flow direction, the kinematic wave equation was derived. Balance of momentum was used in an *ad-hoc* manner to obtain an expression for the mass flux of ice in terms of actual glacier depth, the two equations complemented by geometric statements made up a full set of equations for the glacier depth. These equations were linearized and subsequently discussed and exploited in detail, thereby virtually completely covering the work developed by Nye. This much is roughly familiar to most applied glaciologists.

In the second part, the problem of time-dependent response of a glacier was analysed from a more fundamental point of view. Attention was restricted to plane flow. By incorporating the fact of slow surface variation and basal topography into the basic equations of mass and momentum balance (through the introduction of the shallow ice approximation), it was possible to find a rational procedure for the derivation of the equations of the free-surface geometry, velocity and stress distributions. By combining the continuity equation and the kinematic boundary condition at the base, the kinematic wave equation is found to apply for plane waves, but the flux function  $Q$  must be calculated from careful considerations of momentum balance. The non-linear equations, which emerge from the application of the perturbation scheme suggested by the shallow ice approximation, were then analysed more closely. It was found that to lowest order, the simple for-

ward wave equation resulted. The flavor of the analysis of this lowest-order theory is 'shock-dynamics' well known, e.g., in gas dynamics. A complete treatment of the initial-boundary-value problem that includes the evolution of the snout position is, however, rather complex. When diffusion is accounted for, these shocks are smoothed out, but difficulties arise with the boundary conditions at the glacier head, as fewer boundary conditions are suggested physically than one would expect to be necessary mathematically. To date, this matter is not clearly understood and needs further study before the non-linear convection-diffusion equation with singular coefficients can be applied to a real problem. Finally, a yet higher-order analysis of time-dependent surface effects in an infinitely-long ice slab indicated that considering diffusion alone might not be sufficient in an analysis of surface waves travelling down-glacier.

Several effects have been ignored, however. Among these we mention three-dimensionality, temperature variation and, above all, waves other than surface waves. In valley glaciers, effects of the side valleys must cause the flow to become three-dimensional. Temperature effects were included above, but only in principle and by treating the temperature as a known function. The restriction to surface waves, finally, was based on the fact that the sliding law and the creep-response function are well behaved functions. *Surges* and *seasonal waves* were therefore excluded from the above analysis. These waves are still not clearly understood, but an analysis that is based on the assumption that the sliding law may, under certain circumstances, cease to be a well-behaved function is given by Fowler [11].

#### REFERENCES

1. Bindschadler, R. A., A time-dependent model of temperate glacier flow and its application to predict changes in the surge-type Variegated Glacier during its quiescent phase. PhD Thesis, University of Washington, 1978.
2. Bindschadler, R. A., W. D. Harrison, C. F. Raymond, and C. Gautet, Thermal regime of a surge-type glacier. *J. Glaciology*, **16**, 251–259, 1976.
3. Bindschadler, R. A., W. D. Harrison, C. F. Raymond, and R. Croson, Geometry and dynamics of a surge-type glacier, *J. Glaciology*, **18**, 181–194, 1977.
4. Budd, W. F., A first simple model for periodically self-surging glaciers. *J. Glaciology*, **14**, 3–21, 1975.
5. Budd, W. F. and D. Janssen, Numerical modelling of glacier systems. Union Géodesique et Géophysique Internationale. Association Internationale d'Hydrologie Scientifique. Symposium Neiges et Glaces. Actes du Colloque de Moscow. *International Association for Scientific Hydrology Publ.*, **104**, 257–291, 1975.
6. Clarke, G. K. C., Thermal regulation of glacier surging. *J. Glaciology*, **16**, 231–250, 1976.
7. Clarke, G. K. C., P. W. Cary, and W. R. Peltier, A creep instability analysis of the Antarctic and Greenland ice sheet. *Can. J. Earth Sci.*, **16**, 182–188, 1979.
8. Courant, R. and K. O. Friedrichs, *Supersonic Flow and Shock Waves*. Applied Mathematical Sciences, Vol. 21, Springer-Verlag, New York. Heidelberg, Berlin, 1976.

9. Finsterwalder, S.. Die Theorie der Gletscherschwankungen. *Zeitschrift für Gletscherkunde*. **2**, 81–102, 1907.
10. Finsterwalder, R., Chamonix Glacier, (letter to editor), *J. Glaciology*, **3**, 547–548, 1959.
11. Fowler, A. C., Waves on glaciers, *J. Fluid Mech.*, **120**, 283–321, 1982.
12. Fowler, A. C. and D. A. Larson. On the flow of polythermal glaciers. Part II: Surface wave analysis, *Proc. Royal Soc. London*, **A370**, 155–171, 1980.
13. Hutter, K., Time dependent surface elevation of an ice slope. *J. Glaciology*, **25**, 247–266, 1980.
14. Hutter, K.. The effect of longitudinal strain on the shear stress of an ice sheet. In defense of using stretched coordinates. *J. Glaciology*, **27**, 39–56, 1981.
15. Jonas, J. J. and F. Müller. Deformation of ice under high internal shear stresses. *Can. J. Earth Science*, **6**, 963–968, 1969.
16. Kluwick, A.. Kinematische Wellen. *Acta Mechanica*, **26**, 15–46, 1977.
17. Langdon, J. and C. F. Raymond. Numerical calculation of adjustment of a glacier surface to perturbations of ice thickness. *Dokl. Acad. Sci. U.S.S.R. Glaciol. Sect.*, **32**, 123–133, 1978.
18. Lick, W.. The propagation of disturbances on glaciers. *J. Geophys. Res.*, **79**, 2181–2197, 1970.
19. Lighthill, M. J. and G. B. Whitham. On kinematic waves: I. Flood movements in long rivers, *Proc. Royal Soc. London*, **A229**, 281–316, 1955.
20. Lighthill, M. J. and G. B. Whitham, On kinematic waves: II. Theory of traffic flow on long crowded roads. *Proc. Royal Soc. London*, **A229**, 318–345, 1955.
21. Lliboutry, L. A.. La dynamique de la Mer de Glace et la vague de 1891–95 d'après les mesures de Joseph Vallot. Union Géodésique et Géophysique Internationale. Association Internationale d'Hydrologie Scientifique. Symposium de Chamonix (1958). Physique du mouvement de la glace, *International Association for Scientific Hydrology Publ.*, **47**, 125–138, 1958.
22. Lliboutry, L. A.. *Traité de glaciologie. Tome II: Glaciers, variations du climat, sols gelés.* Masson. Paris, 1965.
23. Lliboutry, L. A.. The glacier theory, in *Advances in Hydrosciences*, Edited by Ven Te Chow, Academic Press. New York. Vol. 7, 81–167, 1971.
24. Lliboutry, L. A.. Instability of temperate ice sheets owing to a feedback mechanism. *Nature*, **203**, 627–629, 1964.
25. Marchi de, L.. La propagation des ondes dans les glaciers. *Zeitschrift für Gletscherkunde*, **5**, 207–211, 1911.
26. Meier, M. F. and J. N. Johnson. The kinematic wave on Nisqually Glacier, Washington. *J. Geophys. Res.*, **67**, 886, 1962.
27. Morland, L. W. and I. R. Johnson. Steady motion of ice sheets. *J. Glaciology*, **25**, 229–246, 1980.
28. Morland, L. W. and I. R. Johnson, Effects of bed inclination and topography on steady isothermal ice sheets, *J. Glaciology*, **25**, 225–246, 1980.
29. Nielsen, L. E.. The ice-dam, powderflow theory of glacier surges. *Can. J. Earth Sci.*, **6**, 955–961, 1969.
30. Nye, J. F.. Surges in glaciers. *Nature*, **181**, 1450–1451, 1958.
31. Nye, J. F.. The response of glaciers and ice sheets to seasonal and climatic changes. *Proc. Roy. Soc. London*, **256A**, 559–584, 1960.
32. Nye, J. F.. On the theory of the advance and retreat of glaciers, *Geophys. J. Roy. Astron. Soc.*, **7**, 431–456, 1963.
33. Nye, J. F.. The response of a glacier to changes in the rate nourishment and wastage. *Proc. Roy. Soc. London*, **275**, 87–112, 1963.
34. Nye, J. F.. The frequency response of glaciers. *J. Glaciology*, **5**, 567–587, 1965.

35. Nye, J. F., A numerical method of inferring the budget history of a glacier from its advance and retreat. *J. Glaciology*, **5**, 589–607, 1965.
36. Palmer, A. C., A kinematic wave model of glacier surge. *J. Glaciology*, **11**, 65–72, 1972.
37. Raymond, C. F., Temperate valley glaciers, in *Dynamics of Snow and Ice Masses*, edited by S. C. Colbeck. Academic Press, New York, pp. 79–139, 1980.
38. Rasmussen, L. A. and W. J. Campell, Comparison of three contemporary flow laws in a three dimensional, time-dependent glacier model. *J. Glaciology*, **12**, 361–374, 1973.
39. Robin, G. de Q., Initiation of glacier surges. *Can. J. Earth Sci.*, **6**, 916–928, 1969.
40. Schytt, V., Some comments on glacier surges in Eastern Svalbard. *Can. J. Earth Sci.*, **6**, 867–873, 1969.
41. Thompson, D. E., Stability of glaciers and ice sheets against flow perturbations. *J. Glaciology*, **24**, 427–441, 1979.
42. Untersteiner, N. and J. F. Nye, Computations of the possible future behavior of Berendon Glacier, Canada. *J. Glaciology*, **7**, 205–213, 1968.
43. Weertman, J., Travelling waves on glaciers, Union Géodesique et Géophysique Internationale, Association Internationale d'Hydrologie Scientifique, Symposium de Chamonix (1958). Physique du mouvement de la glace. *International Association for Scientific Hydrology, Publ.*, **47**, 162–168, 1958.
44. Whitham, G. B., *Linear and Nonlinear Waves*. John Wiley-Interscience, New York, 1974.
45. Szidarowski, F. and S. Yakowitz, *Principles and Procedures of Numerical Analysis*, Plenum Press, New York, London, 1978.
46. Yuen, D. A. and G. Schubert, The role of shear heating in the dynamics of large ice masses. *J. Glaciology*, **24**, 195–212, 1979.

## **Chapter 7**

# **THREE-DIMENSIONAL AND LOCAL FLOW EFFECTS IN GLACIERS AND ICE SHEETS**

### *1. Introduction*

The investigations of ice-flow problems which have been undertaken in this book so far, have been rather qualitative and thus theoretical because only plane flow was considered and, furthermore, very simple glacier geometries were assumed. Either conditions near the strictly parallel-sided ice slab were analysed or the top and bottom surfaces were assumed to vary slowly in the horizontal directions. Three important problems, however, remained untouched; they are:

- (i) Valley glaciers are bounded by mountain sides. These flanks affect the flow and their influence is all the greater, the narrower the valley. Hence, ice flow in a channel of a finite cross-section should be analysed. As a first approximation, flow in a cylindrical channel provides sufficient indications as to the order of magnitude of the boundedness effect of the valley.
- (ii) The analyses of ice sheets were performed in Chapters 5 and 6 for plane motion, and it was shown that real ice sheets spread in both horizontal directions. In order to be able to predict real ice-sheet geometries, the solution procedures of Chapters 5 and 6 should, therefore, be generalized to include both horizontal dimensions.
- (iii) Most ice-flow problems in glaciers that are relevant in engineering, are of a *local* nature and so the simplifications of a nearly-parallel-sided ice slab or the shallow-ice approximation do not apply. Under these circumstances, the full two- or three-dimensional boundary-value problem must be solved, but the complexity of these problems is generally so immense that no analytic solutions can be found. Numerical techniques, of which finite differences and finite elements are two alternatives, must then be resorted to. The latter profits from the existence of variational principles.

These, then, are the general topics to be discussed in this chapter. The rectilinear flow in a cylindrical channel will be analysed first. The

developments follow mainly Nye [18] who presented the first numerical analysis for channels of rectangular, semi-elliptical, and parabolic cross-sections. We shall, however, go one step further and present an approximate analysis for the velocity distribution in the middle part of the cross-section of a wide valley glacier. The formulas for the velocity distribution of this limited case are easy to explore and can be corroborated with field data.

In a further section, we develop an approximate theory of the motion of ice sheets. The basis of this approximation is the shallow-ice approximation, but two-dimensional spreading is also considered. The method follows closely the Morland-Johnson scheme of Chapters 5 and 6, and the systematic derivation of the non-linear partial differential equation and its associated margin conditions appear for the first time in this book. A numerical exploration of the problem for a steady-state, two-dimensional surface profile remains an untouched problem, left for further research.

Finite-element techniques have not been widely used in glaciology, the reason probably being that the non-linear constitutive relationship and the three-dimensionality of the practically-meaningful problems make the numerical-solution scheme an extremely difficult one. The finite-element specialist knows, however, that derivations of numerical schemes are substantially simplified when the equations governing the boundary-value problem under consideration are derivable from a function by setting its first variation to zero. We present the variational principles that are applicable for glacier and ice-sheet flows and state their conditions of validity. The analysis closely parallels that of Johnson [13, 14]. It is found that his variational theorems do not include a non-linear sliding law. Other theorems should therefore be found which cover this case, but these, not being presently available leaves the application of the weighted residuals principle as the only other alternative.

We do not demonstrate how the variational principles are applied to real finite-element approximations. The reader must find this out from the available literature (see, e.g., Zienkiewicz [27]). However, we briefly indicate to what problems finite-element techniques have been applied so far and what inferences can be drawn from them.

## 2. *Effect of Valley Sides on the Motion of a Glacier*

Real ice flow is seldom planar; it always reflects some notion of three dimensionality. In mountain glaciers this effect must be particularly pronounced as the glaciers flow in valleys, and the ice is supported from the sides as well as from the bottom. The effect of the sides is that the velocity not only varies with depth but, equally, also sidewise, resulting in a three-dimensional velocity profile.

The effect of the side walls of a glacier on its flow mechanism is expected

to be of dominant importance, more important than are, for instance, the effects of variations in surface slope and inclination of the bed. To analyse the problem, we ignore surface variations and assume rectilinear flow in a cylindrical channel of an arbitrary, but well defined cross-section. The general problem of steady motion in such an open channel is a complicated one, since, in general, the flow and temperature distribution are coupled. When temperature variations are ignored, the ice-flow problem becomes a purely mechanical one and is substantially simplified. Further simplifications are introduced by restricting attention to no-slip at the boundary, but this assumption can be relatively easily removed.

Before we present the equations governing this flow, a word of caution should be raised regarding the tacit assumption of a rectilinear flow. As is well known to people in non-Newtonian fluid mechanics, rectilinear channel flow does not always exist. There are certain laws that necessarily entail transverse circulation in steady-channel flow. A scrutiny of the literature, see Green and Rivlin [7] and Truesdell and Noll [25], shows that such a secondary flow only arises for constitutive relationships of stress whose coefficients depend not only on the second but also on the third stress-deviator invariant. The creep law

$$\mathbf{D} = f(t'_{II})\mathbf{t}', \quad (7.1)$$

in which  $\mathbf{D}$  is stretching,  $\mathbf{t}'$  stress deviator and  $t'_{II}$  its second invariant, does not fall into this category. Caution must also be observed for the more general constitutive relationships (2.70). These also exhibit the complexity which may exclude rectilinear flow. Incidentally, the existence or absence of evidence of secondary flow features may be taken as an argument for selecting the constitutive relationship accordingly. There is no observational evidence of secondary flow in Alpine glaciers, although some indications of secondary flow on a glacier in Northern Canada has been reported by Shaw [23, 24], however. We shall not be concerned with these secondary flow effects in this section.

To present the governing equations, a Cartesian coordinate system is chosen as in Figure 7.1, where  $x$  is down-glacier on the flat top surface,  $y$  transverse and  $z$  horizontal across the channel width. Equations are non-dimensionalized as before. Lengths are made non-dimensional with a typical length  $D$  within the cross-section, stresses are scaled with  $\rho g D$  and velocities with a typical longitudinal velocity  $U$ . As before, dimensionless quantities will be indicated by overbars or Greek letters. For instance, Equation (7.1) becomes

$$\bar{\mathbf{D}} = \bar{\mathfrak{F}}(\tau'_{II})\bar{\boldsymbol{\sigma}}', \quad (7.2)$$

in which  $\bar{\mathfrak{F}}$  is the dimensionless creep-response function. The only non-trivial velocity component in rectilinear flow is  $\bar{u}$ , the component in  $\bar{x}$ -

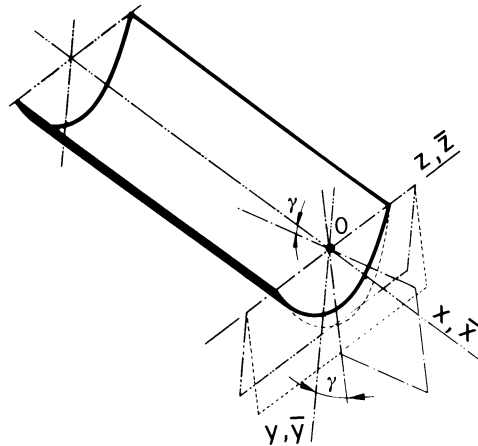


FIG. 7.1. Perspective view of a cylindrical channel. The coordinate  $x$  is measured down-glacier on the flat surface,  $y$  is transverse and  $z$  horizontal. Indicated is also the vertical plane, forming an angle  $\gamma$  relative to cross sectional planes.

direction. The matrix for  $\bar{\mathbf{D}}$  in the  $(\bar{x}, \bar{y}, \bar{z})$ -coordinate system is therefore given by

$$\bar{\mathbf{D}} = \begin{bmatrix} 0 & \frac{1}{2} \frac{\partial \bar{u}}{\partial \bar{y}} & \frac{1}{2} \frac{\partial \bar{u}}{\partial \bar{z}} \\ \frac{1}{2} \frac{\partial \bar{u}}{\partial \bar{y}} & 0 & 0 \\ \frac{1}{2} \frac{\partial \bar{u}}{\partial \bar{z}} & 0 & 0 \end{bmatrix}, \quad (7.3)$$

in which  $\partial \bar{u} / \partial \bar{x}$  has been set to zero. Henceforth, in this section, such  $\bar{x}$ -derivatives will tacitly be omitted. Equations (7.2) and (7.3) together imply that  $\sigma'$  has vanishing normal components which necessarily requires that

$$\sigma_x = \sigma_y = \sigma_z.$$

The proof of this statement which is straightforward, is left to the reader. Moreover, (7.2) and (7.3) imply that  $\tau_{yz}' = 0$  so that the only non-trivial equilibrium equations and stress-stretching relationships assume the form

$$\frac{\partial \tau_{xy}}{\partial \bar{y}} + \frac{\partial \tau_{xz}}{\partial \bar{z}} + \sin \gamma = 0, \quad \frac{\partial \sigma_y}{\partial \bar{y}} + \cos \gamma = 0, \quad \frac{\partial \sigma_z}{\partial \bar{z}} = 0, \quad (7.4)$$

and

$$\frac{\partial \bar{u}}{\partial \bar{y}} = 2\bar{\mathfrak{F}}(\tau'_{ll})\tau_{xy}, \quad \frac{\partial \bar{u}}{\partial \bar{z}} = 2\bar{\mathfrak{F}}(\tau'_{ll})\tau_{xz}, \quad (7.5)$$

with  $\tau'_{ll} = \tau_{xy}^2 + \tau_{xz}^2$ .

Boundary conditions are

$$\begin{aligned}\tau_{xy} &= 0, & \sigma_y &= -\bar{p}^{\text{atm}}, \quad \text{at } \bar{y} = 0, \\ \bar{u} &= \mathbb{C}|\tau|^m, \quad \text{at } \bar{y} = \bar{y}_B(\bar{x}).\end{aligned}\tag{7.6}$$

A straightforward integration of (7.4)<sub>2,3</sub> subject to boundary condition (7.6)<sub>2</sub>, yields

$$\sigma_x = \sigma_y = \sigma_z = -\bar{p}^{\text{atm}} - \cos \gamma \bar{y}. \tag{7.7}$$

The problem is then completed by integrating (7.4)<sub>1</sub>, (7.5), subject to the remaining boundary conditions (7.6).

#### (a) *Solutions in special cases*

One solution to the above boundary-value problem has previously been determined, namely the response of an infinitely-wide ice sheet to its own weight. There are other limiting cases to which analytical solutions can be found. Among them are the infinitely deep narrow channel and the semi-circular channel. Perturbations of these limiting cross-sectional profiles give the very wide and deep rectangle and the slightly elliptical cross-section. Solutions to the limiting cases were constructed by Nye [18] and the flow down the slightly elliptical channel was approximately analysed by Chester (see the Appendix in Nye [18]). The solutions of the very wide and deep rectangle are still not fully known, however.

(α) *Exact solutions for the limiting cases.* Here, we briefly discuss the three special solutions mentioned above, namely

- (i) the infinitely-wide channel of depth 1\*,
- (ii) the infinitely-deep channel of width 2\*,
- (iii) the semi-circle of radius 1\*.

Hence, the surface width of the semi-circle is the same as the width of the infinitely-deep channel and the infinitely-wide channel is half as deep as the infinitely-deep channel is wide.

(i) Solutions for this case have been determined in Chapter 3 already and we only need to quote the results [see (3.77)–(3.81)]

$$\begin{aligned}\tau_{xz} &= \sin \gamma \bar{y}, \quad \tau_{xy} = 0, \\ \bar{u} &= \mathbb{C} \sin^m \gamma + 2 \int_{\bar{y}}^1 \mathfrak{F}(\sin^2 \gamma \xi^2) \xi \sin \gamma d\xi \\ &= \mathbb{C} \sin^m \gamma + \frac{2 \sin^n \gamma}{n+1} \{1 - \bar{y}^{n+1}\},\end{aligned}\tag{7.8}$$

\*These lengths are in non-dimensional coordinates.

where the second expression for  $\bar{u}$  obtains when  $\mathfrak{F}(x) = x^{(n-1)/2}$ , which corresponds to Glen's power law. The term involving  $C$  is the sliding velocity which for the no-slip condition will vanish.

(ii) The infinitely deep channel of width 2 can be treated by recognizing that in this case  $\bar{y}$ -derivatives of the velocity field will vanish but  $\bar{z}$ -derivatives will not. (7.5)<sub>1</sub> thus implies  $\tau_{xy} = 0$  and, consequently, in view of (7.4)<sub>1</sub>

$$\tau_{xz} = -\sin \gamma \bar{z}, \quad \tau_{xy} = 0, \quad (7.9)$$

in which the constant of integration has been set to zero as  $\tau_{xz}$  must be odd in  $\bar{z}$  because of symmetry reasons. With the results (7.9), the second of Equations (7.5) may be integrated subject to the boundary conditions at the wall (7.6)<sub>3</sub>. Thus, the solution is, in this case,

$$\begin{aligned} \tau_{xy} &= 0, \quad \tau_{xz} = -\sin \gamma \bar{z}, \\ \bar{u} &= C \sin^m \gamma + 2 \int_{\bar{z}}^1 \mathfrak{F}(\sin^2 \gamma \xi^2) \sin \gamma \xi \, d\xi \\ &= C \sin^m \gamma + \frac{2 \sin^m \gamma}{(n+1)} \{1 - |z|^{n+1}\}, \end{aligned} \quad (7.10)$$

in agreement with (7.8). Indeed the solutions of cases (i) and (ii) can be brought into full correspondence simply by interchanging the role of the  $\bar{y}$ - and the  $\bar{z}$ -axes. In other words, although gravity is taken into account and seems to give its direction a certain preference, this preference is not borne out by the solution. The reason is that the flow in a channel under gravity is exactly the same as the flow of the same fluid through a closed pipe whose cross-section is symmetrical about the free surface, if its pressure gradient is given by  $\sin \gamma$ .

(iii) Semi-circular cross-section: The above two cases lie at two extremes. They have the same maximum shear stresses and similar velocity profiles (one goes over to the other by simply interchanging  $\bar{y}$  with  $\bar{z}$ ). The semi-circular cross-section can be regarded as intermediate between the two. To derive the solution for this case, Equations (7.4)<sub>1</sub>, (7.5) and (7.6) must be written in cylindrical coordinates. In polar coordinates  $(\bar{r}, \theta)$  (see Figure 7.2), the boundary-value problem (7.4)<sub>1</sub>, (7.5) and (7.6) can be written as:

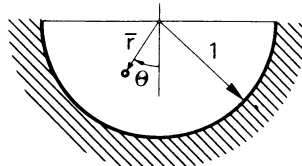


FIG. 7.2. Semi-circular cross-section of radius 1. Coordinates are  $\bar{r}$  and  $\theta$ .

Field equations:

$$\begin{aligned} \frac{1}{\bar{r}} \frac{\partial(\bar{r}\tau_{rx})}{\partial \bar{r}} + \frac{1}{\bar{r}} \frac{\partial \tau_{\theta x}}{\partial \theta} + \sin \gamma &= 0, \\ \frac{\partial \bar{u}}{\partial \bar{r}} &= 2\mathfrak{F}(\tau'_{II})\tau_{rx}, \quad \frac{1}{\bar{r}} \frac{\partial \bar{u}}{\partial \theta} = 2\mathfrak{F}(\tau'_{II})\tau_{\theta x}. \end{aligned} \quad (7.11)$$

Boundary conditions:

$$\begin{aligned} \tau_{\theta x} &= 0, \quad \text{on } \theta = \pm \frac{\pi}{2}, \\ \bar{u} &= \mathbb{C}\tau_{rx}^m \quad \text{on } \bar{r} = 1. \end{aligned} \quad (7.12)$$

Here,  $\tau_{rx}$  and  $\tau_{\theta x}$  are the only non-trivial physical components of the stress deviator in polar coordinates and  $\tau'_{II}$  is, as before, the second stress-deviator invariant. We try a solution which is independent of the angle  $\theta$ . This yields  $\tau_{\theta x} = 0$  and thus,  $(7.11)_1$  can be integrated to give

$$\tau_{rx} = -\frac{\bar{r}}{2} \sin \gamma + \frac{C}{\bar{r}}, \quad (7.13)$$

$C$  being a constant of integration. But  $\tau_{rx}$  is regular at  $\bar{r} = 0$ , and hence we necessarily have  $C = 0$ . Substitution of  $(7.13)$  into  $(7.11)_2$ , finally reveals a differential equation for  $\bar{u}$  subject to the boundary condition  $(7.12)_2$ . Its integration is straightforward. Collectively, the results for the semi-circle therefore read

$$\begin{aligned} \tau_{rx} &= -\frac{\bar{r}}{2} \sin \gamma, \quad \tau_{\theta x} = 0, \\ \bar{u} &= \mathbb{C} \left( \frac{1}{2} \right)^m \sin^m \gamma + 2 \int_{\bar{r}}^1 \mathfrak{F} \left( \frac{\bar{r}^2}{4} \sin^2 \gamma \right) \frac{\bar{r}}{2} \sin \gamma \, d\bar{r} \\ &= \mathbb{C} \left( \frac{1}{2} \right)^m \sin^m \gamma + 2 \left( \frac{\sin \gamma}{2} \right)^n \frac{1}{n+1} (1 - \bar{r}^{n+1}). \end{aligned} \quad (7.14)$$

Solution  $(7.14)$  may be thought of as intermediate between  $(7.8)$  and  $(7.10)$ . This is borne out very clearly if the stress components  $\tau_{xy}$  and  $\tau_{xz}$  are calculated; this gives\*

$$\tau_{xy} = \tau_{xz} = -\frac{1}{2} \sin \gamma \bar{z}.$$

Comparing this with the results stated in  $(7.8)$  and  $(7.10)$ , respectively, it is seen that the stresses  $\tau_{xy}$  and  $\tau_{xz}$  of the semi-circular cross-section lie exactly at the arithmetic mean of the solution to the infinitely-wide and infinitely-deep channel. The velocity, however, is more reduced than by a factor of two,

\*To evaluate these notice that for  $\theta = 0$   $\tau_{rx} = \tau_{xy}$  and for  $\theta = \pi/2$   $\tau_{rx} = \tau_{xz}$ . Since  $\tau_{rx}$  is independent of  $\theta$  the result is immediate.

indicating the major effect on the flux exerted by the walls. It is now interesting to see what inferences could be drawn for other, more general cross-sections.

( $\beta$ ) *Solution for a slightly off-circular channel.* When the boundary deviates only slightly from that of a semi-circle, a perturbation technique similar to the one used in obtaining solutions to the nearly parallel-sided ice slab is suggested. The technique is due to Chester, who constructed an approximate solution for the flow in a slightly elliptical cross-section, which was presented by Nye [18]. As a practical problem, the slightly elliptical-cross section is of little relevance. However, the example allows a clear demonstration of the use of a perturbation method and, moreover, the solutions can be used against other numerical solution procedures, as, for instance, finite difference and finite element schemes.

With the cross-section only slightly deviating from the semi-circle it is to be expected that the stress and velocity distribution will differ from that of a semi-circle by only a small margin. Hence, (7.11) will be used as field equations. Boundary conditions will be similar to those listed in (7.12) and the total solution will be composed of two contributions, namely the unperturbed flow with flow independent of  $\theta$  as listed in (7.14), and a perturbed solution, which is only a small correction to the above zeroth-order solution. Consequently, we write

$$\begin{aligned}\tau_{rx} &= \tau_{rx}^{(0)} + \varepsilon \tau_{rx}^{(1)} + \dots, & \tau_{\theta x} &= \varepsilon \tau_{\theta x}^{(1)} + \dots, \\ \bar{u} &= \bar{u}^{(0)} + \varepsilon \bar{u}^{(1)} + \dots,\end{aligned}\quad (7.15)$$

in which  $\varepsilon$  is a measure for the deviation of  $\bar{r} = \bar{r}_B(\theta)$  from the circle  $\bar{r} = 1$ . Hence

$$\varepsilon = \max_{-\pi/2 \leq \theta \leq \pi/2} |1 - \bar{r}_B(\theta)|.$$

The representations (7.15) are a first-order approximation of a full ‘Taylor series expansion’ of the solution in the parameter  $\varepsilon$ , in which the zeroth-order quantities satisfy (7.14). Substituting (7.15) into (7.11), expanding emerging expressions into powers of  $\varepsilon$ , and collecting terms of like powers of  $\varepsilon$  will yield a hierarchy of differential equations for the  $m$ th-order quantities. We are only interested in the first-order approximation and then obtain the differential equations:

$$\begin{aligned}\frac{\partial(\bar{r}\tau_{rx}^{(1)})}{\partial \bar{r}} + \frac{\partial \tau_{\theta x}^{(1)}}{\partial \theta} &= 0, \\ \frac{\partial \bar{u}^{(1)}}{\partial \bar{r}} &= 2[\tilde{\mathfrak{F}}(\tau_{ll}^{(0)}) + 2\tilde{\mathfrak{F}}'(\tau_{ll}^{(0)})\tau_{ll}^{(0)}]\tau_{rx}^{(1)}, \\ \frac{1}{\bar{r}} \frac{\partial \bar{u}^{(1)}}{\partial \theta} &= 2\tilde{\mathfrak{F}}(\tau_{ll}^{(0)})\tau_{\theta x}^{(1)},\end{aligned}\quad (7.16)$$

in which  $\tau_{II}^{(0)} = \frac{1}{4}\bar{r}^2 \sin^2 \gamma$ . Eliminating the first-order stresses, finally gives

$$\bar{r}^2 \frac{\partial^2 \bar{u}^{(1)}}{\partial \bar{r}^2} + \left\{ 1 - \frac{\bar{r}(\partial/\partial \bar{r})[\ ]}{2[\ ]} \right\} \bar{r} \frac{\partial \bar{u}^{(1)}}{\partial \bar{r}} + \frac{[\ ]}{\mathfrak{F}(\tau_{II}^{(0)})} \frac{\partial^2 \bar{u}^{(1)}}{\partial \theta^2} = 0, \quad (7.17)$$

where  $[\ ]$  is a shorthand notation for the bracketed term in (7.16). For a power-law fluid, (7.17) can be shown to reduce to the differential equation

$$\bar{r}^2 \frac{\partial^2 \bar{u}^{(1)}}{\partial \bar{r}^2} + \bar{r}(2-n) \frac{\partial \bar{u}^{(1)}}{\partial \bar{r}} + n \frac{\partial^2 \bar{u}^{(1)}}{\partial \theta^2} = 0. \quad (7.18)$$

The differential equation (7.18) must be solved subject to the appropriate boundary condition at the channel wall. In order not to unduly complicate the ensuing calculations we shall assume *no-slip*. Thus we must have

$$\bar{u}^{(0)} + \varepsilon \bar{u}^{(1)} = 0, \quad \text{at } \bar{r} = \bar{r}_b = 1 + \varepsilon R, \quad (7.19)$$

where  $R$  is given by the following Fourier-series expansion

$$R = \sum_{v=0}^{\infty} (a_v \sin v\theta + b_v \cos v\theta), \quad (7.20)$$

in which  $a_v$  and  $b_v$  are known Fourier coefficients. With the aid of (7.14), (7.19) can be written as

$$\begin{aligned} \varepsilon \bar{u}^{(1)}(\bar{r}_b) &= \varepsilon \bar{u}^{(1)}(1) + \mathcal{O}(\varepsilon^2) = 2 \int_1^{1+\varepsilon R} \mathfrak{F}\left(\frac{\bar{r}^2}{4} \sin^2 \gamma\right) \frac{\bar{r}}{2} \sin \gamma \, d\bar{r} \\ &= 2 \left[ \mathfrak{F}\left(\frac{\sin^2 \gamma}{4}\right) \frac{\sin \gamma}{2} \right] \varepsilon R + \mathcal{O}(\varepsilon^2) \end{aligned}$$

or

$$\bar{u}^{(1)}(1) = \mathfrak{F}\left(\frac{\sin^2 \gamma}{4}\right) \sin \gamma R + \mathcal{O}(\varepsilon) = 2 \left( \frac{\sin \gamma}{2} \right)^n R + \mathcal{O}(\varepsilon). \quad (7.21)$$

This is the boundary condition for  $\bar{u}^{(1)}$ . Notice that (7.21) is a condition valid at  $\bar{r} = 1$  rather than the true boundary  $\bar{r} = \bar{r}_B$ .

To solve (7.18), subject to the boundary condition (7.21), a separation of variables solution is sought. Writing, therefore

$$\bar{u}^{(1)} = \sum_{v=0}^{\infty} \{ F_v(\bar{r}) \sin v\theta + G_v(\bar{r}) \cos v\theta \}, \quad (7.22)$$

and substituting this representation into (7.18) and collecting coefficients of the sine and cosine functions yields

$$\bar{r}^2 f_v'' + \bar{r}(2-n)f_v' - v^2 n f_v = 0, \quad v = (0), 1, 2, \dots, \quad (7.23)$$

where  $f_v$  stands for  $F_v$  and  $G_v$ , respectively. This is a second-order ordinary differential equation for  $f_v$  whose solutions must be of the form  $f_v \propto \bar{r}^m$ .

The exponent  $m$  is easily calculated by substitution into (7.23) and reads

$$m_v = \frac{1}{2} \{ (n - 1) \pm \sqrt{(n - 1)^2 + 4nv^2} \}. \quad (7.24)$$

Of the two possibilities, only that with the positive square root sign applies because the other exponent would be negative, and the corresponding solution would become singular at  $\bar{r} = 0$ . We thus obtain as a solution

$$\bar{u}^{(1)} = \sum_{v=0}^{\infty} \{ c_v \bar{r}^{m_v} \sin v\theta + d_v \bar{r}^{m_v} \cos v\theta \},$$

in which  $c_v$  and  $d_v$  are coefficients to be determined from the boundary condition (7.21), implying that

$$c_v = 2 \left( \frac{\sin \gamma}{2} \right)^n a_v, \quad d_v = 2 \left( \frac{\sin \gamma}{2} \right)^n b_v, \quad v = (0), 1, 2, 3 \dots$$

This completes the formal solution for the perturbation velocity which now reads

$$\bar{u}^{(1)} = 2 \left( \frac{\sin \gamma}{2} \right)^n \sum_{v=0}^{\infty} \{ a_v \bar{r}^{m_v} \sin v\theta + b_v \bar{r}^{m_v} \cos v\theta \}. \quad (7.25)$$

where  $a_v$  and  $b_v$  are the Fourier coefficients of the periphery equation (7.20) and the exponents  $m_v$  are the positive solutions of (7.24).

For a slightly elliptical channel one has

$$\bar{r}_b = 1 + \varepsilon \sin^2 \theta = 1 + \frac{\varepsilon}{2} (1 - \cos 2\theta) \Rightarrow R = \frac{1}{2} (1 - \cos 2\theta).$$

Consequently, most coefficients in (7.25) vanish; indeed  $a_v = 0$  for all  $v \geq 0$ ,  $b_0 = \frac{1}{2}$ ,  $b_1 = 0$ ,  $b_2 = -\frac{1}{2}$  and  $b_v = 0$  for all  $v > 2$ . Hence the perturbed velocity field in this case becomes

$$\bar{u}^{(1)} = \left( \frac{\sin \gamma}{2} \right)^n (1 - \bar{r}^c), \quad (7.26)$$

where

$$c = \frac{1}{2} [n - 1 + \sqrt{n^2 + 14n + 1}]. \quad (7.27)$$

With the aid of (7.16)<sub>2,3</sub> it is now straightforward to calculate the perturbed stresses  $\tau_{rx}^{(1)}$  and  $\tau_{\theta x}^{(1)}$ . When these are combined with the lowest order stresses (7.14)<sub>1,2</sub> and, furthermore, the corrected velocity is evaluated, the following results for the total solution are obtained

$$\begin{aligned} \tau_{rx} &= -\frac{\sin \gamma}{2} \left\{ \bar{r} + \frac{\varepsilon c}{2n} \bar{r}^{c-n} \cos 2\theta \right\}, \\ \tau_{\theta x} &= \varepsilon \frac{\sin \gamma}{2} \bar{r}^{c-n} \sin 2\theta, \\ \bar{u} &= \frac{2}{n+1} \left( \frac{\sin \gamma}{2} \right)^n \left\{ 1 - \bar{r}^{n+1} + \varepsilon \frac{n+1}{2} (1 - \bar{r}^c \cos 2\theta) \right\}. \end{aligned} \quad (7.28)$$

This is Chester's solution, see Nye [18]. It applies for a slightly elliptical cross-section, a temperature-independent power flow law and no-slip at the wall. For  $n = 3$  Equation (7.28) become

$$\begin{aligned}\tau_{rx} &= -\frac{\sin \gamma}{2} \{ \bar{r} + 0.768\epsilon \bar{r}^{1.606} \cos 2\theta \}, \\ \tau_{\theta x} &= \epsilon \frac{\sin \gamma}{2} \bar{r}^{1.606} \sin 2\theta, \\ \bar{u} &= \frac{\sin^3 \gamma}{16} \{ 1 - \bar{r}^4 + 2\epsilon(1 - \bar{r}^{4.606} \cos 2\theta) \}.\end{aligned}\quad (7.29)$$

The velocity at the origin (this is the maximum velocity) is  $\bar{u}(0) = (1 + 2\epsilon)\bar{u}^{(0)}(0)$ . Notice how the variation of  $\tau_{rx}$  with  $\bar{r}$  departs from linearity by the addition of a term proportional to  $\bar{r}^{1.606}$ . This means that  $\partial \tau_{rx} / \partial \bar{r}$  at the origin is unchanged by the perturbation and retains the value  $-\sin \gamma / 2$  appropriate to the semi-circle.

The above analysis can, in principle, be easily extended to include viscous sliding at the channel wall. A bit more complicated would be extensions for general creep functions  $\mathfrak{F}$ , since in this case the differential equation (7.17) would have to be solved, analytic solutions to which are not readily available. Nevertheless, such solutions are of value because they can be used to check numerical solution procedures valid under more general flow situations.

(v) *A note on very deep and wide channels.* Inspired by the success of finding approximate solutions for the rectilinear flow in a slightly off-semicircular cross-section, one could be tempted to use a similar approach for a channel which is either very wide or very deep. For instance, if  $2L$  is width and  $D$  is depth the ratio  $D/L$  is a measure for the aspect ratio of the channel. For very large  $D/L$  the channel is narrow and deep, for small  $D/L$  it is wide but relatively shallow.

A perturbation scheme based on the smallness of the aspect ratio (or its inverse) which follows the above procedure unfortunately fails. A more complicated solution procedure must be followed in order to construct a valid approximation. The method is known as *matched asymptotic expansions* and well known to boundary-layer fluid dynamicists.

To briefly see what is involved, consider the flow of a Newtonian fluid through a very wide channel. The gravity-driven slow flow of this fluid through a channel is governed by the *Poisson equation* for the velocity  $u$

$$\nabla^2 u + \frac{\rho g \sin \gamma}{\mu} = 0, \quad (7.30)$$

where  $\mu$  is the viscosity (the remaining quantities being the same as before)  $u$  is the physical velocity,  $\nabla^2$  the Laplacian. Assume further that (7.30) is

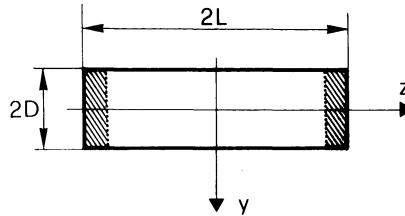


FIG. 7.3. Rectangular channel of depth  $2D$  and width  $2L$ . It is assumed that the aspect ratio  $D/L$  is much smaller than unity.

solved in a very wide rectangle subject to zero velocity at the walls, see Figure 7.3.

In (7.30) the fact that  $D/L \ll 1$  is not accounted for. Physically we would expect, however, that with the exception of the regions very near to the side walls, the vertical velocity gradients for  $u$  are very much larger than horizontal gradients. This interpretation is borne out very clearly by the so-called *soap film analogy*. According to this analogy, the transverse deflection of a soap film spanned over a frame and loaded perpendicular to the undeformed plane of the film is governed by the same boundary-value problem as the velocity field  $u$ . For a frame of rectangular form, it is then intuitively clear that the variation of the deflection with  $y$  must for most part of the rectangle be much larger than corresponding variations in the  $z$ -direction. Exceptions are the regions close to  $|z| = L$  because the boundary condition forces the deflection to its appropriate value at the boundary. The entire rectangle may therefore be divided into subregions. In the regions far from the side walls, horizontal gradients are unimportant and may, to lowest order, be ignored. In the boundary layers close to the side walls, horizontal gradients are dominant for they must cause the deflection to satisfy the boundary condition. Here another approximate solution technique applies. Of course, as one moves away from the side wall this solution must naturally merge into the outer solution, valid far from the side boundary. Mathematically, this perturbation technique is termed singular and the approximate series are called matched asymptotic expansions. For the details, the reader is referred to the specialized literature (see Cole [1], Nayfeh [16], van Dyke [3]). Originally the idea goes back to Prandtl [20].

For the Poisson equation, approximate solutions using matched asymptotic expansions are well known. Unfortunately, if one tries to use the same singular perturbation scheme for the non-Newtonian fluid, one finds that an approximate analytic solution far from the side walls can still be found. In the boundary layer the differential equations are wholly recovered, whereby they do not simplify and defy an analytic solution.

In spite of this unfortunate result, the perturbation technique is a useful one and of practical relevance because it allows an approximate deter-

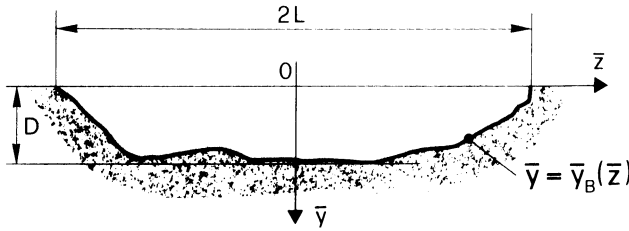


FIG. 7.4. A channel with very wide cross section, but arbitrary shape.

mation of the longitudinal velocity profile for wide valley glaciers, however, to the exclusion of the regions near the side flanks. Below we give the flavor of this (incomplete) approximate analysis.

We consider a very wide cylindrical channel as shown in Figure 7.4 and seek an approximate solution to the differential equations

$$\left. \begin{aligned} \frac{\partial \tau_{xy}}{\partial \bar{y}} + \frac{\partial \tau_{xz}}{\partial \bar{z}} + \sin \gamma &= 0, \\ \frac{\partial \bar{u}}{\partial \bar{y}} &= 2\mathfrak{F}(\tau_{II})\tau_{xy}, \\ \frac{\partial \bar{u}}{\partial \bar{z}} &= 2\mathfrak{F}(\tau_{II})\tau_{xz}, \end{aligned} \right\} \quad \tau_{II} = \tau_{xy}^2 + \tau_{xz}^2, \quad (7.31)$$

subject to the boundary conditions

$$\left. \begin{aligned} \tau_{xy} &= 0, \quad \text{on } \bar{y} = 0, \\ \bar{u} &= \mathbb{C}(\tau_{xy}^2 + \tau_{xz}^2)^{m/2}, \quad \text{on } \bar{y} = \bar{y}_b(\bar{z}). \end{aligned} \right\} \quad (7.32)$$

In order to incorporate the aspect ratio  $\varepsilon = D/L$  into the above equations, a stretching of coordinates is introduced according to

$$\bar{z} = \varepsilon Z. \quad (7.33)$$

Equations (7.31) then read

$$\left. \begin{aligned} \frac{\partial \tau_{xy}}{\partial \bar{y}} + \varepsilon \frac{\partial \tau_{xz}}{\partial Z} + \sin \gamma &= 0, \\ \frac{\partial \bar{u}}{\partial \bar{y}} &= 2\mathfrak{F}(\tau_{II})\tau_{xy}, \quad \varepsilon \frac{\partial \bar{u}}{\partial Z} = 2\mathfrak{F}(\tau_{II})\tau_{xz}, \end{aligned} \right\} \quad (7.34)$$

while (7.32) remains unchanged. A solution to (7.32) and (7.34) may be sought in the form of the perturbation expansions

$$(\tau_{xy}, \tau_{xz}, \bar{u}) = \sum_{v=0}^{\infty} \varepsilon^v (\tau_{xy}^{(v)}, \tau_{xz}^{(v)}, \bar{u}^{(v)}), \quad (7.35)$$

but in view of the remarks made earlier, the emerging solutions will not

be valid uniformly in the region where (7.31) and (7.32) are solved. Substitution of (7.35) into (7.34) and collecting terms of like powers in  $\varepsilon$ , as usual, yields to lowest order

$$\begin{aligned}\frac{\partial \tau_{xy}^{(0)}}{\partial \bar{y}} + \sin \gamma &= 0, & \tau_{xz}^{(0)} &\equiv 0, \\ \frac{\partial \bar{u}^{(0)}}{\partial \bar{y}} &= 2\mathfrak{F}(\tau_{xy}^{(0)2})\tau_{xy}^{(0)},\end{aligned}\quad (7.36)$$

with

$$\begin{aligned}\tau_{xy}^{(0)} &= 0, & \text{on } \bar{y} = 0, \\ \bar{u}^{(0)} &= \mathbb{C}|\tau_{xy}^{(0)}|^m, & \text{on } \bar{y} = \bar{y}_B(Z).\end{aligned}$$

and to first order

$$\begin{aligned}\frac{\partial \tau_{xy}^{(1)}}{\partial \bar{y}} &= 0, \\ \frac{\partial \bar{u}^{(1)}}{\partial \bar{y}} &= 2[\mathfrak{F}(\tau_{xy}^{(0)2}) + 2\mathfrak{F}'(\tau_{xy}^{(0)2})\tau_{xy}^{(0)2}]\tau_{xy}^{(1)}, \\ \frac{\partial \bar{u}^{(0)}}{\partial Z} &= 2\mathfrak{F}(\tau_{xy}^{(0)2})\tau_{xz}^{(1)},\end{aligned}\quad (7.37)$$

with

$$\begin{aligned}\tau_{xy}^{(1)} &= 0, & \text{on } \bar{y} = 0, \\ \bar{u}^{(1)} &= \mathbb{C}m|\tau_{xy}^{(0)}|^{m-1}\tau_{xy}^{(1)}, & \text{on } \bar{y} = \bar{y}_B(Z),\end{aligned}$$

Higher-order equations could equally be obtained. It is easily demonstrated that the solution to (7.36) is given by

$$\begin{aligned}\tau_{xy}^{(0)} &= -\sin \gamma \bar{y}, & \tau_{xz}^{(0)} &= 0, \\ \bar{u}^{(0)} &= \mathbb{C}(\sin \gamma \bar{y}_B(Z))^m + 2 \int_{\bar{y}}^{\bar{y}_B(Z)} \mathfrak{F}(\sin^2 \gamma \xi) \sin \gamma \xi d\xi.\end{aligned}\quad (7.38)$$

Formally it agrees with the results (7.8) which are valid for the infinitely wide rectangle, but the velocity distribution in (7.38) varies with  $z$ , and thus depth variations across the channel are accounted for.

The solution to the boundary value problem (7.37) is  $\tau_{xy}^{(1)} = 0$ ,  $\bar{u}^{(1)} = 0$  and

$$\begin{aligned}\tau_{xy}^{(1)} &= \frac{1}{2\mathfrak{F}(\sin^2 \gamma \bar{y}^2)} \left\{ \mathbb{C}m(\sin \gamma \bar{y}_B(Z))^{m-1} + \right. \\ &\quad \left. + 2\mathfrak{F}(\sin^2 \gamma \bar{y}_B^2(Z)) \sin \gamma \bar{y}_B(Z) \right\} \frac{\partial \bar{y}_B}{\partial Z}.\end{aligned}\quad (7.39)$$

This expression for  $\tau_{xz}^{(1)}$  is singular at the free surface when a power flow law is used, but remains finite for all  $\mathfrak{F}$  with  $\mathfrak{F}(0) \neq 0$ . On the other hand, since  $\bar{u}^{(1)} = \tau_{xy}^{(1)} = 0$ ,  $\bar{u}$  and  $t_{xy}$  are known to first order in  $\varepsilon$ . In other words, *in the outer region*

$$\tau_{xy} = -\sin \gamma \bar{y} + \mathcal{O}(\varepsilon^2),$$

$$\tau_{xz} = \varepsilon \tau_{xy}^{(1)} + \mathcal{O}(\varepsilon^2),$$

$$\bar{u} = \mathbb{C}(\sin \gamma \bar{y}_B(Z))^m + 2 \int_{\bar{y}}^{\bar{y}_B(Z)} \mathfrak{F}(\sin^2 \gamma \xi^2) \sin \gamma \xi \, d\xi + \mathcal{O}(\varepsilon^2), \quad (7.40)$$

where  $\tau_{xy}^{(1)}$  is given by (7.39). This result is interesting for several reasons. Firstly, it is a practical one because it provides a rule for the evaluation of the velocity profile in the central part of a wide valley glacier, provided the bottom profiles are known. Except in the neighborhood of the side flanks, (7.40) is regarded as a reasonable approximation with an error in the order of  $\varepsilon^2$ . Secondly, although a complete solution would involve techniques of matched asymptotic expansion, the complete outer solution (7.40) has been found and all constants of integration could be determined without resorting to the boundary-layer solution. One says in this case that the boundary layers are *passive*. Thirdly, although  $\tau_{xz}$  is singular at the free surface for a power-law fluid, the expression for the velocity is always regular and thus meaningful.

(b) *A useful result for symmetrical channels with no boundary slip*

All foregoing calculations were performed for special channels, either very wide or deep ones, or nearly semi-circular. Here we use dimensional and symmetry arguments for cross-sections which enjoy the symmetry properties as explained below. The argument allows us to deduce a formula for the maximum velocity at the center of the top surface. The method is limited, however, as it only applies when there is no slip and when the creep response function  $\mathfrak{F}$  has the special property that  $\mathfrak{F}(ab) = \mathfrak{F}(a)\mathfrak{F}(b)$ . This limitation is a disadvantage.

Consider, as before, the flow of ice through a channel of *symmetrical* cross-section. It is permissible to complement a given cross-section by the method of images by reflecting the cross-section about the  $\bar{z}$ -axis as shown in Figure 7.5. Consider now the flow of ice through this closed doubly-symmetric cross-section with pressure gradient  $\sin \gamma$ . It is then obvious that the streamwise velocity at the origin 0 in Figures 7.5a and 7.5b are the same, since profiles are the same and can be brought into coincidence by a rotation of one cross-section about  $90^\circ$ . Suppose now we reduce the linear dimensions of the cross-section in Figure 7.5b by a factor  $w$  so that it becomes of depth  $D$  and half width  $w^{-1}D$ , see Figure 7.5c. The question is: how does the velocity at the origin in Figure 7.5c relate to the corresponding velocity in Figure 7.5a?

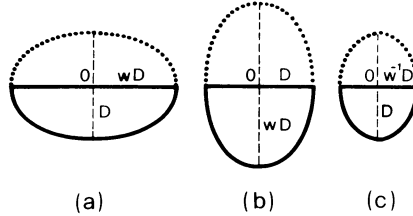


FIG. 7.5. Semi-elliptical channels illustrating the similarity arguments. (Redrawn from [18].)

The answer is: *For a power law fluid,  $\mathfrak{F}(x) = x^{(n-1)/2}$ ,*

$$\bar{u}_a = \bar{u}_b = w^{n+1} \bar{u}_c.$$

Because the cross-sections in Figures 7.5a and 7.5c have the same depth but different widths, this can also be written as

$$\bar{u}(w) = w^{n+1} \bar{u}(w^{-1}). \quad (7.41)$$

To prove (7.41) it suffices to scale equations (7.4) and (7.5) such that in scaled coordinates the cross-sections of Figures 7.5b and 7.5c are of the same size, since they are similar. Stretching the coordinates in Figure 7.5c requires that  $y_1 = w\bar{y}$ ,  $z_1 = w\bar{z}$ . Equation (7.4)<sub>1</sub> then becomes

$$w \left[ \frac{\partial \tau_{xy}^c}{\partial y_1} + \frac{\partial \tau_{xz}^c}{\partial z_1} \right] + \sin \gamma = 0,$$

which agrees with the corresponding equilibrium equation for the cross section of Figure 7.5b provided that  $\tau_{xy}^b = w\tau_{xy}^c$ , etc. Using these results in (7.5)<sub>1</sub> yields

$$w \frac{\partial \bar{u}^c}{\partial y_1} = 2\mathfrak{F}(\tau_{II}^c)\tau_{xy}^c = 2\mathfrak{F}\left(\frac{\tau_{II}^b}{w^2}\right) \frac{\tau_{xy}^b}{w}.$$

Further inferences can only be drawn for creep functions  $\mathfrak{F}$  satisfying the relation  $\mathfrak{F}(ab) = \mathfrak{F}(a)\mathfrak{F}(b)$ . The power law obeys such a relationship, but its generalizations usually do not. With this restriction, the last equation implies

$$\frac{w^2}{\mathfrak{F}(1/w^2)} \frac{\partial \bar{u}^c}{\partial y_1} = 2\mathfrak{F}(\tau_{II}^b)\tau_{xy}^b = \frac{\partial \bar{u}^b}{\partial \bar{y}}. \quad (7.42)$$

from which the result (7.41) is now immediate.

The careful derivation of the result brings about the conditions of validity of similarity laws (7.41). Besides symmetry about the two axes, the ice is not allowed to slide over the bed. But even then solutions may depend on size. The size effect occurs for all non-Newtonian fluids unless

they belong to a limited class that can be characterized by  $\mathfrak{F}(ab) = \mathfrak{F}(a)\mathfrak{F}(b)$ . Only in this limited situation can the velocity at the origin of the cross-section in Figure 7.5a be related to that of Figure 7.5c. Unfortunately, this limits the usefulness of the similarity argument considerably.

Consider an elliptical channel and assume a power flow law for which (7.41) is valid. For  $w \rightarrow \infty$  the elliptical channel becomes infinitely wide, and the velocity of this infinitely wide channel will be the same as for the infinitely wide channel with uniform depth. Hence, from (7.8)

$$\bar{u}(\infty) = \frac{2 \sin^n \gamma}{n+1}.$$

On the other hand, for  $w = 1$  the elliptical channel becomes circular, and thus (7.41) implies

$$\bar{u}(1) = \frac{2(\sin \gamma/2)^n}{n+1} = \left(\frac{1}{2}\right)^n \bar{u}(\infty).$$

Finally,

$$\bar{u}(w) = w^{n+1} \bar{u}(\infty), \quad \text{as } w \rightarrow 0.$$

Thus in Figure 7.6 (curve for ellipses) we know the behavior of the curve near the origin, we know its value at  $w = 1$ , and we know its asymptotic value as  $w \rightarrow \infty$ . It is also straightforward to show that

$$\frac{d\bar{u}}{dw}(w=1) = \frac{n+1}{2} \left(\frac{1}{2}\right)^n \bar{u}(\infty),$$

and it would be possible to derive conditions on higher derivatives at  $w = 1$ , but the entire function cannot be determined this way. Formula (7.41) and ensuing formulas obtained with the similarity argument, are useful because the calculation of  $\bar{u}$  for  $w > 1$  must not be done if those for  $0 \leq w \leq 1$  are available.

Not for all doubly-symmetric cross-sections will Equation (7.41) automatically hold. Condition for (7.41) to hold is that cross-sections can be brought into congruence by (i) a rotation of  $90^\circ$  and/or (ii), a similarity

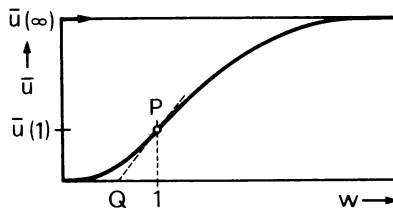


FIG. 7.6. The velocity at the origin of a semi-elliptical cross-section,  $\bar{u}$ , plotted as a function of  $w$ , the ratio of half-width to depth. ( $n = 3$ ). (Redrawn from [18].)

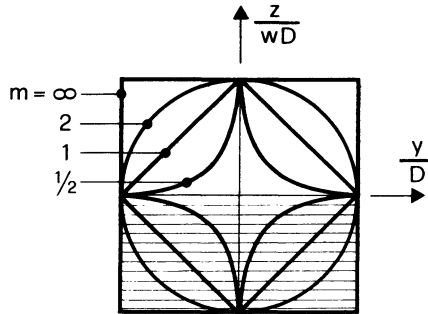


FIG. 7.7. Typical form of hyper-ellipses for various parameters  $m$  and for  $w = 1$ .

With  $m = \infty$  rectangles are obtained;  $m = 2$  corresponds to ellipses,  $m = 1$  gives triangular profiles. For  $m \leq 1$  the profiles are pointed at the bottom.

transformation. These conditions are, for instance, satisfied for the *hyper-ellipses*, defined by

$$\left(\frac{|\bar{y}|}{a}\right)^m + \left(\frac{|\bar{z}|}{wa}\right)^m = 1,$$

and plotted in Figure 7.7 for various values of  $m$ . Figure 7.6 shows the curve  $\bar{u}(w)$  for the case  $m = 2$  corresponding to the elliptic cross-section. Results for the forward velocity at the origin of the coordinate system have been calculated numerically as explained below and are shown in Figure 7.9. These results are due to Nye [18].

### (c) Numerical solution – discussion of results

In this section we discuss a numerical solution scheme that applies for the channels considered in this chapter. The equations to be solved are :

$$\begin{aligned} \frac{\partial \tau_{xy}}{\partial \bar{y}} + \frac{\partial \tau_{xz}}{\partial \bar{z}} + \sin \gamma &= 0, \\ \left. \begin{aligned} \frac{\partial \bar{u}}{\partial \bar{y}} &= 2\mathfrak{F}(\tau_{II})\tau_{xy}, \\ \frac{\partial \bar{u}}{\partial \bar{z}} &= \mathfrak{F}(\tau_{II})\tau_{xz}, \end{aligned} \right\} \quad \tau_{II} &= \tau_{xy}^2 + \tau_{xz}^2, \end{aligned} \quad (7.43)$$

subject to the boundary conditions

$$\begin{aligned} \tau_{xy} &= 0, \quad \text{on } \bar{y} = 0, \\ \bar{u} &= \mathbb{C}\tau_{II}^{m/2}, \quad \text{on } \bar{y} = \bar{y}_B(\bar{z}). \end{aligned} \quad (7.44)$$

It turns out that it is more convenient to scale variables with the ‘pressure

gradient'  $\sin \gamma$  and to work with the variables

$$T_y = \frac{\tau_{xy}}{\sin \gamma}, \quad T_z = \frac{\tau_{yz}}{\sin \gamma}, \quad U = \frac{\bar{u}}{2 \sin^n \gamma}. \quad (7.45)$$

The boundary value problem (7.43), (7.44) can then simply be written as

$$\begin{aligned} \frac{\partial T_x}{\partial \bar{y}} + \frac{\partial T_z}{\partial \bar{z}} + 1 &= 0, \\ \frac{\partial U}{\partial \bar{y}} &= \mathfrak{F}'(T_y^2 + T_z^2)T_y, \\ \frac{\partial U}{\partial \bar{z}} &= \mathfrak{F}'(T_y^2 + T_z^2)T_z, \end{aligned} \quad (7.46)$$

and

$$\begin{aligned} T_y &= 0, \quad \text{on } \bar{y} = 0, \\ U &= \mathbb{C}'(T_y^2 + T_z^2)^{m/2}, \quad \text{on } \bar{y} = \bar{y}_B(\bar{z}). \end{aligned}$$

in which

$$\mathfrak{F}'(T_y^2 + T_z^2) = \frac{\mathfrak{F}(\tau_{yy}/\sin^2 \gamma)}{\sin^{n-1} \gamma}, \quad \mathbb{C}' = \frac{\mathbb{C}}{2 \sin^{n-m} \gamma}. \quad (7.47)$$

For instance,

$$\mathfrak{F}' = \left[ (T_y^2 + T_z^2)^{(n-1)/2} + \frac{k}{\sin^{n-1} \gamma} \right] / (1 + k)$$

and for Glen's power law this is independent of the inclination angle. When also assuming the no-slip condition, (7.46) will be independent of  $\gamma$ . It was for this restricted case that Nye proposed the following solution procedure :

Introduce the *stress function*  $\Phi$  which is such that

$$T_y = \frac{\partial \Phi}{\partial \bar{z}} - \frac{1}{2}\bar{y}, \quad T_z = -\frac{\partial \Phi}{\partial \bar{y}} - \frac{1}{2}\bar{z}. \quad (7.48)$$

The equilibrium equation (7.46)<sub>1</sub> is then automatically satisfied. Differentiating Equations (7.46)<sub>2,3</sub> with respect to  $\bar{z}$  and  $\bar{y}$  respectively and subtracting the resulting equations allows to eliminate the velocity  $U$ . When simultaneously expressing the stress components in terms of the stress function, one arrives at the equation

$$A \frac{\partial^2 \Phi}{\partial \bar{y}^2} + 2B \frac{\partial^2 \Phi}{\partial \bar{y} \partial \bar{z}} + C \frac{\partial^2 \Phi}{\partial \bar{z}^2} = 0, \quad (7.49)$$

with

$$\begin{aligned}
 A &= \bar{\mathfrak{F}}'(\arg) + 2 \frac{d\bar{\mathfrak{F}}'(\arg)}{d(\arg)} \left( \frac{\partial \Phi}{\partial \bar{y}} + \frac{1}{2} \bar{z} \right)^2, \\
 B &= 2 \frac{d\bar{\mathfrak{F}}'(\arg)}{d(\arg)} \left( \frac{\partial \Phi}{\partial \bar{y}} + \frac{1}{2} \bar{z} \right) \left( \frac{\partial \Phi}{\partial \bar{z}} - \frac{1}{2} \bar{y} \right), \\
 C &= \bar{\mathfrak{F}}'(\arg) + 2 \frac{d\bar{\mathfrak{F}}'(\arg)}{d(\arg)} \left( \frac{\partial \Phi}{\partial \bar{z}} - \frac{1}{2} \bar{y} \right)^2, \\
 \arg &= \left( \frac{\partial \Phi}{\partial \bar{z}} - \frac{1}{2} \bar{y} \right)^2 + \left( \frac{\partial \Phi}{\partial \bar{y}} + \frac{1}{2} \bar{z} \right)^2.
 \end{aligned} \tag{7.50}$$

The reader may show himself that for a *power law fluid* with  $n \neq 1$

$$\begin{aligned}
 A &= \left( \frac{\partial \Phi}{\partial \bar{z}} - \frac{1}{2} \bar{y} \right)^2 + n \left( \frac{\partial \Phi}{\partial \bar{y}} + \frac{1}{2} \bar{z} \right)^2, \\
 B &= 2 \left( \frac{\partial \Phi}{\partial \bar{y}} + \frac{1}{2} \bar{z} \right) \left( \frac{\partial \Phi}{\partial \bar{z}} - \frac{1}{2} \bar{y} \right), \\
 C &= \left( \frac{\partial \Phi}{\partial \bar{y}} + \frac{1}{2} \bar{z} \right)^2 + n \left( \frac{\partial \Phi}{\partial \bar{z}} - \frac{1}{2} \bar{y} \right)^2.
 \end{aligned} \tag{7.51}$$

Equation (7.49) is of the form known as *quasilinear*, that is, it is linear in the second-order derivatives of  $\Phi$ . This quasilinearity makes it possible to use an iterative procedure in the numerical solution scheme.

With a rectangular finite difference mesh as shown in Figure 7.8 and with *centered* finite difference approximations of the  $\bar{y}$ - and  $\bar{z}$ -derivatives of  $\Phi$ , it is clear that the finite difference approximation of (7.49) will involve the value of  $\Phi$  at point 2 only in the second derivatives.\* The result is that (7.49) becomes an equation involving  $\Phi_2$  and the values of  $\Phi$  at the eight neighboring mesh points, and that in this equation only the first power of  $\Phi_2$  occurs. One may then solve for  $\Phi_2$  in terms of the neighboring values. Starting from an initial guess for  $\Phi$  in the entire mesh, one may then, point by point, improve the values in all mesh points in succession until further use of the formulas produces no changes to the number of significant figures.

\*Notice that

$$\begin{aligned}
 \left. \frac{\partial^2 \Phi}{\partial \bar{y}^2} \right|_2 &\simeq \frac{\Phi_1 - 2\Phi_2 + \Phi_3}{2\Delta \bar{y}^2}, & \left. \frac{\partial^2 \Phi}{\partial \bar{z}^2} \right|_2 &= \frac{\Phi_4 - 2\Phi_2 + \Phi_5}{2\Delta \bar{z}^2} \\
 \left. \frac{\partial \Phi}{\partial \bar{y}} \right|_2 &= \frac{\Phi_1 - \Phi_3}{2\Delta \bar{y}}, & \left. \frac{\partial \Phi}{\partial \bar{z}} \right|_2 &= \frac{\Phi_4 - \Phi_5}{2\Delta \bar{z}}
 \end{aligned}$$

corroborating the above statement.

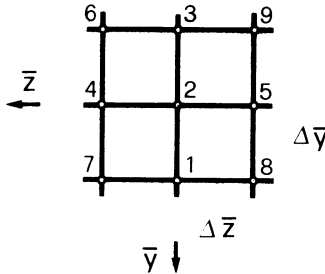


FIG. 7.8. Finite difference mesh for the numerical solution of Equation (7.49).

Having found  $\Phi$  the stresses can be obtained from (7.48) by differentiation, and subsequently  $U$  follows by integration from  $(7.46)_{2,3}$  by using the boundary condition  $(7.46)_5$ .

Integration of (7.49) affords knowledge of  $\Phi$  at the channel wall. Here we shall only indicate briefly how this boundary condition can be expressed as an equation in  $\Phi$ . We start with Equation  $(7.46)_5$  and evaluate  $dU$  along the basal boundary. This yields

$$\begin{aligned} & \frac{\partial U}{\partial \bar{y}} d\bar{y} + \frac{\partial U}{\partial \bar{z}} d\bar{z} \\ &= C' m (T_y^2 + T_z^2)^{(m-2)/2} \times \\ & \quad \times \left\{ T_y \left[ \frac{\hat{c} T_y}{\hat{c} \bar{y}} d\bar{y} + \frac{\hat{c} T_y}{\hat{c} \bar{z}} d\bar{z} \right] + T_z \left[ \frac{\hat{c} T_z}{\hat{c} \bar{y}} d\bar{y} + \frac{\hat{c} T_z}{\hat{c} \bar{z}} d\bar{z} \right] \right\}. \end{aligned}$$

$\partial U / \partial \bar{y}$  and  $\partial U / \partial \bar{z}$  can be replaced by the right-hand sides of  $(7.46)_{2,3}$ . If this is done and the last equation is rearranged, the following expression is obtained

$$\begin{aligned} & \mathfrak{F}'(0) \left[ \frac{d\bar{y}_B}{dz} T_y + T_z \right] \\ &= C' m (T_y^2 + T_z^2)^{(m-2)/2} \left\{ \frac{d\bar{y}_B}{dz} \left[ T_y \frac{\hat{c} T_y}{\hat{c} \bar{y}} + T_z \frac{\hat{c} T_z}{\hat{c} \bar{y}} \right] + \left[ T_y \frac{\hat{c} T_y}{\hat{c} \bar{z}} + T_z \frac{\hat{c} T_z}{\hat{c} \bar{z}} \right] \right\}, \end{aligned} \quad (7.52)$$

an equation which now can be expressed in terms of  $\Phi$ . When there is no sliding at the base then  $C' = 0$ , and (7.52) may be written as

$$\frac{\partial \Phi / \partial \bar{y} + \frac{1}{2} \bar{z}}{\partial \Phi / \partial \bar{z} - \frac{1}{2} \bar{y}} = -\tan \Phi. \quad (7.52a)$$

At the basal boundary points, the finite difference approximations must also obey Equations (7.52) and at the free surface one must have  $\partial U / \partial \bar{y} = 0$ .

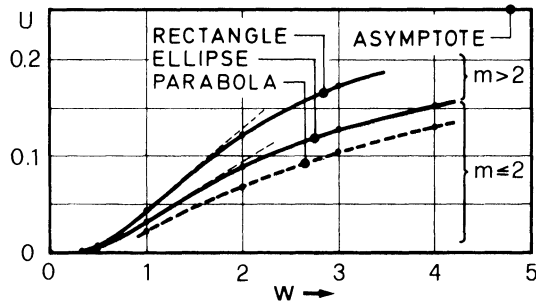


FIG. 7.9. Maximum dimensionless velocity  $U$  in a rectangular, semi-elliptical and parabolic cross section plotted against  $w$ , the ratio of half-width of depth for a power flow law with  $n = 3$ . (Redrawn from [18].)

or  $\Phi = \text{constant}$ , and the same condition must also hold at a symmetry line. In the integration procedure explained above, these boundary conditions should be observed, of course.

The numerical solution procedure described above was used by Nye [18] to find the velocity and stress distribution in cross-sections of rectangular, semi-elliptical and parabolic cross-sections. Nye used a power law fluid with  $n = 3$  and assumed no-slip at the basal boundary. Some of his results are summarized in Figure 7.9. It shows the maximum velocity at the origin of the coordinate system as a function of  $w$ . Results are shown for rectangles, semi-ellipses and parabolas. It is seen that with growing  $w$   $U$  grows in all three cases approaching the value for the infinitely wide channel as  $w$  becomes asymptotically large. The approach of this asymptotic limit is, however, slow and cross-sections with  $w \leq 5$  should still be treated as having a finite width. It follows that side-wall effects will only be negligible for channels, which are at least 10 times as wide as they are deep. Reynaud [21] repeated the analysis for parabolic cross-sections by allowing for basal sliding, but the sliding law he used is different from ours.

Of particular interest are the surface velocities along a transverse line and the velocity distribution down the  $\bar{y}$ -axis. Of further interest are the stress  $T_z$  on the  $\bar{z}$ -axis (that is on the free surface) and finally the distribution of the stress  $T_y$  down the  $\bar{y}$ -axis. In Figure 7.10 the surface velocity is plotted on a transverse line parameterized for various cross-sections. These velocity curves show the distortion of a transverse line drawn on the glacier surface along the  $\bar{z}$ -axis. There are interesting differences between the results for the hyper-ellipses and for parabolas. For instance, for rectangles the line is always convex down glacier, for parabolas it is convex down glacier in the center, but concave at the edges. The curvature changes and there is a point of inflection. This can be understood as soon as the results for the shear stresses are known. We shall come back to this in a moment.

Next, let us look at the velocity distribution on the  $\bar{y}$ -axis. For various

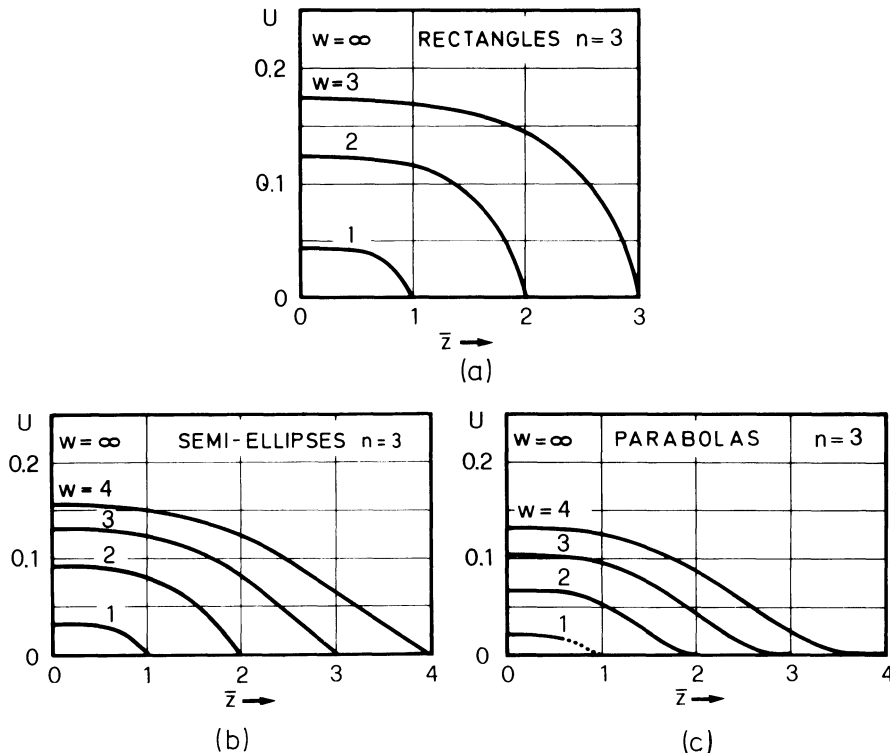


FIG. 7.10. Forward velocity distribution at the free surface plotted against distance  $\bar{z}$  from the symmetry point. Results are shown for several values of the aspect ratio ( $w = 1, 2, 3, 4, \dots, \infty$ ) and three different types of cross-sections. The upper bound  $U = 0.25$  applies for infinitely-wide channels. (Redrawn from [18].)

aspect ratios (parameterized by  $w$ ) these are shown in Figure 7.11, for rectangles, semi-ellipses and parabolas. For  $w = \infty$  the profiles are the same in all three cases, but for  $w < \infty$  there is a marked influence of the shape of the cross-section on the vertical-velocity distribution. In particular for a fixed value of  $w$  velocities are smallest for the parabolas and largest for the rectangle.

Shear stresses being related to the velocity gradient according to (7.46), qualitative information about the distribution of  $T_z$  at the free surface across the channel and of  $T_y$  along the symmetry line should be obtainable from Figures 7.10 and 7.11. Qualitatively,  $T_z$  at the free surface across the channel behaves like  $\partial U / \partial \bar{z}$ . It can be inferred from Figure 7.10, therefore, that  $T_z$  must be monotonically increasing with  $\bar{z}$  for rectangular cross-sections, but this is certainly not so for parabolic cross-sections. Indeed, at the point of inflection  $T_z$  must go through a relative maximum, and it

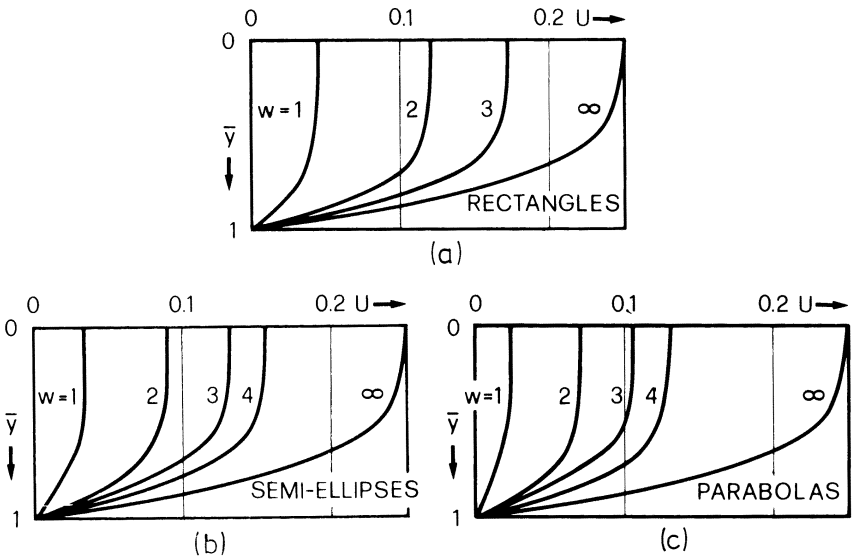


FIG. 7.11. Velocity distribution along the symmetry axis for several values of the parameter ( $w = 1, 2, 3, 4, \dots \infty$ ) for rectangles (a), semi-ellipses (b), and parabolas (c). For  $w = \infty$ , the profiles are identical in the three cases, but differ substantially from each other when  $w < \infty$ . (Redrawn from [18].)

is seen from Figure 7.10 that this is the case for all  $w$  drawn for semi-ellipses and parabolas. Corroboration is provided by Figure 7.12 in which the dimensionless shear stress  $T_z$  at the surface is plotted along the  $\bar{z}$ -axis. It is seen from this figure that the transverse distribution of the shear stress  $T_z$  for parabolas is qualitatively substantially different from that of rectangles

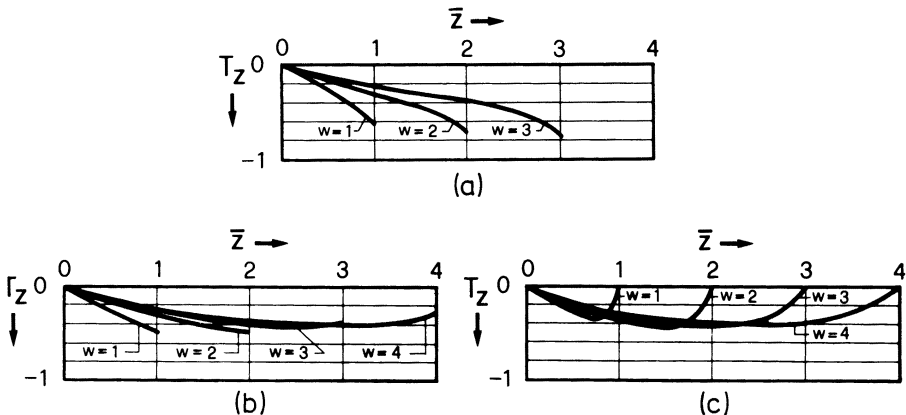


FIG. 7.12. Shear stress  $T_z$  at the free surface plotted for  $w = 1, 2, 3, 4$  for rectangular (a), semi-elliptic (b), and parabolic (c) cross-sections. (Redrawn from [18].)

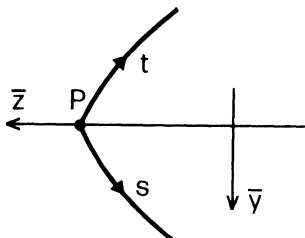


FIG. 7.13. Close-up of the side wall and its symmetric extension at the far left side of the channel when the bottom curve does not perpendicularly meet the coordinate  $\bar{z}$ . On all boundary points, the velocity  $U$  must vanish implying that in  $P \partial U / \partial s$  and  $\partial U / \partial t$  will vanish.

or semi-ellipses. Firstly, for rectangles and semi-ellipses, the shear stress  $|T_z|$  is zero at the symmetry line ( $\bar{z} = 0$ ), increases steadily and assumes a non-vanishing value at the side wall. Whereas for rectangular cross-sections the value of  $|T_z|$  assumes the maximum at the side wall; this is not necessarily so for semi-elliptic channels. Indeed, for  $w = 3$  and  $w = 4$ ,  $|T_z|$  at the surface assumes a maximum at an intermediate point. Contrary to this behavior, for parabolas the shear stress  $|T_z|$  vanishes at the side wall. The maximum must for these cases therefore lie at an intermediate point. This is indeed so and there is a reason for this behavior. To find it, note that  $U$  must vanish along the boundary of the extended closed cross-section. If we now look at the side wall close to the free surface (Figure 7.13), the boundary of the extended cross-section has a kink at the point where the side wall and the free glacier surface intersect. Hence, since  $U$  must vanish at the boundary so must  $\partial U / \partial \bar{z}$  and  $\partial U / \partial \bar{y}$  at the point  $P$ . This must be so, because for no-slip quite obviously  $\partial U / \partial s|_P = 0$  and  $\partial U / \partial t|_P = 0$ . From the constitutive relations (7.46) it then immediately follows that at such corners  $T_z = 0$  and  $T_y = 0$ . It is now also clear that the velocity curves in Figure 7.10 must change from being convex down-glacier in the center to concave towards the side wall and must have a point of inflection for all those cross-sections whose boundaries do not meet the free glacier surface at a right angle. For, according to (7.46), the shear stress assumes a relative maximum where the velocity gradient changes sign. These are the points of inflection.

Lastly, let us look at the distribution of the shear stresses  $T_y$  along the  $\bar{y}$ -axis (the axis of symmetry). In Figure 7.14 we have plotted  $T_y$  along this axis for various aspect ratios of the cross-sections involved. For rectangles, semi-ellipses, and parabolas the shear stress  $T_y$  grows monotonically with depth and assumes its maximum at the lowest point of the channel. Interesting, however, is the different qualitative behavior of  $T_y$  for relatively small values of  $w$ , say  $w = 1$ . Whereas for semi-ellipses  $T_y$  varies along  $\bar{y}$  in an essentially linear fashion, this is not so for rectangles and parabolas. In these cases the curves  $T_y(\bar{y})$  are bent, however with different signs of the

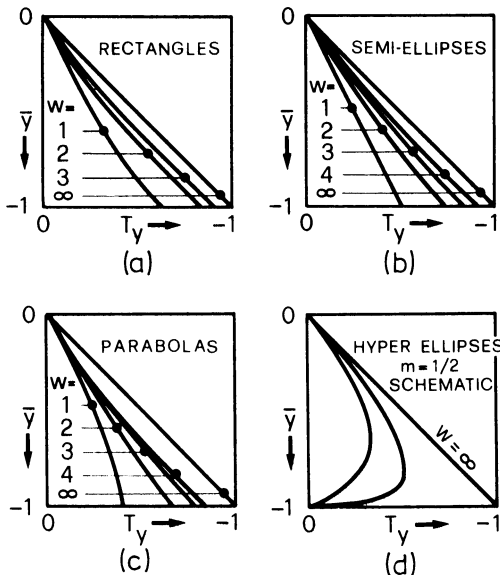


FIG. 7.14. Shear-stress distribution  $T_y$  along the symmetry line for several values of the aspect ratio parameter  $w$ . Results are shown for rectangles (a), semi-ellipses (b) and parabolas (c). Results depend strongly on cross-sectional shape, as indicated with further qualitative results for hyper-ellipses with  $m = 1/2$ . These suggest that the maximum stress  $T_y$  may not necessarily arise at the boundary. (Partly redrawn from [18].)

curvature. Qualitatively this can be understood. For the more pointed the cross-section is at the lowest point, the smaller must be the shear stress  $T_y$ . Indeed, if the cross-section would have a kink at the lowest point (as is the case for hyper-ellipses with  $0 < m < 1$ )  $T_y$  would have to vanish in the lowest point. For these cases the maximal shear stresses  $T_y$  would lie within the glacier and not at the base.

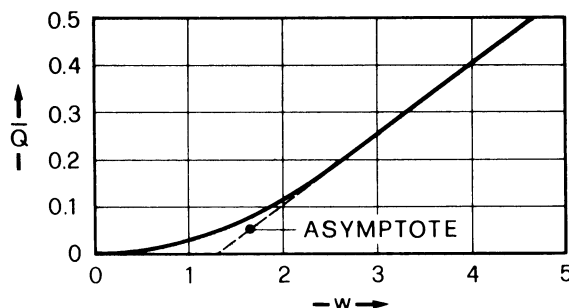


FIG. 7.15. Dimensionless discharge for a parabolic bed profile plotted against the parameter  $w$ , characterizing the aspect ratio. (Redrawn from [18].)

There are many more results that can be derived from the above numerical analysis. An important one is a relationship for the discharge  $\bar{Q}$  which obtains by integrating the velocity distribution over the cross-section. Since parabolic cross-sections are closest to real valley profiles, Nye restricted attention to these. He looked at a non-dimensional  $\bar{Q}$  defined by

$$\bar{Q} = \frac{Q}{(\rho g D \sin \gamma)^n D^3}, \quad (7.53)$$

and evaluated  $\bar{Q}$  as a function of  $w$ . The  $\bar{Q}(w)$ -plot is given in Figure 7.15. The limiting cases  $w \rightarrow 0$  and  $w \rightarrow \infty$  can be treated analytically by looking at the very wide but shallow and the very deep but narrow channel. Nye [18] finds for a power law fluid with  $n = 3$

$$\begin{aligned} \bar{Q} &\simeq \frac{4}{35} w^5, \quad \text{as } w \rightarrow 0, \\ \bar{Q} &\simeq 0.1478 w - 0.187, \quad \text{as } w \rightarrow \infty; \end{aligned} \quad (7.54)$$

comparison with numerical results shows that the asymptotic representation (7.54)<sub>2</sub> is sufficiently accurate for  $w \gtrsim 3$ .

Another result obtained for the parabolic cross-section is also very useful. To explain it consider two mean velocities,  $\langle u \rangle_c$ , averaged over the cross-section and  $\langle u \rangle_s$  averaged over the surface at a given cross-section. Nye finds that for the parabola (and no sliding at the base) the ratio of the two nearly equals unity,  $\langle u \rangle_c / \langle u \rangle_s \simeq 1$ , with deviations smaller than 10%. This seems to be an important result, for it means that the mean velocity of a glacier and, therefore, if the cross-section is known, the discharge may be inferred purely from measurements on the glacier surface. This rule certainly applies also when sliding is involved. For suppose that the entire motion consisted of bed slip, so that the glacier moved forward as a rigid body. Then certainly  $\langle u \rangle_c / \langle u \rangle_s \equiv 1$ . Thus the result applies at both extremes and is presumably a good approximation for intermediate cases.

For several other details including the application to the kinematic wave theory, the reader is referred to the paper by Nye [18]. An application using a sliding law that depends on the water table is given by Reynaud [21].

### 3. Three-dimensional Flow Effects in Ice Sheets

Section 2 of this chapter dealt with the effects of boundedness of the cross-sections in valley glaciers. It was demonstrated that the side walls have a dominant effect on the stress and velocity distributions which should not be ignored in actual problems.

Here we shall go to the other extreme and look at three-dimensional ice flow on ice sheets. In Chapters 5 and 6 such sheets were looked at from an idealized point of view. Flow conditions were regarded as planar and, therefore, results could, only be qualitatively correct. Real ice sheets are bounded from either side. They should, strictly speaking, be considered as shallow ice masses on the globe. To describe their evolution in the large, the governing equations of ice-flow dynamics should be developed in spherical coordinates using an assumption of shallowness similar to the shallow-ice approximation applied before. We shall work instead in Cartesian coordinates  $(\bar{x}, \bar{y}, \bar{z})$ . This is not a restriction because the curvature of the bed can be taken into account, if desired, by adjusting the profile accordingly.

It was demonstrated in Chapters 5 and 6 that by introducing the shallow-ice approximation problems will usually arise at the margins. In particular, margin slopes are either infinite, and then make the assumptions of the shallow-ice approximation invalid in these regions, or when finite margin slopes are enforced, the sliding law must become singular as the margin is approached. These difficulties can equally be expected to arise here, and therefore the suggested approach can, at most, be a hint to how calculations could proceed when a three-dimensional attempt at ice-sheet dynamics is made.

A further word of caution is necessary. Since ice sheets generally extend over several hundred to thousand kilometers, the climate and hence the accumulation function, as well as geothermal heat, will vary considerably so that the ice will be *polythermal*, divided into subregions of cold and temperate ice, respectively. The correct treatment of ice sheets is therefore a thermo-mechanical model including phase-change problems. Decoupling of the mechanical from the thermal problem is not possible in general. If such a decoupling is assumed below and estimates of the temperature distribution are treated as known, this must be regarded as a drastic simplification whose limitation should be borne in mind. Furthermore, ice sheets are not necessarily wholly grounded but may frequently contain a non-negligible floating portion. Such shelves will be ignored below and the entire ice sheet therefore will be regarded as *grounded*. Finally, a last simplification, which is not entirely justified but can relatively easily be removed, is that the ground is assumed to be perfectly rigid and thus cannot deform under the weight of the ice.

#### (a) Basic equations

The ice sheet will be referred to a Cartesian coordinate system  $\bar{x}, \bar{y}, \bar{z}$ , where  $\bar{x}$  and  $\bar{z}$  are horizontal and  $\bar{y}$  is vertical as shown in Figure 7.16. The top surface and the base will be denoted by  $\bar{y} = \bar{y}_s(\bar{x}, \bar{z})$  and  $\bar{y} = \bar{y}_b(\bar{x}, \bar{z})$ , respectively. We shall work in dimensionless coordinates, as before in

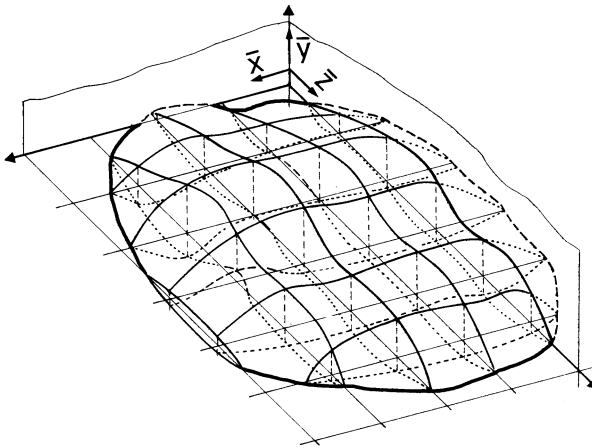


FIG. 7.16. Sketch of a three-dimensional ice sheet. It is bounded in both horizontal directions.

Chapters 3 to 6. The governing field equations are the balance of momentum and mass and the constitutive relations for stress (this assumes that the thermal and mechanical effects are decoupled). These equations read:

**Balance of mass**

$$\frac{\partial \bar{u}}{\partial \bar{x}} + \frac{\partial \bar{v}}{\partial \bar{y}} + \frac{\partial \bar{w}}{\partial \bar{z}} = 0. \quad (7.55)$$

**Balance of momentum:**

$$\begin{aligned} -\frac{\partial \bar{p}}{\partial \bar{x}} + \frac{\partial \sigma_x}{\partial \bar{x}} + \frac{\partial \tau_{xy}}{\partial \bar{y}} + \frac{\partial \tau_{xz}}{\partial \bar{z}} + g_x &= 0, \\ \frac{\partial \tau_{xy}}{\partial \bar{x}} - \frac{\partial \bar{p}}{\partial \bar{y}} + \frac{\partial \sigma_y}{\partial \bar{y}} + \frac{\partial \tau_{yz}}{\partial \bar{z}} + g_y &= 0, \\ \frac{\partial \tau_{xz}}{\partial \bar{x}} + \frac{\partial \tau_{yz}}{\partial \bar{y}} - \frac{\partial \bar{p}}{\partial \bar{z}} + \frac{\partial \sigma_z}{\partial \bar{z}} + g_z &= 0, \end{aligned} \quad (7.56)$$

**Constitutive relations:**

$$\frac{\partial \bar{u}}{\partial \bar{x}} = \mathbb{G} \tilde{\mathfrak{F}}(\tau_{II}) \sigma_x,$$

$$\frac{\partial \bar{u}}{\partial \bar{y}} + \frac{\partial \bar{v}}{\partial \bar{x}} = 2 \mathbb{G} \tilde{\mathfrak{F}}(\tau_{II}) \tau_{xy},$$

$$\frac{\partial \bar{u}}{\partial \bar{z}} + \frac{\partial \bar{w}}{\partial \bar{x}} = 2G\tilde{\mathfrak{F}}(\tau_{II})\tau_{xz}, \quad (7.57)$$

$$\frac{\partial \bar{v}}{\partial \bar{y}} = G\tilde{\mathfrak{F}}(\tau_{II})\sigma_y,$$

$$\frac{\partial \bar{v}}{\partial \bar{z}} + \frac{\partial \bar{w}}{\partial \bar{y}} = 2G\tilde{\mathfrak{F}}(\tau_{II})\tau_{yz},$$

$$\frac{\partial \bar{w}}{\partial \bar{z}} = G\tilde{\mathfrak{F}}(\tau_{II})\sigma_z,$$

with

$$\tau_{II} = \frac{1}{2}\sigma_{ij}\sigma_{ij} = \frac{1}{2}(\sigma_x^2 + \sigma_y^2 + \sigma_z^2) + \tau_{xy}^2 + \tau_{yz}^2 + \tau_{zx}^2. \quad (7.58)$$

In these equations,  $(\bar{u}, \bar{v}, \bar{w})$  are the velocities in the  $(\bar{x}, \bar{y}, \bar{z})$  directions,  $\bar{p}$  is pressure and  $g_x, g_y, g_z$  are the components of the gravity vector in the three spatial directions. If the  $(\bar{x}, \bar{z})$ -plane is horizontal and curvature effects of the earth can be ignored, then in this system of coordinates  $g_x = g_z = 0$  and  $g_y = -1$ . The components  $\sigma_x, \tau_{xy}$ , etc. are those of the stress deviator (this is different from the notation before),  $\tilde{\mathfrak{F}}$  is the creep-response function, assumed to be a function of the second stress deviator invariant  $\tau_{II}$  and the temperature (through the Arrhenius factor), but temperature estimates are assumed known.  $\tilde{\mathfrak{F}}$  may therefore also be regarded as position dependent, but this dependency will not be made explicit. Finally  $G$  is a pure number and generally large; for details see Chapters 3 and 5.

The boundary conditions that Equations (7.55)–(7.58) are subject to, are:  
At the free surface:  $\bar{y} = \bar{y}_s(\bar{x}, \bar{z}, \bar{t})$

$$\left. \begin{aligned} \frac{\partial \bar{y}_s}{\partial \bar{t}} + \frac{\partial \bar{y}_s}{\partial \bar{x}}\bar{u} + \frac{\partial \bar{y}_s}{\partial \bar{z}}\bar{w} - \bar{v} &= \mathfrak{U}(\bar{x}, \bar{y}_s, \bar{z}), \\ -(-\bar{p} + \sigma_x)\frac{\partial \bar{y}_s}{\partial \bar{x}} + \tau_{xy} - \tau_{xz}\frac{\partial \bar{y}_s}{\partial \bar{z}} &= \bar{p}^{\text{atm}}\frac{\partial \bar{y}_s}{\partial \bar{x}}, \\ -\tau_{xy}\frac{\partial \bar{y}_s}{\partial \bar{x}} + (-\bar{p} + \sigma_y) - \tau_{yz}\frac{\partial \bar{y}_s}{\partial \bar{z}} &= -\bar{p}^{\text{atm}}, \\ -\tau_{xz}\frac{\partial \bar{y}_s}{\partial \bar{x}} + \tau_{yz} - (-\bar{p} + \sigma_z)\frac{\partial \bar{y}_s}{\partial \bar{z}} &= \bar{p}^{\text{atm}}\frac{\partial \bar{y}_s}{\partial \bar{z}}. \end{aligned} \right\} \quad (7.59)$$

The first of Equations (7.59) is the kinematic surface condition, the remaining three equations state that the only non-vanishing boundary traction is atmospheric pressure.

The three-dimensional form of the bottom-sliding condition is not entirely trivial and so we present its derivation in greater detail. To this

end let  $\mathbf{n}$  be the exterior unit vector normal to the bottom surface. The viscous sliding law must then relate the velocity vector  $\bar{\mathbf{u}}$  with the shear traction at the base. A relation of the form  $\bar{\mathbf{u}} = -f(-p\mathbf{1} + \boldsymbol{\sigma}) \cdot \mathbf{n}$  where  $f$  depends on the shear traction, cannot hold, since it does not satisfy the tangency condition  $\mathbf{n} \cdot \mathbf{u} = 0$ . However, when we introduce

$$\tau_* \equiv (-\bar{p}\mathbf{1} + \boldsymbol{\sigma}) - [\mathbf{n} \cdot (-\bar{p}\mathbf{1} + \boldsymbol{\sigma}) \cdot \mathbf{n}] \mathbf{1} = \boldsymbol{\sigma} - [\mathbf{n} \cdot \boldsymbol{\sigma} \cdot \mathbf{n}] \mathbf{1}$$

and postulate a sliding law of the form

$$\bar{\mathbf{u}} = -f\tau_* \cdot \mathbf{n}. \quad (7.60a)$$

the tangency condition is automatically satisfied. Incidentally, the vector  $\tau_* \cdot \mathbf{n}$  is that portion of the traction vector which is tangential to the basal surface. All that is needed to make Equation (7.60a) non-linear is to assume  $f$  to be dependent on  $(\tau_* \cdot \mathbf{n})^2$  so that the general sliding law must have the form

$$\bar{\mathbf{u}} = -f((\tau_* \cdot \mathbf{n})^2)\tau_* \cdot \mathbf{n}. \quad (7.60b)$$

In general,  $f$  may also depend on position, temperature and/or water pressure etc. For a Weertman-type sliding law  $f(x) = Cx^{(n-1)/2}$ . The application to our particular coordinates is now straightforward. With

$$\mathbf{n} = \frac{1}{Y} \left( \frac{\partial \bar{y}_S}{\partial \bar{x}}, -1, \frac{\partial \bar{y}_B}{\partial \bar{z}} \right), \quad Y = \sqrt{1 + \left( \frac{\partial \bar{y}_B}{\partial \bar{x}} \right)^2 + \left( \frac{\partial \bar{y}_B}{\partial \bar{z}} \right)^2}$$

the bottom boundary conditions assume the following form:

$$\begin{aligned} & \left[ \frac{\partial \bar{y}_B}{\partial \bar{x}} \bar{u} + \frac{\partial \bar{y}_B}{\partial \bar{z}} \bar{w} - \bar{v} = 0 \right], \\ & \bar{u} = -\frac{f((\tau_* \cdot \mathbf{n})^2)}{Y} \left\{ \sigma_x^* \frac{\partial \bar{y}_B}{\partial \bar{x}} - \tau_{xy}^* + \tau_{xz}^* \frac{\partial \bar{y}_B}{\partial \bar{z}} \right\}, \\ & \bar{v} = -\frac{f((\tau_* \cdot \mathbf{n})^2)}{Y} \left\{ \tau_{xy}^* \frac{\partial \bar{y}_B}{\partial \bar{x}} - \sigma_y^* + \tau_{yz}^* \frac{\partial \bar{y}_B}{\partial \bar{z}} \right\}, \\ & \bar{w} = -\frac{f((\tau_* \cdot \mathbf{n})^2)}{Y} \left\{ \tau_{xz}^* \frac{\partial \bar{y}_B}{\partial \bar{x}} - \tau_{yz}^* + \sigma_z^* \frac{\partial \bar{y}_B}{\partial \bar{z}} \right\}. \end{aligned} \quad (7.61)$$

Equation (7.61)<sub>1</sub> expresses that the basal velocity is tangential to the base. This condition is already incorporated in the remaining boundary conditions (7.61) and is not needed unless  $f \rightarrow \infty$ . It will, however, be of help later on when the equation for the surface profile is derived. The remaining equations (7.61) are the sliding law; for  $f \equiv 0$  they include the no-slip condition.

It is easily seen that the field equations (7.55)–(7.57) comprise a set of 10 partial differential equations for the 10 unknowns  $\bar{u}, \bar{v}, \bar{w}, \sigma_x, \tau_{xy}, \dots, \tau_{yz}, \bar{p}$ . The kinematic surface condition contains the further unknown  $\bar{y}_S(\bar{x}, \bar{z}, \bar{t})$ .

The entire problem thus involves 11 unknowns; subject to the boundary conditions (7.59) and (7.61) and complemented by initial conditions and conditions at the margin, the initial boundary-value problem should be solvable, at least in principle.

We know, however, from Chapter 6 that boundary conditions at the margins are not clearly understood, and so we restrict ensuing considerations to *steady* situations. In this case margin conditions are simply that  $\bar{y}_S = \bar{y}_B$ .

(b) *Decoupling of the stress-velocity problem from the problem of surface profile*

Ice sheets are shallow regions which spread in horizontal directions. They are often dome-like and show little preference of a distinct horizontal direction. Hence, and to the exclusion of localized features, surface and bottom topography vary slowly in both horizontal directions, so that a stretching of the horizontal coordinates according to

$$\xi = \varepsilon \bar{x}, \quad \zeta = \varepsilon \bar{z}, \quad \eta = \bar{y} \quad (7.62)$$

is suggested, in which  $\varepsilon$  is a small parameter, to be determined later on. Relations (7.62) are part of the *shallow ice approximation* and will be complemented by scaling time and the transverse velocity  $\bar{v}$  according to

$$\bar{t} = \varepsilon t, \quad V = \frac{1}{\varepsilon} \bar{v}. \quad (7.63)$$

In what follows, we shall also write  $U = \bar{u}$ ,  $W = \bar{w}$  and  $\mathfrak{A} = \bar{a}/\varepsilon$ . With the above transformations (7.62), (7.63), the field equations can be written in the form

$$\begin{aligned} -\varepsilon \frac{\partial \bar{p}}{\partial \xi} + \varepsilon \frac{\partial \sigma_x}{\partial \xi} + \frac{\partial \tau_{xy}}{\partial \eta} + \varepsilon \frac{\partial \tau_{xz}}{\partial \zeta} + \varepsilon g_1 &= 0, \\ \varepsilon \frac{\partial \tau_{xy}}{\partial \xi} - \frac{\partial \bar{p}}{\partial \eta} + \frac{\partial \sigma_y}{\partial \eta} + \varepsilon \frac{\partial \tau_{yz}}{\partial \zeta} - g_2 &= 0, \\ \varepsilon \frac{\partial \tau_{xz}}{\partial \xi} + \frac{\partial \tau_{yz}}{\partial \eta} - \varepsilon \frac{\partial \bar{p}}{\partial \zeta} + \varepsilon \frac{\partial \sigma_z}{\partial \zeta} + \varepsilon g_3 &= 0, \\ \frac{\partial U}{\partial \xi} + \frac{\partial V}{\partial \eta} + \frac{\partial W}{\partial \zeta} &= 0, \\ \varepsilon \frac{\partial U}{\partial \xi} = \mathbb{G} \tilde{\mathfrak{F}}(\tau_{II}) \sigma_x, \quad \frac{\partial U}{\partial \eta} + \varepsilon^2 \frac{\partial V}{\partial \xi} &= 2 \mathbb{G} \tilde{\mathfrak{F}}(\tau_{II}) \tau_{xy}, \\ \varepsilon \frac{\partial U}{\partial \zeta} + \varepsilon \frac{\partial W}{\partial \xi} &= 2 \mathbb{G} \tilde{\mathfrak{F}}(\tau_{II}) \tau_{xz}, \quad \varepsilon \frac{\partial V}{\partial \eta} = \mathbb{G} \tilde{\mathfrak{F}}(\tau_{II}) \sigma_y, \\ \varepsilon^2 \frac{\partial V}{\partial \zeta} + \frac{\partial W}{\partial \eta} &= 2 \mathbb{G} \tilde{\mathfrak{F}}(\tau_{II}) \tau_{yz}, \quad \varepsilon \frac{\partial W}{\partial \zeta} = \mathbb{G} \tilde{\mathfrak{F}}(\tau_{II}) \sigma_z, \end{aligned} \quad (7.64)$$

in which  $g_x = \varepsilon g_1$ ,  $g_y = -g_2$ ,  $g_z = \varepsilon g_3$ , and  $g_2$  is order unity, while  $g_1$  and  $g_3$  are order unity or smaller in general.

Similarly, the boundary conditions (7.59) and (7.61) can be transformed and written in terms of the variables (7.62) and (7.63). One obtains:

*At the free surface*:  $\bar{y} = \bar{y}_S(\xi, \zeta, t)$

$$\begin{aligned} \frac{\partial \bar{y}_S}{\partial t} + \frac{\partial \bar{y}_S}{\partial \xi} U + \frac{\partial \bar{y}_S}{\partial \zeta} W - V &= \mathfrak{A}, \\ -\varepsilon(-\bar{p} + \sigma_x) \frac{\partial \bar{y}_S}{\partial \xi} + \tau_{xy} - \varepsilon \tau_{xz} \frac{\partial \bar{y}_S}{\partial \zeta} &= \varepsilon \bar{p}^{\text{atm}} \frac{\partial \bar{y}_S}{\partial \xi}, \\ -\varepsilon \tau_{xy} \frac{\partial \bar{y}_S}{\partial \xi} + (-\bar{p} + \sigma_y) - \varepsilon \tau_{yz} \frac{\partial \bar{y}_S}{\partial \zeta} &= -\bar{p}^{\text{atm}}, \\ -\varepsilon \tau_{xz} \frac{\partial \bar{y}_S}{\partial \xi} + \tau_{yz} - (-\bar{p} + \sigma_z) \frac{\partial \bar{y}_S}{\partial \zeta} &= \varepsilon \bar{p}^{\text{atm}} \frac{\partial \bar{y}_S}{\partial \zeta}. \end{aligned} \quad (7.65)$$

*At the bottom surface*:  $\bar{y} = \bar{y}_B(\xi, \zeta)$

$$\begin{aligned} \left[ \frac{\partial \bar{y}_B}{\partial \xi} U + \frac{\partial \bar{y}_B}{\partial \zeta} W - V = 0 \right], \\ U &= -\frac{f}{Y} \left\{ \sigma_x^* \varepsilon \frac{\partial \bar{y}_B}{\partial \xi} - \tau_{xy}^* + \tau_{xz}^* \varepsilon \frac{\partial \bar{y}_B}{\partial \zeta} \right\}, \\ \varepsilon V &= -\frac{f}{Y} \left\{ \tau_{xy}^* \varepsilon \frac{\partial \bar{y}_B}{\partial \xi} - \sigma_y^* + \tau_{yz}^* \varepsilon \frac{\partial \bar{y}_B}{\partial \zeta} \right\}, \\ W &= -\frac{f}{Y} \left\{ \tau_{xz}^* \varepsilon \frac{\partial \bar{y}_B}{\partial \xi} - \tau_{yz}^* + \sigma_z^* \varepsilon \frac{\partial \bar{y}_B}{\partial \zeta} \right\}, \end{aligned} \quad (7.66)$$

in which  $f$ ,  $Y$  and the components of  $\sigma_*$  involve the parameter  $\varepsilon$ , as can be seen from the definition of  $\sigma_*$  and  $Y$ . In order not to overload formulas, we have refrained from making this dependence explicit.

Equations (7.64) to (7.66) are now in a form suitable for the lowest-order approximation to be treated here. Before such an approximate treatment can be given, the parameter  $\varepsilon$  must be expressed in terms of  $\mathbb{G}$ . To find this relationship, let us return to Equations (7.64), in particular the force balances in the horizontal directions, (7.64)<sub>1,3</sub>. For vanishing  $g_1$  a lowest order force balance in the  $\xi$ -direction requires the transverse stress gradient  $\partial \tau_{xy}/\partial \eta$  to vanish unless  $\tau_{xy}$  is  $\mathcal{O}(\varepsilon)$ . In this case, transverse shear-stress gradients can be balanced by the horizontal pressure gradient  $\partial \bar{p}/\partial \xi$ . Similarly, in Equation (7.64)<sub>3</sub>; here transverse shear stress gradients  $\partial \tau_{yz}/\partial \eta$

can balance the horizontal pressure gradient  $\partial\bar{p}/\partial\zeta$  only provided that  $\tau_{yz} = \mathcal{O}(\varepsilon)$ . We assume such order of magnitude relationships to hold; they are plausible from the basic approximate shear-stress formula according to which the shear stresses are proportional to the surface inclination angle, which is small after all. It then follows from the sixth and ninth of Equations (7.64), since  $\partial U/\partial\eta$  and  $\partial W/\partial\eta$  are  $\mathcal{O}(1)$  that

$$\mathbb{G}\mathcal{O}(\mathfrak{F}(\cdot)\tau_{xy}) = \mathcal{O}(1), \quad \mathbb{G}\mathcal{O}(\mathfrak{F}(\cdot)\tau_{yz}) = \mathcal{O}(1). \quad (7.67)$$

Assuming further (and momentarily)  $\sigma_x, \sigma_y, \sigma_z$  and  $\tau_{xz}$  to be  $\mathcal{O}(\varepsilon)$  or smaller it follows that  $\mathfrak{F}(\cdot)$  is  $\mathcal{O}(1)$  for a finite viscosity law, but  $\mathfrak{F}(\cdot) = \mathcal{O}(\varepsilon^{n-1})$  for a power flow law with exponent  $n$ . Hence (7.67) may be written as  $\mathbb{G}\cdot\mathcal{O}(\varepsilon^\alpha) = \mathcal{O}(1)$  or when solved for  $\varepsilon$

$$\varepsilon = \mathcal{O}(\mathbb{G}^{-\alpha}),$$

where  $\alpha = 1$  for a finite viscosity law and  $\alpha = n$  for a power flow law. Henceforth, we shall use the value  $\mathbb{G} = \varepsilon^\alpha, \alpha \geq 1$ .

Considering this relationship between  $\mathbb{G}$  and  $\varepsilon$  we shall now simplify the boundary-value problem (7.64)–(7.66) by ignoring all terms of order higher than and equal to  $\varepsilon$ . From (7.64)<sub>5,7,8,10</sub> it then follows that  $\sigma_x, \sigma_y, \sigma_z$  and  $\tau_{xz}$  are all  $\mathcal{O}(\varepsilon^2)$  thereby corroborating our earlier assumption, so that to lowest order we have

$$\sigma_x = \sigma_y = \sigma_z = \tau_{xz} = 0.$$

Furthermore, the field equations reduce to

$$\begin{aligned} -\frac{\partial\bar{p}}{\partial\xi} + \frac{\partial T_x}{\partial\eta} + g_1 &= 0, & -\frac{\partial\bar{p}}{\partial\eta} - g_2 &= 0, \\ \frac{\partial T_z}{\partial\eta} - \frac{\partial\bar{p}}{\partial\zeta} + g_3 &= 0, & \frac{\partial U}{\partial\xi} + \frac{\partial V}{\partial\eta} + \frac{\partial W}{\partial\zeta} &= 0, \\ \frac{\partial U}{\partial\eta} &= 2\mathbb{F}(T_x^2 + T_z^2)T_x, & \frac{\partial W}{\partial\zeta} &= 2\mathbb{F}(T_x^2 + T_z^2)T_z, \end{aligned} \quad (7.68)$$

in which  $T_x = \tau_{xy}/\varepsilon$  and  $T_z = \tau_{yz}/\varepsilon$  are  $\mathcal{O}(1)$  and  $\mathbb{F}$  is defined by

$$\mathbb{F}(T_x^2 + T_z^2) = \varepsilon^{1-\alpha}\mathfrak{F}(\varepsilon^2(T_x^2 + T_z^2)) [ = \mathcal{O}(1) ]. \quad (7.69)$$

A similar reduction is possible with the boundary conditions. Deleting for the moment the kinematic surface condition (7.65)<sub>1</sub>, the boundary conditions of stress at the free surface reduce to

$$\bar{p} = \bar{p}^{\text{atm}}, \quad T_x = -\bar{p}^{\text{atm}}\frac{\partial\bar{y}_S}{\partial\xi}, \quad T_z = -\bar{p}^{\text{atm}}\frac{\partial\bar{y}_S}{\partial\zeta}, \quad \text{on } \bar{y} = \bar{y}_S(\xi, \zeta, \ell), \quad (7.70)$$

and those at the base become

$$\begin{aligned} V &= U \frac{\partial \bar{y}_B}{\partial \xi} + W \frac{\partial \bar{y}_B}{\partial \zeta}, \\ U &= C' [T_x^2 + T_z^2]^{(m-1)/2} T_x, \\ W &= C' [T_x^2 + T_z^2]^{(m-1)/2} T_z, \end{aligned} \quad (7.71)$$

where  $C' = \epsilon^m C$  is  $\mathcal{O}(1)$  for the viscous sliding to be significant.

Let us pause here for a moment and point at the significance of the simplified boundary-value problem (7.68), (7.70) and (7.71). Assuming that the surface profile is known, the equations can easily be integrated for the stresses  $T_x$ ,  $T_z$  and the velocities  $U$ ,  $V$ ,  $W$ . Once these quantities are known, the functional relationship valid at the surface obtained for the velocity components, can be used in the kinematic surface condition to obtain an equation governing the surface geometry. It has, thus, indeed been possible to uncouple the stress-velocity problem from the surface-geometry problem.

In order to explicitly demonstrate the integrability of Equations (7.67)–(7.71) let us look at the simplified case in which  $g_1 = g_3 = 0$ ,  $g_2 = 1$ . We shall also ignore the influence of the atmospheric pressure which is negligibly small anyhow. It then follows from (7.68)<sub>2</sub> and (7.70)<sub>1</sub> that

$$\bar{p} = (\bar{y}_S - \eta). \quad (7.72)$$

With this result (7.68)<sub>1,3</sub> can now be integrated subject to the boundary conditions (7.70)<sub>2,3</sub>. Indeed, with

$$\frac{\partial T_x}{\partial \eta} = \frac{\partial \bar{y}_S}{\partial \xi}, \quad \frac{\partial T_z}{\partial \eta} = \frac{\partial \bar{y}_S}{\partial \zeta}$$

one easily deduces that

$$T_x = -\frac{\partial \bar{y}_S}{\partial \xi}(\bar{y}_S - \eta), \quad T_z = -\frac{\partial \bar{y}_S}{\partial \zeta}(\bar{y}_S - \eta). \quad (7.73)$$

By considering the equilibrium equations and their associated boundary conditions of stress, it has been possible to determine the complete stress distribution. Equation (7.72) gives the overburden pressure, which increases linearly with depth and (7.73) provides formulas for the horizontal shear stresses. These formulas are very important as they generalize the famous shear-stress formula for two dimensions according to which shear stress is proportional to surface inclination and depth. Our non-dimensionalization and the stretching transformations have been such that, to lowest order, these dependencies are recovered. Indeed, (7.73) states that the two horizontal shear-stress components are proportional to depth and surface gradient

*in the direction of the stress component.* Moreover,  $T_x$  and  $T_z$  may change sign at positions where  $\partial \bar{y}_S / \partial \xi$  and  $\partial \bar{y}_S / \partial \zeta$  go through zero. Equation (7.71) then implies that the corresponding component of the sliding velocity will vanish. Later on it will be shown that  $U$  and  $V$  vanish at all depths in positions where  $\partial \bar{y}_S / \partial \xi = 0$  and  $\partial \bar{y}_S / \partial \zeta = 0$ , respectively. This result is of very practical significance, for it implies the following important facts which can be tested by observation :

- (i) At any given position the horizontal velocity vector does not change direction with depth, or the ratio of the two horizontal velocity components is only a function of  $\xi, \zeta$  but not  $\eta$ .
- (ii) At any position the direction of the velocity vector is that of the steepest descent of the surface profile.
- (iii) A dome or a trough is the location of zero velocity.

The proof of these statements is as follows: Assume that the Cartesian coordinate system has been chosen such that at the point under consideration  $\partial \bar{y}_S / \partial \zeta = 0$ . Then the  $\zeta$ -axis is parallel to the tangent to the lines of equal height. The orthogonal trajectories of these mark the steepest descent and thus are tangential to the  $\zeta$ -axis at the point under question. Hence  $|T_x|$  assumes a non-vanishing maximum and  $T_z = 0$ . Therefore, since the velocity component in the  $\zeta$ -direction vanishes at all depths if  $T_z = 0$ , statements (i) and (ii) are immediate and (iii) follows when the surface is horizontal in all directions.

There still remains the proof that the horizontal velocity cannot turn with depth in this simplest approximate theory. To this end, let us return to Equations (7.68)<sub>5,6</sub> and substitute the results (7.73). We then obtain

$$\begin{aligned} \frac{\partial U}{\partial \eta} &= -2\mathbb{F}(\mathcal{X}^2(\eta)) \frac{\partial \bar{y}_S}{\partial \xi} (\bar{y}_S - \eta) \equiv g_\xi(\eta), \\ \frac{\partial W}{\partial \eta} &= -2\mathbb{F}(\mathcal{X}^2(\eta)) \frac{\partial \bar{y}_S}{\partial \zeta} (\bar{y}_S - \eta) \equiv g_\zeta(\eta), \end{aligned} \quad (7.74)$$

where

$$\mathcal{X}^2(\eta) = (\bar{y}_S - \eta)^2 \left[ \left( \frac{\partial \bar{y}_S}{\partial \xi} \right)^2 + \left( \frac{\partial \bar{y}_S}{\partial \zeta} \right)^2 \right]. \quad (7.75)$$

The right-hand sides of (7.74) are known functions of  $\eta$  (and  $\xi, \zeta$  and  $\mathcal{X}$  whose dependence is not indicated). Defining

$$g_\xi^{(1)} = \int_{\bar{y}_B}^\eta g_\xi(\bar{\eta}) d\bar{\eta}, \quad g_\zeta^{(1)} = \int_{\bar{y}_B}^\eta g_\zeta(\bar{\eta}) d\bar{\eta} \quad (7.76)$$

integration of (7.74), subject to the boundary conditions (7.71)<sub>2,3</sub> reveals that

$$\begin{aligned} U(\xi, \zeta, \eta, \ell) &= -g_\xi^{(1)}(\eta) - C' |\mathcal{X}(\bar{y}_B)|^{m-1} \frac{\partial \bar{y}_S}{\partial \xi} (\bar{y}_S - \bar{y}_B), \\ W(\xi, \zeta, \eta, \ell) &= -g_\zeta^{(1)}(\eta) - C' |\mathcal{X}(\bar{y}_B)|^{m-1} \frac{\partial \bar{y}_S}{\partial \zeta} (\bar{y}_S - \bar{y}_B). \end{aligned} \quad (7.77)$$

Substituting these expressions for  $U$  and  $W$  into the continuity equation (7.68)<sub>4</sub> results in an integrable equation for  $V$ , an expression which could easily be deduced by also applying the kinematic boundary condition (7.71)<sub>1</sub> at the base. We shall not do it here since the vertical velocity components are small anyhow and, furthermore, will not be needed in the determination of the surface geometry.

Observe that  $g_\xi$  vanishes with  $\partial \bar{y}_S / \partial \xi$  and so does  $g_\xi^{(1)}$ , irrespective of the value of  $\eta$ . Therefore, (7.77)<sub>1</sub> implies that  $U = 0$  whenever  $\partial \bar{y}_S / \partial \xi = 0$ . Similarly  $W = 0$  whenever  $\partial \bar{y}_S / \partial \zeta = 0$ . The horizontal velocity vector has a vanishing component in the direction of the lines of equal height. The ice flow is in the direction of the steepest descent of the top surface. This provides the *a posteriori* information for the proof of the above statements (i)–(iii).\*

### (c) The equation describing the surface geometry

Having determined the stress and the velocity fields there remains the derivation of the equation governing the surface geometry. To this end consider the continuity equation (7.68)<sub>4</sub> and integrate it with respect to  $\eta$  between  $\eta = \bar{y}_B$  and  $\eta = \bar{y}_S$ . This yields

$$\int_{\bar{y}_B}^{\bar{y}_S} \frac{\partial U}{\partial \xi} d\eta + \int_{\bar{y}_B}^{\bar{y}_S} \frac{\partial W}{\partial \zeta} d\eta + V(\bar{y}_S) - V(\bar{y}_B) = 0,$$

or after interchanging differentiation and integration with Leibnitz's rule,

$$\begin{aligned} \frac{\partial}{\partial \xi} \int_{\bar{y}_B}^{\bar{y}_S} U d\eta + \frac{\partial}{\partial \zeta} \int_{\bar{y}_B}^{\bar{y}_S} W d\eta - U(\bar{y}_S) \frac{\partial \bar{y}_S}{\partial \xi} - W(\bar{y}_S) \frac{\partial \bar{y}_S}{\partial \zeta} + V(\bar{y}_S) + \\ + \left[ U(\bar{y}_B) \frac{\partial \bar{y}_B}{\partial \xi} + W(\bar{y}_B) \frac{\partial \bar{y}_B}{\partial \zeta} - V(\bar{y}_B) \right] = 0. \end{aligned} \quad (7.78)$$

The term in square brackets vanishes in view of (7.71)<sub>1</sub>. Adding (7.78) to (7.65)<sub>1</sub> yields

$$\frac{\partial \bar{y}_S}{\partial \ell} + \frac{\partial Q_\xi}{\partial \xi} + \frac{\partial Q_\zeta}{\partial \zeta} = \mathfrak{A},$$

with

$$Q_\xi \equiv \int_{\bar{y}_B}^{\bar{y}_S} U d\eta, \quad Q_\zeta \equiv \int_{\bar{y}_B}^{\bar{y}_S} W d\eta. \quad (7.79)$$

\*Partial observational proof of these statements is given in Figure 5.4a on p. 267.

This is the differential equation we were looking for. Equation (7.79)<sub>1</sub> is the spatially two-dimensional form of the *kinematic wave equation*. For steady problems it reduces to the equation

$$\frac{\partial Q_\xi}{\partial \xi} + \frac{\partial Q_\zeta}{\partial \zeta} = \mathfrak{A}(\xi, \zeta, \bar{y}_S). \quad (7.80)$$

As seen from (7.77), it is of second order. With the aid of (7.77) and

$$g_\xi^{(2)} = \int_{\bar{y}_B}^{\bar{y}_S} g_\xi^{(1)}(\eta) d\eta, \quad g_\zeta^{(2)} = \int_{\bar{y}_B}^{\bar{y}_S} g_\zeta^{(1)}(\eta) d\eta, \quad (7.81)$$

it may also be written in the form

$$\begin{aligned} & \frac{\partial}{\partial \xi} \left[ g_\xi^{(2)} \left( \bar{y}_S, \frac{\partial \bar{y}_S}{\partial \xi}, \frac{\partial \bar{y}_S}{\partial \zeta} \right) + C' |\mathcal{X}(\bar{y}_B)|^{m-1} (\bar{y}_S - \bar{y}_B)^2 \frac{\partial \bar{y}_S}{\partial \xi} \right] + \\ & + \frac{\partial}{\partial \zeta} \left[ g_\zeta^{(2)} \left( \bar{y}_S, \frac{\partial \bar{y}_S}{\partial \xi}, \frac{\partial \bar{y}_S}{\partial \zeta} \right) + C' |\mathcal{X}(\bar{y}_B)|^{m-1} (\bar{y}_S - \bar{y}_B)^2 \frac{\partial \bar{y}_S}{\partial \zeta} \right] = -\mathfrak{A}, \end{aligned} \quad (7.82)$$

in which the structure of a second-order equation becomes evident. It involves  $\bar{y}_S$  and  $\bar{y}_B$  separately and cannot be written as an equation for the difference  $(\bar{y}_S - \bar{y}_B)$ . So, the bed profile is not simply superimposed on a corresponding flat-bed surface profile. However, (7.82) is singular at the margin unless  $C'$  is singular as  $(\bar{y}_S - \bar{y}_B)^{-m}$ , as the margin is approached. When solving (7.82), a procedure should therefore be known on how (7.82) is handled close to the margins. This is a difficult question on its own.

#### (d) The margin conditions

For ice sheets under plane deformation, it was demonstrated in Chapter 5 that a power series solution to the differential equation corresponding to (7.82) had to be constructed close to the lower margin. Integration had to start from this margin using this power series representation and continued using a forward integrator. It was then seen that the solution failed to be uniformly valid, because close to the upper margin slope changes became large, contradicting the shallow-ice approximation. This suggests that margin conditions must be very difficult in this more general two-dimensional case.

The difficulty with the solution of Equation (7.82) is that the location of the margin is not known in advance; it must be guessed. This groundline is a closed curve in the  $(\xi, \zeta)$  plane, and Equation (7.82) close to a point of this line may be written in the local coordinates  $(n, s)$ , which are, respectively, perpendicular ( $n$ ) and parallel ( $s$ ) to it. On the groundline  $(\bar{y}_S - \bar{y}_B)$  does not change with  $s$  and a power-series solution can be constructed to evaluate  $\bar{y}_S$  a small distance inside the ice sheet. Using a numerical

scheme (as, for instance, a finite-difference approximation),  $\bar{y}_S$  may then be determined further inside the ice sheet. In this process, in a number of inner points  $\bar{y}_S$  will be calculated twice, and the two values will not be the same, in general. Let the number of these conflicting points be  $N$ . To arrive at the consistent integration scheme one must, in a second step, leave the value of  $\bar{y}_S$  in  $N$  points at the preselected margin unspecified. The finite difference equations of (7.82) are then solvable and yield a value for  $\bar{y}_S$  at the  $N$  'margin-points'. If in one of these points  $\bar{y}_S = \bar{y}_B$  then the point is indeed a margin point; otherwise it is not. Depending on the sign of  $\bar{y}_S - \bar{y}_B$ , the domain of the ice sheet must be extended or reduced. The process of integration must be repeated with this new estimated groundline until no further iterations are required.

This process is bound to be difficult, has not been performed so far, but a study of the margin conditions is urgently needed if a proper prediction of ice-sheet geometry should ever be possible.

#### 4. *Variational Principles*

The analysis of the ice-flow problems of the preceding sections dealt with situations which lie at two extremes of the three-dimensional effects. On the one hand, a rectilinear unidirectional flow in cylindrical channels of arbitrary cross-sections was considered, and it was shown that the boundedness of ice flow by valley sides had a dominant quantitative effect on the flux. On the other hand, ice sheets were looked at. These are shallow ice masses which spread in the horizontal directions over 100 to 1000 times their thickness. Globally, the flow in such sheets cannot be assumed to be planar. Ice spreads in both horizontal directions and a spatially three-dimensional formulation is necessary. With the aid of the shallow ice approximation, it was possible to reduce the stress-velocity problem to simple quadratures (if the surface geometry is known) and the problem of ice-sheet topography to a non-linear partial differential equation in two independent variables – the coordinates in the horizontal direction.

There is one important class of problems, which so far has not been given the necessary attention – localized features. There are many important practical problems which are of a local nature: stress and velocity distributions in glaciers close to an ice fall; in an ice mass shortly before breaking-off; formation of arches in hanging glaciers; ice forces on structures, etc. All these phenomena are truly three-dimensional. Analytical solutions are not available, and approximate techniques used previously are invalid. Numerical solution schemes must be found in these instances, the most obvious ones being the finite-element technique. It has not been greatly popularized in glaciology, but there is no doubt about its usefulness.

Derivation of finite-element formulations profits from the existence

of a *variational principle*. In this section we shall present several versions of a fundamental variational principle which is useful in ice-flow problems when the following conditions are satisfied:

(i) The constitutive relation for the stress deviator falls into the class

$$\begin{aligned}\boldsymbol{\sigma}' &= -\frac{2}{3}D_{II}\phi_1(D_{II}, D_{III}, \vartheta)\mathbf{1} + \phi_2(D_{II}, D_{III}, \vartheta)\mathbf{D} + \phi_1(D_{II}, D_{III}, \vartheta)\mathbf{D}^2, \\ \mathbf{D} &= -\frac{2}{3}\sigma'_{II}g(\sigma'_{II}, \sigma'_{III}, \vartheta)\mathbf{1} + f(\sigma'_{II}, \sigma'_{III}, \vartheta)\boldsymbol{\sigma}' + g(\sigma'_{II}, \sigma'_{III}, \vartheta)\boldsymbol{\sigma}'^2,\end{aligned}\quad (7.83)$$

in which the coefficient functions depend on the second and third invariants of  $\mathbf{D}$  or  $\boldsymbol{\sigma}'$ , respectively and on temperature. The coefficients are not entirely free, as the stress deviator  $\boldsymbol{\sigma}'$  or stretching  $\mathbf{D}$  must be derivable from 'potentials' as follows\*

$$\boldsymbol{\sigma} = \frac{\partial \Gamma(\mathbf{D})}{\partial \mathbf{D}}, \quad \mathbf{D} = \frac{\partial \hat{\Gamma}(\boldsymbol{\sigma}')}{\partial \boldsymbol{\sigma}'}. \quad (7.84)$$

The constitutive relation used for ice previously falls into the class (7.83), (7.84).

(ii) If the ice is cold, the temperature distribution must be *known*, so that its dependence in (7.83) can be replaced by a position-dependence.

(iii) The geometry of the region under consideration is fixed and the boundary consists of two non-intersecting parts, on which boundary conditions of velocity and stress apply, respectively. The boundary condition of velocity is limited insofar as one must either prescribe the velocity or else use a linear viscous sliding law.

These conditions imply that problems of changing boundaries cannot be handled when using the variational principles presented below. However, this is not a serious drawback because the boundaries in local problems are generally well defined.

In the following developments the reader is assumed to know the basic ideas of calculus of variations, see Weinstock [26] or Lanczos [15]. Modern methods of variational mechanics are rather sophisticated, see, e.g., the book on variational methods in theoretical mechanics by Oden and Reddy [19]. We shall be less ambitious and remain on the level of elementary variational calculus. The developments in this section are again more easily performed in tensor notation. Cartesian tensor notation will therefore be used; doubly repeated indices will denote summation, and partial differentiation with respect to a space variable will be indicated by a comma preceding the respective index. Our presentation follows Johnson [13], [14].

#### (a) Fundamental variational theorem

As before, we shall work in dimensionless coordinates. The governing

\*This amounts to requiring that Onsager relations hold in a non-linear theory.

equations of the boundary-value problem under consideration are

$$\begin{aligned}\bar{u}_{i,i} &= 0, \\ \sigma'_{ij,j} - \bar{p}_{,i} + g_i &= 0, \quad \text{where } g_i = \frac{\partial U(\bar{u}_k)}{\partial \bar{u}_i}, \\ \sigma'_{ij} &= \frac{\partial \Gamma(\bar{D}_{kl})}{\partial \bar{D}_{ij}} \text{ or } \bar{D}_{ij} = \frac{\partial \hat{\Gamma}(\sigma'_{kl})}{\partial \sigma_{ij}}.\end{aligned}\quad (7.85)$$

These equations must be solved in a region  $\mathcal{V}$  of the three-dimensional space subject to the following boundary conditions on the non-overlapping regions  $\partial\mathcal{V}_\sigma$  and  $\partial\mathcal{V}_u$  of the boundary  $\partial\mathcal{V}$ :

$$\begin{aligned}\bar{u}_i + \frac{\partial \psi_u(\sigma_k^{(n)})}{\partial \sigma_i^{(n)}} &= 0, \quad \text{on } \partial\mathcal{V}_u, \\ \sigma'_{ij} n_j - \bar{p} n_i + \frac{\partial \psi_\sigma(\bar{u}_k)}{\partial \bar{u}_i} &= 0, \quad \text{on } \partial\mathcal{V}_\sigma.\end{aligned}\quad (7.86)$$

In these equations variables which look familiar have the usual meaning. Of these we only repeat that  $\sigma'$  is the stress *deviator* and  $\sigma$  the total stress.  $\sigma^{(n)} = \sigma \cdot \mathbf{n}$  is the stress vector at the boundary with exterior unit normal  $\mathbf{n}$ .  $\psi_u$  and  $\psi_\sigma$  are known functions of their variables defined over the boundary;  $\Gamma$  and  $\hat{\Gamma}$  are the creep response ‘potentials’ and  $g_i$  the externally applied body force, which we assume to be derivable from a velocity potential  $U$ . If the external body force is constant, then one simply has  $U = g_i \bar{u}_i$ ; further for  $\psi_u \equiv 0$  (7.86)<sub>1</sub> expresses the no-slip condition and when  $\psi_u$  is a certain power law of its argument the Weertman-type sliding law is obtained (see, however, later conclusions). Similarly, when  $\psi_\sigma$  is a linear homogeneous form in  $\bar{u}$ , (7.86)<sub>2</sub> describes how the tractions are prescribed along the boundary.

Consider the functional

$$\begin{aligned}\mathfrak{J} &= \int_{\mathcal{V}} \left\{ \left[ \frac{1}{2} (\bar{u}_{i,j} + \bar{u}_{j,i}) - \bar{D}_{ij} \right] \sigma'_{ij} - U + \Gamma - \bar{p} \bar{u}_{i,i} \right\} dV - \\ &\quad - \int_{\partial\mathcal{V}_u} [\sigma_i^{(n)} \bar{u}_i + \psi_u] dA + \int_{\partial\mathcal{V}_\sigma} \psi_\sigma dA,\end{aligned}\quad (7.87)$$

where the volume integral is over the entire volume of the fluid and the surface integrals over the regions  $\partial\mathcal{V}_\sigma$  and  $\partial\mathcal{V}_u$ , respectively. The boundary is assumed to be sufficiently smooth to permit application of Gauss’ theorem. Assume the fields in (7.87) to be differentiable (as much as we need) and let

us perform the variational of  $\mathfrak{J}$  by varying all quantities independently. We then find:

$$\begin{aligned} \delta\mathfrak{J} = & \int_V \left\{ \left[ \frac{1}{2}(\bar{u}_{i,j} + \bar{u}_{j,i}) - \bar{D}_{ij} \right] \delta\sigma'_{ij} + \delta\bar{u}_{i,j}\sigma'_{ij} - \delta\bar{D}_{ij}\sigma'_{ij} - \right. \\ & \left. - \frac{\partial U}{\partial \bar{u}_i} \delta\bar{u}_i + \frac{\partial \Gamma}{\partial \bar{D}_{ij}} \delta\bar{D}_{ij} - \delta\bar{p}\bar{u}_{i,j} - \bar{p}\delta\bar{u}_{i,i} \right\} dV - \\ & - \int_{\partial V_u} \left\{ \delta\sigma_{ij}n_j\bar{u}_i + \sigma_i^{(n)}\delta\bar{u}_i + \frac{\partial \psi_u}{\partial \sigma_i^{(n)}} \delta\sigma_{ij}n_j \right\} dA + \int_{\partial V_\sigma} \frac{\partial \psi_\sigma}{\partial \bar{u}_i} \delta\bar{u}_i dA. \end{aligned} \quad (7.88)$$

The symbol  $\delta$  is used as a prefix to the variable that is varied, so that  $\delta\bar{u}_i$  is an arbitrary (but differentiable) function. Equation (7.88) can be transformed by using Gauss' theorem as follows:

$$\begin{aligned} \int_V \delta\bar{u}_{i,j}\sigma'_{ij} dV &= \int_V [(\delta\bar{u}_i\sigma'_{ij})_j - \delta\bar{u}_i\sigma'_{ij,j}] dV \\ &= \int_{\partial V} \delta\bar{u}_i\sigma'_{ij}n_j dA - \int_V \delta\bar{u}_i\sigma'_{ij,j} dV, \\ \int_V \bar{p}\delta\bar{u}_{i,i} dV &= \int_V [(\bar{p}\delta\bar{u}_i)_{,i} - \delta\bar{u}_i\bar{p}_{,i}] dV \\ &= \int_{\partial V} \bar{p}\delta\bar{u}_i n_i dA - \int_V \delta\bar{u}_i\bar{p}_{,i} dV. \end{aligned} \quad (7.89)$$

Replacing the respective terms in (7.88) by the expressions on the right-hand side of (7.89), we obtain

$$\begin{aligned} \delta\mathfrak{J} = & \int_V \left\{ \left[ \frac{1}{2}(\bar{u}_{i,j} + \bar{u}_{j,i}) - \bar{D}_{ij} \right] \delta\bar{u}_i - \left( \sigma'_{ij,j} + \frac{\partial U}{\partial \bar{u}_i} - \bar{p}_{,i} \right) \delta\bar{u}_i + \right. \\ & \left. + \left( -\sigma'_{ij} + \frac{\partial \Gamma}{\partial \bar{D}_{ij}} \right) \delta\bar{D}_{ij} - \bar{u}_{i,i}\delta\bar{p} \right\} dV + \\ & + \int_{\partial V_u} \left\{ - \left[ \bar{u}_i + \frac{\partial \psi_u}{\partial \sigma_i^{(n)}} \right] \delta\sigma_i^{(n)} - (\sigma_i^{(n)} - \sigma'_{ij}n_j + \bar{p}n_i)\delta\bar{u}_i \right\} dA + \\ & + \int_{\partial V_\sigma} \left( \frac{\partial \psi_\sigma}{\partial \bar{u}_i} + \sigma'_{ij}n_j - \bar{p}n_i \right) \delta\bar{u}_i dA. \end{aligned} \quad (7.90)$$

In order to make the functional  $\mathfrak{J}$  stationary, one must have  $\delta\mathfrak{J} = 0$  for all admissible variations of the fields. We shall let all fields vary arbitrarily and then claim that (7.85) are the Euler–Lagrange equations of the functional

$\mathfrak{J}$  and (7.86) the associated natural boundary conditions. Indeed,  $\delta\mathfrak{J} = 0$  for all variations subject to zero variation at the boundary implies

$$\left. \begin{aligned} \bar{D}_{ij} &= \frac{1}{2}(\bar{u}_{i,j} + \bar{u}_{j,i}), & \sigma'_{ij} &= \frac{\partial \Gamma}{\partial \bar{D}_{ij}} \\ \sigma'_{ij,j} - \bar{p}_{,i} + \frac{\partial U}{\partial \bar{u}_i} &= 0, & \bar{u}_{i,i} &= 0 \end{aligned} \right\} \text{ in } \mathcal{V}, \quad (7.91)$$

which are Equations (7.85). By choosing the variations of the basic fields in a second step now such that they are arbitrary at the boundary, the boundary conditions (7.86) are obtained.

The Euler–Lagrange equations of the functional  $\mathfrak{J}$  agree with Equations (7.85) provided that the stress deviator is given as a function of stretching according to (7.85)<sub>3</sub>, but not vice versa, (7.85)<sub>4</sub>. This second case being the more common one in glaciology, let us also present a functional  $\mathfrak{H}$  whose Euler–Lagrange equations will correspond to (7.85) and the natural boundary conditions to (7.86) with a stress-strain rate relationship as given by (7.85)<sub>4</sub>. To this end we must only introduce the *Legendre transformation*

$$\Gamma(\bar{D}_{kl}) - \bar{D}_{ij}\sigma'_{ij} = -\hat{\Gamma}(\sigma'_{kl}) \quad (7.92)$$

and replace  $\Gamma$  in (7.87) by  $\hat{\Gamma}$ . The functional  $\mathfrak{J}$  (denoted by  $\mathfrak{H}$  after this transformation) then reads

$$\begin{aligned} \mathfrak{H} = \int_{\mathcal{V}} & \left[ \frac{1}{2}(\bar{u}_{i,j} + \bar{u}_{j,i})\sigma'_{ij} - U - \hat{\Gamma} - \bar{p}\bar{u}_{i,i} \right] dV - \\ & - \int_{\partial\mathcal{V}_u} [\sigma_i^{(n)}\bar{u}_i + \psi_u] dA + \int_{\partial\mathcal{V}_\sigma} \psi_\sigma dA, \end{aligned} \quad (7.93)$$

from which we easily deduce that

$$\begin{aligned} \delta\mathfrak{H} = \int_{\mathcal{V}} & \left\{ \frac{1}{2}(\bar{u}_{i,j} + \bar{u}_{j,i})\delta\sigma'_{ij} + \delta\bar{u}_{i,j}\sigma'_{ij} - \frac{\partial U}{\partial \bar{u}_i}\delta\bar{u}_i - \right. \\ & \left. - \frac{\partial \hat{\Gamma}}{\partial \sigma'_{ij}}\delta\sigma'_{ij} - \bar{p}\delta\bar{u}_{i,i} - \bar{u}_{i,i}\delta\bar{p} \right\} dV - \\ & - \int_{\partial\mathcal{V}_u} \left[ \delta\sigma_i^{(n)}\bar{u}_i + \sigma_i^{(n)}\delta\bar{u}_i + \frac{\partial \psi_u}{\partial \sigma_i^{(n)}}\delta\sigma_i^{(n)} \right] dA + \int_{\partial\mathcal{V}_\sigma} \frac{\partial \psi_\sigma}{\partial \bar{u}_i}\delta\bar{u}_i dA, \end{aligned}$$

or

$$\begin{aligned} \delta\mathfrak{H} = \int_{\mathcal{V}} & \left\{ \left[ \frac{1}{2}(\bar{u}_{i,j} + \bar{u}_{j,i}) - \frac{\partial \hat{\Gamma}}{\partial \sigma'_{ij}} \right] \delta\sigma'_{ij} - \right. \\ & \left. - \left[ \sigma'_{ij,j} - \bar{p}_{,i} + \frac{\partial U}{\partial \bar{u}_i} \right] \delta\bar{u}_i - \bar{u}_{i,i}\delta\bar{p} \right\} dV + \end{aligned} \quad (7.94)$$

$$\begin{aligned}
& + \int_{\partial\mathcal{V}_u} \left\{ - \left[ \bar{u}_i + \frac{\partial\psi_u}{\partial\sigma_i^{(n)}} \right] \delta\sigma_i^{(n)} + [-\sigma_i^{(n)} + \sigma'_{ij}n_j - \bar{p}n_i] \delta\bar{u}_i \right\} dA + \\
& + \int_{\partial\mathcal{V}_\sigma} \left\{ \sigma'_{ij}n_j - \bar{p}n_i + \frac{\partial\psi_\sigma}{\partial\bar{u}_i} \right\} \delta\bar{u}_i dA,
\end{aligned}$$

in which the formulas (7.89) have again been used. As seen from this expression,  $\delta\mathfrak{H} = 0$  implies the equilibrium equation (7.85) but with the constitutive relationship  $\frac{1}{2}(\bar{u}_{i,j} + \bar{u}_{j,i}) = \partial\hat{\Gamma}/\partial\sigma'_{ij}$ . Hence, the definition of  $\bar{D}_{ij}$ , which in (7.91) was obtained as one set of Euler–Lagrange equations, is naturally implied here.

It should be emphasized that there are no admissibility conditions other than differentiability in obtaining stationary conditions of the functionals  $\mathfrak{J}$  and  $\mathfrak{H}$ . In an approximate method such as the finite element method, this means that interpolation functions which only satisfy the inter-element continuity conditions can be chosen, and no other conditions such as compatibility or equilibrium equations need be satisfied. The functionals  $\mathfrak{J}$  and  $\mathfrak{H}$  are therefore suitable for *low continuity hybrid finite element formulations* in which attention is focussed on both stress and velocity distributions.

The variational theorems based on the functionals  $\mathfrak{J}$  and  $\mathfrak{H}$  have the disadvantage of not corresponding to a minimum or maximum principle. Such principles can, however, be deduced from  $\mathfrak{J}$  and  $\mathfrak{H}$  by invoking further admissibility conditions. This, generally amounts to the imposition of higher smoothness requirements.

### (b) Variational principle for velocities

Consider the case that the variations are subject to the admissibility conditions

$$\begin{aligned}
\bar{u}_{i,i} &= 0, & \bar{D}_{ij} &= \frac{1}{2}(\bar{u}_{i,j} + \bar{u}_{j,i}), & \sigma'_{ij} &= \frac{\partial\Gamma}{\partial\bar{D}'_{ij}}, \quad \text{in } \mathcal{V}, \\
\bar{u}_i + \frac{\partial\psi_u}{\partial\sigma_i^{(n)}} &= 0, & \text{on } \partial\mathcal{V}_u,
\end{aligned} \tag{7.95}$$

which we assume to be met automatically by the fields. This means that in an approximate treatment, the interpolation function would have to satisfy the continuity equation and the boundary conditions of velocity. The relation for  $\bar{D}_{ij}$  serves as a definition and the constitutive relation for  $\sigma'_{ij}$  has to be thought of as being substituted in the equilibrium equations. Conditions (7.95) do not suffice to obtain a variational principle for velocities alone, we also need to assume that the following transformation for the boundary condition (7.95)<sub>4</sub> exists:

$$\sigma_i^{(n)}\bar{u}_i + \psi_u(\sigma_i^{(n)}) = -\hat{\psi}_u(\bar{u}_i). \tag{7.96}$$

Using (7.95) and (7.96) in (7.87) yields

$$\begin{aligned}\mathfrak{J}_u = & \int_{\mathcal{V}} \left\{ -U(\bar{u}_i) + \Gamma\left(\frac{1}{2}(\bar{u}_{i,j} + \bar{u}_{j,i})\right) \right\} dV + \\ & + \int_{\partial\mathcal{V}_\sigma} \psi_\sigma(\bar{u}_i) dA + \int_{\partial\mathcal{V}_u} \hat{\psi}_u(\bar{u}_i) dA.\end{aligned}\quad (7.97)$$

To find the conditions of stationarity subject to (7.95) and (7.96) we remark that with the exception of  $\bar{u}_{i,i} = 0$  these conditions are already taken into account in (7.97). When evaluating  $\delta\mathfrak{J}_u = 0$  it must be observed, therefore, that  $\bar{u}_i$  is solenoidal. We take this condition into account by a Lagrangian parameter  $\bar{p}$ , write  $\tilde{\mathfrak{J}}_u = \mathfrak{J}_u - \int_{\mathcal{V}} \bar{p} \bar{u}_{i,i} dV$  and form  $\delta\tilde{\mathfrak{J}}_u = 0$ . This yields

$$\begin{aligned}\delta\tilde{\mathfrak{J}}_u = & \int_{\mathcal{V}} \left\{ -\frac{\partial U}{\partial \bar{u}_i} - \left( \frac{\partial \Gamma}{\partial \bar{D}_{ij}} \right)_{,j} + \bar{p}_{,i} \right\} \delta \bar{u}_i dV + \\ & + \int_{\partial\mathcal{V}_u} \left\{ \frac{\partial \Gamma}{\partial \bar{D}_{ij}} n_j - \bar{p} n_i + \frac{\partial \hat{\psi}_u}{\partial \bar{u}_i} \right\} \delta \bar{u}_i dA + \\ & + \int_{\partial\mathcal{V}_\sigma} \left\{ \frac{\partial \Gamma}{\partial \bar{D}_{ij}} n_j - \bar{p} n_i + \frac{\partial \psi_\sigma}{\partial \bar{u}_i} \right\} \delta \bar{u}_i dA,\end{aligned}\quad (7.98)$$

in which  $\bar{D}_{ij}$  is an abbreviation for  $\frac{1}{2}(\bar{u}_{i,j} + \bar{u}_{j,i})$ . Using (7.96) in the first surface integral, it is seen that the Euler–Lagrange equations and natural boundary conditions are

$$\begin{aligned}\left( \frac{\partial \Gamma}{\partial \bar{D}_{ij}} \right)_{,j} - \bar{p}_{,i} + \frac{\partial U}{\partial \bar{u}_i} &= 0, \quad \text{in } \mathcal{V}, \\ \sigma_i^{(n)} = \frac{\partial \Gamma}{\partial \bar{D}_{ij}} n_j - \bar{p} n_i &= 0, \quad \text{on } \partial\mathcal{V}_u, \\ \frac{\partial \Gamma}{\partial \bar{D}_{ij}} n_j - \bar{p} n_i + \frac{\partial \psi_\sigma}{\partial \bar{u}_i} &= 0, \quad \text{on } \partial\mathcal{V}_\sigma,\end{aligned}\quad (7.99)$$

which is the original boundary-value problem, expressed in terms of velocities only. The form of Equations (7.99) suggests that the Lagrangian parameter can be interpreted as a pressure.

There are further variants of the variational  $\mathfrak{J}_u$  which are obtained by restricting  $\Gamma$  and  $\psi_u$  to special forms. We shall not be concerned with these and refer the reader to Johnson [13, 14].

### (c) Reciprocal variational theorem

The above variational theorem for velocities corresponds in non-linear elasticity to the ‘principle of minimum of potential energy’. There is a prin-

ciple which is dual or complementary to this; it is a principle involving *stresses*. Admissibility conditions that must be fulfilled by the fields are now the equilibrium equations and the boundary conditions of stress. These equations were the Euler–Lagrange equations and the natural boundary conditions in the velocity principle. We thus expect that the admissibility conditions of the velocity principle will become here the Euler–Lagrange equations. Starting equation to deduce the appropriate functional is the functional  $\mathfrak{H}$  given in (7.93).

Using Gauss' theorem in the integral

$$\int_{\mathcal{V}} \left[ \frac{1}{2} (\bar{u}_{i,j} + \bar{u}_{j,i}) \sigma'_{ij} - \bar{p} \bar{u}_{i,i} \right] dV,$$

we leave it as an exercise for the reader to show that the functional given in (7.93) may also be written as

$$\begin{aligned} \mathfrak{H} = & \int_{\mathcal{V}} \left\{ \left[ -\bar{u}_i \sigma'_{ij,j} + \bar{p}_{,i} \bar{u}_i - \frac{\partial U}{\partial \bar{u}_i} \bar{u}_i \right] + \frac{\partial U}{\partial \bar{u}_i} \bar{u}_i - U - \hat{\Gamma} \right\} dV + \\ & + \int_{\partial \mathcal{V}_u} \left\{ [\sigma'_{ij} n_j \bar{u}_i - \bar{p} n_i \bar{u}_i - \sigma_i^{(n)} \bar{u}_i] - \psi_u \right\} dA + \\ & + \int_{\partial \mathcal{V}_\sigma} \left\{ \left[ \bar{u}_i \sigma'_{ij} n_j - \bar{p} n_i \bar{u}_i + \frac{\partial \psi_\sigma}{\partial \bar{u}_i} \bar{u}_i \right] - \frac{\partial \psi_\sigma}{\partial \bar{u}_i} \bar{u}_i + \psi_\sigma \right\} dA. \end{aligned} \quad (7.100)$$

We now assume that the fields satisfy as admissibility conditions the equilibrium equations (7.85)<sub>2</sub> and the boundary conditions of stresses (7.86)<sub>2</sub> and  $\sigma_i^{(n)} = \sigma_{ij} n_j$ . Under these conditions the terms in braces in (7.100) vanish and  $\mathfrak{H}$  becomes

$$\begin{aligned} \mathfrak{H}_\sigma = & \int_{\mathcal{V}} \left\{ \frac{\partial U}{\partial \bar{u}_i} \bar{u}_i - U - \hat{\Gamma} \right\} dV - \\ & - \int_{\partial \mathcal{V}_u} \psi_u dA + \int_{\partial \mathcal{V}_\sigma} \left\{ - \frac{\partial \psi_\sigma}{\partial \bar{u}_i} \bar{u}_i + \psi_\sigma \right\} dA. \end{aligned} \quad (7.101)$$

The Euler–Lagrange equations of this functional, when the stress fields are subject to the admissibility conditions mentioned above, are

$$\bar{u}_{i,i} = 0, \quad \bar{D}_{ij} = \frac{\partial \Gamma}{\partial \sigma'_{ij}} \quad (7.102)$$

and its natural boundary conditions are (7.86)<sub>1</sub>. One can prove this directly by calculating  $\delta \mathfrak{H}_\sigma$  using Lagrangian multipliers to account for the admis-

sibility conditions. Thus we form

$$\begin{aligned}\tilde{\mathfrak{H}}_\sigma &= \mathfrak{H}_\sigma - \int_V \bar{u}_i^* \left[ \sigma'_{ij,j} - \bar{p}_{,i} + \frac{\partial U}{\partial \bar{u}_i} \right] dV + \\ &\quad + \int_{\partial \mathcal{V}_u} \bar{u}_i^* [\sigma'_{ij} n_j - \bar{p} n_i - \sigma_i^{(n)}] dA + \\ &\quad + \int_{\partial \mathcal{V}_\sigma} \bar{u}_i^* \left[ \sigma'_{ij} n_j - \bar{p} n_i + \frac{\partial \psi_\sigma}{\partial \bar{u}_i} \right] dA,\end{aligned}\tag{7.103}$$

where  $\bar{u}_i^*$  are Lagrangian parameters, and then find

$$\begin{aligned}\delta \tilde{\mathfrak{H}}_\sigma &= \int_V \left\{ \frac{\partial^2 U}{\partial \bar{u}_i \partial \bar{u}_j} \bar{u}_i \delta \bar{u}_j - \frac{\partial \hat{\Gamma}}{\partial \sigma'_{ij}} \delta \sigma'_{ij} - \right. \\ &\quad \left. - \bar{u}_i^* \left[ \underline{\delta \sigma'_{ij,j} - \delta \bar{p}_{,i}} + \frac{\partial^2 U}{\partial \bar{u}_i \partial \bar{u}_j} \delta \bar{u}_j \right] \right\} dV - \\ &\quad - \int_{\partial \mathcal{V}_u} \left\{ \frac{\partial \psi_u}{\partial \sigma_i^{(n)}} \delta \sigma_i^{(n)} - \bar{u}_i^* [\delta \sigma'_{ij} n_j - \delta \bar{p} n_i - \delta \sigma_i^{(n)}] \right\} dA + \\ &\quad + \int_{\partial \mathcal{V}_\sigma} \left\{ - \frac{\partial^2 \psi_\sigma}{\partial \bar{u}_i \partial \bar{u}_j} \bar{u}_i \delta \bar{u}_j + \bar{u}_i^* \left[ \delta \sigma'_{ij} \bar{u}_j - \delta \bar{p} \bar{u}_i + \frac{\partial^2 \psi_\sigma}{\partial \bar{u}_i \partial \bar{u}_j} \delta \bar{u}_j \right] \right\} dA = 0.\end{aligned}$$

Using Gauss' theorem for the underlined terms, it is possible to write  $\delta \tilde{\mathfrak{H}}_\sigma$  as follows (many terms cancel)

$$\begin{aligned}\delta \tilde{\mathfrak{H}}_\sigma &= \int_V \left\{ [\bar{u}_i - \bar{u}_i^*] \frac{\partial^2 U}{\partial \bar{u}_i \partial \bar{u}_j} \delta \bar{u}_j + \right. \\ &\quad \left. + \left[ \frac{1}{2} (\bar{u}_{i,j}^* + \bar{u}_{j,i}^*) - \frac{\partial \hat{\Gamma}}{\partial \sigma'_{ij}} \right] \delta \sigma'_{ij} - \bar{u}_{i,i} \delta \bar{p} \right\} dV - \\ &\quad - \int_{\partial \mathcal{V}_u} \left\{ \frac{\partial \psi_u}{\partial \sigma_i^{(n)}} + \bar{u}_i^* \right\} \delta \sigma_i^{(n)} dA + \\ &\quad + \int_{\partial \mathcal{V}_\sigma} \frac{\partial^2 \psi_\sigma}{\partial \bar{u}_i \partial \bar{u}_j} (\bar{u}_i^* - \bar{u}_i) \delta \bar{u}_i dA = 0,\end{aligned}$$

from which we immediately conclude that

$$\begin{aligned}\bar{u}_{i,i}^* &= 0, \quad \frac{1}{2} (\bar{u}_{i,j}^* + \bar{u}_{j,i}^*) = \frac{\partial \hat{\Gamma}}{\partial \sigma'_{ij}}, \quad \text{in } \mathcal{V}, \\ \bar{u}_i^* - \frac{\partial \psi_u}{\partial \sigma_i^{(n)}} &= 0, \quad \text{on } \partial \mathcal{V}_u, \\ \bar{u}_i &= \bar{u}_i^* \quad \text{in } \mathcal{V} \cup \partial \mathcal{V}_u.\end{aligned}\tag{7.104}$$

Thus, the Lagrangian parameter agrees with the true velocity field. Since the roles of admissibility conditions and Euler equations are interchanged for the variational principles corresponding to functionals  $\mathfrak{J}_u$  given by (7.97) and  $\mathfrak{H}_\sigma$  given by (7.101), one speaks of these principles as being reciprocal.

(d) *Maximum and minimum principles*

Let  $\bar{u}_i$ ,  $\bar{D}_{ij}$ ,  $\sigma_{ij}$ ,  $\sigma'_{ij}$  and  $\bar{p}$  be solutions of the boundary-value problem (7.85) and (7.86) and let  $\delta\bar{u}_i$ ,  $\delta\bar{D}_{ij}$ , etc. be admissible variations of these quantities. Introduce  $\bar{u}_i + \delta\bar{u}_i$ ,  $\bar{D}_{ij} + \delta\bar{D}_{ij}$ , etc. into the functionals (7.87) and (7.93), respectively and expand the resulting expressions in powers of the variations. Considering that for the solution of the boundary-value problem  $\delta\mathfrak{J} = 0$  and  $\delta\mathfrak{H} = 0$  we then may write  $\mathfrak{J}$  and  $\mathfrak{H}$  as

$$\mathfrak{J} = \mathfrak{J}_0 + \delta^2 \mathfrak{J}_2 + \delta^3 \mathfrak{J}_3 + \dots, \quad \mathfrak{H} = \mathfrak{H}_0 + \delta^2 \mathfrak{H}_2 + \delta^3 \mathfrak{H}_3 + \dots, \quad (7.105)$$

in which  $\delta^i$  indicates that the variations occur in products or powers of order  $i$  and  $\mathfrak{J}_0$  and  $\mathfrak{H}_0$  are constants. Under usual circumstances the second variations do not vanish so that the sign of  $\delta^2 \mathfrak{J}_2$  or  $\delta^2 \mathfrak{H}_2$  indicates a local maximum or minimum. As can be inferred from (7.87) and (7.93) the second variations of  $\mathfrak{J}$  and  $\mathfrak{H}$  have the following form:

$$\begin{aligned} \delta^2 \mathfrak{J}_2 = & \int_V \left\{ \left[ \frac{1}{2} (\delta\bar{u}_{i,j} + \delta\bar{u}_{j,i}) - \delta\bar{D}_{ij} \right] \delta\sigma'_{ij} - \frac{1}{2} \frac{\partial^2 U}{\partial\bar{u}_i \partial\bar{u}_j} \delta\bar{u}_i \delta\bar{u}_j + \right. \\ & + \left. \frac{\partial^2 \Gamma}{\partial\bar{D}_{ij} \partial\bar{D}_{kl}} \delta\bar{D}_{ij} \delta\bar{D}_{kl} - \delta\bar{p} \delta\bar{u}_{i,i} \right\} dV - \\ & - \int_{\partial V_u} \left\{ \delta\sigma_i^{(n)} \delta\bar{u}_i + \frac{\partial^2 \psi_u}{\partial\sigma_i^{(n)} \partial\sigma_j^{(n)}} \delta\sigma_i^{(n)} \delta\sigma_j^{(n)} \right\} dA + \\ & + \int_{\partial V_\sigma} \frac{\partial^2 \psi_\sigma}{\partial\bar{u}_i \partial\bar{u}_j} \delta\bar{u}_i \delta\bar{u}_j dA \end{aligned} \quad (7.106)$$

and

$$\begin{aligned} \delta^2 \mathfrak{H}_2 = & \int_V \left\{ \frac{1}{2} (\delta\bar{u}_{i,j} + \delta\bar{u}_{j,i}) \delta\sigma'_{ij} - \frac{1}{2} \frac{\partial^2 U}{\partial\bar{u}_i \partial\bar{u}_j} \delta\bar{u}_i \delta\bar{u}_j - \right. \\ & - \left. \frac{1}{2} \frac{\partial^2 \hat{\Gamma}}{\partial\sigma'_{ij} \partial\sigma'_{kl}} \delta\sigma'_{ij} \delta\sigma'_{kl} - \delta\bar{p} \delta\bar{u}_{i,i} \right\} dV - \\ & - \int_{\partial V_u} \left[ \delta\sigma_i^{(n)} \delta\bar{u}_i + \frac{1}{2} \frac{\partial^2 \psi_u}{\partial\sigma_i^{(n)} \partial\sigma_j^{(n)}} \delta\sigma_i^{(n)} \delta\sigma_j^{(n)} \right] dA + \\ & + \int_{\partial V_\sigma} \frac{1}{2} \frac{\partial^2 \psi_\sigma}{\partial\bar{u}_i \partial\bar{u}_j} \delta\bar{u}_i \delta\bar{u}_j dA. \end{aligned} \quad (7.107)$$

We wish to find sufficient conditions such that  $\delta\mathfrak{J} = 0$  and  $\delta\mathfrak{H} = 0$  are either

maximum or minimum principles. According to the theory of calculus of variations,  $\delta\mathfrak{J} = 0$  is a local minimum or maximum according to whether  $\delta^2\mathfrak{J}$  is negative or positive. When the fields are subject to differentiability conditions only, nothing can be inferred from (7.106) and (7.107), but from the dual principles for velocities and stresses, respectively, such statements do evolve.

Let the fields in (7.106), therefore, satisfy the admissibility conditions of the principle for velocities,

$$\left. \begin{aligned} \delta\bar{u}_{i,i} &= 0, & \delta\bar{D}_{ij} &= \frac{1}{2}(\delta\bar{u}_{i,j} + \delta\bar{u}_{j,i}), \\ \delta\sigma'_{ij} &= \frac{\partial^2\Gamma}{\partial\sigma'_{ij}\partial\sigma'_{kl}}\delta\sigma'_{kl} & & \\ \delta\bar{u}_i + \frac{\partial^2\psi_u}{\partial\sigma_i^{(n)}\partial\sigma_j^{(n)}}\delta\sigma_k^{(n)} &\equiv 0, & \text{on } \partial\mathcal{V}_u. & \end{aligned} \right\} \text{in } \mathcal{V}, \quad (7.108)$$

Upon substitution into (7.106) the second variational  $\delta^2\mathfrak{J}_u$  of  $\mathfrak{J}_u$  is obtained. It reads

$$\begin{aligned} \delta^2\mathfrak{J}_u &= \int_{\mathcal{V}} \left\{ -\frac{1}{2} \frac{\partial^2 U}{\partial\bar{u}_i\partial\bar{u}_j} \delta\bar{u}_i \delta\bar{u}_j + \frac{1}{2} \frac{\partial^2\Gamma}{\partial\bar{D}_{ij}\partial\bar{D}_{kl}} \delta\bar{D}_{ij} \delta\bar{D}_{kl} \right\} dV + \\ &+ \int_{\partial\mathcal{V}_u} \frac{1}{2} \frac{\partial^2\psi_u}{\partial\sigma_i^{(n)}\partial\sigma_j^{(n)}} \delta\sigma_i^{(n)} \delta\sigma_j^{(n)} dA + \int_{\partial\mathcal{V}_\sigma} \frac{1}{2} \frac{\partial^2\psi_\sigma}{\partial\bar{u}_i\partial\bar{u}_j} \delta\bar{u}_i \delta\bar{u}_j dA. \end{aligned} \quad (7.109)$$

This is a symmetric quadratic form in the variables  $\delta\bar{u}_i$ ,  $\delta\bar{D}_{ij}$ ,  $\delta\sigma_i^{(n)}$  defined on the respective regions  $\mathcal{V}$ ,  $\partial\mathcal{V}_u$ ,  $\partial\mathcal{V}_\sigma$  and sufficient conditions for a (maximum) minimum are that the matrices

$$\frac{\partial^2 U}{\partial\bar{u}_i\partial\bar{u}_j}, \frac{\partial^2\Gamma}{\partial\bar{D}_{ij}\partial\bar{D}_{kl}}, \frac{\partial^2\psi_u}{\partial\sigma_i^{(n)}\partial\sigma_j^{(n)}}, \frac{\partial^2\psi_\sigma}{\partial\bar{u}_i\partial\bar{u}_j} \quad (7.110)$$

be (negative) positive semi-definite and at least one of them should not be identically zero.

On the other hand, when the admissibility conditions are those of the reciprocal variational principle, the variations must satisfy

$$\begin{aligned} \delta\sigma'_{ij,j} - \delta\bar{p}_{,i} + \frac{\partial^2 U}{\partial\bar{u}_i\partial\bar{u}_j} \delta\bar{u}_j &\equiv 0, & \text{in } \mathcal{V}, \\ \delta\sigma'_{ij} n_j - \delta\bar{p} n_i + \frac{\partial\psi_\sigma}{\partial\bar{u}_i\partial\bar{u}_j} \delta\bar{u}_j &\equiv 0, & \text{on } \partial\mathcal{V}_\sigma, \\ \delta\sigma_i^{(n)} - \delta\sigma_{ij} n_j + \delta\bar{p} n_i &= 0, & \text{on } \partial\mathcal{V}_u. \end{aligned} \quad (7.111)$$

To invoke these identities in (7.107), the latter relation must first be transformed by applying Gauss' theorem to the underlined terms. When this is

done and when (7.111) are invoked in the emerging equations, it is straightforward to show that  $\delta \mathfrak{H}_\sigma$  is given by

$$\begin{aligned} \delta \mathfrak{H}_\sigma = & \int_V \left\{ \frac{1}{2} \frac{\partial^2 U}{\partial \bar{u}_i \partial \bar{u}_j} \delta \bar{u}_i \delta \bar{u}_j - \frac{1}{2} \frac{\partial^2 \Gamma}{\partial \sigma'_{ij} \partial \sigma'_{kl}} \delta \sigma'_{ij} \delta \sigma'_{kl} \right\} dV - \\ & - \int_{\partial V_u} \frac{\partial^2 \psi_u}{\partial \sigma_i^{(n)} \partial \sigma_j^{(n)}} \delta \sigma_i^{(n)} \delta \sigma_j^{(n)} dA - \int_{\partial V_\sigma} \frac{\partial^2 \psi_\sigma}{\partial \bar{u}_i \partial \bar{u}_j} \delta \bar{u}_i \delta \bar{u}_j dA. \end{aligned} \quad (7.112)$$

It is seen from this that the conditions for  $\mathfrak{H}_\sigma$  to take on a minimum (maximum) at its extreme value are that the matrices

$$\frac{\partial^2 U}{\partial \bar{u}_i \partial \bar{u}_j}, -\frac{\partial^2 \Gamma}{\partial \sigma'_{ij} \partial \sigma'_{kl}}, -\frac{\partial^2 \psi_u}{\partial \sigma_i^{(n)} \partial \sigma_j^{(n)}}, -\frac{\partial^2 \psi_\sigma}{\partial \bar{u}_i \partial \bar{u}_j} \quad (7.113)$$

be either positive (negative) definite or identically zero, not all being identically zero.

It is interesting to apply the admissibility conditions (7.108) of the 'velocity principle' in the 'stress principle' (7.107). We then obtain

$$\begin{aligned} \delta^2 \mathfrak{H}_u = & \int_V \left\{ \delta \bar{D}_{ij} \delta \sigma'_{ij} - \frac{1}{2} \frac{\partial^2 U}{\partial \bar{u}_i \partial \bar{u}_j} \delta \bar{u}_i \delta \bar{u}_j - \frac{1}{2} \frac{\partial^2 \Gamma}{\partial \sigma'_{ij} \partial \sigma'_{kl}} \delta \sigma'_{ij} \delta \sigma'_{kl} \right\} dV - \\ & - \int_{\partial V_u} \frac{1}{2} \frac{\partial^2 \psi_u}{\partial \sigma_i^{(n)} \partial \sigma_j^{(n)}} \delta \sigma_i^{(n)} \delta \sigma_j^{(n)} dA + \int_{\partial V_\sigma} \frac{1}{2} \frac{\partial^2 \psi_\sigma}{\partial \bar{u}_i \partial \bar{u}_j} \delta \bar{u}_i \delta \bar{u}_j dA. \end{aligned} \quad (7.114)$$

However,  $\bar{D}_{ij}$  can be expressed in terms of  $\hat{\Gamma}$ , in view of (7.85)<sub>4</sub>, and when this is done, Equation (7.112) is identical with the negative of (7.114),

$$\delta^2 \mathfrak{H}_u = -\delta^2 \mathfrak{J}_\sigma. \quad (7.115)$$

It may be concluded, therefore, that the reciprocal principle is a maximum (minimum) principle under the same condition that the velocity principle is a minimum (maximum).

Assume now that the boundary-value problem (7.85) and (7.86) has a unique solution, and that conditions hold sufficient to ensure that the velocity principle is a minimum principle and the reciprocal principle is a maximum principle. We then conclude that the extremum value of  $\mathfrak{J}$  has the following bounds

$$\mathfrak{H}_\sigma \leq \mathfrak{J}_0 \leq \mathfrak{J}_u, \quad (7.116)$$

where  $\mathfrak{H}_\sigma$  and  $\mathfrak{J}_u$  are functions of any admissible trial function given by (7.97) and (7.107). Inequalities (7.116) may be used to find upper and lower bounds for the exact solution of the boundary-value problem (7.85) and (7.86).

The inequalities need no proof but can, perhaps, be better understood by recalling the maximum and minimum properties of  $\mathfrak{J}$  and  $\mathfrak{H}$ , respectively. Since  $\mathfrak{J}$  has a minimum whenever an exact solution of the boundary-value

problem (7.85) and (7.86) is found,  $\mathfrak{J}_u$  for any approximate solution will be larger than  $\mathfrak{J}_0$ . Similarly, since  $\mathfrak{H}$  is a maximum for the exact solution,  $\mathfrak{H}_\sigma$  will approach  $\mathfrak{J}_0$  from below. This explains the inequalities (7.116).

(e) *Adoption of the variational principles to ice problems*

To apply the above theoretical findings to problems in ice mechanics we must identify the functions  $U$ ,  $\Gamma$ ,  $\hat{\Gamma}$ ,  $\psi_u$  and  $\psi_\sigma$ . From the adoption of such functional relations the application to ice flow problems is then immediate.

In (7.85), the body force  $g_i$  was defined as the derivative of  $U$  with respect to velocity. If we choose

$$U = g_i(x)\bar{u}_i, \quad (7.117)$$

the momentum balance (7.85)<sub>2</sub> reduces to a simple force balance as used in all glaciology problems;  $g_i(x)$  may be position-dependent if desired.

The applicability of the variational principles also hinges on the existence of the functions  $\Gamma$  and  $\hat{\Gamma}$ , respectively. For a Newtonian fluid  $\sigma' = 2\mu\mathbf{D}$ , where  $\mu$  is the constant viscosity, these functions are given by the *quadratic forms*

$$\Gamma = \mu\bar{D}_{ij}\bar{D}_{kl}, \quad \hat{\Gamma} = \frac{1}{4\mu}\sigma'_{ij}\sigma'_{kl}. \quad (7.118)$$

With this choice of  $\Gamma$ , the variational principle is attributed to Helmholtz.

For the non-Newtonian fluid law

$$\begin{aligned} \bar{D}_{ij} &= \mathfrak{F}(\tau'_{ll})\sigma'_{ij}, & \tau'_{ll} &= \frac{1}{2}\sigma'_{ij}\sigma'_{ij}, \\ \sigma'_{ij} &= 2\mu(\bar{D}_{ll})\bar{D}_{ij}, & D'_{ll} &= \frac{1}{2}\bar{D}_{ij}\bar{D}_{ij} \end{aligned} \quad (7.119)$$

the ‘potentials’  $\Gamma$  and  $\hat{\Gamma}$  are given by

$$\Gamma = 2 \int_0^{\bar{D}_{ll}} \mu(\xi) d\xi, \quad \hat{\Gamma} = \int_0^{\tau'_{ll}} \mathfrak{F}(\xi) d\xi. \quad (7.120)$$

It is easily checked that the constitutive relations (7.119) are obtained when (7.120) are appropriately differentiated, but (7.120) must also conform with the Legendre transformation (7.92), otherwise the functionals  $\mathfrak{J}$  and  $\mathfrak{H}$  do not have the same extreme values. This is assured by formulas (7.120). Functions  $\mu$  and  $\mathfrak{F}$  are shown to depend only on one single variable (the second tensor invariant). They may, however, also be position-dependent without violating the validity of the variational principles. A temperature-dependent Arrhenius factor may therefore be incorporated in either  $\mu$  or  $\mathfrak{F}$ . For the constitutive law  $\mathfrak{F} = (\xi^{(n-1)/2} + k)/(1+k)$  we have

$$\hat{\Gamma}(\tau'_{ll}) = \frac{1}{1+k} \left\{ \frac{2}{n+1} (\tau'_{ll})^{(n+1)/2} + k\tau'_{ll} \right\}. \quad (7.121)$$

The reader may easily derive expressions for his own  $\mu$  or  $\mathfrak{F}$ .

The variational theorems apply even to the more general constitutive relationships of the Reiner–Rivlin type, see Johnson [14]. We shall not be concerned with these as they have not yet found applications in ice dynamics problems.

Next, we need to consider the ‘boundary functions’  $\psi_u$ ,  $\psi_\sigma$  and  $\hat{\psi}_u$ , respectively, in terms of which the boundary conditions (7.86) are prescribed. On the free surface,  $\partial\mathcal{V}_u$ , where the stresses are prescribed, we may choose  $\psi_\sigma \equiv 0$  and then obtain the conditions of a stress-free boundary. When

$$\psi_\sigma(\bar{u}_k) = \bar{p}^{\text{atm}} \bar{u}_k n_k, \quad (7.122)$$

where  $\bar{p}^{\text{atm}}$  is the atmospheric pressure and the boundary condition evolving from (7.86)<sub>2</sub> is

$$\sigma'_{ij} n_j - \bar{p} n_i = -\bar{p}^{\text{atm}} n_i, \quad (7.123)$$

which is the well-known boundary condition of stress.

Consider next the basal boundary condition (7.86)<sub>1</sub>. Here we must prescribe  $\psi_u$ . For  $\psi_u \equiv 0$  (7.86)<sub>1</sub> implies  $\bar{u}_i = 0$  on  $\partial\mathcal{V}_u$ , corresponding to no-slip. However, we want to apply our variational principle when sliding is permitted. For instance, when  $\psi_u$  is linear in its argument with position-dependent coefficient  $\psi_u = -\bar{u}_i^* \sigma_i^{(n)}$  then (7.86)<sub>1</sub> corresponds to  $\bar{u}_i = \bar{u}_i^*$ , where  $\bar{u}_i^*$  is a prescribed function of position on  $\partial\mathcal{V}_u$ . Equation (7.96) implies in this case  $\hat{\psi}_u \equiv 0$  and the  $\hat{\psi}_u$ -dependent term in the velocity functional  $\mathfrak{J}_u$  drops out. The variational principle for velocities does not involve stress in this case. This form of the variational principle has been elegantly used by Fowler [6] in a theory of sliding without cavity formation.

The appropriate form of the traction dependent sliding law has been given by formulas (7.60) and (7.61) of this chapter. It is

$$\bar{\mathbf{u}} + f \tau_*^{(n)} = 0, \quad \tau_*^{(n)} = \boldsymbol{\sigma}^{(n)} - \mathbf{n} \cdot \boldsymbol{\sigma}^{(n)}, \quad (7.124)$$

in which  $f$  is a function of the magnitude of  $\tau_*^{(n)}$ . We shall now demonstrate that the function  $\psi_u$  only exists for a sliding law in which  $f$  is at most a function of position. To this end, assume  $\psi_u$  exists. Comparing (7.124) with (7.86) then implies that

$$\frac{\partial \psi_u}{\partial \sigma_i^{(n)}} = f [(\tau_*^{(n)})^2] \tau_{*i}^{(n)}. \quad (7.125)$$

The left-hand side of this relation is the gradient of the scalar  $\psi_u$  in stress space, and so should be the right-hand side of (7.125). Existence of  $\psi_u$  therefore requires the integrability conditions,

$$\frac{\partial^2 \psi_u}{\partial \sigma_i^{(n)} \partial \sigma_j^{(n)}} = \frac{\partial^2 \psi_u}{\partial \sigma_j^{(n)} \partial \sigma_i^{(n)}}$$

to hold or

$$f \frac{\partial \tau_{*i}^{(n)}}{\partial \sigma_j^{(n)}} + 2f' \tau_{*i}^{(n)} \tau_{*k}^{(n)} \frac{\partial \tau_{*k}^{(n)}}{\partial \sigma_j^{(n)}} = f \frac{\partial \tau_{*j}^{(n)}}{\partial \sigma_i^{(n)}} + 2f' \tau_{*j}^{(n)} \tau_{*k}^{(n)} \frac{\partial \tau_{*k}^{(n)}}{\partial \sigma_i^{(n)}}, \quad (7.126)$$

in which  $f'$  is the derivative of  $f$  with respect to its argument. In view of (7.124)<sub>2</sub>

$$\frac{\partial \tau_{*i}^{(n)}}{\partial \sigma_j^{(n)}} = \delta_{ij} - n_i n_j,$$

this implies that the integrability conditions (7.126) are only fulfilled provided that  $f$  does not depend on  $\tau_*^{(n)}$ . We conclude that *the variational principles derived above apply only for a linear sliding law, no-slip or when the velocity is prescribed*. Numerically, this is a disadvantage, as flow and stress problems can only be solved in this case by using iterative procedures. An alternative procedure is, of course, to search for another variational principle in which a non-linear viscous sliding law is obtained as a natural boundary condition or else to use the principle of weighted residuals to derive the approximate (finite element) schemes. To our knowledge this has not been done so far.

### 5. Discussion of Some Finite-element Solutions

In the context of glacier flow, finite-element calculations have been performed under different situations by Emery and Mirza [3, 4], Hooke *et al.* [8], Iken [9, 10], and Nguyen [17]. Of these authors, only Hooke *et al.* use the above variational principle (for velocity), and for this reason they must restrict the boundary conditions at the base to no-slip or, alternatively, prescribe tangential velocity. Iken uses a code based on a hybrid stress model for the linear-elasticity equations (which also applied for slow linear viscous fluids). This procedure requires the introduction of non-linear creep behavior by a method of successive approximation and thus also allows the introduction of a viscous sliding law. Emery, Mirza and Nguyen employ an ‘incremental initial strain finite element formulation’, and claim to be able to model realistic creep behavior by following the measured creep curves in uniaxial compression tests. They further incorporate failure mechanisms and are thus, at least in principle, able to deal with the problem of crack or crevasse formations. Finally, they also include a sliding mechanism. Scrutiny of these authors’ published work, however, reveals that, firstly, the two- or three-dimensional extensions of the uniaxial creep behavior remains conjectural for ice, at least to date, and, secondly, the sliding mechanism is incorporated by an *ad-hoc* procedure as the ice rock interface is replaced by a thin layer of soft ice. It is not clear how this procedure relates to a viscous sliding law. Furthermore, all calculations known to us pertain to *plane motion*. We are

forced to conclude that a three-dimensional numerical formulation of ice-flow problems, which incorporates an independent viscous-sliding law relating tangential velocity with tangential traction still does not exist.

As stated above, Hooke *et al.* use the variational principle for velocity and are forced to use the no-slip or the prescribed velocity-boundary condition. Following common usage in glaciology, they restrict considerations to a power creep law, but allow both phenomenological parameters to vary with position, thus incorporating an known temperature-dependency in their model. They test their program against known analytic solutions (of Chapter 3) and then apply it to the flow of the Barnes Ice Cap comparing numerical results with observed flow in boreholes. Implementation of the finite-element program profited from field observations insofar as the structure of the wedge-shaped Barnes Ice Cap may be subdivided into two sub-domains of different ice texture. There is a band of white ice which owes its color to a high concentration of air bubbles and thus reduces the ice density and, consequently, also the apparent viscosity of the ice. In contrast, the surrounding blue ice is denser and more viscous.

The entire domain was divided into quadrilateral domains in such a way that the white ice was distinct from the blue ice. Nodes within the domain and on the boundary were placed to coincide with points where the velocity is known from triangulation and bore-hole deformation data and temperature measurements established the temperature distribution in the domain. A stress-free boundary condition was used on the upper surface and a no-slip boundary condition at the frozen bed.

It is not appropriate to copy the study of Hooke *et al.* in this place; for that the reader is referred to the original literature. The authors' results, however, imply the following conclusions:

A satisfactory match of calculated and observed longitudinal velocities along two distinct flow directions could only be achieved by incorporating into the flow a position-dependence which enters the Arrhenius factor independent of its temperature dependency. In other words, introducing the position-dependent material flow law through a position-dependent temperature variation does not suffice. Hooke *et al.* found the parameters in the power law that match the observed longitudinal-velocity profile by trial and error and they rightly conclude

that in the absence of measurements which can be used to 'tune' the models, the calculated velocities must be used with considerable caution. Also, tuning such models by adjusting temperature gradients or spatial variation of flow-law parameters, for example, to better match field data, is a somewhat uncertain process.

In addition to the documented differences between the blue and the white ice, the structural heterogeneity and non-uniformity of the blue ice is reflected in flow behavior which varies from place to place. There is no

justification for this. One possible suggestion is that the discrepancies could be traced to stress-induced anisotropies. For these no material law is known to date, however. Even in case that longitudinal velocity components of the model calculations could be brought into coincidence with observed data, calculated vertical velocity components at the surface did not agree with the observed data. The observed velocity components were rather smooth while the calculated velocities showed an unrealistic fluctuation. The reasons for these fluctuations are to be sought in the finite-element discretization; the problem can probably be remedied by using other approximate techniques. Since the Barnes Ice Cap is a shallow flat ice sheet, application of the approximate-stress formulas of the shallow-ice approximation (based on the MJ-transformations, see Chapter 5) would be enlightening.

Emery and Mirza [4], apparently, have also applied their incremental 'initial strain finite element formulation' to the Barnes Ice Cap. They incorporate sliding and fracture mechanics and give hints of the suitability of their procedure. Their conclusions, to be able to predict normal flow conditions as well as surge-type behavior, are largely conjectural and of little help for a better understanding, unless they provide corroboration in further numerical work. Such studies would, indeed, be helpful.

Hooke *et al.*'s procedure seems to be defective in that the authors apply the finite-element method to a problem where a simpler approach is possible. With the provision of alterations implied by such an approach or by effects that have been ignored (three-dimensional flow) their study, however, indicates that the simple flow law used to model flow in glaciers and ice sheets should not be used in a *local* sense but rather in a *global* sense.

Problems of a local nature, but still plane flow, are analysed by Iken [9, 10] in two different papers pertaining to (i) the movement of a large ice mass before breaking off and (ii) the effect of subglacial water pressure on the sliding velocity. In her first paper, Iken studies the front portion of an idealized glacier bordering a shallow lake which undercuts the steep cliff causing calving about once a year (in the event of Grubengletscher). The ice mass breaks off from the main ice body under the effect of its own weight. The process starts in the zone of maximum tensile stress, which exists some distance from the cliff as a consequence of the horizontal gradient of longitudinal stress. A crack is formed which opens under the ensuing creeping motion of the ice mass, leading to further crack propagation, step by step, until the final breaking-off arises. This process is numerically simulated. The idealized geometry is shown in Figure 7.17. The ice is assumed to adhere to its bed (except far distant from the cliff). At the top surface, along the two faces of the crack and the vertical front of the lamella, a stress-free state is applied and hydrostatic pressure is implemented at the ice-water interface. The assumed breaking mechanism consists of two alternating processes, namely, (i) formation of a crack which stops at a certain depth and (ii) growth

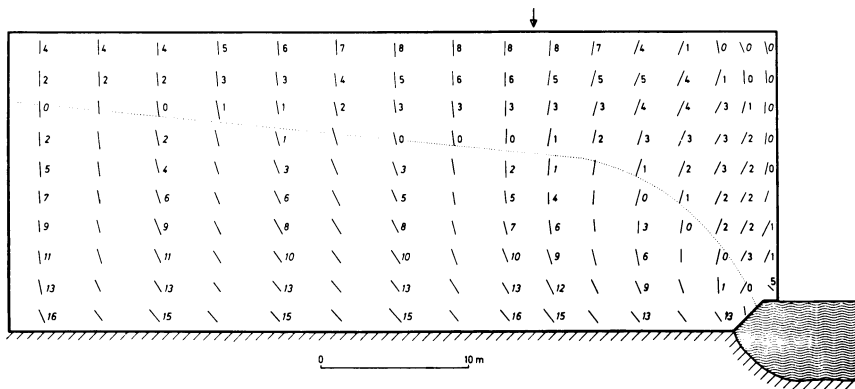


FIG. 7.17. Model of ice cliff undercut by shallow lake at the right-hand edge.

Numbers are values of the more-tensile principal stress  $\sigma_1$  in tenths of bar, upright numbers indicate tension, slanting numbers compression. The dotted line is the boundary between tensile and compressive values of  $\sigma_1$ . Line elements indicate direction perpendicular to  $\sigma_1$ . Below the arrow a crack will be introduced, from [9]. Reproduced from the *Journal of Glaciology* by permission of the International Glaciological Society.

of stress at the base of the crack until further crack propagation is possible. In process (i) the criterion for a crack to open, or to open up further, is the maximum principal stress becoming tensile. It opens in the direction perpendicular to the principal tensile stress and stops where this stress vanishes. The tensile stresses at the tip of a crack grow by the creeping motion set forth in the lamella, which leads to an increasing overhang of the lamella until finally it breaks off. Stress concentrations at the crack tip are ignored as it is assumed that, once the crack has stopped it becomes blunted and therefore a principal tensile stress greater than a critical value is necessary to trigger further propagation.

The hybrid stress finite-element code used by Iken applies for linear viscous flow models. However, by implementing an iterative procedure and adjusting, element by element, the viscosity according to the (constant) stress state present in the element, the non-Newtonian fluid law used in this book can approximately be accounted for.

Calculations were started with a crack-free cliff. Figure 7.17 shows the result of the calculation for the unbroken ice block under its own weight. Line elements indicate directions perpendicular to the principal tensile stress, the dotted line is the boundary between tensile (upright numbers) and compressive values (slanted numbers) of the larger of the two principal stresses  $\sigma_1$ , and the arrow indicates where a crack will be introduced. This crack will be parallel to the indicated principal stress direction and will extend (roughly vertical in the figure) down to the dotted line. Once the crack

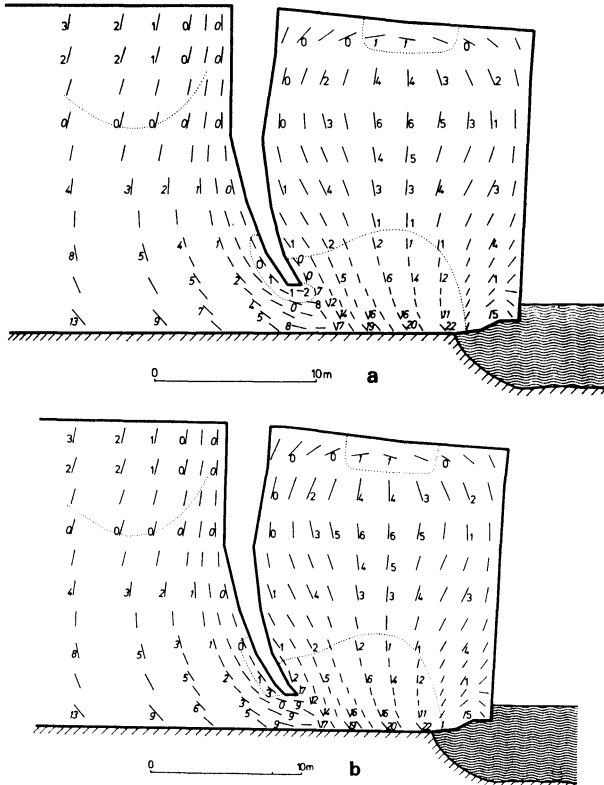


FIG. 7.18. (a) Later stage with overhanging lamella. Crack is unstable (i.e., stress below crack tip is tensile). (b) Same overhang of lamella as in Figure 7.18a. Crack is deeper and stable, from [9]. Reproduced from the *Journal of Glaciology* by permission of the International Glaciological Society.

is introduced, the stress state in the block changes, requiring re-calculation and a possible correction of crack geometry until a stable crack is formed; that is to say, a crack below which the largest principal stresses are compressive. When this stage of the calculation is reached, the deformation of the lamella can be analysed, for associated with a certain configuration is a velocity distribution which, in a certain selected small-time increment, gives rise to a deformation and thus the opening of the crack. Stresses and velocities are then calculated at this new time, and the result of the calculations at this stage either will or will not yield a compressive maximum principal stress below the crack. In the former case, the velocity field (multiplied with a further time increment) results in a new geometry of ice block and lamella and the calculation cannot again be repeated. In the other case, the crack length must be extended until a new configuration is found with a

compressive maximum principal stress below the crack tip. Two such situations are shown in Figure 7.18, one with a crack that does not lead to an acceptable stress and one with an acceptable crack length. This process of step-by-step approximation is very elaborate but will eventually lead to breaking-off, Figure 7.19.

This calculation would serve little purpose were it not for obtaining qualitative information regarding the forecast of the time of breaking-off. The model namely allows calculation of the velocity-time relationship of a representative point on the lamella, say the midpoint on the top surface. To a high degree of accuracy, this relationship has the hyperbolic form

$$v - v_c = \frac{B}{(t_A - t)^D}, \quad (7.127)$$

where  $v_c$ ,  $B$ ,  $t_A$  and  $D$  are constants. Such a functional relationship has been proposed and used by Roethlisberger [22] in connection with the forecast of the breaking-off of a large ice mass on a hanging glacier in Switzerland. The time of breaking-off has been predicted quite accurately by extrapolation of the velocity-time function measured in the preceding months. Iken's finite-element simulation developed for a different situation showed (7.127) to be reasonable from a more fundamental point of view, giving the practitioner confidence for his *ad-hoc* procedure. For further implications, the reader is referred to Iken [9].

In her second paper, Iken [10] uses a Newtonian fluid model in a study of the effect of water pressure on the sliding mechanism. Since sliding has not been carefully studied in this book, as it is both mathematically and physically difficult, it would be hard to fully appreciate the conclusions of this important paper. Very briefly, the paper analyses the opening process

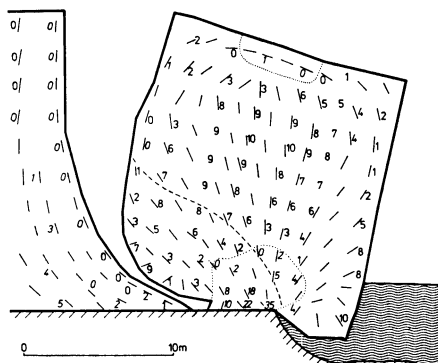


FIG. 7.19. Lamella shortly before breaking-off, the broken line shows a possible surface of shear fracture, from [9]. Reproduced from the *Journal of Glaciology* by permission of the International Glaciological Society.

of cavities formed at the lee-sides of a wavy rockbed. If the water pressure exceeds a certain threshold, cavities form and reach a new steady state corresponding to the given water pressure. The process of cavity formation is accompanied by a substantial increase of longitudinal ice velocity. For an idealized sinusoidal bed, this opening process and the associated flow field is modelled using a Newtonian fluid.

In conclusion, it might be said that very little has been done so far on numerical glacier and ice-sheet flow and nothing at all on three-dimensional effects. However, it is clear that the dynamics of glaciers and large ice masses would largely profit from numerical studies. If this chapter has been successful in triggering the interest its purpose is well achieved.

#### REFERENCES

1. Cole, J. D., *Perturbation Methods in Applied Mathematics*, Blaisdell Publishing Co., Waltham, Mass., Toronto, London, 1968.
2. Courant, R. and D. Hilbert, *Methods of Mathematical Physics, Vol. II. Partial Differential Equations*, Interscience, New York, London, 1962.
3. van Dyke, M., *Perturbation Methods in Fluid Mechanics*, The Parabolic Press, Stanford, California, 1975.
4. Emery, J. J., Simulation of slope creep, *Dev. Geotech. Eng.*, **14A**, 669–691, 1978.
5. Emery, J. J. and F. A. Mirza, Finite element method simulation of large ice mass flow behavior, in *IUTAM Symposium on the 'Physics and Mechanics of Ice'*, edited by P. Tryde, Springer Verlag, Berlin, pp. 82–92, 1980.
6. Fowler, A. C., A theoretical treatment of the sliding of glaciers in the absence of cavitation, *Phil. Trans. Royal Soc. London.*, **298**, 637–685, 1981.
7. Green, A. E. and R. S. Rivlin, Steady flow of non-Newtonian fluids through tubes, *Quart. J. Appl. Math.*, **14**, 299–308, 1956.
8. Hooke, R. L., C. F. Raymond, R. L. Hotchkiss, and R. J., Gustafson, Calculations of velocity and temperature in a polar glacier using the finite element method, *J. Glaciology*, **24**, 131–146, 1979.
9. Iken, A., Movement of a large ice mass before breaking off, *J. Glaciology*, **19**, 595–605, 1977.
10. Iken, A., The effect of the subglacial water pressure on the sliding velocity of a glacier in an idealized numerical model, *J. Glaciology*, **27**, 407–421, 1981.
11. Johnson, I. R., The steady profile of an axisymmetric ice sheet, *J. Glaciology*, **27**, 25–37, 1982.
12. Johnson, I. R., Steady ice sheet flow, thesis submitted to the University of East Anglia in application for the degree of Doctor of Philosophy, pp. 135, 1981.
13. Johnson, M. W., Some variational theorems for non-Newtonian flow, *Phys. Fluids*, **3**, 871–878, 1960.
14. Johnson, M. W., On variational principles for non-Newtonian fluids, *Trans. Soc. Rheology*, **5**, 9–21, 1961.
15. Lanczos, C., *The Variational Principles of Mechanics*, University of Toronto Press, 1964.
16. Nayfeh, A. H., *Perturbation Methods*, John Wiley, New York, London, Sidney, Toronto, 1973.
17. Nguyen, T. Q., Simulation of ice flow using the finite element method, Master of Engineering dissertation, McMaster University, Hamilton, Ontario, 1976.

18. Nye, J. F., The flow of a glacier in a channel of rectangular, elliptic or parabolic cross-section. *J. Glaciology*, **5**, 661–690, 1965.
19. Oden, J. T. and J. N. Reddy, *Variational Methods in Theoretical Mechanics*, Universitext, Springer-Verlag, Berlin, Heidelberg, New York, 1976.
20. Prandtl, L., Ueber Flüssigkeitsbewegung bei sehr kleiner Reibung. *Proc. III. Intern. Math. Congr. Heidelberg*, 1904.
21. Reynaud, L., Flow of a valley glacier with a solid friction law, *J. Glaciology*, **12**, 251–258, 1973.
22. Roethlisberger, H., Ice avalanches, *J. Glaciology*, **19**, 669–671, 1977, abstract.
23. Shaw, J. and R. C. Freschauf, A kinematic discussion of the formation of glacier fluting, *Canadian Geographer*, **17**, 19–35, 1973.
24. Shaw, J., Till body morphology and structure related to glacier flow, *Boreas*, **6**, 189–201, 1977.
25. Truesdell, C. and W. Noll, The nonlinear field theories of mechanics, in *Handbuch der Physik*, Vol. III/3, edited by S. Flügge, Springer-Verlag, Berlin, 1965.
26. Weinstock, R., *Calculus of Variation With Applications to Physics and Engineering*, McGraw-Hill, New York, Toronto, London, 1952.
27. Zienkiewicz, D. C., *The Finite Element Method in Engineering Science*, McGraw-Hill, London, 1971.

## Appendix

### DETAILED CALCULATIONS PERTAINING TO HIGHER-ORDER STRESSES IN THE SHALLOW-ICE APPROXIMATION

In this Appendix, explicit formulas will be derived for the functions  $T_1, \dots, T_7, T$  and for the derivatives of  $U^{(0)}$  listed in Chapter 5, p. 280–281. Calculations are only sketched. They follow Hutter [16] of Chapter 5 but extend the calculations to temperature profiles which may be dependent on a length coordinate. The functions  $T_1, \dots, T_7$  occur in formulas (5.53), (5.54) and (5.55) in connection with the evaluation of the basal shear stress. From Formula (5.41a)

$$U^{(0)}(\xi, \eta, \ell) = 2 \sin \gamma \int_{\bar{y}_B}^{\eta} \tilde{\mathfrak{F}}(x(\bar{\eta}), \hat{\mathfrak{G}}(\bar{\eta})) \times \\ \times (\bar{y}_S - \bar{\eta}) d\bar{\eta} + C \sin^m \gamma \bar{D}^m. \quad (A1)$$

Here,  $C, m, \gamma$  are constants;  $\bar{y}_B = \bar{y}_B(\xi)$ ,  $\bar{y}_S = \bar{y}_S(\xi, \ell)$  and  $\bar{D} = \bar{y}_S - \bar{y}_B$  are known functions of  $\xi$  and  $\ell$ , respectively. Furthermore,  $\tilde{\mathfrak{F}}$  is a prescribed function of its arguments  $x$  and  $\hat{\mathfrak{G}}$ ;  $\hat{\mathfrak{G}}$  is a prescribed temperature distribution  $\hat{\mathfrak{G}} = \hat{\mathfrak{G}}(\xi, \eta, \ell)$  and

$$x = \sin^2 \gamma (\bar{y}_S(\xi, \ell) - \eta)^2.$$

Strictly, therefore, both  $x$  and  $\hat{\mathfrak{G}}$  are functions of the three variables  $\xi, \eta$  and  $\ell$ .

A straightforward differentiation of (A1) with respect to  $\xi$  shows that

$$\frac{\partial U^{(0)}}{\partial \xi} = U_{11}^{(0)} \frac{\partial \bar{y}_S}{\partial \xi} - \frac{d\bar{y}_B}{d\xi} U_{21}^{(0)}, \\ \frac{\partial^2 U^{(0)}}{\partial \xi^2} = U_{12}^{(0)} \frac{\partial^2 \bar{y}_S}{\partial \xi^2} + U_{22}^{(0)} \left( \frac{\partial \bar{y}_S}{\partial \xi} \right)^2 - U_{32}^{(0)} \frac{\partial \bar{y}_S}{\partial \xi} \frac{d\bar{y}_B}{d\xi} - \\ - U_{42}^{(0)} \frac{d^2 \bar{y}_B}{d\xi^2} + U_{52}^{(0)} \left( \frac{d\bar{y}_B}{d\xi} \right)^2, \quad (A2)$$

where the coefficient functions are functions of  $\xi, \bar{y}_S, \bar{y}_B, \eta$  and/or equivalently, of  $\xi, \eta$  and  $z$ . They are given by

$$\begin{aligned}
U_{11}^{(0)} &= U_{12}^{(0)} = 4 \sin^3 \gamma \int_{\bar{y}_B}^{\eta} (\bar{y}_S - \eta')^2 \tilde{\mathfrak{F}}_x(x(\eta'), \hat{g}(\eta')) d\eta' + \\
&\quad + 2 \sin \gamma \int_{\bar{y}_B}^{\eta} \tilde{\mathfrak{F}}_x(x(\eta'), \hat{g}(\eta')) d\eta' + Cm \sin^m \gamma \bar{D}^{m-1}; \\
U_{21}^{(0)} &= U_{42}^{(0)} = 2 \sin \gamma \tilde{\mathfrak{F}}_x(x(\bar{y}_B), \hat{g}(\bar{y}_B)) \bar{D} + Cm \sin^m \gamma \bar{D}^{m-1}, \\
U_g^{(0)} &= 2 \sin \gamma \int_{\bar{y}_B}^{\eta} \tilde{\mathfrak{F}}_g(x(\eta'), \hat{g}(\eta')) (\bar{y}_S - \eta') \frac{\partial \hat{g}(\eta')}{\partial \xi} d\eta', \\
U_{22}^{(0)} &= 12 \sin^3 \gamma \int_{\bar{y}_B}^{\eta} \tilde{\mathfrak{F}}_x(x(\eta'), \hat{g}(\eta')) (\bar{y}_S - \eta') d\eta' + \\
&\quad + 8 \sin^5 \gamma \int_{\bar{y}_B}^{\eta} \tilde{\mathfrak{F}}_{xx}(x(\eta'), \hat{g}(\eta')) (\bar{y}_S - \eta')^3 d\eta' + Cm(m-1) \sin^m \gamma \bar{D}^{m-2}, \\
U_{32}^{(0)} &= 2U_{52}^{(0)} = 4 \sin \gamma \tilde{\mathfrak{F}}_x(x(\bar{y}_B), \hat{g}(\bar{y}_B)) + 8 \sin^3 \gamma \bar{D}^2 \tilde{\mathfrak{F}}_x(x(\bar{y}_B), \hat{g}(\bar{y}_B)) + \quad (A3) \\
&\quad + 2Cm(m-1) \sin^m \gamma \bar{D}^{m-2}, \\
U_{62}^{(0)} &= 4 \sin \gamma \int_{\bar{y}_B}^{\eta} \tilde{\mathfrak{F}}_g(x(\eta'), \hat{g}(\eta')) \frac{\partial \hat{g}(\eta')}{\partial \xi} d\eta' + \\
&\quad + 8 \sin \gamma \int_{\bar{y}_B}^{\eta} \tilde{\mathfrak{F}}_{xg}(x(\eta'), \hat{g}(\eta')) \frac{\partial \hat{g}(\eta')}{\partial \xi} d\eta', \\
U_{72}^{(0)} &= 4 \sin \gamma \bar{D} \tilde{\mathfrak{F}}_g(x(\bar{y}_B), \hat{g}(\bar{y}_B)) \frac{\partial \hat{g}(\bar{y}_B)}{\partial \xi}, \\
U_{gg}^{(0)} &= 2 \sin \gamma \int_{\bar{y}_B}^{\eta} \tilde{\mathfrak{F}}_g(x(\eta'), \hat{g}(\eta')) \frac{\partial^2 \hat{g}(\eta')}{\partial \xi^2} d\eta' + \\
&\quad + 2 \sin \gamma \int_{\bar{y}_B}^{\eta} \tilde{\mathfrak{F}}_{gg}(x(\eta'), \hat{g}(\eta')) (\bar{y}_S - \eta') \left( \frac{\partial \hat{g}(\eta')}{\partial \xi} \right)^2 d\eta'.
\end{aligned}$$

In these formulas  $\tilde{\mathfrak{F}}_x$  and  $\tilde{\mathfrak{F}}_g$  denote the derivative of  $\tilde{\mathfrak{F}}$  with respect to the first and second variables. For temperate ice, no temperature-dependency occurs and, consequently,  $\tilde{\mathfrak{F}}_g = 0$ . In this case  $U_g^{(0)} = U_{gg}^{(0)} = U_{62}^{(0)} = U_{72}^{(0)} = 0$ .

Substituting relations (A2) into Equation (5.52) it is then easy to see that

$$\begin{aligned}
\tau^{(2)} &= T_1 \frac{\partial \bar{y}_S}{\partial \xi} - T_2 \frac{d \bar{y}_B}{d \xi} + T_3 \frac{\partial^2 \bar{y}_S}{\partial \xi^2} - T_4 \frac{d^2 \bar{y}_B}{d \xi^2} + \quad (A4) \\
&\quad + T_5 \left( \frac{\partial \bar{y}_S}{\partial \xi} \right)^2 + T_6 \frac{\partial \bar{y}_S}{\partial \xi} \frac{d \bar{y}_B}{d \xi} + T_7 \left( \frac{d \bar{y}_B}{d \xi} \right)^2 + T_8,
\end{aligned}$$

in which  $T_1, \dots, T_7, T_8$  are the following expressions:

$$\begin{aligned}
T_1 &= \frac{2U_{\hat{s}}^{(0)}(\eta)}{\tilde{\mathfrak{F}}(0, \hat{\mathfrak{G}}(\bar{y}_S))} - 4 \sin^2 \gamma \int_{\eta}^{\bar{y}_S} \frac{(\bar{y}_S - \eta') U_{\hat{s}}^{(0)}(\eta') \tilde{\mathfrak{F}}_x(x(\eta'), \hat{\mathfrak{G}}(\eta'))}{[\tilde{\mathfrak{F}}(x(\eta'), \hat{\mathfrak{G}}(\eta'))]^2} d\eta' + \\
&\quad + 2 \int_{\eta}^{\bar{y}_S} \frac{U_{62}^{(0)}(\eta') \eta' d\eta'}{\tilde{\mathfrak{F}}(x(\eta'), \hat{\mathfrak{G}}(\eta'))}, \\
T_2 &= 2 \int_{\eta}^{\bar{y}_S} \frac{U_{72}^{(0)}(\eta') \eta' d\eta'}{\tilde{\mathfrak{F}}(x(\eta'), \hat{\mathfrak{G}}(\eta'))}, \\
T_3 &= \sin \gamma \left[ \left( \bar{y}_S^2 - \frac{\bar{y}_S^2}{2} \right) - \left( \bar{y}_S \eta - \frac{\eta^2}{2} \right) \right] + 2 \int_{\eta}^{\bar{y}_S} \frac{U_{12}^{(0)}(\eta') \eta' d\eta'}{\tilde{\mathfrak{F}}(x(\eta'), \hat{\mathfrak{G}}(\eta'))}, \\
T_4 &= 2 \int_{\eta}^{\bar{y}_S} \frac{U_{42}^{(0)}(\eta') \eta' d\eta'}{\tilde{\mathfrak{F}}(x(\eta'), \hat{\mathfrak{G}}(\eta'))}, \\
T_5 &= \sin \gamma (\bar{y}_S - \eta) + \frac{2U_{11}^{(0)}(\eta)}{\tilde{\mathfrak{F}}(x(\eta), \hat{\mathfrak{G}}(\eta))} + 2 \int_{\eta}^{\bar{y}_S} \frac{U_{22}^{(0)}(\eta') \eta' d\eta'}{\tilde{\mathfrak{F}}(x(\eta'), \hat{\mathfrak{G}}(\eta'))} - \\
&\quad - 4 \sin^2 \gamma \int_{\eta}^{\bar{y}_S} \frac{(\bar{y}_S - \eta') \tilde{\mathfrak{F}}_x(x(\eta'), \hat{\mathfrak{G}}(\eta'))}{[\tilde{\mathfrak{F}}(x(\eta'), \hat{\mathfrak{G}}(\eta'))]^2} U_{11}^{(0)}(\eta') d\eta', \\
T_6 &= - \frac{2U_{21}^{(0)}(\eta)}{\tilde{\mathfrak{F}}(x(\eta), \hat{\mathfrak{G}}(\eta))} - 2 \int_{\eta}^{\bar{y}_S} \frac{U_{32}^{(0)}(\eta') \eta' d\eta'}{\tilde{\mathfrak{F}}(x(\eta'), \hat{\mathfrak{G}}(\eta'))} + \\
&\quad + 4 \sin^2 \gamma \int_{\eta}^{\bar{y}_S} \frac{(\bar{y}_S - \eta') \tilde{\mathfrak{F}}_x(x(\eta'), \hat{\mathfrak{G}}(\eta'))}{[\tilde{\mathfrak{F}}(x(\eta'), \hat{\mathfrak{G}}(\eta'))]^2} U_{21}^{(0)}(\eta') d\eta', \\
T_7 &= \int_{\eta}^{\bar{y}_S} \frac{U_{32}^{(0)}(\eta') \eta' d\eta'}{\tilde{\mathfrak{F}}(x(\eta'), \hat{\mathfrak{G}}(\eta'))}, \quad T_8 = 2 \int_{\eta}^{\bar{y}_S} \frac{U_{99}^{(0)}(\eta') \eta' d\eta'}{\tilde{\mathfrak{F}}(x(\eta'), \hat{\mathfrak{G}}(\eta'))}.
\end{aligned} \tag{A5}$$

Here for brevity only the  $\eta$ -dependency of the functions  $U_{ij}^{(0)}$  is made explicit. Strictly speaking, these functions depend on  $\xi, \eta$  and  $\zeta$ . Consequently,  $T_1, \dots, T_7$  and  $T_8$  must also depend on these variables. Notice also that  $T_1$  and  $T_2$  must vanish in a temperate glacier. It can be seen that the evaluation of  $\tau^{(2)}$  can be achieved by quadratures only. Of course, explicit calculations depend on the form of the function  $\tilde{\mathfrak{F}}$  and, for most practical cases, closed-form representations of the respective integrals cannot be found. For

$$\tilde{\mathfrak{F}}(x, \hat{\mathfrak{G}}) = \tilde{\mathfrak{F}}(x) = \frac{x^{(n-1)/2} + k}{1 + k}, \tag{A6}$$

where  $k$  is a constant dependent on  $n$ , explicit functional relationships for  $T_i$  ( $i = 1, \dots, 7$ ) can, however, be found. Observing then, that

$$\begin{aligned}\mathfrak{F}_x(\sin^2 \gamma(\bar{y}_S - \eta)^2) &= \frac{n-1}{2} \frac{1}{1+\mathbb{k}} [\sin^2 \gamma(\bar{y}_S - \eta)^2]^{(n-3)/2}, \\ \mathfrak{F}'_{xx}(\sin^2 \gamma(\bar{y}_S - \eta)^2) &= \frac{(n-1)(n-3)}{4} \frac{1}{1+\mathbb{k}} [\sin^2 \gamma(\bar{y}_S - \eta)^2]^{(n-5)/2},\end{aligned}\quad (\text{A7})$$

functions (A3) can be calculated with reasonable effort. The result is

$$\begin{aligned}U_{11}^{(0)} &= \frac{2\mathbb{k}}{1+\mathbb{k}} \sin \gamma(\eta - \bar{y}_B) + \frac{2 \sin^n \gamma}{1+\mathbb{k}} [(\bar{y}_S - \bar{y}_B)^n - (\bar{y}_S - \eta)^n] + \\ &\quad + \mathbb{C}m \sin^m \gamma(\bar{y}_S - \bar{y}_B)^{m-1}, \\ U_{21}^{(0)} &= \frac{2\mathbb{k}}{1+\mathbb{k}} \sin \gamma(\bar{y}_S - \bar{y}_B) + \frac{2 \sin^n \gamma}{1+\mathbb{k}} (\bar{y}_S - \bar{y}_B)^n + \mathbb{C}m \sin^m \gamma(\bar{y}_S - \bar{y}_B)^{m-1}, \\ U_{12}^{(0)} &= U_{11}^{(0)}, \\ U_{22}^{(0)} &= \frac{2n}{1+\mathbb{k}} \sin^n \gamma [(\bar{y}_S - \bar{y}_B)^{n-1} - (\bar{y}_S - \eta)^{n-1}] + \mathbb{C}m(m-1) \sin^m \gamma(\bar{y}_S - \bar{y}_B)^{m-2}, \\ U_{32}^{(0)} &= \frac{4}{1+\mathbb{k}} [n \sin^n \gamma(\bar{y}_S - \bar{y}_B)^{n-1} + \mathbb{k}] + 2\mathbb{C}m(m-1) \sin^m \gamma(\bar{y}_S - \bar{y}_B)^{m-2}, \\ U_{52}^{(0)} &= \frac{1}{2} U_{32}^{(0)}.\end{aligned}\quad (\text{A8})$$

The evaluation of the functions  $T_i$  ( $i = 1, \dots, 7$ ) is more involved and there is no justification to give all pertinent details. What obtains reads as follows:

$$\begin{aligned}T_1 &= 4 \sin \gamma(\eta - \bar{y}_B) + \frac{4}{\mathbb{k}} \sin^n \gamma [(\bar{y}_S - \bar{y}_B)^n - (\bar{y}_S - \eta)^n] + \\ &\quad + \frac{2(1+\mathbb{k})}{\mathbb{k}} \mathbb{C}m \sin^m \gamma(\bar{y}_S - \bar{y}_B)^{m-1}, \\ T_2 &= 4 \sin \gamma(\bar{y}_S - \bar{y}_B) + \frac{4}{\mathbb{k}} \sin^n \gamma(\bar{y}_S - \bar{y}_B)^n + \\ &\quad + \frac{2(1+\mathbb{k})}{\mathbb{k}} \mathbb{C}m \sin^m \gamma(\bar{y}_S - \bar{y}_B)^{m-1}, \\ T_3 &= \sin \gamma \left[ \frac{\bar{y}_S^2}{2} - \left( \bar{y}_S \eta - \frac{\eta^2}{2} \right) \right] + \\ &\quad + 4\mathbb{k}^{1/(n-1)} \left\{ \left[ (\bar{y}_S - \bar{y}_B) + \frac{1}{\mathbb{k}} \sin^{n-1} \gamma(\bar{y}_S - \bar{y}_B)^n \right] \mathbb{G}_n(\mathcal{X}) - \frac{\mathbb{k}^{1/(n-1)} \mathcal{X}^2}{\sin \gamma} \right\} + \\ &\quad + 2(1+\mathbb{k}) \mathbb{C}m \sin^m \gamma(\bar{y}_S - \bar{y}_B)^{m-1} \frac{\mathbb{k}^{(2-n)/(n-1)}}{\sin \gamma} \mathbb{G}_n(\mathcal{X}),\end{aligned}$$

$$\begin{aligned}
T_4 &= \frac{\mathbb{k}^{(2-n)/(n-1)}}{\sin \gamma} \{4 \sin \gamma (\bar{y}_S - \bar{y}_B) [\sin^{n-1} \gamma (\bar{y}_S - \bar{y}_B)^{n-1} + \mathbb{k}] + \\
&\quad + \mathbb{C}m(1+\mathbb{k}) \sin^m \gamma (\bar{y}_S - \bar{y}_B)^{m-1}\} \mathbb{G}_n(\mathcal{X}), \\
T_5 &= \sin \gamma (\bar{y}_S - \eta) + 2I_1 - 4 \sin^2 \gamma I_3 + I_5, \\
T_6 &= 4 \sin^2 \gamma I_2 - 2I_4 - I_6, \\
T_7 &= I_4,
\end{aligned} \tag{A9}$$

in which

$$\begin{aligned}
\mathcal{X} &= \frac{\sin \gamma}{\mathbb{k}^{1/(n-1)}} (\bar{y}_S - \eta), \\
I_1 &= \frac{\mathbb{k}^{(2-n)/(n-1)}}{\sin \gamma} \mathbb{G}_n(\mathcal{X}) \{2n \sin^n \gamma (\bar{y}_S - \bar{y}_B)^{n-1} + \\
&\quad + \mathbb{C}m(m-1)(1+\mathbb{k}) \sin^m \gamma (\bar{y}_S - \bar{y}_B)^{m-2}\} - 2n^{(1-n-1)}(\mathcal{X} - \mathbb{G}_n(\mathcal{X})), \\
I_2 &= \frac{-1}{2\mathbb{k} \sin \gamma} [2\mathbb{k}(\bar{y}_S - \bar{y}_B) + 2 \sin^{n-1} \gamma (\bar{y}_S - \bar{y}_B)^n + \\
&\quad + \mathbb{C}m(1+\mathbb{k}) \sin^{m-1} \gamma (\bar{y}_S - \bar{y}_B)^{m-1}] \frac{1}{\mathcal{X}^{n-1} + 1}, \\
I_3 &= I_2 - [\mathbb{2k}^{n/(n-1)}(\mathbb{G}_n(\mathcal{X}) - \mathcal{X}) + \mathbb{k}^{n/(n-1)}Z_n(\mathcal{X})] \frac{1}{2\mathbb{k} \sin^2 \gamma}, \\
I_4 &= \mathbb{k}^{(2-n)/(n-1)} \mathbb{G}_n(\mathcal{X}) \{4[n \sin^n \gamma (\bar{y}_S - \bar{y}_B)^{n-1} + \mathbb{k}] + \\
&\quad + 2\mathbb{C}m(m-1) \sin^m \gamma (\bar{y}_S - \bar{y}_B)^{m-1}\}, \\
I_5 &= 4 \sin \gamma (\eta - \bar{y}_B) + \frac{4}{\mathbb{k}} \sin^n \gamma [(\bar{y}_S - \bar{y}_B)^n - (\bar{y}_S - \eta)^n] + \\
&\quad + \frac{2(1+\mathbb{k})}{\mathbb{k}} \mathbb{C}m \sin^m \gamma (\bar{y}_S - \bar{y}_B)^{m-1}, \\
I_6 &= 4 \sin \gamma (\bar{y}_S - \bar{y}_B) + \frac{4}{\mathbb{k}} \sin^n \gamma (\bar{y}_S - \bar{y}_B)^n + \frac{2(1+\mathbb{k})}{\mathbb{k}} \mathbb{C}m \sin^m \gamma (\bar{y}_S - \bar{y}_B)^{m-1},
\end{aligned} \tag{A10}$$

with

$$\begin{aligned} \mathbb{G}_n(x) &= \begin{cases} \ln(x+1), & n = 2, \\ \tan^{-1}(x) & n = 3, \end{cases} \\ Z_n(x) &= \begin{cases} x - \frac{1}{x+1} - 2\ln(1+x), & n = 2, \\ \frac{2x^3}{1+x^2} + \frac{3x}{1+x^2} - 3\tan^{-1}(x), & n = 3. \end{cases} \end{aligned} \quad (\text{A11})$$

## AUTHOR INDEX

- Aikilov, G. P., 157, 185  
Anderson, D. L., 100, 103, 107, 110, 114  
Arrhenius, S. A., 59, 93, 95, 97, 125, 151,  
153, 160–161, 474  
Assur, A., 97, 100–105, 109–110, 115  
  
Barnes, P. D., 93, 94, 110  
Bass, R., 55, 110  
Batchelor, G. K., 104, 110, 201, 253  
Begbie, G. H., 55, 110  
Bellman, R. E., 157, 184, 249, 253  
Benjamin, T. B., 244, 253  
Benney, D. J., 244, 253, 273, 331.  
Bentley, C. R., 50, 254  
Bergmann, L., 55, 114  
Bindschadler, R. A., 243, 253, 335, 421  
Bingham, E. C., 91–92, 110  
Bird, R. G., 138, 184  
Björnsson, H., 142, 184  
Bland, D. R., 63, 110  
Bodvarsson, G., 292, 294, 331  
Boltzmann, L., 57, 59, 95, 125, 151  
Born, M., 110  
Boshinskiy, A. N., 168, 184  
Bourgoin, J. P., 189, 253  
Brill, R., 58, 63, 72–73, 75, 77–81, 112  
Bromwich, J. T. I., 74, 359  
Brown, J. H., 107, 110  
Budd, W. F., 122, 168, 184, 189–190,  
192, 204, 208, 214–215, 220, 226, 244,  
253–254, 258–259, 264, 266, 271, 282,  
298, 331, 335, 421  
Bulirsch, R., 292, 301, 331  
Burgers, J. M., 72–74, 76, 415  
Butkowich, T. R., 106–107, 110  
  
Campell, W. I., 335, 423  
Cary, P. W., 421  
  
Carlslaw, H. S., 144, 184  
Cauchy, A. -L., 7, 15, 52  
Cayley, A., 31  
Chadwick, P., 4, 46  
Chester, W., 428, 431, 434  
Christensen, M. R., 63, 69, 111  
Clapeyron, E., 44–46, 126, 129, 143, 151,  
153–154  
Clarke, G. K. C., 168–169, 172, 174–176,  
178–179, 184, 244, 254, 336, 421  
Clausius, R. J. E., 33–35, 37–38, 44–46,  
126, 129, 143, 151, 153–154  
Clough, J. W., 189, 254  
Colbeck, S. C., 92, 110, 318, 324–325,  
331, xxv  
Cole, J. D., 219, 254, 277, 331, 435, 482  
Coleman, B. D., 63, 110  
Coles, N. E., 58, 111  
Collins, L. F., 189, 254, 258, 264, 331  
Coon, M., 109–110  
Courant, R., 391, 394, 421, 482  
Craik, A. D. D., 244, 254  
Crosson, R., 421  
  
Dantl, G., 55, 111  
Day, A. W., 63, 111  
De Quervain, M., 73, 113  
Dickins, D. F., 93, 113  
Dirac, P. M. A., 364  
Dorsey, N. E., 54, 111  
Duhem, P. M. M., 33–35, 37–38  
Dyke van M., 219, 254, 435, 482  
Dykins, J. E., 107, 111  
  
Einstein, A., 104, 111  
Emery, J. J., 476, 478, 482  
Erickson, J. L., 29, 32, 99  
Eshelby, J. D., 104, 111

- Euler, L., 6, 15, 465–466, 469, 471  
 Evans, R. J., 92, 110, 318, 324–325, 331  
 Eyring, H., 91–95, 111  
 Fick, A., 128–129  
 Findley, W. N., 111  
 Finsterwalder, S., 243, 254, 335, 347, 422  
 Fourier, J., 31, 68, 71, 124, 130, 202–203,  
   230, 365, 367, 370, 374  
 Fowler, A. C., 122, 126, 128, 134, 139,  
   140, 142, 144, 165–166, 178–179, 184,  
   243, 254, 259–260, 273, 331, 336, 352,  
   380, 388, 392, 396, 398–400, 403, 421–422,  
   475, 482  
 Frank, C. F., 142, 186  
 Frankenstein, G., 102, 111  
 Freschauf, R. C., 483  
 Friedrichs, K. O., 273, 331, 391, 394, 421  
 Froude, W., 149, 153–154  
 Fukuda, A., 112  
 Garner, R., 102, 111  
 Garofalo, S., 93–95, 111  
 Gauss, C. F., 464–465, 469–470, 472  
 Gautet, C., 421  
 Geiringer, H., 185  
 Gerrard, J. A. F., 185  
 Glasstone, S., 95, 111  
 Glen, J. W., 49, 51, 55, 57–58, 81–86,  
   89–92, 95, 111–112, 119, 141, 149, 151,  
   153, 158, 182, 218, 223, 277, 317–318,  
   324, 343–344, 415, 417, 429  
 Gold, L. W., 54, 81, 111  
 Green, A. E., 426, 482  
 Green, R. E., 52, 55, 111  
 Greenberg, M. D., 68, 111  
 Greub, W., 47  
 Griggs, T. D., 58, 111  
 Grigoryan, S. S., 122, 134, 168, 184–185  
 Gross, B., 63, 111  
 Gurtin, M. E., 63, 111  
 Gustafson, R. J., 482  
 Hamilton, W. R., 31  
 Harrison, W. D., 421  
 Hashin, Z., 105  
 Hawkes, I., 107, 112  
 Heaviside, O., 65, 359  
 Helmholtz, H. L., 65  
 Higashi, A. S., 59, 112  
 Hilbert, D., 482  
 Hobbs, P. V., 49, 54–55, 57, 60, 84, 112  
   xxv  
 Hodge, S. M., 190, 254  
 Hooke, R. L., 54, 60, 476–478, 482  
 Hotchkiss, R. L., 482  
 Howick, E. E., 107, 110  
 Humphreys, W. S., 50  
 Hutter, K., 34, 47, 62, 92, 97, 102, 104–105,  
   112, 122, 126, 141–142, 162, 179, 185–187,  
   189, 214–215, 220, 243, 254, 259, 273,  
   275, 281, 288, 331, 336, 403, 422, 484  
 Iken, A., 142, 185, 476, 478, 481–482  
 Jeger, J. C., 144, 184  
 Jellinek, H. H. G., 58, 63, 72–73, 75, 77–81,  
   112  
 Jenssen, D., 298, 331, 421  
 John, B. S., xxv  
 Johnson, I. R. N., 259–260, 309–310,  
   314–315, 317–318, 320, 322, 324, 326,  
   328–332, 334–336, 422, 425, 463, 468,  
   475, 482  
 Jona, F., 55, 112  
 Jonas, J. J., 336, 422  
 Jones, S. J., 58, 111–112  
 Kalaba, R. E., 157, 184, 249, 253  
 Kamb, B., 45, 47, 120, 139–141, 185  
 Kantorovich, L. W., 157, 185  
 Kaplan, W., 68, 112  
 Kasser, P., 185  
 Keller, J. B., 273, 331  
 Kelvin, Thompson, W. Lord, 72–73, 75,  
   77, 79  
 Kingery, W. D., 110–112  
 Kirchhoff, G., 7, 22, 40, 56, 98  
 Kluwick, A., 334, 422  
 Koptsik, V. A., 114  
 Korteweg, D. J., 415  
 Krass, M. S., 122, 179, 182, 185–186  
 Kröner, E., 62, 112  
 Kuo, S. S., 80–81, 112  
 Kutta, W. M., 157, 209, 377  
 LaChapelle, R., 120, 185  
 Lagrange, J. -L., 6, 465–466, 468–470  
 Lai, J. S., 63, 111  
 Laitone, E. V., 273, 332  
 Lamé, G., 61–62, 65  
 Lanczos, C., 75, 112, 463, 482  
 Landauer, J. K., 110  
 Langdon, J., 335, 422

- Langleben, M. P., 100, 103, 112–113  
 Laplace, P. S., 68–69, 215, 358  
 Larson, D. A., 122, 126, 128, 134, 142, 144,  
     166, 179, 184, 243, 254, 260, 273, 331,  
     336, 352, 380, 388, 392, 396, 398–400,  
     403, 422  
 Legendre, A. M., 65, 466, 474  
 Legerer, F., 112, 254  
 Leibnitz, G. W., 262, 264, 380, 460  
 Leightfoot, E. N., 184  
 Lick, W., 243, 254, 335, 422  
 Lighthill, M. J., 334–335, 339, 422  
 Lile, R. C., 49, 82, 112  
 Lin, C. C., 244, 246, 254  
 Little, E. M., 113  
 Libloutry, L. A., 92, 112, 129, 140–142,  
     168, 171, 185, 189, 215, 243, 254, 258,  
     331, 335, 341–342, 345, 356–358, 362,  
     422, xxv  
 Lockett, F. J., 63, 112  
 Lord, M. E., 249  
 Lovitt, W. V., 70, 112  
 Ludford, G. S. S., 185  
  
 Mackenzie, J. K., 104, 113  
 Mae, S., 112  
 Mahaffy, M. W., 298, 331  
 Mälzer, H., 183, 254  
 Mantis, T. H., 54, 113  
 Marchi de L., 335, 422  
 Mathews, W. R., 179, 185  
 Matthew, W. H., 142, 185  
 Mavko, G. M., 113  
 Maxwell, J. C., 29, 72–73, 75, 77, 79  
 McInnes, B. J., 190, 244, 254  
 McKinnon, L., 55, 111  
 Meier, M. F., 190, 254, 335, 422  
 Mellor, M., 81, 84, 90, 95, 107, 112–113  
 Michel, B., 49, 113, xxv  
 Mirza, F. A., 476, 478, 482  
 Mises, R., 144, 185  
 Mohaghegh, M. M., 109–110  
 Morland, W. L., 33, 49, 82, 85, 89–92,  
     95, 99, 113–114, 125, 140, 186, 253, 260,  
     309–310, 314–315, 317–318, 320, 322,  
     324, 326, 328–329, 332, 334, 336, 422, 425  
 Morris, E. M., 215, 254  
 Müller, I., 4, 21, 31, 47, 301, 336, 422  
 Muncaster, R. G., 47  
  
 Nakaya, U., 63, 71, 73, 113  
 Navier, C. L. M. H., 29, 207  
  
 Nayfeh, A. H., 219, 254, 435, 482  
 Neave, K. G., 168, 186  
 Nevel, D. E., 73, 76–78, 113  
 Newton, I., 29, 84, 91, 159, 213–214,  
     301, 439, 474, 479  
 Nguyen, T. Q., 476, 482  
 Nielsen, L. E., 422  
 Nitsan, C. V., 184  
 Noll, W., 4, 21, 27, 29, 426, 483  
 Norton, F. H., 83, 113  
 Nur, A., 105, 113  
 Nusselt, W., 138, 153, 154  
 Nye, J. F., 85–87, 89–90, 92, 97, 113, 119,  
     122, 139–140, 142, 158, 160, 166–168,  
     186, 189, 190, 230, 243, 254–255, 258,  
     264, 292–293, 298, 322–323, 332, 335,  
     341–342, 348, 357, 360, 362, 375, 377,  
     398–399, 404–405, 420, 422–423, 425,  
     428, 431, 434, 441, 445, 450, 483  
  
 Oden, J. T., 463, 483  
 Olunloyo, V. O. S., 141, 185–186  
 Onaran, K., 63, 111  
 Onsager, L., 463  
 Orowan, E., 258, 292, 294, 332  
 Orr, W. M. F., 246  
  
 Palmer, A. C., 336, 423  
 Paterson, W. S. B., 179, 184, 186, 294,  
     297, 332, xxv  
 Peltier, W. R., 421  
 Penny, A. H., 55, 61, 113  
 Perutz, M. F., 57, 111, 185  
 Peyton, H. R., 106–107, 113  
 Piola, G., 7, 22, 40, 56, 98  
 Pipkin, A. C., 63, 113  
 Planck, M., 95  
 Poisson, S. D., 61–62, 80, 105, 434–435  
 Porter, C. K., 254  
 Post, A., 190, 254  
 Poston, T., 186  
 Pounder, E. R., 100, 103, 112–113  
 Prandtl, L., 91–95, 113, 138, 151, 154, 435,  
     483  
  
 Ramseier, R. O., 93, 113  
 Rasmussen, L. A., 335, 423  
 Raymond, C. F., 335–336, 421–423, 482  
 Read, W. T., 69, 114  
 Reddy, J. N., 463, 483  
 Redheffer, R., 68, 114  
 Reiner, M., 32, 125, 475  
 Reynaud, L., 445, 450, 483

- Reynolds, O., 137–138, 154, 251  
 Richardson, C., 101, 114  
 Rigsby, G. P., 58, 86, 114  
 Ritz, C., 185  
 Rivlin, R. S., 29, 32, 99, 125, 426, 475, 482  
 Robin, G. de Q., 168, 171–172, 186, 189–190, 199, 216–217, 226, 244, 255, 258–259, 266, 332, 336, 423  
 Robinson, E. S., 189, 255  
 Roch, A., 185  
 Rossberg, D., 110  
 Röthlisberger, H., 61–63, 114, 142, 186, 481, 483  
 Runge, C. D. T., 157, 209, 377  
 Saidler, J. K., 111  
 Savage, J. C., 168, 179, 186  
 Savel'ev, B. A., 100, 114  
 Schaefer, C., 55, 114  
 Scherrer, P., 55, 112  
 Schlichting, H., 137–138, 186, 201, 255  
 Schubert, G., 160, 163, 165, 172, 174, 178–179, 187, 336, 423  
 Schwarz, J., 103–108, 114  
 Schytt, V., 336, 423  
 Scott, M. R., 249  
 Sharp, R. P., 179, 186  
 Shaw, J., 426, 483  
 Shreve, R. L., 186  
 Shubnikov, A. V., 114  
 Shumskiy, P. A., 80–81, 114, 122, 179, 182, 185–186, 258, 332, xxv  
 Smith, F. I. P., 244, 254  
 Smith, G. D., 85, 90–92, 95, 114, 125  
 Smith, G. F., 31–32, 47, 98  
 Smith, J. H., 81, 84, 113  
 Sokolnikoff, I., 114  
 Sokolnikov, I., 68, 114  
 Sommerfeld, A., 246  
 Spring, U., 33, 49, 82, 99, 112–114, 126, 142, 162, 185–187, 220, 254  
 Stalinski, P., 113  
 Stefan, J., 144  
 Steinemann, S., 58, 81, 83–85, 90, 92, 95, 114  
 Sternberg, E., 63, 111  
 Stewart, I., 186  
 Stewart, N. E., 184  
 Stieljes, T. J., 64, 68  
 Stoer, J., 292, 331  
 Stoker, J. J., 273, 332  
 Stokes, J. J., 29, 207  
 Sugden, D. E., xxv, 297, 332  
 Swithinbank, C. W. M., 189, 255  
 Szidarovski, F., 157, 187, 292, 332, 375, 423  
 Tabor, D., 110  
 Taylor, G. I., 104, 114  
 Testa, R., 81, 90, 95, 113  
 Thomas, R. H., 179, 187  
 Thompson, D. E., 92, 114, 190, 243, 249–250, 252, 255, 336, 423  
 Toupin, R. A., 4, 47  
 Traetteberg, A., 111  
 Tricomi, F. G., 70, 114  
 Truesdell, C. A., 4, 6, 21, 29–30, 47, 426, 483  
 Untersteiner, N., 375, 423  
 Vialov, S. S., 292, 294, 332  
 Voigt, W., 61, 72, 114  
 Volterra, V., 57, 63, 70, 114  
 Voytkovskiy, K. F., 54, 114  
 de Vries, G., 415  
 Walker, J. C. F., 110  
 Van der Waerden, B. L., 31, 47  
 Wang, C. C., 6, 21, 31, 47, 98, 114  
 Watts, H. R., 249  
 Weeks, W. F., 100–101, 103–110, 114–115  
 Weertman, J., 95, 115, 140–142, 171–172, 179, 182, 187, 190, 218, 223, 225–226, 228–229, 234–235, 237–240, 244, 255, 274, 293, 298, 329, 332, 335, 343, 392, 423, 464  
 Wehausen, J. V., 273, 332  
 Weinstock, R., 463, 483  
 Wengefeld, P., 137, 187  
 Whitham, G. B., 144, 187, 273, 332, 334–335, 339, 347, 391, 394, 415, 422–423  
 Williams, M. F., 92, 115, 179, 185, 187  
 Wu, T. T., 104, 115  
 Yakowitz, S., 157, 187, 292, 332, 375, 423  
 Yih, C. C., 244, 255  
 Yosida, Z., 192, 255  
 Young, T., 61–62, 80, 103, 105, 109, 112  
 Yuen, D. A., 160, 163, 165, 172, 174, 178–179, 187, 336, 423  
 Zener, C., 63, 115  
 Ziegler, G., 110  
 Zienkiewicz, D. C., 425, 483  
 Zotikov, I. A., 171, 187  
 Zubov, N. N., 100, 115

## SUBJECT INDEX

- ablation, 134, 171, 178, 188, 187, 327  
ablating margin, 308  
accumulation, 122, 135, 161, 176, 193, 294, 298, 309, 327  
equilibrium point, 135, 297  
rate, 135, 161, 193, 287, 298, 302  
accumulation, 122, 132, 156, 165–166, 168, 171, 179, 181, 188, 199, 212, 241, 245, 295, 297–298, 308–310, 315, 325, 327, 333–337, 339, 351, 357, 367, 390  
and ablation, 122, 132, 135, 161, 176, 193, 294, 297–298, 308–309, 327  
balance of, 180  
equilibrium point, 135, 297  
flux function, 202, 385  
function, 133, 135, 202, 295–296, 319, 321–323, 326–327, 329, 347, 363, 365, 385, 451  
longitudinal variations, 217  
parameter, 227  
point, 135, 297  
rate, 135, 150, 152, 156, 161, 168, 179, 188–189, 193, 202, 212, 217–218, 240, 242, 259, 294–298, 301–302, 308, 314, 352, 355, 362–363, 365, 367, 369, 374  
steady state, 202, 214, 240  
time dependent, 242  
uniform, 327  
admissible, 19, 41, 124  
thermodynamically, 19, 41  
variations, 471  
admissibility conditions, 467, 469–471  
advance, 122, 369  
and retreat, 122, 335, 397  
advancing glacier, 260, 358  
rate of, 396  
snout, 396  
advection, 172, 176–177  
parameter, 169, 178  
heat, 226  
advection heating, 176  
strain, 176  
transverse, 17, 196, 226  
aging, 64  
amplitude, 191–253  
basal, 234–235  
longitudinal, 236–237  
normal stress, 234–235  
perturbation, 231  
shear stress, 231–234  
stress, 230, 236  
surface, 237, 241  
transverse stress, 236  
velocity, 236–237, 241  
analysis,  
beam, 107  
dimensional, 137  
elastic, 107  
Fourier, 202, 370  
frequency, 374  
harmonic, 202, 242  
limit, 219  
limit load, 110  
perturbation, 165  
stability, 165, 178, 190, 243, 252  
surface wave, 243  
anisotropy, 48, 82  
effects, 60  
stress induced, 98–99  
air, 48, 63  
bubbles, 63  
entrained, 63

- antarctica, 48, 266, 333  
     ice cap, 48, 271  
     Vostoc Mirny, 296–297
- Arrhenius, 59, 85, 95, 97, 149  
     factor, 95, 146, 151, 160–162, 269,  
         282, 453, 474, 477  
     function, 85  
     law, 97  
     number, 149, 153
- Arctic, 179, 333  
     ice, 48, 103, 271  
     antarctic, 179  
     sea, 103
- asymptotic, 139, 152, 219  
     expansions, 413, 434–435, 438  
     behavior, 364  
     limit, 310  
     matched asymptotic expansions, 139,  
         152, 219, 413, 434–435, 438  
     representation, 373, 450  
     stable, 349
- atmosphere, 133–134, 137, 182, 188, 333  
 atmospheric heat flux, 133, 135, 156, 174  
     moisture, 135  
     pressure, 145, 148, 152, 262, 263  
     stress, 133
- attenuation, 56
- avalance, powder snow, 9
- balance (laws), 30, 124, 127, 129, 146,  
     269, 334, 420, 452  
     accumulation, 180  
     angular momentum, 315  
     energy, 3, 14, 17, 30, 127, 146, 334  
     entropy, 7, 10, 33  
     equations of, 7, 126–127, 131, 183  
     force, 292, 474  
     global, 13, 131, 334  
     local, 131  
     mass, 3, 14, 17, 124–129, 146, 294,  
         298, 328, 334, 339, 420, 452  
     momentum, 3, 14, 17–18, 30, 124–  
         128, 146, 269, 298, 334–335,  
         420, 452, 474  
     water, 129
- Barnes Ice cap, 477–478
- base, 120, 176, 184, 212, 243, 257, 268  
     free, 184  
     frozen, 176  
     mean, 212  
     smoothed, 257
- basal,  
     amplitude, 234, 235
- boundary conditions, 239, 312, 475  
 drainage, 310  
 friction number, 153  
 heat flux, 160  
 ice, 244  
     normal stress, 234, 235  
 plane, 59  
 shear, 140, 155, 189, 231, 257, 273,  
     280, 281, 287, 293, 484  
 shear stress, 259, 260, 264, 276, 279  
 sliding, 58, 140, 233, 238, 248, 279,  
     400  
 softening, 244  
 stress, 140, 155, 189, 230, 235, 256,  
     273, 280, 281, 287, 293, 484  
 temperature, 164, 175, 177, 336  
 traction, 139  
 transfer function, 222  
 undulation, 222  
 variation, 336  
 velocity, 140, 248, 325
- beam, 107, 108  
 analysis, 107  
 cantilever, 108  
 elastic, 107  
 simply supported, 107, 108  
 test, 108
- bearing capacity, 39, 92, 110
- bed, 138, 140, 206, 298, 326  
     flat, 322, 326  
     horizontal, 322, 329  
     inclination, 319, 326  
     mean, 329  
     roughness, 140, 141, 206  
     topography, 329
- bedrock, 123, 294, 310  
 interface, 123, 310  
 perturbations, 189  
 profile, 300, 301  
 slope, 189  
 surface, 138
- bifurcation,  
     mechanism, 142  
     states, 177  
     points, 175
- biharmonic, 201
- Bingham body, 91, 92
- binary mixture, 9, 122, 126, 127, 128
- Boltzmann,  
     constant, 57, 59, 95, 125, 151  
     equation, 95
- bore-hole, 477

- Bosson, glacier de, 243, 335  
 bounded memory, 27, 56, 99  
 boundary,  
   basal, 239, 312, 475  
   bottom, 454  
   cold, 134  
   flow, 137, 139  
   inner, 139  
 boundary conditions, 120, 122, 131–138,  
   140–144, 147, 152, 154, 156,  
   166, 175, 180, 181, 191, 192,  
   196, 201, 203, 217, 223, 233,  
   234, 236, 239, 242, 244–246,  
   261, 268, 271, 272, 274, 277,  
   280, 299, 311, 312, 316, 346,  
   356, 379, 405, 420, 428, 430,  
   436, 453, 454, 456, 460, 466,  
   468, 469, 475  
 kinematic, 180, 242, 244, 299, 420,  
   460  
 mechanical, 120, 141  
 for moisture, 137  
 natural, 468, 469  
 (no) slip, 233, 234, 438  
 smoothed out, 139, 140  
 thermal, 122, 132, 134, 136, 138, 147,  
   181  
 top, 312  
 Weertman-type, 223  
 boundary layer, 121, 129, 136–139, 438  
 boundary-value problem, 148, 162, 168,  
   190, 192–194, 198–200, 208,  
   210, 212–214, 242–244, 260,  
   273, 291, 298, 310, 346, 347,  
   384, 409, 429, 464, 468, 471,  
   473  
 first order, 200  
 initial, 291, 346, 347, 384  
 two-point, 160, 174, 208, 243, 291  
 brine, 99, 100, 106  
 content, 99, 100, 103–105  
 drainage, 101  
 fraction, 100  
 inclusion, 49, 100, 102, 103  
 liquid, 99  
 volume of, 100–109  
 Bromwich contour, 74, 359  
 Burger's model, 72, 73, 74, 76  
   equation, 415  
 Calving mechanism, 304  
 Camp Century, 171  
 capacity, bearing, 4, 39, 92, 110  
 Cartesian,  
   coordinate system, 4  
   Tensor, 4  
 catastrophe theory, 175  
 Cauchy–Green deformation tensor, 21, 40  
   right, 21, 40  
 Cauchy's lemma, 7  
 Cauchy stress, 7, 31, 52, 124  
   deviator, 124  
 cavity,  
   formation, 121, 139–142, 475, 482  
   sliding with/without, formation, 121,  
   140–142, 475  
 cavitation, sliding with, 121, 140  
 channel,  
   circular, 431  
   cylindrical, 424  
   elliptical, 433, 440  
   flow, 426  
   infinitely deep, 428  
   infinitely wide, 428, 440, 445  
   intraglacial, 126, 142  
   rectangular, 435  
   semi-circular, 428  
   semi-elliptical, 439  
   symmetrical, 438  
 characteristic, 144, 386, 388, 389, 393–  
   397  
 diagram, 394  
 length, 354  
 method, 347, 382, 385  
 parameter, 347, 385  
 slopes, 394  
 solution, 387, 391  
 speed, 352, 353  
 time, 148, 150, 151  
 velocity, 150  
 Clausius–Clapeyron, 126, 129, 143, 153,  
   154  
 constant, 151  
 equation, 126, 129, 143, 154  
 number, 153, 154  
 Clausius–Duhem inequality, 33–40  
 cliff, 304, 478, 479  
 climate, 122, 333, 335, 362, 363, 367  
 climatic changes, 333, 335, 362, 363  
 coldness, 148  
 compatibility, 467  
 compliance, elastic, 55  
 compression, 41, 76, 81  
   bulk, 61

- combined, 89
- equilateral, 88
- modulus, 61
  - uniaxial, 41, 87–93, 476
- compressible, 30, 34, 42
  - body, 125, 126
  - fluid, 34, 42
- compressive, 348
  - stress, 98
- component,
  - longitudinal, 299
  - mixture, 104
  - one component body, 99
  - shear stress, 458
  - tangential, 143
  - velocity, 143, 299
- composite material, 99, 100, 102
- concave ice divide, 321
- concentration, 102
  - stress, 100, 102, 479
- condition,
  - admissibility, 467–470
  - basal, 239, 312, 475
  - bottom, 454
  - bottom sliding, 453
  - boundary, Neumann type, 17, 120, 122, 130, 132–138, 140–144, 147, 152, 154, 156, 166, 175, 180, 181, 183, 191, 192, 196, 201, 203, 217, 223, 233, 234, 236, 239, 242, 244–246, 261, 268, 271, 272, 274, 277, 280, 299, 311, 312, 316, 346, 356, 379, 406, 420, 428, 430, 436, 453, 454, 456, 460, 466, 468, 469, 475
  - integrability, 475, 476
  - inter-element continuity, 467
  - jump, 17, 42, 131–143
  - kinematic, 145, 179, 180, 192, 215, 242, 244, 269, 272, 298, 299, 310, 311, 379–382, 420, 453, 454, 458, 460
  - margin, 461
  - no slip, 120, 138, 192, 233, 429
  - regularity, 346
  - shock, 389
  - sliding, 199, 220
  - thermal, 119, 122, 132, 134, 136, 147, 181, 188
- conduction,
  - heat, 31, 124, 182
- heat, equation, 182
- law of heat, 31, 124
- conducting,
  - body, 125
  - fluid, 29, 31, 34, 37, 42, 45, 46
- conductivity,
  - heat, 31, 39, 40, 124, 130
  - thermal, 151, 163
- configuration, 25, 52, 57
  - natural, 25
  - present, 4
  - reference, 4, 22, 25, 52, 53, 57
- conservation laws, *see* balance laws
- constitutive equation (relation), 18–20, 28–30, 32, 41, 48, 52, 70, 71, 91, 99, 124–125, 128–130, 146, 156, 259, 269, 298, 317, 339, 378, 452, 467
  - for heat flux, 26
  - for internal energy, 26
  - Fick-type, 129
  - isotropic, 32
  - linear, 70
  - non-linear, 140
  - Reiner–Rivlin, 125
- constitutive theory, 48, 126
- constraint condition, 30
- continuum, 4, 20, 33, 94, 99
  - mechanics, 20, 99
  - thermodynamics, 33
- continuity,
  - equation, 34, 129, 269, 299, 380, 381, 460
  - interelement, 467
- convection, 138, 168, 172, 178
  - forced, 138
  - heat, 168
  - longitudinal, 172
  - transverse, 178
- convection-diffusion equation, 401, 421
- convergence, 200, 361, 366, 372
  - radius of, 374
- convolution,
  - integral, 68
  - Laplace, 68, 363
  - operator, 68
  - Stieltjes, 68, 70
  - theorem, 363
- Coriolis acceleration, 21
- correspondence principle (elastic-visco-elastic), 68, 69
- crack, 48, 126, 478, 480

- boundary, 126
- internal, 48
- penny-shaped, 105
- propagation, 478
- creep, 32, 57–103, 168, 178, 476
  - behavior, 103, 476
  - curve, 32, 58, 67, 76, 82, 83
  - function, 57, 63–79, 124, 149, 221, 281, 392, 434, 439
  - instability, 168, 178
  - linear, 81
  - multiaxial, 41, 80, 89
  - (non) Newtonian, 84
  - polycrystalline, 77
  - primary, 76
  - rate, 85
  - relaxation, 63, 65, 69, 70
  - response, 124, 149, 281, 317, 392, 464
  - secondary, 76, 82–85, 89, 91, 99
  - state, 84, 91, 93, 94
  - steady, 82–85, 91–99
  - tertiary, 76–85, 119
  - test, 58, 67, 75, 77, 81–89
  - transient, 82
  - uniaxial, 99, 476
- crystal,
  - hexagonal, 22, 57, 60
  - ice, 51–60, 81, 99, 106
  - single ice, 56, 60, 81, 106
  - structure, 49, 51
- cusp, 175, 389
  - catastrophe, 389
- current, 121, 137, 154, 188
  - ocean, 121, 137, 154, 155, 188
  - speed, 154
- Dashpot, 72, 73
- deformation, 11, 23, 40, 52, 118, 126, 477
  - bore-hole, 477
  - Cauchy–Green tensor, 21, 40
  - creep, 81
  - gradient, 23, 24, 26, 52
  - tensor, 11, 40, 52
  - viscous, 126
- density, 30, 127
  - jump, 129
  - total mass, 127
- derivative,
  - material, 6
  - normal, 137
- destabilization, 240
- deviator, 32, 69, 80–90, 124–130
- Cauchy stress, 124, 149, 175, 215, 426, 453, 464
- invariant, 86–90, 124, 130, 149, 167, 179, 453
- Piola–Kirchhoff stress, 98
  - stress, 32, 69, 80–90, 98, 124–130, 149, 179, 215, 426, 453, 464
- differential equation, 19, 201–216, 247, 268, 274, 280, 368, 436
  - ordinary, 203, 216
  - partial, 201
- diffusion, 127, 130, 346, 347, 356, 360–362, 396, 400, 402–405, 416, 418, 420, 421
  - equation, 129, 403
  - number, 151, 153
  - thermal, 151, 153, 163
- diffusive,
  - process, 102
  - flux, 128, 133
  - model, 353
- diffusivity, 128, 129, 353, 401
  - thermal, 163
- dilute suspension, 104
- Dirac pulse, 364
- discharge, 160, 337, 343, 370, 449
- discontinuous,
  - glacier profile, 393
- discontinuity, 16–17, 131, 132, 141, 390
  - jump, 16–17, 390
  - surface, 131, 132
- discretization, finite element, 478
- disinclination, 54
- dislocation, 48, 54
- dispersion, 415, 418–420
- dissipation, 34, 126, 151–153, 165, 291
  - postulate, 34
  - energy, 151, 153
  - frictional, 165
  - number, 151, 153
  - viscous, 291
- distribution,
  - stress, 449, 458
  - temperature, 120, 218, 290, 292
  - velocity, 162, 163, 193, 326, 445, 447, 450
- divergence theorem, 13
- dome, 266, 455, 459
  - D-Cape-Poinsett, 266
- drag, 9, 120, 136–139, 155, 188
- drainage, 137
  - basal, 310
  - brine, 101

- eigenfunction, 246–248  
eigenvalue, 246, 247  
    problem, 244, 245, 250  
elastic,  
    analysis, 107  
    anisotropy, 60  
    beam, 107  
    behavior, 52, 54, 60, 67, 100  
    body, 28, 51  
    compliance, 55  
    constants, 54, 61  
    constituents, 104  
    correspondence principle, 69, 80  
    ice, 60, 61  
    inclusion, 104  
    material, 28, 53  
    modulus, 69, 103, 104, 109  
    plastic, 100  
    polycrystalline ice, 60, 61  
    properties, 56, 103  
    response, 104  
    solid, 53  
    viscoelastic correspondence principle,  
        69, 80, 100  
elasticity,  
    compliance, 55  
    constant, 51, 61  
    modulus of, 109  
element,  
    finite, 98, 467, 476, 478  
    hybrid, 467  
    incremental, 476  
    surface, 16  
    vectorial surface, 16  
elevation, geographical, 314  
ellipse, 441  
embankment, 310  
energy,  
    activation, 59, 84, 95, 125, 151, 160  
        163  
    balance of, 3, 14, 17, 30, 127, 146, 334  
    barrier, 95, 96  
    body, 127  
    budget, 136  
    dissipation, 151, 153  
    equation, 3, 14, 18, 34, 126, 129, 151,  
        156, 167, 194, 269  
    free, 20, 26, 31, 38, 40, 52–54  
    function(al), 26, 53  
    flux, 136, 333  
    Helmholtz free, 40, 65  
    internal, 10, 18–38, 124–130  
jump, 18, 44, 133–136  
kinetic, 10, 133  
melting, 127  
potential, 468  
production, 126–129  
thermal, 95  
total specific, 10  
supply, 34  
temperature, 136  
Enthalpy, free, 38  
Entropy,  
    balance, 7, 10, 33  
    flux, 10, 33  
    inequality, 34  
    jump, 18  
    principle, 20, 33, 34  
    production, 9, 17, 33  
    specific, 9  
    supply, 10, 33  
    surface, 17  
equilibrium,  
    ablation/accumulation, point, 135, 297  
    chemical, 43  
    equations of, 178, 257, 261, 427, 439,  
        458, 467, 469  
heat flux, 36  
phase, 43  
position, 95, 96  
stress, 36  
surface, 43, 284  
thermal, 99, 101  
thermostatic, 36–43  
equipresence, rule of, 35  
error function, 170  
Euclidean,  
    space, 4  
    transformation, 20  
Euler–Cauchy equation, 15  
Euler–Lagrange equation, 465–471  
Eulerian description, 16  
    formulation, 6  
    variable, 6  
evaporation, 122  
evolution equation, 130  
exponential integral, 76, 79  
extending-compressing flow, 166, 180  
fading memory, 27, 74–77  
failure, 100–109, 476  
    mechanism, 476  
    strength, 100–108  
    stress, 109

- fan, expansion, 393–397  
 Fick-type constitutive equation, 128, 144  
 field,  
     dimensionless, equations, 150  
     equations, 19, 122, 124–126, 148,  
         149, 166, 191, 195, 203, 242,  
         245, 271, 312, 379, 405, 430,  
         452, 455  
 film,  
     liquid, 139, 273  
     soap, analogy, 435  
 filter function, 203, 206, 207, 220–229  
 finite,  
     bed inclination, 314, 319  
     difference, 98, 431, 443, 462  
     element, 98, 467–478  
     hybrid, element, 467, 479  
     jump, 16  
     mesh, 443, 444  
     slope, 322  
     strain, 476, 478  
     velocity, 306–309  
     viscosity creep (function), 119, 253,  
         313, 316–319  
 flexural,  
     strength, 105–108  
     wave velocity, 103  
 flow,  
     boundary, 137, 139  
     channel, 426  
     compressing, 166, 180  
     extending, 168, 180  
     generalized, law, 158, 223, 417  
     geothermal heat, 139  
     Glen's, law, 85, 92, 93, 141, 200, 218,  
         223, 236, 250, 253, 277, 283,  
         313, 317, 318, 343, 413, 415,  
         417, 418, 442  
     ice sheet, 425  
     instability, 239–250  
     inner (outer), 137–140  
     law, 85, 92, 119, 141, 158, 163, 182,  
         200, 218, 223, 236, 244, 250,  
         253, 259, 277, 283, 288, 289,  
         291, 313, 317, 318, 343, 392,  
         413, 415–418, 434, 442  
     lines, 181  
     outer, 137–140, 303, 438  
     plastic, 258, *see also* creep  
     Prandtl–Eyring, law, 92  
     rectilinear, 426, 462  
     secondary, 93, 426
- steady, 138, 387, 426  
 turbulent, 138  
 fluid,  
     boundary layer, 434  
     compressible, 34, 42  
     heat conducting, 29, 31, 34, 37, 42,  
         45, 46  
     incompressible, 31, 37, 38, 46, 86, 184  
     linear, non-linear, 86, 91  
     linear viscous, 476  
     Maxwell (generalized), 72  
     (non) Newtonian, 124, 201, 204, 213,  
         244, 246, 249, 426, 434, 435,  
         439, 479, 481, 482  
     power law, 438–450  
     Reiner–Rivlin, 32  
     stability, 244  
     thermoelastic, 28  
     viscoelastic, 33  
     viscosity, 104  
     viscous, 4, 18, 31, 34, 37, 42, 45–48,  
         66, 86, 119, 244, 246, 329
- flux,  
     accumulation, function, 202, 293–299,  
         310, 385, 392  
     atmospheric heat, 135  
     diffusive, 128, 133  
     energy, 133–136  
     entropy, 10, 33  
     Fick-type, 144  
     geothermal heat, 163, 252, 333  
     heat, 31, 36, 124, 133–138, 153, 252,  
         333  
     mass, 133, 188, 293, 295, 319, 378  
     moisture, 128, 135, 143, 144
- force,  
     balance, 296, 474  
     external, 124  
     frictional, 143  
     gravity, 120  
     longitudinal, 257  
     path dependent, 97  
     restoring, 97  
     shearing, 96
- Fourier,  
     analysis, 370  
     constitutive relation, 130  
     cosine decomposition, 284  
     cosine integral, 71  
     series, 242  
     sine integral, 71  
     transform, 71, 202
- fracture, 481

- frame,  
   dependent, 21  
   indifference, 21, 22, 29, 52  
   (non) inertial, 21  
   of reference, 4  
   rule of material, indifference, 21, 22,  
     29  
 freezing, 101, 136–138, 245  
   of brine, 101  
   melting, 122, 136, 180  
   point, 101, 138  
   rate, 136  
   temperature, 102, 145  
 frequency, 54, 96, 203, 365, 374  
   of activation, 96  
   analysis, 374  
 friction,  
   basal, 153  
   bottom, 325  
   effect, 155  
   factor, 137  
   viscous, 182  
 frictional,  
   coefficient, 151, 314  
   dissipation, 165  
   force, 143  
   heat, 126  
   power, 143  
 Froude number, 149, 153, 154  
 function,  
   accumulation, 135, 202, 295, 296,  
     319, 321–323, 326, 327, 329,  
     347, 363, 365, 385, 451  
 Arrhenius, 85  
 creep, 57, 63, 65, 66–70, 76, 77, 79,  
     124, 149, 221, 281, 309, 310,  
     392, 426, 434, 439, 453  
 drainage, 310  
 enthalpy, 38  
 error, 170  
 filter, 203, 206, 207, 220–226, 228,  
     229  
 flux, 202, 293–297, 299, 310, 385,  
     392  
 generalized, 381  
 Green's, 370  
 Heavyside, 65, 363  
 isotropic, 30–32, 98  
 relaxation, 63–66, 68–70, 72–75, 77,  
     79, 80, 103  
 response, 80, 124, 141, 149, 281, 306,  
     317, 318, 392  
   stream, 200, 201, 213, 216, 236, 246,  
     381  
   stress, 200, 201, 213, 215, 216, 442  
   transfer, 203, 206, 207, 220  
   viscoelastic response, 80, 124  
 functional, 19, 464–474  
   constitutive, 26  
   equation, 19  
   heat flux, 26  
   isotropic, 26  
   material, 20, 21  
   scalar, 26  
   tensorial, 26  
   vectorial, 26  
 fusion,  
   heat of, 43, 127, 132, 151  
   latent heat of, 43, 127, 132, 151  
   number, 153  
 Gauss theorem (divergence theorem), 13,  
     464  
 geothermal,  
   flow, 139  
   heat, 139, 252, 333  
   heat flux, 161–165, 172, 177  
 Gibbs relation, 36, 40  
 glacier, 18, 119, 120, 134, 135, 183, 253,  
     256, 333, 425, 478  
   advance, 260, 358  
   de Bosson, 243, 335  
   cirque, 309  
   hanging, 462  
   mountain, 122, 425  
   Nisqually, 335  
   polythermal, 127, 141, 143, 330  
   retreat, 122  
   de Saint Sorlin, 362  
   steep, 269, 309, 310  
   subpolar, 244  
   surge, 335  
   temperate, 120, 121, 282, 344  
   valley, 119, 120, 297, 336, 337, 341,  
     346, 369, 424, 438  
   waves on, 260, 378  
 Glen's flow law, 83, 85, 92, 93, 141, 151,  
     200, 218, 223, 236, 250, 253,  
     277, 283, 313, 316–318, 343,  
     413, 415, 417, 418, 429, 442  
   generalized, 223, 417  
   number, 149, 153  
 gliding, 157, 293, 334, 343, 344  
   mechanism, 334

- speed, 158  
 surface, 158, 192  
 velocity, 158, 159  
 global balance laws, 13, 131, 334  
 gradient,  
     deformation, 23, 24, 26, 52  
     horizontal, 456, 457  
     longitudinal, 244, 336  
     pressure, 429, 456, 457  
     shear stress, 313, 456  
     stress, 244, 336  
     temperature, 23–26, 86  
     velocity, 29, 446  
 grain, 22, 48, 63, 102, 126  
     boundaries, 63, 102, 126  
     crystal, 60  
 Green's function, 370  
 Greenland, 48  
 Grubengletscher, 478  
  
 harmonic, 57, 202, 215, 242, 265  
     analysis, 202, 252  
     excitation, 57  
     perturbation, 202, 216  
     undulation, 265  
 head, 297, 303, 330, 346, 361  
 heat,  
     advection, 226  
     conduction, 31, 34, 37, 42, 45, 46, 86,  
         124, 125  
     conductivity, 31, 39, 40, 124, 130  
     convective, 168  
     equation, 173, 176, 182  
     flow, 7  
     flux, 31, 36, 133–138, 153, 252, 333  
     frictional, 126  
     geothermal, 139, 252, 333  
     latent, of fusion, 43, 127, 132, 151  
     specific, 39, 124, 126, 151  
     strain, 126  
     supply, 10  
     transfer, 136–138, 151, 173, 176  
 heat flux,  
     atmospheric, 133, 156, 174  
     basal, 160  
     geothermal, 161–165, 172, 177  
 jump in, 143  
 material, 22  
 vector, 7, 19, 31, 124, 129  
 heating, strain, 161–178  
 Heaviside,  
     function, 65, 363  
  
     pulse, 359  
     Helmholtz free energy, 40, 65  
     hereditary effects, 19, 41  
     homogeneous body, 52  
     Hooke's law, 60, 67  
     hybrid finite element, 467–479  
     hyper-ellipses, 294, 441–449  
  
 Ice,  
     ablation, 321  
     arctic, 103  
     basal, 244  
     bedrock, 123, 283, 310  
     cap, 48, 63, 189, 266–297  
     cold, 123–129, 134–150, 183, 192,  
         231, 291, 400  
     crystal, 51, 56, 60, 81, 99, 106  
     divide, 309, 314, 316, 320, 322, 329  
     dome, 309  
     elastic, 60, 61  
     floating, 4, 49, 71, 92, 121, 122, 137,  
         155, 179, 188  
     freshwater, 99  
     hexagonal, 49, 52  
     *Ih, Ic*, 49–60  
     lake, 49, 71  
     molten, 175  
     ordinary, 49, 50, 63  
     parallel-sided, slab, 119, 145, 147, 154,  
         161, 183, 184, 188, 190, 196,  
         218, 219, 230, 252, 256, 276,  
         424  
     plastic, 91, 92, 155, 295, 298  
     plates, 49, 92, 137  
     polar, 171  
     polycrystalline, 22, 60, 61, 63, 65, 77,  
         81–83, 85, 86, 93, 94, 99, 100  
     polythermal, 127, 145  
     reservoir, 310, 327  
     sea, 99–110  
     shallow, approximation, 243, 256, 257,  
         268, 270, 273, 276, 279, 292,  
         298, 303, 309, 311, 313, 334,  
         379, 400, 405, 424, 451, 455,  
         461, 462, 478, 484  
     sheets, 4, 119, 120, 122, 123, 135,  
         144, 148, 159, 162, 168, 171,  
         183, 188, 256, 259, 260, 284,  
         291, 293, 297, 309, 330, 333,  
         379, 403, 424, 425, 428, 450–  
         452, 455, 461, 462, 478

- shelf, 121, 122, 124, 155, 167, 179, 181, 188
- slab, 119, 145, 147, 154, 161, 183, 184, 188, 190, 191, 196, 218, 219, 230, 256, 276, 404, 416, 424
- standard sea, 100–102
- temperate, 123, 126, 127, 129, 131, 132, 135, 136, 138–141, 145, 146, 149, 156, 160, 233, 237, 238, 288, 291, 303, 343, 451
- water interface, 121–123, 134, 136–138, 147, 153, 155, 179, 181, 182, 283, 310
- sheet, 425
- rock interface, 147
- viscoelastic, 70
- viscous, 66
- impurity, 63, 129
- inclination, 221–265, 316–319, 338
  - angle, 221, 230, 260, 264, 338
  - bed, 316, 319
  - surface, 258, 259, 338
- inclusion,
  - of brine, 49, 100–103
  - elastic, 104
  - elliptical, 104
- incompressible, 30, 86, 89, 125, 130
  - heat conducting fluid, 31, 37, 38, 46, 86, 124
- indifference, material frame, 21–29, 52
- inelastic behavior, 56
- inequality,
  - Clausius–Duhem, 33–40
  - entropy, 34
  - residual, 35, 37
- inertial, 21, 244, 249
- inflection point, 76
- inner flow, 139, 140, *see also* boundary layer flow
  - instability, 168–180, 240, 249, 259, 394, 398
  - creep, 168, 178
  - flow, 250
- integrability condition, 475, 476
- integration, 157, 209, 377
  - Runge–Kutta, 377
- inviscid, 139
- isostatic depression, 297
- isotropic, 24, 34–40, 60, 68, 82
  - behavior, 56
  - body, 25, 26, 48, 100, 103
- constitutive response, 25, 30–32
- function, 30–32, 98
- viscoelastic body, 56, 80
- jump, 16, 45, 131, 392, 397, 403
  - condition, 17, 18, 42, 131–143
  - energy, 18, 44, 134
  - entropy, 18
  - heat flux, 143
  - mass, 18
  - moisture, 137, 143
  - momentum, 18, 133, 136
- Kelvin,
  - body, 72, 73, 79
  - generalized, body, 72
  - solid, 75
  - temperature, 124
- kinematic,
  - boundary condition, 145, 179, 180, 192, 215, 242, 244, 269, 272, 298, 299, 310, 311, 379–382, 420, 453, 454, 458, 460
  - equation, 132, 133, 136, 273, 292, 315, 336, 339, 342, 381, 413, 420, 461
  - surface condition, 132, 136, 145, 179, 192, 215, 269, 272, 273, 292, 298, 310, 311, 315, 379–382, 413, 453, 454, 458
  - wave, 122, 160, 190, 243, 334–336, 339, 342, 350, 377, 378, 381, 398, 415, 461
- Korteweg–de Vries equation, 415
- lag, phase-angle, 203–237
- Lagrangian,
  - description, 7, 18
  - multiplier, 469
  - parameter, 468–471
  - strain tensor, 52, 53, 98
- lake ice, 49, 71, 137
- Lamé constants, 61–65
- Laplace,
  - convolution, 68, 363
  - transform, 68–73, 358, 363
- latent heat, 43, 127, 132, 151
- lattice dynamics, 55
- layer, 121–140
  - boundary, 121, 129, 136–140
    - inner, 139
    - outer, 139
    - thermal, 138

- Legendre transformation, 466, 474  
 Leibnitz' rule, 262, 264, 380, 460  
 lemma, Cauchy, 7  
 limit, 110, 219, 310  
     analysis, 219  
     asymptotic, 310  
     load, 110  
 lines of equal height, 459  
 liquid, 99, 139, 207, 214, 273  
     brine, 99  
     film, 139, 273  
     Navier-Stokes, 207  
     (non) Newtonian, 214  
 logarithmic decrement, 56  
 lubrication, 139, 244  
  
 margin, 299–330, 381, 383, 402, 404, 455  
     ablation, 308  
     condition, 461  
     slope, 302, 322  
     surface, 319  
     velocity, 302, 306, 307, 319, 327  
  
 Mass,  
     balance of, 9, 14, 18, 30, 124–129, 294, 298, 328, 334, 339, 378, 420, 452  
     body, 127  
     density, 7  
     flux, 133, 188, 293, 315, 319, 378  
     fraction, 128  
     jump condition of, 18  
     production, 127, 128  
     water mass, 129  
  
 material, 7  
     behavior, 49, 309  
     composite, 102  
     description, 18  
     elastic, 28, 53  
     frame indifference, 21, 22, 29, 52  
     function, 141, 317, 318  
     functional, 20, 21  
     heat flux, 22  
     ideally plastic, 155, 295  
     incompressible, 30  
     memory, 27, 99  
     objectivity, 20  
     plastic, 92, 155, 258, 295  
     properties, 49, 221, 268, 279, 297, 298, 303  
     of the rate type, 27  
     one-component, 9, 99  
  
     response, 1–120, 141, 317, 318, 324  
     rule of, frame indifference, 20, 21  
     science, 48, 52, 53, 98, 45–110  
     simple, 18, 20, 27  
     symmetry, 22, 27  
     matrix, orthogonal, 25  
     maximum-minimum principle, 480  
     Maxwell, 29, 72–80  
         body, 72, 73  
         fluid, 29, 70  
         generalized, body, 72  
     measurements,  
         frequency, 54  
         logarithmic decrement, 56  
     mechanism,  
         bifurcation, 142  
         calving, 304  
         dislocation, 95  
         failure, 476  
         gliding, 334  
     Meighen ice cap, 296, 297  
     melting, 44–46, 120–180, 227  
         curve, 141  
         energy, 127  
         formula, 44–46  
         freezing, 122, 136, 180  
         point, 99, 120, 123, 137, 141, 172, 174–176  
         pressure, 44–46, 151  
         rate, 121, 135–137, 143  
         surface, 123, 129, 132, 138, 143, 144  
         temperature, 99, 127, 151, 156, 164, 165, 172, 227  
     meltwater, 142  
     memory, 27, 74–77, 99, 369  
         bounded, 99  
         fading, 27, 74, 76, 77  
     Mer de Glace, 243, 258, 335  
     mixture, 9, 122–134  
         binary, 9, 122, 126, 127, 128  
         component, 104  
         concept, 132  
         ice water, 134  
         incompressible, 128  
     modulus, 61–80, 103–105, 366, 367  
         bulk, 61  
         complex, 71  
         compression, 61  
         effective elastic, 104  
         elastic, 69, 103–109  
         Young's, 61–67, 80, 103  
     moisture, 128–149, 183, 221

- boundary condition, 137  
 content, 128–131, 135, 137, 144,  
     146, 149, 183, 221  
 diffusion, 128  
 diffusive flux, 128, 135, 143, 144  
 jump condition, 137, 143  
 molecule, 51, 175  
 momentum, 9  
     balance of, 14, 18, 124, 125, 269, 474  
     balance of angular, 14  
     jump, 18, 133  
     production, 9  
     supply, 9  
 motion, 5, 52  
 moulin, 121, 126  
 Müller's method, 301  
  
 Nabla operator, 26  
 Navier–Stokes, 29, 207  
 Nevel's ice model, 76  
 Newton, 9  
 Newtonian (non-),  
     behavior, 29, 84, 92, 158, 201, 277  
     creep, 84  
     fluid, 29, 124, 201, 204, 213, 244,  
         246, 249, 426, 434, 435, 439,  
         474, 479, 481, 482  
 Nisqually glacier, 335  
 non-local hereditary effects, 19  
 non-polar theory, 10  
 Nusselt number, 138, 153, 154  
  
 objective, 30, 32  
     stress rate, 30, 32  
 objectivity, 22  
     rule of, 22  
 ocean, 121, 137, 153–155, 179, 182,  
     188  
 one-component material, 9  
 Onsager, 40, 463  
  
 part, skewsymmetric, 29  
 partial fraction, 363  
 permutation symbol, 10  
 perturbation, 178, 218, 236–252, 329,  
     368, 370, 398, 413, 420, 428  
     analysis, 165  
     expansion, 189, 193, 273, 287, 341,  
         405  
     harmonic, 202, 216  
     method, 198–274, 407, 414, 431–435  
     series, 290  
  
 phase, 15, 41–46, 125–137, 206–208,  
     220–237  
 angle, 206–208, 220–237, 366  
 change, 15, 41–46, 125–134, 143,  
     451  
 change discontinuity, 100  
 diagram, 99–101, 121  
 equilibrium, 43  
 lag, 206, 220–237, 366  
 shift, 203  
 surface of, change, 42, 43, 131–134,  
     143  
 phenomenological, 3, 17, 30, 100, 110,  
     266, 334–342  
     constant, 100, 266  
     law, 30, 339  
     relation, 3, 17, 342  
 pillbox, 16, 17  
 Piola–Kirchhoff,  
     deviator, 98  
     first stress, 7, 98  
 Plande's constant, 95  
 plastic behavior, 51, 91, 92, 100, 105,  
     135, 295–298  
 plates, 49, 92, 137  
 Poisson's,  
     equation, 434, 435  
     ratio, 61, 62, 77, 80, 105  
 pole, 74, 75, 359  
 polycrystalline, 22, 60–100  
     aggregate, 56  
     behavior, 60  
     creep, 77  
     elastic body, 60, 61  
     ice, 22, 60–65, 77, 81–86, 93–100  
 polynomial, 92, 287, 317–326, 356,  
     363  
 polythermal,  
     glaciers, 127, 141, 143, 330  
     ice, 120–145, 191, 451  
 porosity,  
     brine, 100–105  
     volume, 100–105  
 porous media, 121  
 postulate, dissipation, 34  
 potential,  
     chemical, 43, 45  
     creep, 464  
     energy, 468  
     thermodynamic, 52, 65  
 power,  
     frictional, 143

- Glen's, law, 91, 119, 137, 159, 163, 291, 308, 313, 317, 324, 369, 392, 416, 429, 434, 439, 442, 443, 450, 477
- Prandtl, 92–95, 138, 151, 154
- Eyring flow law, 92–95
- number, 138, 151, 154
- precipitation, 122, 333
- pressure,
- atmospheric, 32, 37, 124, 181, 453
  - contact, 121
  - extra, 38
  - horizontal, 456, 457
  - hydrostatic, 121, 478
  - melting, 44–46
  - over burden, 121, 155, 191, 235, 292
  - water, 121, 136, 243
- profile,
- bedrock, 300, 301
  - effective, 244
  - equilibrium surface, 287
  - inversion (temperature), 172, 218
  - surface, 284, 296, 298, 315, 321, 328, 352, 403, 455
  - temperature, 16, 171, 172, 218
- propagation, 25, 48–56, 103, 272, 336, 478
- crack, 478
- elastic wave, 56, 103
- ultrasonic pulse, 51
- wave, 25, 48, 51, 272, 336
- protuberance,
- bedrock, 188, 189
  - bottom, 220, 256
- quadrilateral element, 477
- quasilinearization, 157
- quasi-Newtonian behavior, 159, 211
- radiation, 10
- reciprocal variational principle, 468, 473
- reciprocity relations of Onsager, 40
- recrystallization, 49, 60, 82, 84
- regelation, 121
- Reiner–Rivlin, 125, 475
- relaxation, 57, 76
- creep, 63–70
- functions, 64–66, 68–70, 72–75, 77, 79, 80
- time, 57, 74–79, 362, 365
- reservoir, 310, 327, 328
- residue theorem, 74, 359
- residual inequality, 35, 37
- response,
- creep, 85, 124, 149, 281, 317, 392, 464
  - frequency, 365
  - functional, 27
  - functions, 80, 124, 141, 149, 281, 306, 317, 318, 392
  - high frequency, 373
  - low frequency, 371
- retardation, 57, 74
- retreat, 122, 335, 369, 397
- Reynold's number, 138, 154, 251
- rheological models, 72–77
- rheology, 140, 208
- ridge, 256
- Rivlin–Ericksen,
- fluid, 29
  - tensor, 29, 99
- rockbed, 139, 152, 155, 188, 202
- actual, 139
- protuberances, 188
- smoothed, 139, 140
- surface, 140
- roughness,
- drag, 120
  - of bed, 140, 141, 206
  - scale, 139
  - surface, 137
  - tensor, 52
- rule,
- Leibnitz', 262, 264, 380
  - of equipresence, 35
  - of material frame indifference, 21
  - of objectivity, 20, 21
- Runge–Kutta, 377
- Saint Sorlin, glacier de, 362
- salinity, 49, 99, 102
- salt, 99–101, 145
- content, 99, 102, 129
  - solid, 99, 100, 101
- scalar valued functional, 26
- isotropic, 26
- scale, 120, 139, 148, 157
- length, 148, 257
- protuberance, 120
- roughness, 139
- scaling, 148, 287, 309–311
- sea,
- arctic, 103
  - ice, 49, 99–110
  - standard, ice, 100–102

- separation,  
   of exponentials, 75  
   of variables, 178  
 series, 290, 356, 376  
   perturbation, 290  
   power, 356, 376  
 Shallow ice approximation, 243, 256, 257,  
   268, 270, 273, 276, 279, 292,  
   298, 303, 309, 311, 313, 334,  
   379, 400, 405, 424, 451, 455,  
   461, 462, 478, 484  
 shear, 41, 80, 87, 89, 90  
   basal, 140, 155, 189, 231, 257, 273,  
   276, 281, 287, 293, 484  
   strength, 108  
   traction, 136, 142, 312  
 shear stress, 59, 137, 140, 155, 179, 189,  
   273, 276, 281, 287, 293, 297,  
   316, 446–448, 484  
   amplitude, 231–234  
   basal, 259–264, 276, 279  
   formula, 259–264, 276–279, 287,  
   294, 316, 457, 458  
 sheet,  
   dome like ice, 309  
   ice, 119, 120, 122, 123, 135, 144, 148,  
   159, 162, 168, 171, 183, 188,  
   256, 259, 260, 284, 291, 293,  
   297, 309, 330, 333, 379, 403,  
   424, 425, 428, 450–452, 455,  
   461, 462, 478  
   polar, 171  
   three dimensional, 452  
 shock, 15, 391–401  
   condition, 389  
   discontinuity, 390  
   dynamics, 421  
   formation, 272  
   multiple, 390–392  
   speed, 402  
 similarity, 400–401  
   argument, 400  
   transformation, 401  
 singular, 42, 283, 291, 302, 303, 308,  
   319, 346, 352, 371  
   perturbation, 152, 219  
   surface, 16, 17, 131–133, 143  
 singularity, 218, 231–234, 278, 283, 350,  
   413  
 pole, 74  
 stress, 142, 221  
 slab,  
   ice, 119, 145, 147, 154, 161, 183, 184,  
   188, 190, 191, 196, 218, 219,  
   230, 256, 276, 404, 416, 424  
   parallel-sided, 119, 120, 145, 147,  
   154, 161, 183, 184, 188, 190,  
   192, 194, 196, 199, 218, 219,  
   230, 245, 258, 276, 283, 291,  
   343, 424  
 sliding,  
   basal, 58, 140, 233, 238, 248, 279,  
   400  
 law, 140–143, 167, 188, 192, 198,  
   199, 204, 210, 212, 222, 228,  
   232, 233, 236, 238, 240, 250,  
   269, 279, 285, 293, 322, 324,  
   343, 392, 417–419, 450, 454,  
   463, 464, 476  
 linear, 324, 476  
 nonlinear, 476  
 perfect, 192  
 stress dependent, 167, 188, 204, 210  
 velocity, 140, 142, 157, 208, 212,  
   223–226, 238  
 viscous, 204, 212, 222, 233, 236, 269,  
   302, 458, 463, 476  
 Weertmann-type, 147, 225, 228, 232,  
   234–240, 285, 293, 343, 392,  
   464  
 with cavitation, 121, 140  
 with cavity formation, 121, 140–142,  
   475  
 slip,  
   boundary condition, 120, 138, 192,  
   233, 234, 429  
 no, 58, 223–241, 287, 426, 432, 445,  
   488, 476  
   perfect, 120, 215, 302  
 slope, 189, 302–322, 358, 328, 314,  
   404  
 bedrock, 189  
   characteristic, 394  
   surface, 258, 259, 328, 404  
 snout, 122, 139, 256, 308, 309, 319, 330,  
   345, 346, 361, 367, 369,  
   388  
   advance, 396  
   condition, 307  
   evolution, 365  
   velocity, 306–309, 315  
   wedge-shaped, 344, 346  
 soap film analogy, 435

- solid,  
     elastic, 4, 53  
     fluid, 18, 27, 99  
     ideally plastic, 4  
     Kelvin, 75  
     precipitation, 122  
     salt, 99–101  
     thermoelastic, 39  
     viscoelastic, 4, 48  
 Sommerfeld equation, 246  
 speed,  
     characteristic, 352, 353  
     crack propagation, 105  
     current, 154  
     gliding, 158  
     ocean, 154  
     of propagation, 131  
     shock, 402  
     surface, 158  
     surface particle, 244, 385  
     wave, 103, 105, 273, 401  
 spring-dashpot, 72, 73  
 stability, 165, 178, 190, 243–253, 341, 352  
     parameter, 169, 177, 178  
     surface wave, 243, 333  
 state,  
     natural, 53, 73  
     variable, 129  
 statistical mechanics, 33, 95  
 steady state, 81–94, 138, 170, 202, 216, 358, 362, 399  
     accumulation, 202, 212, 240  
     analysis, 252  
     creep, 82–85, 91–99, 212, 240  
     profile, 287–298, 309, 322, 330, 357  
     temperature profile, 170, 217  
 steepest descent, 459  
 Stefan problem, 144  
 Stieltjes convolution, 68, 70  
 strain,  
     hardening, 59  
     heating, 126, 161, 162, 165, 168–170, 172, 176, 178  
     history, 66  
     Lagrangian, 52, 53, 98  
     linear, 60  
     longitudinal, 168, 231, 259, 266, 268, 281,  
     rate, 32, 76, 84–92, 99, 105, 167, 168, 259, 266, 268  
     tensor, 52, 98  
     softening, 59, 60, 244  
 strength,  
     failure, 100–108  
     flexural, 105–109  
     tensile, 107, 109  
 stress,  
     amplitude, 230, 236  
     atmospheric, 133  
     basal, 140, 155, 189, 230, 235, 256, 273, 276, 281, 287, 293, 484  
     Cauchy, 7, 31, 52, 124  
     compressive, 98  
     concentration, 100, 479  
     deviator, 32, 69, 80, 86–88, 90, 98, 124, 128, 130, 149, 179, 215, 268, 426, 453, 463  
     extra, 36–38  
     failure, 109  
     function, 200–216, 442  
     induced anisotropy, 49, 98  
     invariants, 86–90, 124, 130, 149, 179, 453  
     multiaxial, 41, 80, 99  
     Piola–Kirchhoff, 7–10, 19, 22, 31, 40, 52, 56, 98  
     rate, 30  
 shear, 59, 137, 140, 154, 179, 189, 273, 276, 281, 287, 293, 297, 316, 446–448, 484  
     singularity, 221  
     uniaxial, 57  
 stretched coordinates, 270, 290  
 stretching, 38, 86, 88, 92, 182, 215, 221, 318, 466  
     coordinate, 151, 303, 378, 436, 439  
     parameter, 270, 273, 284, 285  
     tensor, 38, 86–89, 124, 130  
 surface,  
     angle, 338  
     amplitude, 237, 241  
     base, 134, 138, 184, 220, 291, 316, 456  
     boundary condition, 134, 145, 179, 192, 215, 269, 272, 298, 310, 311, 316, 379, 380–382, 453, 454, 458  
     bulges, 335  
     datum, 337, 362  
     discharge, 136  
     elevation, 190  
     entropy production, 17  
     free, 122, 123, 132–135, 138, 147, 152, 166, 184, 192, 197, 243, 263, 446, 453, 456

- geometry, 122, 297, 303, 460  
 gliding, 158  
 kinematic equation, 132, 136, 269, 272, 273, 292, 298, 310, 311, 315, 370, 380, 381, 382, 413, 453, 454, 458  
 margin, 319  
 melting, 123, 129, 132, 138, 143, 144 of discontinuity, 131, 132 of phase change, 42, 43, 131, 134, 143 of singularity, 131–133 rigid, 143 roughness, 137 strain, 259, 266, 268 temperature, 134, 152, 156, 160 undulations, 189, 190 velocity, 150, 161, 164, 236–241, 256, 268, 379, 417 wave, 190, 243, 260, 272, 333, 336, 377, 380, 385, 404, 417 wave speed, 158, 385 wave stability, 333 suspension, 104 supercritical, 165  
 temperate,  
   cold, transition, 142  
   ice, 123, 126, 127, 129, 131, 132, 135, 136, 138–141, 145, 146, 149, 156, 160, 233, 237, 238, 288, 291, 303, 343, 451 temperature,  
   absolute, 9, 95  
   basal, 164, 175, 177, 336 freezing, 102, 145 Kelvin, 124 melting, 99, 127, 151, 156, 164, 165, 172, 227 inversion profile, 218 tensor,  
   antisymmetric, 8  
   Cartesian, 4  
   Cauchy stress, 9, 31 deviator, 87 extra stress, 37 invariant, 31, 87, 167 Piola–Kirchhoff, 22, 40, 52, 56 Rivlin–Erickson, 99 rotation, 52 strain, 15, 52, 53, 98 stretching, 15, 38, 86–89, 124, 130 symmetric, 31 tensorial, 26, 98 function, 98 functional, 26 thermodynamic(s), 1–47 admissible process, 41 irreversible, 10 process, 19, 34, 35 potential, 52, 65 second law of, 10, 17, 20, 33 thermoelastic body, 28, 40 thermostatic equilibrium, 36–43, 99 third invariant, 80, 87 topography, 120, 297, 329, 455 bottom, 155 smoothed-out, 120, 139, 140, 192, 257 tracer, 127 traction, 133, 136, 142, 230, 312 transfer,  
   coefficient, 136–138, 151 function, 203–207, 220 heat, 136–138, 151, 173, 176 transform,  
   fast Fourier, 202 Fourier cosine, 71 Fourier sine, 71 Laplace, 69, 73, 358, 363 transformation,  
   Euclidean, 20 isotropic, 24 MJ, 311–313, 441, 478 orthogonal, 24–25 shallow ice, 313 similarity, 401 stretching, 270, 273, 311, 406, 458 symmetry, 24 unimodular, 25 transition,  
   cold-temperate, 142 transport theorem, 16 transverse,  
   ad- (con)vection, 171, 178, 196, 226 velocity, 168, 236, 237, 239, 240, 275, 287 triple point, 121 turbulent, 138 two-component mixture, 41, 104 two-point value problem, 160, 174, 208, 243, 291 ultrasonic, 51, 55 undulations,  
   basal, 222

- bottom, 212, 217, 220, 226, 229, 231, 245
- surface, 189, 190
- uniaxial,
  - compression, 41, 87–93, 476
  - creep, 99, 476
  - strain, 57
  - stress, 57
- unidirectional flow, 462
- uniform(ly)
  - accumulation, 327
  - flow, 202
  - valid solution, 301
- unimodular, 25, 27
- variational,
  - calculus, 463
  - principle, 425, 462, 463, 467, 474, 476, 477
  - theorem, 463–475
- varying,
  - slowly, 270, 278, 279, 292
- vector,
  - differential equation, 209, 210, 247
  - gravity, 453
  - heat flux, 7, 19, 31, 124, 129
- vein, 102
- velocity,
  - barycentric, 127
  - basal, 140, 248, 325
  - boundary condition, 194, 477
  - characteristic, 150
  - diffusion, 128
  - jump, 133
  - longitudinal, 188, 218, 236–239, 299, 303, 311, 482
  - margin, 306, 307, 319, 327
  - shock, 390, 391
  - sliding, 142, 157, 208, 212, 223, 224, 226, 238, 248, 314, 429, 478
  - snout, 302, 306–309, 315
  - surface, 150, 161, 164, 236–241, 256, 268, 397, 417
- viscoelastic, 33, 41, 49, 56, 63, 80, 100, 105
  - constant, 78, 79
  - correspondence principle, 69, 80
  - functions, 80
  - linear, body, 63–70, 100
- viscous,
  - body, 28, 51, 100, 110, 125, 126
  - compressible body, 34, 42, 125, 126
- creep, 81
- dissipation, 291
- drag, 120
  - aerodynamic, 9
- fluid, 31–48, 66, 86, 91, 119, 244, 246, 329
- friction, 182
- heat conducting fluid, 4, 18, 28, 31, 34, 37, 42, 45, 46, 125
- incompressible body, 31, 37, 46, 86
- (non) Newtonian fluid, 124, 244, 246
- sliding, 204, 212, 222, 223, 236, 269, 302, 458, 463, 476
- thermoelastic body, 28
- viscosity, 56, 98, 104, 137, 317
  - bulk, 56, 104
  - effective, 218, 244
  - kinematic, 137
  - logarithmic, law, 91–93
- viscotropic, 98
- Volterra integral equation, 70
- water, 41, 129
  - balance of, 129
  - content, 121
  - ice, interface, 51, 121–123, 136–138, 147, 153, 155, 179, 181, 182
  - table, 142
  - trapped, 243
- wave,
  - body, 103
  - equation, 336, 339, 342, 377, 381, 420, 461
  - flexural, 103
  - kinematic, 122, 160, 190, 243, 334–336, 339, 342, 350, 377, 378, 381, 398, 415, 420, 461
  - lengths, 203, 207, 208, 212, 220–222, 226, 228, 230–240, 243, 265, 266, 407
  - paths, 350–352
  - seasonal, 190, 260, 336, 385, 421
  - speed, 103, 105, 273, 401
  - surface, 189, 190, 245, 260, 272, 336, 377, 380, 404, 417
  - ultrasonic, 51
- wavenumber, 245, 250, 251
- Wilkes ice cap, 266
- yield stress, 258
- Young's modulus, 61–67, 80, 103